Vol. 26, No. 8

EMERGING INFECTIOUS DISEASES®

CDC
CENTERS FOR DISEASE CONTROL AND PREVENTION

Parasitic Infections

August 2020

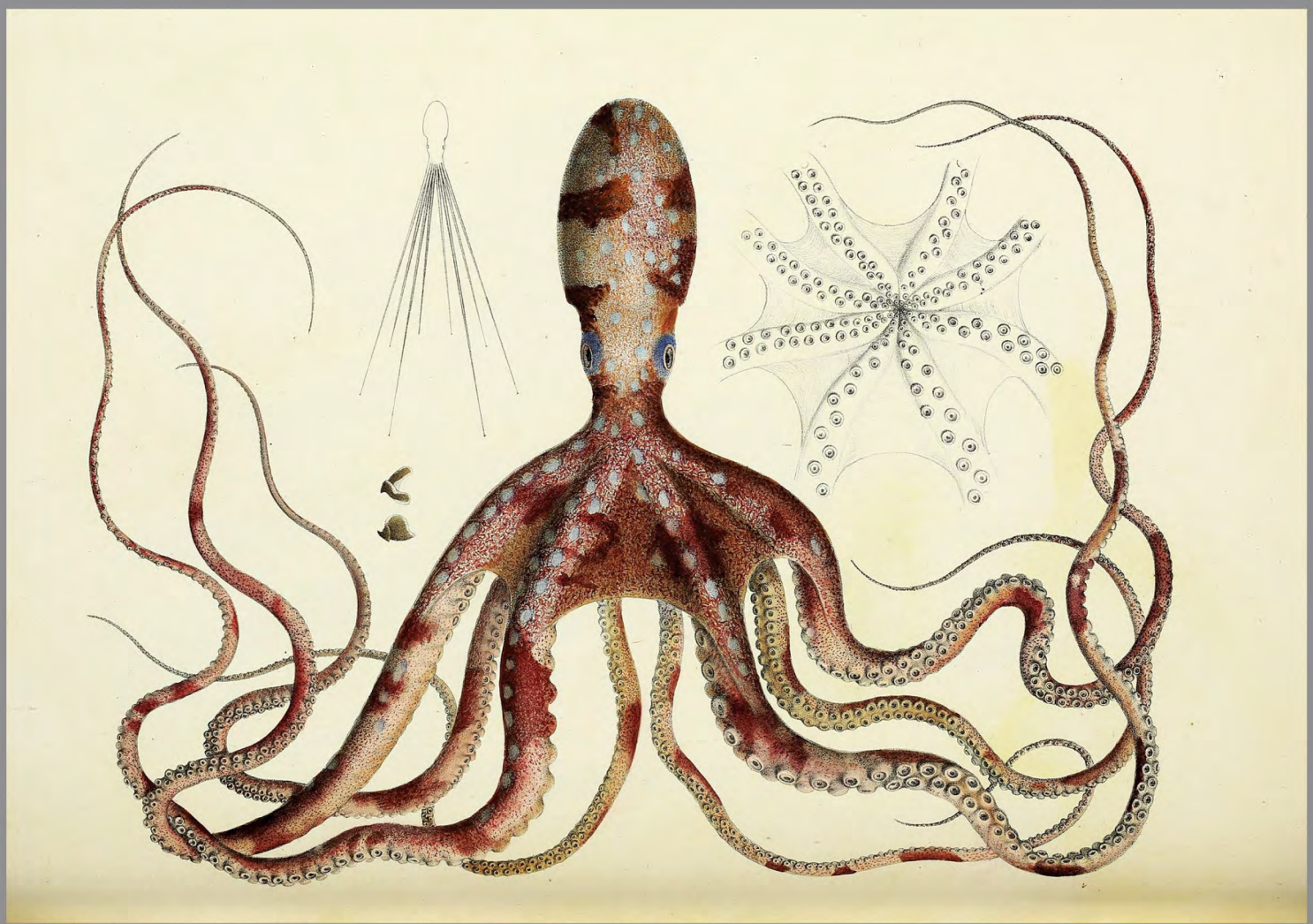

A.E. d'Audebard de baron de Férussac (1786–1836) and Alcide Dessalines d' Orbigny (1802–1857). Plate 24 from *Natural, General and Particular History of the Acetabuiferous Cephalopods Living* (1835). Ink on paper. Public domain image from Biodiversity Heritage Library. Holding institution: Smithsonian Libraries, Washington DC, USA.

EMERGING INFECTIOUS DISEASES®

Emerging Infectious Diseases is published monthly by the Centers for Disease Control and Prevention, 1600 Clifton Rd NE, Mailstop H16-2, Atlanta, GA 30329-4027, USA. Telephone 404-639-1960; email, eideditor@cdc.gov

EMERGING INFECTIOUS DISEASES®

Parasitic Infections **August 2020**

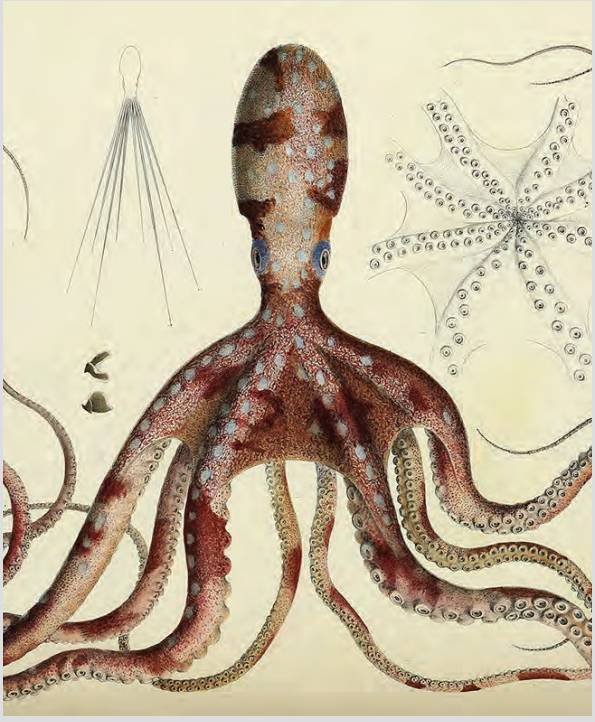

On the Cover

A. E. d'Audebard de baron de Férussac (1786–1836) and Alcide Dessalines d' Orbigny (1802–1857). Plate 24 from ***Natural, General and Particular History of the Acetabuiferous Cephalopods Living*** (detail).

About the Cover p. 1965

Synopses

Research

Dispatches

EMERGING INFECTIOUS DISEASES®
August 2020

Research Letters

EMERGING INFECTIOUS DISEASES®
August 2020

Comment Letters

Retraction Letter

Books and Media

About the Cover

Etymologia

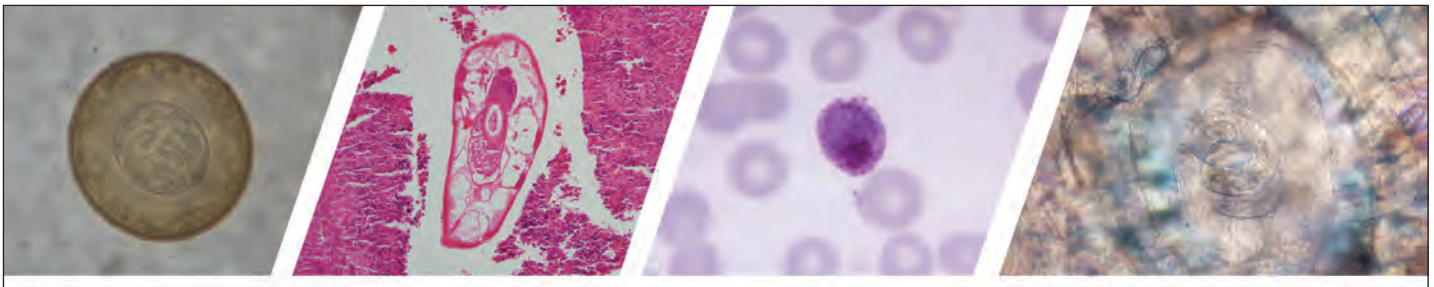

DPDx

Diagnostic Assistance and Training in Laboratory Identification of Parasites

A free service of CDC available to laboratorians, pathologists, and other health professionals in the United States and abroad

- Diagnosis from photographs of worms, histological sections, fecal, blood, and other specimen types
- Expert diagnostic review
- Formal diagnostic laboratory report
- Submission of samples via secure file share

Visit the DPDx website for information on laboratory diagnosis, geographic distribution, clinical features, parasite life cycles, and training via Monthly Case Studies of parasitic diseases.

www.cdc.gov/dpdx
dpdx@cdc.gov

U.S. Department of Health and Human Services
Centers for Disease Control and Prevention

CS272346-DE

Association of Dengue Virus and *Leptospira* Co-Infections with Malaria Severity

Rajendra Mandage,[1] Charandeep Kaur,[1] Atreyi Pramanik,[1] Vinod Kumar,[2] Parul Kodan, Adarsh Singh, Sounak Saha, Shivam Pandey, Naveet Wig, Ravindra Mohan Pandey, Manish Soneja, Pragyan Acharya

Plasmodium infections are co-endemic with infections caused by other agents of acute febrile illnesses, such as dengue virus (DENV), chikungunya virus, *Leptospira* spp., and *Orientia tsutsugamushi*. However, co-infections may influence disease severity, treatment outcomes, and development of drug resistance. When we analyzed cases of acute febrile illness at the All India Institute of Medical Sciences, New Delhi, India, from July 2017 through September 2018, we found that most patients with malaria harbored co-infections (*Plasmodium* mixed species and other pathogens). DENV was the most common malaria co-infection (44% of total infections). DENV serotype 4 was associated with mild malaria, and *Leptospira* was associated with severe malaria. We also found the presence of *P. knowlesi* in our study population. Therefore, in areas with a large number of severe malaria cases, diagnostic screening for all 4 DENV serotypes, *Leptospira*, and all *Plasmodium* species should be performed.

In tropical countries, including India, acute febrile illnesses (AFIs) constitute a group of infections with similar manifestations, such as fever, malaise, body aches, chills, hepatic and renal dysfunction, and central nervous system effects. The causative agents of AFI can be bacterial (e.g., *Orientia tsutsugamushi, Leptospira,* and *Salmonella enterica* serovar Typhi), parasitic (protozoans of the apicomplexa family), or viral (e.g., dengue virus [DENV], chikungunya virus [CHIKV], influenza A[H1N1] virus) (*1*–*4*). Distinguishing between the causative agents of AFIs can be difficult. In tropical climates, several AFI pathogens, such as malaria parasites, DENV, and CHIKV, occur in the same areas and during the same seasons (*5*), making it possible that >1 pathogen can infect the same person. Indeed, recent retrospective analyses based on persons hospitalized with an AFI have uncovered malaria co-infections with dengue, chikungunya, and leptospirosis in different populations across the world (*6*–*14*).

Despite the increasing realization that co-infections may contribute to the course and outcome of malaria, only a few studies have investigated the prevalence and nature of co-infections (*14*–*20*), which limits our ability to manage and understand AFIs, as follows. First, we do not know the spectrum of infections that a person with an AFI may harbor, leading to inadequate drug therapy. Treatment strategies based on diagnosis of a single pathogen may lead to inadvertent exposure of the undetected pathogen to antimicrobial agents, thereby contributing to generation of antimicrobial-resistant species. Second, lack of adequate data on co-infections in clinical and field settings can misdirect the field of drug and vaccine development. Pathogens such as malaria parasites, DENV, and *Orientia* spp. have host immune-modulatory effects (*21*). Therefore, co-infections can aid or antagonize each other in terms of evading host immune responses. These interactions may have major effects on immune responses to vaccine candidates and need to be known during design of effective vaccination strategies (*22*). Third, we do not know how interactions of co-infecting pathogens lead to diverse disease outcomes affecting organ function and ultimately mortality. In India, the prevalence of malaria parasites, DENV, and CHIKV resembles the global prevalence and co-endemicity of these pathogens (*5*).

Author affiliations: All India Institute of Medical Sciences, New Delhi, India (R. Mandage, C. Kaur, A. Pramanik, P. Kodan, S. Pandey, N. Wig, R.M. Pandey, M. Soneja, P. Acharya); Nehru Shatabdi Chikitsalaya, Singrauli, India (V. Kumar); Indian Institute of Technology, Kharagpur, West Bengal, India (A. Singh, S. Saha)

DOI: https://doi.org/10.3201/eid2608.191214

[1]These authors contributed equally to this article.

[2]Work was conducted at the All India Institute of Medical Sciences, New Delhi.

Malaria infections in India are reportedly caused by *Plasmodium falciparum*, *P. vivax, P. ovale*, and *P. malariae* (*23*). Several studies have also reported the occurrence of *P. vivax* severe malaria in India as well as in Southeast Asia and South America (*23*–*25*). Our objective with this study was to define the spectrum of co-infections in patients with an AFI associated with malaria admitted to the All India Institute of Medical Sciences, New Delhi, India, a tertiary care research hospital.

Materials and Methods

Study Participants and Sample Collection

For our prospective study, we recruited patients with an AFI (history of fever, i.e., temperature >38°C that had persisted for ≥2 days without an identified source) from the Department of Medicine at All India Institute of Medical Sciences from July 2017 through September 2018. Every admitted consenting AFI patient was tested by PCR for all 5 *Plasmodium* species (*P. falciparum*, *P. vivax, P. malaria*, *P. ovale*, and *P. knowlesi*), DENV, CHIKV, *O. tsutsugamushi,* and *Leptospira*. The study was approved by the institute research ethics committee (reference no. IEC-55/07.10.2016, RP7/2017).

For each participant, we collected information about geographic location (Figure) and completed a standard questionnaire (including demographic information, history, general physical examination findings, systemic examination findings, and clinical investigation findings). To determine presumptive clinical diagnoses and treatments, we reviewed medical chart records corresponding to each participant.

All patient data were anonymized to protect confidentiality. Blood samples were collected and subjected to microscopy, rapid diagnostic testing, and PCR analysis for all 5 pathogens (5 species of

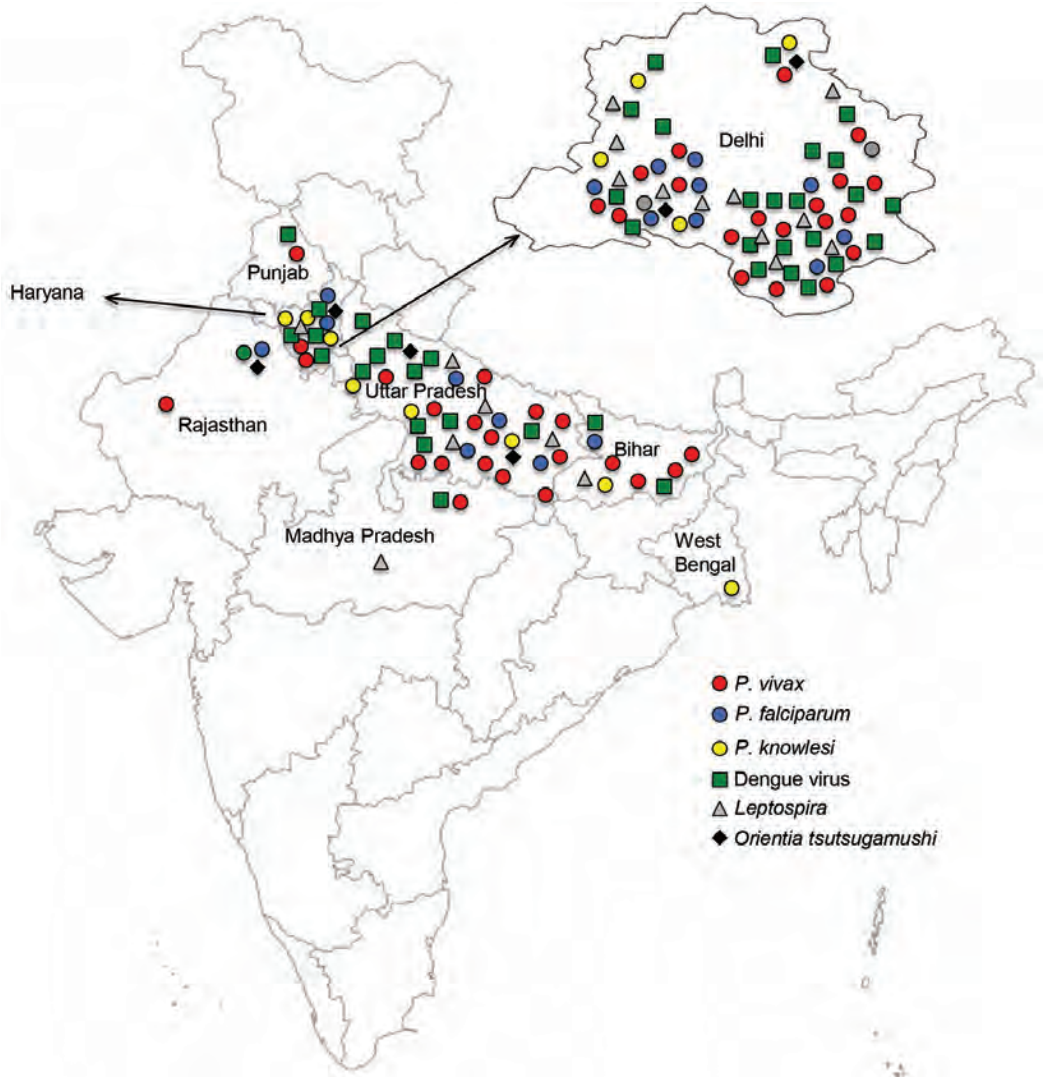

Figure. Locations of malaria patients with co-infections, India, July 2017–September 2018. Close-up view of Delhi state is provided.

Plasmodium, DENV, CHIKV, *Leptospira,* and *Orientia*). Typhoid testing was not conducted for patients with no abdominal pain or diarrhea. None of the patients recruited for this study showed indications for typhoid testing.

For microscopic examinations, we used peripheral blood smears (Giemsa-stained thick and thin smears) and a 3-band rapid diagnostic test kit (SD Bioline Malaria Ag Pf/Pan kit; Standard Diagnostics, Inc., https://www.alere.com/en/home.html). The rapid diagnostic test detects antigens specific to histidine-rich protein II from *P. falciparum* and pan-*Plasmodium* lactate dehydrogenase from *P. vivax*, *P. malariae*, or *P. ovale*.

Patients positive for malaria by PCR were classified as having severe malaria according to World Health Organization 2015 guidelines (https://www.who.int/docs/default-source/documents/publications/gmp/guidelines-for-the-treatment-of-malaria-eng.pdf?sfvrsn=a0138b77_2). These guidelines define severe malaria as creatinine level >3 mg/dL, bilirubin level >3 mg/dL, bicarbonate level <15 mmol/L, hemoglobin level <7 g/dL for adults and <5 g/dL for children, parasite count 10%, hypoglycemia <2.2 mM, substantial bleeding, impaired consciousness, shock, prostration (defined as myalgia and arthralgia), multiple convulsions, and pulmonary edema) (*26*). The remaining patients were classified as having mild malaria.

DNA Extraction and PCR Analyses

From participating AFI patients, we collected 5 mL of venous blood into EDTA tubes for PCR analysis. We extracted DNA from whole blood by using a QiaAmp DNA Mini Kit (QIAGEN, https://www.qiagen.com) according to the manufacturer's instructions. To detect DENV and CHIKV, we extracted RNA from TRIzol by using the isopropanol method, and we synthesized complementary DNA from RNA by using a Verso cDNA Synthesis Kit (Thermo Fisher Scientific, https://www.thermofisher.com) according to the manufacturer's recommendations. We analyzed all samples for the presence of all 5 human *Plasmodium* species, *O. tsutsugamushi, Leptospira,* DENV, and CHIKV. All samples were also subjected to microscopy and rapid diagnostic testing (for PfHRP2 and PvLDH genes) for malaria diagnosis. The diagnosis of DENV and its serotypes was conducted by using serotype-specific PCR primers. The presence of other infectious agents, such as *O. tsutsugamushi*, *Leptospira*, and CHIKV was detected by PCR (Appendix Table 1, https://wwwnc.cdc.gov/EID/article/26/8/19-1214-App1.pdf). Randomly selected representative PCR products were subjected to Sanger sequencing to confirm species identity (Appendix Table 2).

We categorized the types of infections or combination of infections in a person as monoinfections, mixed infections, or co-infections. Monoinfections are defined as infections with 1 species of *Plasmodium,*

Table 1. Frequency of co-infections with *Plasmodium* spp. and DENV serotypes 1–4, *Leptopsira* spp., and *Orientia tsutsugamushi*, India, July 2017–September 2018*

Pathogen	No. co-infections
All *Plasmodium*-positive infections, n = 66	
P. falciparum alone	10
P. vivax alone	34
P. knowlesi alone	5
P. vivax + *P. knowlesi*	4
P. falciparum + *P. vivax*	10
P. falciparum + *P. knowlesi*	1
P. falciparum + *P. vivax* + *P. knowlesi*	2
Plasmodium + bacteria co-infections, n = 17	
Plasmodium + *O. tsutsugamushi*	5
Plasmodium + *Leptospira*	11
Plasmodium + *Leptospira* + *O. tsutsugamushi*	1
Plasmodium + DENV co-infections, n = 40	
Plasmodium + DENV, all serotypes	40
Plasmodium + DENV-1	8
Plasmodium + DENV-3	5
Plasmodium + DENV-4	20
Plasmodium + DENV-1 + DENV-3	1
Plasmodium + DENV-1 + DENV-4	2
Plasmodium + DENV-3 + DENV-4	1
Plasmodium + DENV-1 + DENV-4 + DENV-3	3
Plasmodium + DENV + bacteria co-infections, n = 11	
Plasmodium + DENV + *Leptospira*	8
Plasmodium + DENV+ *O. tsutsugamushi*	2
Plasmodium + DENV + *Leptospira* + *O. tsutsugamushi*	1

**P. malariae* and *P. ovale* were not detected in the study population. DENV, dengue virus.

mixed infections with >1 *Plasmodium* species, and co-infections with *Plasmodium* species and other bacterial or viral infections.

Determination of Patient Locations and Construction of Map of India

We were able to retrieve location data for 82 patients. We constructed a map of India based on the official maps provided by the Survey of India (http://www.surveyofindia.gov.in/pages/display/235-political-map-of-india), as described previously (*26*). In brief, we downloaded an India map shapefile (http://www.indianremotesensing.com/2017/01/Download-India-shapefile-with-kashmir.html) and generated the final image by using Microsoft PowerPoint (https://www.microsoft.com) to map each patient to their local area. In addition, the 12 patients with *P. knowlesi* infection were asked to answer questions about time of malaria infection (as recorded in our dataset), travel outside India in 2 years preceding the malaria infection, visits from abroad by friends/relatives, and any previous malaria infections (possibility of recurrence/relapse).

Statistical Analyses

We recorded data on a predesigned form and managed the data in a Microsoft Excel spreadsheet and checked all entries for possible manual errors. We summarized categorical variables by frequency (%) and age as means. We used χ^2 or Fisher exact tests, or both, as appropriate, to compare frequencies between 2 groups and the Student *t*-test to compare age distribution between 2 groups. We evaluated accuracy of microscopy and rapid diagnostic testing methods by using PCR as a reference for malaria diagnosis. For each of the 2 tests, we computed sensitivity, specificity, positive predictive value, negative predictive value, positive likelihood ratio, and negative likelihood ratio by using PCR as a reference. We also computed 95% CIs for each measure computed to determine the strength of association of various co-infections with malaria severity. We used bivariate and multivariate logistic regression methods to determine the odds ratio (95% CI) for each co-infection by using Stata version 15.0 statistical software (https://www.stata.com). We considered $p<0.05$ to be statistically significant. We created a patient baseline characteristics table by using the R version 3.4.3 package tableone (*27*). The tableone package summarizes categorical data in the form of counts and percentages and summarizes continuous data in the form of means and SDs.

Results

Spectrum of Co-infections and *Plasmodium* Mixed Species Infections in Patients with Malaria

We analyzed the prevalence of various co-infections and *Plasmodium* mixed-species infections in the 66 *Plasmodium*-positive samples (Table 1). *P. vivax* accounted for most (76%) (50/66) infections, whereas *P. falciparum* accounted for 35% (23/66). *P. knowlesi* was detected in 18% (12/66) of infections (Table 1); *P. malariae* and *P. ovale* were not detected in our study.

From the 66 *Plasmodium*-positive patients, 40 (60%) samples indicated a DENV co-infection with or without other co-infecting pathogens, and 29 (44%) indicated exclusive *Plasmodium*/DENV co-infections. *Plasmodium* co-infections with bacteria were found for 16 (25%) patients: *Leptospira* infections for 11 (17%) of the 66 and *O. tsutsugamushi* for 5 (8%) (Table 1).

Mapping indicated that locations of the malaria patients in our study spanned the entire northern region of India, including the states of Rajasthan, Haryana, Punjab, Delhi, Uttar Pradesh, Bihar, and West Bengal (Figure). Patients with *P. knowlesi* infection originated from Delhi, Haryana, Uttar Pradesh, and West Bengal. Most patients with dengue infections originated from Delhi and Uttar Pradesh. Of the 12 patients with *P. knowlesi* infection, 5 had not traveled abroad or had direct contact with any visitors from abroad for at least 2 years before admission. No information was available for the remaining 7 patients (Appendix Table 3).

Patient Baseline Characteristics

Detailed hematologic and biochemical parameters for all patients were retrieved from medical records (Table 2; Appendix Table 4). Differences between severe and mild malaria patients were found in hemoglobin

Table 2. Comparison of blood parameters for patients with mild or severe malaria, India, July 2017–September 2018*

Parameter	Mild disease, mean (± SD), n = 33†	Severe, mean (± SD), n = 33‡
Hemoglobin, g/dL	12.11 (± 3.22)	9.89 (± 2.96)
Hematocrit, %	36.45 (± 9.48)	29.93 (± 8.95)
Platelets, $\times 10^3/\mu L$	87.00 (± 54.73)	76.69 (± 66.24)
Leukocytes, $\times 10^3$ cells/μL	6.07 (± 3.20)	10.53 (± 6.98)
Erythrocytes, $\times 10^6$ cells/μL	4.26 (± 1.34)	3.69 (± 0.95)
Creatinine, mg/dL	0.90 (± 0.41)	3.37 (± 3.41)

*In each group, 26 patients were male. Mean (± SD) ages were 32.03 (± 15.99) y for those with mild disease and 28.81 (± 13.99) y for those with severe disease.

levels (9.89 g/dL vs. 12.11 g/dL), hematocrit (29.93% vs. 36.45%), platelet counts (76.69 vs. 87 × 10^3/μL), leukocyte counts (10.53 vs. 6.07) × 10^3 cells/μL), and creatinine levels (3.37 vs. 0.90). Each group contained 26 male patients; mean age for severe malaria patients was 28 years and for mild malaria patients was 32 years.

Association of Co-infecting Pathogens with Malaria Severity

We found that co-infection with DENV serotype 4 (DENV-4) was associated with mild malaria (adjusted odds ratio [aOR] 0.3, 95% CI 0.4–5.0), whereas infection with *Leptospira* (aOR 1.6, 95% CI 0.4–6.8) or *O. tsutsugamushi* (aOR 1.1, 95% CI 0.1–7.8) was associated with severe malaria. *P. vivax* or *P. knowlesi* monoinfection was also associated with severe malaria (aOR 2.5, 95% CI 0.9–7.2) (Table 3). Other categories of *Plasmodium* mixed-species infections did not show any strong association with malaria severity (Appendix Table 5). However, the species of *Plasmodium* may confound some of these analyses.

Relative Performance of Malaria Diagnostic Procedures

All 99 patients were tested for *Plasmodium* species by microscopy (8 positive results), rapid diagnostic testing (26 positive), and PCR (66 positive) (Table 4). Almost 50% of the *P. vivax* infections escaped detection by both microscopy and rapid testing. *P. knowlesi* was detectable solely by PCR. In addition, rapid diagnostic testing was able to detect only 1 of 18 *Plasmodium* mixed-species infections (Table 4). The diagnostic performance of microscopy and rapid diagnostic testing was calculated, and each was found to have poor sensitivity compared with PCR (Appendix Table 6).

Discussion

Among patients hospitalized with AFI at the All India Institute of Medical Sciences during July 2017–September 2018, the major circulating *Plasmodium* species was *P. vivax* and malaria/DENV co-infections predominated. A high number of severe malaria cases reported to the institute are from northern India. Among the 5 *Plasmodium* species known to infect humans, in our study population we detected *P. falciparum*, *P. vivax*, and *P. knowlesi* but found no evidence of *P. malariae* or *P. ovale*. Most AFI patients in this study originated from northern India across the states of Rajasthan, Haryana, Punjab, Delhi, Uttar Pradesh, Bihar, and West Bengal. The burden of co-infecting pathogens in patients with malaria was revealed by a combination of complete blood work (peripheral blood smear analysis, rapid diagnostic testing, serum renal and liver function testing) and in-depth molecular assays (PCR amplification of *Plasmodium* species–specific genes followed by Sanger sequencing). We found a very high percentage of *Plasmodium*/DENV co-infections in our study population. This finding can be partly attributed to the highly sensitive PCR diagnostic methods used.

A recent meta-analysis of the prevalence of DENV/ *Plasmodium*/CHIKV co-infections spanning 7 geographic regions (southern Asia, Africa, Southeast Asia, South America, North America, the Caribbean, and the Middle East) showed that DENV/ *Plasmodium* co-infections have been reported in 19 countries, including India; DENV/CHIKV co-infections have been reported in 24 countries including India; CHIKV/*Plasmodium* co-infections have been reported in 6 countries with only a single co-infection reported from India; and DENV/CHIKV/ *Plasmodium* co-infections have been reported in 3 countries (*5*). According to that meta-analysis, the average reported prevalence of DENV/*Plasmodium* co-infection in India is ≈6.5%, which is much lower than that detected by our study. However, a more detailed analysis from the eastern India state of Odisha

Table 3. Frequency of co-infections and mixed infections in patients with severe and mild malaria, India, July 2017–September 2018*

Co-infections	No. malaria cases		p value	Unadjusted OR (95% CI)	Adjusted OR (95% CI)
	Severe, n = 33	Mild, n = 33			
DENV			≤0.08		
Neg for DENV	14	12		Referent	Referent
Pos for DENV-4	6	14		0.34 (0.1–1.2)	0.3 (0.4–5.0)
Pos for other DENV serotypes: 1, 3, 1+3, 4+3	13	7		1.6 (0.5–2.5)	1.4 (0.4–4.9)
Leptospira			≤0.5		
Absent	26	29			
Present	7	4		1.9 (0.5–7.4)	1.6 (0.4–6.8)
Orientia tsutsugamushi			≤0.5		
Absent	30	31		Referent	Referent
Present	3	2		1.6 (0.2–9.9)	1.1 (0.1–7.8)
Malaria parasite types			≤0.1		
Plasmodium mixed infections	17	10		Referent	Referent
P. vivax/*P. knowlesi* monoinfection	16	23		2.4 (0.9–6.7)	2.5 (0.9–7.2)

*Bivariate and multivariate logistic regression analysis was used to determine the strength of association of various co-infections and mixed malaria infections with malaria severity. DENV, dengue virus.; neg, negative; pos, positive; OR, odds ratio.

Table 4. Summary of detection of *Plasmodium* species by RDT, microscopy and PCR, India, July 2017–September 2018*

Parasites	RDT, no. (%)	Microscopy, no. (%)	PCR, no. (%)
Plasmodium negative	73 (71.7)	90 (90.9)	33 (33.3)
Plasmodium positive	26 (28.3)	9 (9.09)	66 (66.7)
P. falciparum	6 (6.06)	2 (2.02)	10 (10.1
P. vivax	14 (14.1)	7 (7.07)	34 (34.3)
P. ovale	0	0	0
P. malariae	0	0	0
P. knowlesi	0	0	5 (5.05)
Mixed *Plasmodium*	1 (1.01)	0	17 (17.2)
Pan-*Plasmodium*	7 (7.07)	0	0

*Percentages are calculated out of all AFI samples (n = 99). RDT, rapid diagnostic test.

shows that this percentage can vary within a year, depending on season, and the highest reported prevalence of DENV/*Plasmodium* co-infections from this region was 31.8% during September–October, an observation similar to ours (*28*).

Although awareness of *Plasmodium*/DENV co-infections is increasing, little information is available about *Plasmodium*/*Leptospira* or *Plasmodium*/*O. tsutsugamushi* co-infections (*13*,*29*). This lack of information is concerning because our study suggests that *Plasmodium*/*Leptospira* co-infections are associated with severe malaria. Prevalence data for co-infections with these pathogens are limited. We emphasize the need for such information because although these pathogens are carried by different vectors, they co-exist in the same geoclimactic habitats that combine a warm, moist environment with dense vegetation and poor socio-economic development (*13*,*29*). The presence of one co-infecting pathogen can influence disease outcomes, treatment outcomes, development of immunity, or drug resistance with regard to infections caused by the other co-infecting pathogen. One example is the predisposition for bacteremia to develop in persons with malaria (*30*).

In most malaria-endemic settings, malaria is still diagnosed by microscopic examination of Giemsa-stained peripheral blood smears and rapid diagnostic testing for parasite antigen. The rapid test is specifically designed to detect *P. falciparum* and *P. vivax* and is extensively used because of its speed and simplicity. For microscopy, diagnostic success depends on the skill of the technicians who observe the peripheral blood smears. We found that rapid tests and microscopy missed most of the *P. vivax*–positive malaria cases and all *P. knowlesi* cases and detected only 1 of 18 *Plasmodium* mixed-species infections. This finding clearly shows the limitations of rapid testing and microscopy for comprehensive detection of malaria parasites, which have been independently observed in several studies and attributed to deletions in the HRP2 and HRP3 genes in the specific case of *P. falciparum* infection (*31*–*34*). This problem is well recognized for healthcare workers and researchers working toward malaria elimination all over the world. Although the rapid diagnostic test for malaria has been shown to be better than microscopic examination of Giemsa-stained peripheral blood smears, PCR has been shown to be far superior to rapid testing for diagnosing low-parasitemia malaria infections (*35*). Our observations were similar; PCR was most sensitive, followed by rapid testing and then microscopy. However, rapid tests have low success rates in areas of low transmission intensities and give rise to a high proportion of false negatives (*36*). In addition, rapid tests fail to detect infections with emerging pathogens, such as the simian parasite species *P. knowlesi* and *P. cynomolgi*, both known to infect humans (*37*). Although recent reports highlight the improvement of rapid tests for *P. knowlesi* detection by use of a cross-reacting pan-parasite lactate dehydrogenase feature, we were unable to detect *P. knowlesi* by using a pan-parasite lactate dehydrogenase–containing rapid test, possibly because of low parasitemia, below the detection limit of the rapid test (*38*). *P. knowlesi*, which was previously believed to be localized to Southeast Asia, has now been reported from various parts of the world as single case reports of travelers' infections from areas including Oceania, Europe, and the Middle East (*39*–*41*). From India, *P. knowlesi* infection has been reported from the Andaman and Nicobar Islands in the context of drug resistance and in a recent study by our group in the context of acute kidney injury (*26*,*42*). Historically, *P. knowlesi* infection was discovered as a naturally occurring human infection in Malaysia in 1965 (*43*). The accurate diagnosis of *P. knowlesi* by use of PCR took ≈40 years from its initial discovery and gave a preliminary indication of the burden of this zoonosis in Sarawak, Malaysia (*44*). Until this point, *P. knowlesi* as a human infection was frequently misdiagnosed as *P. vivax*, *P. malariae*, or *P. falciparum* infection.

To assess whether the infections originated locally, we surveyed the *P. knowlesi* patients in our study group for the possibility of travel abroad or

interaction with visitors from abroad within their family. The patients who responded to our questionnaire do not appear to have traveled abroad or to have had direct contact with anyone visiting them from abroad, suggesting local presence of *P. knowlesi*. However, unknown sources of travel from Southeast Asia, a neighbor to India, cannot be ruled out. Currently, testing for *P. knowlesi* is not included in diagnostic procedures in India, irrespective of diagnostic method (microscopy, rapid diagnostic test, or PCR), because it has not been widely reported. However, India is known to harbor both the potential vector for *P. knowlesi*, the *Anopheles dirus* mosquito, as well as the reservoir, pig-tailed macaques (*Macaca nemestrina*), thereby making India a potential ecosystem for the proliferation of this zoonotic *Plasmodium* species (*45*). Furthermore, the populations of *Macaca mulatta* macaques and related species have recently expanded in northern India, particularly in the state of Uttar Pradesh, which may explain the appearance of *P. knowlesi* in our study population representative of these areas, whereas it was not reported earlier (*45*). A recent report has also demonstrated the presence of *P. falciparum* parasites in monkey populations from India, indicating freely occurring undetected zoonotic transfer of the malaria parasites across reservoirs and hosts. Therefore, healthcare workers and national programs should incorporate all species of malaria parasites known to infect humans, in their diagnostic portfolio.

In conclusion, our study clearly showed that microscopy and rapid diagnostic testing gave false-negative results for most mixed-species infections and completely missed *P. knowlesi* infections, co-infections and mixed *Plasmodium* infections were highly prevalent in patients with malaria, *Plasmodium*/DENV co-infections were the most common co-occurring pathogens in our study population, *P. knowlesi* infections were present in India, *Plasmodium*/DENV4 co-infections were associated with mild malaria, and *Plasmodium*/*Leptospira* infections were associated with severe malaria. Although the ORs support the above findings, the 95% CIs for these associations were wide. CIs reflect the uncertainty of the estimated effect, and wider intervals suggest greater uncertainty. The wide 95% CIs in this study suggest that although trends were observed, additional data points are needed to determine the effect size of these associations. Wider prevalence studies investigating malaria co-infections are needed.

The government of India has recently declared a goal of malaria elimination by 2030, which will be a major step toward global malaria eradication because India serves as a major *Plasmodium* reservoir, contributing to almost 4% of malaria-related deaths globally. Therefore, to make malaria elimination possible, we offer 2 recommendations based on our observations in this study, particularly for tertiary healthcare centers or centers where the burden of severe malaria cases is high. First, malaria elimination efforts will need to include strategies for malaria elimination in humans as well as animal reservoirs. Second, efforts toward the development of novel diagnostics for malaria must be renewed, and AFI diagnoses must include screening for all 5 *Plasmodium* species, *Leptospira*, and all 4 DENV serotypes.

This work was funded by the Science and Engineering Research Board Early Career Research (grant no. ECR/2016/000833 to P.A.). R.M. was supported by the Department of Biotechnology for a Research Associate fellowship.

About the Author

Dr. Mandage is a postdoctoral fellow working in the laboratory of Dr. Acharya in the Department of Biochemistry, All India Institute of Medical Sciences, New Delhi, India.

References

1. Raina S, Raina RK, Agarwala N, Raina SK, Sharma R. Coinfections as an aetiology of acute undifferentiated febrile illness among adult patients in the sub-Himalayan region of north India. J Vector Borne Dis. 2018;55:130–6. https://doi.org/10.4103/0972-9062.242560
2. Susilawati TN, McBride WJH. Acute undifferentiated fever in Asia: a review of the literature. Southeast Asian J Trop Med Public Health. 2014;45:719–26.
3. Joshi R, Kalantri SP. Acute undifferentiated fever: management algorithm [cited 2020 May 29]. http://apiindia.org/wp-content/uploads/pdf/monograph_2015_update_on_tropical_fever/001_acute_undifferentiated_fever.pdf
4. Ahmad S, Dhar M, Mittal G, Bhat NK, Shirazi N, Kalra V, et al. A comparative hospital-based observational study of mono- and co-infections of malaria, dengue virus and scrub typhus causing acute undifferentiated fever. Eur J Clin Microbiol Infect Dis. 2016;35:705–11. https://doi.org/10.1007/s10096-016-2590-3
5. Salam N, Mustafa S, Hafiz A, Chaudhary AA, Deeba F, Parveen S. Global prevalence and distribution of coinfection of malaria, dengue and chikungunya: a systematic review. BMC Public Health. 2018;18:710. https://doi.org/10.1186/s12889-018-5626-z
6. Manock SR, Jacobsen KH, de Bravo NB, Russell KL, Negrete M, Olson JG, et al. Etiology of acute undifferentiated febrile illness in the Amazon basin of Ecuador. Am J Trop Med Hyg. 2009;81:146–51. https://doi.org/10.4269/ajtmh.2009.81.146
7. Capeding MR, Chua MN, Hadinegoro SR, Hussain IIHM, Nallusamy R, Pitisuttithum P, et al. Dengue and other common causes of acute febrile illness in Asia: an active surveillance study in children. PLoS Negl Trop Dis. 2013;7:e2331. https://doi.org/10.1371/journal.pntd.0002331

8. Mueller TC, Siv S, Khim N, Kim S, Fleischmann E, Ariey F, et al. Acute undifferentiated febrile illness in rural Cambodia: a 3-year prospective observational study. PLoS One. 2014;9:e95868. https://doi.org/10.1371/journal.pone.0095868
9. Chipwaza B, Mugasa JP, Selemani M, Amuri M, Mosha F, Ngatunga SD, et al. Dengue and chikungunya fever among viral diseases in outpatient febrile children in Kilosa district hospital, Tanzania. PLoS Negl Trop Dis. 2014;8:e3335. https://doi.org/10.1371/journal.pntd.0003335
10. Chrispal A, Boorugu H, Gopinath KG, Chandy S, Prakash JAJ, Thomas EM, et al. Acute undifferentiated febrile illness in adult hospitalized patients: the disease spectrum and diagnostic predictors - an experience from a tertiary care hospital in South India. Trop Doct. 2010;40:230–4. https://doi.org/10.1258/td.2010.100132
11. Singh R, Singh SP, Ahmad N. A study of etiological pattern in an epidemic of acute febrile illness during monsoon in a tertiary health care institute of Uttarakhand, India. J Clin Diagn Res. 2014;8:MC01–03. https://doi.org/10.7860/JCDR/2014/8965.4435
12. Lindo J, Brown PD, Vickers I, Brown M, Jackson ST, Lewis-Fuller E. Leptospirosis and malaria as causes of febrile illness during a dengue epidemic in Jamaica. Pathog Glob Health. 2013;107:329–34. https://doi.org/10.1179/2047773213Y.0000000112
13. Mørch K, Manoharan A, Chandy S, Chacko N, Alvarez-Uria G, Patil S, et al. Acute undifferentiated fever in India: a multicentre study of aetiology and diagnostic accuracy. BMC Infect Dis. 2017;17:665. https://doi.org/10.1186/s12879-017-2764-3
14. Barua A, Yeolekar ME. Concurrent dengue and malaria coinfection: observations from a central Mumbai hospital. Int J Infect Dis. 2016;45:165. https://doi.org/10.1016/j.ijid.2016.02.393
15. Arya SC, Mehta LK, Agarwal N, Agarwal BK, Mathai G, Moondhara A. Episodes of concurrent dengue and malaria [cited 2020 May 29]. https://apps.who.int/iris/bitstream/handle/10665/164116/dbv29p208.pdf;jsessionid=B3A6898DEDC1ECA2FB605F977C3F0E6E?sequence=1
16. Mushtaq M, Qadri MI, Rashid A, Bin, Qadri MI, Rashid A. Concurrent infection with dengue and malaria: An unusual presentation. Case Rep Med. 2013;2013:1–2. https://doi.org/10.1155/2013/520181
17. Barua A, Gill N. A comparative study of concurrent dengue and malaria infection with their monoinfection in a teaching hospital in Mumbai. J Assoc Physicians India. 2016;64:49–52.
18. Carme B, Matheus S, Donutil G, Raulin O, Nacher M, Morvan J. Concurrent dengue and malaria in Cayenne Hospital, French Guiana. Emerg Infect Dis. 2009;15:668–71. https://doi.org/10.3201/eid1504.080891
19. Kaushik RM, Varma A, Kaushik R, Gaur KJBS. Concurrent dengue and malaria due to *Plasmodium falciparum* and *P. vivax*. Trans R Soc Trop Med Hyg. 2007;101:1048–50. https://doi.org/10.1016/j.trstmh.2007.04.017
20. Alam A, Dm M. A case of cerebral malaria and dengue concurrent infection. Asian Pac J Trop Biomed. 2013;3:416–7. https://doi.org/10.1016/S2221-1691(13)60087-8
21. Choi JH, Cheong TC, Ha NY, Ko Y, Cho CH, Jeon JH, et al. *Orientia tsutsugamushi* subverts dendritic cell functions by escaping from autophagy and impairing their migration. PLoS Negl Trop Dis. 2013;7:e1981. https://doi.org/10.1371/journal.pntd.0001981
22. Frosch AEP, John CC. Immunomodulation in *Plasmodium falciparum* malaria: experiments in nature and their conflicting implications for potential therapeutic agents. Expert Rev Anti Infect Ther. 2012;10:1343–56. https://doi.org/10.1586/eri.12.118
23. Anvikar AR, Shah N, Dhariwal AC, Sonal GS, Pradhan MM, Ghosh SK, et al. Epidemiology of *Plasmodium vivax* malaria in India. Am J Trop Med Hyg. 2016;95(Suppl):108–20. https://doi.org/10.4269/ajtmh.16-0163
24. Sharma VP, Dev V, Phookan S. Neglected *Plasmodium vivax* malaria in northeastern states of India. Indian J Med Res. 2015;141:546–55.
25. van Hellemond JJ, Rutten M, Koelewijn R, Zeeman AM, Verweij JJ, Wismans PJ, et al. Human *Plasmodium knowlesi* infection detected by rapid diagnostic tests for malaria. Emerg Infect Dis. 2009;15:1478–80. https://doi.org/10.3201/eid1509.090358
26. Kaur C, Pramanik A, Kumari K, Mandage R, Dinda AK, Sankar J, et al. Renal detection of *Plasmodium falciparum*, *Plasmodium vivax* and *Plasmodium knowlesi* in malaria associated acute kidney injury: a retrospective case-control study. BMC Res Notes. 2020;13:37. https://doi.org/10.1186/s13104-020-4900-1
27. Pollard TJ, Johnson AEW, Raffa JD, Mark RG. tableone: An open source Python package for producing summary statistics for research papers. JAMIA Open. 2018;1:26–31. https://doi.org/10.1093/jamiaopen/ooy012
28. Rao MRK, Padhy RN, Das MK. Prevalence of dengue viral and malaria parasitic co-infections in an epidemic district, Angul of Odisha, India: an eco-epidemiological and cross-sectional study for the prospective aspects of public health. J Infect Public Health. 2016;9:421–8. https://doi.org/10.1016/j.jiph.2015.10.019
29. Borkakoty B, Jakharia A, Biswas D, Mahanta J. Co-infection of scrub typhus and leptospirosis in patients with pyrexia of unknown origin in Longding district of Arunachal Pradesh in 2013. Indian J Med Microbiol. 2016;34:88–91. https://doi.org/10.4103/0255-0857.174116
30. Chau JY, Tiffany CM, Nimishakavi S, Lawrence JA, Pakpour N, Mooney JP, et al. Malaria-associated L-arginine deficiency induces mast cell-associated disruption to intestinal barrier defenses against nontyphoidal *Salmonella* bacteremia. Infect Immun. 2013;81:3515–26. https://doi.org/10.1128/IAI.00380-13
31. Kumar N, Pande V, Bhatt RM, Shah NK, Mishra N, Srivastava B, et al. Genetic deletion of HRP2 and HRP3 in Indian *Plasmodium falciparum* population and false negative malaria rapid diagnostic test. Acta Trop. 2013;125:119–21. https://doi.org/10.1016/j.actatropica.2012.09.015
32. Pati P, Dhangadamajhi G, Bal M, Ranjit M. High proportions of *pfhrp2* gene deletion and performance of HRP2-based rapid diagnostic test in *Plasmodium falciparum* field isolates of Odisha. Malar J. 2018;17:394. https://doi.org/10.1186/s12936-018-2502-3
33. Berhane A, Anderson K, Mihreteab S, Gresty K, Rogier E, Mohamed S, et al. Major threat to malaria control programs by plasmodium falciparum lacking histidine-rich protein 2, Eritrea. Emerg Infect Dis. 2018;24:462–70. https://dx.doi.org/10.3201/eid2403.171723
34. Mussa A, Talib M, Mohamed Z, Hajissa K. Genetic diversity of *Plasmodium falciparum* histidine-rich protein 2 (PfHRP2) and its effect on the performance of PfHRP2-based rapid diagnostic tests. BMC Res Notes. 2019;12:334. https://doi.org/10.1186/s13104-019-4361-6
35. Megnekou R, Djontu JC, Nana BC, Bigoga JD, Fotso M, Fogang B, et al. Accuracy of One Step malaria rapid diagnostic test (RDT) in detecting *Plasmodium falciparum* placental malaria infection in women living in Yaoundé, Cameroon. Malar J. 2018; 17:450. https://doi.org/10.1186/s12936-018-2595-8

36. Watson OJ, Sumner KM, Janko M, Goel V, Winskill P, Slater HC, et al. False-negative malaria rapid diagnostic test results and their impact on community-based malaria surveys in sub-Saharan Africa. BMJ Glob Heal. 2019;4:e001582. https://doi.org/10.1136/bmjgh-2019-001582
37. Anstey NM, Grigg MJ. Zoonotic malaria: the better you look, the more you find. J Infect Dis. 2019;219:679–81. https://doi.org/10.1093/infdis/jiy520
38. Grigg MJ, William T, Barber BE, Parameswaran U, Bird E, Piera K, et al. Combining parasite lactate dehydrogenase-based and histidine-rich protein 2-based rapid tests to improve specificity for diagnosis of malaria due to *Plasmodium knowlesi* and other *Plasmodium* species in Sabah, Malaysia. J Clin Microbiol. 2014;52:2053–60. https://doi.org/10.1128/JCM.00181-14
39. Figtree M, Lee R, Bain L, Kennedy T, Mackertich S, Urban M, et al. *Plasmodium knowlesi* in human, Indonesian Borneo. Emerg Infect Dis. 2010;16:672–4. https://doi.org/10.3201/eid1604.091624
40. Ehrhardt J, Trein A, Kremsner P, Frank M. *Plasmodium knowlesi* and HIV co-infection in a German traveller to Thailand. Malar J. 2013;12:283. https://doi.org/10.1186/1475-2875-12-283
41. Kantele A, Marti H, Felger I, Müller D, Jokiranta TS. Monkey malaria in a European traveler returning from Malaysia. Emerg Infect Dis. 2008;14:1434–6. 10.3201/eid1409.080170 https://doi.org/10.3201/eid1409.080170
42. Tyagi RK, Das MK, Singh SS, Sharma YD. Discordance in drug resistance-associated mutation patterns in marker genes of *Plasmodium falciparum* and *Plasmodium knowlesi* during coinfections. J Antimicrob Chemother. 2013;68:1081–8. https://doi.org/10.1093/jac/dks508
43. Huff CG. The primate malarias. Am J Trop Med Hyg. 1972;21:602–3. https://doi.org/10.4269/ajtmh.1972.21.602
44. Singh B, Kim Sung L, Matusop A, Radhakrishnan A, Shamsul SSG, Cox-Singh J, et al. A large focus of naturally acquired *Plasmodium knowlesi* infections in human beings. Lancet. 2004;363:1017–24. https://doi.org/10.1016/S0140-6736(04)15836-4
45. Mewara A, Sehgal R. Guest commentary: *Plasmodium knowlesi*—need to diagnose in India. Trop Parasitol. 2017;7:2–4.

Address for correspondence: Pragyan Acharya, Lab 3002, Department of Biochemistry, All India Institute of Medical Sciences, New Delhi 110029, India; email: pragyan.acharya@aiims.edu

US CDC Real-Time Reverse Transcription PCR Panel for Detection of Severe Acute Respiratory Syndrome Coronavirus 2

Xiaoyan Lu, Lijuan Wang, Senthilkumar K. Sakthivel, Brett Whitaker, Janna Murray, Shifaq Kamili, Brian Lynch, Lakshmi Malapati, Stephen A. Burke, Jennifer Harcourt, Azaibi Tamin, Natalie J. Thornburg, Julie M. Villanueva, Stephen Lindstrom

Severe acute respiratory syndrome coronavirus 2 (SARS-CoV-2) was identified as the etiologic agent associated with coronavirus disease, which emerged in late 2019. In response, we developed a diagnostic panel consisting of 3 real-time reverse transcription PCR assays targeting the nucleocapsid gene and evaluated use of these assays for detecting SARS-CoV-2 infection. All assays demonstrated a linear dynamic range of 8 orders of magnitude and an analytical limit of detection of 5 copies/reaction of quantified RNA transcripts and 1 x $10^{-1.5}$ 50% tissue culture infectious dose/mL of cell-cultured SARS-CoV-2. All assays performed comparably with nasopharyngeal and oropharyngeal secretions, serum, and fecal specimens spiked with cultured virus. We obtained no false-positive amplifications with other human coronaviruses or common respiratory pathogens. Results from all 3 assays were highly correlated during clinical specimen testing. On February 4, 2020, the Food and Drug Administration issued an Emergency Use Authorization to enable emergency use of this panel.

On December 31, 2019, an outbreak of an unexplained acute respiratory disease, later designated coronavirus disease (COVID-19), was reported in Wuhan, China (*1*). On January 7, 2020, a novel coronavirus, severe acute respiratory syndrome coronavirus 2 (SARS-CoV-2), previously known as 2019-nCoV, was identified as the causative agent of the outbreak (*2*). On January 10, 2020, a SARS-CoV-2 genome sequence was shared with the global scientific community through an online resource (*3*). The virus was genetically most closely related to SARS-CoV and SARS-related bat and civet coronaviruses within the family *Betacoronavirus*, subgenus *Sarbecovirus* (*4*,*5*).

To support the potential public health emergency response to COVID-19, the Centers for Disease Control and Prevention (CDC) developed and validated a real-time reverse transcription PCR (rRT-PCR) panel based on this SARS-CoV-2 genome sequence (*3*). The panel targeted the nucleocapsid protein (N) gene of SARS-CoV-2. The rRT-PCR panel was validated under the Clinical Laboratory Improvement Amendments (https://www.cms.gov/Regulations-and-Guidance/Legislation/CLIA) for CDC use for diagnosis of SARS-CoV-2 from respiratory clinical specimens. On January 20, 2020, the CDC rRT-PCR panel confirmed an early case of COVID-19 in the United States (*6*). The US Food and Drug Administration issued an Emergency Use Authorization to enable emergency use of the CDC rRT-PCR panel as an in vitro diagnostic test for SARS-CoV-2 (https://www.fda.gov/news-events/press-announcements/fda-takes-significant-step-coronavirus-response-efforts-issues-emergency-use-authorization-first). From January 18 through February 27, as part of the COVID-19 response, CDC tested 2,923 specimens from 998 persons for SARS-CoV-2.

As of April 22, ≈2,400,000 confirmed COVID-19 cases and ≈169,000 associated deaths had been identified globally, including ≈770,000 cases and ≈37,000 deaths in the United States (*7*). We describe the design and validation of the CDC rRT-PCR panel and present comprehensive data on its performance with

Author affiliations: Centers for Disease Control and Prevention, Atlanta, Georgia, USA (X. Lu, B. Whitaker, S.A. Burke, J. Harcourt, A. Tamin, N.J. Thornburg, J.M. Villanueva, S. Lindstrom); Synergy America, Inc., Atlanta (L. Wang, S. Kamili); Eagle Contracting, Atlanta (S.K. Sakthivel, J. Murray, B. Lynch); Leidos, Atlanta (L. Malapati); Battelle, Atlanta (S.A. Burke)

DOI: https://doi.org/10.3201/eid2608.201246

multiple specimen types and clinical specimens tested during the early CDC COVID-19 response.

Materials and Methods

SARS-CoV-2 Cultured Virus and Other Respiratory Pathogens

SARS-CoV-2 was isolated in Vero cells from a respiratory specimen from an early US COVID-19 patient (*8*). We measured infectious virus titer of virus stock by 50% tissue culture infectious dose ($TCID_{50}$) (2.01×10^6 $TCID_{50}$/mL) and inactivated the virus by gamma irradiation. The inactivated stock virus was used as reference material for assay evaluation. Cell culture stocks or clinical specimens containing other respiratory viruses/bacteria were used to evaluate assay specificity. Ten nasopharyngeal swab samples that had been collected in 2018 (before COVID-19) and were negative for respiratory viruses were also available for assay specificity evaluation.

Clinical Specimens

We used the rRT-PCR panel for SARS-CoV-2 to test 2,923 clinical specimens collected from January 18 through February 27, 2020, from persons under investigation from 43 states and territories in the United States. Specimens included 2,437 specimens collected from 998 persons suspected to be infected who either met the initial definition of a COVID-19 person under investigation (*9*), were a close contact with a laboratory-confirmed COVID-19 case-patient, or had been repatriated to the United States from Wuhan, China, or the Diamond Princess cruise ship from Japan; and 486 specimens that were serially collected over time from 28 persons with COVID-19 confirmed at CDC. Respiratory specimens (90.2%) included nasopharyngeal swab samples (n = 1,220) and oropharyngeal swab samples (n = 1,208) in viral transport medium, nasal swab/wash samples (n = 7), sputum (n = 197), bronchoalveolar lavage fluid (n = 2), lung tissues (n = 2), tracheal aspirate (n = 1), and bronchial wash samples (n = 1). Nonrespiratory specimens (9.8%) included serum (n = 156), urine (n = 72), stool (n = 54), cerebrospinal fluid (n = 2), and pericardial fluid (n = 1).

Specimen Processing and Nucleic Acid Extraction

We extracted total nucleic acid from 120 µL of respiratory specimens by using the EZ1 DSP Virus Kit (QIAGEN, https://www.qiagen.com) following the manufacturer's instructions and collected 120 µL elution volumes. We processed sputum specimens by adding equal volumes of 10 mM of freshly prepared No-Weigh Thermo Scientific Pierce dithiothreitol (Thermo Fisher Scientific, https://www.thermofisher.com) and incubating them at room temperature for 30 min with intermittent mixing or until the specimens were sufficiently liquefied for extraction. We processed stool specimens by preparing 10% suspensions by adding 100 µL of liquid stool or ≈100 mg of solid stool to 900 µL of phosphate-buffered saline, pH 7.4 (Thermo Fisher Scientific), pulse vortexing for 30 s, and centrifuging at 4,000 × *g* for 10 min at 4°C. We then carefully removed the clarified supernatant for extraction. To demonstrate successful nucleic acid recovery and reagent integrity, we extracted human specimen control consisting of cultured A549 cells concurrently with the test specimens as a procedural control. We either tested extracts immediately or stored them at ≤-70°C until use.

Primers and Probes

We aligned the N gene sequence from the publicly available SARS-CoV-2 genome (GenBank accession no. MN908947) with other coronavirus sequences available from GenBank by using MAFFT version 7.450 implemented in Geneious Prime (Geneious Biologics, https://www.geneious.com). We designed multiple primer/probe sets targeting regions in the 5′, middle, and 3′ regions of the N gene sequence with the aid of Primer Express software version 3.0.1 (Thermo Fisher Scientific). We selected 3 candidate gene regions, designated N1, N2, and N3, for further study (Table 1). N1 and N2 were designed to specifically detect SARS-CoV-2, and N3 was designed to universally detect all currently recognized clade 2 and 3 viruses within the subgenus *Sarbecovirus* (*4*), including SARS-CoV-2, SARS-CoV, and bat- and civet-SARS–like CoVs. BLASTn (http://www.ncbi.nlm.nih.gov/blast/Blast.cgi) analysis demonstrated no major combined similarity of primers and probes of each assay with other coronaviruses (OC43, 229E, HKU1, NL63, and Middle East respiratory syndrome coronavirus [MERS-CoV]) or microflora of humans that would potentially yield false-positive results. We synthesized all primers and probes by using standard phosphoramidite chemistry techniques at the CDC Biotechnology Core Facility. We labeled hydrolysis probes at the 5′ end with 6-carboxy-fluorescein (FAM) and at the 3′ end with Black Hole Quencher 1 (Biosearch Technologies, https://www.biosearchtech.com).

In Vitro RNA Transcript and Viral Template Control

Double-stranded DNA containing a 5′-T7 RNA polymerase promoter sequence (TAATACGACTCACTATAGGG) and the SARS-CoV-2 complete N gene

Table 1. Assay primer/probe sequences for the US CDC rRT-PCR panel for detection of SARS-CoV-2*

Assay	Genome target	Genome location	Primers and probes†	Sequence, 5′→3′	Amplicon size, bp	Assay use
N1	Nucleocapsid gene	28303–28322‡	Forward primer	GACCCCAAAATCAGCGAAAT	73	SARS-CoV-2
		28374–28351‡	Reverse primer	TCTGGTTACTGCCAGTTGAATCTG		
		28325–28348‡	Probe	ACCCCGCATTACGTTTGGTGGACC		
N2	Nucleocapsid gene	29180–29199‡	Forward primer	TTACAAACATTGGCCGCAAA	67	SARS-CoV-2
		29246–29228‡	Reverse primer	GCGCGACATTCCGAAGAA		
		29204–29226‡	Probe	ACAATTTGCCCCCAGCGCTTCAG		
N3	Nucleocapsid gene	28697–28718‡	Forward primer	GGGAGCCTTGAATACACCAAAA	72	SARS-CoV-2, SARS-CoV, and other *Sarbecoviruses*§
		28768–28748‡	Reverse primer	TGTAGCACGATTGCAGCATTG		
		28720–28743‡	Probe	AYCACATTGGCACCCGCAATCCTG		
RP¶	Human RNase P gene	50–68#	Forward primer	AGATTTGGACCTGCGAGCG	65	Sample quality control
		114–95#	Reverse primer	GAGCGGCTGTCTCCACAAGT		
		71–93#	Probe	TTCTGACCTGAAGGCTCTGCGCG		

*CDC, Centers for Disease Control and Prevention; N, nucleocapsid protein gene; RP, ribonuclease P gene; rRT-PCR, real-time reverse transcription PCR; SARS-CoV-2, severe acute respiratory coronavirus 2.
†Probes labeled at the 5′-end with the reporter molecule 6-carboxyfluorescein (FAM) and at the 3′-end with Black Hole Quencher 1 (Biosearch Technologies Inc., https://www.biosearchtech.com).
‡Nucleotide numbering based on SARS-CoV-2 (accession no. MN908947).
§Bat- and civet-SARS–like coronaviruses.
¶Primer/probe sequences from (*10*).
#Nucleotide numbering based on human RP mRNA (accession no. NM_006413).

sequence was synthesized by Integrated DNA Technologies (https://www.idtdna.com**)**. We transcribed the DNA by using the MEGAscript T7 Transcription Kit (Thermo Fisher Scientific). The RNA transcripts were purified by using the MEGAclear Transcription Clean-Up Kit (Thermo Fisher Scientific) and quantified with a Qubit fluorometer by using a Qubit RNA HS Assay Kit (Thermo Fisher Scientific). We used the RNA transcript for subsequent assay evaluation and positive template control.

rRT-PCR Assay

We performed all rRT-PCR testing by using the TaqPath 1-Step RT-qPCR Master Mix, CG (Thermo Fisher Scientific). Each 20-μL reaction contained 5 μL of 4X Master Mix (Thermo Fisher Scientific), 0.5 μL of 5 μmol/L probe, 0.5 μL each of 20 μmol/L forward and reverse primers, 8.5 μL of nuclease-free water, and 5 μL of nucleic acid extract. We conducted amplification in 96-well plates on an Applied Biosystems 7500 Fast Dx Real-Time PCR Instrument (Thermo Fisher Scientific). Thermocycling conditions consisted of 2 min at 25°C for uracil-DNA glycosylase incubation, 15 min at 50°C for reverse transcription, 2 min at 95°C for activation of the Taq enzyme, and 45 cycles of 3 s at 95°C and 30 s at 55°C. We set the threshold in the middle of exponential amplification phase in log view. A positive test result was defined as an exponential fluorescent curve that crossed the threshold within 40 cycles (cycle threshold [C_t] <40).

Test Algorithm

For routine specimen testing, we ran all 3 SARS-CoV-2 assays simultaneously along with the human ribonuclease P gene (RP) assay to monitor nucleic acid extraction, specimen quality, and presence of reaction inhibitors. To monitor assay performance, we included positive template controls, no-template controls, and human specimen controls in all runs. When all controls exhibited expected performance, we considered a specimen to be positive for SARS-CoV-2 if all assay amplification curves crossed the threshold line within 40 cycles (C_t <40). If all 3 assay results were negative, the test result was reported as negative. If all 3 assay results were not positive, an inconclusive test result was recorded and retesting was required. If both initial and retest results were inconclusive, the final result was reported as inconclusive.

Results

Assay Efficiency

We prepared serial 10-fold dilutions of quantified RNA transcript in 10 mmol/L Tris-HCl buffer containing 50 ng/μL of yeast tRNA (Thermo Fisher Scientific) and tested them by each assay. A linear amplification was achieved over an 8-log dynamic range from 5 to 5 × 10^7 copies/reaction for all 3 assays; calculated efficiency ranged from 99.4% to 102.6% (Figure 1).

Analytical Sensitivity (Limits of Detection)

SARS-CoV-2 RNA Transcripts

We tested serial 2-fold dilutions of quantified RNA transcript prepared in buffer as above by each assay in 24 replicates/dilution. The highest dilution of transcript at which all replicates were positive was

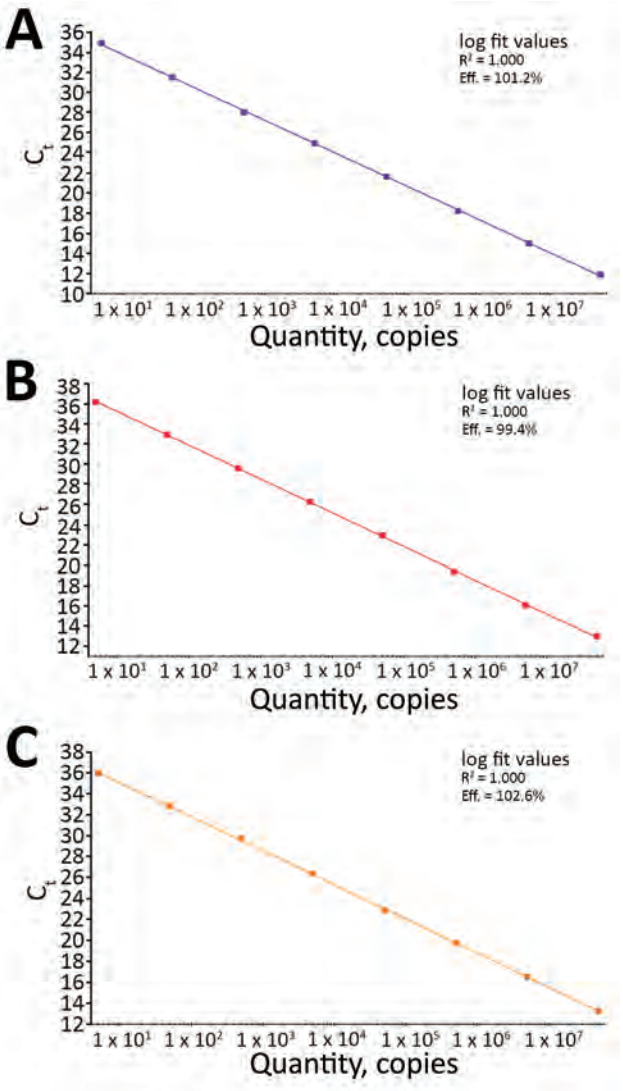

Figure 1. Linear regression analysis of serial 10-fold dilutions of synthetic RNA transcripts of the nucleocapsid gene (N) ranging from 5 to 5 × 10^7 copies/reaction tested by the N1 (A), N2 (B), and N3 (C) assays in the US Centers for Disease Control and Prevention real-time reverse transcription PCR panel for detection of severe acute respiratory syndrome coronavirus 2. For each assay, R^2 indicates calculated linear correlation coefficients and eff. indicates amplification efficiencies. C_t, cycle threshold.

defined as the limit of detection (LoD) for each assay. The LoDs for all assays were 5 RNA transcript copies/reaction (Table 2), which is consistent with that previously demonstrated (*11*).

SARS-CoV-2 Genomic RNA

We tested serial half-log dilutions of SARS-CoV-2 RNA extracted from inactivated cultured virus and prepared in buffer as above in triplicate by each assay (Table 3). For all 3 assays, the LoD was ≈1 × $10^{-1.5}$ $TCID_{50}$/mL.

Table 2. Limits of detection of the US CDC rRT-PCR panel for detection of SARS-CoV-2 with RNA transcripts*

Copies/ reaction	No. positive tests/no. (%) reaction replicates		
	N1	N2	N3
20	24/24 (100)	24/24 (100)	24/24 (100)
10	24/24 (100)	24/24 (100)	24/24 (100)
5	24/24 (100)	24/24 (100)	24/24 (100)
2.5	23/24 (95.8)	16/24 (66.7)	15/24 (62.5)
1.25	15/24 (62.5)	8/24 (33.3)	3/24 (12.5)

*CDC, Centers for Disease Control and Prevention; N, nucleocapsid protein gene; rRT-PCR, real-time reverse transcription PCR; SARS-CoV-2, severe acute respiratory coronavirus 2.

SARS-CoV-2 Spiked in Different Clinical Matrices

Serial half-log dilutions of SARS-CoV-2 were spiked in different specimen matrices contrived from pooled human clinical specimens: 10 serum samples, 10 nasopharyngeal swab samples, 10 oropharyngeal swab samples, 10 sputum samples, and 10 stool suspensions (prepared as 10% suspensions). The LoDs for all assays ranged from 1.0 × $10^{-1.5}$ to 1.0 × 10^{-1} $TCID_{50}$/mL across all specimen matrices (Table 4). Negative results were obtained for all 3 assays with all pooled negative specimen matrices.

Assay Reproducibility

We evaluated assay reproducibility by using 3 contrived respiratory specimens constructed from pooled nasopharyngeal swabs and spiked with high (1.0 × 10^3 $TCID_{50}$/mL), moderate (1.0 × 10^1 $TCID_{50}$/mL), and low (1.0 × 10^{-1} $TCID_{50}$/mL) concentrations of virus. We extracted the contrived specimens, and tested them in triplicate against each assay on 3 different days. Interassay variation was low for all assays (coefficient of variation range for N1, 1.8%–3.7%; N2, 2.3%–2.8%; N3, 1.1%–1.3%; RP, 0.9%–1.5%) (Table 5).

Analytical Specificity

In Silico Analysis Against Available SARS-CoV-2 Genome Sequences

We evaluated the primer/probe sequences of the 3 assays against 7,158 genome sequences available from the Global Initiative on Sharing All Influenza Data (GISAID, https://www.gisaid.org) as of April 14, 2020. Nucleotide mismatches in the primer/probe regions with frequency ≥0.1% were sporadic among viruses (Table 6). Except for 1 nucleotide mismatch with frequency >1% (1.55%) at the eighth position of the N3 forward primer, frequency of all other mismatches was <1%. These nucleotide mismatches would not be expected to affect reaction performance. No viruses were found to have >1 mismatch in any primer/probe region.

Table 3. Limits of detection of the US CDC rRT-PCR panel for detection of SARS-CoV-2 with extracted SARS-CoV-2 virus RNA*

Virus concentration,	N1 C_t				N2 C_t				N3 C_t			
$TCID_{50}$	Test 1	Test 2	Test 3	Call rate	Test 1	Test 2	Test 3	Call rate	Test 1	Test 2	Test 3	Call rate
$1 \times 10^{0.5}$	27.5	27.1	27.4	3/3	29.2	28.9	28.7	3/3	28.3	28.3	28.2	3/3
1×10^{0}	30.9	29.4	29.9	3/3	31.2	31.1	31.1	3/3	30.0	30.0	30.0	3/3
$1 \times 10^{-0.5}$	30.7	30.9	31.1	3/3	33.0	32.7	32.3	3/3	31.4	31.4	32.5	3/3
1×10^{-1}	33.0	32.4	32.9	3/3	34.4	34.3	34.7	3/3	34.6	32.3	33.3	3/3
$1 \times 10^{-1.5}$	34.4	33.6	35.6	3/3	36.3	36.1	37.6	3/3	35.4	35.8	35.6	3/3
1×10^{-2}	37.2	36.1	Neg	2/3	39.0	Neg	Neg	1/3	36.1	Neg	Neg	1/3
$1 \times 10^{-2.5}$	36.2	36.3	Neg	2/3	38.8	37.6	Neg	2/3	37.1	Neg	Neg	1/3
1×10^{-3}	Neg	Neg	Neg	0/3	Neg	Neg	Neg	0/3	Neg	Neg	Neg	0/3

*Call rate indicates each assay performed in triplicate. CDC, Centers for Disease Control and Prevention; C_t, cycle threshold; N, nucleocapsid protein gene; neg, negative; rRT-PCR, real-time reverse transcription PCR; SARS-CoV-2, severe acute respiratory coronavirus 2; $TCID_{50}$, 50% tissue culture infectious dose.

Cross-Reactivity with Other Respiratory Pathogens and Human Microbial Flora

We evaluated the specificity of the SARS-CoV-2 rRT-PCR assay with purified nucleic acid obtained from a collection of respiratory pathogen isolates or positive clinical specimens, including human coronaviruses 229E, OC43, NL63, HKU1, SARS-CoV, and MERS-CoV (Table 7). We also tested 10 nasopharyngeal swabs samples collected in 2018 before COVID-19 was identified. Except for the N3 assay, which was reactive with SARS-CoV RNA as expected, we observed no false-positive results for any pathogens and specimens tested.

Clinical Specimen Testing

Specimens from Persons with Suspected Cases

Among the 2,437 clinical specimens collected from 998 persons with suspected cases for initial SARS-CoV-2 diagnostic testing, 81 (3.32%) specimens (42 nasopharyngeal, 33 oropharyngeal, 5 sputum, 1 BAL) collected from 46 persons with suspected cases were positive and 2,355 (96.64%) specimens were negative (Table 8). We did not detect SARS-CoV-2 RNA in any of the 74 serum and 10 urine specimens tested.

Serially Collected Specimens from Persons with Laboratory-Confirmed COVID-19

Of 486 specimens serially collected from 28 persons with laboratory-confirmed COVID-19, results were SARS-CoV-2 positive for 142 (29.22%) samples (60 nasopharyngeal, 42 oropharyngeal, 13 sputum, 1 tracheal aspirate, 22 stool, and 4 serum) (Table 8). We detected SARS-CoV-2 RNA in serum of 2 of 15 persons with laboratory-confirmed COVID-19 for whom serum was available for testing. For 1 of those case-patients, serum was collected 14 days after symptom onset and tested positive. For the other case-patient, a total of 10 serum samples were collected. Of those, specimens collected on days 9, 11, and 13 were positive; specimens collected on days 3, 19, 22, 25, and 28 were negative; and specimens collected on days 6 and 16 had inconclusive results. A total of 22 stool specimens collected from 7 case-patients were positive. We detected no SARS-CoV-2 RNA in any of the 62 urine specimens collected.

Specimens with Positive Results According to the SARS-CoV-2 rRT-PCR Assay

Of the 223 clinical specimens with positive results by all 3 rRT-PCR assays, C_t values obtained by the N1, N2, and N3 assays correlated well with each other (N1 vs. N2, $R^2 = 0.94$; N1 vs. N3, $R^2 = 0.97$; N2 vs. N3, $R^2 = 0.96$) (Figure 2). Among the 71 pairs of nasopharyngeal and oropharyngeal specimens collected simultaneously from the 46 persons with suspected cases or from persons with laboratory-confirmed COVID-19 and any positive nasopharyngeal/oropharyngeal specimen, both nasopharyngeal and oropharyngeal samples were positive for 31 (43.67%); nasopharyngeal was positive but oropharyngeal was negative for 24 (33.80%); oropharyngeal was positive but nasopharyngeal was negative for 7 (9.86%); nasopharyngeal was positive but oropharyngeal was inconclusive for 5 (7.04%); and oropharyngeal was positive but nasopharyngeal was inconclusive for 4 (5.63%).

Inconclusive SARS-CoV-2 rRT-PCR Results

Inconclusive results were obtained for 40 (1.37%) of 2,923 specimens tested, including 1 (0.04%) of 2,437, from a person with a suspected case at initial testing, and 39 (8.02%) of 486 specimens collected for follow-up investigation from persons with laboratory-confirmed COVID-19. All specimens with inconclusive results had C_t values >35 (Table 9). Of these, 35 (87.5%) specimens were collected ≥7 days after symptom onset. Times from symptom onset to collection were unknown for the other 5 (12.5%) specimens.

Quality Control Data

Among 185 no-template controls and 219 human specimen controls included with specimen testing, negative results were obtained for all (100%) controls for N1, N2, and N3 assays and expected RP values were observed for human specimen controls. C_t values obtained from positive template control of 185 runs were in the expected range (data not shown).

Table 4. Performance of the US CDC rRT-PCR panel for detection of SARS-CoV-2 with various specimen matrices spiked with SARS-CoV-2*

	N1 C_t				N2 C_t				N3 C_t				RP C_t			
Virus titer, $TCID_{50}$†	Test 1	Test 2	Test 3	Call rate	Test 1	Test 2	Test 3	Call rate	Test 1	Test 2	Test 3	Call rate	Test 1	Test 2	Test 3	Call rate
$1 \times 10^{0.5}$																
NP	30.4	29.9	29.9	3/3	30.3	30.5	30.5	3/3	30.0	29.6	29.7	3/3	26.0	26.1	26.1	3/3
OP	30.1	29.7	29.7	3/3	30.7	30.8	30.5	3/3	29.6	29.5	29.5	3/3	30.0	30.3	30.2	3/3
Sputum	30.3	30.1	30.4	3/3	31.2	31.5	31.7	3/3	30.5	30.0	30.4	3/3	24.9	24.8	25.1	3/3
Serum	30.1	29.7	29.8	3/3	31.1	31.0	31.1	3/3	29.8	29.8	29.6	3/3	29.1	28.6	28.3	3/3
Stool	30.7	30.5	30.7	3/3	31.7	31.9	31.7	3/3	30.7	29.9	30.2	3/3	34.9	35.1	35.7	3/3
1×10^{0}																
NP	32.1	30.8	30.4	3/3	32.3	32.0	31.6	3/3	31.3	30.7	30.9	3/3	24.5	24.2	25.0	3/3
OP	31.6	31.3	31.4	3/3	32.8	32.3	32.2	3/3	30.8	31.3	31.1	3/3	29.3	29.2	29.5	3/3
Sputum	32.0	32.0	31.8	3/3	33.1	32.9	32.7	3/3	31.7	31.4	32.1	3/3	24.3	24.3	24.6	3/3
Serum	32.2	30.8	31.4	3/3	32.4	32.6	33.1	3/3	31.2	31.3	31.3	3/3	28.1	28.2	27.5	3/3
Stool	32.1	32.3	32.0	3/3	33.6	33.9	33.5	3/3	32.1	32.0	32.1	3/3	34.6	35.1	34.5	3/3
$1 \times 10^{-0.5}$																
NP	33.7	32.5	33.9	3/3	34.1	33.9	35.5	3/3	33.2	32.6	33.5	3/3	25.3	25.4	25.5	3/3
OP	33.6	33.6	33.1	3/3	34.4	34.4	34.6	3/3	33.5	33.0	32.0	3/3	29.2	29.4	29.6	3/3
Sputum	35.1	33.4	33.0	3/3	35.0	34.2	34.8	3/3	33.5	33.4	33.2	3/3	24.0	24.2	24.3	3/3
Serum	33.4	32.2	33.3	3/3	35.2	34.1	33.9	3/3	32.7	32.7	33.1	3/3	28.3	28.2	29.3	3/3
Stool	35.0	35.3	35.3	3/3	36.2	36.4	35.3	3/3	34.2	34.6	34.0	3/3	33.4	36.2	35.0	3/3
1×10^{-1}																
NP	33.9	34.0	34.6	3/3	36.0	36.2	36.5	3/3	34.1	34.3	35.1	3/3	25.6	25.6	25.9	3/3
OP	33.4	33.3	33.6	3/3	35.9	36.7	35.3	3/3	34.5	34.3	35.1	3/3	29.2	29.3	29.3	3/3
Sputum	35.2	35.0	36.2	3/3	36.8	36.8	35.3	3/3	35.3	35.2	35.1	3/3	24.1	24.1	24.3	3/3
Serum	37.5	35.3	34.8	3/3	36.4	37.2	36.3	3/3	35.2	33.7	34.3	3/3	28.3	28.3	28.6	3/3
Stool	36.1	35.8	36.0	3/3	37.3	37.9	38.1	3/3	35.8	35.6	34.7	3/3	34.1	33.9	34.2	3/3
$1 \times 10^{-1.5}$																
NP	35.6	36.8	35.9	3/3	39.9	36.8	37.6	3/3	36.7	35.1	35.7	3/3	26.1	26.3	26.6	3/3
OP	36.2	35.2	Neg	2/3	36.8	38.0	Neg	2/3	Neg	Neg	Neg	0/3	29.3	29.3	29.6	3/3
Sputum	36.9	36.3	Neg	2/3	39.1	39.5	38.4	3/3	35.8	38.2	Neg	2/3	23.9	24.2	24.2	3/3
Serum	36.8	36.5	36.4	3/3	38.4	39.1	36.9	3/3	35.6	36.2	Neg	2/3	27.9	28.2	27.4	3/3
Stool	Neg	Neg	Neg	0/3	39.2	38.1	37.5	3/3	35.5	38.1	38.0	3/3	34.2	33.3	35.6	3/3
1×10^{-2}																
NP	Neg	Neg	Neg	0/3	39.4	Neg	Neg	1/3	Neg	Neg	Neg	0/3	25.5	25.7	25.8	3/3
OP	Neg	Neg	Neg	0/3	38.5	38.0	Neg	2/3	37.1	Neg	Neg	1/3	29.4	29.3	29.4	3/3
Sputum	36.1	Neg	Neg	1/3	38.2	38.5	Neg	2/3	37.1	37.5	Neg	2/3	24.0	24.0	24.1	3/3
Serum	37.5	Neg	Neg	1/3	39.9	Neg	Neg	1/3	38.9	Neg	Neg	1/3	28.2	27.9	27.2	3/3
Stool	Neg	Neg	Neg	0/3	39.1	Neg	Neg	1/3	38.1	Neg	Neg	1/3	33.5	35.1	34.6	3/3
$1 \times 10^{-2.5}$																
NP	36.2	Neg	Neg	1/3	38.9	Neg	Neg	1/3	Neg	Neg	Neg	0/3	26.3	26.5	26.6	3/3
OP	Neg	Neg	Neg	0/3	Neg	Neg	Neg	0/3	Neg	Neg	Neg	0/3	29.0	29.2	29.2	3/3
Sputum	37.4	Neg	Neg	1/3	Neg	Neg	Neg	0/3	36.7	Neg	Neg	1/3	24.0	24.2	24.4	3/3
Serum	36.4	Neg	Neg	1/3	38.4	Neg	Neg	1/3	Neg	Neg	Neg	0/3	28.1	28.2	27.2	3/3
Stool	37.6	Neg	Neg	1/3	Neg	Neg	Neg	0/3	Neg	Neg	Neg	0/3	33.4	34.1	35.5	3/3
1×10^{-3}																
NP	Neg	Neg	Neg	0/3	Neg	Neg	Neg	0/3	Neg	Neg	Neg	0/3	26.8	26.7	27.0	3/3
OP	Neg	Neg	Neg	0/3	Neg	Neg	Neg	0/3	Neg	Neg	Neg	0/3	29.2	29.4	29.1	3/3
Sputum	Neg	Neg	Neg	0/3	Neg	Neg	Neg	0/3	Neg	Neg	Neg	0/3	23.9	24.1	24.3	3/3
Serum	Neg	Neg	Neg	0/3	Neg	Neg	Neg	0/3	Neg	Neg	Neg	0/3	28.2	28.3	27.9	3/3
Stool	Neg	Neg	Neg	0/3	Neg	Neg	Neg	0/3	Neg	Neg	Neg	0/3	34.1	35.0	35.0	3/3
0																
NP	Neg	Neg	Neg	0/3	Neg	Neg	Neg	0/3	Neg	Neg	Neg	0/3	25.0	25.2	24.8	3/3
OP	Neg	Neg	Neg	0/3	Neg	Neg	Neg	0/3	Neg	Neg	Neg	0/3	28.6	28.3	28.5	3/3
Sputum	Neg	Neg	Neg	0/3	Neg	Neg	Neg	0/3	Neg	Neg	Neg	0/3	23.1	23.0	23.1	3/3
Serum	Neg	Neg	Neg	0/3	Neg	Neg	Neg	0/3	Neg	Neg	Neg	0/3	27.6	27.8	27.7	3/3
Stool	Neg	Neg	Neg	0/3	Neg	Neg	Neg	0/3	Neg	Neg	Neg	0/3	33.5	33.8	33.2	3/3

*Call rate indicates each assay performed in triplicate. CDC, Centers for Disease Control and Prevention; C_t, cycle threshold; N, nucleocapsid protein gene; neg, negative; NP, nasopharyngeal; OP, oropharyngeal; RP, ribonuclease P gene; rRT-PCR, real-time reverse transcription PCR; SARS-CoV-2, severe acute respiratory coronavirus 2; $TCID_{50}$, 50% tissue culture infectious dose.
†50% tissue culture infectious dose/mL.

Table 5. Reproducibility of the US CDC rRT-PCR panel for detection of SARS-CoV-2 with respiratory specimen matrix spiked with SARS-CoV-2*

Virus titer, $TCID_{50}$	N1 C_t			N2 C_t			N3 C_t			RP C_t		
	Test 1	Test 2	Test 3	Test 1	Test 2	Test 3	Test 1	Test 2	Test 3	Test 1	Test 2	Test 3
Day 1												
1.0×10^3	21.1	21.1	21.0	21.5	21.2	21.5	21.0	21.1	21.1	26.0	25.9	26.1
1.0×10^1	27.8	27.6	27.5	28.6	28.6	28.9	27.6	27.3	27.7	26.0	25.8	26.1
1.0×10^{-1}	35.6	33.8	33.8	34.7	34.2	34.5	34.0	34.5	33.7	26.4	26.4	26.4
Day 2												
1.0×10^3	21.8	21.8	21.8	21.6	21.5	21.6	21.2	21.1	21.2	26.5	26.3	26.3
1.0×10^1	28.4	28.3	28.5	29.4	29.3	29.0	28.1	28.0	28.1	26.7	26.7	26.67
1.0×10^{-1}	37.6	35.7	34.0	36.0	34.7	34.9	34.1	33.8	34.5	26.8	26.3	26.2
Day 3												
1.0×10^3	20.8	20.7	20.8	20.6	20.4	20.6	20.7	20.6	20.7	26.8	26.7	26.9
1.0×10^1	27.1	27.6	27.3	27.5	27.6	27.4	27.2	27.3	27.3	26.6	26.8	26.8
1.0×10^{-1}	34.2	33.9	34.1	33.1	33.5	34.9	33.2	34.2	33.5	26.6	26.9	26.7
Summary results	Mean	SD	CV	Mean	SD	CV	Mean	SD	CV	Mean	SD	CV
1.0×10^3	21.2	0.5	2.2%	21.2	0.5	2.3%	21.0	0.2	1.1%	26.4	0.4	1.4%
1.0×10^1	27.8	0.5	1.8%	28.5	0.8	2.8%	27.6	0.4	1.3%	26.5	0.4	1.5%
1.0×10^{-1}	34.7	1.3	3.7%	34.5	0.8	2.5%	33.9	0.4	1.2%	26.5	0.2	0.9%

*Specimen matrix constructed from combined nasopharyngeal swabs obtained from 10 persons. CDC, Centers for Disease Control and Prevention; C_t, cycle threshold; neg, negative; CV, coefficient of variation; N, nucleocapsid protein gene; RP, ribonuclease P gene; rRT-PCR, real-time reverse transcription PCR; SARS-CoV-2, severe acute respiratory coronavirus 2; $TCID_{50}$, 50% tissue culture infectious dose.
†50% tissue culture infectious dose/mL.

Discussion

The COVID-19 pandemic has affected multiple countries, causing severe illness and death, with sustained and efficient person-to-person community transmission, and it continues to pose a serious public health threat. Rapid and reliable laboratory diagnosis of SARS-CoV-2 infection is a critical component of public health interventions to mitigate this threat.

Our assay design and validation strategy were guided by several principles. First, we based assay designs on previous diagnostic assays that had been developed for detection of MERS-CoV (*12*) and SARS-CoV (*10*) and targeted the N gene. Because of the relative abundance of N gene subgenomic mRNA produced during virus replication (*13*), rRT-PCR assays targeting the N gene of coronaviruses could theoretically achieve enhanced diagnostic sensitivity. One study also showed that the N gene–based rRT-PCR assay was more sensitive than the open reading frame (ORF) 1 assay for detection of SARS-CoV-2 in clinical specimens (*14*). Second, we designed rRT-PCR assays on the basis of limited genetic information available soon after the emergence of SARS-CoV-2, when it was announced that a novel coronavirus of zoonotic origin was described as being similar to bat-SARS–like CoVs and only 1 SARS-CoV-2 sequence was publicly available. The N3 assay was intentionally designed to universally detect SARS-CoV-2 and other SARS-like sarbecoviruses to ensure detection of SARS-CoV-2 as this virus evolves over time and to improve early identification of future emerging novel coronaviruses from this high-risk subgenus. After completion of this study, the sequence of a new bat-SARS–like CoV, RaTG13 (EPI_SL_402131), was released on GISAID. Detected in 2013 from China, this virus appears to be the nearest bat precursor of SARS-CoV-2 (*15*), having 96% genome and 97% N gene sequence identity with SARS-CoV-2. All 3 assays are predicted to detect the RaTG13 strain. Third, we designed and used multiple assays for routine specimen screening to confirm virus detection when present at low concentrations and to reduce the possibility of false-negative results caused by polymorphisms within the binding sites of the target sequences, which might occur as the virus evolves. Fourth, we validated all assays by using multiple specimen types, including upper and lower respiratory specimens, serum, and stool samples, all of which have been shown to be diagnostically valuable for detection of SARS-CoV and MERS-CoV (*10*,*16*).

Table 6. Nucleotide mismatches among 7,158 SARS-CoV-2 genome sequences found in the primer and probe regions included in the US CDC rRT-PCR panel for detection of SARS-CoV-2*

Primer/probe	N1 probe	N1 reverse		N2 forward	N3 forward		N3 probe		N3 reverse
Location, 5′→3′	3	15	21	4	8	10	5	17	14
Mismatch nucleotide	C>T	G>T	T>C	C>T	T>C	G>T	C>T	C>T	C>A
No. sequences	39	22	33	7	111	7	7	9	22
Mismatch frequency, %†	0.54	0.31	0.46	0.10	1.55	0.10	0.10	0.13	0.31

*CDC, Centers for Disease Control and Prevention; N, nucleocapsid protein gene; rRT-PCR, real-time reverse transcription PCR; SARS-CoV-2, severe acute respiratory coronavirus 2.
†Only mismatches with frequency ≥0.10% are shown.

Table 7. Cross-reactivity of the US CDC rRT-PCR panel for detection of SARS-CoV-2 against other respiratory pathogens*

Pathogen (strain)	Source	Other respiratory pathogens, rRT-PCR (C_t)	SARS-CoV-2 rRT-PCR N1	N2	N3 (C_t)
Adenovirus C1 (Ad.71)	Virus isolate	Pos (14.0)	Neg	Neg	Neg
Bocavirus	Clinical specimen	Pos (14.9)	Neg	Neg	Neg
Coronavirus 229E	Virus isolate	Pos (9.6)	Neg	Neg	Neg
Coronavirus OC43	Virus isolate	Pos (12.9)	Neg	Neg	Neg
Coronavirus HKU1	Clinical specimen	Pos (22.3)	Neg	Neg	Neg
Coronavirus MERS	Virus isolate	Pos (14.3)	Neg	Neg	Neg
Coronavirus NL63	Clinical specimen	Pos (21.9)	Neg	Neg	Neg
Coronavirus SARS (Urbani)	Virus isolate	Pos (27.3)	Neg	Neg	Pos (26.3)†
Enterovirus D68	Virus isolate	Pos (21.3)	Neg	Neg	Neg
Human metapneumovirus (CAN 99–81)	Virus isolate	Pos (13.8)	Neg	Neg	Neg
Influenza A H1N1 (A/India/2012)	Virus isolate	Pos (14.7)	Neg	Neg	Neg
Influenza A H3N1 (A/Texas/2012)	Virus isolate	Pos (10.7)	Neg	Neg	Neg
Influenza B (B/Massachusetts/1999)	Virus isolate	Pos (8.4)	Neg	Neg	Neg
Parainfluenza 1 (C35)	Virus isolate	Pos (17.2)	Neg	Neg	Neg
Parainfluenza 2 (Greer)	Virus isolate	Pos (17.1)	Neg	Neg	Neg
Parainfluenza 3 (C-43)	Virus isolate	Pos (20.4)	Neg	Neg	Neg
Parainfluenza 4a (M-25)	Virus isolate	Pos (16.7)	Neg	Neg	Neg
Parainfluenza 4b (CH 19503)	Virus isolate	Pos (18.2)	Neg	Neg	Neg
Respiratory syncytial virus (Long)	Virus isolate	Pos (15.1)	Neg	Neg	Neg
Rhinovirus 1A	Virus isolate	Pos (15.9)	Neg	Neg	Neg
Mycoplasma pneumoniae	Cultured bacteria	Pos (20.7)	Neg	Neg	Neg
Streptococcus pneumoniae	Cultured bacteria	Pos (21.1)	Neg	Neg	Neg

*CDC, Centers for Disease Control and Prevention; C_t, cycle threshold; neg, negative;pos, positive; MERS, Middle East respiratory syndrome; N, nucleocapsid protein gene; rRT-PCR, real-time reverse transcription PCR; SARS-CoV-2, severe acute respiratory coronavirus 2.
†N3 assay designed for universal detection of clade 2 and 3 within *Sarbecovirus* subgenus including SARS-CoV-2, SARS-CoV, and bat- and civet-SARS–like coronaviruses.

A study of SARS-CoV-2 viral load in upper respiratory tract specimens of infected patients showed that viral loads were higher in the nasopharynx than in the throat (*17*). Our study also showed a higher detection rate for nasopharyngeal swab samples than for oropharyngeal swab samples, although in some cases, viral load was higher in oropharyngeal than in nasopharyngeal swab samples. Our limited sputum data showed that SARS-CoV-2 seems to be more often detected and with higher viral loads in lower respiratory tract specimens than in upper respiratory tract specimens, especially later in the course of infection (72.22% positivity rate for sputum compared with 46.51% for nasopharyngeal and 30.00% for oropharyngeal samples in serial follow-up specimens). This phenomenon could be explained by the active replication of SARS-CoV-2 in the lungs,

Table 8. Test results for 2,923 human specimens determined by the US CDC real-time RT-PCR panel for detection of SARS-CoV-2*

Specimens	Specimens for initial laboratory diagnosis, no. (%) Positive	Negative	Inconclusive	Total	Serial follow-up specimens from laboratory-confirmed positive cases, no. (%) Positive	Negative	Inconclusive	Total
Upper respiratory tract								
NP swab	42 (3.85)	1,048 (96.06)	1 (0.09)	1,091 (100)	60 (46.51)	50 (38.76)	19 (14.73)	129 (100)
OP swab	33 (3.09)	1,035 (96.91)	0	1,068 (100)	42 (30.00)	86 (61.43)	12 (8.57)	140 (100)
Nasal swab/wash	0	7 (100)	0	7 (100)	0	0	0	0
Lower respiratory tract								
Sputum	5 (2.79)	174 (97.21)	0	179 (100)	13 (72.22)	3 (16.67)	2 (11.11)	18 (100)
BAL	1 (50)	1 (50)	0	2 (100)	0	0	0	0
Bronchial wash	0	1 (100)	0	1 (100)	0	0	0	0
Tissue, lung	0	2 (100)	0	2 (100)	0	0	0	0
Tracheal aspirate	0	0	0	0	1 (100)	0	0	1 (100)
Other								
Serum	0	74 (100)	0	74 (100)	4 (4.88)	76 (92.68)	2 (2.44)	82 (100)
Stool	0	0	0	0	22 (40.74)	28 (51.85)	4 (7.41)	54 (100)
Urine	0	10 (100)	0	10 (100)	0	62 (100)	0	62 (100)
Pleural fluid	0	1 (100)	0	1 (100)	0	0	0	0
CSF	0	2 (100)	0	2 (100)	0	0	0	0
Total	81 (3.32)	2,355 (96.64)	1 (0.04)	2,437 (100)	142 (29.22)	305 (62.76)	39 (8.02)	486 (100)

*BAL, bronchoalveolar lavage; CDC, Centers for Disease Control and Prevention; CSF, cerebrospinal fluid; NP, nasopharyngeal; OP, oropharyngeal; rRT-PCR, real-time reverse transcription PCR; SARS-CoV-2, severe acute respiratory coronavirus 2.

where the SARS-CoV-2 angiotensin–converting enzyme 2 receptor predominates (*18*). Similar to findings for SARS-CoV (*19*), our results showed that the SARS-CoV-2 RNA detection rate was high in the serial follow-up stool specimens collected from case-patients with laboratory-confirmed COVID-19. In contrast, SARS-CoV and MERS-CoV could be detected in serum/blood during the early prodromal phase of infection (*12*,*20*), whereas SARS-CoV-2 RNA was not detected in any of the serum specimens during the initial testing, although it was detected in serum collected from 2 (13.3%) case-patients ≥9 days after symptom onset. Similarly, whereas SARS-CoV and MERS-CoV RNA have been detected in urine (*16*,*19*), SARS-CoV-2 RNA was not detected in urine in our study nor has detection been reported (*21*).

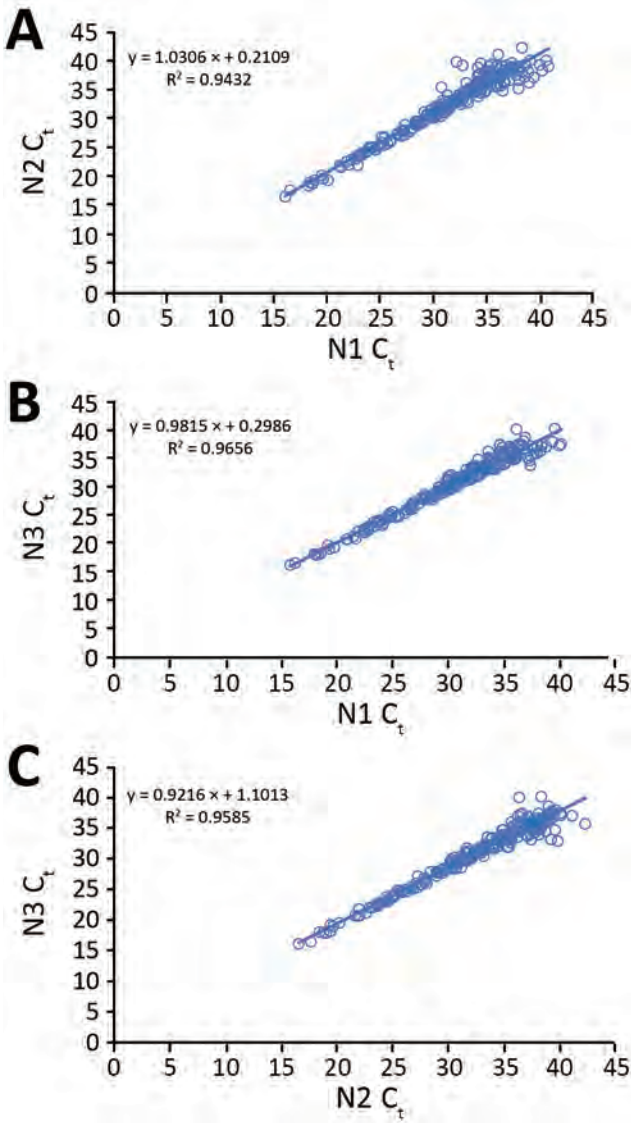

Figure 2. Comparison of the N1, N2, and N3 assays in the US Centers for Disease Control and Prevention real-time reverse transcription PCR panel for detection of SARS-CoV-2 with 223 SARS-CoV-2–positive clinical specimens. Linear regression lines were fitted to C_t values, with regression equations and coefficients of determination (R^2). A) N1 vs. N2; B) N1 vs. N3; C) N2 vs. N3. C_t, cycle threshold; SARS-CoV-2, severe acute respiratory syndrome coronavirus 2.

All specimens with inconclusive results in our study had C_t values >35, with reactivity not attributable to 1 individual assay, indicating that the viral RNA levels in the specimens were at the LoD of the assay. All specimens with inconclusive results were collected either ≥7 days after symptom onset or from repatriates who had been quarantined on the Diamond Princess cruise ship for ≈2 weeks before specimen collection. Inconclusive results most likely resulted from low viral loads, especially in upper respiratory tract specimens collected later in the course of infection. This observation is supported by another study, which showed that SARS-CoV-2 actively replicated in the oropharynx during the first 5 days after symptoms onset only (*21*). If inconclusive results are obtained, collection of additional specimens and specimen types may be warranted for accurate diagnosis.

All 3 SARS-CoV-2 rRT-PCR assays proved to be both sensitive and specific with high reproducibility. The earliest specimens from US COVID-19 case-patients were confirmed by virus isolation, whole-genome or partial gene sequencing, or both (*22*) (GenBank accession nos. MN985325, MN988713, MN994467–8, MN997409, MT027062–4, MT039887–8, MT044257–8, MT106052–4, MT118835, MT159705–22, and MT184907–13), although not all positive follow-up specimens detected by rRT-PCR assays were confirmed by independent assays. An independent comparison study showed that the CDC N2 and N3 assays performed well among 7 assays targeting the N gene that were evaluated and posted by the World Health Organization (Y. Jung, unpub. data, https://www.biorxiv.org/content/10.1101/2020.02.25.964775v1). In another study that compared 7 assays, the N2 assay was shown to be among the most sensitive (*23*). However, both studies used enzyme chemistries not optimized by CDC for testing, and we did not observe difference in sensitivity among the 3 assays in our study.

To expedite reagent kit manufacturing by removal of the N3 assay from the panel, we analyzed results of 2,437 specimens for initial COVID-19 testing when only N1 and N2 assay results were used for interpretation. Positive and negative test results showed 100% agreement to interpretation with all 3 assays. Only 1 (0.04%) specimen with an inconclusive result, which was positive for N2 at initial testing and positive for

N3 at retesting, would be reported as negative if the N3 assay was excluded from result interpretation of the CDC panel. This analysis demonstrates that interpretation of only N1 and N2 assay results agreed totally (99.96%) with the original results, and removal of the N3 assay from the panel would have a negligible effect on the ability of the test to detect positive specimens. The analytical LoD of the panel remained the same for detection of SARS-CoV-2 with or without the N3 assay included, and sensitivity of the panel was not affected. The benefits of testing with only N1 and N2 assays include simplified diagnosis of COVID-19 with fewer reactions for each patient specimen as well as increased testing throughput and reduced reagent cost, although removal of the N3 assay from the panel limits the ability to detect other SARS-like coronaviruses. Accordingly, the N3 assay has been removed from CDC testing interpretation, and current recommendations are to test with the N1 and N2 assays only (*11*). Because SARS-CoV-2 is an RNA virus with an estimated evolutionary rate of $\approx 1.8 \times 10^{-3}$ substitutions/site/year (*24*), performance of the assays included in the CDC panel will be monitored as SARS-CoV-2 continues to circulate and evolve over time. Therefore, assay designs included in the CDC panel are subject to change to account for future genetic mutations in the SARS-CoV-2 genome that may affect test sensitivity.

Table 9. Inconclusive test results for human specimens with the US CDC real-time RT-PCR panel for detection of SARS-CoV-2*

	Initial test, C_t			Retest, C_t			
Specimen ID	N1	N2	N3	N1	N2	N3	Days after onset
Specimen from suspected cases							
NP1	Neg	39.3	Neg	Neg	Neg	36.9	Unknown†
Serial follow-up specimens from laboratory-confirmed COVID-19 cases							
NP1	36.1	39.8	Neg	Neg	Neg	37.5	15
NP2	39.6	39.6	Neg	36.9	38.5	Neg	16
NP3	41.6	Neg	Neg	37.8	Neg	39.4	12
NP4	38.1	Neg	Neg	37.0	38.5	Neg	14
NP5	Neg	37.8	36.1	Neg	38.3	36.8	16
NP6	Neg	40.1	Neg	Neg	37.5	37.0	22
NP7	Neg	38.3	36.1	37.2	Neg	Neg	13
NP8	38.3	Neg	36.0	36.7	38.1	Neg	22
NP9	Neg	39.9	Neg	Neg	38.7	Neg	25
NP10	Neg	Neg	36.4	Neg	Neg	37.6	11
NP11	36.6	Neg	36.2	Neg	38.0	Neg	13
NP12	37.5	39.2	Neg	Neg	38.9	36.0	15
NP13	36.9	Neg	39.5	Neg	36.9	37.0	13
NP14	36.4	40.2	Neg	36.2	Neg	Neg	17
NP15	37.0	Neg	Neg	Neg	37.2	Neg	18
NP16	Neg	39.1	35.8	38.0	37.3	Neg	11
NP17	35.4	37.9	Neg	Neg	38.7	36.9	16
NP18	Neg	37.8	36.1	36.7	37.2	Neg	Unknown‡
NP19	35.5	39.0	Neg	39.8	Neg	Neg	Unknown‡
OP1	Neg	38.0	Neg	35.9	Neg	Neg	18
OP2	36.3	38.2	Neg	38.4	Neg	Neg	20
OP3	Neg	39.1	Neg	Neg	38.4	37.8	11
OP4	Neg	38.2	37.3	35.8	Neg	36.0	10
OP5	Neg	37.2	36.7	37.7	Neg	Neg	7
OP6	Neg	Neg	36.5	38.1	Neg	Neg	9
OP7	Neg	Neg	38.4	Neg	Neg	36.6	9
OP8	37.2	38.2	Neg	37.2	Neg	36.8	11
OP9	Neg	37.6	38.1	Neg	Neg	39.3	15
OP10	36.6	38.0	Neg	Neg	39.3	Neg	9
OP11	Neg	Neg	Neg	Neg	Neg	Neg	Unknown‡
OP12	Neg	37.8	Neg	37.6	Neg	37.6	Unknown‡
Sputum 1	Neg	42.9	37.3	Neg	Neg	38.6	10
Sputum 2	38.0	Neg	Neg	36.1	38.2	Neg	12
Serum 1	39.8	Neg	Neg	Neg	39.6	Neg	6
Serum 2	38.1	Neg	Neg	Neg	Neg	35.8	16
Stool 1	Neg	Neg	38.3	Neg	40.1	Neg	21
Stool 2	Neg	38.8	Neg	36.9	39.2	Neg	13
Stool 3	36.0	Neg	Neg	37.3	Neg	Neg	15
Stool 4	Neg	39.9	Neg	37.7	Neg	35.8	9

*CDC, Centers for Disease Control and Prevention; C_t, threshold cycle; COVID-19, coronavirus disease; N, nucleocapsid protein gene; neg, negative; NP, nasopharyngeal; OP, oropharyngeal; rRT-PCR, real-time reverse transcription PCR; SARS-CoV-2, severe acute respiratory coronavirus 2.
†Repatriated from Diamond Princess Cruise Ship, Japan.
‡Repatriated from Diamond Princess Cruise Ship and confirmed positive in Japan.

In conclusion, the CDC rRT-PCR panel for detection of SARS-CoV-2 demonstrated high sensitivity and specificity for detecting 5 RNA copies/reaction with no observed false-positive reactivity, and it facilitated rapid detection of SARS-CoV-2 infections in humans. These assays have proven to be valuable for rapid laboratory diagnosis and support, clinical management, and infection prevention and control of COVID-19.

Acknowledgments

We thank those who contributed substantially to this effort, including Nicky Sulaiman, Mathew Esona, Sung-Sil Moon, Yange Zhang, Jennifer Thomas, Laurel Jenkins, Mila Cohen, Hsin Chien, How-Yi Chang, Shannon York, and Nazia Kamal. We also thank all authors who have kindly shared genome data on GISAID.

Names of specific vendors, manufacturers, or products are included for public health and informational purposes; inclusion does not imply CDC endorsement of the vendors, manufacturers, or products. X.L. and S.L. have submitted the technology to the CDC Technology Transfer Office to ensure public health access to the technology and to facilitate its access to commercial developers.

About the Author

Ms. Lu is a research microbiologist with the National Center for Immunization and Respiratory Diseases, CDC, in Atlanta, Georgia. Her research interests include development and application of novel technologies to study the molecular epidemiology of human respiratory viruses, including adenoviruses, rhinoviruses, and emerging coronaviruses.

References

1. World Health Organization. Pneumonia of unknown cause–China [cited 2020 Mar 1]. https://www.who.int/csr/don/05-january-2020-pneumonia-of-unkown-cause-china
2. Zhu N, Zhang D, Wang W, Li X, Yang B, Song J, et al.; China Novel Coronavirus Investigating and Research Team. A novel coronavirus from patients with pneumonia in China, 2019. N Engl J Med. 2020;382:727–33. https://doi.org/10.1056/NEJMoa2001017
3. Zhang Y-Z. Novel 2019 coronavirus genome. Virological. 2020 Jan 10 [cited 2020 Mar 1]. http://virological.org/t/novel-2019-coronavirus-genome/319
4. Lu R, Zhao X, Li J, Niu P, Yang B, Wu H, et al. Genomic characterisation and epidemiology of 2019 novel coronavirus: implications for virus origins and receptor binding. Lancet. 2020;395:565–74. https://doi.org/10.1016/S0140-6736(20)30251-8
5. Chan JF, Kok KH, Zhu Z, Chu H, To KK, Yuan S, et al. Genomic characterization of the 2019 novel human-pathogenic coronavirus isolated from a patient with atypical pneumonia after visiting Wuhan. Emerg Microbes Infect. 2020;9:221–36. https://doi.org/10.1080/22221751.2020.1719902
6. Holshue ML, DeBolt C, Lindquist S, Lofy KH, Wiesman J, Bruce H, et al.; Washington State 2019-nCoV Case Investigation Team. First case of 2019 novel coronavirus in the United States. N Engl J Med. 2020;382:929–36. https://doi.org/10.1056/NEJMoa2001191
7. World Health Organization. Coronavirus disease 2019 (COVID-19) situation report-93 [cited 2020 Apr 22]. https://www.who.int/docs/default-source/coronaviruse/situation-reports/20200422-sitrep-93-covid-19.pdf?sfvrsn=35cf80d7_4
8. Harcourt J, Tamin A, Lu X, Kamili S, Sakthivel SK, Murray J, et al. Severe acute respiratory syndrome coronavirus 2 from patient with 2019 novel coronavirus disease, United States. Emerg Infect Dis. 2020 Mar 11 [Epub ahead of print]. https://doi.org/10.3201/eid2606.200516
9. Centers for Disease Control and Prevention. Health Alert Network: update and interim guidance on outbreak of 2019 novel coronavirus (2019-nCoV) in Wuhan, China [cited 2020 Apr 16]. https://emergency.cdc.gov/han/han00426.asp
10. Emery SL, Erdman DD, Bowen MD, Newton BR, Winchell JM, Meyer RF, et al. Real-time reverse transcription-polymerase chain reaction assay for SARS-associated coronavirus. Emerg Infect Dis. 2004;10:311–6. https://doi.org/10.3201/eid1002.030759
11. Centers for Disease Control and Prevention. CDC 2019-novel coronavirus (2019-nCoV) real-time RT-PCR diagnostic panel [cited 2020 Mar 1]. https://www.fda.gov/media/134922/download
12. Lu X, Whitaker B, Sakthivel SK, Kamili S, Rose LE, Lowe L, et al. Real-time reverse transcription-PCR assay panel for Middle East respiratory syndrome coronavirus. J Clin Microbiol. 2014;52:67–75. https://doi.org/10.1128/JCM.02533-13
13. Moreno JL, Zúñiga S, Enjuanes L, Sola I. Identification of a coronavirus transcription enhancer. J Virol. 2008;82:3882–93. https://doi.org/10.1128/JVI.02622-07
14. Chu DKW, Pan Y, Cheng SMS, Hui KPY, Krishnan P, Liu Y, et al. Molecular diagnosis of a novel coronavirus (2019-nCoV) causing an outbreak of pneumonia. Clin Chem. 2020;66:549–55. https://doi.org/10.1093/clinchem/hvaa029
15. Zhou P, Yang XL, Wang XG, Hu B, Zhang L, Zhang W, et al. A pneumonia outbreak associated with a new coronavirus of probable bat origin. Nature. 2020;579:270–3. https://doi.org/10.1038/s41586-020-2012-7
16. Al-Abdely HM, Midgley CM, Alkhamis AM, Abedi GR, Lu X, Binder AM, et al. Middle East respiratory syndrome coronavirus infection dynamics and antibody responses among clinically diverse patients, Saudi Arabia. Emerg Infect Dis. 2019;25:753–66. https://doi.org/10.3201/eid2504.181595
17. Zou L, Ruan F, Huang M, Liang L, Huang H, Hong Z, et al. SARS-CoV-2 viral load in upper respiratory specimens of infected patients. N Engl J Med. 2020;382:1177–9. https://doi.org/10.1056/NEJMc2001737
18. Hamming I, Timens W, Bulthuis ML, Lely AT, Navis G, van Goor H. Tissue distribution of ACE2 protein, the functional receptor for SARS coronavirus. A first step in understanding SARS pathogenesis. J Pathol. 2004;203:631–7. https://doi.org/10.1002/path.1570
19. Chan KH, Poon LL, Cheng VC, Guan Y, Hung IF, Kong J, et al. Detection of SARS coronavirus in patients with suspected SARS. Emerg Infect Dis. 2004;10:294–9. https://doi.org/10.3201/eid1002.030610
20. Grant PR, Garson JA, Tedder RS, Chan PK, Tam JS, Sung JJ. Detection of SARS coronavirus in plasma by real-time RT-PCR. N Engl J Med. 2003;349:2468–9. https://doi.org/10.1056/NEJM200312183492522

21. Wölfel R, Corman VM, Guggemos W, Seilmaier M, Zange S, Müller MA, et al. Virological assessment of hospitalized cases of coronavirus disease 2019. Nature. 2020 Apr 1 [Epub ahead of print].
22. Kujawski SA, Wong KK, Collins, JP. Clinical and virologic characteristics of the first 12 patients with coronavirus disease 2019 (COVID-19) in the United States. Nat Med. 2020 Apr 23 [Epub ahead of print]. https://doi.org/10.1038/s41591-020-0877-5
23. Nalla AK, Casto AM, Huang MW, Perchetti GA, Sampoleo R, Shrestha L, et al. Comparative performance of SARS-CoV-2 detection assays using seven different primer/probe sets and one assay kit. J Clin Microbiol. 2020 Apr 8 [Epub ahead of print].
24. Li X, Wang W, Zhao X, Zai J, Zhao Q, Li Y, et al. Transmission dynamics and evolutionary history of 2019-nCoV. J Med Virol. 2020;92:501–11. https://doi.org/10.1002/jmv.25701

Address for correspondence: Stephen Lindstrom, Centers for Disease Control and Prevention, 1600 Clifton Rd NE, Mailstop G04, Atlanta, GA 30329-4027, USA; email: sql5@cdc.gov

Coronavirus Disease Outbreak in Call Center, South Korea

Shin Young Park, Young-Man Kim, Seonju Yi, Sangeun Lee, Baeg-Ju Na, Chang Bo Kim, Jung-il Kim, Hea Sook Kim, Young Bok Kim, Yoojin Park, In Sil Huh, Hye Kyung Kim, Hyung Jun Yoon, Hanaram Jang, Kyungnam Kim, Yeonhwa Chang, Inhye Kim, Hyeyoung Lee, Jin Gwack, Seong Sun Kim, Miyoung Kim, Sanghui Kweon, Young June Choe, Ok Park, Young Joon Park, Eun Kyeong Jeong

We describe the epidemiology of a coronavirus disease (COVID-19) outbreak in a call center in South Korea. We obtained information on demographic characteristics by using standardized epidemiologic investigation forms. We performed descriptive analyses and reported the results as frequencies and proportions for categoric variables. Of 1,143 persons who were tested for COVID-19, a total of 97 (8.5%, 95% CI 7.0%–10.3%) had confirmed cases. Of these, 94 were working in an 11th-floor call center with 216 employees, translating to an attack rate of 43.5% (95% CI 36.9%–50.4%). The household secondary attack rate among symptomatic case-patients was 16.2% (95% CI 11.6%– 22.0%). Of the 97 persons with confirmed COVID-19, only 4 (1.9%) remained asymptomatic within 14 days of quarantine, and none of their household contacts acquired secondary infections. Extensive contact tracing, testing all contacts, and early quarantine blocked further transmission and might be effective for containing rapid outbreaks in crowded work settings.

Since the first imported case of coronavirus disease (COVID-19) was confirmed in South Korea on January 20, 2020, a sharp increase in the number of COVID-19 cases has been observed, with most infections being reported from specific clusters (*1*). Outbreaks of COVID-19 related to mass gathering, religious activities, workplaces, and hospitals have accounted for the largest portion cases in the national outbreak (*1*).

In March 2020, the Korea Centers for Disease Control and Prevention (KCDC), South Korea's national-level public health authority, was informed about a cluster of cases of COVID-19 in a call center located in a commercial–residential mixed-use building (building X) in the capital city of Seoul. We describe the epidemiology of this COVID-19 outbreak and detail the containment efforts to limit the spread of the disease.

Materials and Methods

Setting

On March 8, the Seoul Metropolitan Government was notified of a confirmed case of COVID-19 in a person who worked in building X; the case reportedly was associated with a possible cluster of cases. On March 9, KCDC and local governments (in Seoul, the city of Incheon, and Gyeonggi Province) formed a joint response team and launched an epidemiologic investigation with contact tracing. Building X is a 19-story floor in one of the busiest urban area of Seoul. Commercial offices are located on the 1st through 11th floors, and residential apartments are located on the 13th through 19th floors. We identified and investigated 922 employees who worked in the commercial offices, 203 residents who lived in the residential apartments, and 20 visitors. The call center is located on the 7th through 9th floors and the 11th floor; it has a total of 811 employees. Employees do not generally go between floors, and they do not have an in-house restaurant for meals.

Case Definition

We defined a patient under investigation (PUI) as one who worked at, lived at, or visited building X during February 21–March 8, 2020. We defined a confirmed

Author affiliations: Korea Centers for Disease Control and Prevention, Cheongju, South Korea (S.Y. Park, Y.-M. Kim, S. Yi, S. Lee, H. Lee, J. Gwack, S.S. Kim, M. Kim, S. Kweon, O. Park, Y.J. Park, E.K. Jeong); Seoul Metropolitan Government, Seoul, South Korea (B.-J. Na, J.-i. Kim, H.S. Kim, Y.B. Kim); Seoul Health Foundation, Seoul (C.B. Kim); Seoul Center for Infectious Disease Control and Prevention, Seoul (Y. Park, I.S. Huh); Incheon Metropolitan City, Incheon, South Korea (H.K. Kim, H.J. Yoon, H. Jang); Gyeonggi Provincial Office, Suwon, South Korea (K. Kim, Y. Chang, I. Kim); Hallym University College of Medicine, Chuncheon, South Korea (Y.J. Choe)

DOI: https://doi.org/10.3201/eid2608.201274

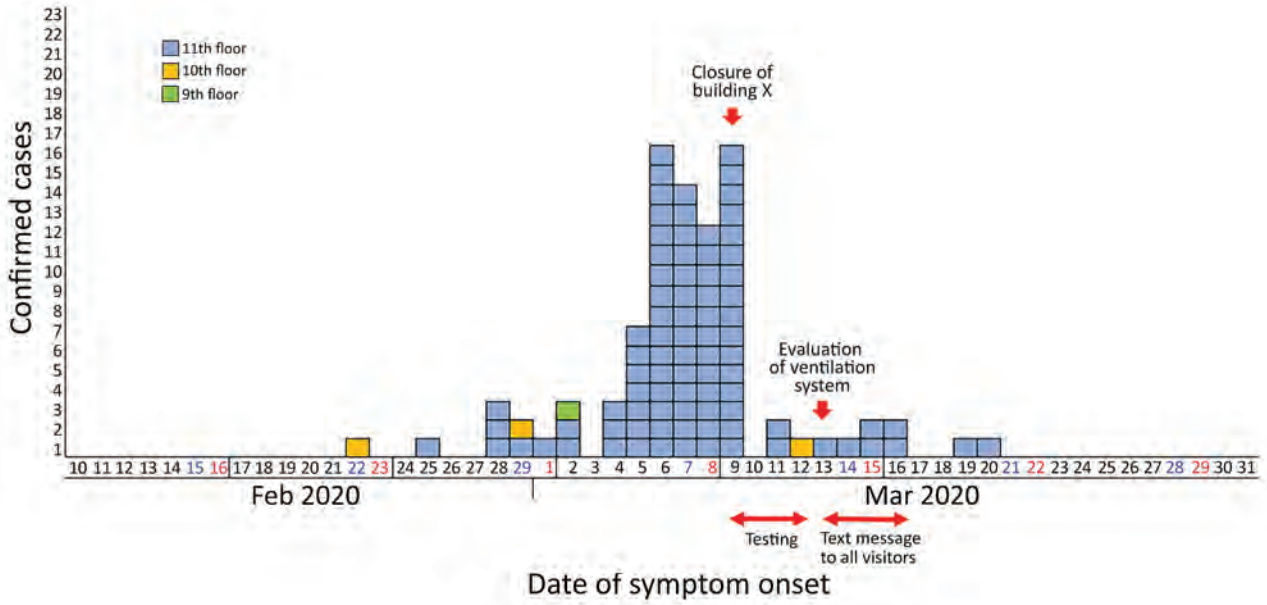

Figure 1. Epidemic curve of a coronavirus disease outbreak in a call center, by date of symptom onset, Seoul, Korea, 2020. Asymptomatic cases are excluded.

case-patient as a PUI with a positive COVID-19 laboratory test. We confirmed the diagnosis of COVID-19 by using real-time reverse transcription PCR assays. We defined a symptomatic case-patient as a confirmed case-patient with symptoms at the time of positive testing, a presymptomatic case-patient as a confirmed case-patient who was asymptomatic at the time of positive testing but later had symptoms during the 14 days of monitoring, and an asymptomatic case-patient as confirmed a case-patient with a positive COVID-19 test result who remained asymptomatic during the entire 14-day period.

Response Measures

Building X was closed on March 9, 2020, immediately after the outbreak was reported. We offered testing to all occupants (office workers and apartment residents) during March 9–12. We collected nasopharyngeal and oropharyngeal swab specimens from PUIs for immediate real-time reverse transcription PCR testing; the average turnaround time was 12–24 hours. Confirmed case-patients were isolated, and negative case-patients were mandated to stay quarantined for 14 days. We followed and retested all test-negative case-patients until the end of quarantine. We also investigated, tested, and monitored household contacts of all confirmed case-patients for 14 days after discovery, regardless of symptoms. During March 13–16, we sent a total of 16,628 text messages to persons who stayed >5 minutes near the building X; we tracked these persons by using cell phone location data. The messages instructed the recipients to avoid contact with others and go to the nearest COVID-19 screening center to get tested.

Data Collection and Analysis

We obtained information on demographic characteristics and presence of symptoms through face-to-face interviews with case-patients, using standardized epidemiologic investigation forms. We performed

Table 1. Attack rate by location during a coronavirus disease outbreak in a call center, Seoul, South Korea, 2020

Location type and floor	Potentially exposed, no. (%)	Confirmed cases, no. (%)	Attack rate, % (95% CI)
Commercial			
1st–6th	84 (7.3)	0	0
7th (call center)	182 (15.9)	0	0
8th (call center)	207 (18.1)	0	0
9th (call center)	206 (18.0)	1 (1.0)	0.5 (0.0–3.1)
10th	27 (2.4)	2 (2.1)	7.4 (1.3–25.8)
11th (call center)	216 (18.9)	94 (96.9)	43.5 (36.9–50.4)
Residential			
13th–19th	201 (17.6)	0	0
Other	20 (1.7)	0	0
Total	1,143	97	8.5 (7.0–10.3)

descriptive analyses reported the results as frequencies and proportions for categoric variables. The investigation was a part of public health response and was not considered research subject to institutional review board approval; therefore, written informed consent by participants was not required.

Results

Of 1,145 PUIs, we tested 1,143 (99.8%) for COVID-19 (922 employees, 201 residents, and 20 visitors) and identified 97 (8.5%, 95% CI 7.0–10.3) confirmed case-patients (Figure 1). Of 857 patients for whom demographic information was available, 620 (72.3%) were women; mean age was 38 years (range 20–80 years). Most (94 [96.9%]) of the confirmed case-patients were working on the 11th-floor call center, which had a total of 216 employees, resulting in an attack rate of 43.5% (95% CI 36.9%–50.4%) (Table 1; Figure 2). Most of the case-patients on the 11th floor were on the same side of the building. Among the 97

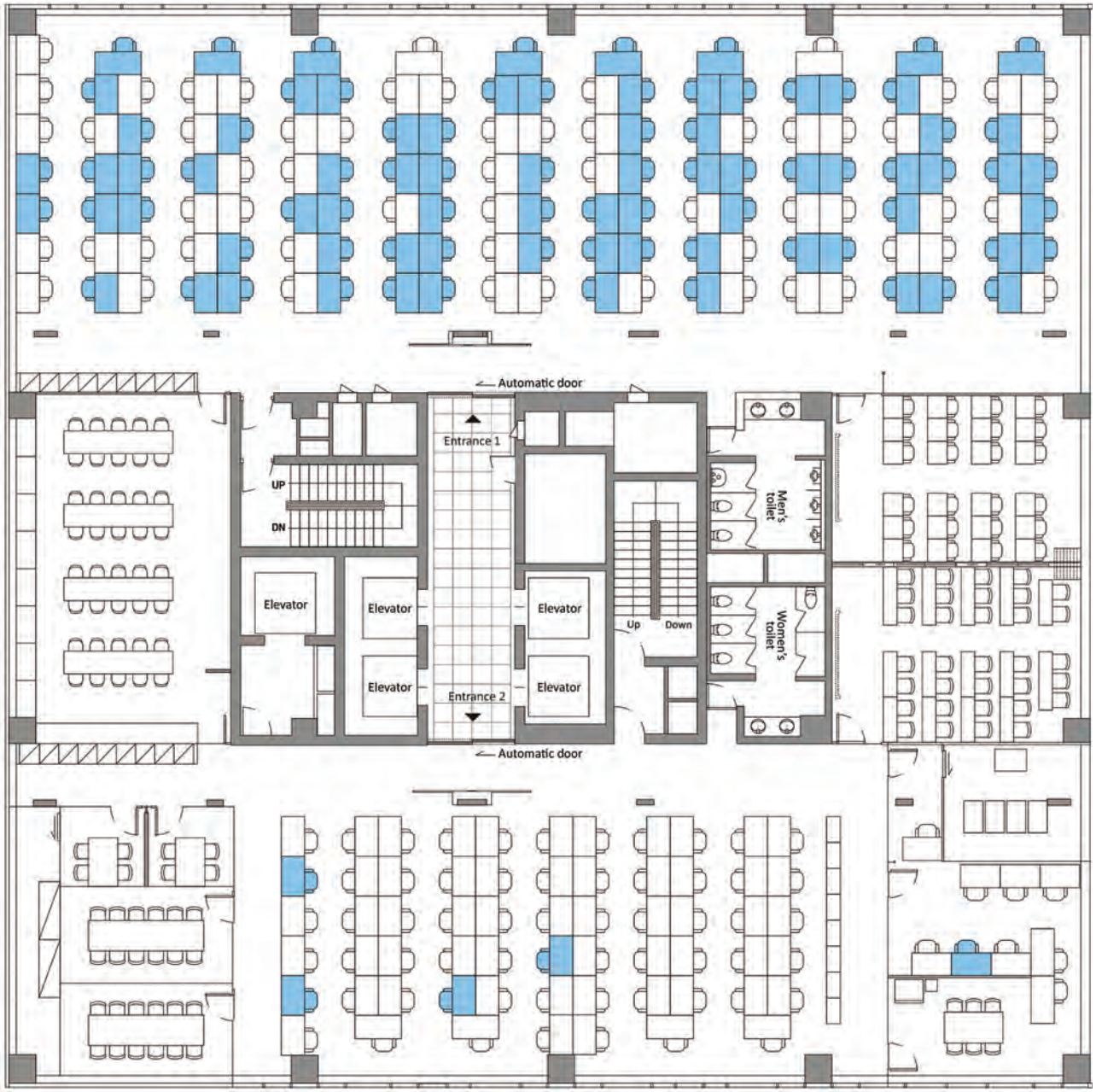

Figure 2. Floor plan of the 11th floor of building X, site of a coronavirus disease outbreak, Seoul, South Korea, 2020. Blue indicates the seating places of persons with confirmed cases.

confirmed case-patients, 89 (91.7%) were symptomatic at the time of investigation and 4 (4.1%) were presymptomatic during the time of investigation but later had onset of symptoms within 14 days of monitoring; 4 (4.1%) case-patients remained asymptomatic after 14 days of isolation.

The first case-patient with symptom onset, who worked in an office on the 10th floor (and reportedly never went to 11th floor), had onset of symptoms on February 22. The second case-patient with symptom onset, who worked at the call center on the 11th floor, had onset of symptoms on February 25. Residents and employees in building X had frequent contact in the lobby or elevators. We were not able to trace back the index case-patient to another cluster or an imported case.

We followed up on a total of 225 household contacts of confirmed COVID-19 case-patients (average 2.3 household members per confirmed case-patient). COVID-19 had occurred in 34 household members who had contact with symptomatic case-patients, translating to a secondary attack rate of 16.2% (Table 2). Among 11 household members of presymptomatic case-patients and 4 household members of asymptomatic case-patients, none had COVID-19 symptoms nor tested positive after 14 days of quarantine.

Discussion

We described the epidemiologic characteristics of a COVID-19 outbreak centered in a call center in South Korea. We identified 97 confirmed COVID-19 case-patients in building X, indicating an attack rate of 8.5%. However, if we restrict our results to the 11th floor, the attack rate was as high as 43.5%. This outbreak shows alarmingly that severe acute respiratory syndrome coronavirus 2 (SARS-CoV-2) can be exceptionally contagious in crowded office settings such as a call center. The magnitude of the outbreak illustrates how a high-density work environment can become a high-risk site for the spread of COVID-19 and potentially a source of further transmission. Nearly all the case-patients were on one side of the building on 11th floor. Severe acute respiratory syndrome coronavirus, the predecessor of SARS-CoV-2, exhibited multiple superspreading events in 2002 and 2003, in which a few persons infected others, resulting in many secondary cases. Despite considerable interaction between workers on different floors of building X in the elevators and lobby, spread of COVID-19 was limited almost exclusively to the 11th floor, which indicates that the duration of interaction (or contact) was likely the main facilitator for further spreading of SARS-CoV-2.

Unique features of this outbreak investigation include a complete 14-day follow-up of close contacts of case-patients after containment measures were implemented. Close contact with an infected person is a well-recognized risk factor for acquiring SARS-CoV-2 (*2*). In a recent US study, the symptomatic secondary attack rate among 445 close contacts of COVID-19 case-patients was 10.5% among household members (*3*). In this outbreak in South Korea, we found that the secondary attack rate within the household was 16.5% among symptomatic index case-patients, which is consistent with other reports.

The role of asymptomatic COVID-19 case-patients in spreading the disease is of great concern. Among 97 confirmed COVID-19 case-patients in this study, 4 (4.1%) remained asymptomatic during the 14-days of monitoring. This rate is lower than the 30.8% rate estimated in previous modeling (*4*). A case-patient series from Beijing, China, indicated that asymptomatic case-patients accounted for 5% (13/262) of patients transferred to a designated COVID-19 hospital (*5*). Our data might represent the likely proportion of asymptomatic COVID-19 infections in the community setting. We also found that, among 17 household contacts of asymptomatic case-patients, none had secondary infections. Previous reports have postulated that SARS-CoV-2 in asymptomatic (or presymptomatic) case-patients might become transmissible to others (*6*); however, given the high degree of self-quarantine and isolation measures that were instituted after March 8 among this cohort, our analyses might have not detected the actual transmissibility in asymptomatic COVID-19 case-patients. Robust mass testing of all suspected case-patients might have prevented asymptomatic transmission because asymptomatic persons were given information about their possible infection and therefore might have self-isolated from their household members.

Table 2. Household secondary attack rate, by presence of symptoms, during a coronavirus disease outbreak in in a call center, Seoul, South Korea, 2020

Symptom status of index patients	Exposed, no. (%)	Confirmed cases, no. (%)	Secondary attack rate, % (95% CI)
Symptomatic	210 (93.3)	34 (100.0)	16.2 (11.6–22.0)
Presymptomatic	11 (4.8)	0	0
Asymptomatic	4 (1.9)	0	0
Total	225	34	15.1 (10.8–20.6)

This outbreak investigation has several limitations. First, we could not track these cases to another cluster, making it difficult to identify the actual index case-patient. Second, not all clinical information was available for all confirmed cases, prohibiting detailed description of clinical syndromes. Date of symptom onset by office seat would be informative in understanding SARS-CoV-2 transmission in close contact area. However, our findings demonstrate the power of screening all potentially exposed persons and show that early containment can be implemented and used in the middle of national COVID-19 outbreak. By testing all potentially exposed persons and their contacts to facilitate the isolation of symptomatic and asymptomatic COVID-19 case-patients, we might have helped interrupt transmission chains. In light of the shift to a global pandemic, we recommend that public health authorities conduct active surveillance and epidemiologic investigation in this rapidly evolving landscape of COVID-19.

In summary, this outbreak exemplifies the threat posed by SARS-CoV-2 with its propensity to cause large outbreaks among persons in office workplaces. Targeted preventive strategies might help mitigate the risk for SARS-CoV-2 infection in these vulnerable group.

Acknowledgments

We thank the relevant ministries (including the Ministry of Interior and Safety, Si/Do, and Si/Gun/Gu), medical staffs in health centers, and medical facilities for their efforts in responding to the COVID-19 outbreak.

The opinions expressed by authors contributing to this journal do not necessarily reflect the opinions of the Korea Centers for Disease Control and Prevention or the institutions with which the authors are affiliated.

About the Author

Ms. Park is a public health officer at the Korea Centers for Disease Control and Prevention. Her main interest is the epidemiologic investigation of infectious diseases.

References

1. COVID-19 National Emergency Response Center, Epidemiology and Case-patient Management Team, Korea Centers for Disease Control and Prevention. Early epidemiological and clinical characteristics of 28 cases of coronavirus disease in South Korea. Osong Public Health Res Perspect. 2020;11:8–14. https://doi.org/10.24171/j.phrp.2020.11.1.03
2. Bajema KL, Oster AM, McGovern OL, Lindstrom S, Stenger MR, Anderson TC, et al.; 2019-nCoV Persons Under Investigation Team; 2019-CoV Persons Under Investigation Team. Persons evaluated for 2019 novel coronavirus—United States, January 2020. MMWR Morb Mortal Wkly Rep. 2020;69:166–70. https://doi.org/10.15585/mmwr.mm6906e1
3. Burke RM, Midgley CM, Dratch A, Fenstersheib M, Haupt T, Holshue M, et al. Active monitoring of persons exposed to patients with confirmed COVID-19—United States, January–February 2020. MMWR Morb Mortal Wkly Rep. 2020;69:245–6. https://doi.org/10.15585/mmwr.mm6909e1
4. Nishiura H, Kobayashi T, Suzuki A, Jung SM, Hayashi K, Kinoshita R, et al. Estimation of the asymptomatic ratio of novel coronavirus infections (COVID-19). Int J Infect Dis. 2020;S1201-9712(20)30139-9. https://doi.org/10.1016/j.ijid.2020.03.020
5. Tian S, Hu N, Lou J, Chen K, Kang X, Xiang Z, et al. Characteristics of COVID-19 infection in Beijing. J Infect. 2020;80:401–6. https://doi.org/10.1016/j.jinf.2020.02.018
6. Tong ZD, Tang A, Li KF, Li P, Wang HL, Yi JP, et al. Potential presymptomatic transmission of SARS-CoV-2, Zhejiang Province, China, 2020. Emerg Infect Dis. 2020;26:1052–4. https://doi.org/10.3201/eid2605.200198

Address for correspondence: Eun Kyeong Jeong, Korea Centers for Disease Control and Prevention, Osong Health Technology Administration Complex, 187, Osongsaengmyeong 2-ro, Osong-eup, Heungdeok-gu, Cheongju-si, Chungcheongbuk-do, 28159, South Korea; email: jeongek@korea.kr

Investigation and Serologic Follow-Up of Contacts of Early Confirmed Case-Patient with COVID-19, Washington, USA

Victoria T. Chu,[1] Brandi Freeman-Ponder,[1] Scott Lindquist, Christopher Spitters, Vance Kawakami, Jonathan W. Dyal, Shauna Clark, Hollianne Bruce, Jeffrey S. Duchin, Chas DeBolt, Sara Podczervinski, Marisa D'Angeli, Kristen Pettrone, Rachael Zacks, Grace Vahey, Michelle L. Holshue, Misty Lang, Rachel M. Burke, Melissa A. Rolfes, Mariel Marlow, Claire M. Midgley, Xiaoyan Lu, Stephen Lindstrom, Aron J. Hall, Alicia M. Fry, Natalie J. Thornburg, Susan I. Gerber, Satish K. Pillai, Holly M. Biggs

We describe the contact investigation for an early confirmed case of coronavirus disease (COVID-19), caused by severe acute respiratory syndrome coronavirus 2 (SARS-CoV-2), in the United States. Contacts of the case-patient were identified, actively monitored for symptoms, interviewed for a detailed exposure history, and tested for SARS-CoV-2 infection by real-time reverse transcription PCR (rRT-PCR) and ELISA. Fifty contacts were identified and 38 (76%) were interviewed, of whom 11 (29%) reported unprotected face-to-face interaction with the case-patient. Thirty-seven (74%) had respiratory specimens tested by rRT-PCR, and all tested negative. Twenty-three (46%) had ELISA performed on serum samples collected ≈6 weeks after exposure, and none had detectable antibodies to SARS-CoV-2. Among contacts who were tested, no secondary transmission was identified in this investigation, despite unprotected close interactions with the infectious case-patient.

Author affiliations: Centers for Disease Control and Prevention, Atlanta, Georgia, USA (V.T. Chu, B. Freeman-Ponder, J.W. Dyal, Kristen Pettrone, R. Zacks, G. Vahey, M.L. Holshue, R.M. Burke, M.A. Rolfes, M. Marlow, C.M. Midgley, X. Lu, S. Lindstrom, A.J. Hall, A.M. Fry, N.J. Thornburg, S.I. Gerber, S.K. Pillai, H.M. Biggs); Washington State Department of Public Health, Shoreline, Washington, USA (S. Lindquist, C. DeBolt, S. Podczervinski, M. D'Angeli, M.L. Holshue, M. Lang); Snohomish Health District, Everett, Washington, USA (C. Spitters, H. Bruce); Public Health—Seattle and King County, Seattle, Washington (V. Kawakami, S. Clark, J.S. Duchin); University of Washington, Seattle (J.S. Duchin)

DOI: https://doi.org/10.3201/eid2608.201423

In December 2019, a viral pneumonia outbreak caused by severe acute respiratory syndrome coronavirus 2 (SARS-CoV-2) emerged in Wuhan, China, before spreading rapidly to other provinces in China and then internationally (*1*). On January 20, 2020, the Centers for Disease Control and Prevention (CDC) confirmed a US case of coronavirus disease (COVID-19), the disease caused by SARS-CoV-2, in a traveler who had recently returned to Washington state from Wuhan (*2*). We investigated contacts of the confirmed case-patient to describe transmission to inform public health recommendations and control measures.

Methods

Washington state and local health officials interviewed the case-patient to identify contacts and activities during time of symptom onset until appropriate isolation of the patient. Because contact investigations for COVID-19 had not been conducted in the United States, the Washington State Department of Health (WA DOH), in consultation with CDC, developed contact definitions based on the best evidence available at the time, which are not necessarily consistent with those currently in use (Table 1). We tailored the contact definitions after the case-patient interview based on the known movement and activities of the case-patient. We categorized contacts into community or healthcare contacts. For this investigation, we defined community contact as any close contact (being within 6 feet of the case-patient) for a prolonged

[1]These authors contributed equally to this article.

Table 1. Contact definitions, number of contacts identified by category, and comments regarding the contact identification process during the contact investigation of an early confirmed US COVID-19 case, Washington, USA, 2020*

Type	Definition†	Contacts	Comments
Community contact	Any close contact (being within 6 feet of the case-patient) for a prolonged time (>10 min), other than office co-worker	0	None
	Being an office co-worker of the case-patient with close contact of any duration	11 office co-workers	None
	Contact with infectious secretions from the case-patient	0	None
	Sharing a healthcare waiting room or area during the same time and up to 2 h after the case-patient was present	31 waiting room patients	7/31 of the waiting room contacts likely overlapped with the case-patient in the waiting room.
Healthcare contact	Any face-to-face interactions between an HCP and the case-patient without the HCP wearing full PPE†	6 HCP	None
	Potential contact with the case-patient's infectious secretions by an HCP without wearing full PPE‡	2 HCP	2 HCP were EVS workers who did not have direct contact with the case-patient. They were included for potential exposure to infectious secretions from the case-patient while cleaning surfaces.

*COVID-19, coronavirus disease; EVS, environmental services; HCP, healthcare personnel; PPE, personal protective equipment.
†Contact definitions were developed on January 21, 2020, before published guidance from CDC for COVID-19 was available. Contacts were identified during the time from the case-patient's symptom onset until the case-patient was appropriately isolated. An airport shuttle driver who had contact with the case-patient before symptom onset was identified during contact tracing but was not included in this investigation. He self-monitored for 14 days and reported remaining asymptomatic.
‡At the time of the investigation, full PPE consisted of gown, gloves, eye protection, and an N95 respirator.

time (>10 minutes); being an office co-worker of the case-patient with close contact of any duration; contact with infectious secretions from the case-patient; or sharing a healthcare waiting room or area during the same time and up to 2 hours after the case-patient was present. Transient community interactions (e.g., grocery store cashiers) were not considered community contacts. Healthcare contact included any face-to-face interaction between healthcare personnel (HCP) and the case-patient without wearing the full personal protective equipment (PPE) that was recommended at the time of the investigation (i.e., gown, gloves, eye protection, and N95 respirator) or potential contact with the case-patient's secretions by HCP without wearing full PPE. HCP who cared for the patient after patient isolation while wearing the full recommended PPE were monitored but not included in this contact investigation report.

The local health departments actively monitored identified contacts during the 14 days after the last exposure date to the case-patient (i.e., the monitoring period). Active monitoring consisted of daily telephone calls or text messages to ask the contacts whether they had measured fever ($\geq$100.4°F or $\geq$38°C) or symptoms including cough, shortness of breath, chills, runny nose, body aches, sore throat, headache, diarrhea, nausea, or vomiting. The local health department supplied thermometers to contacts without a home thermometer. Contacts who developed signs or symptoms during the monitoring period were assessed as persons under investigation (PUIs) for SARS-CoV-2 infection, and nasopharyngeal (NP) and oropharyngeal (OP) swabs were obtained for testing.

Concurrently with mandatory active monitoring, CDC, WA DOH, and the local health departments conducted an enhanced contact investigation. This investigation was implemented after the urgent public health activities of identifying contacts and initiating active monitoring procedures were begun and was voluntary. The enhanced contact investigation included an in-depth interview using a standardized questionnaire and collection of NP and OP specimens and serum samples. We approached all identified community and healthcare contacts by telephone for participation. For contacts who agreed, we conducted the interview by telephone or during in-person household visits, depending on the contact availability at the time of the initial outreach. The questionnaire included demographic characteristics, medical history, and type and duration of the exposure to the case-patient. Exposure types assessed on the questionnaire were "physically within 6 feet of the case-patient," "had face-to-face interaction," "had direct physical contact," and "traveled in the same vehicle, sitting within 6 feet of the case-patient." For HCP, we also obtained data regarding healthcare-specific exposures and PPE use during the encounter. For all asymptomatic contacts who agreed, we collected NP and OP specimens and serum samples during the monitoring period to test for SARS-CoV-2 by molecular and serologic methods. We tested symptomatic contacts under PUI protocols. We approached participants in the initial enhanced investigation ≈6 weeks

after last exposure to the case-patient for collection of follow-up serum samples.

NP and OP swabs were shipped to CDC and tested for SARS-CoV-2 using a real-time reverse transcription PCR (rRT-PCR) assay with 3 targets (N1, N2, and N3), as previously described (*3*). The human RNase P gene was used as an internal human gene to confirm RNA quality. Serum samples were tested at CDC using a SARS-CoV-2 ELISA with a recombinant SARS-CoV-2 spike protein (courtesy of Dr. Barney Graham, National Institutes of Health, Bethesda, MD, USA) as an antigen (*4*). Protein ELISA 96-well plates were coated with 0.15 μg/mL of recombinant SARS-CoV-2 spike protein and ELISA was carried out as previously described (*5*). An optimal cutoff optical density value of 0.4 was determined for >99% specificity and 96% sensitivity (B. Freeman et al., unpub. data; https://www.biorxiv.org/content/10.1101/2020.04.24.057323v1). Specimens with total SARS-CoV-2 antibody titers ≥400 were considered seropositive. Serum samples from the case-patient were used as a positive control and commercially available serum collected before January 2020 from an uninfected person as a negative control.

This public health investigation was determined to be non-research by CDC and WA DOH. Thus, it was not subject to review by either institutional review board.

Results

The case-patient, a 35-year-old man, was asymptomatic when he returned home to Washington from Wuhan on January 15, 2020 (*2*). During the next 2 days, he developed a cough (day 1 of illness) and chills (day 2) while continuing to work in an office setting. He reported feeling feverish on day 3, a weekend day. On day 4, he went to an urgent care clinic, where he was identified as meeting the PUI criteria at the time for COVID-19; NP and OP swabs and serum samples were collected and sent to CDC for SARS-CoV-2 testing (*6*). Upon laboratory confirmation as a COVID-19 case-patient (day 5), he was hospitalized for isolation and clinical observation (Figure 1).

The investigation identified 50 contacts of the case-patient while he was symptomatic, including 42 community contacts (11 office co-workers and 31 waiting room contacts at the urgent care clinic) and 8 healthcare contacts (Table 1). The case-patient lived alone, so he had no household contacts. Among the 50 contacts, the median age was 44 years (range <1–86 years); 25 (50%) were male. All 50 contacts were actively monitored daily. Eight (16%) developed symptoms, including cough (n = 6), headache (n = 5), runny nose (n = 5), sore throat (n = 4), or fever (n = 1), during their monitoring period and were assessed as PUIs; none required hospitalization (Table 2).

Of the 50 contacts, 38 (76%) participated in the voluntary enhanced contact investigation and completed the standardized questionnaire interview (Figure 2). Among these, 24 (63%) had ≥1 underlying condition, including asthma (n = 10; 26%), hypertension (n = 7; 18%), type 2 diabetes mellitus (n = 4; 11%), or pregnancy/postpartum (n = 2; 5%) (Table 3).

Eleven office co-workers were identified as having had close contact (≤6 feet) with the case-patient. Four (36%) co-workers were exposed over the course of 1 day and 7 (64%) were exposed over the course of 2 days. The duration of close contact ranged from 2 to 90 minutes (<10 minutes, n = 2; 10–15 minutes, n = 3; 60–90 minutes, n = 6). All 11 co-workers reported face-to-face interaction with the case-patient, and 6 (55%) had direct physical contact (e.g., shaking hands, touching shoulder). Although the case-patient admitted symptoms of cough while at the office, no co-workers recalled being within 6 feet of the case-patient while he was coughing. On day 2 of illness, the case-patient attended a 2-hour lunch with 7 co-workers. Three co-workers traveled in the same vehicle as the symptomatic case-patient for a total of 30 minutes on the way to and from lunch.

All 8 HCP had interactions with the case-patient without wearing the full recommended PPE. One HCP was a public health employee who briefly visited the case-patient's home and had a face-to-face conversation without wearing PPE; however, further details of this HCP's exposure were not available because the contact did not participate in the enhanced contact investigation. The remaining 7 HCP worked at the urgent care clinic where the patient initially sought care: a receptionist, medical assistant, nurse, physician assistant, radiograph technician, and 2 environmental services (EVS) workers.

All 7 HCP at the urgent care clinic participated in the enhanced contact investigation. Of those, 5 (71%) had face-to-face interaction with the case-patient; the case-patient was wearing a facemask for most encounters. Duration of exposure among HCP ranged from 5 to 25 minutes (<10 minutes, n = 1; 10–15 minutes, n = 3; 15–30 minutes, n = 1). Three HCP had direct physical contact with the case-patient while the HCP was wearing a facemask and no gloves; HCP 1 positioned the case-patient for chest radiograph imaging, HCP 2 took the patient's vital signs, and HCP 3 examined the case-patient and performed an OP exam. When obtaining the NP and OP swabs, HCP 3 wore an N95 respirator, face shield, and gloves but no gown. HCP 4 had

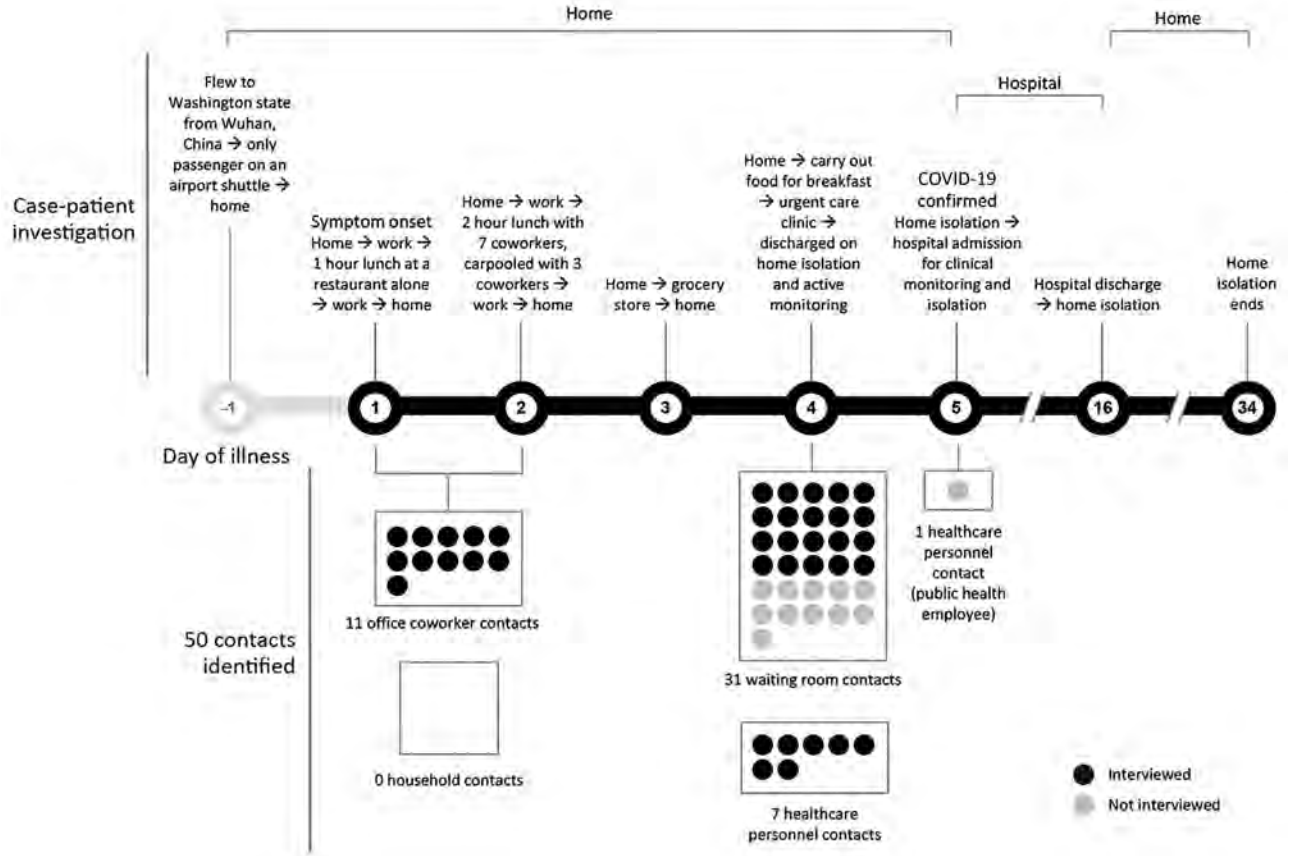

Figure 1. Case-patient investigation and contact identification during the investigation of an early confirmed US COVID-19 case, Washington, USA, 2020. The case-patient was asymptomatic when he arrived home from Wuhan, China. The next day, he developed a cough (day 1), followed by chills (day 2) and a subjective fever (day 3). When he arrived at the urgent care clinic (day 4), he was given a facemask and sat in the waiting room for ≈20 minutes. He was evaluated in a standard examination room, and received a chest radiograph in a radiology room down the hallway from the exam room. The case-patient was identified as meeting the Centers for Disease Control and Prevention (CDC) criteria at the time for a person under investigation for COVID-19, and specimens (nasopharyngeal and oropharyngeal swabs and serum samples) were collected for testing (*6*). He was clinically stable and discharged home pending SARS-CoV-2 test results. When COVID-19 was confirmed (day 5), the case-patient was admitted to a hospital for observation and isolation. After 11 days, he was discharged to home isolation until 2 negative sets of nasopharyngeal and oropharyngeal specimens were obtained ≥24 hours apart, in accordance with CDC guidance at the time (*7*). Persons exposed during transient interactions, such as restaurant waitstaff and persons encountered at the grocery store, were not considered community contacts. COVID-19, coronavirus disease.

direct physical contact while wearing an N95 respirator and gloves when drawing blood and processing specimens. Neither HCP wearing N95 respirators had been fit tested within the last year. The EVS workers cleaned the clinic >8 hours after the case-patient left the urgent care clinic. While cleaning, 1 EVS worker wore gloves consistently but the other did not.

The 31 waiting room contacts included patients and persons accompanying them who were likely to be in the waiting room at the same time as the case-patient or up to 2 hours after the case-patient was taken to a room. According to the sign-in sheet, ≈7 contacts overlapped in the waiting room with the case-patient. Because the case-patient was anonymous to the waiting room contacts, the 20 (65%) interviewed waiting room contacts were unable to describe their exposure type and duration. However, they consistently described being given a facemask if they had respiratory symptoms, staying >6 feet apart from other waiting room patients, and sitting <30 minutes in the waiting room. The case-patient said that he did not interact directly with any of the waiting room contacts.

Of the 50 contacts, 37 (74%) had NP and OP specimens collected and tested for SARS-CoV-2; 33 (66%) had specimens collected once, and 4 (8%) had specimens collected twice (Table 3). Of the 8 (16%) contacts who were assessed as PUIs during the investigation, all were tested for SARS-CoV-2 infection while symptomatic. Among asymptomatic contacts, the NP and OP specimens were collected a median of 11 days (range

9–13 days) from the last date of exposure. All NP and OP specimens tested negative for SARS-CoV-2 by rRT-PCR, including those from PUIs. Serum samples were obtained from 32 (64%) of the 50 contacts (Table 3). Initial serum was obtained from 28 (56%) contacts, and follow-up serum was obtained from 23 (46%) contacts; none had detectable antibodies to SARS-CoV-2.

Discussion

This investigation identified no secondary cases among close contacts of this early US COVID-19 case-patient by molecular or serologic methods. Systematic contact tracing initiated soon after case confirmation identified office co-workers, HCP, and persons who overlapped in an urgent care clinic waiting area as contacts of the symptomatic case-patient with potential risk for infection. All 50 contacts were actively monitored daily for development of signs or symptoms consistent with COVID-19 and were assessed as PUIs if signs or symptoms developed. During the 14 days after last exposure of the identified contacts, testing of respiratory specimens by rRT-PCR of all symptomatic contacts (PUIs) and most asymptomatic contacts revealed no evidence of secondary transmission. Serum specimens collected ≈6 weeks after the last exposure for 23 (46%) contacts showed no evidence of SARS-CoV-2 antibodies, providing additional confirmation that secondary transmission did not occur among tested contacts.

The lack of transmission among contacts in this investigation is similar to findings reported in other early systematic contact investigations of case-patients with COVID-19 in January and February, in which only close household contacts were infected (*8*–*11*). One potential explanation for the lack of transmission among tested contacts may be the nature of the community exposures to the case-patient compared with the more intimate and continuous exposures that would typically be experienced by household contacts. Given the current situation of sustained community transmission of SARS-CoV-2, it is of interest that there was no evidence of transmission to co-workers, despite a 60–90 minute lunch together and travel together in a car while the case-patient was symptomatic, albeit with mild symptoms (*12*).

Similar to other reported COVID-19 case-patients, this case-patient had SARS-CoV-2 detected from NP and OP specimens at very low cycle threshold values (NP 18–19, OP 21–22) at the time of first testing at the urgent care clinic (day 4 of illness), indicating a high viral load (*2*,*13*). Of note, the case-patient wore a facemask in the urgent care clinic waiting room and during most of the healthcare encounters, except during examination and respiratory specimen collection. In addition, HCP who interacted with the case-patient all wore partial PPE, which included a facemask or an unfitted N95 respirator. Influenza studies found that patients or HCP wearing a facemask is associated with a reduced risk of nosocomial transmission (*14*). A COVID-19 contact investigation described 35 HCP who wore facemasks during a prolonged exposure to an aerosol-generating procedure for a patient with COVID-19; none acquired infection (*15*). These investigations suggest that facemasks worn by the case-patient or the HCP might have helped prevent secondary transmission of COVID-19 in the healthcare setting, although additional studies are needed.

A unique aspect of our contact investigation was the inclusion of serologic testing, which strengthened the conclusion that secondary transmission did not occur among tested contacts. Molecular testing detects viral RNA present in an active infection and is dependent on sampling location, technique, and the timing. Although the serologic assay used does not necessarily confirm current infection, it enables detection of seroconversion, indicating a history of SARS-CoV-2 infection. SARS-CoV-2 antibodies are detectable in most persons with COVID-19 within 1–3 weeks after illness onset, although more data are needed to determine whether all persons infected with SARS-CoV-2 develop detectable antibodies (*16*,*17*). Use of serologic testing complements molecular diagnostics and adds to the ability to detect

Table 2. Demographic characteristics, clinical symptoms, and laboratory testing of PUIs for COVID-19 related to an early confirmed US COVID-19 case, Washington, USA, 2020*

Characteristic	PUI, N = 8
Age, y, median (range)	41.5 (21–58)
Sex	
M	2
F	6
Contact group	
Office co-workers	2
Healthcare personnel	2
Waiting room contacts	4
Clinical symptoms	
Days from last case-patient exposure to symptom onset, median (range)	5.5 (1–11)
Cough	6
Headache	5
Runny nose	5
Sore throat	4
Body aches	3
Fever	1
Chills	1
Shortness of breath	0
Laboratory testing	
PUIs with respiratory specimens	8
PUIs with initial serum specimens	4
PUIs with follow-up serum specimens	5

*Values are no. persons except as indicated. COVID-19, coronavirus disease; PUIs, persons under investigation.

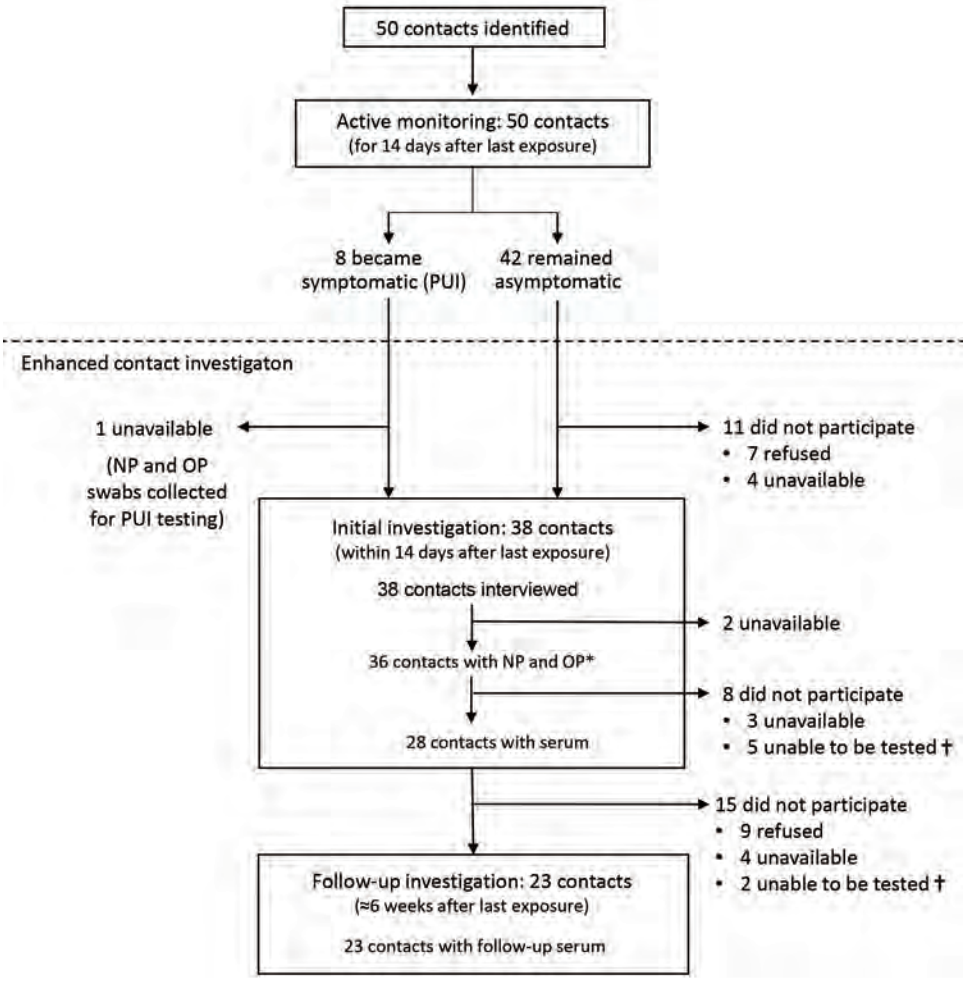

Figure 2. Contact investigation flowchart of identified contacts, active monitoring, and participation in the enhanced contact investigation of an early confirmed US coronavirus disease case, Washington, USA, 2020. NP, nasopharyngeal; OP, oropharyngeal; PUI, person under investigation. *Includes contacts from whom specimens obtained for PUI testing. †Specimens were unable to be tested if blood could not be obtained (n = 5) or if the standard specimen requirements for testing were not met (n = 2).

asymptomatic infections or infections that occurred in persons who did not have testing performed during the acute phase of illness.

This contact investigation had limitations. The investigation involved a single case; thus, only transmissions related to specific interactions for a single case are assessed. The case-patient had no household contacts, and all HCP contacts reported using at least partial PPE. Therefore, these findings cannot be generalized for persons with other types of contacts. Furthermore, not all contacts were tested. Testing was biased toward contacts who knew the case-patient personally (office co-workers) or provided direct care for the case-patient (HCP). Most contacts were tested by rRT-PCR assay at one point during their monitoring period; we cannot exclude that timing of NP and OP swab collection could have affected the ability to capture asymptomatic infection. In addition, details of the exposure history, particularly exposure duration and frequency, are subject to recall bias. Contacts of the case-patient before symptom onset were not included in this investigation, including airplane contacts from the day before the case-patient's symptom onset. Finally, contact identification could have been incomplete. We cannot rule out the possibility that certain interactions not captured in the contact investigation, including those classified as transient interactions, could have resulted in transmission, although unprotected prolonged exposures described in this report did not result in transmission.

This contact investigation provides detailed exposure information regarding prolonged close interactions among tested contacts that did not result in secondary transmission of SARS-CoV-2. Multiple factors likely influence transmissibility of a given COVID-19 case-patient, including viral load, symptom severity, aerosol generation, host factors in the case-patient and contact, use of protective equipment (e.g., facemask use by the case-patient), and exposure type, timing, duration, setting, and frequency. Further investigations are needed to

Table 3. Demographic characteristics, underlying medical conditions, exposures, and SARS-CoV-2 testing among contacts of an early confirmed US COVID-19 case participating in the enhanced contact investigation, Washington, USA, 2020*

Characteristic	All contacts, N = 38	Community contacts		Healthcare contacts
		Office co-workers, n = 11	Waiting room contacts, n = 20	Healthcare personnel, n = 7†
Age, y, median (range)	45 (0–78)	39 (24–62)	53.5 (<1–78)	36 (30–56)
Sex				
M	21 (55)	9 (82)	9 (45)	3 (43)
F	17 (45)	2 (18)	11 (55)	4 (57)
Race				
White	27 (71)	2 (18)	18 (90)	7 (100)
Asian	8 (21)	8 (73)	0	0
Black	0	0	0	0
Not specified	3 (8)	1 (9)	2 (10)	0
Ethnicity				
Hispanic/Latino	5 (13)	0	3 (15)	2 (29)
Not Hispanic/Latino	28 (74)	10 (91)	14 (70)	4 (57)
Not specified	5 (13)	1 (9)	3 (15)	1 (14)
Underlying medical conditions‡				
None	15 (39)	8 (73)	3 (15)	4 (57)
Asthma	10 (26)	3 (27)	4 (20)	3 (43)
Diabetes mellitus, type 2	4 (11)	0	4 (20)	0
Hypertension	7 (18)	1 (9)	6 (30)	0
Coronary artery disease	1 (3)	0	1 (5)	0
Immunosuppressive condition or therapy	1 (3)	0	1 (5)	0
Pregnant or postpartum§	2 (5)	0	1 (5)	1 (14)
Exposure type¶				
Face-to-face interaction	16/18 (89)	11 (100)	NA	5 (71)
Direct physical contact	10/18 (56)	6 (55)	NA	4 (57)
Physically within 6 feet	16/18 (89)	11 (100)	NA	5 (71)
Within 6 feet while case-patient was coughing or sneezing	3/18 (17)	0	NA	3 (43)
Touched object handled by the case-patient	13/18 (72)	10 (91)	NA	3 (43)
In the same room	14/18 (78)	9 (82)	NA	5 (71)
Traveled in the same vehicle	3/18 (17)	3 (28)	NA	0
Active monitoring				
Days from last exposure to start of active monitoring, median (range)	4 (1–7)	6 (5–7)	4 (4–5)	1 (1–1)
Assessed as PUI during monitoring period†	7 (18)	2 (18)	4 (20)	1 (14)
Days from last exposure until symptom onset among PUIs	5 (1–11)	6 (1–11)	4.5 (3–11)	6 (6–6)
Laboratory testing				
Any testing (rRT-PCR or serology)	37 (97)	11 (100)	19 (95)	7 (100)
Enhanced contact investigation: initial specimen collection within 14 d after last exposure to case-patient				
Contacts with respiratory specimens#	36 (95)	11 (100)	19 (95)	6 (86)
Contacts with serum specimens	28 (74)	8 (73)	14 (75)	6 (86)
Days from last exposure to initial specimen collection (respiratory and serum specimens) among asymptomatic contacts, median (range)	11 (9–13)	10 (10–11)	11 (10–13)	9 (9–11)
Enhanced contact investigation: follow-up serum, ≈6 weeks after last exposure to case-patient				
Contacts with follow-up serum specimens	23 (61)	9 (82)	10 (50)	4 (57)
Days from last exposure to follow-up serum collection, median (range)	46 (44–49)	47 (46–47)	46 (44–49)	46 (45–47)

*Values are no. persons except as indicated. COVID-19, coronavirus disease; HCP, healthcare personnel; NA, not asked; PUI, person under investigation; rRT-PCR, real-time reverse transcription PCR.
†One HCP PUI was not available for interview and was not included in this table. Nasopharyngeal and oropharyngeal specimens were collected for this PUI testing, and were negative by rRT-PCR for SARS-CoV-2. No serum specimens were collected.
‡Some contacts had >1 underlying medical condition.
§Postpartum was defined as within 6 weeks after delivery.
¶Exposure types were not asked for waiting room contacts, as the case-patient was anonymous to the waiting room contacts.
#Included respiratory specimens obtained for PUI testing.

determine host factors and exposures associated with increased transmission.

Contact investigations coupled with laboratory testing remain crucial public health tools for identifying, isolating, and preventing additional COVID-19 cases. Serologic methods, in addition to molecular detection, are a valuable tool in improving our understanding of the rate of asymptomatic infection. Understanding more about the occurrence of asymptomatic and presymptomatic infection and its contribution to

SARS-CoV-2 transmission is critical for guiding community mitigation strategies and infection prevention and control recommendations.

Acknowledgments

We thank the following persons at the Washington State Department of Health: Elyse Bevers, Mike Boysun, Tia Dostal, Jessica Gant, Romesh Gautom, Nicholas Graff, Cynthia Harry, Brian Hiatt, Esther Lam, Larissa Lewis, Kathy Lofy, Jasmine Matheson, Patricia Montgomery, Denny Russell, John Wiesman; and at the Centers for Disease Control and Prevention: Sharad Aggarwal, Catherine Bozio, How-Yi Chang, Hsin Chien, Mila Cohen, Rebecca Dahl, Mathew Esona, Leora Feldstein, Paul Gastanaduy, Rashi Gautam, Ruth Link-Gelles, Connor Hoff, Jennifer Hunter, Laurel Jenkins, Nazia Kamal, Shifaq Kamili, Michelle Kautz, Lindsay Kim, Steven Langerman, Jessica Leung, Brian Lynch, Lakshmi Malapati, Claire Mattison, Allison Miller, Ruth Moro, Janna' Murray, Manisha Patel, Makisha Rogan, Senthil Kumar Sakthivel, Sarah E. Smith-Jeffcoat, Jennifer Thomas, Lijuan Wang, John Watson, Brett Whitaker, and Shannon York.

About the Author

Dr. Chu is an Epidemic Intelligence Service officer and Dr. Freeman-Ponder is a Laboratory Leadership Service fellow in the Division of Viral Diseases, National Center for Immunization and Respiratory Diseases, Centers for Disease Control and Prevention, Atlanta, GA, USA. Dr. Chu's research interests include viral respiratory and vaccine-preventable diseases, and Dr. Freeman-Ponder's research interests include immunological and molecular epidemiologic studies of infectious diseases.

References

1. Huang C, Wang Y, Li X, Ren L, Zhao J, Hu Y, et al. Clinical features of patients infected with 2019 novel coronavirus in Wuhan, China. Lancet. 2020;395:497–506. https://doi.org/10.1016/S0140-6736(20)30183-5
2. Holshue ML, DeBolt C, Lindquist S, Lofy KH, Wiesman J, Bruce H, et al.; Washington State 2019-nCoV Case Investigation Team. First case of 2019 novel coronavirus in the United States. N Engl J Med. 2020;382:929–36. https://doi.org/10.1056/NEJMoa2001191
3. Centers for Disease Control and Prevention. CDC 2019-novel coronavirus (2019-nCoV) real-time RT-PCR diagnostic panel; 2020 [cited 2020 Mar 30]. https://www.fda.gov/media/134922/download
4. Wrapp D, Wang N, Corbett KS, Goldsmith JA, Hsieh CL, Abiona O, et al. Cryo-EM structure of the 2019-nCoV spike in the prefusion conformation. Science. 2020;367:1260–3. https://doi.org/10.1126/science.abb2507
5. Trivedi S, Miao C, Al-Abdallat MM, Haddadin A, Alqasrawi S, Iblan I, et al. Inclusion of MERS-spike protein ELISA in algorithm to determine serologic evidence of MERS-CoV infection. J Med Virol. 2018;90:367–71. https://doi.org/10.1002/jmv.24948
6. Centers for Disease Control and Prevention. Update and interim guidance on outbreak of 2019 novel coronavirus (2019-nCoV) in Wuhan, China; 2020 Jan 17 [cited 2020 Apr 5]. https://emergency.cdc.gov/han/han00426.asp
7. Kujawski SA, Wong KK, Collins JP, Epstein L, Killerby ME, Midgley CM, et al.; COVID-19 Investigation Team. Clinical and virologic characteristics of the first 12 patients with coronavirus disease 2019 (COVID-19) in the United States. Nat Med. 2020 Apr 23 [Epub ahead of print]. https://doi.org/10.1038/s41591-020-0877-5
8. Bernard Stoecklin S, Rolland P, Silue Y, Mailles A, Campese C, Simondon A, et al.; Investigation Team. First cases of coronavirus disease 2019 (COVID-19) in France: surveillance, investigations and control measures, January 2020. Euro Surveill. 2020;25:2000094. https://doi.org/10.2807/1560-7917.ES.2020.25.6.2000094
9. Burke RM, Midgley CM, Dratch A, Fenstersheib M, Haupt T, Holshue M, et al. Active monitoring of persons exposed to patients with confirmed COVID-19—United States, January–February 2020. MMWR Morb Mortal Wkly Rep. 2020;69:245–6. http://dx.doi.org/10.15585/mmwr.mm6909e1
10. Ghinai I, McPherson TD, Hunter JC, Kirking HL, Christiansen D, Joshi K, et al.; Illinois COVID-19 Investigation Team. First known person-to-person transmission of severe acute respiratory syndrome coronavirus 2 (SARS-CoV-2) in the USA. Lancet. 2020;395:1137–44. http://dx.doi.org/10.1016/S0140-6736(20)30607-3
11. Scott SE, Zabel K, Collins J, Hobbs KC, Kretschmer MJ, Lach M, et al. First mildly ill, non-hospitalized case of coronavirus disease 2019 (COVID-19) without viral transmission in the United States—Maricopa County, Arizona, 2020. Clin Infect Dis. 2020 Apr 2 [Epub ahead of print]. https://doi.org/10.1093/cid/ciaa374
12. Centers for Disease Control and Prevention. Coronavirus disease 2019 (COVID-19) cases in the U.S.; 2020 [cited 2020 Apr 20]. https://www.cdc.gov/coronavirus/2019-ncov/cases-updates/cases-in-us.html
13. Zou L, Ruan F, Huang M, Liang L, Huang H, Hong Z, et al. SARS-CoV-2 viral load in upper respiratory specimens of infected patients. N Engl J Med. 2020;382:1177–9. https://doi.org/10.1056/NEJMc2001737
14. Cheng VC, To KK, Tse H, Hung IF, Yuen KY. Two years after pandemic influenza A/2009/H1N1: what have we learned? Clin Microbiol Rev. 2012;25:223–63. https://doi.org/10.1128/CMR.05012-11
15. Ng K, Poon BH, Kiat Puar TH, Shan Quah JL, Loh WJ, Wong YJ, et al. COVID-19 and the risk to health care workers: a case report. Ann Intern Med. 2020 Mar 16 [Epub ahead of print]. https://doi.org/10.7326/L20-0175
16. Zhao J, Yuan Q, Wang H, Liu W, Liao X, Su Y, et al. Antibody responses to SARS-CoV-2 in patients of novel coronavirus disease 2019. Clin Infect Dis. 2020 Mar 28 [Epub ahead of print]. https://doi.org/10.1093/cid/ciaa344
17. To KK-W, Tsang OT-Y, Leung W-S, Tam AR, Wu T-C, Lung DC, et al. Temporal profiles of viral load in posterior oropharyngeal saliva samples and serum antibody responses during infection by SARS-CoV-2: an observational cohort study. Lancet Infect Dis. 2020;20:565–74. https://doi.org/10.1016/S1473-3099(20)30196-1

Address for correspondence: Victoria Chu, Centers for Disease Control and Prevention, 1600 Clifton Dr NE, Mailstop H24-5, Atlanta, GA 30329-4027, USA; email: pgz4@cdc.gov

Characteristics and Outcomes of Coronavirus Disease Patients under Nonsurge Conditions, Northern California, USA, March–April 2020

Jessica Ferguson,[1] Joelle I. Rosser,[1] Orlando Quintero, Jake Scott, Aruna Subramanian, Mohammad Gumma, Angela Rogers, Shanthi Kappagoda

Limited data are available on the clinical presentation and outcomes of coronavirus disease (COVID-19) patients in the United States hospitalized under normal-caseload or nonsurge conditions. We retrospectively studied 72 consecutive adult patients hospitalized with COVID-19 in 2 hospitals in the San Francisco Bay area, California, USA, during March 13–April 11, 2020. The death rate for all hospitalized COVID-19 patients was 8.3%, and median length of hospitalization was 7.5 days. Of the 21 (29% of total) intensive care unit patients, 3 (14.3% died); median length of intensive care unit stay was 12 days. Of the 72 patients, 43 (59.7%) had underlying cardiovascular disease and 19 (26.4%) had underlying pulmonary disease. In this study, death rates were lower than those reported from regions of the United States experiencing a high volume of COVID-19 patients.

Health officials in China first reported a cluster of cases of a new acute respiratory illness associated with a seafood market in Wuhan, China, on December 31, 2019 (*1*). Less than 1 month later, cases of what would become known as coronavirus disease (COVID-19) were reported in patients in northern California, USA (*2*). In the San Francisco Bay area counties of Alameda and Santa Clara, COVID-19 cases in travelers returning from Wuhan were confirmed on January 28 and January 31, respectively. As of May 5, 2020, a total of 1,809 laboratory-confirmed cases have occurred in Alameda County (population 1.7 million) and 2,555 cases in Santa Clara County (population 1.9 million); however, these numbers probably vastly underestimate the disease incidence because of the lack of widespread testing in the region early in the epidemic (*3*,*4*). Studies from China and Europe have described the clinical presentation of COVID-19, but data from the United States are still emerging (*5*–*9*). In addition, current data from the United States have primarily come from hospitals working under high-volume or surge conditions. In this study, we describe the characteristics and outcomes of patients hospitalized in northern California with COVID-19 early in the epidemic under nonsurge conditions.

Methods

Study Design and Oversight

We conducted a retrospective chart review of demographic and clinical data for patients admitted to our 2 partner institutions, Stanford University Hospital (SUH) and Stanford Health Care-ValleyCare (ValleyCare), during March 13–April 11, 2020, with follow up through May 2, 2020. SUH is an academic medical center with 600 beds, including 119 intensive care unit (ICU) beds, located in Palo Alto, Santa Clara County. ValleyCare is a community hospital with 167 beds, including 22 ICU beds, in Pleasanton, Alameda County. The Stanford Health Care Institutional Review Board approved this study.

Inclusion and Exclusion Criteria

We sequentially enrolled all patients ≥18 years of age who were hospitalized for ≥24 hours and had reverse transcription PCR (RT-PCR)–confirmed severe acute respiratory syndrome coronavirus 2 (SARS-CoV-2) during the study period. Our study comprised patients who spent ≥1 nights in the hospital; we excluded

Author affiliations: Stanford Health Care, Stanford, California, USA (J. Ferguson, J.I. Rosser, O. Quintero, J. Scott, A. Subramanian, A. Rogers, S. Kappagoda); Stanford University, Stanford (M. Gumma)

DOI: https://doi.org/10.3201/eid2608.201776

[1]These authors contributed equally to this article.

patients seen only in the emergency department and discharged in <24 hours.

Data Sources and Collection

We used the electronic medical record system, EpicSystems (https://www.epic.com) to extract data on clinical symptoms and signs, laboratory test results, and outcomes. We collected and managed study data using REDCap electronic data capture tools hosted at Stanford University (*10*,*11*).

Laboratory Testing

All laboratory data were ordered as part of routine clinical care. SARS-CoV-2 infection was confirmed using RT-PCR, which was validated on nasopharyngeal, oropharyngeal, endotracheal aspirate, and bronchoalveolar lavage samples.

Definitions

We recorded the date of the earliest reported symptom. Diabetes was defined by any preadmission medication prescription for diabetes or documented hemoglobin A1C ≥6.5% (reference <5.7%). Admission tests refers to laboratory studies collected within the first 24 hours of admission. We defined admission chest radiograph as one done within 24 hours after hospital arrival and admission chest computed tomography as one performed within 48 hours after hospital arrival. Radiographic findings were based on the radiology report in the electronic medical record. We defined acute respiratory distress syndrome using the Berlin Criteria (presence of acute respiratory failure with bilateral pulmonary infiltrates, ratio of arterial oxygen tension to fraction of inspired oxygen <300 with ≥5 cm water of positive-end expiratory pressure, and absence of cardiogenic pulmonary edema) (*12*). We defined acute kidney injury as an increase in serum creatinine during admission of 1.5 times baseline (*13*). We defined cardiomyopathy as an ejection fraction assessed on transthoracic echocardiogram of <50% or ≥10% decrease from the baseline ejection fraction if the result of a prior echocardiogram within the past 2 years was available. We defined central line–associated bloodstream infection using National Healthcare Safety Network criteria (*14*).

Data Analysis

We conducted all analyses using R version 3.6.2 (https://www.r-project.org). The 4 patients who remained hospitalized at the end of the study period were right-censored on May 2 and included in length-of-stay calculations. We performed Mann-Whitney U tests for continuous variables and Fisher exact tests for categorical variables, all using a type I error of 0.05.

Results

Demographic Characteristics

A total of 72 SARS-CoV-2–positive patients were admitted during March 13–April 11, 2020. Twelve were admitted to ValleyCare Hospital and 60 to Stanford Hospital. Twenty-two (30.6%) patients were Hispanic or Latino, 20 (27.8%) were Asian or Asian-American, 19 (26.4%) were white, and 4 (5.6%) were black (Table 1). Most (51 [70.8%]) patients came from stable housing situations with family. Twelve (16.7%) lived in a skilled nursing facility, assisted living, group home, or unstable living situation, and 1 (1.4%) lived alone.

Concurrent Conditions

Forty-three (59.7%) patients had underlying cardiovascular disease, and 19 (26.4%) had underlying pulmonary disease. Thirty-six percent had no cardiovascular or pulmonary disease. Among the ICU patients, in univariate analysis, only diabetes was significantly associated with ICU admission.

The most common concurrent conditions among all 72 patients were hypertension (36.1%), hyperlipidemia (34.7%), and diabetes (27.8%). Twenty-three non-ICU (45.1%) and 6 ICU (28.6%) patients had no known cardiovascular disease. The most common respiratory concurrent conditions were asthma (7 patients) or chronic obstructive pulmonary disease (3). Tobacco use did not differ between non-ICU and ICU patients.

Six (8.3%) patients had an immunocompromising condition. These conditions included 3 with active malignancies, 2 solid organ transplant recipients, and 1 patient with systemic sclerosis.

Before admission, 20 (27.8%) patients had been prescribed azithromycin. Two (2.8%) patients had been prescribed hydroxychloroquine to target COVID-19. No patients were on long-term hydroxychloroquine for other indications. Twenty-six (36.1%) patients, including 5 (23.8%) treated in the ICU, had no known concurrent conditions.

Characteristics at Admission

At admission, the most common symptoms were fever (73.6%), dry cough (58.3%), and shortness of breath (56.9%) (Table 2). Patients also commonly reported nonspecific influenza-like symptoms of fatigue, myalgias, nausea, and diarrhea. Few (5.6%) patients reported altered sensation of taste or smell. ICU patients were more likely to have fever

Table 2. Clinical characteristics and laboratory and radiographic findings for COVID-19 patients, northern California, 2020

Characteristic	COVID-19 patients			p value
	All, n = 72	Non-ICU, n = 51	ICU, n = 21	
Symptoms, no. (%)				
Fever	53 (73.6)	37 (72.5)	16 (76.2)	1.00
Chills	25 (34.7)	15 (29.4)	10 (47.6)	0.18
Cough, dry	42 (58.3)	28 (54.9)	14 (66.7)	0.44
Cough, productive	15 (20.8)	12 (23.5)	3 (14.3)	0.53
Shortness of breath	41 (56.9)	29 (56.9)	12 (57.1)	1.00
Chest pain/pressure	8 (11.1)	6 (11.8)	2 (9.5)	1.00
Fatigue	26 (36.1)	21 (41.2)	5 (23.8)	0.19
Myalgias	32 (44.4)	19 (37.3)	13 (61.9)	0.07
Arthralgias	1 (1.4)	1 (2.0)	0	1.00
Headache	14 (19.4)	9 (17.6)	5 (23.8)	0.53
Sore throat	10 (13.9)	5 (9.8)	5 (23.8)	0.14
Nasal congestion/rhinorrhea	7 (9.7)	3 (5.9)	4 (19.0)	0.18
Nausea	17 (23.6)	15 (29.4)	2 (9.5)	0.13
Vomiting	7 (9.7)	7 (13.7)	0	0.01
Diarrhea	19 (26.4)	13 (25.5)	6 (28.6)	0.78
Altered sense of taste/smell	4 (5.6)	3 (5.9)	1 (4.8)	1.00
Other†	16 (22.2)	11 (21.6)	5 (23.8)	NP
Vital signs				
Medium max temp in first 24 h, °C (IQR)	38.1 (37.3–38.8)	37.8 (37.2–38.7)	38.6 (38.6–39.3)	<0.05
Temperature ≥38.2°C, no. (%)	34 (47.2)	19 (37.3)	15 (71.4)	<0.05
Room air SaO2, no. (%)				
SaO2 ≥94	42 (58.3)	36 (70.6)	6 (28.6)	<0.05
Median SaO2	30 (41.7)	15 (29.4)	15 (71.4)	
<94 RR (IQR)	20 (18–22)	19 (18–20)	22 (18–27)	<0.05
Laboratory results, median (IQR)‡				
Leukocytes, K/μL	5.6 (4.3–7.8)	5.7 (4.4–8.1)	5.2 (4.0–7.0)	0.40
ANC, n = 71	3,890 (2,705–5,835)	3,875 (2,630–5,725)	4140 (2930–6430)	0.42
ALC, n = 71	910 (580–1,235)	915 (592–1,335)	890 (520–1,090)	0.47
Platelets, K/μL	194 (160–256)	198 (162–265)	183 (157–250)	0.40
Sodium, mmol/L	136 (133–138)	136 (132–139)	136 (134–137)	1.00
Potassium, mmol/L	3.8 (3.7–4.2)	3.9 (3.7–4.2)	3.8 (3.6–4.0)	0.31
Creatinine, mg/dL	0.89 (0.67–1.07)	0.89 (0.73–1.07)	0.89 (0.66–1.07)	0.69
Glucose, mg/dL	108 (98–124)	107 (96–120)	114 (102–147)	0.18
AST, U/L	45.5 (31.8–63.5)	45.0 (29.0–59.5)	52.0 (38.0–82.0)	0.04
ALT, U/L	36.5 (23.8–56.2)	35.0 (22.5–51.5)	49.0 (34.0–58.0)	0.09
CK, total, U/L	119 (55–360)	53 (48–70)	282 (174–774)	0.01
LDH, U/L	394 (251–492)	344 (250–442)	430 (299–522)	0.03
Ferritin, ng/mL	824 (453–1643)	612 (304–1030)	1422 (817–1944)	0.04
CRP >0.5 ng/dL, no./total (%)	36/41 (87.8)	21/26 (80.8)	15/15 (100)	0.14
IL-6 >5 pg/mL, no./total (%)	5/7 (71.4)	3/3 (100)	2/4 (50.0)	0.43
Procalcitonin >0.5 ng/mL, no./total (%)	4/47 (8.5)	3/33 (9.1)	1/14 (7.1)	1.0
D-dimer >0.5 μg/mL, no./total (%)	20/26 (76.9)	14/19 (73.7)	6/7 (85.7)	1.0
Troponin >0.055 ng/mL, no./total (%)	2/45 (4.4)	1/31 (3.2)	1/14 (7.1)	0.53
Radiology, no. (%)				
Chest radiograph				
Diffuse/patchy bilateral infiltrates	45 (62.5)	26 (51.0)	19 (90.5)	<0.05§
Focal consolidation	11 (15.3)	9 (17.6)	2 (9.5)	NP
Pleural effusion	4 (5.6)	2 (3.9)	2 (9.5)	
Clear	11 (15.3)	11 (21.6)	0	
Other¶	5 (6.9)	4 (7.8)	1 (4.8)	
Chest computed tomography scan				
Diffuse/multifocal/GGO/opacities	11 (15.3)	8 (15.7)	3 (14.3)	
Diffuse consolidations	4 (5.6)	3 (5.9)	1 (4.8)	
Focal consolidation	2 (2.8)	2 (3.0)	0	

*ALC, absolute lymphocyte count; ALT, alanine aminotransferase; ANC, absolute neutrophil count; AST, aspartate aminotransferase; CK, creatinine kinase; COVID-19, coronavirus disease; CRP, C-reactive protein; GGO, ground glass opacities; IL-6, interleukin-6; IQR, interquartile range; LDH, lactate dehydrogenase; NP, test not performed; RR, respiratory rate.
†Altered mental status, dizziness, night sweats, anorexia, and abdominal pain.
‡Reference ranges: leukocytes, 4.0–11.0 K/μL; ANC, 1,700–6,700 cells/μL; ALC, 1,000–3,000 cells/μL; platelets, 150–400 K/μL; sodium, 135–145 mmol/L; potassium, 3.5–5.5 mmol/L; creatinine, 0.67–1.17 mg/dL; glucose, 70–100 mg/dL; AST, 10–50 U/L; ALT, 10–50 U/L; CK, total <190 U/L; LDH, 135–225 U/L; ferritin 30–400 ng/mL; CRP <0.5 ng/dL; IL-6, ≤5 pg/mL; procalcitonin, ≤0.5 ng/mL; D-dimer, <0.5 μg/mL; troponin <0.055 ng/mL.
§Compares diffuse/patchy bilateral infiltrates with all other categories combined.
¶Bibasilar opacities and interstitial markings.

documented within 24 hours after admission and had higher temperatures recorded. Of 48 patients who had a multiplex PCR–based respiratory viral panel performed within 24 hours after admission, 2 had a viral co-infection (1 patient with respiratory syncytial virus and 1 with both respiratory syncytial virus and rhinovirus).

Abnormal results of chest imaging were more common in patients requiring ICU admission. Among patients admitted to the ICU, 19 (90.5%) had an initial chest radiograph with diffuse or patchy bilateral opacities, compared with 26 (51.0%) of non-ICU patients. None of the patients admitted to the ICU had normal-appearing chest radiograph result at admission. Overall, very few patients had a chest computed tomography scan performed within the first 48 hours of hospitalization.

Treatments

Patients most commonly received remdesivir (44.4% of all patients and 76.2% of ICU patients), azithromycin, or both during hospitalization (Table 3). Four ICU patients received tocilizumab, and 1 received leronlimab. Among the 12 patients seen at ValleyCare,

Table 3. Complications, interventions, and outcomes of COVID-19 patients, northern California, 2020*

Variable	COVID-19 patients			p value
	All, n = 72	Non-ICU, n = 51	ICU, n = 21	
Complications, no. (%)				
Acute respiratory distress syndrome	13 (18.0)	0	13 (61.9)	NP
Arrhythmia†	6 (8.3)	0	6 (28.6)	
Ventilator- or hospital-associated pneumonia	5 (6.9)	0	5 (23.8)	
Acute kidney injury	4 (5.6)	0	4 (19.0)	
Catheter-related bloodstream infection	2 (2.8)	0	2 (9.5)	
Cardiomyopathy‡	2 (2.8)	0	2 (9.5)	
Highest level of oxygen support required, no. (%)				
None	29 (40.3)	28 (54.9)	1 (4.8)	Referent
Oxygen by nasal cannula	22 (30.6)	21 (41.2)	1 (4.8)	1.0
High-flow nasal cannula	2 (2.8)	1 (2.0)	1 (4.8)	0.13
Nonrebreather mask	6 (8.3)	1 (2.0)	5 (23.8)	<0.05
Mechanical ventilation	13 (18.1)	0	13 (61.9)	NP
Median duration of mechanical ventilation, d§ (IQR)		NP	17 (13–29)	NP
Interventions, no. (%)				
Use of a paralytic agent	7 (9.7)	0	7 (33.3)	NP
Use of proning	6 (8.3)	1 (2.0)	5 (23.8)	
Tracheostomy	6 (8.3)	0	6 (28.6)	
Use of vasopressors	13 (18.1)	0	13 (61.9)	
Use of renal replacement therapy¶	4 (5.6)	0	4 (19.0)	
Inhaled nitric oxide	4 (5.6)	0	4 (19.0)	
Treatment, no. (%)				
Azithromycin	33 (45.8)	19 (37.3)	14 (66.7)	<0.05
Remdesivir	32 (44.4)	15 (29.4)	16 (76.2)	<0.05
Hydroxychloroquine	16 (22.2)	11 (21.6)	5 (23.8)	1.0
Systemic glucocorticoids	5 (6.9)	3 (5.9)	2 (9.5)	0.63
Tocilizumab	4 (5.6)	0	4 (19.0)	<0.05
Other#	11 (15.3)	8 (15.7)	3 (14.3)	NP
Any antimicrobial drug	48 (66.7)	28 (54.9)	19 (90.5)	<0.05
Any antifungal drug	1 (1.4)	0	1 (4.8)	0.29
Median length of stay,** d (IQR)				
Hospitalization	7.5 (4–13)	5 (3–9)	17 (11–30)	
ICU	NP	NP	12 (5–28)	
Disposition, no. (%)				
Discharged from hospital				
Home	53 (73.6)	43 (84.3)	10 (47.6)	0.35††
SN/LTAC facility	9 (12.5)	5 (9.8)	4 (19.0)	
Died or discharged with hospice	6 (8.3)	3 (5.9)	3 (14.3)	
Remains hospitalized	4 (5.6)	0	4 (19.0)	

*COVID-19, coronavirus disease; ICU, intensive care unit; IQR, interquartile range; LTAC, long-term acute care; NP, test not performed; SN, skilled nursing.
†Includes 2 atrial fibrillation with rapid ventricular response, 2 supraventricular tachycardia, 2 bradycardia.
‡New ejection fraction <50% after previously normal ejection fraction on echocardiogram in the preceding 2 y and/or >10% decrease in ejection fraction from baseline.
§Includes 1 patient who remained on mechanical ventilation at discharge to LTAC facility on April 7, 2020.
¶Newly requiring renal replacement therapy during admission.
#Zinc, n = 11; leronlimab, n = 1.
**Length of stay includes 4 patients who remained hospitalized on the study end date with censoring date of May 2, 2020.
††Comparison of death or discharged with hospice in ICU and non-ICU patients (Fisher exact test).

in addition to supportive care, 11 (91.7%) received hydroxychloroquine, 11 (91.7%) received zinc, and 5 (41.7%) received azithromycin. No patients received convalescent plasma, lopinavir/ritonavir, chloroquine, or intravenous gamma globulin during the study period. A trial of prone positioning was used for 2 hypoxic, nonintubated patients, in accordance with institutional protocol (*15*).

Complications

No major complications developed in the patients who never required ICU care during hospitalization (non-ICU patients) (Table 3). Acute respiratory distress syndrome developed in 13 (61.9%) ICU patients. No patients were treated with intravenous pulmonary vasodilators or extracorporeal membrane oxygenation. Arrhythmias developed in 6 ICU patients, 4 with supraventricular tachycardia, including atrial fibrillation or atrial flutter, and 2 with bradycardia, including complete heart block requiring a permanent pacemaker that developed in 1.

Outcomes

Five (6.9%) patients died, and 1 patient was discharged to hospice. Fifty-three (73.6%) patients were discharged home, and 9 (12.5%) were discharged to a skilled nursing facility or long-term acute care hospital. At the end of the study period (May 2, 2020), 4 remained hospitalized awaiting placement in a skilled nursing facility or long-term acute care hospital. Of the 6 patients who died or were discharged to hospice, median age was 83.5 years. Median length of hospitalization for all patients was 7.5 days (interquartile range [IQR] 4–13 days).

Among ICU patients, 3 (14.3%) died; median length of hospitalization was 17 days (IQR 11–30 days). Thirteen (61.9%) ICU patients required mechanical ventilation for a median of 17 days (IQR 13–29 days), and 6 (28.6%) patients underwent tracheostomy. All 4 patients who remained hospitalized had required ICU admission; however, all had improved by the end of the study period, and none still required mechanical ventilation or ICU level of care.

Discussion

We found a lower overall death rate (8.3%) than for the largest US studies thus far, which reported 17.5%–21% death rates (J.A. Lewnard et al., unpub. data, https://doi.org/10.1101/2020.04.12.20062943; C.M. Petrilli et al., unpub. data, https://doi.org/10.1101/2020.04.08.20057794) (*16*). The death rate for ICU patients of 14.3% was also lower than previously reported rates within the United States (45%–50%) (C.M. Petrilli et al., unpub. data, https://doi.org/10.1101/2020.04.08.20057794) (*17*). These results are based on censoring 4 patients who remained hospitalized at the end of the study period, all of whom no longer required ICU level of care and awaited placement in rehabilitation or long-term acute care facilities. Although our sample size is small, this difference in death rates might be attributed to nonsurge conditions. Patient volumes did not exceed normal operating capacity in the 2 hospitals during the study period, which might signify that patients were admitted who might not merit hospitalization in conditions where hospital beds were limited. Disease severity was probably lower in the population in our study; 71% (51/72) of patients required only nasal cannula supplemental oxygen or no oxygen during admission. In addition, the substantial number of patients treated with remdesivir might have contributed to the lower death rate. Preliminary data from recent clinical trials suggest remdesivir use may be associated with reduced mortality (*18*,*19*).

The presenting symptoms and laboratory findings of the patients in our study are similar to those noted in the studies from China published earlier in the COVID-19 pandemic despite the finding that our patient population probably had greater racial and ethnic diversity (*6*–*9*). As seen in prior studies, respiratory complaints were the most common presenting symptoms; however, 5 (6.9%) patients in our study did not have respiratory symptoms of cough or shortness of breath. This finding emphasizes the importance of capturing nonrespiratory symptoms on COVID-19 screening questionnaires.

California in general, and the San Francisco Bay area in particular, have had a longstanding housing affordability crisis (*20*). Seven (9.7%) patients in our study lacked a safe place to isolate at home because of crowded living conditions (no separate bedroom), living with an immunocompromised person, or both. These circumstances also might have contributed to lower hospitalization death rates because patients with mild disease required hospital admission.

One important context for this study is the difference in the standard of care at the 2 institutions. When our institutions began seeing COVID-19 patients, the Centers for Disease Control and Prevention and the World Health Organization had published clinical care guidelines emphasizing supportive care as the standard of care and recommended using experimental therapies only as part of a randomized controlled trial (*21*,*22*). Both of our study sites are involved in clinical trials of the novel

antiviral agent remdesivir but began enrolling at different times: March 14 at SUH and April 9 at ValleyCare. This difference in implementation led to nonuniform use of hydroxychloroquine, azithromycin, and zinc between SUH and ValleyCare. At both study sites, azithromycin was commonly prescribed to outpatients before admission, despite lack of evidence of clinical efficacy. Detailed national guidelines from the Society for Critical Care Medicine were published on March 20 and from the Infectious Disease Society of America on April 11 (*23*,*24*). Notable differences in the standard of care were seen even between our 2 affiliated hospitals, perhaps reflecting the initial lack of national guidelines.

Our study has several limitations. Overall case numbers were low, probably because of early and decisive public health interventions in our community (*25*). This observational study is not powered or designed to analyze treatment efficacy of the experimental therapies given. Analysis of the efficacy of remdesivir, received by most critically ill patients in this cohort, will be conducted as part of a multisite clinical trial. Four patients remained hospitalized at the conclusion of the study period, and final outcomes could therefore not be reported. Thus, the duration of hospitalization is weighted toward patients who had shorter admissions and outcomes of a subset of prolonged hospital courses were not captured. Our results most likely are not generalizable to hospitals with excessive COVID-19 caseloads or with fewer resources for high acuity patients.

In summary, we found that under nonsurge conditions, the overall death rate and the death rate for ICU patients were lower than those previously reported in the United States. The differences in treatment strategy between the 2 hospitals in this study highlight the need for standardized, well-publicized guidelines for new pathogens early on in an epidemic.

J.I.R. is supported by National Institutes of Health Training Grant 5T32AI052073-14.

A.S. and S.K. are involved in a clinical trial of remdesivir sponsored by Gilead Pharmaceuticals.

About the Authors

Dr. Ferguson is an infectious diseases fellow at Stanford Health Care. Her research interests include immunocompromised and transplant infectious diseases. Dr. Rosser is an infectious diseases fellow at Stanford Health Care. Her primary research interest is studying the impact of climate change and globalization on emerging infectious diseases.

References

1. World Health Organization. Novel Coronavirus (2019-NCoV) Situation Report 1. 21 January 2020 [cited 2020 May 11]. https://www.who.int/docs/default-source/coronaviruse/situation-reports/20200121-sitrep-1-2019-ncov.pdf
2. Bialek S, Boundy E, Bowen V, Chow N, Cohn A, Dowling N, et al.; CDC COVID-19 Response Team. COVID-19 Response Team. Severe outcomes among patients with coronavirus disease 2019 (COVID-19)—United States, February 12–March 16, 2020. MMWR Morb Mortal Wkly Rep. 2020;69:343–6. https://doi.org/10.15585/mmwr.mm6912e2
3. ArcGIS. Alameda County COVID-19 dashboard [cited 2020 May 5]. https://ac-hcsa.maps.arcgis.com/apps/opsdashboard/index.html#/948c67558cff414dbbee1a78fcbab1c9
4. Santa Clara County Public Health Emergency Operations Center. Santa Clara County coronavirus (COVID-19) data dashboard [cited 2020 May 5]. https://www.sccgov.org/sites/covid19/Pages/dashboard.aspx
5. Grasselli G, Zangrillo A, Zanella A, Antonelli M, Cabrini L, Castelli A, et al.; COVID-19 Lombardy ICU Network. Baseline characteristics and outcomes of 1591 patients infected with SARS-CoV-2 admitted to ICUs of the Lombardy region, Italy. JAMA. 2020;323:1574. https://doi.org/10.1001/jama.2020.5394
6. Guan WJ, Ni ZY, Hu Y, Liang WH, Ou CQ, He JX, et al.; China Medical Treatment Expert Group for Covid-19. Clinical characteristics of coronavirus disease 2019 in China. N Engl J Med. 2020;382:1708–20. https://doi.org/10.1056/NEJMoa2002032
7. Li LQ, Huang T, Wang YQ, Wang ZP, Liang Y, Huang TB, et al. COVID-19 patients' clinical characteristics, discharge rate, and fatality rate of meta-analysis. J Med Virol. 2020;92:577–83 [Epub ahead of print]. https://doi.org/10.1002/jmv.25757
8. Ruan Q, Yang K, Wang W, Jiang L, Song J. Clinical predictors of mortality due to COVID-19 based on an analysis of data of 150 patients from Wuhan, China. Intensive Care Med. 2020 Mar 3 [Epub ahead of print]. https://doi.org/10.1007/s00134-020-05991-x.
9. Yang X, Yu Y, Xu J, et al. Clinical course and outcomes of critically ill patients with SARS-CoV-2 pneumonia in Wuhan, China: a single-centered, retrospective, observational study. Lancet Respir Med. 2020 Feb 24 [Epub ahead of print]. https://doi.org/10.1016/S2213-2600(20)30079-5
10. Harris PA, Taylor R, Minor BL, Elliott V, Fernandez M, O'Neal L, et al.; REDCap Consortium. The REDCap consortium: building an international community of software platform partners. J Biomed Inform. 2019;95:103208. https://doi.org/10.1016/j.jbi.2019.103208
11. Harris PA, Taylor R, Thielke R, Payne J, Gonzalez N, Conde JG. Research electronic data capture (REDCap)—a metadata-driven methodology and workflow process for providing translational research informatics support. J Biomed Inform. 2009;42:377–81. https://doi.org/10.1016/j.jbi.2008.08.010
12. Ranieri VM, Rubenfeld GD, Thompson BT, Ferguson ND, Caldwell E, Fan E, et al.; ARDS Definition Task Force. Acute respiratory distress syndrome: the Berlin definition. JAMA. 2012;307:2526–33.
13. Lopes JA, Jorge S. The RIFLE and AKIN classifications for acute kidney injury: a critical and comprehensive review. Clin Kidney J. 2013;6:8–14. https://doi.org/10.1093/ckj/sfs160
14. Centers for Disease Control and Prevention. 2020 National Healthcare Safety Network (NHSN) patient safety

component manual. 2020 Jan [cited 2020 Apr 14]. https://www.cdc.gov/nhsn/pdfs/pscmanual/pcsmanual_current.pdf
15. Stanford Medicine COVID-19 Critical Care Task Force. Proning non-intubated patient [cited 2020 May 11]. https://sites.google.com/view/stanford-covid/home/proning-non-intubated-patient
16. Richardson S, Hirsch JS, Narasimhan M, Crawford JM, McGinn T, Davidson KW, et al.; and the Northwell COVID-19 Research Consortium. Presenting characteristics, comorbidities, and outcomes among 5700 patients hospitalized with COVID-19 in the New York City area. JAMA. 2020. https://doi.org/10.1001/jama.2020.6775
17. Arentz M, Yim E, Klaff L, Lokhandwala S, Riedo FX, Chong M, et al. Characteristics and outcomes of 21 critically ill patients with COVID-19 in Washington state. JAMA. 2020;323:1612. https://doi.org/10.1001/jama.2020.4326
18. Gilead. Gilead announces results from phase 3 trial of investigational antiviral remdesivir in patients with severe COVID-19 [cited 2020 May 4]. https://www.gilead.com/news-and-press/press-room/press-releases/2020/4/gilead-announces-results-from-phase-3-trial-of-investigational-antiviral-remdesivir-in-patients-with-severe-covid-19
19. National Institute of Allergy and Infectious Diseases. NIH clinical trial shows remdesivir accelerates recovery from advanced COVID-19 [cited 2020 May 4]. http://www.niaid.nih.gov/news-events/nih-clinical-trial-shows-remdesivir-accelerates-recovery-advanced-covid-19
20. California Department of Housing and Community Development. California's housing future: challenges and opportunities. Final statewide housing assessment 2025. February 2018 [cited 2020 Apr 14]. https://www.hcd.ca.gov/policy-research/plans-reports/docs/SHA_Final_Combined.pdf
21. Centers for Disease Control and Prevention. Coronavirus disease 2019 (COVID-19). Interim clinical guidance for management of patients with confirmed coronavirus disease (COVID-19) [cited 2020 Mar 28]. https://www.cdc.gov/coronavirus/2019-ncov/hcp/clinical-guidance-management-patients.html
22. World Health Organization. Clinical management of severe acute respiratory infection when novel coronavirus (NCoV) infection is suspected [cited 2020 Mar 28]. https://www.who.int/publications-detail/clinical-management-of-severe-acute-respiratory-infection-when-novel-coronavirus-(ncov)-infection-is-suspected
23. Alhazzani W, Møller MH, Arabi YM, Loeb M, Gong MN, Fan E, et al. Surviving Sepsis Campaign: guidelines on the management of critically ill adults with coronavirus disease 2019 (COVID-19). Crit Care Med. 2020 Mar 27 [Epub ahead of print]. https://doi.org/10.1097/CCM.0000000000004363
24. Bhimraj A, Morgan RL, Hirsch Shumaker A, Lavergne V, Baden L, Cheng VCC, et al. Infectious Diseases Society of America guidelines on the treatment and management of patients with COVID-19. Clin Infect Dis. 2020 Apr 27 [Epub ahead of print]. http://doi.org/10.1093/cid/ciaa478
25. City and County of San Francisco Department of Public Health. Order of the health officer no. C19-07b [cited 2020 May 11]. https://www.sfdph.org/dph/alerts/files/HealthOfficerOrder-C19-07b-ShelterInPlace-03312020.pdf

Address for correspondence: Shanthi Kappagoda, Stanford Health Care, Division of Infectious Diseases and Geographic Medicine, 300 Pasteur Dr, L-134, Stanford, CA 94305, USA; email: skappago@stanford.edu

Tuberculosis in Internationally Displaced Children Resettling in Harris County, Texas, USA, 2010–2015[1]

Gabriella S. Lamb,[2] Andrea T. Cruz, Elizabeth A. Camp, Michelle Javier, Jessica Montour, Tamisha Piper, Umair A. Shah, Jeffrey R. Starke

Medscape EDUCATION ACTIVITY

In support of improving patient care, this activity has been planned and implemented by Medscape, LLC and Emerging Infectious Diseases. Medscape, LLC is jointly accredited by the Accreditation Council for Continuing Medical Education (ACCME), the Accreditation Council for Pharmacy Education (ACPE), and the American Nurses Credentialing Center (ANCC), to provide continuing education for the healthcare team.

Medscape, LLC designates this Journal-based CME activity for a maximum of 1.00 ***AMA PRA Category 1 Credit(s)™***. Physicians should claim only the credit commensurate with the extent of their participation in the activity.

Successful completion of this CME activity, which includes participation in the evaluation component, enables the participant to earn up to 1.0 MOC points in the American Board of Internal Medicine's (ABIM) Maintenance of Certification (MOC) program. Participants will earn MOC points equivalent to the amount of CME credits claimed for the activity. It is the CME activity provider's responsibility to submit participant completion information to ACCME for the purpose of granting ABIM MOC credit.

All other clinicians completing this activity will be issued a certificate of participation. To participate in this journal CME activity: (1) review the learning objectives and author disclosures; (2) study the education content; (3) take the post-test with a 75% minimum passing score and complete the evaluation at http://www.medscape.org/journal/eid; and (4) view/print certificate. For CME questions, see page 1968.

Release date: July 17, 2020; Expiration date: July 17, 2021

Learning Objectives

Upon completion of this activity, participants will be able to:

- Distinguish recommendations from the Centers for Disease Control and Prevention regarding screening for tuberculosis (TB) among immigrant children
- Identify rates of discrepancy between results of the tuberculin skin test and interferon-gamma release assays in the current study
- Analyze results of TB testing among immigrant children in the current study
- Evaluate risk factors for a positive TB test among immigrant children

CME Editor

Deborah Wenger, MBA, Copyeditor, Emerging Infectious Diseases. *Disclosure: Deborah Wenger, MBA, has disclosed no relevant financial relationships.*

CME Author

Charles P. Vega, MD, Health Sciences Clinical Professor of Family Medicine, University of California, Irvine School of Medicine, Irvine, California. *Disclosure: Charles P. Vega, MD, has disclosed the following relevant financial relationships: served as an advisor or consultant for Johnson & Johnson Pharmaceutical Research & Development, LLC; GlaxoSmithKline; served as a speaker or a member of a speakers bureau for Genentech; GlaxoSmithKline.*

Authors

Disclosures: ***Gabriella S. Lamb, MD, MPH; Andrea T. Cruz, MD, MPH; Elizabeth A. Camp, PhD; Michelle Javier, MD; Jessica Montour, MPH; Tamisha Piper MPAS, PA-C;*** and ***Umair A. Shah, MD, MPH,*** *have disclosed no relevant financial relationships.* ***Jeffrey R. Starke, MD,*** *has disclosed the following relevant financial relationships: served as an advisor or consultant for Otsuka Pharmaceuticals.*

Author affiliations: Baylor College of Medicine, Houston, Texas, USA (G.S. Lamb, A.T. Cruz, E.A. Camp, M. Javier, J.R. Starke); US Committee for Refugees and Immigrants, Austin, Texas, USA (J. Montour); Harris County Public Health Refugee Health Screening Program, Houston (T. Piper, U.A. Shah)

[1]Preliminary results from this study were presented at the North American Union TB Conference, February 28–March 3, 2018, Chicago, IL, USA.

[2]Current affiliation: Harvard Medical School, Boston, Massachusetts, USA.

DOI: https://doi.org/10.3201/eid2608.190793

US guidelines have recommended testing children emigrating from high tuberculosis-incidence countries with interferon-gamma release assays (IGRAs) or tuberculin skin tests (TSTs). We describe the Harris County (Texas) Public Health Refugee Health Screening Program's testing results during 2010–2015 for children <18 years of age: 5,990 were evaluated, and 5,870 (98%) were tested. Overall, 364 (6.2%) children had ≥1 positive test: 143/1,842 (7.8%) were tested with TST alone, 129/3,730 (3.5%) with IGRA alone, and 92/298 (30.9%) with both TST and IGRA. Region of origin and younger age were associated with positive TST or IGRA results. All children were more likely to have positive results for TST than for IGRA (OR 2.92, 95% CI 2.37–3.59). Discordant test results were common (20%) and most often were TST+/IGRA– (95.0%), likely because of bacillus Calmette-Guérin vaccination. Finding fewer false positives supports the 2018 change in US immigration guidelines that recommends using IGRAs for recently immigrated children.

The World Health Organization (WHO) has estimated that there were 1 million tuberculosis (TB) cases and 234,000 tuberculosis-related deaths among children in 2017 (*1*). An estimated additional 67 million children were infected with *Mycobacterium tuberculosis* (*2*). Testing of children emigrating from high- to low-incidence countries can provide benefit to individual patients and to the community by identifying patients for whom providing treatment would reduce the risk of progression to disease and thus decrease the reservoir for future contagious disease cases.

Not all recently arrived children are at equal risk for TB infection. Refugees, asylees, and victims of human trafficking (VHTs) may be at highest risk as the result of prolonged periods of displacement, undernutrition, poor sanitation, and poor access to medical care (*3*). In the United States, special immigrant visa (SIV) holders are predominantly children of persons from Afghanistan or Iraq who served as military translators and do not typically live in congregate settings (*4*,*5*), potentially placing them at lower risk for TB exposure. Those with parole classification most commonly emigrated from Cuba, a country with a low incidence of TB (*6*–*8*).

In 2018, the Centers for Disease Control and Prevention (CDC) updated the preimmigration guidelines for TB testing for immigrants to the United States, recommending that children 2–14 years of age who come from high TB-incidence countries (>20 cases/100,000 population) be tested with an interferon-gamma release assay (IGRA) rather than a tuberculin skin test (TST) (*9*). Previously, because of resource restrictions, TSTs were performed more commonly in many countries, and 9%–35% of refugee children tested positive (*10*–*15*). However, in a large study, almost two thirds of children with positive preimmigration TST results had negative IGRA results on postimmigration testing (*11*), indicating that many positive TST results likely were caused by prior vaccination with bacillus Calmette-Guérin (BCG).

Almost 10% of refugees, asylees, parolees, or SIV holders in the United States resettle in Texas, and almost 25% of those resettle in Harris County (which includes Houston) (*16*). Texas is also a human trafficking hub, with many internationally trafficked persons passing through the state (*17*). We describe the comparative epidemiology of positive TSTs and IGRAs in children of different immigration classifications cared for through the Harris County Public Health Refugee Health Screening Program.

Methods

The Harris County Public Health Refugee Health Screening Program performs intake screening for TB, HIV, and pathogenic parasites and performs other routine laboratory screenings for all refugees, asylees, identified VHTs, parolees, and SIV holders resettling in the county. We performed a cross-sectional study of children 0–18 years of age who were evaluated by this program during January 1, 2010–December 31, 2015. We obtained demographic information, TB exposure history, symptom screening, and testing results from the Harris County Public Health Refugee Health Screening Program and the US Committee for Refugees and Immigrants (although the data originated from the Texas Department of State Health Services when the Texas Refugee Health Program resided there). All children were seen in a clinic run by the Harris County Public Health Refugee Health Screening Program. At this visit, demographic information and testing before immigration were obtained from the family and overseas records. Children not tested before immigration or who had no overseas records were tested during the clinic visit. Most of the children with a positive test for TB infection were evaluated at the Texas Children's Hospital TB Clinic where additional testing and, if indicated, treatment were provided by 3 of the authors of this article (G.S.L., A.T.C., and J.R.S.).

Immigration classification was determined by the US Committee for Refugees and Immigrants. Immigration classifications are defined by US Citizenship and Immigration Services (Table 1) (*18*–*22*). We used WHO definitions for regions of origin (*23*). We predicted that refugees, asylees, and VHTs would be higher-risk groups for TB infection because they were

Table 1. Definitions of immigration classifications, United States

Immigration classification	Definition
Refugee	A person located outside the United States who demonstrates he or she was persecuted or has a fear of persecution because of race, religion, nationality, political opinion, or membership in a particular social group and is not firmly resettled in another country (*18*).
Asylee (asylum seeker)	Any person who meets the definition of a refugee and is already in the United States or seeking admission at a port of entry (*19*).
Parolee (Cuban and Haitian Family Reunification Parole Programs)	Persons from Cuba and Haiti who have family members who are US citizens or lawful permanent residents, who are able to come to the United States without waiting for immigrant visas to become available (*20*).
Special immigrant visa (holders	There are many categories; however, the children included in this study are children of Iraqi and Afghan translators who are interpreters who have worked with the US Armed Forces or under the chief of mission authority at the US embassy in Baghdad or Kabul (*21*).
Victim of human trafficking	A person who has been recruited, harbored, or transported for compelled labor or commercial sex acts through the use of force, fraud, or coercion (*22*).

more likely to have lived in congregate settings. We predicted the lower-risk groups to be parolees and SIVs because of their residence in lower TB-incidence nations and not living in congregate settings. Although overseas vaccination data were unavailable, we assumed that children were BCG immunized because most children emigrated from countries where universal BCG vaccination is practiced.

Clinicians in the Harris County Public Health Refugee Health Screening Program performed initial TB testing. Providers were able to choose the type of TB testing used; they typically used the TST in children <5 years of age and an IGRA in children ≥5 years of age (*24*). TST results were considered positive if there was ≥10 mm of induration, unless the child was living with HIV or had contact with a person with pulmonary TB, in which case the threshold was ≥5 mm of induration (*25*). The main IGRA used was the T-SPOT.*TB* (Oxford Immunotec, https://www.tspot.com), for which a result was defined as positive if ≥8 spots were noted in either well (*24*). A positive QuantiFERON Gold-In Tube (QIAGEN, https://www.qiagen.com) result was defined as an antigen-nil value of ≥0.35 IU/mL (*24*).

We classified children with positive test(s) for infection as TB infected, likely TB uninfected, or having TB disease. These classifications were determined by 2 authors (ATS and JRS) at the time each child was seen. In the first 2 categories, children had normal physical examinations and 2-view chest radiographs. We classified children as having TB infection if they had a positive IGRA result (IGRA+), if they had a positive TST result (TST+) and no IGRA was done (not all TST+ children had IGRAs performed), or if the IGRA result was indeterminate/invalid. We typically defined children as being likely uninfected if they were TST+/IGRA–, had normal physical examination findings and normal chest radiographs, and had no known contacts with TB disease or if they had negative tests with normal physical examination findings and chest radiographs. However, we did not classify all children who were TST+/IGRA– as being uninfected; some of these children were classified as having TB infection, most commonly because of young age (<2 years). TB disease was diagnosed in children who had clinical, physical examination, or radiographic findings consistent with TB disease (*26*).

We created 3 models to determine which factors were independently associated with positive tests of infection: a positive TST result, a positive IGRA result, and any positive TB test result (TST or IGRA). We compared demographic characteristics and other categorical variables among the higher-risk and lower-risk groups for statistically significant differences by the χ^2 test or Fisher exact test for dichotomous variables and Wilcoxon rank-sum or Kruskal-Wallis test for continuous variables. We included any factor with a p value ≤0.25 in the binary regression model. We created the final model using a backward-step approach. To assess secular trends in usage and positivity, we analyzed monthly totals using linear regression and the Wilcoxon signed-rank test. A p value <0.05 was considered significant.

We conducted all analyses using the SPSS Statistics 25 (IBM, https://www.ibm.com). We obtained institutional review board approval from the Harris County Public Health Department and Baylor College of Medicine (Houston, TX, USA).

Results

During the study period, the Harris County Public Health Refugee Health Screening Program evaluated 5,990 children (Table 2), 98% (5,870) of whom received ≥1 test of TB infection (Table 3): IGRA, 3,730 (63.5%); TST, 1,842 (31.4%); both TST and IGRA, 298 (5.1%). In the TST and IGRA group, 206 (69.1%) were TST–/IGRA–, 29 (9.7%) TST+/IGRA+, 57 (19.1%) TST+/IGRA–, 3 (1.0%) TST+/IGRA indeterminate/invalid, and 3 (1.0%) TST–/IGRA+ (Figure 1). Discrepant test results occurred in 60 (20.1%) children tested with both TST and IGRA.

Table 2. Demographic variables of internationally displaced children, Harris County, Texas, USA, 2010–2015*

		Immigration classification					
		Higher-risk groups			Lower-risk groups		
Category	Variable	Refugee, n = 4,246	Asylee, n = 173	VHT, n = 16	Parolee, n = 851	SIV holder, n = 704	p value
Demographics	Age, y, median (IQR)	8 (4–12)	9 (5–12)	11.5 (7–15)	9 (5–13)	4 (2–8)	<0.001†
	Female sex	2,025 (47.7)	81 (46.8)	7 (43.8)	404 (47.5)	304 (43.2)	0.281‡
WHO region of origin	Eastern Mediterranean	1,414 (33.3)	89 (51.4)	0	0	704 (100.0)	<0.001‡
	Southeast Asia	1,416 (33.3)	7 (4.0)	1 (6.3)	0	0	
	Africa	1,202 (28.3)	40 (23.1)	0	0	0	
	America	183 (4.3)	31 (17.9)	12 (75.0)	851 (100.0)	0	
	Western Pacific	18 (0.4)	2 (1.2)	1 (6.3)	0	0	
	European	13 (0.3)	4 (2.3)	2 (12.5)	0	0	
Underlying conditions	HIV infected	22 (0.5)	0	0	1 (0.1)	2 (0.3)	<0.001‡
	Pathogenic parasites detected in feces	328 (17.1)	18 (11.3)	2 (12.5)	98 (12.5)	115 (17.9)	<0.001‡

*Values are no. (%) except as indicated. Percentages reflect those for whom the information was available. IQR, interquartile range; SIV, special immigrant visa; VHT, victim of human trafficking; WHO, World Health Organization.
†p value using Kruskal-Wallis test.
‡p value using χ^2 test.

Overall, 364 children (6.2%) had ≥1 positive TB test. Among these children, 325 (89.3%) received diagnoses of TB infection, 35 (9.6%) were considered likely uninfected, and 4 (1.1%) received diagnoses of TB disease (Figure 1). The 35 children with a positive test who were considered likely uninfected were all TST+/IGRA–. In addition, 22 (38.6%) children who were TST+/IGRA– were classified as having TB infection, typically earlier in the study period because of young age, variability in provider practice, or both (Figure 1).

The Texas Children's Hospital Tuberculosis Clinic in Houston cares for most of children in Harris County with TB disease. According to a chart review, none of the children who had TB infection or who were considered likely uninfected had TB disease developed during the following 4–9 years (2,427 person-years of follow-up). Furthermore, we cross-referenced the public health records for Harris County and found that none of these children had been reported to have TB disease develop.

We found 3 factors to be associated with a either a positive TST or IGRA: region of origin, age group, and HIV status. Immigration classification was associated with a positive TB test result on univariate analysis, but this association did not hold true on multivariate analysis. Children, irrespective of immigration classification and from all regions and age groups, had greater odds of having a positive TST result than a positive IGRA result (OR 2.92, 95% CI 2.79–3.59).

Immigration Classification

On univariate analysis, irrespective of test performed, children determined to have a higher-risk immigration classification had nearly 3 times the odds of having a positive TST or IGRA compared with those with lower-risk immigration classifications (OR 2.68, 95% CI 1.94–3.68). Specifically, children with higher-risk immigration classifications had twice the odds of having a positive TST (OR 2.14, 95% CI 1.45–3.15) and nearly 4 times the odds of having a positive IGRA (OR 3.84, 95% CI 2.21–6.68) compared with children with

Table 3. Tests for TB infection performed and test results by immigration classification in migrant children, Harris County, Texas, USA, 2010–2015*

	Immigration classification						
	Higher-risk groups			Lower-risk groups			
Category	Refugee, n = 4,246	Asylee, n = 173	VHT, n = 16	Parolee, n = 851	SIV holder, n = 704	OR (95% CI)	p value†
Test(s) performed							
TST alone	1,381 (32.5)	30 (17.3)	1 (6.3)	168 (19.7)	300 (42.6)	1.08 (0.96–1.23)	<0.001
IGRA alone	2,558 (60.2)	137 (79.2)	15 (93.8)	642 (75.4)	349 (49.6)	1.12 (0.99–1.26)	
TST and IGRA	204 (4.8)	4 (2.3)	0	22 (2.6)	29 (4.1)	1.45 (1.06–1.98)	
Result							
TST positive	196/1,589 (12.3)	4/35 (11.4)	0	7/190 (3.7)	25/329 (7.6)	2.14 (1.45–3.15)	<0.001
IGRA positive	142/2,819 (5.0)	5/141 (3.5)	0	5/664 (0.8)	9/389 (2.3)	3.84 (2.21–6.68)	<0.001
Total positive tests	311 (7.3)	9 (5.2)	0	10 (1.2)	34 (4.8)	2.67 (1.94–3.68)	<0.001

*Values are no. (%) or no. positive/no. tested (%) except as indicated. IGRA, interferon gamma release assay; OR, odds ratio; SIV, special immigrant visa; TST, tuberculin skin test; VHT, victim of human trafficking.
†p value using χ^2 test.

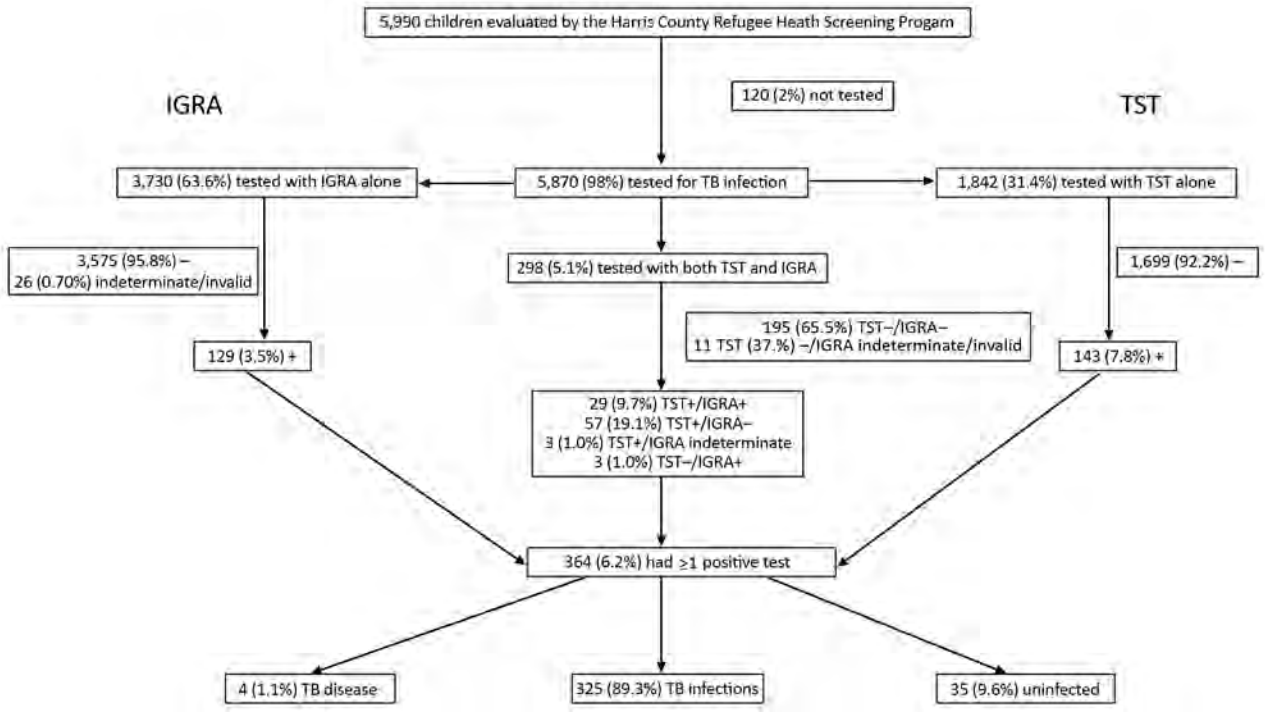

Figure 1. Consort diagram of TST and IGRA results in internationally displaced children over a 6-year period, Harris County, Texas, USA, 2010–2015. The percentage reported for TB disease, infection, and uninfected are the percentage of persons who had ≥1 positive test. IGRA, interferon gamma release assay; TST, tuberculin skin test; TB, tuberculosis; +, positive; –, negative.

lower-risk immigration classifications (Table 3). These differences were not seen on multivariate analysis.

All children, regardless of immigration classification, had greater odds of a positive result for TST compared with IGRA (OR 2.92, 95% CI 2.79–3.59). This difference was more pronounced among those with lower-risk classification (OR 4.81, 95% CI 2.54–9.10) than those with higher-risk classification (OR 2.68, 95% 2.15–3.35).

Region of Origin

On multivariate analysis, region of origin was a notable correlate for a positive test of TB infection. TST and IGRA positivity varied by region of origin. Using children from Southeast Asia as a reference group, we found that children from eastern Mediterranean countries (adjusted odds ratio [aOR] 0.48, 95% CI 0.33-0.70) and the Americas (aOR 0.19, 95% CI 0.09–0.39) had reduced odds for a positive TST result compared with children from Southeast Asia. Similarly, children from eastern Mediterranean countries (aOR 0.34, 95% CI 0.21-0.53) and the Americas (aOR 0.12, 95% CI 0.06–0.25) had reduced odds for a positive IGRA result compared with children from Southeast Asia (Table 4). Using the IGRA result as the reference, we found the odds of having a positive TST result to be greater in children from eastern Mediterranean countries (OR 3.99, 95% CI 2.59–6.16) and the Americas (OR 4.15, 95% CI 1.62–10.62) (Figure 2, panel A).

Age Group

TST and IGRA positivity varied by age group. Using children <2 years of age as the reference group, on multivariate analysis, we found that children 2–5 years of age had reduced odds for a positive TST result (aOR 0.40, 95% CI 0.26–0.61) and children 2–10 years of age had reduced odds for a positive IGRA result (2–5 years, aOR 0.26, 95% CI 0.11–0.60; 6–10 years, aOR 0.41, 95% CI 0.20–0.85) (Table 4).

Using the IGRA result as the reference, we found that all children, regardless of age, had greater odds of having a positive TST than a positive IGRA (OR 2.92, 95% CI 2.79–3.59). Children 6–10 years of age had the greatest odds of having a positive TST result compared with a positive IGRA result (OR 5.47, 95% CI 3.45–8.69) (Figure 2, panel B).

HIV Infection

On multivariate analysis, we found that children living with HIV had 3 times the odds for a positive TST result compared with children who were HIV uninfected

Table 4. Factors associated with a positive result for TST, IGRA, or both in 5,870 migrant children, Harris County, Texas, USA, 2010–2015*

Characteristic	TST model			IGRA model			TST and IGRA combined model		
	No.†	aOR (95% CI)	p value	No.†	aOR (95% CI)	p value	No.†	aOR (95% CI)	p value
Age, y									
<2	53	Referent		10	Referent		55	Referent	
2–5	75	0.40 (0.26–0.61)	<0.001	13	0.26 (0.11–0.60)	0.002	81	0.36 (0.24–0.54)	<0.001
6–10	43	0.72 (0.45–1.07)	0.25	35	0.41 (0.20–0.85)	0.02	74	0.28 (0.18–0.42)	<0.001
11–14	34	0.68 (0.39–1.21)	0.19	56	1.05 (0.52–2.12)	0.90	85	0.55 (0.37–0.83)	0.004
>14	27	0.77 (0.44–1.35)	0.36	47	1.35 (0.66–2.77)	0.41	69	0.72 (0.48–1.10)	0.13
Region of origin									
Southeast Asia	99	Referent		62	Referent		149	Referent	
E. Mediterranean	74	0.48 (0.33–0.70)	<0.001	30	0.34 (0.21–0.53)	<0.001	98	0.44 (0.33–0.59)	<0.001
Africa	49	0.69 (0.45–1.07)	0.10	61	1.02 (0.70–1.49)	0.91	100	0.81 (0.61–1.09)	0.17
Americas	10	0.19 (0.09–0.39)	<0.001	8	0.12 (0.06–0.25)	<0.001	17	0.14 (0.08–0.23)	<0.001
HIV positive	5	2.99 (1.01–8.87)	0.049	2	–	–	7	5.57 (2.23–13.90)	<0.001

*aOR, adjusted odds ratio; E., Eastern; IGRA, interferon gamma release assay; TST, tuberculin skin test; –, numbers too small to enable performance of these tests.
†Number in group with a positive TB test result.

(aOR 2.99, 95% CI 1.01–8.87). HIV infection was not associated with a positive IGRA result (Table 4).

Discussion

In the United States, 66% of reported TB cases occur among foreign-born persons, a rate 13 times higher than for persons born in the United States (*27*). Previous studies, mostly using the TST, found a prevalence of TB infection of 9%–35% among refugee children (*10*–*15*). However, positive results were less common in our cohort, likely because of the variety of immigration classifications included and expanded IGRA use.

We found that the prevalence of positive results for tests of TB infection varied by region of origin and age and that all children in the study had greater odds of a positive result from TST than from IGRA. Immigration classification was not associated with positive results for TB infection. We also found discordance between TST and IGRA results across the pediatric age spectrum, suggesting that the effect of BCG vaccination on TST positivity may be more prolonged than typically expected (*28*). In addition, potentially confounding our results, children who received TSTs before and after immigration may

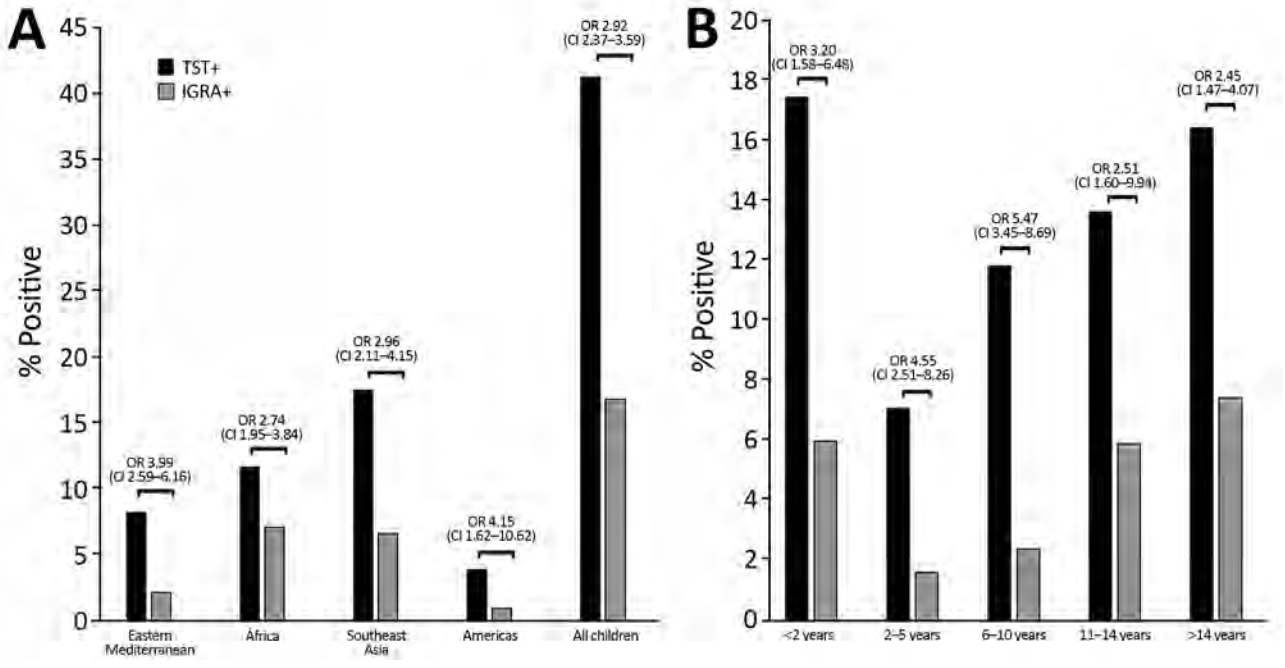

Figure 2. Comparison of TST and IGRA results (using IGRAs as reference) in internationally displaced children over a 6-year period, Harris County, Texas, USA, 2010–2015. A) By location; B) by age. Brackets indicate ORs and 95% CIs between categories. IGRA, interferon gamma release assay; OR, odds ratio; TST, tuberculin skin test.

have had immunologic boosting, resulting in falsely positive TSTs and IGRAs (*29*).

Region of origin was a notable risk factor for positive TB test results. Children from Southeast Asia had greater odds of having a positive result for TST, IGRA, or both than did children from eastern Mediterranean countries and the Americas, but we found no difference for these children compared with those from Africa. This finding is consistent with known epidemiologic risk factors: the prevalence of TB disease is high in countries in Africa and Southeast Asia, and Southeast Asia has a higher prevalence of TB disease than eastern Mediterranean countries and Cuba (where most children from the Americas region originated) (*30*).

Age was another noteworthy risk factor for positive TB test results. Children <2 years and >14 years of age had a higher prevalence of positive results for TST, IGRA, or both compared with children 2–14 years of age. Older children (>14 years of age) in our cohort had increased prevalence of positive TB test results by both the TST and IGRA, which more likely represented true TB infection because of the children's greater time outside the home and cumulative exposure to adults with infectious pulmonary TB (*30*–*34*). The higher frequency of positive tests in children <2 years of age, on the other hand, is more difficult to explain. Higher TST positivity in children <2 years of age likely represented greater cross-reactivity with BCG, given the temporal proximity to vaccination or potential boosting if children had serial TSTs performed (before and after immigration). However, BCG immunization cannot explain the increased prevalence of positive IGRA results in these young children. Furthermore, these data contradict previous studies that demonstrate that older children are more likely to have TB infection (*30*–*34*). One possible explanation is that IGRA-positive children <2 years of age in our cohort had more prolonged exposure to an adult family member with infectious pulmonary TB in the home, because very young children spend more time in the home than their school-aged counterparts. To date, IGRAs have not been used routinely for the diagnosis of TB infection in children <2 years of age because of a paucity of data on test performance (*35*).

Most previous estimates of the prevalence of TB infection in immigrant children used the TST as the test of choice, given an initial paucity of pediatric data and the scarcity and cost of IGRAs. Our findings paralleled the results of a recent study using IGRA testing, which estimated that 5.6% of immigrant children had TB infection, compared with previous estimates of 22% based on TST testing (*36*). American Academy of Pediatrics guidelines currently recommend IGRA use down to 2 years of age (*35*); some experts recommend using IGRAs in children as young as 1 year of age. Use of IGRAs rather than the TST would likely reduce false positive tests and allow for TB infection therapy to be targeted to those who would most benefit.

The CDC does not recommend tiered testing (that is, obtaining an IGRA if a TST result is positive) for TB infection. However, at times, the initial test of infection, selected either by choice or by necessity, is not the optimal test, particularly for a BCG-immunized child. In our study, all children had greater odds of having a positive TST result compared with a positive IGRA test regardless of immigration classification, region of origin, or age. In addition, we had almost 300 children in whom both TSTs and IGRAs were obtained, of whom 20% had discordant results, mostly TST+/IGRA–. Our findings are consistent with a prior study that demonstrated that for BCG-immunized children who have immigration-related testing, false positive TST results are common, and IGRAs should be the tests of choice for this patient population (*10*).

Discordance between TST and IGRA results was seen in all age groups. Although false-positive results are an expected limitation of TST use among BCG-vaccinated children, the impact of BCG vaccine in causing falsely positive TST results has typically been thought to be temporally related to BCG vaccine receipt, which in most countries is a single dose immediately after birth. However, discordant TST and IGRA results in older children suggest either that the effect of some strains of BCG on the TST result lasts longer than previously recognized (*28*) or that the effect of nontuberculous mycobacteria infections that also can cause a falsely positive TST result may be underestimated in children from developing nations. A third possibility is that immunologic boosting as a result of repeat skin testing before and after immigration may have resulted in false positive TSTs (*29*). Concerns about false positive TST results are considered in updated 2018 guidelines (*9*) for TB testing before immigration, thereby suggesting use of IGRAs for all persons ≥2 years of age.

Our study has limitations. Although we have follow-up data from the Texas Children's Hospital TB clinic for most children evaluated for a positive test of TB infection, we do not have data for some children evaluated at other clinics or for children

whose test for TB infection was negative. BCG vaccination status was not routinely documented; thus, the presumption of false-positive TSTs secondary to cross-reactivity with BCG assumes that most children were BCG-immunized. We assumed BCG vaccination because this vaccination is recommended in the national immunization programs of 95% of countries from which these children emigrated (*37*). HIV infection was rare in our cohort, precluding drawing meaningful conclusions regarding positive results for TST, IGRA, or both in HIV-infected children from our data. Finally, these data may not be generalizable to all immigrant children relocating to the United States because this study included predominantly children from TB high-burden countries (*9*).

In summary, the prevalence of positive TB test results in this cohort of children was lower than previously reported, and TB disease was rare. The lower prevalence of positive tests of TB infection in this childhood population likely stems from the predominant use of IGRA testing. The TST and IGRA results are frequently discrepant, particularly among those with lower-risk immigration classification, younger children who have received a BCG vaccine, and those from lower-burden countries.

As a result of these data and our experience, we advocate for other health jurisdictions to implement the routine use of IGRA testing for all children, regardless of immigration classification, region of origin, or age, who are evaluated as part of the immigration process to the United States. We also advocate for use of confirmatory IGRA testing in BCG-immunized children with no known TB contacts who have positive TST results. Use of IGRA as opposed to TST in BCG-immunized children would reduce false-positive test results and enable TB infection therapy to be targeted to those who would most benefit.

Acknowledgments

We thank our colleagues in the Harris County Public Health Refugee Health Screening Program, City of Houston Tuberculosis Program, and the US Committee for Refugees and Immigrants for their collaboration in caring for our children.

About the Author

Dr. Lamb is an assistant in medicine at Boston Children's Hospital and a Clinical Instructor at Harvard Medical School, Boston, Massachusetts, USA. Her research interests are in *Mycobacteria* and epidemiology.

References:

1. World Health Organization. Global TB report 2018 [cited 2019 Feb 25]. https://apps.who.int/iris/bitstream/handle/10665/274453/9789241565646-eng.pdf
2. Dodd PJ, Gardiner E, Coghlan R, Seddon JA. Burden of childhood tuberculosis in 22 high-burden countries: a mathematical modelling study. Lancet Glob Health. 2014; 2:e453–9. https:// doi.org/10.1016/S2214-109X(14)70245-1
3. De Bruijn B. The living conditions and well-being of refugees. United Nations Development Program, New York City 2018 [cited 2019 Feb 25]. http://hdr.undp.org/sites/default/files/hdrp_2009_25.pdf
4. US Citizenship and Immigration Services. Special immigrants [cited 2019 Feb 25]. https://www.uscis.gov/humanitarian/special-immigrants
5. Coburn N, Sharan T. Out of harm's way? Perspectives of the special immigrant visa program for Afghanistan, July 2016 [cited 2019 Feb 25]. http://www.hollingscenter.org/wp-content/uploads/2016/09/SIV-Full-Report.pdf
6. World Health Organization. Tuberculosis country profiles: Cuba [cited 2019 Feb 25]. https://extranet.who.int/sree/Reports?op=Replet&name=%2FWHO_HQ_Reports%2FG2%2FPROD%2FEXT%2FTBCountryProfile&ISO2=CU&LAN=EN&outtype=html
7. Wasem RE. Immigration policy on Haitian migrants. Congressional Research Service, May 17, 2011 [cited 2019 Feb 25]. https://fas.org/sgp/crs/row/RS21349.pdf
8. Krogstad JM. Surge in Cuban immigration to U.S. continued through 2016. Pew Research Center, January 13, 2017 [cited 2019 Feb 25]. http://www.pewresearch.org/fact-tank/2017/01/13/cuban-immigration-to-u-s-surges-as-relations-warm
9. Centers for Disease Control and Prevention. Tuberculosis technical instructions for panel physicians; 2018 [cited 2019 Mar 14]. https://www.cdc.gov/immigrantrefugeehealth/exams/ti/panel/tuberculosis-panel-technical-instructions.html?CDC_AA_refVal=https%3A%2F%2Fwww.cdc.gov%2-Fimmigrantrefugeehealth%2Fexams%2Fti%2Fpanel%2Ftuberculosis-implementation.html
10. Taylor EM, Painter J, Posey DL, Zhou W, Shetty S. Latent tuberculosis infection among immigrant and refugee children arriving in the United States: 2010. J Immigr Minor Health. 2016;18:966–70. https://doi.org/10.1007/s10903-015-0273-2
11. Hayes EB, Talbot SB, Matheson ES, Pressler HM, Hanna AB, McCarthy CA. Health status of pediatric refugees in Portland, ME. Arch Pediatr Adolesc Med. 1998;152:564–8. https://doi.org/10.1001/archpedi.152.6.564
12. Geltman PL, Radin M, Zhang Z, Cochran J, Meyers AF. Growth status and related medical conditions among refugee children in Massachusetts, 1995–1998. Am J Public Health. 2001;91:1800–5. https://doi.org/10.2105/AJPH.91.11.1800
13. Sheikh M, Pal A, Wang S, MacIntyre CR, Wood NJ, Isaacs D, et al. The epidemiology of health conditions of newly arrived refugee children: a review of patients attending a specialist health clinic in Sydney. J Paediatr Child Health. 2009;45:509–13. https://doi.org/10.1111/j.1440-1754.2009.01550.x
14. Gray K, Wood N, Gunasekera H, Sheikh M, Hazelton B, Barzi F, et al. Vitamin D and tuberculosis status in refugee children. Pediatr Infect Dis J. 2012;31:521–3. https://doi.org/10.1097/INF.0b013e3182456c55
15. Lucas M, Nicol P, McKinnon E, Whidborne R, Lucas A, Thambiran A, et al. A prospective large-scale study of methods for the detection of latent *Mycobacterium tuberculosis*

infection in refugee children. Thorax. 2010;65:442–8. https://doi.org/10.1136/thx.2009.127555
16. US Department of State Bureau of Population, Refugees, and Migration. Refugee Processing Center; 2018 [cited 2019 Feb 25]. http://ireports.wrapsnet.org
17. Busch-Armendariz N, Nale NL, Kamerr-Kerwick M, Kellison JB, Torres MIM, Cook-Heffron L, et al. Human trafficking by the numbers: the initial benchmark of prevalence and economic impact for Texas. The University of Texas at Austin, School of Social Work, Institute on Domestic Violence and Sexual Assault; 2016 [cited 2019 Feb 25]. https://repositories.lib.utexas.edu/bitstream/handle/2152/44597/idvsa-2016-human-trafficking-by-the-numbers.pdf
18. US Citizenship and Immigration Services. Refugees [cited 2019 Mar 18]. https://www.uscis.gov/humanitarian/refugees-asylum/refugees
19. US Citizenship and Immigration Services. Asylum [cited 2019 Mar 18]. https://www.uscis.gov/humanitarian/refugees-asylum/asylum
20. US Citizenship and Immigration Services. The Cuban family reunification parole program [cited 2019 Mar 18]. https://www.uscis.gov/humanitarian/humanitarian-parole/cuban-family-reunification-parole-program
21. US Department of State – Bureau of Consular Affairs. Special immigrant visas (SIVs) for Iraqi and Afghan translators/interpreters [cited 2019 Mar 18]. https://travel.state.gov/content/travel/en/us-visas/immigrate/siv-iraqi-afghan-translators-interpreters.html
22. National Human Trafficking Hotline. Federal law [cited 2019 Mar 25]. https://humantraffickinghotline.org/what-human-trafficking/federal-law
23. World Health Organization Member States. Regional offices [cited 2019 Feb 25] https://www.who.int/about/regions/en
24. Mazurek GH, Jereb J, Vernon A, LoBue P, Goldberg S, Castro K; IGRA Expert Committee; Centers for Disease Control and Prevention (CDC). Updated guidelines for using interferon gamma release assays to detect *Mycobacterium tuberculosis* infection—United States, 2010. MMWR Recomm Rep. 2010;59(RR-5):1–25.
25. Lewinsohn DM, Leonard MK, LoBue PA, Cohn DL, Daley CL, Desmond E, et al. Official American Thoracic Society/Infectious Diseases Society of America/Centers for Disease Control and Prevention clinical practice guidelines: diagnosis of tuberculosis in adults and children. Clin Infect Dis. 2017;64:e1–33. https://doi.org/10.1093/cid/ciw694
26. Graham SM, Cuevas LE, Jean-Philippe P, Browning R, Casenghi M, Detjen AK, et al. Clinical case definitions for classification of intrathoracic tuberculosis in children: an update. Clin Infect Dis. 2015;61(Suppl 3):S179–87. https://doi.org/10.1093/cid/civ581
27. Centers for Disease Control and Prevention. Tuberculosis—United States, 2018. *MMWR*. 2019 [cited 2019 May 10]. https://www.cdc.gov/mmwr/volumes/68/wr/mm6811a2.htm
28. Seddon JA, Paton J, Nademi Z, Keane D, Williams B, Williams A, et al. The impact of BCG vaccination on tuberculin skin test responses in children is age dependent: evidence to be considered when screening children for tuberculosis infection. Thorax. 2016;71:932–9. https://doi.org/10.1136/thoraxjnl-2015-207687
29. van Zyl-Smit RN, Zwerling A, Dheda K, Pai M. Within-subject variability of interferon-g assay results for tuberculosis and boosting effect of tuberculin skin testing: a systematic review. PLoS One. 2009;4:e8517. https://doi.org/10.1371/journal.pone.0008517
30. World Health Organization. Tuberculosis country profile [cited 2019 Feb 25]. https://www.who.int/tb/country/data/profiles/en/
31. Pediatric Tuberculosis Collaborative Group. Targeted tuberculin skin testing and treatment of latent tuberculosis infection in children and adolescents. Pediatrics. 2004;114(s4):1175–201. https://doi.org/10.1542/peds.2004-0809
32. Seddon JA, Shingadia D. Epidemiology and disease burden of tuberculosis in children: a global perspective. Infect Drug Resist. 2014;7:153–65.
33. Young J, O'Connor ME. Risk factors associated with latent tuberculosis infection in Mexican American children. Pediatrics. 2005;115:e647–53. https://doi.org/10.1542/peds.2004-1685
34. Gounder CR, Driver CR, Scholten JN, Shen H, Munsiff SS. Tuberculin testing and risk of tuberculosis infection among New York City schoolchildren. Pediatrics. 2003;111:e309–15. https://doi.org/10.1542/peds.111.4.e309
35. American Academy of Pediatrics Committee on Infectious Diseases. Red Book: report of the Committee on Infectious Diseases. Elk Grove Village (IL): American Academy of Pediatrics; 2018.
36. Howley MM, Painter JA, Katz DJ, Graviss EA, Reves R, Beavers SF, et al.; Tuberculosis Epidemiologic Studies Consortium. Evaluation of QuantiFERON-TB gold in-tube and tuberculin skin tests among immigrant children being screened for latent tuberculosis infection. Pediatr Infect Dis J. 2015;34:35–9. https://doi.org/10.1097/INF.0000000000000494
37. The BCG World Atlas 2nd Edition [cited 2019 Mar 14]. http://www.bcgatlas.org

Address for correspondence: Gabriella Lamb, Harvard Medical School, 333 Longwood Ave, Boston, MA 02115, USA; email: gabriella.lamb@childrens.harvard.edu

Epidemiology of Legionnaires' Disease, Hong Kong, China, 2005-2015

Yiu-Hong Leung, Chau-Kuen Lam, Yung-Yan Cheung, Chi-Wai Chan, Shuk-Kwan Chuang

We reviewed findings of clinical, epidemiologic, and environmental investigations for 288 confirmed case-patients with Legionnaires' disease reported in Hong Kong, China, during January 2005–December 2015. We found that chronic renal failure/impairment (adjusted odds ratio [aOR] 4.09), chronic pulmonary diseases (aOR 3.22), malignancy (aOR 3.04), and heart diseases (aOR 2.15) were independently associated with a higher risk for severe Legionnaires' disease. However, patients with hyperlipidemia had a lower risk for severe outcome (aOR 0.17). *Legionella* positivity rate was 22% for 1,904 water samples collected. We found a higher positivity rate in summer months (28%-30%), which corroborated with months of highest rainfalls. Our novel finding that Legionnaires' disease patients with hyperlipidemia had a lower risk for severe outcome deserves further study to confirm the observation and ascertain the underlying reason.

Legionnaires' disease is caused by bacteria of the species *Legionella*, of which *Legionella pneumophila* serogroup 1 (Lp1) is the most virulent and the most common cause of disease (*1*). Legionnaires' disease is transmitted mainly by inhalation of infectious aerosols; microaspiration of contaminated water is another possible mode of transmission (*2*,*3*).

Aerosol-generating systems, including cooling towers, whirlpools, decorative fountains, humidifiers or respiratory equipment, have been linked to Legionnaires' disease cases and outbreaks (*4*,*5*). In particular, cooling towers are the most commonly reported source of infection for Legionnaires' disease outbreaks, and hundreds of persons were affected in some outbreaks (*5*,*6*).

In Hong Kong, Legionnaires' disease has been a notifiable infectious disease since 1994. Medical practitioners are required by law to report suspected or confirmed cases to the Centre for Health Protection (CHP) of the Department of Health. A confirmed case is defined as illness in a patient who had pneumonia and confirmatory laboratory results, including detection of Lp1 antigen in urine, detection of *Legionella* species nucleic acid or culture positive for *Legionella* species in respiratory specimens, or demonstration of a ≥4-fold increase in antibody titer against *L. pneumophila* in paired serum specimens. In this study, we reviewed the clinical, epidemiologic and environmental investigation findings for all confirmed Legionnaires' disease cases reported during January 2005–December 2015.

Author affiliation: Hong Kong Department of Health, Hong Kong, China

DOI: https://doi.org/eid2608.191244

Materials and Methods

CHP conducted an epidemiologic investigation for all reported cases. We interviewed patients or their proxies and their attending doctors to obtain clinical and exposure history. We retrieved medical records of the patients to obtain supplementary clinical information, including complication and relevant microbiological and laboratory results.

In 2016, CHP adopted a risk-based strategy for environmental investigation and sampling for Legionnaires' disease cases that environmental investigation and sampling from potential sources will be conducted only if certain criteria are met (e.g., definite nosocomial case). Before that time, environmental investigation and sampling were conducted for all case-patients except those who had not stayed in Hong Kong during the entire incubation period.

Sample Collection

We conducted joint field visits with engineers of the Electrical and Mechanical Services Department to the patients' residence. We collected water samples and environmental swab specimens from potential sources, including water outlets in kitchens and bathrooms of residence, and other aerosol generating system identified (e.g., humidifier or respiratory equipment). During field visits, we also looked for aerosol–generating systems, such as decorative fountains or fresh

water cooling towers near patients' residence. Water samples and environmental swab specimens would then be collected from these systems as appropriate. If patients had been exposed to other aerosol-generating systems in other places, such as workplace, club house, or recreational facilities, we would also conduct field visits to these places to collect water samples and environmental swab specimens.

Water samples were sent to the Public Health Laboratory Centre of CHP for testing of total *Legionella* count. Environmental swab specimens for detection of *Legionella* species were tested by culture. We performed molecular typing of *L. pneumophila* isolates from human and environmental samples by using pulsed-field gel electrophoresis and later by *Legionella* sequence-based typing according to the 7-gene protocol from the European Working Group for *Legionella* Infections sequence-based typing scheme (http://www.hpa-bioinformatics.org.uk/legionella/legionella_sbt/php/sbt_homepage.php).

Data Collection

We reviewed case records of all confirmed Legionnaires' disease cases in the study period. We retrieved information including sociodemographic characteristics (age, sex, ethnicity, smoking history, and occupation), medical history, clinical manifestations, and relevant laboratory and microbiological results from case records. We obtained population occupation data for the 2011 Hong Kong Population Census from the Census and Statistics Department.

Data Analysis

We defined severe cases as those in patients who required admission to the intensive care unit for management of Legionnaires' disease or in patients who died from this disease. Other cases were regarded as mild cases.

We entered all data into a spreadsheet by using Excel version 2010 (https://www.microsoft.com). For bivariate analysis, we computed crude odds ratio for sociodemographic and other variables that might predict severe illness. We used logistic regression for multivariate analysis. We used SPSS Statistics 14.0 (https://www.ibm.com) for all data analyses.

Results

A total of 288 confirmed Legionnaires' disease cases were reported during the study period. The annual number of cases ranged from 11 to 66, and the annual incidence ranged from 0.16 cases/100,000 population to 0.91 cases/100,000 population (Figure 1). Cases with an onset during April–October accounted for 77% of all cases. However, more cases occurred during June–August (Figure 2).

Sociodemographic Characteristics and Clinical Manifestations

Median age of the patients was 64 years (range 25–96 years, interquartile range 56–74 years), and 88% of case-patients were >50 years of age. A total of 86% of patients were male, 93% were Chinese, and 61% patients were either smokers or former smokers.

Information on occupation was unknown for 3 patients. A total of 164 patients (58%) were economically inactive (housewives, retired, or unemployed). Among the 121 working patients, 12% worked as drivers and 9% worked as security guards. The corresponding percentage of persons who worked in these occupations among the total working population in the 2011 Hong Kong Population Census was 4% for drivers and 3% for security guards.

Most (230, 80%) patients had a history of chronic medical illnesses. Hypertension (56%), diabetes (38%), and heart diseases (24%) were the most commonly reported illnesses (Table 1). All except 1 patient

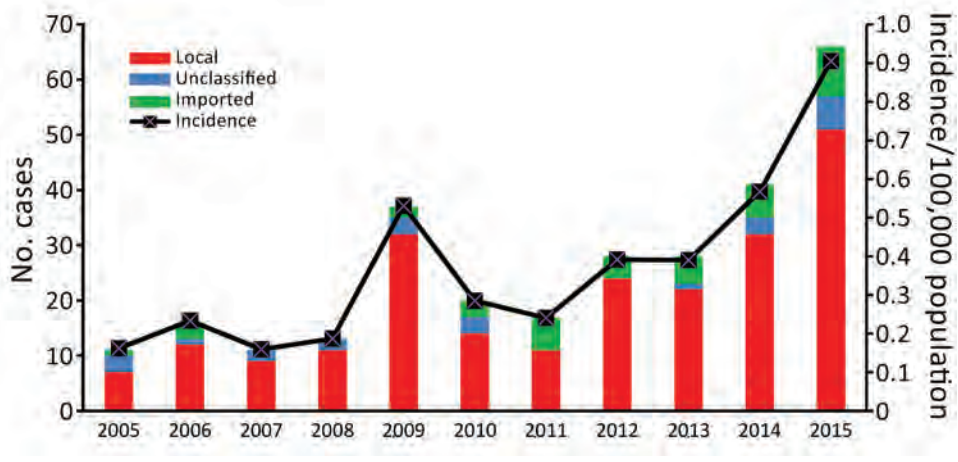

Figure 1. Annual number and incidence of Legionnaires' disease cases, Hong Kong, China, 2005–2015.

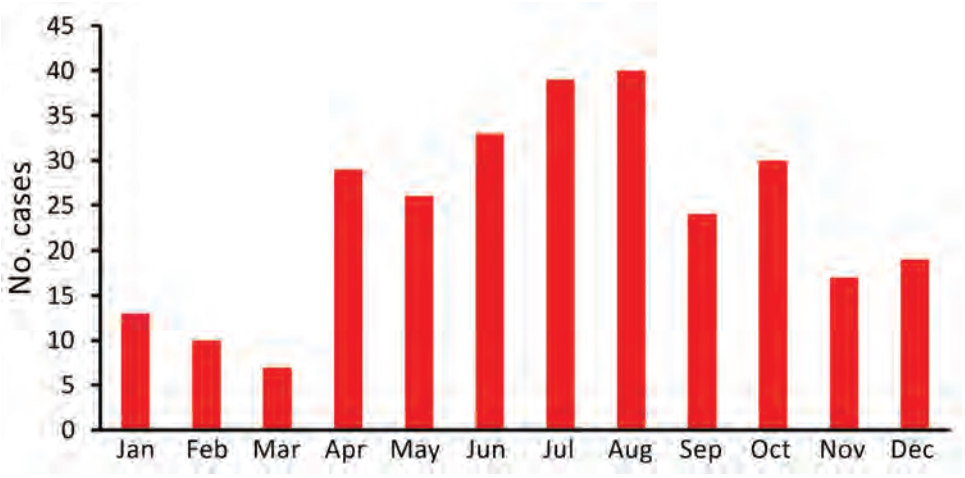

Figure 2. Number of Legionnaires' disease cases by month of onset, Hong Kong, China, 2005–2015. The onset date for 1 case was unknown.

required hospital admission, and the duration of hospital stay ranged from 2 to 125 days (median 12 days). Fever (94%), cough (85%), and shortness of breath (65%) were the most commonly reported symptoms. Gastrointestinal symptoms were reported only by ≈20% of patients.

Respiratory failure developed in 119 (41%) patients, among whom 99 patients required intubation and mechanical ventilation. Deterioration of renal function developed in 149 (52%) patients, of whom 58 (39%) patients required renal replacement therapy. Other reported complications included septic shock (29%), acute coronary syndrome (6%), gastrointestinal bleeding (4%), and rhabdomyolysis (3%). A total of 114 (40%) patients required admission to an intensive care unit for management. A total of 42 patients died from Legionnaires' disease. The case-fatality rate was 15%.

A total of 124 patients were classified as having severe cases and 164 patients as having mild cases. We showed by using bivariate analysis that patients with chronic renal failure/impairment, chronic pulmonary diseases, heart diseases, and hyperlipidemia had major associations with severe disease (Table 1). We showed by using multivariate analysis that patients with chronic renal failure/impairment (adjusted odds ratio [aOR] 4.09, 95% CI 1.81–9.27), chronic pulmonary diseases (aOR 3.22, 95% CI 1.10–9.42), malignancy (aOR 3.04, 95% CI 1.17–7.91), and heart diseases (aOR 2.15, 95% CI 1.12–4.13) were independently associated with a higher risk for severe disease. In contrast, patients who had hyperlipidemia had lower risk for severe outcome (aOR 0.17, 95% CI 0.08–0.40).

Microbiological Investigation

We provide the annual number of Legionnaires' disease cases by confirmatory microbiological testing (Figure 3). Before 2008, ≈36%–63% of cases were confirmed by serologic analysis. Subsequently, most cases were confirmed by urine antigen test (UAT). An increasing number of cases since 2011 were also confirmed by PCR for respiratory specimens. Overall, 74% cases were confirmed by UAT, 16% by serologic analysis, and 9% by PCR. For the 26 case-

Table 1. Bivariate and multivariate analysis of factors associated with severe outcome of Legionnaires' disease cases, Hong Kong, China, 2005–2015

Factor	Total, no. (%), n = 288	Severe, no. (%), n = 124	Mild, no. (%), n = 164	Crude odds ratio (95% CI)	Adjusted odds ratio (95% CI)
Male sex	248 (86)	108 (87)	140 (85)	1.16 (0.59–2.29)	1.43 (0.61–3.36)
Age >64 y	140 (49)	67 (54)	73 (45)	1.47 (0.92–2.34)	1.17 (0.66–2.05)
Smoker/former smoker	173 (61)*	79 (65)	94 (58)	1.38 (0.85–2.25)	1.55 (0.86–2.78)
History of chronic medical illnesses					
Chronic renal failure/impairment	46 (16)	30 (24)	16 (10)	2.95 (1.53–5.71)	4.09 (1.81–9.27)
Chronic pulmonary diseases	22 (8)	15 (12)	7 (4)	3.09 (1.22–7.82)	3.22 (1.10–9.42)
Malignancy	25 (9)	15 (12)	10 (6)	2.12 (0.92–4.89)	3.04 (1.17–7.91)
Heart diseases	69 (24)	40 (32)	29 (18)	2.22 (1.28–3.84)	2.15 (1.12–4.13)
Hyperlipidemia	53 (18)	13 (11)	40 (24)	0.36 (0.19–0.71)	0.17 (0.08–0.40)
Diabetes	109 (38)	49 (40)	60 (37)	1.13 (0.70–1.83)	0.94 (0.52–1.69)
Hypertension	161 (56)	77 (62)	84 (51)	1.56 (0.97–2.51)	1.62 (0.88–2.96)
Immunosuppression	22 (8)	10 (8)	12 (7)	1.11 (0.46–2.66)	0.75 (0.28–2.00)

*Information for 4 patients was unknown.

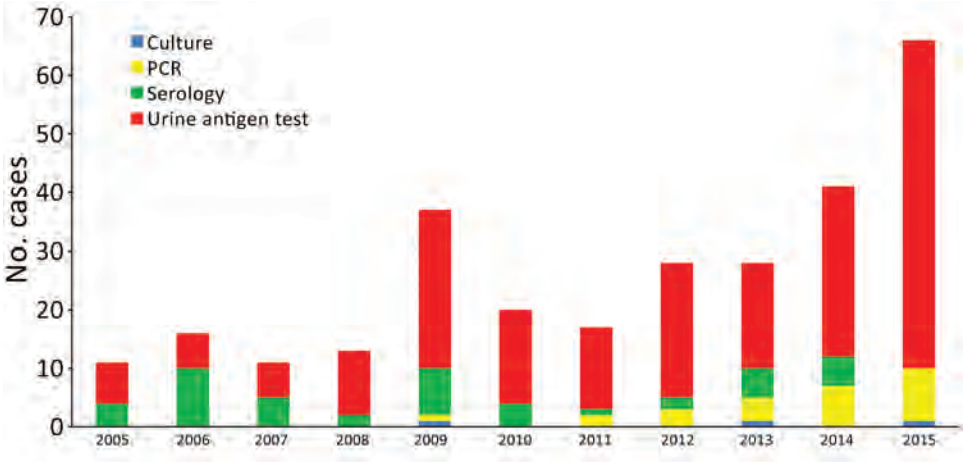

Figure 3. Number of Legionnaires' disease cases by confirmatory microbiological testing, Hong Kong, China, 2005–2015.

patients given a diagnosis by PCR, 18 of them also had a UAT performed; only 2 of these patients had a positive result.

We analyzed respiratory specimens for *Legionella* culture for 166 (58%) patients and *L. pneumophila* was isolated for 71 (43%) patients. Among them, 69 had Lp1, 1 had *L. pneumophila* nonserogroup 1 (non-Lp1), and 1 had an unknown *L. pneumophila* serogroup. Among 16 case-patients given a diagnosis by PCR and negative UAT results, a respiratory specimen from 1 patient was culture positive for non-Lp1 and a specimen from another patient was positive for an unknown Lp serogroup. Another 2 patients had Lp1 nucleic acid detected by additional molecular testing.

Environmental Investigations

Among the 288 cases, 256 had environmental investigations performed. A total of 1,904 water samples and 892 environmental swab specimens were collected from potential sources. The overall *Legionella* positivity rate for water samples was 22% (425/1,904), and it was generally higher for samples collected during June–August (28%–30%) (Table 2). Environmental investigations were conducted at 243 households; 85 (35%) had ≥1 water sample positive for *Legionella* species.

Regarding environmental swab specimens, 127 (14%) were positive for *Legionella* species. For collection sites, surface of water tap aerator, internal surface of water tap, shower head, or shower hose constituted ≈80% (101/127) of the positive samples. The positivity rate for water taps was 22% and that for showers was 6% (Table 3). In addition, we found that >30% of samples collected from water filters were positive for *Legionella* species. From the 240 households with environmental swab specimens collected, 56 (23%) had ≥1 environmental swab specimen positive for *Legionella* species.

Source of Infection

We found that 78% (225) of case-patients contracted the infection locally, and 14% (39) cases were classified as imported cases (Figure 1). The source of infection of the remaining 8% of case-patients was regarded as unclassified because patients had stayed in Hong Kong and outside Hong Kong during the incubation period and had no exposure history for epidemiologic classification.

There were 3 nosocomial cases in patients who had stayed in a hospital for the entire incubation period. Disinfection of the relevant potable water system in the hospital by superheating and flushing and/or shock hyperchlorination was performed for all 3 case-patients. In addition, 11 case-patients were residents of long-term care facilities. Environmental investigations conducted failed to identify the source of infection for any of these case-patients.

All 288 patients had sporadic cases for which no outbreak was identified. Molecular typing was performed for 25 case-patients; only 1 case-patient had matching human and environmental samples. The patient was a 66 year-old retired man who had multiple illnesses. Lp1 was isolated from his tracheal aspirate and bronchoalveolar lavage; a water sample collected from his kitchen water tap, which had a filter; and a swab sample from the container of a respirator in his home. We found that the Lp1 isolates from the patient and the water samples had indistinguishable patterns by pulsed-field gel electrophoresis.

Discussion

The incidence of Legionnaires' disease in Hong Kong increased during the study period, showing a >4-fold increase from 0.16 cases/100,000 population during 2005 to 0.91 cases/100,000 population during 2015. A similar increasing trend has been observed in the United States and countries in Europe since the 2000s.

In the United States, the incidence of legionellosis increased from 0.42 cases/100,000 population during 2000 to 1.62 cases/100,000 population during 2014 (*7*). In Europe, Legionnaires' disease incidence increased from 0.54 cases/100,000 population during 2000 to 1.4 cases/100,000 population during 2015 (*8*,*9*).

The true incidence of Legionnaires' disease was reported to be underestimated (*4*,*10*). The exact reason for the increasing incidence of Legionnaires' disease is not known but is believed to be related to the increasing population of persons at high risk for infection, improved diagnosis and reporting, and increased use of UAT (*11*).

In Hong Kong, increasing incidence of Legionnaires' disease during the study period might be related to increased use of more sensitive diagnostic tests. During 2005–2008, the average percentage of cases diagnosed by UAT was 50%, which increased to 78% during 2009–2015. The number of UATs performed showed an increase of 127% during 2015 compared with 2010; the annual increase was 11%–28%. The percentage positive results for UATs performed in the corresponding period decreased from 1.2% to 0.9%. In contrast, the number of reported Legionnaires' disease cases increased from 20 during 2010 to 66 during 2015.

We also observed an increased number of cases diagnosed by PCR from 2011 onward. Among the 18 PCR-diagnosed cases for which a UAT was performed, only 2 showed positive UAT results, which implied that 16 of these PCR-diagnosed cases would not have been diagnosed if PCR had not been performed. With the development of commercially available multiplex PCR assays for respiratory pathogens, including *Legionella* species (*12*), it is expected that the Legionnaires' disease incidence will continue to increase, and the percentage of Legionnaires' disease cases diagnosed by PCR will also increase.

The clinical and epidemiologic characteristics of Legionnaires' disease cases in Hong Kong were similar to those reported in other localities. Legionnaires' disease incidence in Hong Kong showed an apparent seasonal trend with peak incidence during summer months. A similar situation has been reported for the United States, Europe, Canada, and Japan (*13*). Associations between legionellosis and several weather variables had been reported; the most consistent results are related to rainfall, and studies have identified small but major increases in risk for legionellosis with increased rainfall after a lag time of 1–2 weeks (*14*). In Hong Kong, ≈80% of rainfall occurred during May–September, and June–August had the greatest rainfall (*15*). Apart from Legionnaires' disease incidence, our study also showed that water samples collected during June–August had the highest *Legionella* positivity rate.

Male sex, age >50 years, smoking, and a history of chronic diseases are well-established risk factors for acquiring Legionnaires' disease (*4*,*10*,*13*). Our study showed consistent findings; 86% of patients were men and 88% of patients were >50 years of age. In addition, 61% of patients were either smokers or former smokers, and 80% had chronic medical illnesses.

In contrast, studies on the factors associated with severe outcome for Legionnaires' disease are less common. Marston et al. reported that older age, male sex, nosocomial infection, immunosuppression, end-stage renal disease, and cancer were independently associated with death caused by Legionnaires' disease (*16*). Chidiac et al. reported that older age and female sex were independent predictors of death for community-acquired legionellosis cases in France (*17*). Our findings demonstrated that age and sex of patients were not associated with severe outcomes, but a history of certain chronic medical illnesses was a major predictor of severe outcomes. We found that chronic renal failure/impairment (aOR 4.09), chronic pulmonary diseases (aOR 3.22), malignancy (aOR 3.04), and heart diseases (aOR 2.15) were independent risk factors for severe disease.

We also found that patients with hyperlipidemia had an 83% lower risk for severe outcomes than persons without this illness. This finding was unexpected. We postulate that this finding might be related to use of statins among patients with hyperlipidemia. In addition to its lipid-lowering effect, statins have been shown to attenuate acute lung injury by modulating neutrophil function, reducing proinflammatory cytokine release, and reducing vascular leak in experimental and animal studies; current evidence suggests that pretreatment with statins might have a beneficial effect in prevention of pneumonia and reducing severity of community-acquired pneumonia (*18*). We found that 66% (35/53) of patients with hyperlipidemia were documented to have used statins. Subgroup analysis showed that a lower percentage of persons who used statins had severe disease (23%, 8/35) than persons who did not use statins (28%, 5/18). However, these results were not significant, which might be caused by the small sample size. Additional studies should be conducted to confirm our hypothesis.

Delay in starting appropriate antimicrobial therapy could also be a risk factor for poor disease outcome. Unfortunately, our data did not capture the date of Legionnaires' disease diagnosis and date of

Table 2. *Legionella* culture results of water samples by month of collection, Hong Kong, China, 2005–2015

Month	No. water samples positive for *Legionella*/no. tested (%)
January	19/109 (17)
February	8/45 (18)
March	6/32 (19)
April	26/155 (17)
May	29/129 (23)
June	49/167 (29)
July	76/275 (28)
August	71/236 (30)
September	26/186 (14)
October	21/178 (12)
November	31/172 (18)
December	63/220 (29)*
Total	425/1,904 (22)

*For 1 case-patient, 39 of 43 water samples collected from patient's workplace were positive for *Legionella* species. The percentage positive for December is 14% if this case-patient is excluded from analysis.

starting appropriate antimicrobial therapy, which is a limitation regarding the analysis of risk factors associated with severe outcome.

In our study, we found that patients who worked as drivers among working patients was overrepresented when compared with the general working population (12% vs. 4%). Several studies had reported being a professional driver as a risk factor for Legionnaires' disease. Den Boer et al. found that being a professional driver was an independent risk factor for Legionnaires' disease in a case–control study of sporadic community-acquired Legionnaires' disease cases in the Netherlands during July 1998–June 2001 (*19*). A study on sporadic Legionnaires' disease cases with onset during 2001–2006 in the United Kingdom also found that professional drivers had ≈5 times increased risk for Legionnaires' disease (*20*).

The underlying reason for the association between working as a driver and Legionnaires' disease is not known, but studies have reported that the air conditioning system, cabin air filter, or windshield washer fluid might be potential sources of transmission for *Legionella* species. Sakamoto et al. reported that a *Legionella* species was detected in 50% of the swab samples collected from the evaporator components of car air conditioning systems (*21*). Alexandropoulou et al. found that 32% of car cabin air filters tested were colonized with *L. pneumophila* (*22*). Another study reported that *Legionella* species was detected in 84% of windshield washer fluid samples collected from elementary school buses, and culturable cells were detected in aerosolized washer fluid during spraying of washer fluid (*23*).

Residential water supplies had been implicated as the source of infection for Legionnaires' disease (*24*). Other studies have reported *Legionella* colonization in 6%–37% of residential potable water systems (*25*–*28*). Our study found that 35% of households had ≥1 water sample positive for *Legionella* species. Our finding was higher than that for another study in Hong Kong, which reported *Legionella* colonization in 22% of households surveyed (*29*). Apart from water samples, we also found that 23% of households had environmental swab specimens positive for *Legionella* species. Despite the high prevalence of households with *Legionella* colonization, matching *Legionella* isolates from human and environmental samples by molecular typing was found for only 1 case.

We also found that 32% of environmental swab specimens collected from water filters, 22% from water taps, and 6% from shower facilities were positive for *Legionella* species, but none of these samples were implicated as the source of infection for the cases in this investigation. Studies on the *Legionella* prevalence in swab samples have been reported rarely in the literature. A study from Japan reported that only 1 of 90 swab samples collected from 19 households were positive for *Legionella* species (*28*). The high prevalence of *Legionella* colonization in water fixtures deserves attention, and further studies are needed to delineate its relationship with Legionnaires' disease in patients.

All cases of Legionnaires' disease during the study period were sporadic, and no outbreak was detected in Hong Kong. The source of infection could not be determined for nearly all cases. However, this result might have been caused by the fact that only ≈10% of cases with environmental investigations conducted had positive isolates from human and environmental samples such that molecular typing could be performed because only 58% of case-patients had lower respiratory tract samples that could be tested for *Legionella* species.

Some patients could not produce lower respiratory tract specimens, and in some instances, samples obtained were used only for bacterial culture. Communication and follow-up with the attending physicians

Table 3. *Legionella* culture results of environmental swab specimens by site of collection, Hong Kong, China, 2005–2015

Site	No. water samples positive for *Legionella*/no. tested (%)
Water tap	74/332 (22)
Water tap aerator	47/248 (19)
Internal surface of water tap	27/84 (32)
Water filter	10/31 (32)
Shower*	27/459 (6)
Shower head	12/295 (4)
Shower hose	14/154 (9)
Water dispenser	2/17 (11)
Other	14/37 (28)
Total	127/892 (14)

*One sample was collected from shower head and shower hose.

and microbiology laboratories should be enhanced such that lower respiratory tract samples are collected for all Legionnaires' disease patients to test for *Legionella* species to facilitate epidemiologic investigations.

In Hong Kong, Legionnaires' disease incidence was increasing during the study period, but all cases were sporadic, and no outbreak was recorded. The apparent upward trend in incidence might be explained by increased use of more sensitive diagnostic tests. Legionnaires' disease patients with chronic renal failure/impairment, chronic pulmonary diseases, malignancy, or heart diseases are at a higher risk for severe disease. Patients who had hyperlipidemia were found to have a lower risk for severe outcome, which is a novel finding that deserves further study to confirm the observation and ascertain the underlying reason. Environmental investigations showed that the *Legionella* positivity rate in water samples was higher in summer months, which corroborated with the seasonality of human infection and months that had greatest rainfall. Surveillance and epidemiologic investigation of Legionnaires' disease cases is crucial in monitoring trends and other epidemiologic characteristics and for outbreak detection, which can contribute to formulation of prevention and control strategies for this disease.

Acknowledgments

We thank the healthcare workers for managing patients with Legionnaires' disease and the staff of the Department of Health and Electrical and Mechanical Services Department for their contributions to the investigation and control of Legionnaires' disease in Hong Kong.

Disclaimer

The opinions expressed by authors contributing to this manuscript do not necessarily reflect the opinions of the Department of Health, Hong Kong, China.

About the Author

Dr. Leung is a public health specialist at the Department of Health, Hong Kong, China. His primary research interests are investigation and control of infectious diseases.

References

1. Stout JE, Yu VL. Legionellosis. N Engl J Med. 1997;337:682–7. https://doi.org/10.1056/NEJM199709043371006
2. Fraser DW. Legionellosis: evidence of airborne transmission. Ann N Y Acad Sci. 1980;353:61–6. https://doi.org/10.1111/j.1749-6632.1980.tb18906.x
3. Blatt SP, Parkinson MD, Pace E, Hoffman P, Dolan D, Lauderdale P, et al. Nosocomial Legionnaires' disease: aspiration as a primary mode of disease acquisition. Am J Med. 1993;95:16–22. https://doi.org/10.1016/0002-9343(93)90227-G
4. Cunha BA, Burillo A, Bouza E. Legionnaires' disease. Lancet. 2016;387:376–85. https://doi.org/10.1016/S0140-6736(15)60078-2
5. van Heijnsbergen E, Schalk JA, Euser SM, Brandsema PS, den Boer JW, de Roda Husman AM. Confirmed and potential sources of *Legionella* reviewed. Environ Sci Technol. 2015;49:4797–815. https://doi.org/10.1021/acs.est.5b00142
6. Walser SM, Gerstner DG, Brenner B, Höller C, Liebl B, Herr CE. Assessing the environmental health relevance of cooling towers: a systematic review of legionellosis outbreaks. Int J Hyg Environ Health. 2014;217:145–54. https://doi.org/10.1016/j.ijheh.2013.08.002
7. Garrison LE, Kunz JM, Cooley LA, Moore MR, Lucas C, Schrag S, et al. Vital signs: deficiencies in environmental control identified in outbreaks of Legionnaires' disease—North America, 2000–2014. MMWR Morb Mortal Wkly Rep. 2016;65:576–84. https://doi.org/10.15585/mmwr.mm6522e1
8. Joseph CA; European Working Group for Legionella Infections. Legionnaires' disease in Europe 2000–2002. Epidemiol Infect. 2004;132:417–24. https://doi.org/10.1017/S0950268804002018
9. European Centre for Disease Prevention and Control. Annual epidemiological report for 2015. Legionnaires' disease [cited 2019 Aug 25]. https://ecdc.europa.eu/sites/portal/files/documents/AER_for_2015-legionnaires-disease_0.pdf
10. Burillo A, Pedro-Botet ML, Bouza E. Microbiology and epidemiology of Legionnaire's disease. Infect Dis Clin North Am. 2017;31:7–27. https://doi.org/10.1016/j.idc.2016.10.002
11. Centers for Disease Control and Prevention. Legionellosis—United States, 2000–2009. MMWR Morb Mortal Wkly Rep. 2011;60:1083–6.
12. Wagner K, Springer B, Imkamp F, Opota O, Greub G, Keller PM. Detection of respiratory bacterial pathogens causing atypical pneumonia by multiplex Lightmix RT-PCR. Int J Med Microbiol. 2018;308:317–23. https://doi.org/10.1016/j.ijmm.2018.01.010
13. Phin N, Parry-Ford F, Harrison T, Stagg HR, Zhang N, Kumar K, et al. Epidemiology and clinical management of Legionnaires' disease. Lancet Infect Dis. 2014;14:1011–21. https://doi.org/10.1016/S1473-3099(14)70713-3
14. Sakamoto R. Legionnaire's disease, weather and climate. Bull World Health Organ. 2015;93:435–6. https://doi.org/10.2471/BLT.14.142299
15. Hong Kong Observatory. Climate of Hong Kong [cited 2019 Aug 25]. https://www.weather.gov.hk/cis/climahk_e.htm
16. Marston BJ, Lipman HB, Breiman RF. Surveillance for Legionnaires' disease. Risk factors for morbidity and mortality. Arch Intern Med. 1994;154:2417–22. https://doi.org/10.1001/archinte.1994.00420210049006
17. Chidiac C, Che D, Pires-Cronenberger S, Jarraud S, Campèse C, Bissery A, et al.; French Legionnaires' Disease Study Group. Factors associated with hospital mortality in community-acquired legionellosis in France. Eur Respir J. 2012;39:963–70. https://doi.org/10.1183/09031936.00076911
18. Chalmers JD, Short PM, Mandal P, Akram AR, Hill AT. Statins in community acquired pneumonia: evidence from experimental and clinical studies. Respir Med. 2010;104:1081–91. https://doi.org/10.1016/j.rmed.2010.04.005
19. Den Boer JW, Nijhof J, Friesema I. Risk factors for sporadic community-acquired Legionnaires' disease. A 3-year national case-control study. Public Health. 2006;120:566–71. https://doi.org/10.1016/j.puhe.2006.03.009

20. Wallensten A, Oliver I, Ricketts K, Kafatos G, Stuart JM, Joseph C. Windscreen wiper fluid without added screenwash in motor vehicles: a newly identified risk factor for Legionnaires' disease. Eur J Epidemiol. 2010;25:661–5. https://doi.org/10.1007/s10654-010-9471-3
21. Sakamoto R, Ohno A, Nakahara T, Satomura K, Iwanaga S, Kouyama Y, et al. Is driving a car a risk for Legionnaires' disease? Epidemiol Infect. 2009;137:1615–22. https://doi.org/10.1017/S0950268809002568
22. Alexandropoulou IG, Konstantinidis TG, Parasidis TA, Nikolaidis C, Panopoulou M, Constantinidis TC. First report of *Legionella pneumophila* in car cabin air filters. Are these a potential exposure pathway for professional drivers? Scand J Infect Dis. 2013;45:948–52. https://doi.org/10.3109/00365548.2013.840917
23. Schwake DO, Alum A, Abbaszadegan M. Automobile windshield washer fluid: a potential source of transmission for *Legionella*. Sci Total Environ. 2015;526:271–7. https://doi.org/10.1016/j.scitotenv.2015.03.122
24. Stout JE, Yu VL, Muraca P, Joly J, Troup N, Tompkins LS. Potable water as a cause of sporadic cases of community-acquired Legionnaires' disease. N Engl J Med. 1992;326:151–5. https://doi.org/10.1056/NEJM199201163260302
25. Stout JE, Yu VL, Yee YC, Vaccarello S, Diven W, Lee TC. *Legionella pneumophila* in residential water supplies: environmental surveillance with clinical assessment for Legionnaires' disease. Epidemiol Infect. 1992;109:49–57.
26. Alary M, Joly JR. Risk factors for contamination of domestic hot water systems by legionellae. Appl Environ Microbiol. 1991;57:2360–7. https://doi.org/10.1128/AEM.57.8.2360-2367.1991
27. Codony F, Alvarez J, Oliva JM, Ciurana B, Company M, Camps N, et al. Factors promoting colonization by legionellae in residential water distribution systems: an environmental case-control survey. Eur J Clin Microbiol Infect Dis. 2002;21:717–21. https://doi.org/10.1007/s10096-002-0789-y
28. Kuroki T, Watanabe Y, Teranishi H, Izumiyama S, Amemura-Maekawa J, Kura F. *Legionella* prevalence and risk of legionellosis in Japanese households. Epidemiol Infect. 2017;145:1398–408. https://doi.org/10.1017/S0950268817000036
29. Cheng VC, Wong SS, Chen JH, Chan JF, To KK, Poon RW, et al. An unprecedented outbreak investigation for nosocomial and community-acquired legionellosis in Hong Kong. Chin Med J (Engl). 2012;125:4283–90.

Address for correspondence: Yiu-Hong Leung, Department of Health, Ste 1101, 11/F, AIA Kowloon Tower, Landmark East, 100 How Ming St, Kwun Tong, Hong Kong, China; email: fansh@graduate.hku.hk

Rise in Babesiosis Cases, Pennsylvania, USA, 2005–2018

David Ingram, Tonya Crook

Babesiosis is an emerging infection in the state of Pennsylvania, and clinicians need to be made aware of its clinical manifestations as well as the risk factors associated with severe disease. Before 2010, our tertiary academic center in central Pennsylvania previously saw zero cases of babesiosis. We saw our first confirmed case of *Babesia* infection acquired in Pennsylvania in 2011; we recorded 2 confirmed cases in 2017 and 4 confirmed cases in 2018. All 4 cases from 2018 were thought to be acquired in southcentral Pennsylvania counties, whereas prior reports of cases were predominately in the southeast and northeast counties of the state.

Babesiosis, a tickborne infection caused by protozoan parasites that infect erythrocytes, has been identified as an emerging infection of concern in the state of Pennsylvania, USA (*1*–*4*). Infection with *Babesia* parasites can cause a range of symptoms, including fever, myalgias, and fatigue. Although many patients are asymptomatic, the infection can be severe in some persons, especially those who are >50 years of age, immunosuppressed, or asplenic (*1*,*5*,*6*).

The most common species known to cause human infection in the United States is *Babesia microti*, which is transmitted by the *Ixodes scapularis* tick (blacklegged tick). Transmission can also occur through blood transfusion; *B. microti* is currently the most common pathogen transmitted through the blood supply in the United States (*7*,*8*). The highest incidence of human infection has been reported in the Northeast and upper Midwest states (*9*). Until fairly recently, few cases of *B. microti* infection have occurred in Pennsylvania. However, new data suggest not only increased prevalence of ticks harboring *B. microti* within the state (*10*) but also a rise in the number of cases seen in clinical practice (*2*–*4*).

Babesiosis is not a mandatory reportable infection in Pennsylvania; however, the Pennsylvania Department of Health does receive reports of cases of babesiosis from healthcare providers that elect to do so. Among these recounted cases, the department has seen a 20-fold increase in the past 12 years (E. Negrón, Pennsylvania Department of Health, pers. comm., 2018 Aug 1). A similar trend was documented in a recent study from February 2019 involving a 4-hospital system in southeastern Pennsylvania, where clinicians saw an increase in cases from ≤7 cases annually during 2008–2014 to 26 cases in 2015 (*4*).

We have suspected a similar increase in the number of cases at our institution, Penn State Milton S. Hershey Medical Center (Hershey, PA, USA), which is a tertiary academic center located in central Pennsylvania. We performed a retrospective review of all of the confirmed cases of babesiosis at our institution for the period 2005–2018 to determine whether we were truly seeing an increased number of cases and to highlight the demographic and clinical characteristics of these patients.

Methods

We obtained a list of all patients who had International Classification of Diseases, 9th Revision (ICD-9) (088.82), and International Classification of Diseases, 10th Revision (ICD-10) (B60.0), diagnostic codes for babesiosis as well as patients that had *Babesia* serologic tests ordered at Hershey Medical Center during 2005–2018. The list consisted of 352 patient encounters, some of which were duplicates. We retrospectively chart reviewed each patient encounter to identify confirmed cases of babesiosis. Only patients who met Centers for Disease Control and Prevention criteria for confirmed cases of babesiosis were included in our study (Table 1): patients who had confirmatory laboratory results (i.e., parasite seen on peripheral smear, positive PCR from blood, or both) and met ≥1 of the objective or subjective clinical evidence criteria. Although we did not use positive serologic test results as a part of our diagnostic criteria, identifying patients who had serologic tests ordered was used to increase the number

Author affiliation: Penn State Health Milton S. Hershey Medical Center, Hershey, Pennsylvania, USA

DOI: https://doi.org/10.3201/eid2608.191293

Table 1. Centers for Disease Control and Prevention criteria for diagnosis of confirmed cases of babesiosis, 2011*

Laboratory criteria for diagnosis	Clinical criteria for diagnosis
Identification of intraerythrocytic *Babesia* organisms by light microscopy in a Giemsa, Wright, or Wright-Giemsa–stained blood smear; OR detection of *Babesia microti* DNA in a whole blood specimen by PCR; OR detection of *Babesia* spp. genomic sequences in a whole blood specimen by nucleic acid amplification; OR Isolation of *Babesia* organisms from a whole blood specimen by animal inoculation.	Objective: ≥1 of the following: fever, anemia, or thrombocytopenia Subjective: ≥1 of the following: chills, sweats, headache, myalgia, or arthralgia.

*Includes cases that have confirmatory laboratory results and meet ≥1 of the objective or subjective clinical evidence criteria, regardless of the mode of transmission (can include clinically manifest cases in transfusion recipients or blood donors). Full case definition available at https://wwwn.cdc.gov/nndss/conditions/babesiosis/case-definition/2011.

of patients in our initial cohort. We noted inconsistencies in the way blood smears and PCR testing were ordered in our electronic medical records, and we wanted to ensure we did not miss any cases.

The *Babesia* serologic testing used at Hershey Medical Center is the indirect fluorescent antibody (IFA) test. This test is specific for *B. microti* species. We considered a titer ≥1:256 to be positive on the basis of the titer value determined to be supportive of the diagnosis of babesiosis according to Centers for Disease Control and Prevention laboratory criteria (*11*). From our initial list of 352 patient encounters, we identified 8 cases of confirmed babesiosis. We maintained demographic, clinical, and laboratory data in a REDCap Electronic Database (*12*). Research protocols were reviewed and approved by the Penn State College of Medicine Institutional Review Board.

The Patients

Demographic Characteristics

Of the 8 confirmed cases of babesiosis seen at our institution, 7 of the cases were acquired in the state of Pennsylvania (Table 2). One case was thought to have been acquired in Massachusetts. Of the 7 cases in Pennsylvania, more than half (4/7) were acquired in south-central Pennsylvania counties; 2 cases were from northeast counties, and 1 case was from a southeast county (Figure 1). No cases were reported during 2005–2010, 1 case was reported in 2011, 1 case in 2015, 2 cases in 2017, and 4 cases in 2018. All cases were diagnosed during the summer months. All but 1 of the patients were ≥60 years of age at the time of diagnosis. The median age at time of diagnosis was 70 years (range 20–77 years), and 75% of the patients were male. Only 1 patient reported a history of tick bite preceding infection. Six of 8 patients reported history of outdoor activity before seeking care. None of the patients had history of recent blood transfusion.

Clinical Manifestations

The cohort included 2 patients with a history of splenectomy and 1 patient with a history of diabetes. Most of the patients were immunocompetent. None of the patients were on immunosuppressive therapy. No HIV patients or posttransplant patients were in the cohort. Most patients reported fever (6/8) and malaise (5/8). Other symptoms included myalgias or arthralgias (2/8), anorexia (2/8), rash (1/8), headache (1/8), nausea or vomiting (1/8), diarrhea (1/8), and respiratory failure (1/8). The average time from symptom onset to diagnosis was 9.7 days. The most common laboratory abnormalities seen were anemia, thrombocytopenia, transaminitis, and hyperbilirubinemia. Anemia was seen in all of the patients; average hemoglobin level was 9.8 g/dL (reference range 13–16 g/dL) (Table 3). Thrombocytopenia was seen in 7/8 patients; average platelet count was 90.8 × 10^9/L (reference range 150–350 × 10^9/L). Most of the patients (6/8) had platelet counts of ≤75. Elevated alanine aminotransferase and aspartate aminotransferase were

Table 2. Demographic characteristics of 8 patients with confirmed babesiosis, Penn State Health Milton S. Hershey Medical Center, Hershey, Pennsylvania, USA, 2005–2018

Patient no.	Age, y/sex	Date patient sought care	Location of infection acquisition*	History of tick bite	History of outdoor activity	History of recent transfusion
1	77/F	2011 Jul 1	Northampton County	No	No	No
2	75/M	2015 Aug 4	Berks County	No	Yes	No
3	70/M	2017 Jun 30	Massachusetts	Yes	Yes	No
4	75/M	2017 Jul 19	Lehigh County	No	Yes	No
5	63/M	2018 Jun 19	York County	No	Yes	No
6	20/M	2018 Jun 27	Cumberland County	No	Yes	No
7	70/F	2018 Jul 2	Lebanon County	No	No	Unknown
8	65/M	2018 Jul 21	Cumberland County	No	Yes	No

*All counties are in Pennsylvania.

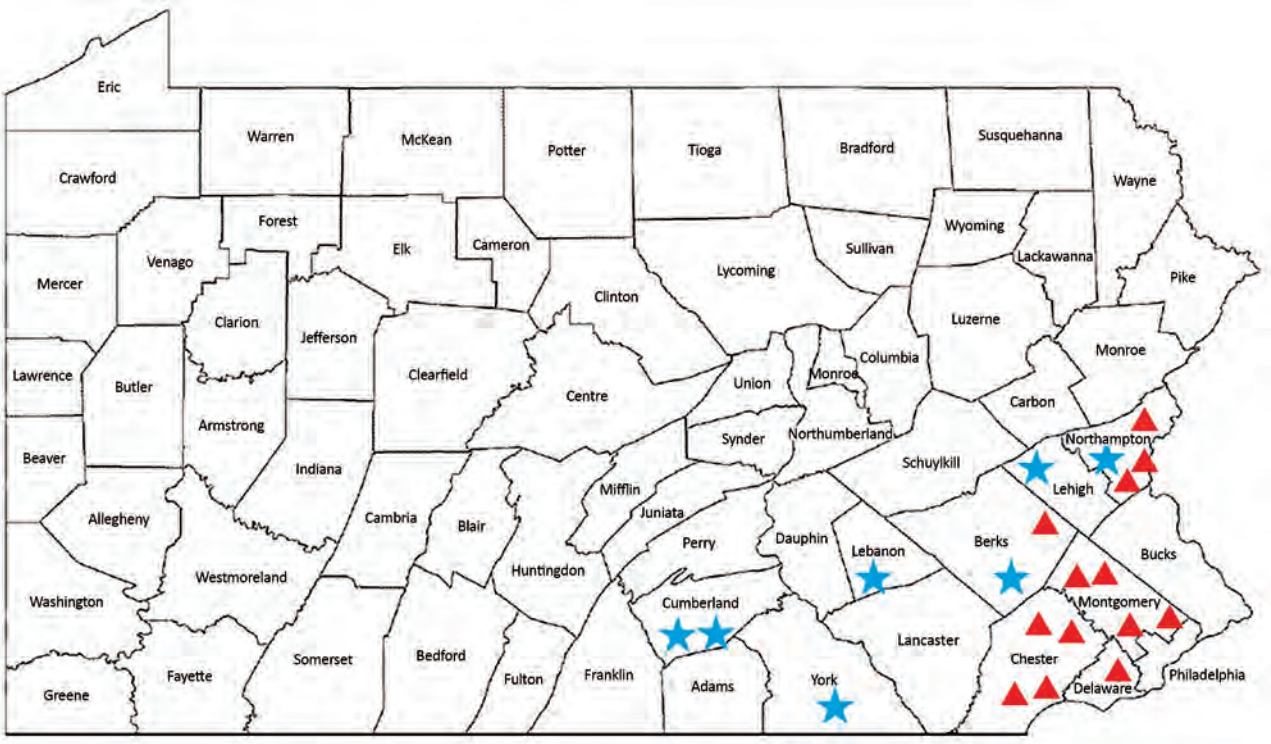

Figure 1. Counties where confirmed babesiosis cases were thought to have been acquired during 2011–2018 according to previous studies (*2*–*4*) compared with cases seen at Penn State Health Milton S. Hershey Medical Center, Hershey, Pennsylvania, USA, during 2005–2018. Red triangles indicate cases from previous studies (not all cases shown); blue stars indicate cases seen at Hershey Medical Center.

seen in 7/8 patients; average alanine aminotransferase was 72 U/L (reference range 0–40 U/L) and average aspartate aminotransferase 176.6 U/L (reference range 0–40 U/L). Hyperbilirubinemia was also seen in 7/8 patients; average bilirubin level was 6.4 mg/dL (reference range 0–1.2 mg/dL).

Diagnosis and Treatment

All 8 patients had blood smears that were positive for identification of intraerythrocytic *Babesia* organisms (Table 4). Most (6/8) patients had an initial parasitemia of >10% (average parasitemia 18%). Three patients had PCR results obtained, all of which were positive. Six of the 8 patients had serologic test results obtained, and serum samples from all 6 patients were reactive for IgG (titers ≥1:256).

Concurrent Lyme disease was noted in half (4/8) of patients. Patients were screened for Lyme disease by using ELISA; if the result was positive, then a Western blot was performed. Patients had Lyme disease diagnosed if they had positive ELISA results and positive IgM or IgG results on Western blot.

Most (7/8) patients received a combination of azithromycin and atovaquone for treatment. Three patients received clindamycin and quinine as part of their treatment; of these 3 patients, 1 patient received clindamycin and quinine alone for the duration of their therapy, and 2 patients were switched to azithromycin and atovaquone because of persistent parasitemia. Two of the patients who received clindamycin and quinine (1 of whom was switched to azithromycin and atovaquone) also required blood

Table 3. Laboratory results for 8 patients with confirmed babesiosis, Penn State Health Milton S. Hershey Medical Center, Hershey, Pennsylvania, USA, 2005–2018

Test	Average (range)	Reference range
Leukocyte, × 10^9 cells/L	8.7 (3.5–17.5)	4–10.4
Hemoglobin, g/dL	9.8 (6.3–11.9)	13–17
Platelets, × 10^9 /L	90.8 (26–307)	150–350
Alanine aminotransferase, U/L	72 (23–185)	0–41
Aspartate aminotransferase, U/L	176.6 (38–733)	0–40
Bilirubin, mg/dL	6.4 (1.0–19.7)	0.0–1.2
Alkaline phosphatase, U/L	94 (58–172)	40–130
Creatinine, mg/dL	2.2 (0.8–4.7)	0.7–1.3

Table 4. Diagnostic results for 8 patients with confirmed babesiosis, Penn State Health Milton S. Hershey Medical Center, Hershey, Pennsylvania, USA, 2005–2018

Patient no.	Smear (% parasitemia)	PCR result	IgG*	Co-infection with *Borrelia burgdorferi*
1	Positive (12)	Not obtained	Not obtained	Yes
2	Positive (45)	Positive	Positive	Yes
3	Positive (40)	Positive	Positive	Yes
4	Positive (11)	Not obtained	Positive	No
5	Positive (16)	Not obtained	Not obtained	No
6	Positive (17)	Positive	Positive	Yes
7	Positive (2)	Not obtained	Positive	No
8	Positive (1)	Not obtained	Positive	No

*IgG serologic test result considered positive if titer ≥1:256.

or platelet transfusions. Five patients underwent red cell exchange transfusions. The average duration of treatment was 18.1 days. The average duration of parasitemia was 9 days, but we only had exact date of clearance for 3 of the 8 patients.

Hospital Course and Complications

Patients were identified as having severe babesiosis if they had parasitemia >10% or if they had intensive care unit (ICU) care, exchange transfusion requirement, intubation, acute respiratory distress syndrome, shock, or dialysis (*4*,*6*,*13*). Six of the 8 patients were classified as having severe infection. These 6 patients all had parasitemia >10%. Five of the 8 patients required ICU care and underwent exchange transfusions. One patient required dialysis, and 2 patients required blood or platelet transfusion. No patients required intubation or pressor support, and all patients survived.

Four of the 6 patients with severe infection had co-infection with *Borrelia burgdorferi* (Lyme disease). The 2 nonsevere patients did not have co-infection. All 6 of the severely ill patients had infectious disease consults during their hospitalization. The 2 patients that were considered not severely ill did not receive an infectious disease consultation. The average length of stay for all patients was 11 days. The average length of stay for patients with severe infection was 12.3 days and for patients with nonsevere infection was 7 days.

Discussion

Our findings further suggest that babesiosis is an emerging infection in the state of Pennsylvania. Data from our institution as well as the Pennsylvania Department of Health show a clear trend toward increasing cases throughout the state (Figure 2). In our study, 7 of the 8 reported cases were thought to be acquired in Pennsylvania. There were no reported cases during 2005–2010 and 1 case in 2011, followed by a steady rise in cases until 2018, when our institution saw 4 cases. The distribution of the areas of suspected infection acquisition makes us question whether we might be seeing a further expansion into central Pennsylvania over time. Over half (4/7) of the cases seen at Hershey Medical Center were acquired in southcentral Pennsylvania counties, and all 4 of those cases were seen most recently in the year 2018 (contrary to previous years, when cases occurred in northeast and southeast counties). These southcentral counties were determined by the home address ZIP codes of infected patients who had no history of travel before seeking care. Previous studies highlighting cases of babesiosis in Pennsylvania included patients from northeast and southeast counties only (*2*–*4*; Figure 1). Whether a westward expansion of babesiosis is truly occurring within the state is difficult to conclude on the basis of our small sample size; nonetheless, these findings warrant further inquiry, and we would be interested to see if other institutions in the southcentral region have noted a similar trend. Because most persons infected with *B. microti* are either asymptomatic or have mild symptoms and diagnostic testing is often not obtained, the actual number of babesiosis cases at our institution was most likely underrepresented. In addition, given our methodology of focusing specifically on babesiosis-related codes in ICD-9 and ICD-10, we might have missed patients that were presumed to be co-infected (i.e., having both Lyme and babesiosis) and treated empirically.

Babesiosis is currently considered endemic in the US states of Connecticut, Massachusetts, Minnesota, New Jersey, New York, Rhode Island, and Wisconsin (*9*). Surveillance data shows a steady rise in babesiosis cases throughout the United States and further geographic expansion (*9*,*13*). When examining neighboring states that are currently endemic for babesiosis, specifically New York and New Jersey, we observed a historical pattern of expansion that might be indicative of what is to come in the state of Pennsylvania. Both states were endemic for Lyme disease, which shares the same vector as babesiosis (blacklegged ticks), before seeing the rise in babesiosis cases (*14*–*20*).

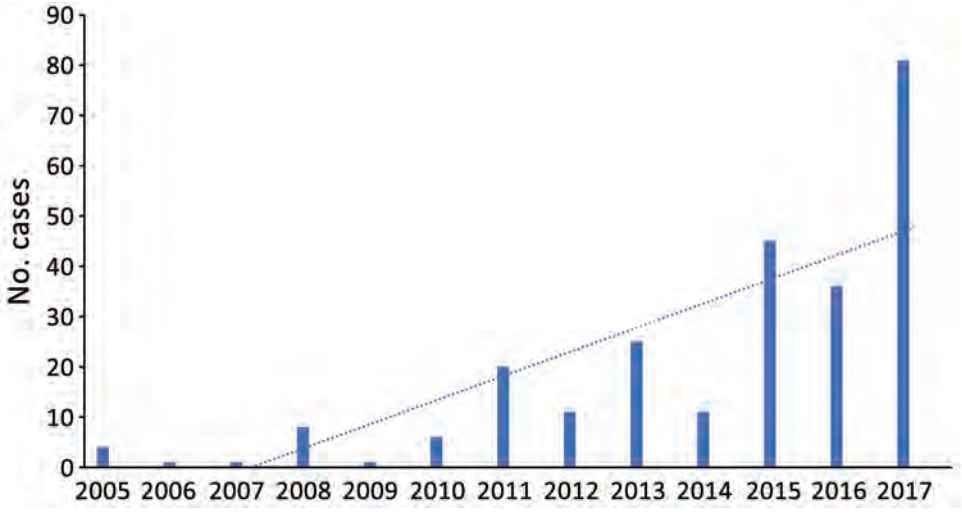

Figure 2. Annual number of babesiosis cases in Pennsylvania, USA, 2005–2017. Includes confirmed cases reported during 2005–2010 based on identification of *Babesia microti* organisms on blood smear and confirmed and probable cases reported during 2011–2017 based on the 2011 Centers for Disease Control and Prevention case definition (https://wwwn.cdc.gov/nndss/conditions/babesiosis/case-definition/2011). Dotted line indicates upward trend of cases over time.

One study suggests that geographic spread of *B. microti* is favored by prior establishment of *B. burgdorferi* (the agent responsible for Lyme disease) and that co-infection (in mice reservoirs) with *B. burgdorferi* increases the likelihood of *B. microti* transmission (*21*). A paper from 1998 documented the presence of *I. scapularis* ticks in 49 of the 67 counties in Pennsylvania (*22*); however, a more recent study from 2015 identified the presence of the tick in all 67 counties (*10*). This same study reported tick infection rates of 47.4% for *B. burgdorferi*, 3.5% for *B. microti*, and 3.3% for *Anaplasma phagocytophilum*. This 3.5% infection rate by *Babesia* was higher than a previously reported rate of 0.7% in a 2010 report (*23*). The reasons for this suspected expansion are thought to be multifactorial, including the results of climatic effects on tick populations, growth of deer populations, and incursion into tick and deer habitats by humans (*13*).

When evaluating the patients treated at Hershey Medical Center, we found that our patients were demographically similar to patients described in prior studies; most patients in our investigation were male (75%) and elderly (median age 70 years). Only 1 patient reported a history of tick bite preceding infection, but most (75%) reported a history of outdoor activity. This finding further stresses the importance of having a high clinical suspicion in elderly patient populations despite absence of tick bite history.

The average number of days of symptoms before diagnosis was ≈10 days, which is a slightly shorter period compared with reports from other studies (*5*,*24*) and might have been because all patients had blood smears obtained early on during admission. The reason for obtaining blood smears was predominately for work-up of new anemia or thrombocytopenia. Most (75%) patients were identified as having severe infection; 6 of the 8 had parasitemia >10%. Five of these 6 patients required ICU care and underwent exchange transfusion. The purpose of ICU care in these patients was for close monitoring and exchange transfusion. No patients required pressor support or mechanical ventilation. The exchange transfusion process consists of removing a patient's red blood cells and replacing them with donor red blood cells and is recommended for babesiosis patients who have parasitemia ≥10%; severe hemolysis (hemoglobin ≤10 g/dL); or pulmonary, hepatic, or renal impairment (*25*). No randomized trials have evaluated the efficacy of red cell exchange therapy; recommendations for this treatment are based on case series that show that parasitemia can be reduced by >50%–90% with red cell exchange therapy (*26*–*28*). Of the patients who required ICU care and exchange transfusion, only 1 of the patients was considered immunocompromised because of history of splenectomy; 1 other patient with severe infection had a history of splenectomy but did not require exchange transfusion. The remaining patients were considered immunocompetent, including 1 patient with diabetes. The unifying risk factor for most patients was older age. The high percentage of patients with severe infection was attributed to our hospital being a large tertiary academic center that received referrals from other hospitals. Some of the cases were referred specifically for evaluation for exchange transfusion. Co-infection with *B. burgdorferi* might have also contributed to severity of infection, given that 4 of the 6 patients with severe infection had serologic test results indicative of Lyme disease. Prior studies have shown increased disease severity and duration of illness in patients co-infected with *B. burgdorferi* and *Babesia* (*29*), which is consistent with the findings in our study.

No deaths occurred in our study cohort. Average length of hospital stay was 11 days. Most patients (7/8) received treatment with azithromycin and atovaquone. Three patients received clindamycin and quinine; 1 patient received clindamycin and quinine alone for the duration of their therapy, and 2 patients were switched to azithromycin and atovaquone because of persistent parasitemia. These 2 patients improved with the azithromycin and atovaquone regimen; however, this outcome might have been attributable to their having undergone exchange transfusion. Historically, clindamycin and quinine was the regimen of choice for the treatment of *B. microti* infection (*1*). Later, azithromycin and atovaquone became recommended for mild to moderate disease because the regimen was shown to be as effective as the combination of clindamycin and quinine and had fewer adverse effects (*25*). Most recently, a study from 2017 suggested that azithromycin plus atovaquone was equally effective for patients with severe infection (*30*).

Conclusions

Ours is yet another article highlighting the emergence of babesiosis in the state of Pennsylvania. Given the nonspecific signs and symptoms associated with the illness and the potential severity of infection, especially in our elderly population, we believe that increased awareness and reporting of this infection is necessary. Clinicians must maintain a high index of suspicion in patients with a nonspecific febrile syndrome despite absence of tick bite history or lack of an immunocompromising condition. Evaluation for co-infections, particularly co-infection with *B. burgdorferi*, should be considered given patients with co-infection appear to have more severe disease.

Acknowledgments

We thank Elizabeth Negrón for her contributions to this study.

Author Bio

Dr. Ingram is a second-year infectious disease fellow at Penn State Health Milton S. Hershey Medical Center. His primary research interests include tickborne infections and medical education.

Dr. Crook is an associate professor at Penn State Health Milton S. Hershey Medical Center and program director of the Penn State Infectious Disease Fellowship. Her research interests include HIV patient care, tickborne infections, and medical education.

References

1. Vannier E, Krause PJ. Human babesiosis. N Engl J Med. 2012;366:2397–407. https://doi.org/10.1056/NEJMra1202018
2. Acosta ME, Ender PT, Smith EM, Jahre JA. *Babesia microti* infection, eastern Pennsylvania, USA. Emerg Infect Dis. 2013;19:1105–7. https://doi.org/10.3201/eid1907.121593
3. Genda J, Negron EA, Lotfipour M, Balabhadra S, Desai DS, Craft DW, et al. Severe *Babesia microti* infection in an immunocompetent host in Pennsylvania. J Investig Med High Impact Case Rep. 2016;4:2324709616663774. https://doi.org/10.1177/2324709616663774
4. Liu HH, Cushinotto L, Giger O, Daum G, McBride P, Negron EA, et al. Increasing babesiosis in southeastern Pennsylvania, 2008–2017. Open Forum Infect Dis. 2019;6:ofz066. https://doi.org/10.1093/ofid/ofz066
5. Hatcher JC, Greenberg PD, Antique J, Jimenez-Lucho VE. Severe babesiosis in Long Island: review of 34 cases and their complications. Clin Infect Dis. 2001;32:1117–25. https://doi.org/10.1086/319742
6. Mareedu N, Schotthoefer AM, Tompkins J, Hall MC, Fritsche TR, Frost HM. Risk factors for severe infection, hospitalization, and prolonged antimicrobial therapy in patients with babesiosis. Am J Trop Med Hyg. 2017;97:1218–25. https://doi.org/10.4269/ajtmh.17-0146
7. Young C, Krause PJ. The problem of transfusion-transmitted babesiosis. Transfusion. 2009;49:2548–50. https://doi.org/10.1111/j.1537-2995.2009.02494.x
8. Levin AE, Krause PJ. Transfusion-transmitted babesiosis: is it time to screen the blood supply? Curr Opin Hematol. 2016; 23:573–80. https://doi.org/10.1097/MOH.0000000000000287
9. Gray EB, Herwaldt BL. Babesiosis surveillance—United States, 2011–2015. MMWR Surveill Summ. 2019;68 (No. SS-6):1–11. https://doi.org/10.15585/mmwr.ss6806a1
10. Hutchinson ML, Strohecker MD, Simmons TW, Kyle AD, Helwig MW. Prevalence rates of *Borrelia burgdorferi* (Spirochaetales: Spirochaetaceae), *Anaplasma phagocytophilum* (Rickettsiales: Anaplasmataceae), and *Babesia microti* (Piroplasmida: Babesiidae) in host-seeking *Ixodes scapularis* (Acari: Ixodidae) from Pennsylvania. J Med Entomol. 2015;52:693–8. https://doi.org/10.1093/jme/tjv037
11. Centers for Disease Control and Prevention. Babesiosis (*Babesia* spp.) 2011 case definition [cited 2020 Mar 5]. https://wwwn.cdc.gov/nndss/conditions/babesiosis/case-definition/2011
12. Harris PA, Taylor R, Thielke R, Payne J, Gonzalez N, Conde JG. Research electronic data capture (REDCap)—a metadata-driven methodology and workflow process for providing translational research informatics support. J Biomed Inform. 2009;42:377–81. https://doi.org/10.1016/j.jbi.2008.08.010
13. Menis M, Forshee RA, Kumar S, McKean S, Warnock R, Izurieta HS, et al. Babesiosis occurrence among the elderly in the United States, as recorded in large Medicare databases during 2006–2013. PLoS One. 2015;10:e0140332. https://doi.org/10.1371/journal.pone.0140332
14. Herwaldt BL, McGovern PC, Gerwel MP, Easton RM, MacGregor RR. Endemic babesiosis in another eastern state: New Jersey. Emerg Infect Dis. 2003;9:184–8. https://doi.org/10.3201/eid0902.020271
15. Apostolou A, Sorhage F, Tan C. Babesiosis surveillance, New Jersey, USA, 2006–2011. Emerg Infect Dis. 2014;20:1407–9. https://doi.org/10.3201/eid2008.131591
16. Filstein MR, Benach JL, White DJ, Brody BA, Goldman WD, Bakal CW, et al. Serosurvey for human babesiosis in New York. J Infect Dis. 1980;141:518–21. https://doi.org/10.1093/infdis/141.4.518

17. Meldrum SC, Birkhead GS, White DJ, Benach JL, Morse DL. Human babesiosis in New York State: an epidemiological description of 136 Cases. Clin Infect Dis. 1992;15:1019–23. https://doi.org/10.1093/clind/15.6.1019
18. Kogut SJ, Thill CD, Prusinski MA, Lee JH, Backerson PB, Coleman JL, et al. *Babesia microti*, upstate New York. Emerg Infect Dis. 2005;11:476–8. https://doi.org/10.3201/eid1103.040599
19. Joseph JT, Roy SS, Shams N, Visintainer P, Nadelman RB, Hosur S, et al. Babesiosis in Lower Hudson Valley, New York, USA. Emerg Infect Dis. 2011;17:843–7. https://doi.org/10.3201/eid1705.101334
20. Linden JV, Prusinski MA, Crowder LA, Tonnetti L, Stramer SL, Kessler DA, et al. Transfusion-transmitted and community-acquired babesiosis in New York, 2004 to 2015. Transfusion. 2018;58:660–8. https://doi.org/10.1111/trf.14476
21. Dunn JM, Krause PJ, Davis S, Vannier EG, Fitzpatrick MC, Rollend L, et al. *Borrelia burgdorferi* promotes the establishment of *Babesia microti* in the northeastern United States. PLoS One. 2014;9:e115494. https://doi.org/10.1371/journal.pone.0115494
22. Dennis DT, Nekomoto TS, Victor JC, Paul WS, Piesman J. Reported distribution of *Ixodes scapularis* and *Ixodes pacificus* (Acari: Ixodidae) in the United States. J Med Entomol. 1998;35:629–38. https://doi.org/10.1093/jmedent/35.5.629
23. Cherepko J, Berry GJ, Keeler SP, Huffman JE. Prevalence of *Borrelia burgdorferi*, *Bartonella* spp., *Bartonella henselae*, *Babesia microti* and *Anaplasma phagocytophila* in *Ixodes scapularis* ticks collected in Monroe County, Pennsylvania, show a risk for co- and tri-infections. J Pa Acad Sci. 2010;84:74–8.
24. Fida M, Challener D, Hamdi A, O'horo J, Abu Saleh O. Babesiosis: a retrospective review of 38 cases in the upper Midwest. Open Forum Infect Dis. 2019;6:ofz311. https://doi.org/10.1093/ofid/ofz311
25. Wormser GP, Dattwyler RJ, Shapiro ED, Halperin JJ, Steere AC, Klempner MS, et al. The clinical assessment, treatment, and prevention of Lyme disease, human granulocytic anaplasmosis, and babesiosis: clinical practice guidelines by the Infectious Diseases Society of America. Clin Infect Dis. 2006;43:1089–134. https://doi.org/10.1086/508667
26. Spaete J, Patrozou E, Rich JD, Sweeney JD. Red cell exchange transfusion for babesiosis in Rhode Island. J Clin Apher. 2009;24:97–105. https://doi.org/10.1002/jca.20197
27. Saifee NH, Krause PJ, Wu Y. Apheresis for babesiosis: therapeutic parasite reduction or removal of harmful toxins or both? J Clin Apher. 2016;31:454–8. https://doi.org/10.1002/jca.21429
28. Nixon CP, Park S, Nixon CE, Reece RM, Sweeney JD. Adjunctive treatment of clinically severe babesiosis with red blood cell exchange: a case series of nineteen patients. Transfusion. 2019;59:2629–35. https://doi.org/10.1111/trf.15346
29. Krause PJ, Telford SR III, Spielman A, Sikand V, Ryan R, Christianson D, et al. Concurrent Lyme disease and babesiosis. Evidence for increased severity and duration of illness. JAMA. 1996;275:1657–60. https://doi.org/10.1001/jama.1996.03530450047031
30. Kletsova EA, Spitzer ED, Fries BC, Marcos LA. Babesiosis in Long Island: review of 62 cases focusing on treatment with azithromycin and atovaquone. Ann Clin Microbiol Antimicrob. 2017;16:26. https://doi.org/10.1186/s12941-017-0198-9

Address for correspondence: David Ingram, Penn State University College of Medicine, 500 University Dr, Rm C6860, Hershey, PA 17033, USA; email: disol1186@gmail.com

Sporadic Creutzfeldt-Jakob Disease among Physicians, Germany, 1993–2018

Peter Hermann,[1] Johannes Treig,[1] Steffen Unkel, Stefan Goebel, Timothy Bunck, Martha Jünemann, Tim Friede, Inga Zerr

Medscape EDUCATION ACTIVITY

In support of improving patient care, this activity has been planned and implemented by Medscape, LLC and Emerging Infectious Diseases. Medscape, LLC is jointly accredited by the Accreditation Council for Continuing Medical Education (ACCME), the Accreditation Council for Pharmacy Education (ACPE), and the American Nurses Credentialing Center (ANCC), to provide continuing education for the healthcare team.

Medscape, LLC designates this Journal-based CME activity for a maximum of 1.00 ***AMA PRA Category 1 Credit(s)™***. Physicians should claim only the credit commensurate with the extent of their participation in the activity.

Successful completion of this CME activity, which includes participation in the evaluation component, enables the participant to earn up to 1.0 MOC points in the American Board of Internal Medicine's (ABIM) Maintenance of Certification (MOC) program. Participants will earn MOC points equivalent to the amount of CME credits claimed for the activity. It is the CME activity provider's responsibility to submit participant completion information to ACCME for the purpose of granting ABIM MOC credit.

All other clinicians completing this activity will be issued a certificate of participation. To participate in this journal CME activity: (1) review the learning objectives and author disclosures; (2) study the education content; (3) take the post-test with a 75% minimum passing score and complete the evaluation at http://www.medscape.org/journal/eid; and (4) view/print certificate. For CME questions, see page 1969.

Release date: July 15, 2020; Expiration date: July 15, 2021

Learning Objectives

Upon completion of this activity, participants will be able to:

- Assess the occurrence of sporadic Creutzfeldt-Jakob disease (sCJD) among physicians in Germany from 1993 to 2018, according to an analysis of occupational data for patients with sCJD in Germany
- Evaluate risk factors for sCJD among physicians in Germany from 1993 to 2018, according to an analysis of occupational data for patients with sCJD in Germany
- Determine the clinical implications of the occurrence of sCJD among physicians in Germany from 1993 to 2018, according to an analysis of occupational data for patients with sCJD in Germany

CME Editor

Karen L. Foster, Technical Writer/Editor, Emerging Infectious Diseases. *Disclosure: Karen L. Foster has disclosed no relevant financial relationships.*

CME Author

Laurie Barclay, MD, freelance writer and reviewer, Medscape, LLC. *Disclosure: Laurie Barclay, MD, has disclosed no relevant financial relationships.*

Authors

Disclosures: ***Peter Hermann, MD; Johannes Treig, MD; Steffen Unkel, PhD; Stefan Goebel, MD; Timothy Bunck, MD; Martha Jünemann, BA; Tim Friede, PhD;*** *and* ***Inga Zerr, MD,*** *have disclosed no relevant financial relationships.*

Author affiliations: University Medical Center Göttingen Department of Neurology, Göttingen, Germany (P. Hermann, J. Treig, S. Goebel, T. Bunck, M. Jünemann, I. Zerr); University Medical Center Göttingen Department of Medical Statistics, Göttingen (S. Unkel, T. Friede); German Center for Neurodegenerative Diseases, Göttingen (I. Zerr)

DOI: https://doi.org/10.3201/eid2608.191159

[1]These authors contributed equally to this article.

We investigated sporadic Creutzfeldt-Jakob disease (sCJD) among physicians in Germany by analyzing occupational information of patients with sCJD recorded by the German CJD Surveillance Unit (1993–2005; 1,250 patients, of whom 4 [0.32%] were physicians) and the National Reference Center for Human Spongiform Encephalopathies (2006–2016; 1,491 patients, of whom 13 [0.87%] were physicians). Among the physicians, we did not identify any neurologists, neurosurgeons, psychiatrists, or pathologists. A cumulative sum test showed an increase in reported physicians over time. Data for 2017–2018 indicated an increased rate of physicians among all notified sCJD cases (5/239 [2.1%]) when we used the total population of Germany as control group. Our data suggest the possibility of an increased risk for sCJD among physicians in Germany. However, we can only speculate about the reasons, and larger multinational studies are needed to replicate the finding and to clarify whether this finding is a general or a country-specific phenomenon.

Creutzfeldt-Jakob disease (CJD) is a syndrome comprising dementia and various neurologic signs and symptoms (*1*) caused by the transmissible misfolded prion protein scrapie (*2*). Reported death rates and incidence rates differ from 1.67 (*3*) to >2 per million person-years (*4*,*5*). In contrast to animal prion diseases (*6*,*7*), transmitted human prion diseases are uncommon. Variant CJD (vCJD) caused by ingestion of beef is rare (231 cases worldwide) (*8*), and its incidence has decreased since 2000 (*9*). Most cases of human prion disease are sporadic CJD (sCJD; 84%–93%), followed by genetic CJD (5%–10%). Only ≤4% are considered to be iatrogenic (iCJD) (*3*,*10*–*12*). Clinical diagnostic criteria of iCJD imply the presence of an iatrogenic risk factor (*13*). Known cases were caused by cadaver-derived growth hormones, dura mater grafts, neurosurgical instrument contamination, and corneal grafts (*12*). On the other hand, iCJD might be overlooked when no classic risk factor is present. Neuropathologic characteristics can identify iCJD only in a subgroup of cases (*14*,*15*). Unrecorded cases related to surgery are likely because an increased risk for sCJD in persons with a history of surgery was reported (*16*); however, data on this issue remain ambiguous (*17*). vCJD transmitted by transfusion of blood products has been reported (*8*), but no confirmed case was recorded among recipients of blood from donors with sCJD (*18*–*20*).

An increased risk for iCJD among caregivers and healthcare professionals has been suggested, but its evaluation is complex (*21*–*24*). Previous studies neither unequivocally displayed nor ruled out relevant increases in risk for CJD among healthcare professionals (*25*,*26*). Furthermore, these investigations were mostly designed as case–control studies, which are prone to bias because of case selection. Therefore, we aimed to evaluate sCJD among physicians using historical epidemiologic data from 25 years of CJD surveillance in Germany and the whole population of that country as controls.

Methods

Study Design and Data Acquisition

In the framework of a retrospective cohort study, we evaluated 4,645 patient files representing all suspected CJD cases reported to the German surveillance group during June 1993–December 2016 about the patient's occupational history to identify physicians of all specialties. In addition and as negative controls, we collected information about other professions.

The centralized assessment of suspected human prion diseases in Germany started in June 1993 and was conducted by the CJD Surveillance Unit of the University Medical Center Goettingen. Since January 2006, health authorities have officially charged this center with CJD surveillance and named it the National Reference Center for Human Transmissible Spongiform Encephalopathies (NRZ-TSE). In Germany, notification of sCJD is required. Health authorities advise clinical institutions to contact the NRZ-TSE for clinical classifications of notified cases. The NRZ-TSE counsels physicians with respect to differential diagnosis and hygienic issues and records clinical data, including the patient's professional background. Specifically, until 2006, physicians from the CJD Surveillance Unit visited and interviewed patients and caregivers using a standardized questionnaire.

Patient Cohorts

We considered all patients in the database for this study. Inclusion criteria for further analyses were diagnosis of probable or definite sCJD according to World Health Organization criteria (*2*) and age ≥35 years. We reviewed all available questionnaires (evaluated by the NRZ-TSE) and medical reports (sent to the NRZ-TSE by treating institution) since 1993 for patient's professions to identify physicians. During 1993–2005, the research group of the University Medical Center Goettingen had to actively search for suspected CJD cases (e.g., through regular newsletters to all neurologic and psychiatric centers in Germany). Most reported patients had been visited by physicians from the research group, and epidemiologic questionnaires were available for analyses. In 2006, the group was assigned as National Reference

Center, leading to a substantial increase in reported cases and resulted in a decrease in the proportion of visitations and interviews. Because of these structural differences, we divided the study cohort into cohort A (reported 1993–2005; 1,250 persons) and cohort B (reported 2006–2016; 1,491 persons) and analyzed them separately.

Population-Based Cohorts

We used publicly available data on the population of Germany to create control groups in each time frame (matching cohorts A and B). Numbers of working and retired physicians were sourced from the database of the German Federal Medical Association (Bundesärztekammer [BÄK], Berlin, Germany), which provides the number of physicians and information about age, sex, specialty, and location. Membership is required for, but is not restricted to, all working physicians and does not expire with retirement. To analyze the entire population, we obtained numbers from the German Federal Office of Statistics.

Data Analyses and Statistical Methods

BÄK data give numbers of physicians in Germany in different age categories. The youngest category was <35 years of age (without further differentiation). Only 10 patients in the sCJD cohort were <35 years of age, and none were physicians. We included only patients and controls ≥35 years of age to achieve approximate age matching between the German physicians and the sCJD cohort. We did not further stratify for age (and sex) because of the low case count among physicians with sCJD. We pooled all data from our sources using Excel 2016 (Microsoft, https://www.microsoft.com). We used Statistica (https://www.statsoft.de) for descriptive analyses and performed further statistical analyses using the statistical software R version 3.4.2 (https://www.r-project.org). We considered results with $p \leq 0.05$ to be significant.

The aims of the study were to evaluate the rate of physicians in the cohort of CJD patients and to investigate a potential risk modification using population-based data. The aims had been framed before data collection. We used Fisher exact test to compare the number of physicians in the cohort of CJD patients and the number of physicians in the population of Germany.

Analyses were performed as follows. To define the number of nonphysicians in the CJD cohort, we considered only patients with known occupation. These analyses were based on the assumption of a corresponding number of physicians in the group of patients with unknown occupation. We further considered all CJD patients assuming that no additional physicians were in the group of patients with unknown occupation. We used the results to perform sensitivity analyses to evaluate the number of physicians in the group of patients with unknown occupation that would be necessary to reach statistical significance using Fisher exact test. We conducted a CUSUM (cumulative sum)–based test for a change point in a time series (*27*) to investigate alterations of the number of reported physicians with CJD over time (per year). Finally, in an additional step, we collected data from 2017 and 2018 and analyzed them to validate results of the previous analyses on the basis of the historical cohorts (1993–2016).

Results

Descriptive Data Analyses: CJD Cohort

Of 4,645 suspected CJD cases during June 1993–December 2016, we classified 2,754 as probable sCJD (1,543) or definite sCJD (1,211). We classified other cases as possible sCJD (2) (156 cases), non-CJD (1,188), genetic prion disease (197), and iCJD (12). A total of 338 reported cases remained unclassified because of incomplete clinical information. We reduced the number of probable and definite sCJD cases to 2,741 after excluding patients <35 years of age. We determined occupation for 1,532 (55.9%) patients, of whom 17 (1.1%) were physicians (Figures 1, 2).

In cohort A (June 1993–December 2005), we classified 539 (43%) of the 1,250 cases as probable sCJD and 711 (57%) as definite sCJD. In cohort B (January 2006–December 2016), we classified 1,000 (67%) of the 1,491 cases as probable sCJD and 491 (33%) as definite sCJD. The mean age of cohort A patients was 66 years (range 35–90 years) and of cohort B patients was 68 years (range 37–93 years). In cohort A, 58% of patients were women; in cohort B, 52%. Information about codon 129 polymorphism was available for 1,039 (83%) cohort A cases and 581 (39%) for cohort B cases (Table 1). For 1,532 (56% in cohorts A and B combined) patients, we were able to evaluate history of occupation before illness (cohort A, 1,093 patients; cohort B, 439). For some patients, ≥2 different professions were recorded (up to 7). We considered occupation as a physician at any point in time. Occupation as a physician was known for 4 cohort A patients (0.3% of all patients; 0.4% of cohort A patients) and 13 cohort B patients (0.9% of all patients; 3% of cohort B patients).

Physicians with sCJD (including patients from the validation cohort 2017–2018) had a broad spectrum of medical specialties. Surgical specialties were present for 14 patients (surgery without information

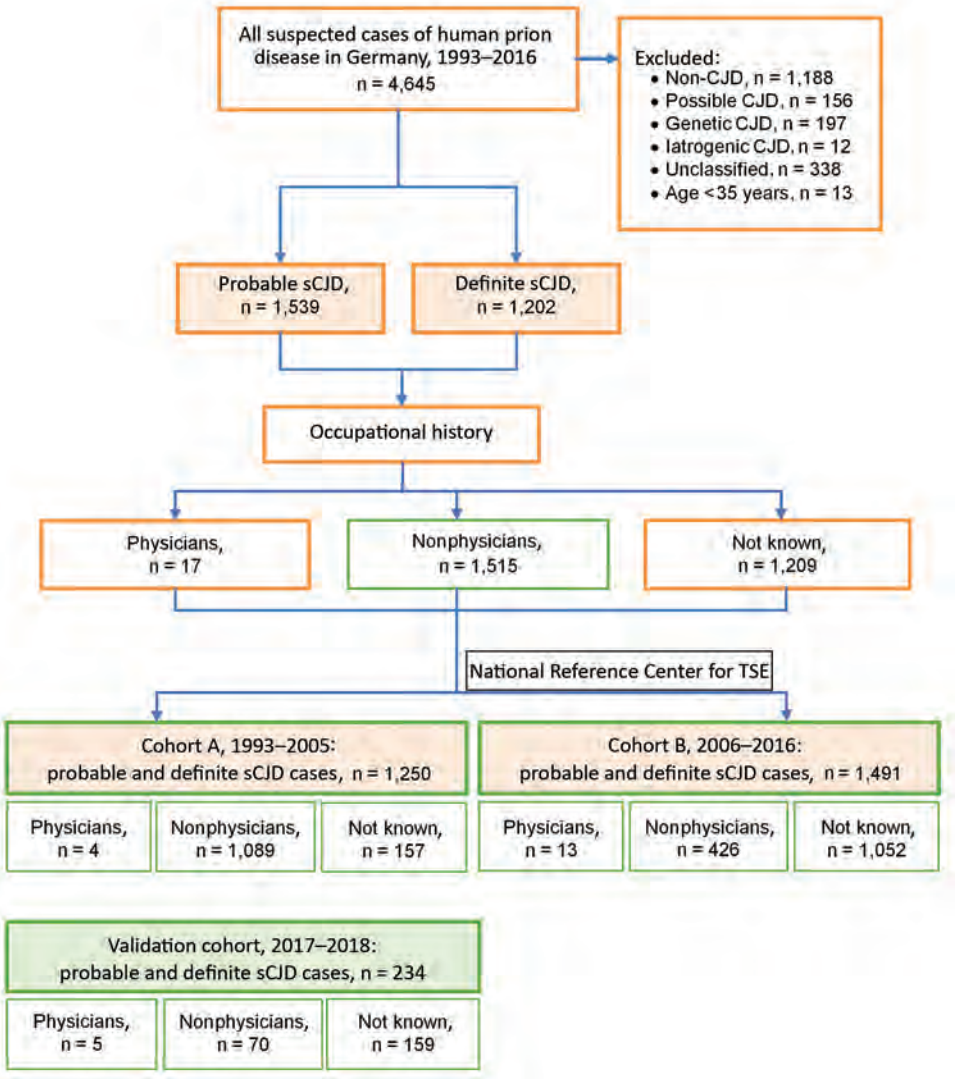

Figure 1. Study cohort and case selection in a study of sCJD among physicians, Germany, 1993–2018. All case numbers are based on the classifications of the German National Reference Center for Human Transmissible Spongiform Encephalopathies (*2*) in February 2019. CJD, Creutzfeldt-Jakob disease; sCJD, sporadic CJD; TSE, transmissible spongiform encephalopathy.

about further specialty, 3 patients; trauma/orthopedic surgery, 5; gynecology and otolangyrology, 2 each; urology and visceral surgery, 1 each). The others had nonsurgical specialties (internal medicine, 5; anesthesiology, podiatry, and general practice, 1 each). Of all physicians with sCJD (1993–2018), 64% had a surgical specialty (Table 2); in 2018, only 31% of all physicians in German had a surgical specialty (*28*). Very long duration of disease occurred only among physicians with surgical specialties (mean 205 days vs. 109 days for nonsurgical specialties; overall 175 days [range 49–809 days]). We identified no hospital in Germany that had employed >1 physician with sCJD, but a complete occupational history was not available for all patients, especially in cohort B. We found no link between a physician and another known sCJD patient, but only limited information was available (Appendix Table, https://wwwnc.cdc.gov/EID/article/26/8/19-1159-App1.pdf). Most patients were not able to give detailed information about this issue because of progressed cognitive impairment. The rate of autopsy-confirmed cases was 55%. Prion typing was performed in only 4 cases.

Descriptive Data Analyses: Population-Based Cohort

The number of physicians in Germany increased from 297,803 in 1993 to 496,240 in 2016 (*29*), a factor of 1.67. For each period corresponding to cohort A (1993–2005) and cohort B (2006–2016), mean values of yearly numbers were calculated that excluded physicians <35 years of age. Mean numbers were 295,556 (range 240,709–345,599) during 1993–2005 and 382,558 (range 349,878–416,311) during 2006–2016. We performed the same calculations considering the entire population of the same age in Germany (*30*): mean 47,907,927 (range 44,336,444–51,243,273)

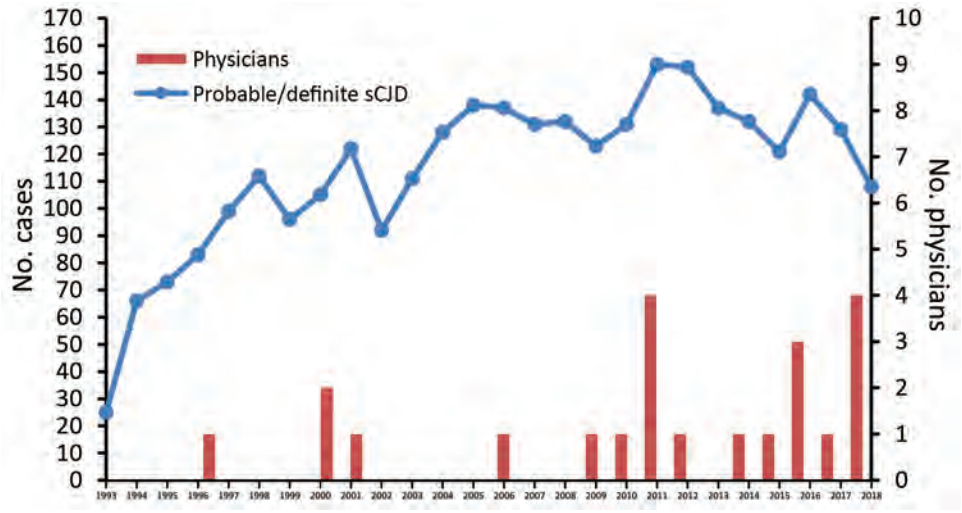

Figure 2. Definite and probable sCJD cases and number of physicians with sCJD, Germany, 1993–2018. All case numbers are based on the classifications of the German National Reference Center for Human Transmissible Spongiform Encephalopathies (*2*) in February 2019. Red bars, number of physicians reported in 1 year; blue line, number of probable and definite sCJD cases per year. sCJD, sporadic Creutzfeldt-Jakob disease.

during 1993–2005 and 51,601,356 (range 51,553,192–51,961,175) during 2006–2016.

Rate of Physicians in sCJD Cohorts and in the Total Population of Germany

We based contingency tables on the numbers of all patients in the study cohort for whom occupation was known (cohort A, 1,093 patients; cohort B, 439 patients), all physicians in the sCJD cohort (cohort A, 4 patients; cohort B, 13 patients), the population of Germany, and all physicians in that population (Table 3). Fisher exact test yielded an odds ratio (OR) of 0.59 (95% CI 0.16–1.52; p = 0.44) for cohort A and OR 4.09 (95% CI 2.16–7.06; p<0.001) for cohort B (Table 3). These results indicate a significantly higher rate of physicians in cohort B than in the total population of Germany.

We based this approach on the assumption of a corresponding proportion of physicians and nonphysicians in the group of sCJD patients without known occupational history. In a second step, we included the entire study cohort, assuming there were no additional physicians in the group of sCJD patients for whom occupational history was not known. Cohort A did not differ significantly from the total population of Germany (OR 0.52 [95% CI 0.14–1.33]; p = 0.27); likewise, cohort B did not differ significantly from the total population of Germany (OR 1.18 [95% CI 0.63–2.02]; p = 0.54). Subsequently, we conducted a sensitivity analysis to determine the number of physicians in the group without known occupation who would be required for a statistically significant difference between the study cohort and the total German population: 9 for cohort A (p = 0.03) and 5 for cohort B (p = 0.047). In a fou rth step, we investigated the change of the rate of reported physicians in the study cohort over time: 0.32% for cohort A (1993–2005) and 0.87% for cohort B. Results of our CUSUM test showed an increase of reported cases (p = 0.04) and identified a change point from 2008 to 2009.

Table 1. Characteristics of sCJD patients, Germany, 1993–2018*

Variable	Cohort A	Cohort B	Validation cohort
Time period	1993 Jun–2005 Dec	2006 Jan–2016 Dec	2017 Jan–2018 Dec
Total, no. (%)	1,250 (100)	1,491 (100)	234 (100)
Definite sCJD	711 (57)	491 (33)	59 (25)
Probable sCJD	539 (43)	1,000 (67)	175 (75)
Mean age, y (range)	66 (35–90)	68 (37–93)	68 (41–91)
Sex			
F	731 (58)	769 (52)	118 (50)
M	519 (42)	722 (48)	116 (50)
Codon 129, no. (%)			
MM	693 (67)	322 (55)	8 (53)†
MV	180 (17)	134 (23)	7 (47)†
VV	166 (16)	125 (22)	0
Occupation known, no. (%)	1,093 (87)	439 (29)	70 (30)
Physicians, no. (% of all patients, % of known occupation)	4 (0.3, 0.4)	13 (0.9, 3)	5 (2.1, 7.1)

*MM, methionine homzygosity; MV, heterozygosity; sCJD, sporadic Creutzfeldt-Jakob disease; VV, valin homozygosity.
†Since 2015, codon 129 analyses were not regularly performed during neuropathologic investigation.

Table 2. Characteristics of physicians with sCJD, Germany, 1993–2018*

Variable	Total, N = 22	Surgical, n = 14	Nonsurgical, n = 8
Population-based %†	100	39	61
Sex, no. (%)			
F	3 (14)	2 (14)	1 (12)
M	19 (86)	12 (86)	7 (88)
Mean age, y (range)	67 (53-83)	65 (53-83)	69 (60–75)
Classification, no. (%)			
Definite	12 (55)	7 (50)	5 (63)
Probable	10 (45)	7 (50)	3 (38)
Mean duration of disease, d (range)§	175 (49-809)	205 (84-809)	109 (49–272)
Codon 129, no.			
MM	7	5	2
VV	2	2	0
MV	2	1	1
NA	11	6	5

*MM, methionine homozygosity; MV, heterozygosity; NA, genotype not available; sCJD, sporadic Creutzfeldt-Jakob disease; VV, valine homozygosity.
†Percentage of surgical and nonsurgical specialties among all physicians in 2018 (*28*).
§Information about disease duration (onset to death) was available for 21 patients,

Postanalytic Evaluation of 2017 and 2018

In 2017 and 2018, a total of 239 sCJD patients were reported (129 in 2017, 110 in 2018). We identified 5 physicians (1 in 2017, 4 in 2018) (Figure 2). Including the entire postanalytic cohort (sCJD patients 2017–2018), regardless of known occupational history and using population data from 2017 (29,30), excluding patients <35 years of age, we found a significantly elevated rate of physicians among sCJD patients (OR 2.61 [95% CI 1.08–6.34]; p = 0.05 by Fisher exact test) (Table 3).

Discussion

Although prion diseases are transmissible, homozygosity for methionine at codon 129 (an intrinsic factor) is the only established risk factor for sCJD (*11*,*31*). Case–control studies have shown slightly elevated ORs for several features; for example, work at an animal laboratory, ophthalmologic surgery (*32*), ingestion of raw meat and brain (*24*), and history of brain surgery (*33*) (Table 4). Being employed as health professionals was a risk in a meta-analysis of case–control studies (*34*) but was not confirmed in a later prospective study (*23*). Because of the methodologic approaches used, most results were nonsignificant or prone to biases (*17*,*43*). Only 1 study used large population-based data from a US death registry (6 million cases screened, 636 CJD cases and 3,180 controls selected) and identified working as a butcher and work in physicians' offices as occupational risk factors (*35*). Other investigations of occupational risk factors for sCJD are not available, but the presence of unpublished data that might show inconclusive or null results cannot be excluded. Data on the development of reported cases over time with respect to occupational history are not available.

In addition to selection bias, the lack of studies that could validate occupational risk factors for sCJD might be caused by multiple comparisons of too many variables causing insignificant results. For this study, we focused on the evaluation of employment as physician as potential risk factor for sCJD. We used data from a prospective epidemiologic

Table 3. Physicians in cohorts of sCJD patients and in the whole population, Germany, 1993–2018*

Variable	Physicians†	Nonphysicians†	OR (95% CI)‡	p value
Cohort A, 1993–2005)				
sCJD patient				
Known occupation	4	1,089	0.59 (0.16–1.52)	0.44
All	4	1,246	0.52 (0.14–1.33)	0.27
German population	295,552	47,611,282		
Cohort B (2006–2016)				
sCJD patient				
Known occupation	13	426	4.09 (2.16–7.06)	<0.001
All	13	1,478	1.18 (0.63–2.02)	0.54
German population	382,545	51,218,372		
Validation cohort (2017-2018)				
All sCJD patients	5	234§	2.61 (1.08–6.33)	0.05
German population	424,413	51,924,527		

*OR, odds ratio; sCJD, sporadic Creutzfeldt-Jakob disease.
†≥35 years of age.
‡By Fisher exact test.
§Information about occupation was available for 88 patients.

Table 4. Review of studies about health professionals and CJD*

Study or report	Observation or sCJD patient
Case–control study	
Wientjens et al., 1996 (*34*)	Observation: 1975–1984 (Japan, United Kingdom, United States), meta-analysis of 3 case–control studies • 178 cases, 333 controls (hospital based, community based, and spouses) • Nonsignificantly increased risk for health professionals (OR 1.5 [95% CI 0.5–4.1])
Van Duijn et al., 1998 (*24*)	Observation: 1993–1995 (France, Germany, Italy, Netherlands, United Kingdom) • 405 cases, 405 controls (hospital-based) • No increased risk for health professionals (OR 0.92 [95% CI 0.69–1.32])
Cocco et al., 2003 (*35*)	Observation: 1984–1995 (United States) • 636 cases, 3,180 controls (population-based from a death registry) • Increased risk for workers in physicians' offices (OR 4.6 [95% CI 1.2–17.6])
Ruegger et al., 2009 (*32*)	Observation: 2001–2004 (Switzerland) • 69 cases, 224 controls (from general practitioners and random digit telephone dialing) • Nonsignificantly increased risk for medical professionals (OR 1.46 [95% CI 0.43–5.15])
Case report	
Schoene et al., 1981 (*36*)	1 neurosurgeon
Miller, 1988 (*37*)	1 histopathologist
Sitwell, 1988 (*38*)	1 histopathologist
Gorman et al., 1992 (*39*)	1 pathologist
Berger et al., 1993 (*40*)	1 internist (with training in pathology 30 y before disease onset)
Weber et al., 1993 (*41*)	1 orthopedic surgeon (handling dura 20–24 y before onset)
Mitrova et al., 2000 (*42*)	1 physician, 5 nurses, 1 medical technician, 1 ambulance driver
Alcalde-Cabero et al., 2012 (*25*)	Observation: 1965–2010; case reports and literature review • 202 health professionals (among 8,321 cases) • 65 physicians (9 general practitioners, 7 surgeons, 7 internists, 4 dentists, 3 ophthalmologists, 2 pathologists), and 137 other health professionals

*OR, odds ratio; sCJD, sporadic Creutzfeldt-Jakob disease.

surveillance database in Germany and population-based data as controls.

Our first analysis showed a significantly elevated rate of physicians in the study cohort (OR 4.09; p<0.001) during 2006–2016 (cohort B), the years in which structured epidemiologic surveillance had been conducted. The exclusion of patients with unknown occupational history represents a case–control design limited by the possibility of selection bias. An occupation as physician may be more likely to be reported than others; on the other hand, only clinical data relevant for case classification were available for many patients from cohort B. The study design for cohort A was more precise because most suspected patients were examined in person in notifying hospitals, whereas for cohort B, only a proportion of sCJD patients (27%) were examined.

Nonetheless, our second analysis of the entire CJD population and found no significant results (OR 0.53 [p = 0.27] for cohort A; OR 1.18 [p = 0.543] for cohort B). Therefore, we performed a sensitivity analysis indicating 5 additional physicians in the group with unknown occupational history (1,052 [71%]) in cohort B who would be necessary for a significant result. This number was higher in cohort A (9 patients), although the number of patients in cohort A with unknown occupation was much smaller (157 [13%]). These findings suggest that the number of reported physicians with sCJD increased in later years, whereas the reported number of sCJD cases was stable. We validated this finding with a CUSUM test (p = 0.04, change point from 2008 to 2009). During 2017–2018, the increased rate of sCJD in physicians was significant, even when we included all 239 reported cases in the analysis (OR 2.61; p = 0.05).

Fourteen of the 22 physicians were surgeons, but none had worked in neurosurgery and only 1 had worked in a neuropathology department for 1 year. This finding is remarkable because the high proportion of surgeons (64%) versus nonsurgeons (36%) in the sCJD group differs from the population control (39% vs. 61%). The apparent differences of clinical characteristics (age of onset, disease duration) might be explained by slightly different distribution of codon 129 genotypes in the 2 groups. Because of the low number of cases, we could not investigate these observations further. In most cases, information about genotype, prion type, and neuropathologic characteristics was insufficient to identify or exclude iCJD. No neurologists or psychiatrists were reported. We could not find regional links within the group of physicians or with other sCJD patients who had received surgical interventions and might have been index patients for obscure iCJD. Thus, we were not able to establish a causal relation between the statistical risk factor (occupation as a physician) and the disease. Nonetheless, this finding must be interpreted with regard to potential incubation times of up to 30 years (*10*) and

incomplete information about residence history in most patients from cohort B.

Although the use of a very large cohort of patients with sCJD and a population-based control group is a strength of our investigation, the study has several limitations. Because of the low number of physicians with sCJD, every bias in the case group would cause an immense effect on statistical analyses (e.g., unrecorded cases, misdiagnosed cases). Thus, we must interpret our results cautiously. Definite (neuropathologic) diagnosis was available only for some cases in our study, but the high accuracy of clinical diagnoses performed by our center has been reported previously (*5*). The altered status of the surveillance group after it was named a National Reference Center in 2006 might be a source of bias. We cannot exclude that the surveillance system in Germany has improved over the years, but the available data of patients' occupations has decreased in recent years (Table 1), which makes an underestimation of the number of physicians before 2006 highly unlikely. An increased awareness for CJD among German physicians resulting in more reported cases in recent years is also unlikely regarding the decreasing worldwide incidence of vCJD since 2000.

Another limitation of our study is the lack of further and more detailed statistical analyses. We could not calculate individual ORs for certain medical specialties. Only an extremely large-scale study pooling data from multiple national reference centers would be capable of doing that. In addition, we were not able to stratify ORs by age and sex. The age cutoff of >35 years was an attempt only to achieve an approximate matching of age in the case and the control groups. On the other hand, recorded physicians with sCJD showed a strong tendency to be male and have an age at onset of 60–75 years. In this context, unstratified analyses might underestimate ORs. Another limitation of the study is that we analyzed only 1 occupational risk factor. Other professionals, such as laboratory scientists or nurses, should be carefully considered, but the lack of data (especially population-based figures) prevented from further analyses.

The high proportion of physicians among patients with sCJD and its increase over the last years were displayed in a statistical model based on data from the population of Germany. We showed that sCJD patients were significantly more likely than the general population to be physicians, suggesting that it might be an occupational risk factor. Previous epidemiologic studies have not clearly identified an elevated risk for sCJD among physicians (Table 4), but the most recent available data are from 2010. Our study yielded significant results only after 2005, and the CUSUM test identified an increased number of physicians with sCJD after 2008. No specialties involved specifically in treating patients with CJD have been reported. Nonetheless, we found that a high proportion of physicians with sCJD were surgeons, although we can only speculate about the reasons. A larger study comprising new data from other countries is needed to clarify whether this finding is a general or a country-specific phenomenon.

Acknowledgments

We thank physicians throughout Germany for case notification and provision of clinical data to the NRZ-TSE and CJD Surveillance Unit.

This study was funded by the Robert Koch Institute through funds from the Federal Ministry of Health (grant no. 1369–341).

About the Author

Dr. Hermann is is a study physician in the NRZ-TSE at the University Medical Center Göttingen. His research interests are diagnostic testing and epidemiology of prion diseases as well as biomarkers of atypical dementia.

References

1. Prusiner SB. Novel proteinaceous infectious particles cause scrapie. Science. 1982;216:136–44. https://doi.org/10.1126/science.6801762
2. Zerr I, Kallenberg K, Summers DM, Romero C, Taratuto A, Heinemann U, et al. Updated clinical diagnostic criteria for sporadic Creutzfeldt-Jakob disease. [Erratum in: Brain. 2012;135] [Pt 4]. Brain. 2009;132:2659–68. https://doi.org/10.1093/brain/awp191
3. Ladogana A, Puopolo M, Croes EA, Budka H, Jarius C, Collins S, et al. Mortality from Creutzfeldt-Jakob disease and related disorders in Europe, Australia, and Canada. Neurology. 2005;64:1586–91. https://doi.org/10.1212/01.WNL.0000160117.56690.B2
4. Glatzel M, Rogivue C, Ghani A, Streffer JR, Amsler L, Aguzzi A. Incidence of Creutzfeldt-Jakob disease in Switzerland. Lancet. 2002;360:139–41. https://doi.org/10.1016/S0140-6736(02)09384-4
5. Hermann P, Laux M, Glatzel M, Matschke J, Knipper T, Goebel S, et al. Validation and utilization of amended diagnostic criteria in Creutzfeldt-Jakob disease surveillance. Neurology. 2018;91:e331–8. https://doi.org/10.1212/WNL.0000000000005860
6. Colby DW, Prusiner SB. Prions. Cold Spring Harb Perspect Biol. 2011;3:a006833. https://doi.org/10.1101/cshperspect.a006833
7. Imran M, Mahmood S. An overview of animal prion diseases. Virol J. 2011;8:493. https://doi.org/10.1186/1743-422X-8-493
8. The National CJD Research & Surveillance Unit. Current data on variant CJD cases worldwide [cited 2019 Aug 8]. http://www.cjd.ed.ac.uk/sites/default/files/worldfigs.pdf

9. Andrews NJ, Farrington CP, Ward HJT, Cousens SN, Smith PG, Molesworth AM, et al. Deaths from variant Creutzfeldt-Jakob disease in the UK. Lancet. 2003;361:751–2. https://doi.org/10.1016/S0140-6736(03)12632-3
10. Brown P, Preece M, Brandel JP, Sato T, McShane L, Zerr I, et al. Iatrogenic Creutzfeldt-Jakob disease at the millennium. Neurology. 2000;55:1075–81. https://doi.org/10.1212/WNL.55.8.1075
11. Heinemann U, Krasnianski A, Meissner B, Varges D, Kallenberg K, Schulz-Schaeffer WJ, et al. Creutzfeldt-Jakob disease in Germany: a prospective 12-year surveillance. Brain. 2007;130:1350–9. https://doi.org/10.1093/brain/awm063
12. Brown P, Brandel J-P, Sato T, Nakamura Y, MacKenzie J, Will RG, et al. Iatrogenic Creutzfeldt-Jakob disease, final assessment. Emerg Infect Dis. 2012;18:901–7. https://doi.org/ 10.3201/eid1806.120116
13. World Health Organization. Global surveillance, diagnosis and therapy of human transmissible spongiform encephalopathies: report of a WHO consultation, Geneva, Switzerland. 1998 Feb 9–11 [cited 2019 Aug 8]. https://apps.who.int/iris/handle/10665/65516
14. Kobayashi A, Parchi P, Yamada M, Mohri S, Kitamoto T. Neuropathological and biochemical criteria to identify acquired Creutzfeldt-Jakob disease among presumed sporadic cases. Neuropathology. 2016;36:305–10. https://doi.org/10.1111/neup.12270
15. Takeuchi A, Kobayashi A, Parchi P, Yamada M, Morita M, Uno S, et al. Distinctive properties of plaque-type dura mater graft-associated Creutzfeldt-Jakob disease in cell-protein misfolding cyclic amplification. Lab Invest. 2016;96:581–7. https://doi.org/10.1038/labinvest.2016.27
16. Ward HJ, Everington D, Cousens SN, Smith-Bathgate B, Gillies M, Murray K, et al. Risk factors for sporadic Creutzfeldt-Jakob disease. Ann Neurol. 2008;63:347–54. https://doi.org/10.1002/ana.21294
17. López FJG, Ruiz-Tovar M, Almazán-Isla J, Alcalde-Cabero E, Calero M, de Pedro-Cuesta J. Risk of transmission of sporadic Creutzfeldt-Jakob disease by surgical procedures: systematic reviews and quality of evidence. Euro Surveill. 2017;22:16–00806. https://doi.org/10.2807/1560-7917.ES.2017.22.43.16-00806
18. Puopolo M, Ladogana A, Vetrugno V, Pocchiari M. Transmission of sporadic Creutzfeldt-Jakob disease by blood transfusion: risk factor or possible biases. Transfusion. 2011;51:1556–66. https://doi.org/10.1111/j.1537-2995.2010.03004.x
19. Urwin PJ, Mackenzie JM, Llewelyn CA, Will RG, Hewitt PE. Creutzfeldt-Jakob disease and blood transfusion: updated results of the UK Transfusion Medicine Epidemiology Review Study. Vox Sang. 2016;110:310–6. https://doi.org/10.1111/vox.12371
20. Crowder LA, Schonberger LB, Dodd RY, Steele WR. Creutzfeldt-Jakob disease lookback study: 21 years of surveillance for transfusion transmission risk. Transfusion. 2017;57:1875–8. https://doi.org/10.1111/trf.14145
21. Brown P, Cervenáková L, McShane L, Goldfarb LG, Bishop K, Bastian F, et al. Creutzfeldt-Jakob disease in a husband and wife. Neurology. 1998;50:684–8. https://doi.org/10.1212/WNL.50.3.684
22. Rudge P, Jaunmuktane Z, Adlard P, Bjurstrom N, Caine D, Lowe J, et al. Iatrogenic CJD due to pituitary-derived growth hormone with genetically determined incubation times of up to 40 years. Brain. 2015;138(Pt 11):3386–99, 20, 21, 22.
23 de Pedro-Cuesta J, Glatzel M, Almazán J, Stoeck K, Mellina V, Puopolo M, et al. Human transmissible spongiform encephalopathies in eleven countries: diagnostic pattern across time, 1993-2002. BMC Public Health. 2006;6:278. https://doi.org/10.1186/1471-2458-6-278
24. van Duijn CM, Delasnerie-Lauprêtre N, Masullo C, Zerr I, de Silva R, Wientjens DP, et al. Case–control study of risk factors of Creutzfeldt-Jakob disease in Europe during 1993-95. European Union (EU) Collaborative Study Group of Creutzfeldt-Jakob disease (CJD). Lancet. 1998;351:1081–5. https://doi.org/10.1016/S0140-6736(97)09468-3
25. Alcalde-Cabero E, Almazan-Isla J, Brandel JP, Breithaupt M, Catarino J, Collins S, et al. Health professions and risk of sporadic Creutzfeldt-Jakob disease, 1965 to 2010. Euro Surveill. 2012;17:20144.
26. Bradford BM, Piccardo P, Ironside JW, Mabbott NA. Human prion diseases and the risk of their transmission during anatomical dissection. Clin Anat. 2014;27:821–32. https://doi.org/10.1002/ca.22403
27. Worsley KJ. The power of likelihood ratio and cumulative sum tests for a change in a binomial probability. Biometrika. 1983;70:455–64. https://doi.org/10.1093/biomet/70.2.455
28. Bundesärztekammer (BÄK). Ärztinnen und Ärzte mit Schwerpunktbezeichnung, BÄK. 2019 [cited 2019 Dec 2]. http://www.gbe-bund.de/oowa921-install/servlet/oowa/aw92/dboowasys921.xwdevkit/xwd_init?gbe.isgbetol/xs_start_neu/&p_aid=3&p_aid=66737473&nummer=614&p_sprache=D&p_indsp=99999999&p_aid=29100768
29. Bundesärztekammer (BÄK). Ärztinnen und Ärzte mit Gebiets- und Facharztbezeichnung, BÄK. 2019 [cited 2019 Feb 27]. http://www.gbe-bund.de/oowa921-install/servlet/oowa/aw92/dboowasys921.xwdevkit/xwd_init?gbe.isgbetol/xs_start_neu/&p_aid=i&p_aid=7768273&nummer=656&p_sprache=D&p_indsp=99999999&p_aid=70341618
30. Statistisches Bundesamt (DESTATIS). Bevölkerung: Deutschland, Stichtag, Altersjahre. 2019 [cited 2019 Feb 27]. http://www-genesis.destatis.de/genesis/online/link/tabellen/12411*
31. Parchi P, Giese A, Capellari S, Brown P, Schulz-Schaeffer W, Windl O, et al. Classification of sporadic Creutzfeldt-Jakob disease based on molecular and phenotypic analysis of 300 subjects. Ann Neurol. 1999;46:224–33. https://doi.org/10.1002/1531-8249(199908)46:2<224::AID-ANA12>3.0.CO;2-W
32. Ruegger J, Stoeck K, Amsler L, Blaettler T, Zwahlen M, Aguzzi A, et al. A case-control study of sporadic Creutzfeldt-Jakob disease in Switzerland: analysis of potential risk factors with regard to an increased CJD incidence in the years 2001–2004. BMC Public Health. 2009;9:18. https://doi.org/10.1186/1471-2458-9-18
33. Zerr I, Brandel JP, Masullo C, Wientjens D, de Silva R, Zeidler M, et al. European surveillance on Creutzfeldt-Jakob disease: a case-control study for medical risk factors. J Clin Epidemiol. 2000;53:747–54. https://doi.org/10.1016/S0895-4356(99)00207-3
34. Wientjens DP, Davanipour Z, Hofman A, Kondo K, Matthews WB, Will RG, et al. Risk factors for Creutzfeldt-Jakob disease: a reanalysis of case-control studies. Neurology. 1996;46:1287–91. https://doi.org/10.1212/WNL.46.5.1287
35. Cocco PL, Caperna A, Vinci F. Occupational risk factors for the sporadic form of Creutzfeldt-Jakob disease. Med Lav. 2003;94:353–63.
36. Schoene WC, Masters CL, Gibbs CJ Jr, Gajdusek DC, Tyler HR, Moore FD, et al. Transmissible spongiform encephalopathy (Creutzfeldt-Jakob disease). Atypical clinical and pathological findings. Arch Neurol. 1981;38:473–7. https://doi.org/10.1001/archneur.1981.00510080035002

37. Creutzfeldt-Jakob disease in histopathology technicians. N Engl J Med. 1988;318:853–4. https://doi.org/10.1056/NEJM198803313181312
38. Creutzfeldt-Jakob disease in histopathology technicians. N Engl J Med. 1988;318:853–4. https://doi.org/10.1056/NEJM198803313181312
39. Gorman DG, Benson DF, Vogel DG, Vinters HV. Creutzfeldt-Jakob disease in a pathologist. Neurology. 1992;42:463. https://doi.org/10.1212/WNL.42.2.463
40. Berger JR, David NJ. Creutzfeldt-Jakob disease in a physician: a review of the disorder in health care workers. Neurology. 1993;43:205–6. https://doi.org/ 10.1212/WNL.43.1_Part_1.205
41. Weber T, Tumani H, Holdorff B, Collinge J, Palmer M, Kretzschmar HA, et al. Transmission of Creutzfeldt-Jakob disease by handling of dura mater. Lancet. 1993;341:123–4. https://doi.org/10.1016/0140-6736(93)92608-V
42. Mitrová E, Belay G. Creutzfeldt-Jakob disease in health professionals in Slovakia. Eur J Epidemiol. 2000;16:353–5. https://doi.org/10.1023/A:1007601313133
43. de Pedro Cuesta J, Ruiz Tovar M, Ward H, Calero M, Smith A, Verduras CA, et al. Sensitivity to biases of case-control studies on medical procedures, particularly surgery and blood transfusion, and risk of Creutzfeldt-Jakob disease. Neuroepidemiology. 2012;39:1–18. https://doi.org/10.1159/000339318

Address for correspondence: Peter Hermann, National Reference Center for TSE, Department of Neurology, University Medical Center Göttingen, Robert-Koch Strasse 40, 37075 Göttingen, Germany; email: peter.hermann@med.uni-goettingen.de

Analysis of MarketScan Data for Immunosuppressive Conditions and Hospitalizations for Acute Respiratory Illness, United States

Manish Patel, Jufu Chen, Sara Kim, Shikha Garg, Brendan Flannery, Zaid Haddadin, Danielle Rankin, Natasha Halasa, H. Keipp Talbot, Carrie Reed

Increasing use of immunosuppressive biologic therapies poses a challenge for infectious diseases. Immunosuppressed patients have a high risk for influenza complications and an impaired immune response to vaccines. The total burden of immunosuppressive conditions in the United States, including those receiving emerging biologic therapies, remains unknown. We used the national claims database MarketScan to estimate the prevalence of immunosuppressive conditions and risk for acute respiratory illnesses (ARIs). We studied 47.2 million unique enrollees, representing 115 million person-years of observation during 2012–2017, and identified immunosuppressive conditions in 6.2% adults 18–64 years of age and 2.6% of children <18 years of age. Among 542,105 ARI hospitalizations, 32% of patients had immunosuppressive conditions. The risk for ARI hospitalizations was higher among enrollees with immunosuppression than among nonimmunosuppressed enrollees. Future efforts should focus on developing improved strategies, including vaccines, for preventing influenza in immunosuppressed patients, who are an increasing population in the United States.

Influenza is a common cause of illness and death in the United States and affects persons of all ages (*1*). Risk for complications from infection is higher in subpopulations, such as persons with immunosuppressive conditions (*2*,*3*). In recent years, an increasing number of patients are receiving biologic or immune-modulating agents with immunosuppressive potential (*4*,*5*). Although data exist on the prevalence of some immunosuppressive conditions, the total burden of these conditions in the United States remains unknown, particularly when considering patients who are receiving emerging immunosuppressive therapies (*6*–*8*).

Influenza vaccination prevents disease and averts severe outcomes, such as hospitalization and death (*1*,*9*). A meta-analysis of observational studies of influenza vaccines identified that pooled vaccine effectiveness was 33%–67% against medically attended, laboratory-confirmed influenza illness in the overall population (*10*). However, a review of immunogenicity studies suggests that antibody responses to inactivated influenza vaccines (IIVs) in persons who are immunocompromised could be suboptimal compared with persons without immunosuppression (*11*).

Clinical effectiveness data are sparse, but a recent observational study demonstrated lower vaccine effectiveness against influenza illness (≈20%) in patients with cancer compared with the general population (≈42%) (*12*,*13*). Increasing efficacy of influenza vaccines in immunosuppressed populations might substantially improve population benefits of influenza vaccines. Establishing a case definition for and quantifying the burden of immunosuppressive conditions might facilitate evaluation and use of influenza vaccines to enhance immune response in this high-risk target group.

IIVs that contain egg-propagated vaccine viruses and a standard dose of 15 μg of hemagglutinin antigen of each virus per dose, without adjuvant, are the most commonly used vaccines worldwide (*14*). In recent years, 2 enhanced IIVs, MF59-adjuvanted standard-dose IIV and a high-dose IIV that contains 4 times the hemagglutinin antigen of each virus compared with the standard-dose IIV, have been developed to improve the immune responses to and efficacy of standard-dose IIVs (*15*,*16*). Both vaccines are currently licensed in the United States for use in

Author affiliations: Centers for Disease Control and Prevention, Atlanta, Georgia, USA (M. Patel, J. Chen, S. Kim, S. Garg, B. Flannery, C. Reed); Vanderbilt University, Nashville, Tennessee, USA (Z. Haddadin, D. Rankin, N. Halasa, H. Keipp Talbot)

DOI: https://doi.org/10.3201/eid2608.191493

older adults (*9*). High-dose IIV has also met prespecified criteria for superior efficacy against laboratory-confirmed influenza compared with standard-dose IIV (*15*,*17*). Although these enhanced IIVs are not yet licensed for use in US patients <65 years of age, some evidence suggests that humoral immune responses to these vaccines might also be greater than responses to standard IIVs in adults 18–64 years of age who have immunosuppressive conditions (*18*,*19*).

In this study, we created and used case definitions for immunosuppressive conditions by using a modified version of an algorithm implemented by previous investigators (*20*). Our primary objective was to determine the prevalence of immunosuppressive conditions in the US population among MarketScan (Truven Health MarketScan, https://marketscan.truvenhealth.com) enrollees <65 years of age. We recognized that International Classification of Diseases (ICD) and drug codes might not accurately capture enrollees with impaired immune systems. Thus, our secondary objective was to explore whether rates of influenza vaccination and hospitalization for acute respiratory infection (ARI) differed between those with and without immunosuppressive conditions identified by our case definitions.

Methods

Data Sources

We analyzed the MarketScan Commercial Claims and Medicare data from August 1, 2012, through July 31, 2017, to explore the prevalence of immunosuppressive conditions. We calculated rates of ARI hospitalizations among these enrollees relative to enrollees without immunosuppressive conditions. MarketScan is a de-identified commercial insurance claims database representing 30–50 million persons per year from >160 large employers and health plans representing all 50 US states (*21*). The Medicare database includes Medicare-eligible retirees with employer-sponsored Medicare Supplemental plans. The database includes healthcare claims with diagnosis and procedure codes for medical encounters and all outpatient prescription medications. Variables we examined included age, sex, influenza vaccination, and medications, as well as codes from the ICD, 9th Revision, Clinical Modification (ICD-9-CM), or ICD, 10th Revision, Clinical Modification (ICD-10-CM), for immunosuppressive conditions (any medical encounter/claim) and hospitalizations for pneumonia, influenza, and diseases of the respiratory system. We restricted our sample to those enrolled and covered by the drug benefit program during the study years.

Immunosuppressive Conditions

Greenberg et al. have previously established an algorithm for identifying patients with active immunosuppression on the basis of ICD and Current Procedural Terminology (CPT) codes in a large database of patients who were acutely ill with sepsis (*20*). We slightly modified the approach by Greenberg et al. to derive a case definition of immunosuppressive conditions based on 6 groups of diseases and 3 classes of medications (Figure 1). The Infection Diseases Society of America has published detailed guidance for the selection and timing of vaccines for persons with specific immunocompromising conditions but does not consider specific ICD codes (*5*). We reviewed those guidelines to identify additional immunocompromising conditions not included in the Greenberg algorithm (sickle cell disease, asplenia, and psoriatic arthritis) and assessed whether inclusion of these conditions would affect our results.

We considered 3 groups of enrollees to be immunosuppressed: 1) persons with symptomatic HIV/AIDS (excluding asymptomatic HIV), hematologic malignancy, or other intrinsic immune conditions; 2) persons with solid malignancy, organ transplant, rheumatologic, or other inflammatory conditions that were deemed immunosuppressed if patients received chemotherapy or an immune modulator; or rheumatologic or other inflammatory conditions who received systemic (nontopical, noninhaled) steroids; 3) any enrollee not in the first 2 groups who received chemotherapy, an immune modulator, or systemic steroids for >14 days (not considered by Greenberg et al.). Enrollees receiving corticosteroids for <14 days were not considered immunosuppressed because most probably were receiving short-term burst doses, which has low immunosuppressive potential (*5*). The 3 enrollee groups were mutually exclusive. Enrollees who did not meet the immunosuppressed case definition were considered nonimmunosuppressed.

We examined data for persons of all ages who had continuous enrollment in 1 insurance plan during 2 consecutive years. We used ICD-9 and ICD-10 codes from any medical encounter/claim to identify immunosuppressive conditions during the 12-month enrollment periods, including influenza seasons from August 1, 2012, through July 31, 2017. Enrollees were considered immunosuppressed during the enrollment year if they had ≥1 hospitalization or 2 separate outpatient visits listing a corresponding ICD-9 code before October 1, 2015 or ICD-10 code after October 1, 2015 (Table 1), or were prescribed 1 of the listed medications during each of the 12 months (August 1–July 31) of the study period (Table 2, https://wwwnc.cdc.

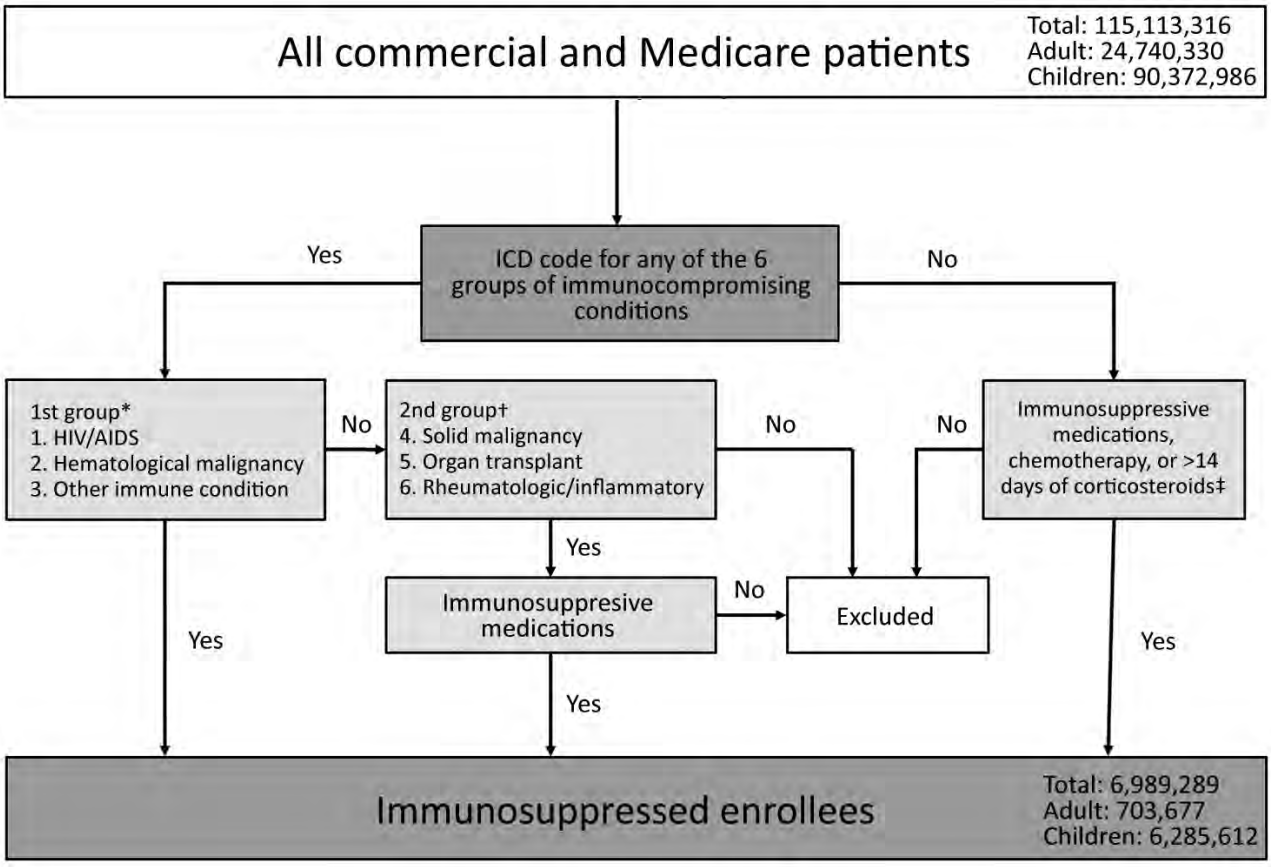

Figure 1. Algorithm for case definitions of immunosuppressive conditions in MarketScan claims database of Commercial and Medicare enrollees, United States, August 2012–July 2017. *These 3 conditions were deemed to be immunosuppressive. †These 3 conditions were deemed to be immunosuppressive only if enrollees were given chemotherapeutic agents or immune-modulating agents or if enrollees who had rheumatologic or inflammatory conditions were receiving systemic corticosteroids. ‡We deemed that enrollees might be given chemotherapeutic agents or immune-modulating agents and not be captured by ICD codes (from the 9th Revision, Clinical Modification, or 10th Revision, Clinical Modification) for the 6 potential immunosuppressive conditions described in the first 2 footnotes. We excluded treatment with corticosteroids for <14 days from these groups to avoid capturing enrollees who might be receiving short-term bursts of corticosteroids (e.g., those with asthma). ICD, International Classification of Diseases.

gov/EID/article/26/8/19-1493-T2.htm). For the purposes of analysis, we considered these persons immunosuppressed for that entire 12-month period.

Acute Respiratory Illness Hospitalizations

All ICD codes that we used for immunosuppressive conditions might not necessarily be specific for conditions that impair immunity. Thus, we also evaluated risk for ARI hospitalization among patients who had immunosuppressive conditions in the MarketScan population. We identified ARI hospitalizations for pneumonia, influenza, and diseases of the respiratory system based on the first 3 discharge diagnosis ICD-9 or ICD-10 codes during August 1–July 31 in the 5 study years. Codes included 460–466 and 480–488 before October 1, 2015 (ICD-9-CM), and J00–J06, J09–J18, and J20–J22 after October 1, 2015 (ICD-10-CM). Data are limited on the validity of these ARI hospitalization codes overall and their position on the discharge diagnosis (22). Using codes in any position improves sensitivity but decreases positive predictive value. To balance sensitivity and specificity, we restricted discharge diagnoses to the first 3 positions and assumed that relative risk for ARI hospitalization between immunosuppressed and nonimmunosuppressed enrollees based on these codes would be unaffected. We inferred that higher relative rates of ARI hospitalizations among immunosuppressed enrollees would support the notion that the cohort of patients identified by our case definitions had some degree of immunosuppression overall.

Influenza Vaccination

We identified enrollees who received influenza vaccine by using CPT codes (Table 3). We assumed that the relative adjusted vaccination rates between

immunosuppressed and nonimmunosuppressed populations would reflect differences in influenza vaccine uptake.

Statistical Analysis

We examined prevalence of immunosuppressive conditions among all enrollees during each influenza season, stratified by age groups (0–8 years, 9–17 years, 18–49 years, and 50–64 years). We calculated relative incidence rates and 95% CIs of ARI hospitalization and influenza vaccination for enrollees with and without immunosuppressive conditions by using a generalized linear model with binomial distribution and log link function. We calculated 95%

Table 1. Conditions and ICD-9-CM and ICD-10-CM codes used to identify enrollees with immunosuppression in MarketScan database, United States, July 2012–August 2017*

Condition	ICD-9 codes	ICD-10 codes
HIV/AIDS†		
HIV/AIDS disease	042	B20-B24
Hematologic malignancy		
Lymphatic and hematopoietic tissue malignancy	200–208	C81-C83; C88-C96
Other immune conditions‡		
Disorders of immune mechanism	279	D89
Neutropenia	288.0	D70
Functional disorders of neutrophils	288.1	D71
Genetic anomalies of leukocytes	288.2	D72.0
Decreased leukocyte count	288.5	D72.81
Leukocyte disease NEC	288.8	D72.89
Leukocyte disease NOS	288.9	D72.9
Myelofibrosis	289.83	D75.81
Blood diseases NEC	289.89	D47.4; D75.89; D75.9; D89.2
Blood diseases NOS	289.9	D75.9; D75.89
Immunologic findings NEC	795.7	R76; R83.4-R87.4; R89.4
Nonspecific immune findings NEC and NOS	795.79	R76; R83.4-R87.4; R89.4
Solid malignancy		
Organ/system malignant tumors	140–199	C00-C07; C11-C19; C22-C80; Z85
Neuroendocrine tumors	209	C7A; C7B; D3A
Neoplasms of uncertain behavior	235–239	D00-D49
Organ transplant§		
Complications of transplanted organ	996.8	T86
Organ transplant status	V42	Z94; Z98.85
Rheumatologic/inflammatory¶		
Sarcoidosis	135	D86
Amyloidosis NOS	277.3	E85
Familial Mediterranean fever	277.31	E85.0; M04
Amyloidosis NEC	277.39	E85.1; E85.3; E85.8
Multiple sclerosis	340	G35
Other CNS demyelination	341	G36; G37.1; G37.3; G37.8; G37.9
Acute infective polyneuritis	357	G61.0; G61.9
Acute myocarditis	422	I40
Polyarteritis nodosa and other	446	M30
Allergic alveolitis/pneumonitis NOS	495.9	T78.40; J67.9
Other alveolar pneumonopathy	516	J84.01; J84.02; J84.09
Enteritis and colitis	555–558	K50-K52
Lupus erythematosus	695.4	L93.0; L93.2; M32
Diffuse connective tissue disease	710	L94; M35.8; M35.9
Arthropathy with infection	711	M12.9; M01.X0; M02.10
Crystal arthropathies	712	M11
Rheumatoid arthritis/inflammatory polyarthropathy	714	M05-M14
Inflammatory spondylopathies	720	M46
Polymyalgia rheumatica	725	M31.5; M35.3

*CNS, central nervous system; ICD9-CM, International Classification of Diseases, 9th Revision, Clinical Modification; ICD-10-CM, International Classification of Diseases, 10th Revision, Clinical Modification; NOS, not otherwise specified; NEC, necrotizing enterocolitis.
†Excludes asymptomatic HIV codes of ICD-9 (V08) and ICD-10 (Z21).
‡Sickle cell disease, asplenia, and psoriatic arthritis were not included in the Greenberg algorithm (*20*) but are considered to have immune deficiencies by Infectious Diseases Society of America guidelines (*5*). Adding these to the algorithm only increased the prevalence of immunosuppressive conditions by 0.1%.
§Bone marrow and peripheral stem cell transplant were considered under organ transplant and only considered immunosuppressed if enrollees were currently being given chemotherapeutic agents or immune modulators. Considering these enrollees under other immune conditions in which immunosuppressed does not require receipt of chemotherapeutic agents or immune modulators would increase the overall prevalence of immunosuppressed by 0.01%.
¶Psoriatic arthritis was not included in the Greenberg algorithm and could be an indication for immunosuppressive treatment. Adding this condition did not increase the prevalence of immunosuppressive conditions.

Table 3. Codes for influenza vaccine used in analysis of MarketScan data for immunosuppressive conditions and hospitalizations for acute respiratory illness, United States

CPT no.*	Vaccine type
90653	Influenza virus vaccine, inactivated, subunit, adjuvanted, for intramuscular use
90654	influenza, seasonal, intradermal, preservative free
90655	Influenza virus vaccine, split virus, no preservative, for children 6–35 mo of age, for intramuscular use
90656	Influenza virus vaccine, split virus, no preservative, for use in persons ≥3 y of age, for intramuscular use
90657	Influenza virus vaccine, split virus, for children 6–35 mo of age, for intramuscular use
90658	Influenza virus vaccine, split virus, for use in persons ≥3 y of age, for intramuscular use
90659	Influenza, whole
90660	Influenza virus vaccine, live, for intranasal use
90661	Influenza virus vaccine, derived from cell cultures, subunit, preservative and antimicrobial drug free, for intramuscular use
90662	Influenza, high dose seasonal
90663	Influenza virus vaccine, pandemic H1N1
90664	Influenza virus vaccine, pandemic formulation, live, for intranasal use
90666	Influenza virus vaccine, pandemic formulation, split virus, preservative free, for intramuscular use
90667	Influenza virus vaccine, pandemic formulation, split virus, adjuvanted, for intramuscular use
90668	Influenza virus vaccine, pandemic formulation, split virus, for intramuscular use
90724	Influenza, unspecified formulation
90470	H1N1 immunization administration (intramuscular, intranasal)
90672	Influenza virus vaccine, quadrivalent, live, for intranasal use
90673	Influenza virus vaccine, trivalent, derived from recombinant DNA (recombinant influenza vaccine 3), hemagglutnin protein only, preservative and antimicrobial drug free, for intramuscular use
90685	Influenza virus vaccine, quadrivalent, split virus, preservative free, when administered to children 6–35 mo of age, for intramuscular use
90686	Influenza virus vaccine, quadrivalent, split virus, preservative free, when administered to children ≥3 y of age, for intramuscular use
90687	Influenza virus vaccine, quadrivalent, when administered to children 6–35 mo of age, for intramuscular use (not recognized by Medicare)
90688	Influenza virus vaccine, quadrivalent, when administered to persons ≥3 y, for intramuscular use (not recognized by Medicare)

*CPT, Current Procedural Terminology.

CIs for incidence rates based on the assumption that incidence rates followed a Poisson distribution. We compared rates for the entire year (August 1–July 31) and for December through March, the 4 months with the highest detection of influenza by surveillance data (23). We selected age, year, and sex, a priori, and adjusted the relative rates of ARI for these factors. We calculated person-time by using the total months each enrollee spent in a health plan supplying data to MarketScan during each study period. We conducted all analyses by using SAS version 9.4 (https://www.sas.com). The p values were 2-sided, and we considered a p value ≤0.05 as being statistically significant.

Results

During August 2012–July 2017, a total of 47.2 million unique enrollees representing 115 million person-years of observation were included in the US MarketScan database (Table 4). Some enrollees did not complete an entire year of follow-up; 87% were enrolled for an entire year and 95% for ≥10 months. Age distribution of all enrollees compared with those with immunosuppressive conditions varied:

Table 4. Prevalence of immunosuppressive conditions by person age and sex for acute respiratory illness in the MarketScan database, United States, July 2012–August 2017

Characteristic	All enrollees, person-years, no. (%)*	Immunosuppressive conditions†	
		Person-years (%)	Prevalence/100 person-years, %
Total	115,113,322 (100)	6,823,509 (100)	5.9
Age, y			
<1–8	11,074,106 (10)	160,137 (2)	1.4
9–17	13,666,230 (12)	474,703 (7)	3.5
18–49	52,413,795 (46)	2,580,737 (38)	4.9
50–64	28,552,259 (25)	2,470,817 (36)	8.
≥65	9,406,932 (8)	1,137,115 (17)	12.1
Sex			
M	55,282,285 (48)	2,597,852 (38)	4.7
F	59,831,037 (52)	4,225,657 (62)	7.1

*Person-time was calculated by using the total months each enrollee spent in a health plan supplying data to MarketScan during the study period. During August 2012–July 2017, a total of 47.2 million unique enrollees were in our MarketScan analysis.
†See Figure 1. Denotes patients had International Classification of Diseases codes for either 3 immunosuppressive conditions OR 3 conditions + immunosuppressive pharmacologic treatment (chemotherapeutic agents or immune-modeling agents or systemic corticosteroids >14 d).

10% versus 2% for those <8 years of age, 12% versus 7% for those 9–17 years of age, 46% versus 38% for those 18–49 years of age, 25% versus 36% for those 50–64 years of age, and 8% versus 17% for those ≥65 years of age) (Table 5).

Among 115 million person-years contributed during the study period, we found a prevalence of 5.9% for immunosuppressive conditions; prevalence was higher for female patients (7.1%) than for male patients (4.7%) (Table 5). Prevalence was 6.2% in the 18–64 year age group and 2.6% among children <18 years of age. Among enrollees with immunosuppressive conditions, 27% had HIV/AIDS, hematologic malignancy, or other intrinsic immune conditions; 36% had solid malignancies, organ transplant, or rheumatologic/inflammatory conditions treated with immunosuppressive medications; and 37% were related to immunosuppressive medications without the presence of an immunosuppressive medical conditions. We noted some increases in prevalence for immunosuppressive conditions during 2012–2017 for each of the age groups (Figure 2). When we included additional conditions not in the Greenberg algorithm (*20*) (sickle cell disease, asplenia, and psoriatic arthritis), our overall results did not change.

During the study period, we identified 542,105 ARI hospitalizations, of which 173,665 (32%) occurred in enrollees who had immunosuppression (Table 6). Annual rates of ARI were 4.2-fold higher among enrollees with immunosuppressive conditions (25.5 cases/1,000 person-years) compared with enrollees without immunosuppressive conditions (4.7 cases/1,000 person-years). When we restricted analysis to only the first 2 immunosuppressed groups without the immunosuppressive medications only group, we found that rates of ARI were 4.25-fold higher. Enrollees with immunosuppressive conditions accounted for 15% of the ARI hospitalizations among children <18 years of age and 38% of the ARI hospitalizations among persons 18–64 years of age.

Age-stratified relative rates of ARI hospitalization adjusted for sex and year were higher among those with immunosuppressive conditions compared with immunocompetent enrollees <1–8 years of age (8.1%, 95% CI 7.8%–8.4%), 9–17 years of age (5.0%, 95% CI 4.7%–5.4%), 18–49 years of age (6.7%, 95% CI 6.5%–6.8%), and 50–64 years of age (4.8%, 95% CI 4.6%–4.9%) (Table 5). The relative rates of ARI hospitalization annually were similar to the relative rates during peak influenza months of December–March. Rates of influenza vaccination were also higher among enrollees 0–8 years of age (1.24-fold), 9–17 years of age (1.29-fold), 18–49 years of age (1.7-fold), and 50–64 years of age (1.4-fold) with immunosuppressive conditions compared with enrollees without immunosuppressive conditions (Table 5).

Discussion

With the availability of new immunotherapy drugs and treatment practices for patients who have malignancies and chronic inflammatory diseases, persons with immunosuppressive conditions could account for an increasing proportion of patients in the United States (*4*,*25*–*28*). A systematic review suggests

Table 5. Acute respiratory illness hospitalizations for patients by age who had immunosuppressive conditions in MarketScan database, United States, July 2012–August 2017*

Characteristic	All ARI hospitalizations		ARI hospitalizations in immunosuppressed persons†		ARI in immunosuppressed versus nonimmunosuppressed persons, relative rate/1,000 person-years (95% CI)‡
	No.	Rate/1,000 person-years	No. (%)	Rate/1,000 person-years	
Year round, August–July					
Age, y					
All	542,105	4.7	173,665 (32.0)	25.5	4.2 (4.0–4.3)
>1–8	50,170	4.5	6,638 (13.2)	41.2	8.1 (7.8–8.4)
9–17	14,388	1.1	2,839 (19.7)	6.0	5.0 (4.7–5.4)
18–49	88,051	1.7	29,136 (33.1)	11.3	6.7 (6.5–6.9)
50–64	142,631	5.0	57,512 (40.3)	23.3	4.8 (4.6–4.9)
≥65	246,865	26.2	77,540 31.4)	68.3	2.1 (2.0–2.1)
Peak influenza season, December–March					
Age, y					
All	240,856	6.3	77,308 (32.1)	34.0	4.3 (4.2–4.5)
<1–8	27,084	7.3	3,408 (12.6)	63.4	7.9 (7.5–8.3)
9–17	5,838	1.3	1,258 (21.5)	7.9	5.7 (5.1–6.4)
18–49	37,190	2.1	12,786 (34.4)	14.8	6.8 (6.8–7.4)
50–64	61,316	6.4	25,491 (41.6)	31.0	5.0 (4.8–5.2)
≥65	109,428	34.9	34,365 (31.4)	90.8	2.1 (2.0–2.2)

*ARI, acute respiratory illness.
†See Figure 1. Immunosuppressive denotes patients had International Classification of Diseases codes for either 3 immunosuppressive conditions OR 3 conditions plus immunosuppressive pharmacologic treatment (chemotherapeutic agents or immune modulators or systemic corticosteroids >14 d).
‡Relative rates of ARI were adjusted for year of hospitalization and sex.

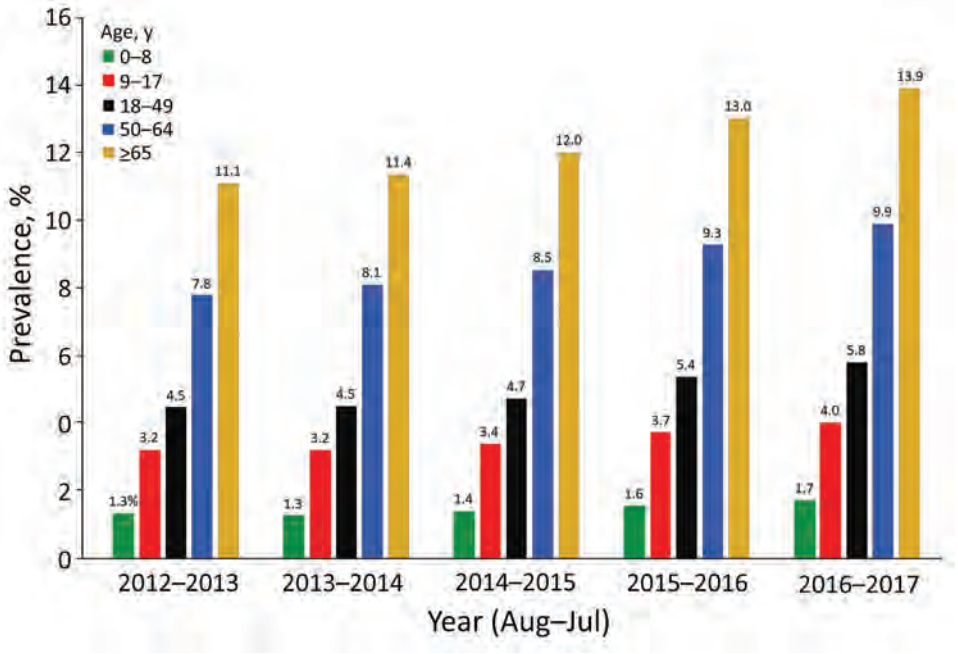

Figure 2. Prevalence of immunosuppressive conditions among children and adults in MarketScan claims database, United States, August 2012–July 2017.

that these patients, especially those who have HIV, solid-organ and stem-cell transplants, and cancer, as well as patients receiving biologic agents, have an increased risk for influenza-related complications and suboptimal immune responses to standard IIV (*11*). Our analysis indicates that ≈6% of the enrollees in a large US claims database had immunosuppressive conditions during 2012–2017, which might represent some 12 million US persons if these rates are similar in the general US population (*29*). We found that risk for ARI hospitalization was 5–8-fold higher among enrollees <65 years of age who we classified as immunosuppressed, which is consistent with results of published studies that documented higher risk for complications from influenza and other pathogens in this patient population (*5*,*30*–*35*). The higher risk for ARI hospitalizations in enrollees with immunosuppression is also consistent with studies demonstrating inferior antibody responses to standard IIVs in immunosuppressed patients. (*11*). Some 38% of all patients 18–64 years of age hospitalized for ARI had immunosuppressive conditions. Our results indicate that immunosuppressed patient groups are disproportionally hospitalized for ARI and likely at high risk for complications from influenza.

Data are limited on whether enhanced vaccines would improve protection against influenza in immunosuppressed patients compared with standard IIVs. Immunosuppressive conditions are heterogeneous, comprising a wide range of immune states, some of which are time-variant, including receipt of immunosuppressive medications. Clinical trials of influenza vaccines typically include healthy persons. Studies assessing vaccine immunogenicity in patients with immunosuppressive conditions usually focus on a few specialized conditions; because of sample size limitations for efficacy endpoints, these studies typically focus on immunogenicity (*18*,*19*,*36*–*41*). A meta-analysis of studies has demonstrated strongly reduced humoral immune responses to standard IIVs in immunosuppressed patients who had HIV, organ transplants, or cancer and those receiving immunosuppressive medications (*11*). The pooled odds of increased antibody titers after IIV ranged from 0.24 to 0.71 among immunosuppressive conditions compared with nonimmunosuppressive conditions (*11*). Studies of high-dose seasonal IIVs have demonstrated consistently stronger antibody responses (1.1–6.7-fold increase in antibody titers) compared with standard IIVs in adults <65 years of age (*18*,*19*,*36*,*38*,*39*). Studies of adjuvanted seasonal IIVs have not consistently resulted in improved immune responses compared with standard IIVs (*19*,*42*–*44*). Although these studies of high-dose IIVs offer hope for improving immune response in immunosuppressed patients, they are not likely to represent the entire spectrum of conditions that might affect the immune system and might not reflect actual clinical efficacy.

Our analysis offers a starting point for identifying patients that clinical trials of healthy participants typically do not capture and in whom protection from standard vaccines might be suboptimal. A great deal of heterogeneity exists in immunosuppressive conditions with varying degrees of immunosuppression and

conditions that affect different components of the immune system. The conditions captured in our analysis probably represent the severe end of the immunosuppression spectrum. For example, we did not assess certain medical conditions associated with lesser degrees of immune suppression, such as diabetes and end-stage renal failure (*45*,*46*). The risk for disease is likely to vary among the immunosuppressive conditions identified in our study. However, from a public health perspective, a case definition of immunosuppression provides a target population for assessing overall risk for disease, rates of vaccination, and protective effects of vaccination.

The increased rate of ARI hospitalizations and influenza vaccination among immunosuppressed enrollees in MarketScan datasets suggests that these codes identified persons at increased risk for severe manifestations of infection. In addition to an increase in severe infections caused by immunosuppression, higher rates of ARI hospitalization might reflect differences in healthcare-seeking patterns or admission practices. Patients who have some immunosuppressive conditions also have had reduced immune responses to standard IIV (*11*) and thus might benefit from improved influenza vaccine strategies. Further research evaluating performance of influenza vaccines among the immunosuppressed cohort could help determine if expanded use of enhanced vaccines is warranted and cost-effective. The case definition for immunosuppressive conditions could also be used to evaluate influenza vaccine effectiveness in hospital-based observational studies or large administrative databases that individually link vaccination records to laboratory confirmed influenza (*12*,*47*). Last, evaluation of antibody and cellular immune responses to enhanced vaccines compared with standard vaccines in patients with these broad range of immunosuppressive conditions could help bridge the evidence gap that is needed to inform licensure and policy decisions for expanding the use of these vaccines.

Our results should be interpreted in the context of several limitations. We used a previously developed set of ICD codes for identifying active immunosuppression in patients who had sepsis, but not all patients with these conditions might have active immunosuppression. For example, although we specified codes that included HIV only when symptomatic, we cannot be certain about the degree of immunosuppression among patients who had ICD codes for symptomatic HIV/AIDS. Conversely, we might have missed other conditions that could be immunosuppressive. However, the approach proposed by Greenberg et al. is a reasonable start because these authors validated these codes of immunosuppression against medical records (sensitivity 87%, specificity 98%) and identified that these patients had higher risk for sepsis (*20*). However, this validation occurred at 1 hospital, and the accuracy of the codes might be affected by temporal differences in coding practices and among medical institutions.

In addition, the switch from ICD-9 to ICD-10 might have affected our case definition and needs further validation against individual medical records. We used a broad definition for ARI hospitalization, which is not specific to risk for influenza risk alone. We also did not expand the use of the ARI discharge codes to beyond the third position because it would reduce the positive predictive value of the code. A review demonstrated that ≈15% of winter ARI hospitalizations are attributable to influenza (*48*). However, the relative differences in respiratory diseases between potentially immunocompromised and non-immunocompromised enrollees was informative and is consistent with the higher risk for severe complications from infectious illnesses, including influenza, in this population. MarketScan vaccination data probably underestimate true influenza vaccine coverage in the population, particularly for persons >65 years of age, because not all vaccinations are billed to insurance companies (*24*). However, the relative vaccination rates for immunosuppressed and nonimmunosuppressed persons were informative and unlikely to be affected.

Our study also considered an enrollee immunosuppressed during the study year if they met

Table 6. Age-specific influenza vaccination coverage and relative rates of coverage in enrollees with and without immunosuppressive conditions in MarketScan database, United States, July 2012–-August 2017

Age, y*	Vaccine coverage, %		Relative rate of vaccination, immunosuppressed versus nonimmunosuppressed, % (95% CI)
	Immunosuppressed	Nonimmunosuppressed	
>1–8	60.1	58.3	1.24 (1.23–1.25)
9–17	47.2	40.5	1.30 (1.29–1.30)
18–49	20.9	14.7	1.72 (1.71–1.73)
50–64	28.9	23.9	1.47 (1.46–1.48)
≥65	30.3	27.9	1.27 (1.26–1.28)

*MarketScan vaccination data probably underestimate true influenza vaccine coverage in the population particularly for persons ≥65 years of age because not all vaccinations are billed to insurance companies (*24*). Relative rates of vaccination between immunosuppressed and nonimmunosuppressed should not be affected.

the case definition at any point in the year, but immunosuppression can be time-variant. Data from MarketScan represents a subset of the US insured population and might not be generalizable to other insured or noninsured populations (*49*,*50*). Claims-based data are also subject to inaccuracies and missingness. Insured patients are likely healthier than uninsured patients and thus our data may underestimate immunosuppression. Although we did not observe substantial increases in prevalence of immunosuppression, prevalence might be higher after the onset of the study period because of increasing coverage of these medications through insurance providers that are captured by MarketScan. Last, although some enrollees dropped out before the end of the 12-month study period, prevalence estimates would be unaffected if drop-out rates were similar between immunosuppressed and nonimmunosuppressed enrollees.

In conclusion, our findings quantify that immunosuppressive conditions, many of which impair immune responses to standard influenza vaccines, affect ≈6% of the enrollees in a large US claims database. Patients identified by our case definitions manifested higher risk for complications from respiratory infections, with 1 in 3 ARI hospitalizations occurring among patients who were immunosuppressed. Consequently, novel strategies to improve efficacy of influenza vaccines in these high-risk patients could substantially reduce the overall burden of severe influenza and hospitalizations in the population.

About the Author

Dr. Patel is a medical epidemiologist with the Influenza Division, National Center for Immunizations and Respiratory Diseases, Centers for Disease Control and Prevention, Atlanta, GA. His primary research interest is prevention and control of influenza.

References

1. Rolfes MA, Flannery B, Chung JR, O'Halloran A, Garg S, Belongia EA, et al.; US Influenza Vaccine Effectiveness (Flu VE) Network, the Influenza Hospitalization Surveillance Network, and the Assessment Branch, Immunization Services Division, Centers for Disease Control and Prevention. Effects of influenza vaccination in the United States during the 2017–2018 influenza season. Clin Infect Dis. 2019;69:1845–53. https://doi.org/10.1093/cid/ciz075
2. Vilchez RA, McCurry K, Dauber J, Lacono A, Griffith B, Fung J, et al. Influenza virus infection in adult solid organ transplant recipients. Am J Transplant. 2002;2:287–91. https://doi.org/10.1034/j.1600-6143.2002.20315.x
3. Memoli MJ, Athota R, Reed S, Czajkowski L, Bristol T, Proudfoot K, et al. The natural history of influenza infection in the severely immunocompromised vs nonimmunocompromised hosts. Clin Infect Dis. 2014;58:214–24. https://doi.org/10.1093/cid/cit725
4. Bersanelli M, Buti S, De Giorgi U, Di Maio M, Giannarelli D, Pignata S, et al. State of the art about influenza vaccination for advanced cancer patients receiving immune checkpoint inhibitors: when common sense is not enough. Crit Rev Oncol Hematol. 2019;139:87–90. https://doi.org/10.1016/j.critrevonc.2019.05.003
5. Rubin LG, Levin MJ, Ljungman P, Davies EG, Avery R, Tomblyn M, et al.; Infectious Diseases Society of America. 2013 IDSA clinical practice guideline for vaccination of the immunocompromised host. Clin Infect Dis. 2014;58:309–18. https://doi.org/10.1093/cid/cit816
6. Harpaz R, Dahl RM, Dooling KL. Prevalence of immunosuppression among US adults, 2013. JAMA. 2016;316:2547–8. https://doi.org/10.1001/jama.2016.16477
7. Satcher Johnson A, Song R, Hall HI. Estimated HIV incidence, prevalence, and undiagnosed infections in US states and Washington, DC, 2010–2014. J Acquir Immune Defic Syndr. 2017;76:116–22. https://doi.org/10.1097/QAI.0000000000001495
8. Miller KD, Nogueira L, Mariotto AB, Rowland JH, Yabroff KR, Alfano CM, et al. Cancer treatment and survivorship statistics, 2019. CA Cancer J Clin. 2019;69:363–85. https://doi.org/10.3322/caac.21565
9. Grohskopf LA, Sokolow LZ, Broder KR, Walter EB, Fry AM, Jernigan DB. Prevention and control of seasonal influenza with vaccines: recommendations of the advisory committee on immunization practices—United States, 2018–19 influenza season. MMWR Recomm Rep. 2018;67:1–20. https://doi.org/10.15585/mmwr.rr6703a1
10. Belongia EA, Simpson MD, King JP, Sundaram ME, Kelley NS, Osterholm MT, et al. Variable influenza vaccine effectiveness by subtype: a systematic review and meta-analysis of test-negative design studies. Lancet Infect Dis. 2016;16:942–51. https://doi.org/10.1016/S1473-3099(16)00129-8
11. Beck CR, McKenzie BC, Hashim AB, Harris RC, Nguyen-Van-Tam JS; University of Nottingham Influenza and the ImmunoCompromised (UNIIC) Study Group. Influenza vaccination for immunocompromised patients: systematic review and meta-analysis by etiology. J Infect Dis. 2012;206:1250–9. https://doi.org/10.1093/infdis/jis487
12. Blanchette PS, Chung H, Pritchard KI, Earle CC, Campitelli MA, Buchan SA, et al. Influenza vaccine effectiveness among patients with cancer: a population-based study using health administrative and laboratory testing data From Ontario, Canada. J Clin Oncol. 2019;37:2795–804. https://doi.org/10.1200/JCO.19.00354
13. Nichols MK, Andrew MK, Hatchette TF, Ambrose A, Boivin G, Bowie W, et al.; Serious Outcomes Surveillance Network of the Canadian Immunization Research Network (CIRN), the Toronto Invasive Bacterial Diseases Network (TIBDN). Influenza vaccine effectiveness to prevent influenza-related hospitalizations and serious outcomes in Canadian adults over the 2011/12 through 2013/14 influenza seasons: a pooled analysis from the Canadian Immunization Research Network (CIRN) Serious Outcomes Surveillance (SOS Network). Vaccine. 2018;36:2166–75. https://doi.org/10.1016/j.vaccine.2018.02.093
14. Vaccines against influenza WHO position paper—November 2012. Wkly Epidemiol Rec. 2012;87:461–76.
15. DiazGranados CA, Dunning AJ, Kimmel M, Kirby D, Treanor J, Collins A, et al. Efficacy of high-dose versus standard-dose influenza vaccine in older adults. N Engl J

Med. 2014;371:635–45. https://doi.org/10.1056/NEJMoa1315727
16. Durando P, Icardi G, Ansaldi F. MF59-adjuvanted vaccine: a safe and useful tool to enhance and broaden protection against seasonal influenza viruses in subjects at risk. Expert Opin Biol Ther. 2010;10:639–51. https://doi.org/10.1517/14712591003724662
17. Food and Drug Administration. October 29, 2014 clinical review—fluzone high-dose [cited 2019 Oct 21]. https://www.fda.gov/vaccines-blood-biologics/vaccines/fluzone-fluzone-high-dose-and-fluzone-intradermal
18. Halasa NB, Savani BN, Asokan I, Kassim A, Simons R, Summers C, et al. Randomized double-blind study of the safety and immunogenicity of standard-dose trivalent inactivated influenza vaccine versus high-dose trivalent inactivated influenza vaccine in adult hematopoietic stem cell transplantation patients. Biol Blood Marrow Transplant. 2016;22:528–35. https://doi.org/10.1016/j.bbmt.2015.12.003
19. Natori Y, Humar A, Lipton J, Kim DD, Ashton P, Hoschler K, et al. A pilot randomized trial of adjuvanted influenza vaccine in adult allogeneic hematopoietic stem cell transplant recipients. Bone Marrow Transplant. 2017;52:1016–21. https://doi.org/10.1038/bmt.2017.24
20. Greenberg JA, Hohmann SF, Hall JB, Kress JP, David MZ. Validation of a method to identify immunocompromised patients with severe sepsis in administrative databases. Ann Am Thorac Soc. 2016;13:253–8.
21. IBM Corporation. IBM Watson Health. Truven Health Analytics, 2020 [cited 2019 Oct 21]. https://truvenhealth.com/portals/0/assets/2017_MarketScan_Databases_Health_Services_Researchers.pdf
22. Barber C, Lacaille D, Fortin PR. Systematic review of validation studies of the use of administrative data to identify serious infections. Arthritis Care Res (Hoboken). 2013;65:1343–57. https://doi.org/10.1002/acr.21959
23. Xu X, Blanton L, Elal AIA, Alabi N, Barnes J, Biggerstaff M, et al. Update: influenza activity in the United States during the 2018–19 season and composition of the 2019–20 influenza vaccine. MMWR Morb Mortal Wkly Rep. 2019;68:544–51. https://doi.org/10.15585/mmwr.mm6824a3
24. Havers FP, Fry AM, Peacock G, Chen J, Reed C. Influenza vaccination coverage in children with neurologic disorders and their siblings, July 2006 to June 2014. Pediatr Infect Dis J. 2018;37:814–6. https://doi.org/10.1097/INF.0000000000001929
25. Chen DS, Mellman I. Oncology meets immunology: the cancer-immunity cycle. Immunity. 2013;39:1–10. https://doi.org/10.1016/j.immuni.2013.07.012
26. Mok MY, Shoenfeld Y. Recent advances and current state of immunotherapy in systemic lupus erythematosus. Expert Opin Biol Ther. 2016;16:927–39. https://doi.org/10.1517/14712598.2016.1171840
27. Reynolds G, Cooles FA, Isaacs JD, Hilkens CM. Emerging immunotherapies for rheumatoid arthritis. Hum Vaccin Immunother. 2014;10:822–37. https://doi.org/10.4161/hv.27910
28. Monaco C, Nanchahal J, Taylor P, Feldmann M. Anti-TNF therapy: past, present and future. Int Immunol. 2015;27:55–62. https://doi.org/10.1093/intimm/dxu102
29. Kaiser Family Foundation, State health facts, 2020 [cited 2017 Aug 21]. https://wwwkfforg/other/state-indicator/distribution-by-age/?dataView=1&currentTimeframe=0&selectedDistributions=adults-19-25–adults-26-34–adults-35-54–adults-55-64&selectedRows=%7B%22wrapups%22:%7B%22united-states%22:%7B%7D%7D%7D&sortModel=%7B%22colId%22:%22Location%22,%22sort%22:%22asc%22%7D
30. Hijano DR, Maron G, Hayden RT. Respiratory viral infections in patients with cancer or undergoing hematopoietic cell transplant. Front Microbiol. 2018;9:3097. https://doi.org/10.3389/fmicb.2018.03097
31. Joshi AY, Iyer VN, Hagan JB, St Sauver JL, Boyce TG. Incidence and temporal trends of primary immunodeficiency: a population-based cohort study. Mayo Clin Proc. 2009;84:16–22. https://doi.org/10.4065/84.1.16
32. Bongartz T, Sutton AJ, Sweeting MJ, Buchan I, Matteson EL, Montori V. Anti-TNF antibody therapy in rheumatoid arthritis and the risk of serious infections and malignancies: systematic review and meta-analysis of rare harmful effects in randomized controlled trials. JAMA. 2006;295:2275–85. https://doi.org/10.1001/jama.295.19.2275
33. Koo S, Marty FM, Baden LR. Infectious complications associated with immunomodulating biologic agents. Infect Dis Clin North Am. 2010;24:285–306. https://doi.org/10.1016/j.idc.2010.01.006
34. Dixon WG, Suissa S, Hudson M. The association between systemic glucocorticoid therapy and the risk of infection in patients with rheumatoid arthritis: systematic review and meta-analyses. Arthritis Res Ther. 2011;13:R139. https://doi.org/10.1186/ar3453
35. Radwan HM, Cheeseman SH, Lai KK, Ellison RT III. Influenza in human immunodeficiency virus-infected patients during the 1997-1998 influenza season. Clin Infect Dis. 2000;31:604–6. https://doi.org/10.1086/313985
36 Bosaeed M, Kumar D. Seasonal influenza vaccine in immunocompromised persons. Hum Vaccin Immunother. 2018;14:1311–22. https://doi.org/10.1080/21645515.2018.1445446
37. Hakim H, Allison KJ, Van de Velde LA, Tang L, Sun Y, Flynn PM, et al. Immunogenicity and safety of high-dose trivalent inactivated influenza vaccine compared to standard-dose vaccine in children and young adults with cancer or HIV infection. Vaccine. 2016;34:3141–8. https://doi.org/10.1016/j.vaccine.2016.04.053
38. Jamshed S, Walsh EE, Dimitroff LJ, Santelli JS, Falsey AR. Improved immunogenicity of high-dose influenza vaccine compared to standard-dose influenza vaccine in adult oncology patients younger than 65 years receiving chemotherapy: A pilot randomized clinical trial. Vaccine. 2016;34:630–5. https://doi.org/10.1016/j.vaccine.2015.12.037
39. McKittrick N, Frank I, Jacobson JM, White CJ, Kim D, Kappes R, et al. Improved immunogenicity with high-dose seasonal influenza vaccine in HIV-infected persons: a single-center, parallel, randomized trial. Ann Intern Med. 2013;158:19–26. https://doi.org/10.7326/0003-4819-158-1-201301010-00005
40. McManus M, Frangoul H, McCullers JA, Wang L, O'Shea A, Halasa N. Safety of high dose trivalent inactivated influenza vaccine in pediatric patients with acute lymphoblastic leukemia. Pediatr Blood Cancer. 2014;61:815–20. https://doi.org/10.1002/pbc.24863
41. Natori Y, Shiotsuka M, Slomovic J, Hoschler K, Ferreira V, Ashton P, et al. A double-blind, randomized trial of high-dose vs standard-dose influenza vaccine in adult solid-organ transplant recipients. Clin Infect Dis. 2018;66:1698–704. https://doi.org/10.1093/cid/cix1082
42. Kumar D, Campbell P, Hoschler K, Hidalgo L, Al-Dabbagh M, Wilson L, et al. Randomized controlled trial of adjuvanted versus nonadjuvanted influenza vaccine in kidney transplant recipients. Transplantation. 2016;100:662–9. https://doi.org/10.1097/TP.0000000000000861
43. Magnani G, Falchetti E, Pollini G, Reggiani LB, Grigioni F, Coccolo F, et al. Safety and efficacy of two types of influenza

vaccination in heart transplant recipients: a prospective randomised controlled study. J Heart Lung Transplant. 2005;24:588–92. https://doi.org/10.1016/j.healun.2004.03.004
44. Ambati A, Einarsdottir S, Magalhaes I, Poiret T, Bodenstein R, LeBlanc K, et al. Immunogenicity of virosomal adjuvanted trivalent influenza vaccination in allogeneic stem cell transplant recipients. Transpl Infect Dis. 2015;17:371–9. https://doi.org/10.1111/tid.12382
45. Beyer WE, Versluis DJ, Kramer P, Diderich PP, Weimar W, Masurel N. Trivalent influenza vaccine in patients on haemodialysis: impaired seroresponse with differences for A-H3N2 and A-H1N1 vaccine components. Vaccine. 1987;5:43–8. https://doi.org/10.1016/0264-410X(87)90008-9
46. Mertz D, Kim TH, Johnstone J, Lam PP, Science M, Kuster SP, et al. Populations at risk for severe or complicated influenza illness: systematic review and meta-analysis. BMJ. 2013;347:f5061. https://doi.org/10.1136/bmj.f5061
47. Shang M, Chung JR, Jackson ML, Jackson LA, Monto AS, Martin ET, et al. Influenza vaccine effectiveness among patients with high-risk medical conditions in the United States, 2012–2016. Vaccine. 2018;36:8047–53. https://doi.org/10.1016/j.vaccine.2018.10.093
48. Buchan SA, Hottes TS, Rosella LC, Crowcroft NS, Tran D, Kwong JC. Contribution of influenza viruses to medically attended acute respiratory illnesses in children in high-income countries: a meta-analysis. Influenza Other Respir Viruses. 2016;10:444–54. https://doi.org/10.1111/irv.12400
49. Kim SC, Solomon DH, Rogers JR, Gale S, Klearman M, Sarsour K, et al. Cardiovascular safety of tocilizumab versus tumor necrosis factor inhibitors in patients with rheumatoid arthritis: a multi-database cohort study. Arthritis Rheumatol. 2017;69:1154–64. https://doi.org/10.1002/art.40084
50. Jensen ET, Cook SF, Allen JK, Logie J, Brookhart MA, Kappelman MD, et al. Enrollment factors and bias of disease prevalence estimates in administrative claims data. Ann Epidemiol. 2015;25:519–525.e2. https://doi.org/10.1016/j.annepidem.2015.03.008

Address for correspondence: Manish Patel, Centers for Disease Control and Prevention, 1600 Clifton Rd NE, Mailstop H24-7, Atlanta, GA 30329-4027, USA; email: mpatel@cdc.gov

CrAssphage as a Novel Tool to Detect Human Fecal Contamination on Environmental Surfaces and Hands

Geun Woo Park, Terry Fei Fan Ng, Amy L. Freeland, Vincent C. Marconi, Julie A. Boom, Mary A. Staat, Anna Maria Montmayeur, Hannah Browne, Jothikumar Narayanan, Daniel C. Payne, Cristina V. Cardemil, Aimee Treffiletti, Jan Vinjé

CrAssphage is a recently discovered human gut–associated bacteriophage. To validate the potential use of crAssphage for detecting human fecal contamination on environmental surfaces and hands, we tested stool samples (n = 60), hand samples (n = 30), and environmental swab samples (n = 201) from 17 norovirus outbreaks for crAssphage by real-time PCR. In addition, we tested stool samples from healthy persons (n = 173), respiratory samples (n = 113), and animal fecal specimens (n = 68) and further sequenced positive samples. Overall, we detected crAssphage in 71.4% of outbreak stool samples, 48%–68.5% of stool samples from healthy persons, 56.2% of environmental swabs, and 60% of hand rinse samples, but not in human respiratory samples or animal fecal samples. CrAssphage sequences could be grouped into 2 major genetic clusters. Our data suggest that crAssphage could be used to detect human fecal contamination on environmental surfaces and hands.

Hygienic practices, including disinfection of environmental surfaces, are important to reduce exposure to pathogens that spread through fecal–oral transmission. Thus, monitoring of human fecal contamination and identifying the source of contamination is an important approach to prevent transmission of gastroenteritis viruses for which humans are the only natural host (e.g., human norovirus) (*1*). Culturable bacteria (e.g., *Escherichia coli*, *Enterococcus* spp., and *Bacteroides* spp.) are widely used as indicators to assess the presence of human fecal contamination of environmental waters (*2*–*5*). However, fecal indicator bacteria are not specific to human fecal contamination (*6*) and have a poor correlation with exposure risk to enteric viruses (*4*,*7*–*9*).

Over the past few decades, several viruses (e.g., human polyomavirus, Aichi virus, norovirus, and human adenovirus) have been studied as human fecal indicators for the detection of sewage-contaminated source and drinking water (*10*–*13*). Recently, both norovirus and adenovirus have been suggested as potential biomarkers of viral contamination to assess hygiene status and potential human health risk of contaminated surfaces and hands of affected persons (*4*,*12*,*14*–*17*). However, the detection of those viruses in indoor environments was relatively rare and inconsistent, making it difficult to estimate indoor hygiene and limiting their applicability for use in both industrial and regulatory settings (*12*,*14*–*17*).

Recently, a new DNA bacteriophage was discovered by computational analysis of publicly accessible human fecal metagenomics data and was named crAssphage, referring to the Cross-Assembly software that was used for its discovery (*18*). The single-stranded circular DNA genome is 97 kbp in size with 80 predicted open reading frames (ORFs) (*18*). Genetically, crAssphage are extremely heterogenous and can be grouped into at least 10 different genera (*18*,*19*). Various bacteria of the phylum *Bacteroidetes* have been proposed as the primary hosts of

Author affiliations: Centers for Disease Control and Prevention, Atlanta, Georgia, USA (G.W. Park, T.F.F. Ng, A.L. Freeland, J. Narayanan, D.C. Payne, C.V. Cardemil, A. Treffiletti, J. Vinjé); Atlanta Veteran Administration Medical Center, Atlanta (V.C. Marconi); Emory University School of Medicine, Atlanta (V.C. Marconi); Texas Children's Hospital, Houston, Texas, USA (J.A. Boom); Cincinnati Children's Hospital Medical Center, Cincinnati, Ohio, USA (M.A. Staat); Cherokee Nation Assurance, Arlington, Virginia, USA (A.M. Montmayeur); Oak Ridge Institute for Science and Education, Oak Ridge, Tennessee, USA (H. Browne)

DOI: https://doi.org/10.3201/eid2608.200346

crAssphage, which was supported by recent findings that phage ΦCrAss001 from human feces could be isolated in *Bacteroides* (*20*). To date, crAssphage has primarily been detected in human stools and rarely in animals (*18*,*21*). In addition, crAssphage can be found at high levels in sewage throughout the year and correlate with the detection of fecal indicators (*E. coli*, enterococcus, human polyomavirus, and somatic coliphage), suggesting they could be used for monitoring human fecal pollution of water (*21*–*25*).

In this study, we aimed to validate the potential use of crAssphage to detect human fecal contamination on environmental surfaces and hands. We tested human stool samples, environmental swab samples, and hand rinse samples collected during norovirus outbreaks, as well as stool samples from persons without acute gastroenteritis (AGE) and saliva and nasal samples from humans with respiratory symptoms. To confirm the specificity of crAssphage for the human gut, we also tested fecal specimens from cats, rats, rhesus monkeys, and husbandry animals (cows, pigs, sheep, and horses).

Materials and Methods

Clinical Samples from Humans

In this study, we used archived fecal specimens that had been collected from patients with AGE from 5 norovirus outbreaks on cruise ships during 2015–2016 (n = 30) and from 12 norovirus outbreaks in long-term care facilities (LTCFs) in Oregon during 2013–2016 (n = 30) (*26*). In addition, we tested 22 vomitus samples from norovirus-positive patients as well as 43 saliva and 48 nasal swab samples from norovirus-negative patients. In addition, stool specimens from 2 cohorts of persons without AGE symptoms were included: adults ≥25 years of age who participated as non-AGE controls in a study to determine the incidence of norovirus in Veteran Affairs Medical Centers (VAMCs) (IRB approval no. 00091065) (*27*) and children ≤5 years of age who participated in the New Vaccine and Surveillance Network (IRB approval no. 6164) (*28*). Because stool samples from the norovirus outbreaks were categorized as public health nonresearch, human subject regulations did not apply.

Fecal Samples from Animals

We obtained fecal samples from 3 laboratory animals (rhesus monkeys [n = 12], rats [n = 4], and cats [n = 2]) without diarrhea from archived collections at the Centers for Disease Control and Prevention (CDC) in Atlanta, Georgia. In addition, fecal DNA extracts from cows (n = 10), sheep (n = 10), horses (n = 10), and pigs (n = 30) were provided by Jeong Kwang Cheol at the University of Florida and Qiuhong Wang at Ohio State University.

Environmental Swab and Hand Rinse Samples

We collected environmental swab samples at the time of disembarkation of 5 cruise ships (cruise ship A–E) that experienced norovirus outbreaks. We sampled hard surfaces, including toilet seats, toilet door handles, telephone handles, television remote controls, and door handles in cabins that had been occupied by passengers who had reported AGE symptoms by using macrofoam swabs (Puritan, https://www.puritanmedproducts.com) as described previously (*29*). On cruise ship B, we sampled the same environmental surfaces again 3 weeks later when no elevation of the number of AGE cases was reported; these samples are expressed as "B, follow up." We collected all swab samples before standard surface cleaning procedures for each ship. We shipped swab samples on dry ice to CDC and stored them at -80°C until testing. We also included in this study archived hand rinse samples collected from 30 norovirus patients in LTCFs (*26*).

Nucleic Acid Extraction and Real-Time PCR Detection of CrAssphage

We extracted total nucleic acid from clinical samples, hand rinse samples, and swabs, as described previously (*26*,*29*; Appendix, https://wwwnc.cdc.gov/EID/article/26/8/20-0346-App1.pdf). We designed oligonucleotide primers and probes on the basis of conserved regions of the DNA polymerase gene (ORF00018) from 43 publicly available crAssphage strains by using the real-time quantitative PCR assay tool from Integrated DNA Technologies (https://www.idtdna.com) (*18*). Primer sequences had no more than 1 mismatch with the prototype CrAssphage genome (GenBank accession no. NC_024711). We tested extracted DNA from clinical and environmental samples by using TaqMan real-time PCR and the AgPath-ID One Step RT-PCR Kit (ThermoFisher Scientific, https://www.thermofisher.com) on an Applied Biosystems 7500 platform (also ThermoFisher Scientific); the oligonucleotide primers (TN201/TN203) and probe (TN202) generated a 146-bp product (Table 1) (Appendix). We amplified the full-length ORF00018 (DNA polymerase) gene of a sample (ship E [stool II] in Figure 1) by using primers CrAssPol-F and CrAsspol-R (Table 1) to generate a 2,428-bp amplicon, as described previously (*30*). In each experiment, we included a 10-fold serial dilution ($10^{5.7}$–$10^{0.7}$ copies/3 μL) of this purified and quantified amplicon to generate a standard curve. The detection limit of

Table 1. Oligonucleotide primers and probe used for detection and typing of crAssphage

Primer or probe	DNA sequence	Position*	Description
CrAssPol_F†	5′-CGG CGG GTT AAT CAA AAT AGA A-3′	8907–8928 (flanking pol)	Forward primer conventional PCR
CrAssPol_R†	5′-GCG GAG AAC CCC ATT TAT TAA TAA G-3′	11334–11310 (flanking pol)	Reverse primer conventional PCR
TN201	5′-ATG TWG GTA RAC AAT TTC ATG TAG AAG-3′	10919–10945 (within pol)	Forward primer real-time PCR
TN203	5′-TCA TCA AGA CTA TTA ATA ACD GTN ACA ACA-3′	11111–11082 (within pol)	Reverse primer real-time PCR and typing PCR
TN202	FAM-5-ACC AGC MGC CAT TCT ACT ACG AGH AC-3-BHQ1	11079–11054 (within pol)	Probe real-time PCR
JP1crasF	5′-TAA AAC TAC WAT TTA TAG AGT TAA TAA AGA TGC STT TAG T-3′	10023–10062 (within pol)	Forward primer typing

*The sequence position was determined against a crAssphage sequence from GenBank (accession no. NC_024711).
†Liang et al. (*30*).

the crAssphage real-time PCR was 0.7 DNA copies per PCR reaction. The average slope and deviation of the standard curves was 3.3626 ± 0.0377 (r^2 ≥0.9926). We calculated the concentration of crAssphage by converting cycle threshold values to DNA copies.

DNA Sequencing of crAssphage

To enable sequencing, we amplified DNA from real-time PCR–positive samples by using oligonucleotide primers JP1crasF/TN203 (Table 1) to generate a 1,089-bp PCR amplicon (Appendix). We sequenced the purified PCR products by using 500-cycle (2 × 250-bp paired-end) MiSeq Reagent Kit (Illumina, https://www.illumina.com). After filtering and trimming raw sequence reads, we assembled contigs by using the de novo assembler SPAdes 3.7.0 (http://cab.spbu.ru/software/spades) (Appendix). We analyzed assembled crAssphage amplicon sequences by read mapping and gene annotation using Geneious 11.1.2 (Biomatters, https://www.geneious.com), as described previously (*31*). The GenBank accession numbers for the strains sequenced in this study are MT475797–824 (Figure 1) and MT475766–96 (Figure 2).

Phylogenetic and Sequence Analyses

We generated multiple sequence alignment of crAssphage sequences by using MUSCLE (*32*) and constructed maximum-likelihood phylogenetic trees by using PhyML (*33*). We used the best nucleotide substitution model analyzed by Smart Model Selection based on

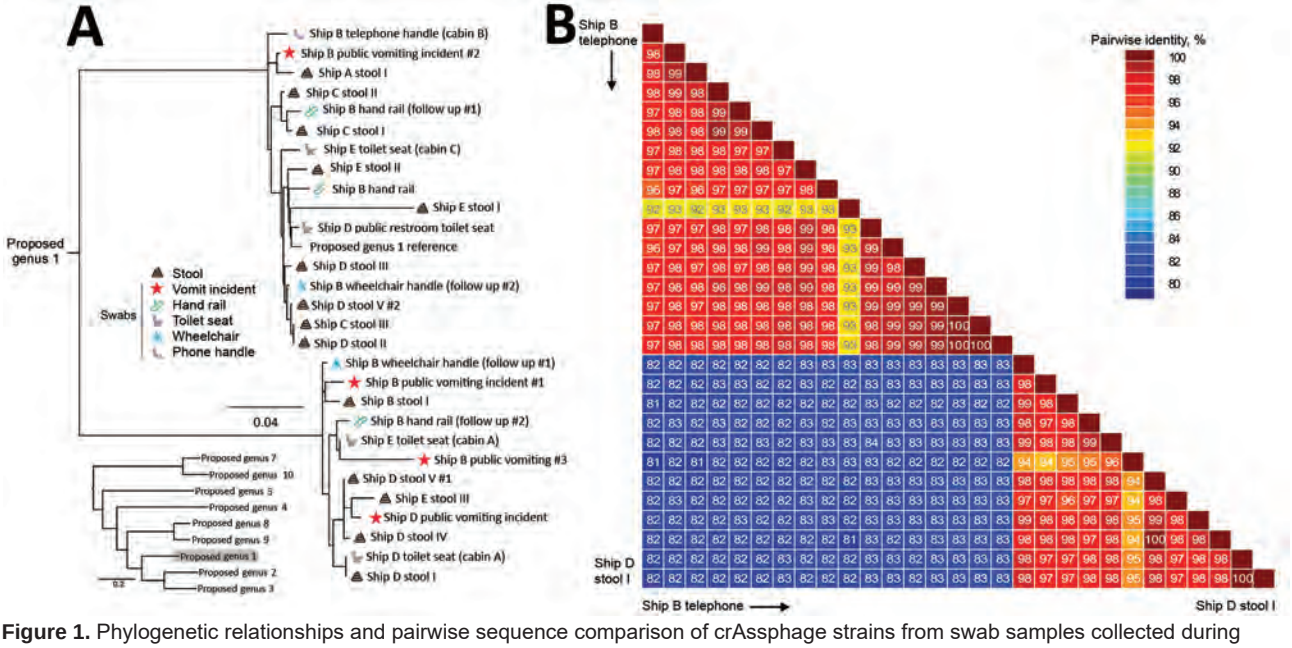

Figure 1. Phylogenetic relationships and pairwise sequence comparison of crAssphage strains from swab samples collected during norovirus outbreaks on cruise ships. A) Phylogeny of crAssphage on cruise ships, showing ship and source for each strain. Inset shows position of cruise ship strains among reference strains; scale bar indicates number of nucleotide changes between sequences. B) Color-coded pairwise identity matrix for crAssphage strains. Each cell includes the percentage identity among 2 sequences (horizontally to the left and vertically at the bottom). Key indicates pairwise identity percentages.

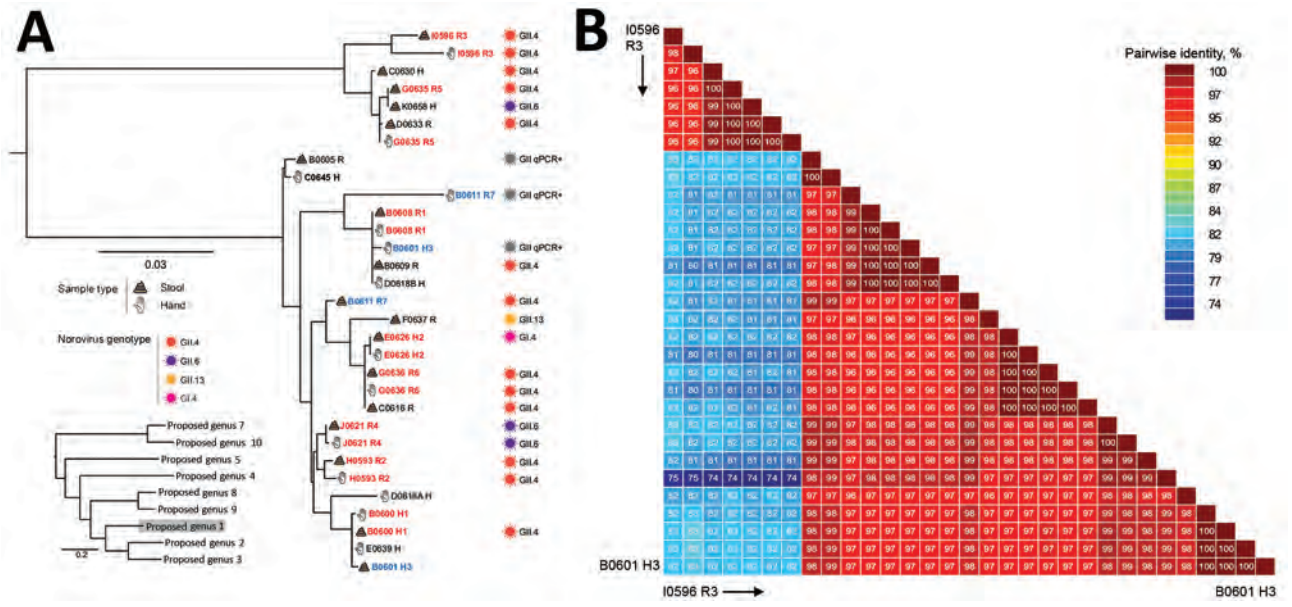

Figure 2. Phylogenetic relationships and pairwise sequence comparison of crAssphage strains from hand rinse samples collected during norovirus outbreaks at long-term care facilities. A) Phylogeny of crAssphage strains. Strain identification includes facility (A–J), strain number, and human source (H, healthcare worker; R, resident) for each isolate. Sample source and genotypes are indicated. Red strain names indicate that both hand and stool sample are genetically related, blue strain names that paired hand and stool samples are genetically distinct. Black strain names indicate hand or stool sample pairs that tested negative for crAssphage. Inset shows position of long-term care strains among reference strains; scale bar indicates number of nucleotide changes between sequences. (B) Color-coded pairwise identity matrix for crAssphage strains. Each cell includes the percentage identity among 2 sequences (horizontally to the left and vertically at the bottom). Key indicates pairwise identity percentages

the Bayesian information criterion (*34*) and calculated pairwise nucleotide identity (NI) between sequences by using the Sequence Demarcation Tool (*35*).

Data Analysis

We determined sensitivity, specificity, and predictive values of crAssphage on norovirus co-infection (or co-contamination) as described previously (*36*). We performed log transformation, followed by the Wilcoxon rank-sum test, to compare the median crAssphage concentration (log_{10} genomic copies per sampled object for surface and hand rinse sample or per gram for stool) between different comparison groups. We used SPSS Statistics 21 (IBM, https://www.ibm.com) for statistical calculations and considered differences with p values <0.05 to be statistically significant (*37*).

Results

Detection of crAssphage in Human and Animal Samples

Overall, we detected crAssphage in 71.4% of human stool samples, including 42 (70.0%) of the 60 stool samples collected from 17 norovirus outbreaks, 46 (48%) of the 96 stool samples from adults ≥25 years of age without AGE symptoms and 53 (68.8%) of the 77 stool samples from children ≤5 years of age with AGE symptoms (Table 2). Specifically, 23 (76.7%) of the 30 stool samples from the 5 norovirus outbreaks on cruise ships tested positive, and 19 (63.3%) of 30 stool samples collected from the 12 norovirus outbreaks in LTCFs tested positive (Table 2). Thirty-nine (65.0%) of the 60 stool samples tested positive for both crAssphage and norovirus. The median concentration of crAssphage per gram of stool ranged from 5.9 (range 2.8–8.9) log_{10} genome copies in samples from norovirus outbreaks to 8.1 (range 3.1–10.3) log_{10} genomic copies in samples from adults without AGE symptoms and 8.4 (range 4.1–10.1) log_{10} genomic copies in samples from children ≤5 years of age without AGE symptoms. All vomitus samples from patients in norovirus outbreaks as well as saliva and nasal swab samples from children with respiratory symptoms tested negative for crAssphage. We did not detect crAssphage in any of the 78 fecal samples from animals.

Detection of crAssphage on Environmental Surfaces on Cruise Ships

We collected a total of 201 swab samples from frequently touched surfaces on 6 cruise ship voyages (5 cruise ships [A–E]) during norovirus outbreaks and

Table 2. Prevalence of crAssphage in stool samples from norovirus outbreaks on cruise ships and in long-term care facilities and healthy controls without acute gastroenteritis

Setting (no. samples)	Age, y, (range)	% CrAssphage (no. positive/no. tested)	crAssphage titer (range)*
Cruise ship voyages† (5)	65.5 (29–88)	76.7% (23/30)	4.5 (3.2–8.9)
Long-term care facilities‡ (12)	63.5 (18–87)	63.3% (19/30)	5.4 (2.8–8.9)
Adults without acute gastroenteritis (96)	59.0 (28–83)	48% (46/96)	8.1 (3.1–10.3)
Children without acute gastroenteritis (77)	1.1 (0.2–5.0)	68.8% (53/77)	8.4 (4.1–10.1)

*$\log_{10}$ genomic copies per gram of stool sample.
†This study.
‡Park et al. (*26*).

1 cruise ship (B, follow up) 3 weeks after a norovirus outbreak). We detected crAssphage DNA in 113 (56.2%) of the swab samples. The rates for each individual cruise ship were as follows: 15.2% (5/33) (cruise ship A); 84.8% (28/33) (cruise ship B); 62.3% (19/31) (cruise ship C); 44.7% (17/38) (cruise ship D); 72.7% (24/33) (cruise ship E); and 60.6% (20/33) (cruise ship (B, follow up).

On Surfaces in Cabins of Norovirus-Positive Patients

A total of 47 (58.8%) of 80 swab samples tested positive for crAssphage; median concentration was 2.5 (0.8–5.6) $\log_{10}$ genomic copies per surface (Table 3). Remote controls had the highest crAssphage contamination (87.5%), followed by toilet seats (68.5%), which had the highest crAssphage titer, 3.3 $\log_{10}$ (1.2–5.6) $\log_{10}$ genomic copies per seat. Of the 80 swab samples, 29 (36.3%) tested positive for norovirus; 11 of those samples also tested positive for crAssphage. The positive predictive value (PPV) of norovirus coinfection of crAssphage-positive samples was 38.0%; the negative predictive value (NPV) was 29.4% (Table 4). Compared with all surfaces sampled, toilet seats (56.3%) in the cabins from AGE-positive passengers had the highest norovirus contamination, with an average concentration of 5.5 (3.1–7.4) $\log_{10}$ genomic copies per surface.

On Surfaces in Public Areas

Of all surfaces in public areas on cruise ships that were sampled, 51.5% (21/64) tested positive for crAssphage; median concentration was 2.4 (1.6–3.2) $\log_{10}$ genomic copies per surface. Five surfaces in public areas (casino chips, a medical center clipboard, gift shop register touch screens, surfaces that were exposed to a public vomiting incident, and edges of a trolley for dirty linen) had contamination of ≥50%. Only 5 surfaces, including a menu folder (cruise ship A), a medical center clipboard (cruise ship A), hand contact surfaces in the public vomiting incident location (cruise ship A), hand rails in the atrium (cruise ship B), and ATM buttons (cruise ship C), tested positive for human norovirus; titers were 1.8–5.1 $\log_{10}$ genomic copies per surface. Two of the 5 norovirus-positive surfaces (a medical center clipboard and a handrail in the atrium) also tested positive for crAssphage. PPV for norovirus co-contamination of crAssphage-positive surfaces was 40.0%; NPV was 67.8.

Three Weeks after a Norovirus Outbreak

Seven (46.7%) of the 15 swab samples collected from cabins on cruise ship B that had been occupied by patients with AGE 3 weeks earlier tested positive for crAssphage, whereas 7 (38.9%) of the 18 surfaces in public areas tested positive. Compared with results from the same cruise ship immediately after the outbreak 3 weeks earlier, the number of crAssphage-positive surfaces decreased from 12 to 7 in public areas of cruise ship B. However, swabs from 6 surfaces (ATM buttons, a buffet utensil, a medical center clipboard, atrium handrails, a wheelchair handle rest in passenger areas, and smoking bar countertop surfaces in the crew smoking room) tested positive for crAssphage again. Two crAssphage-positive swab samples collected from a handrail (ship B handrail, follow-ups 1 and 2) and a wheelchair (ship B wheelchair, follow-ups 1 and 2) on cruise ship B contained multiple crAssphage sequences (Figure 1). These sequences were genetically distinct from those detected during the norovirus outbreak on the same cruise ship 3 weeks earlier (voyage B), suggesting not persistence of previous fecal material but more recent contamination with human fecal matter. In contrast, norovirus contamination on surfaces decreased from 24.2% (8/33) during the outbreak to 3.0% (1/33) 3 weeks later.

Contamination of Hands with crAssphage during Norovirus Outbreaks in LTCFs

In total, 18 (60.0%) of 30 hand rinse samples tested positive for crAssphage, including samples from 7 healthcare workers (HCWs) and 11 residents. Both hand rinse and stool samples from 15 norovirus patients (4 HCWs and 11 residents) tested positive for crAssphage (Appendix Table). In a previous study, we reported that 14 (46.7%) of 30 hand rinse samples

tested positive for norovirus, including 3 HCWs and 11 residents (*26*). Overall, 2 (28.6%) of 7 crAssphage-positive hand rinse samples from HCWs and 8 (72.7%) of 11 from residents tested positive for human norovirus. The PPV was 72.7% and the NPV 25.0% for co-contamination of crAssphage-positive hands of residents with norovirus, whereas for HCWs the PPV was 66.7% and NPV 58.3%.

Sequence and Phylogenetic Analysis of crAssphage

Of the 42 PCR-positive stool samples, 30 (71.4%) were successfully sequenced and the titer of the remaining 12 samples was too low. Sequences from several crAssphage were identical (e.g., ship Dstool V# 1 and ship D stool IV, and ship C stool III and ship D stool II) (Figure 1). Overall, crAssphage sequences detected in samples from cruise ships rarely clustered closely together (Figure 1), whereas crAssphage from LTCFs were more closely related, with near-identical sequences (99%–100% NI) (Figure 2).

From the cruise ship outbreaks, 13 (56.5%) of the 23 crAssphage-positive stool samples and 10 (8.8%) of 113 crAssphage-positive swab samples were sequenced successfully. Phylogenetic analysis showed that crAssphage sequences could be grouped in 2 genetic clusters within proposed genus 1 (*19*) (Figure 1). Several samples contained multiple crAssphage sequences, including multiple stool samples with >1 sequence (ship D), swab samples from a wheelchair and a handrail each containing 2 sequences (ship B, follow up), and a swab sample from a public vomiting event (ship B) containing 3 different crAssphage sequences.

From the crAssphage in LTCFs, 17 (89.5%) of 19 stool samples and 13 (72.2%) of 18 positive hand rinse samples were successfully sequenced. The sequences could be grouped in 2 clusters that had <83% NI (Figure 2, panel A). Within each cluster, crAssphage was genetically diverse, with pairwise NI ranging from 96% to 100% (Figure 2, panel B). Identical crAssphage sequences were detected in paired hand rinse and stool samples from 5 persons (3 residents [G0636, B0608, and J0621] and 2 HCWs [E0626 and B0600]) (Figure 2). Among those persons, 2 residents [G0636, and J0621] had identical norovirus sequences in paired hand and stool samples as well. In contrast, crAssphage sequences in stool samples from 2

Table 3. Prevalence of crAssphage and human norovirus on environmental surfaces on 5 cruise ships with norovirus outbreaks

	CrAssphage		Norovirus	
Sampled objects†	No. positive/total no. (%)	Concentration* (range)	No. positive/total no. (%)	Concentration* (range)
Cabins of norovirus-positive patients				
Toilet seats[P]	11/16 (68.5)	3.3 (1.2–5.6)	9/16 (56.3)	5.5 (3.1–7.4)
Toilet door handles[M]	7/16 (43.75)	2.3 (1.0–3.1)	5/16 (31.3)	5.1 (3.7–5.7)
Telephone handles[P]	9/16 (56.4)	2.4 (1.7–3.5)	3/16 (18.8)	4.9 (4.9–5.5)
Remote control surfaces[P]	14/16 (87.5)	2.6 (1.4–4.1)	5/16 (31.3)	3.6 (2.9–5.1)
Cabin door handles[M]	6/16 (37.5)	2.0 (0.8–3.4)	6/16 (37.5)	4.4 (3.1–6.0)
Overall	47/80 (58.8)	2.5 (0.8–5.6)	29/80 (36.3)	4.8 (3.1–7.4)
Public area (passenger area)				
ATM buttons[P]	2/3 (66.6)	2.8 (2.4–3.4)	1/3 (33.3)	1.8
Menu folder[L]	2/5 (40)	1.9(1.7–2.1)	1/5 (20.0)	4.9
Condiment containers[M]	2/5 (40)	2.2(2.1–2.3)	0/5 (0)	
Buffet utensils[M]	1/2 (50)	1.6	0/2 (0)	
Ice cream handle[P]	1/4 (25.0)	2.2	0/3 (0)	
Casino chips[P]	3/5 (60)	2.7 (2.1–2.8)	0/5 (0)	
Medical center clipboards[P]	3/5 (60)	2.3 (2.1–2.5)	1/5 (20)	5.1
Gift shop register touch screens[P]	3/5 (60)	3.0 (2.7–3.0)	0/5 (0)	
Youth center toys[P]	2/4 (50.0)	2.1 (2.1–2.2)	0/4 (0)	
Atrium hand rails[W]	2/5 (40.0)	3.0 (2.1–3.9)	1/5 (20)	4.1
Internet café keyboards[P]	3/5 (60)	1.8(1.8–2.5)	0/5 (0)	
Wheelchair handle rests[P]	2/5 (25)	2.9 (2.0–3.8)	0/5 (0)	
Hand contact surfaces exposed to public vomiting incident[M]	2/4 (50)	3.2 (2.8–3.5)	1/4 (25)	4.3
Toilet seat surfaces in public rest room[P]	3/3 (100)	4.7 (2.4–4.7)	0/3 (0)	0
Overall	21/64 (51.5)	2.4 (1.6–3.2)	5/64 (7.8)	3.3 (1.8–5.1)
Public area (crew area)				
Time clock machines[P]	3/5 (60)	2.2 (2.1–2.5)	0/5 (0)	
Edges of trolley for dirty linens[P]	5/5 (100)	2.3 (1.8–3.2)	0/5 (0)	
Elevator buttons in food service areas[P]	3/5 (60)	2.3 (2.1–3.1)	0/5 (0)	
Computer keyboard[P]	2/5 (40)	2.3 (2.0–2.5)	0/5 (0)	
Countertop surfaces in crew smoking room[W]	2/5 (40)	2.3(2.1–2.5)	0/5 (0)	
Overall	15/25 (60)	2.3 (1.8–3.2)	0/25 (0)	

[1]$\log_{10}$ genomic copies per sampled object.
[2]Each superscripted character indicates surface material of sampled object as follows: P, plastic; M, metal; W, wood; and L, leather.

Table 4. Sensitivity, specificity, and predictive values of norovirus co-contamination on crAssphage positive environmental surfaces and hand rinse samples*

Setting	Sample type	Source (no. samples)	Sensitivity, %	Specificity, %	PPV, %	NPV, %
Cruise ship†	Swab sample	Case cabin (80)	23.4	45.5	38.0	29.4
		Public area (64)	9.5	93.0	40.0	67.8
		Overall (144)	19.1	72.4	38.2	50.0
LTCFs‡	Hand rinse sample	Resident (15)	72.7	25.0	72.7	25.0
		HCW (15)	28.6	87.5	66.7	58.3
		Overall (30)	55.6	66.7	71.4	50.0

*HCW, healthcare worker; LTCF, long-term care facility; NPV, negative predictive value; PPV, positive predictive value.
†This study
‡Park et al. (*26*).

patients (resident D0611 and HCW B0601) did not match their corresponding hand rinse sample. Also, norovirus was detected only in the hand sample, not a stool sample, from HCW B0601. A single crAssphage sequence was detected on hands from 2 HCWs (D0645 and C0639), and 2 genetically different crAssphages were detected on the hand from 1 HCW (D0618), whereas all stool samples from these 3 HCW tested crAssphage negative.

The median concentration of crAssphage in the 30 stool samples that could be sequenced was 6.5 (range 2.8–8.9) $\log_{10}$ genomic copies per gram of stool, compared with 3.9 (range 3.2–6.6) copies for samples that could not be sequenced ($p<0.001$). Viral load of crAssphage detected in environmental samples that could be sequenced was 3.5 (2.0–5.4) $\log_{10}$ genomic copies ($n = 10$), compared with 2.3 (range 0.6–5.6) copies ($n = 103$) for samples that could not be sequenced.

Discussion

We detected crAssphage in >60% of stool samples from patients with AGE during norovirus outbreaks as well in at least half of stool samples from healthy populations but not in other clinical materials (vomitus, saliva, or nasal rinse) or fecal specimens from animals. The high prevalence of crAssphage on surfaces and hands in norovirus outbreak settings suggests that these phages can be used as an indicator to monitor human fecal contamination of environmental sources other than sewage-contaminated water (*21*–*25*). CrAssphage contamination was also frequently found on environmental surfaces in public areas of cruise ships both during and after norovirus outbreaks, suggesting a potential role of crAssphage in monitoring fecal contamination on surfaces in common settings that could be targeted for enhanced cleaning and disinfection practices.

CrAssphage can be classified into 4 subfamilies, which can be further divided into 10 candidate genera (*18*,*19*). In agreement with data from previous studies (*19*,*38*), we found genetically different phages in stools and environmental surfaces from different norovirus outbreaks. The extreme genetic diversity of crAssphage could help to determine possible contamination sources. For example, crAssphage strains in stool samples collected from the same LTCFs during outbreaks displayed a strong degree of interpersonal variation. Thus, identical crAssphage sequences found in stool and hand rinse samples of the same person suggest self-contamination, whereas different sequences suggest possible contamination with fecal material from someone else. On the basis of these assumptions, we concluded that the hands of most LTCF residents were frequently self-contaminated, whereas the hands of HCWs were more likely cross-contaminated, either by contact with frequently touched environmental surfaces or by assisting norovirus patients, highlighting the need to strictly adhere to hand hygiene practices and to take additional contact precautionary measures during norovirus outbreaks.

This study has several limitations. First, although we designed our PCR assay to detect crAssphage based on a larger number of sequences than were used in previous studies (*21*,*23*,*30*,*39*), only viruses from 1 of the 10 recognized crAssphage genera were detected, suggesting that crAssphage from other genera would likely have been missed. Second, because gastroenteritis viruses such as norovirus are often transmitted through vomitus or aerosols, use of crAssphage during outbreaks might be limited (*40*–*42*). Finally, because crAssphage assay was not validated with other domestic animals that share human-occupied spaces (e.g., dogs), nonhuman fecal contamination could not completely be ruled out.

CrAssphage are strongly correlated with bacterial species related to *Bacteroidetes* but are not associated with diarrheal disease in adults (*38*,*43*). Thus, the presence of crAssphage does not correlate with norovirus contamination but rather with human fecal contamination. Detection of crAssphage on environmental surfaces might help to better assess exposure risk for human norovirus in public areas (e.g., on cruise ships) as well as help to identify

frequently touched surfaces that are often fecally contaminated as key sites for enhanced cleaning practices. Sequence analysis of crAssphage in paired hand rinse and stool samples provided laboratory evidence that hands of several persons were likely cross-contaminated with fecal material from other patients, suggesting that crAssphage can be used as a tool to monitor fecal contamination patterns. Because we did not test crAssphage contamination before or after cleaning of environmental surfaces, or assess hand hygiene practices performed by the staff in the LTCFs during the norovirus outbreaks, we recommend additional studies to guide prevention measures, such as enhanced cleaning (e.g., use of the US Environmental Protection Agency's registered products of list G).

Acknowledgments

We thank Suxiang Tong, Sungsil Moon, and Yuhuan Wang, Peixin Fan, Kwang Cheol, and Jeong Qiuhong Wang for providing human clinical samples or animal fecal (or DNA) samples. We also thank Matthew Jaqua, John Oh, Rachele Cruz, Sandra Martin, Keenan Williamson, Catherine Yen, and Elizabeth De Nardo for coordinating enrollment and data/sample collection during the norovirus outbreaks in long-term care facilities; LaDonna Grenz, Marjorie Yungclass, Laura Tsaknaridis, and Vanda Makris for assistance with testing and shipping of samples; and Vincent R. Hill for critical reading the manuscript.

About the Author

Dr. Park is a microbiologist at the National Calicivirus Laboratory in the Division of Viral Diseases, National Center for Immunization and Respiratory Diseases, Centers for Disease Control and Prevention, Atlanta, Georgia. His research interests include environmental surveillance and disinfection of noroviruses and other viral gastroenteritis viruses.

References

1. Bányai K, Estes MK, Martella V, Parashar UD. Viral gastroenteritis. Lancet. 2018;392:175–86. https://doi.org/10.1016/S0140-6736(18)31128-0
2. Harwood VJ, Staley C, Badgley BD, Borges K, Korajkic A. Microbial source tracking markers for detection of fecal contamination in environmental waters: relationships between pathogens and human health outcomes. FEMS Microbiol Rev. 2014;38:1–40. https://doi.org/10.1111/1574-6976.12031
3. Julian TR, MacDonald LH, Guo Y, Marks SJ, Kosek M, Yori PP, et al. Fecal indicator bacteria contamination of fomites and household demand for surface disinfection products: a case study from Peru. Am J Trop Med Hyg. 2013;89:869–72. https://doi.org/10.4269/ajtmh.12-0425
4. Mattioli MC, Davis J, Mrisho M, Boehm AB. Quantification of human norovirus GII on hands of mothers with children under the age of five years in Bagamoyo, Tanzania. Am J Trop Med Hyg. 2015;93:478–84. https://doi.org/10.4269/ajtmh.14-0778
5. Fiksdal L, Maki JS, LaCroix SJ, Staley JT. Survival and detection of *Bacteroides* spp., prospective indicator bacteria. Appl Environ Microbiol. 1985;49:148–50. https://doi.org/10.1128/AEM.49.1.148-150.1985
6. Sinton LW, Finlay RK, Hannah DJ. Distinguishing human from animal faecal contamination in water: a review. N Z J Mar Freshw Res. 1998;32:323–48. https://doi.org/10.1080/00288330.1998.9516828
7. Haramoto E, Kitajima M, Hata A, Torrey JR, Masago Y, Sano D, et al. A review on recent progress in the detection methods and prevalence of human enteric viruses in water. Water Res. 2018;135:168–86. https://doi.org/10.1016/j.watres.2018.02.004
8. Malla B, Ghaju Shrestha R, Tandukar S, Sherchand JB, Haramoto E. Performance evaluation of human-specific viral markers and application of pepper mild mottle virus and CrAssphage to environmental water samples as fecal pollution markers in the Kathmandu Valley, Nepal. Food Environ Virol. 2019;11:274–87. https://doi.org/10.1007/s12560-019-09389-x
9. De Giglio O, Caggiano G, Bagordo F, Barbuti G, Brigida S, Lugoli F, et al. Enteric viruses and fecal bacteria indicators to assess groundwater quality and suitability for irrigation. Int J Environ Res Public Health. 2017;14:558. https://doi.org/10.3390/ijerph14060558
10. Jiang SC. Human adenoviruses in water: occurrence and health implications: a critical review. Environ Sci Technol. 2006;40:7132–40. https://doi.org/10.1021/es060892o
11. Rachmadi AT, Torrey JR, Kitajima M. Human polyomavirus: advantages and limitations as a human-specific viral marker in aquatic environments. Water Res. 2016;105:456–69. https://doi.org/10.1016/j.watres.2016.09.010
12. Leone CM, Dharmasena M, Tang C, DiCaprio E, Ma Y, Araud E, et al. Prevalence of human noroviruses in commercial food establishment bathrooms. J Food Prot. 2018;81:719–28. https://doi.org/10.4315/0362-028X.JFP-17-419
13. Kitajima M, Haramoto E, Phanuwan C, Katayama H. Prevalence and genetic diversity of Aichi viruses in wastewater and river water in Japan. Appl Environ Microbiol. 2011;77:2184–7. https://doi.org/10.1128/AEM.02328-10
14. Ganime AC, Leite JP, Figueiredo CE, Carvalho-Costa FA, Melgaço FG, Malta FC, et al. Dissemination of human adenoviruses and rotavirus species A on fomites of hospital pediatric units. Am J Infect Control. 2016;44:1411–3. https://doi.org/10.1016/j.ajic.2016.04.207
15. Ganime AC, Carvalho-Costa FA, Santos M, Costa Filho R, Leite JP, Miagostovich MP. Viability of human adenovirus from hospital fomites. J Med Virol. 2014;86:2065–9. https://doi.org/10.1002/jmv.23907
16. Oristo S, Rönnqvist M, Aho M, Sovijärvi A, Hannila-Handelberg T, Hörman A, et al. Contamination by norovirus and adenovirus on environmental surfaces and in hands of conscripts in two Finnish garrisons. Food Environ Virol. 2017;9:62–71. https://doi.org/10.1007/s12560-016-9262-4
17. Maunula L, Kaupke A, Vasickova P, Söderberg K, Kozyra I, Lazic S, et al. Tracing enteric viruses in the

European berry fruit supply chain. Int J Food Microbiol. 2013;167:177–85. https://doi.org/10.1016/j.ijfoodmicro.2013.09.003
18. Dutilh BE, Cassman N, McNair K, Sanchez SE, Silva GG, Boling L, et al. A highly abundant bacteriophage discovered in the unknown sequences of human faecal metagenomes. Nat Commun. 2014;5:4498. https://doi.org/10.1038/ncomms5498
19. Guerin E, Shkoporov A, Stockdale SR, Clooney AG, Ryan FJ, Sutton TDS, et al. Biology and taxonomy of crAss-like bacteriophages, the most abundant virus in the human gut. Cell Host Microbe. 2018;24:653–664.e6. https://doi.org/10.1016/j.chom.2018.10.002
20. Shkoporov AN, Khokhlova EV, Fitzgerald CB, Stockdale SR, Draper LA, Ross RP, et al. ΦCrAss001 represents the most abundant bacteriophage family in the human gut and infects *Bacteroides intestinalis*. Nat Commun. 2018;9:4781. https://doi.org/10.1038/s41467-018-07225-7
21. Stachler E, Kelty C, Sivaganesan M, Li X, Bibby K, Shanks OC. Quantitative CrAssphage PCR assays for human fecal pollution measurement. Environ Sci Technol. 2017;51:9146–54. https://doi.org/10.1021/acs.est.7b02703
22. Stachler E, Akyon B, de Carvalho NA, Ference C, Bibby K. Correlation of crAssphage qPCR markers with culturable and molecular indicators of human fecal pollution in an impacted urban watershed. Environ Sci Technol. 2018;52:7505–12. https://doi.org/10.1021/acs.est.8b00638
23. García-Aljaro C, Ballesté E, Muniesa M, Jofre J. Determination of crAssphage in water samples and applicability for tracking human faecal pollution. Microb Biotechnol. 2017;10:1775–80. https://doi.org/10.1111/1751-7915.12841
24. Ahmed W, Payyappat S, Cassidy M, Besley C, Power K. Novel crAssphage marker genes ascertain sewage pollution in a recreational lake receiving urban stormwater runoff. Water Res. 2018;145:769–78. https://doi.org/10.1016/j.watres.2018.08.049
25. Ahmed W, Lobos A, Senkbeil J, Peraud J, Gallard J, Harwood VJ. Evaluation of the novel crAssphage marker for sewage pollution tracking in storm drain outfalls in Tampa, Florida. Water Res. 2018;131:142–50. https://doi.org/10.1016/j.watres.2017.12.011
26. Park GW, Williamson KJ, DeBess E, Cieslak PR, Gregoricus N, De Nardo E, et al. High hand contamination rates during norovirus outbreaks in long-term care facilities. Infect Control Hosp Epidemiol. 2018;39:219–21. https://doi.org/10.1017/ice.2017.274
27. Cardemil CV, Kambhampati A, Grytdal S, Rodriguez-Barradas MC, Vargas B, Beenhouwer DO, et al. Incidence of norovirus and rotavirus from multisite active surveillance in Veteran's Affairs hospitals, December 2016–February 2018: results from the SUPERNOVA network. Open Forum Infect Dis. 2018;5(Suppl 1):S49. https://doi.org/10.1093/ofid/ofy209.118
28. Payne DC, Staat MA, Edwards KM, Szilagyi PG, Gentsch JR, Stockman LJ, et al. Active, population-based surveillance for severe rotavirus gastroenteritis in children in the United States. Pediatrics. 2008;122:1235–43. https://doi.org/10.1542/peds.2007-3378
29. Park GW, Chhabra P, Vinjé J. Swab sampling method for the detection of human norovirus on surfaces. J Vis Exp. 2017;120. https://doi.org/10.3791/55205
30. Liang Y, Jin X, Huang Y, Chen S. Development and application of a real-time polymerase chain reaction assay for detection of a novel gut bacteriophage (crAssphage). J Med Virol. 2018;90:464–8. https://doi.org/ 10.1002/jmv.24974
31. Montmayeur AM, Ng TF, Schmidt A, Zhao K, Magaña L, Iber J, et al. High-throughput next-generation sequencing of polioviruses. J Clin Microbiol. 2017;55:606–15. https://doi.org/10.1128/JCM.02121-16
32. Edgar RC. MUSCLE: multiple sequence alignment with high accuracy and high throughput. Nucleic Acids Res. 2004;32:1792–7. https://doi.org/10.1093/nar/gkh340
33. Guindon S, Dufayard JF, Lefort V, Anisimova M, Hordijk W, Gascuel O. New algorithms and methods to estimate maximum-likelihood phylogenies: assessing the performance of PhyML 3.0. Syst Biol. 2010;59:307–21. https://doi.org/10.1093/sysbio/syq010
34. Lefort V, Longueville JE, Gascuel O. SMS: Smart Model Selection in PhyML. Mol Biol Evol. 2017;34:2422–4. https://doi.org/10.1093/molbev/msx149
35. Muhire BM, Varsani A, Martin DP. SDT: a virus classification tool based on pairwise sequence alignment and identity calculation. PLoS One. 2014;9:e108277. https://doi.org/10.1371/journal.pone.0108277
36. Trevethan R. Sensitivity, specificity, and predictive values: foundations, pliabilities, and piftalls in research and practice. Front Public Health. 2017;5:1–7. https://doi.org/10.3389/fpubh.2017.00307
37. Wittkowski KM, Song T. Nonparametric methods for molecular biology. Methods Mol Biol. 2010;620:105–53. https://doi.org/10.1007/978-1-60761-580-4_2
38. Edwards RA, Vega AA, Norman HM, Ohaeri M, Levi K, Dinsdale EA, et al. Global phylogeography and ancient evolution of the widespread human gut virus crAssphage. Nat Microbiol. 2019;4:1727–36. https://doi.org/10.1038/s41564-019-0494-6
39. Cinek O, Mazankova K, Kramna L, Odeh R, Alassaf A, Ibekwe MU, et al. Quantitative CrAssphage real-time PCR assay derived from data of multiple geographically distant populations. J Med Virol. 2018;90:767–71. https://doi.org/10.1002/jmv.25012
40. Kirby AE, Streby A, Moe CL. Vomiting as a symptom and transmission risk in norovirus illness: evidence from human challenge studies. PLoS One. 2016;11:e0143759. https://doi.org/10.1371/journal.pone.0143759
41. Verani M, Bigazzi R, Carducci A. Viral contamination of aerosol and surfaces through toilet use in health care and other settings. Am J Infect Control. 2014;42:758–62. https://doi.org/10.1016/j.ajic.2014.03.026
42. Barker J, Jones MV. The potential spread of infection caused by aerosol contamination of surfaces after flushing a domestic toilet. J Appl Microbiol. 2005;99:339–47. https://doi.org/10.1111/j.1365-2672.2005.02610.x
43. Liang YY, Zhang W, Tong YG, Chen SP. crAssphage is not associated with diarrhoea and has high genetic diversity. Epidemiol Infect. 2016;144:3549–53. https://doi.org/10.1017/S095026881600176X

Address for correspondence: Geun Woo Park, Centers for Disease Control and Prevention, 1600 Clifton Rd NE, Mailstop H18-7, Atlanta, GA 30329-4027 USA; email: gpark@cdc.gov

Evaluating the Effectiveness of Social Distancing Interventions to Delay or Flatten the Epidemic Curve of Coronavirus Disease

Laura Matrajt, Tiffany Leung

By April 2, 2020, >1 million persons worldwide were infected with severe acute respiratory syndrome coronavirus 2. We used a mathematical model to investigate the effectiveness of social distancing interventions in a mid-sized city. Interventions reduced contacts of adults ≥60 years of age, adults 20–59 years of age, and children ≤19 years of age for 6 weeks. Our results suggest interventions started earlier in the epidemic delay the epidemic curve and interventions started later flatten the epidemic curve. We noted that, while social distancing interventions were in place, most new cases, hospitalizations, and deaths were averted, even with modest reductions in contact among adults. However, when interventions ended, the epidemic rebounded. Our models suggest that social distancing can provide crucial time to increase healthcare capacity but must occur in conjunction with testing and contact tracing of all suspected cases to mitigate virus transmission.

Severe acute respiratory syndrome coronavirus 2 (SARS-CoV-2) emerged in Wuhan, China, in December 2019 (*1*), and in March 2020, the World Health Organization declared coronavirus disease (COVID-19) a pandemic (*2*). By April 2, 2020, COVID-19 had spread to >181 countries worldwide, and >1 million confirmed cases of COVID-19 and >50,000 deaths had been reported globally (*3*).

On January 21, 2020, the first case of COVID-19 in the United States was identified in a traveler who had recently returned to Washington from Wuhan (*4*,*5*). By March 14, Washington had reported 642 confirmed cases and 40 deaths associated with COVID-19 (*6*). In response to the rapid spread of the virus, on March 12, 2020, approximately 7 weeks after the first confirmed case in the state, the governor of Washington announced a set of interventions in 3 counties (*7*,*8*). More stringent prohibitions were soon imposed, followed by a shelter-in-place order lasting ≥6 weeks beginning on March 25, 2020 (*9*). Similar interventions have been enacted in other US states and in countries in Europe (*10*,*11*,*12*).

We used an epidemic mathematical model to quantify the effectiveness of social distancing interventions in a medium-sized city in the United States or Europe by using Seattle, Washington, as an example. We provide estimates for the proportion of cases, hospitalizations, and deaths averted in the short term and identify key challenges in evaluating the effectiveness of these interventions.

Methods

We developed an age-structured susceptible-exposed-infectious-removed model to describe the transmission of SARS-CoV-2 (Appendix). We divided the population into 10 age groups: 0–5, 6–9, 10–19, 20–29, 30–39, 40–49, 50–59, 60–69, 70–79, and ≥80 years of age. We calibrated the model to the age distribution of the population of the Seattle metropolitan area by using data from the US Census Bureau (*13*). For each age group, we divided the population into compartments: susceptible (*S*) for persons who could be infected; exposed (*E*) for persons who have been exposed but are not yet infectious; infectious (*I*); and removed (*R*) for persons who have recovered or died (Table; Figure 1). We only considered symptomatic infections on the basis of estimates that <1% of infections are asymptomatic (*15*). We assumed only 20% of the cases would be identified because 80% of cases are reported to be mild and would probably be undocumented (*16*,*17*). We used previously reported case-fatality and hospitalization rates by age group (*16*,*18*). We used the contact matrix for 6 age groups computed by Wallinga et al. (*19*) and extended it to 10 age groups (Appendix).

We used January 21, 2020, the day the first case was identified in Washington, as the first day of our simulation on the basis of the analysis by T. Bedford

Fred Hutchinson Cancer Research Center, Seattle, Washington, USA

DOI: https://doi.org/10.3201/eid2608.201093

Table. Description of parameters used in the susceptible-exposed-infectious-removed mathematical model for evaluating the effectiveness of social distancing interventions on coronavirus disease*

Parameter	Meaning	Value	Range	Reference
$1/\sigma$	Mean latent period	5.16 days	4.5–5.8 days	(*14*)
$1/\gamma$	Mean infectious period	5.02 days	3–9 days	†
β	Transmission coefficient	Calculated	NA	NA
C	Contact matrix	NA	NA	(*19*)
N	Total population	3.5 million	NA	(*13*)

*NA, not applicable.
†Q. Bi, unpub. data, https://www.medrxiv.org/content/10.1101/2020.03.03.20028423v3.

(*20*). By using genomic epidemiology of the first 2 COVID-19 cases identified in Washington, Bedford found that SARS-CoV-2 had been circulating locally for 6 weeks before the second case was identified in the state (*20*).

We modeled social distancing by reducing the contact rates in an age group for 6 weeks, corresponding to the policy in Washington in mid-March (*7*,*8*,*21*). We divided the population into 3 major groups for social distancing interventions: children, persons ≤19 years of age; adults 20–59 years of age; and adults ≥60 years of age.

We investigated the effectiveness of 4 scenarios of social distancing. The first was distancing only for adults ≥60 years of age, in which contacts for this group were reduced by 95%. The rationale for this scenario is that older adults are at highest risk for hospitalization and death and should have the most drastic restrictions in their contacts. Similar policies were implemented in early April in some countries, such as Sweden (*22*). In the second scenario, adults ≥60 years of age would reduce social contacts by 95% and children would reduce contacts by 85%, assuming that most of the contacts of children occur at school and would be reduced due to school closures. This scenario corresponds to an intervention in which the high-risk group is fully protected. In addition, it reduces the contact rates for children, who are known to be a major part of the chain of transmission for other respiratory infectious diseases. Research indicates that children are infected with SARS-CoV-2 as often as adults (Q. Bi, unpub. data, https://www.medrxiv.org/content/10.1101/2020.03.03.20028423v3) but seem to have much milder symptoms (*23*). At this point, whether their infectiousness also is reduced is unclear. In the third scenario, adults ≥60 years of age reduce contacts by 95% and adults <60 years of age reduce contacts by 25%, 75%, or 95%. This scenario corresponds to a policy in which high-risk age groups still are protected and younger adults are somewhat restricted in their contacts. However, persons in essential businesses can continue working and children can resume school, which is crucial considering school closures have been shown to have an adverse effect on the economy (*24*). In the fourth scenario, contacts are reduced for every group; adults ≥60

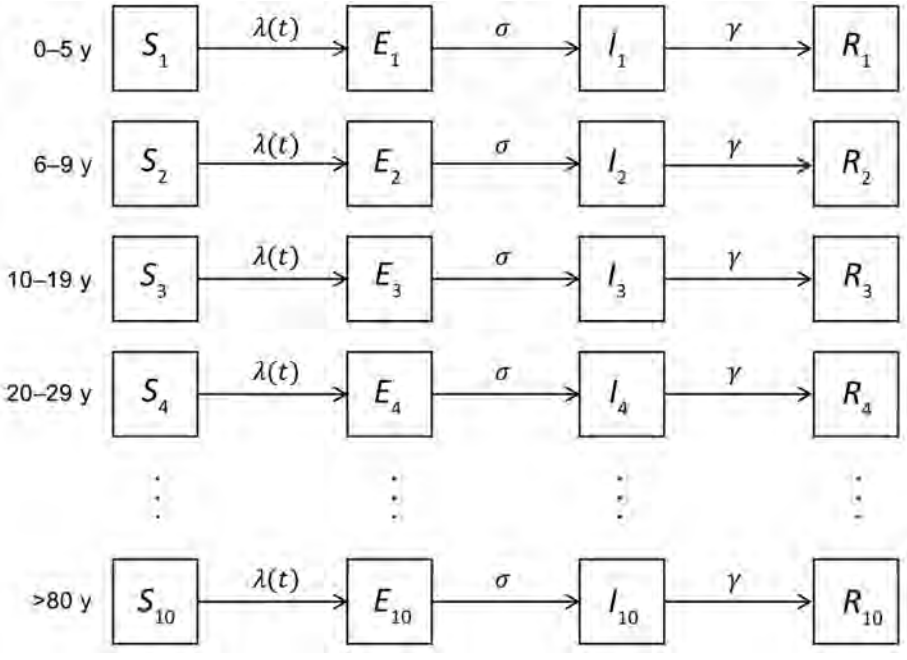

Figure 1. Mathematical model illustrating study population divided into 10 age groups and stratified as susceptible (*S*), exposed (*E*), infectious (*I*), and removed (*R*) from coronavirus disease epidemic. Susceptible persons become exposed at the force of infection $\lambda(t)$, progress to become infectious at rate, σ, and are removed from infecting others at rate, γ.

years of age reduce contacts by 95%, children by 85%, and adults <60 years of age by 25%, 75%, or 95%. This scenario represents many interventions currently in place throughout the world.

To quantify the uncertainty around our results, we performed 1,000 simulations varying 3 parameters: the basic reproduction number (R_0), the latent period, and the duration of infectiousness (Appendix). For each statistic in the results, we computed the error bars by removing the top and bottom 2.5% of the simulations.

Results

Estimates for the duration of infectiousness for SARS-CoV-2 range from 5 to 20 days (*25*; Q. Bi, unpub. data, https://www.medrxiv.org/content/10.1101/2020.03.03.20028423v3). Therefore, we analyzed the influence of the duration of infectiousness on the effectiveness of the social distancing interventions. We kept all other parameters fixed but considered an epidemic with infectious periods of 5, 6, 7, or 8 days, which correspond to the most plausible values (*25*; Q. Bi, unpub. data, https://www.medrxiv.org/content/10.1101/2020.03.03.20028423v3).

In our model, when the infectious period was set to a shorter time of 5 days, the epidemic peaked at 100 days after the introduction of the first case. As we extended the infectious period, the epidemic took much longer to take off (Figure 2) because we kept a fixed R_0, so that a longer infectious period implied a smaller infectious rate. When we used the longest infectious period of 8 days, we noted the epidemic peaked 128 days after the first case was introduced. Therefore, early interventions delay the epidemic but do not substantially change the pool of susceptible persons, which allows similar-sized epidemics to occur later (Figure 2).

We then considered the delay of the epidemic under the 4 social distancing interventions and different infectious periods (Figure 2). As expected, the fourth social distancing strategy, the one applied to all age groups, delayed the epidemic the longest, >50 days, compared with a baseline of using no interventions. Targeting adults ≥60 years of age and children delayed the epidemic by ≈10 days, regardless of infectious period. Targeting adults <60 and ≥60 years of age delayed the epidemic by 41 days when we set the infectious period to 8 days and delayed it 39 days

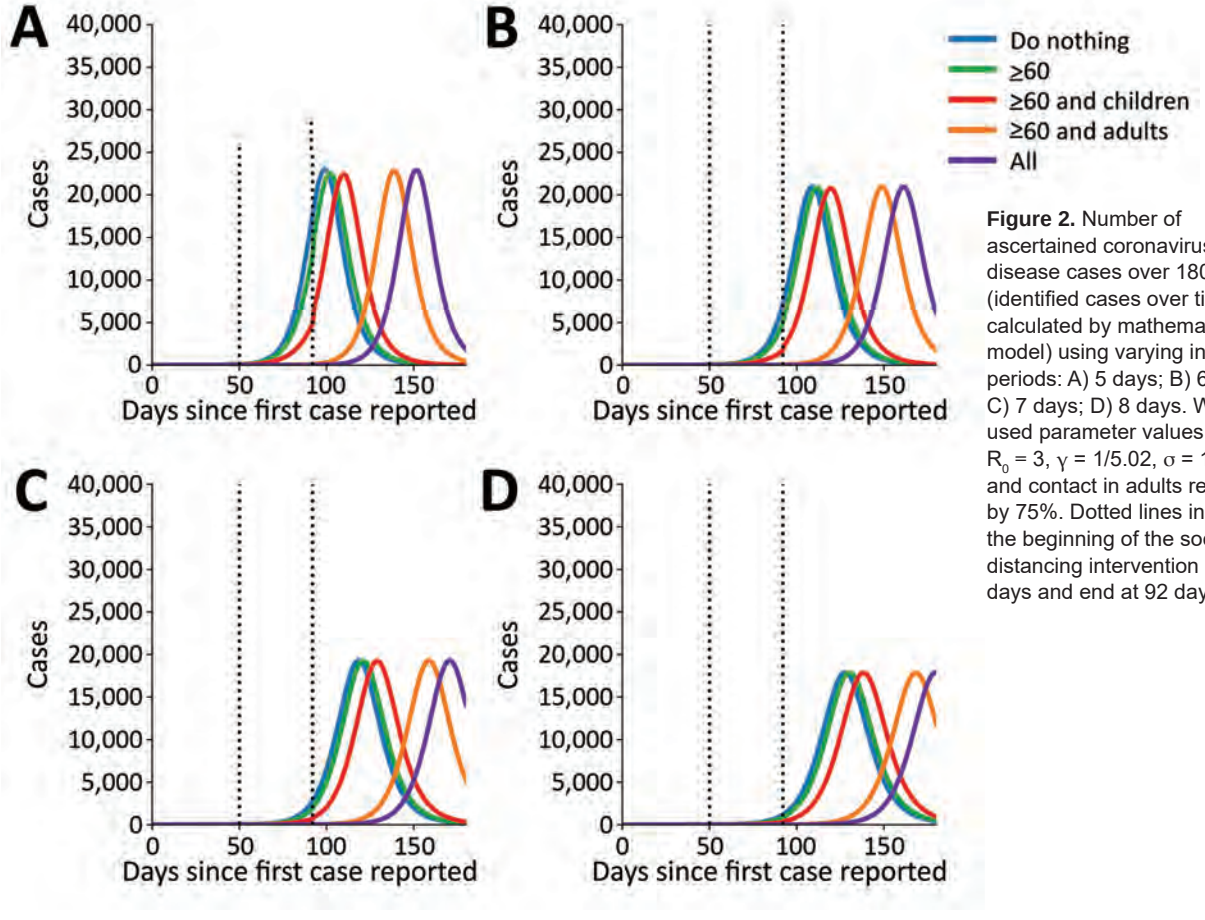

Figure 2. Number of ascertained coronavirus disease cases over 180 days (identified cases over time calculated by mathematical model) using varying infectious periods: A) 5 days; B) 6 days; C) 7 days; D) 8 days. We used parameter values of $R_0 = 3$, $\gamma = 1/5.02$, $\sigma = 1/5.16$, and contact in adults reduced by 75%. Dotted lines indicate the beginning of the social distancing intervention at 50 days and end at 92 days.

when we set the infectious period to 5 days. Social distancing of only adults ≥60 years of age only delayed the epidemic by 2 days, regardless of infectious period (Appendix Table 1). The infectious period did not substantially affect the peak epidemic height compared with baseline.

We examined the effectiveness of the 3 social distancing interventions in adults and the timeframe in which interventions began. We considered social distancing interventions starting 50 days (Figure 3, panels A, C, E) and 80 days (Figure 3, panels B, D, F) after the first case was identified and reduction in adult contacts by 25% (Figure 3, panels A, B), 75% (Figure 3, panels C, D), and 95% (Figure 3, panels E, F). We found that the effect of interventions was dramatically different when started early in the epidemic curve, before the exponential phase of the epidemic, rather than later.

When we started interventions on day 50, we saw a delay in the epidemic regardless of the level of reductions in contact in the adult population, with little change in the magnitude of the epidemic peak. In comparison, when we began the interventions later, during the exponential phase of the epidemic, all interventions flattened epidemic curve. The strategy of reducing the contacts only of adults ≥60 years of age resulted in a moderate reduction of 5,000 (21%) fewer cases at the epidemic peak compared with baseline. Limiting contact for adults ≥60 years of age, as expected, is the only intervention for which there was minimal rebound after the intervention was lifted (Figure 3, panels B, D, F) because older adults make up only 16% of the population and have substantially fewer contacts than the other age groups.

We found that the strategy targeting adults ≥60 years of age and children resulted in 10,500 (45%) fewer cases than baseline at the epidemic peak (Figure 3, panels B, D, F), emphasizing the fact that children are the age group with the highest number of contacts in our model. By comparison, when we applied the adults-only strategy, we saw 11,000 (47%) fewer cases than baseline at the epidemic peak for 25% reduction in contacts in adults <60 years of age (Figure 3, panel B). When we reduced contact by 75% in this age group, the peak epidemic cases dropped by 21,000 (91%). When we reduced contact by 95% in this age group, we noted 22,500 (98%) fewer cases (Figure 3, panels D, F), and the epidemic curve grew at a slower rate in both instances. Of the 4 intervention scenarios, the strategy involving all age-groups decreased the epidemic peak the most and showed the slowest growth rate, which we expected because contacts in all age groups are reduced. Even when we used a lower reduction in contacts of 25% in adults <60 years of age, we noted 16,000 (69%) fewer cases at the epidemic peak (Figure 3, panel B). With

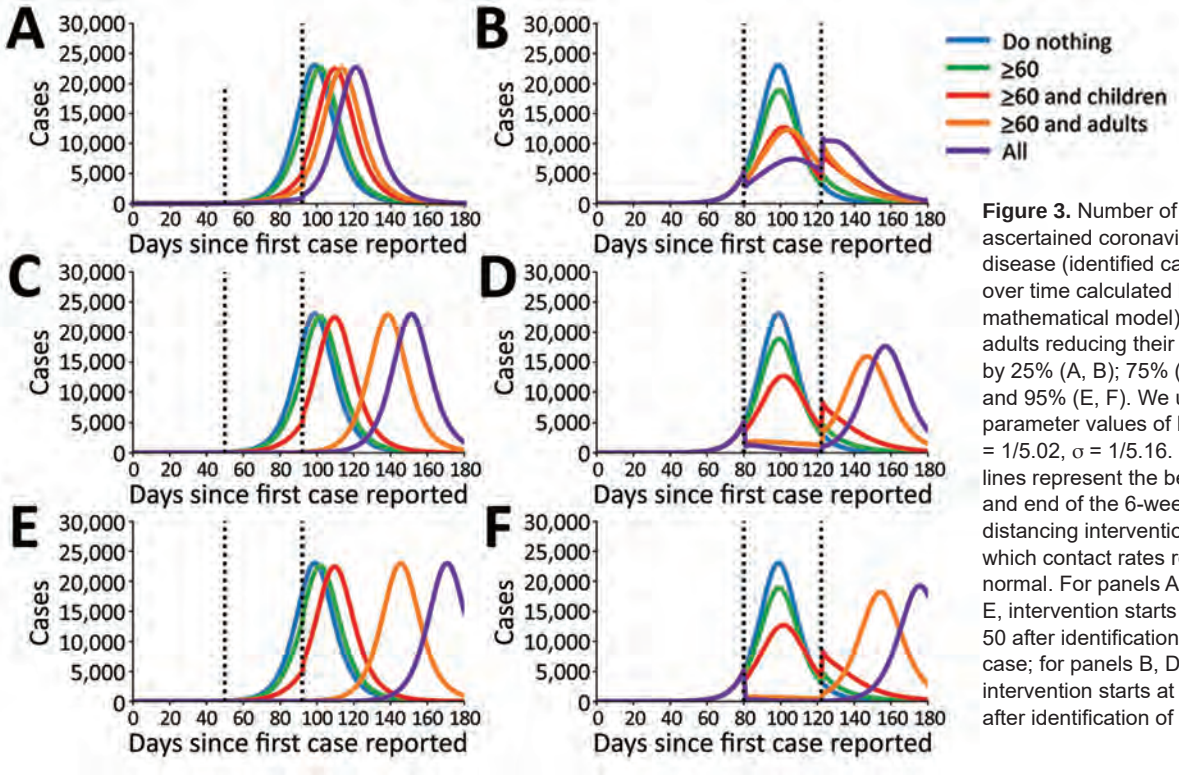

Figure 3. Number of ascertained coronavirus disease (identified cases over time calculated by mathematical model) with adults reducing their contact by 25% (A, B); 75% (C, D); and 95% (E, F). We used parameter values of $R_0 = 3$, $\gamma = 1/5.02$, $\sigma = 1/5.16$. Dotted lines represent the beginning and end of the 6-week social distancing interventions, after which contact rates return to normal. For panels A, C, and E, intervention starts at day 50 after identification of first case; for panels B, D, and F, intervention starts at day 80 after identification of first case.

higher reduction in contacts (95%) in adults <60 years of age, the strategy involving all age groups mitigated nearly all cases at the epidemic peak (Figure 3, panel F). However, our results suggest that all interventions can result in new epidemic curves once the interventions are lifted.

Next, we considered the effects of social distancing interventions over the first 100 days of the epidemic and assumed that the social distancing interventions started on day 50, which corresponds to the approximate date when social distancing interventions started in Washington. To investigate the sensitivity of the model to the chosen parameters, we ran 1,000 simulations (Appendix). We obtained curves that varied widely for both the number of cases and the duration and timing of the epidemic (Appendix Figures 1–3). We ran simulations with the mean parameter values (R_0 = 3, an infectious period lasting 5 days, and a latent period of 5.1 days). We then observed the number of cases and proportion of cases, hospitalizations, and deaths averted during the first 100 days. We noted that reducing the contacts of adults ≥60 years of age averted only 18% of cases for the whole population (Figure 4) but averted 50% of cases for this age group (Appendix Figure 4). In addition, this intervention reduced the overall number of hospitalizations by 30% and reduced deaths by 39% for the whole population (Figure 4) and hospitalizations and deaths by ≥49% for the adults ≥60 years of age (Appendix Figures 5, 6). Adding a social distancing intervention in children slowed the epidemic curve (Figure 3) and reduced the overall hospitalizations by ≥64% (Figure 4) and by ≥53% across all age groups (Appendix Figures 5, 6).

When only 25% of adults <60 years of age changed their contact habits, all interventions rebounded as soon as the intervention was lifted (Figure 3, panel A). Surprisingly, cases, and hence hospitalizations and deaths, can be reduced by 90% during the first 100 days if all groups reduce

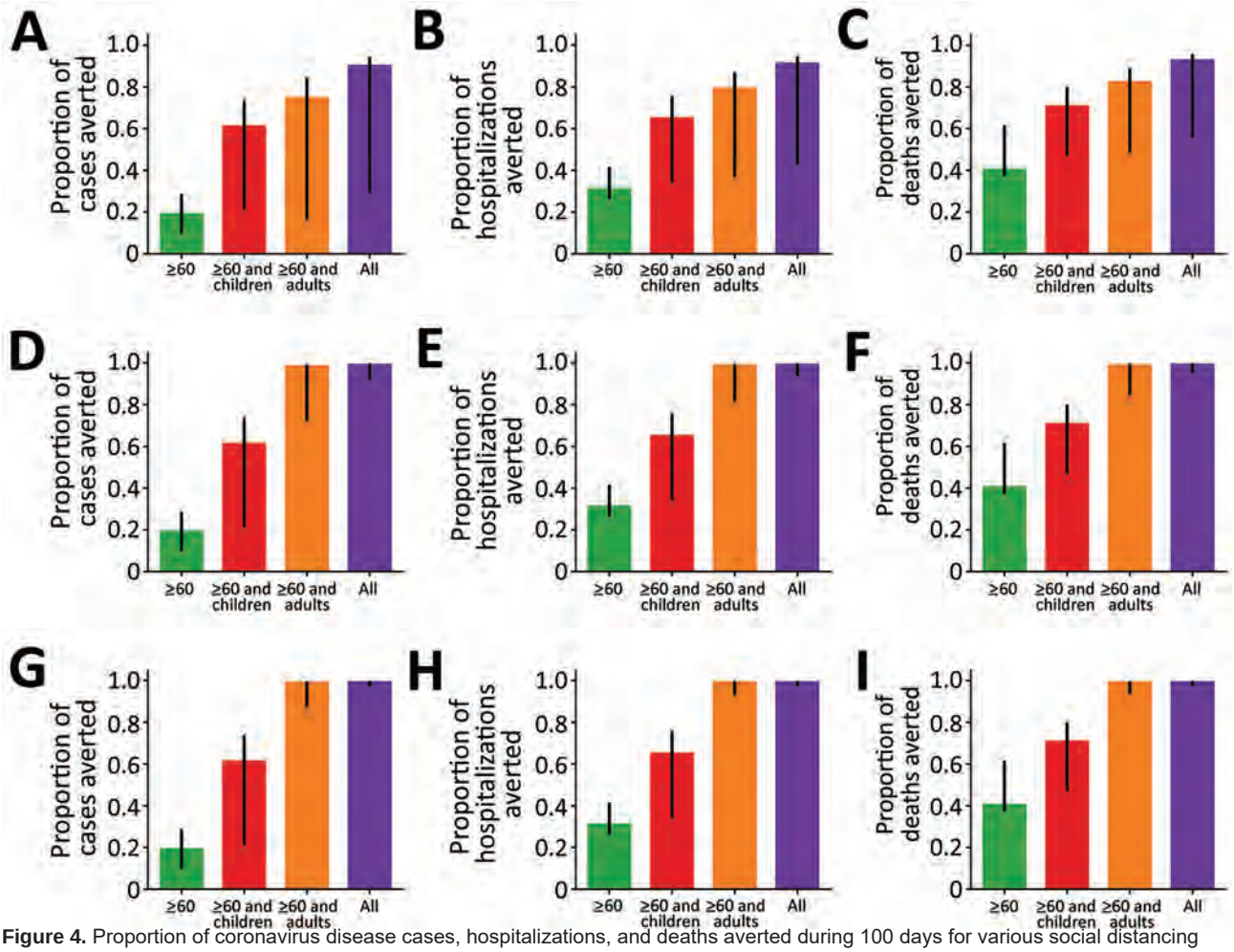

Figure 4. Proportion of coronavirus disease cases, hospitalizations, and deaths averted during 100 days for various social distancing scenarios in which adults reduce their contact by 25% (A–C); 75% (D–F); and 95% (G–I). We used parameter values of R_0 = 3, γ = 1/5.02, σ = 1/5.16. Error bars represent results of 1,000 parameter simulations with the top and bottom 2.5% simulations removed.

their contacts with others, even when adults do so by only 25% (Figure 4, panel A). In this scenario, the reduction in the number of cases, hospitalizations, and deaths was evenly distributed across all age groups (Appendix Figure 4, panel A, Figure 5, panel A, Figure 6, panel A). When adults <60 years of age reduced contacts by 75%, cases, hospitalizations, and deaths rebounded immediately after the end of the intervention, except in the intervention in which contact was reduced for all groups (Figure 3, panel C). As expected, adult groups had the greatest reductions in cases, hospitalizations, and deaths from this intervention (Appendix Figure 5, panel B, Figure 6, panel B). When adults <60 years of age reduced contacts by ≥75%, the strategies that reduced the contacts of adults only and that reduced the contacts of everyone averted ≥98% of cases, hospitalizations and deaths during the first 100 days (Figure 4, panels E, F). Further, when we reduced the contact rate of adults by ≥75%, the strategy targeting all adults and the strategy targeting everyone mitigated the outbreak (Figure 3, panels C, E; Figure 4; Appendix Figure 4, panels B, C, Figure 5, panels B, C, Figure 6, panels B, C). However, our model suggests that the epidemic would rebound even in these scenarios. Of note, the error bars were much larger when adults reduced their contact rates by 25%, and this uncertainty tended to smooth out as the adults further reduced their contact rates.

Discussion

The term "flatten the curve," originating from the Centers for Disease Control and Prevention (*26*), has been used widely to describe the effects of social distancing interventions. Our results highlight how the timing of social distancing interventions can affect the epidemic curve. In our model, interventions put in place and lifted early in the epidemic only delayed the epidemic and did not flatten the epidemic curve. When an intervention was put in place later, we noted a flattening of the epidemic curve. Our results showed that the effectiveness of the intervention will depend on the ratio of susceptible, infected, and recovered persons in the population at the beginning of the intervention. Therefore, an accurate estimate of the number of current and recovered cases is crucial for evaluating possible interventions. As of April 2, 2020, the United States had performed 3,825 tests for SARS-CoV-2 per 1 million population (*27*). By comparison, Italy had performed 9,829 tests/1 million population (*27*). Expanding testing capabilities in all affected countries is critical to slowing and controlling the pandemic.

Some evidence suggests that persons who recover from COVID-19 will develop immunity to SARS-CoV-2 (*28*). However, at this point the duration of immunity is unclear. If immunity lasts longer than the outbreak, then waning immunity will not affect the dynamics of the epidemic. Furthermore, persons who recover from COVID-19 could re-enter the workforce and help care for the most vulnerable groups. However, if immunity is short-lived, for instance on the order of weeks, persons who recover could become re-infected, and extensions to social distancing interventions might be necessary.

We used a mathematical model to quantify short-term effectiveness of social distancing interventions by measuring the number of cases, hospitalizations, and deaths averted during the first 100 days under 4 social distancing intervention scenarios and assuming different levels of reduction in the contacts of the adult population. When we investigated the short-term effects of social distancing interventions started early in the epidemic, our models suggest that the intervention involving all age groups would consistently decrease the number of cases considerably and delay the epidemic the most. Of note, with ≥25% reduction in contact rates for the adult population, combined with 95% reduction in older adults, the number of hospitalizations and deaths could be reduced by >78% during the first 100 days, a finding that agrees with previous reports (*29*,*30*).

Our results must be interpreted with caution. Hospitalizations and deaths averted during the first 100 days in our model would likely occur later if the interventions are lifted without taking any further action, such as widespread testing, self-isolation of infected persons, and contact tracing. As in any model, our assumptions could overestimate the effect of the interventions. However, quantifying the short-term effects of an intervention is vital to help decision makers estimate the immediate number of resources needed and plan for future interventions.

Our simulations suggest that even in the more optimistic scenario in which all age groups reduce their contact rates by ≥85%, the epidemic is set to rebound once the social distancing interventions are lifted. Our results suggest that social distancing interventions can give communities vital time to strengthen healthcare systems and restock medical supplies, but these interventions, if lifted too quickly, will fail to mitigate the current pandemic. Other modeling results also have suggested that extended periods of social distancing would be needed to control transmission (*18*). However, sustaining social distancing interventions over several months might not be feasible economically and

socially. Therefore, a combination of social distancing interventions, testing, isolation, and contact tracing of new cases is needed to suppress transmission of SARS-CoV-2 (*31*,*32*). In addition, these interventions must happen in synchrony around the world because a new imported case could spark a new outbreak in any given region.

Our results suggest that the SARS-CoV-2 infectious period has an extraordinary influence in the modeled speed of an epidemic and in the effectiveness of the interventions considered. However, current estimates of the infectious period range from 5 to 20 days (*25*; Q. Bi, unpub. data, https://www.medrxiv.org/content/10.1101/2020.03.03.20028423v3). Of note, all estimates of the infectious period were made on the basis of PCR positivity, which does not necessarily translate to viability or infectivity of the virus (*33*). We urgently need studies to definitively define the duration of infectiousness of SARS-CoV-2.

Our work has several limitations and should be interpreted accordingly. First, deterministic mathematical models tend to overestimate the final size of an epidemic. Further, deterministic models always will predict a rebound in the epidemic once the intervention is lifted if the number of exposed or infectious persons is >0. To avoid that problem, we forced our infected compartments to 0 if they had <1 person infected at any given time. Second, we considered the latent period to be equal to the incubation period, but others have suggested that presymptomatic transmission is occurring (L. Tindale, unpub. data, https://www.medrxiv.org/content/10.1101/2020.03.03.20029983v1) and SARS-CoV-2 is shed for a prolonged time after symptoms end (*34*). Whether virus shed by convalescent persons can infect others currently is unclear. Further, we considered that mild and severe cases would be equally infectious and our model could be overestimating the total number of infections, which would amplify the effect of social distancing interventions. We also considered infected children and adults to be equally infectious, and our model could be overestimating the effect of social distancing in persons <19 years of age. Strong evidence suggests that children have milder COVID-19 symptoms than adults and might be less infectious (*23*). More studies are needed clarify the role children play in SARS-CoV-2 transmission. In our models, we assumed death and hospitalization rates would be similar to those experienced in Wuhan, where older age groups have been the most affected. Because different countries have different population structures and different healthcare infrastructure, including varying numbers of hospital beds, ventilators, and intensive care unit beds, effects of social distancing interventions could vary widely in different places.

Our results align with an increasing number of publications estimating the effects of interventions against COVID-19. Several researchers have investigated how social distancing interventions in Wuhan might have affected the trajectory of the outbreak (*30*,*35*,*36*; J. Zhang, unpub. data, https://www.medrxiv.org/content/10.1101/2020.03.19.20039107v1). Others have investigated the effect of similar measures elsewhere and concluded that social distancing interventions alone will not be able to control the pandemic (*37*,*38*; M.A. Acuña-Zegarra, unpub. data, https://www.medrxiv.org/content/10.1101/2020.03.28.20046276v1; N.G. Davies, unpub. data, medrxiv.org/content/10.1101/2020.04.01.20049908v1; S. Kissler, unpub. data, https://www.medrxiv.org/content/10.1101/2020.03.22.20041079v1).

Taken together, our results suggest that more aggressive approaches should be taken to mitigate the transmission of SARS-CoV-2. Social distancing interventions need to occur in tandem with testing and contact tracing to minimize the burden of COVID-19. New information about the epidemiologic characteristics of SARS-CoV-2 continues to arise. Incorporating such information into mathematical models such as ours is key to providing public health officials with the best tools to make decisions in uncertain times.

Acknowledgments

This article was preprinted at https://www.medrxiv.org/content/10.1101/2020.03.27.20044891v2.

We thank Dobromir Dimitrov for helpful discussions. We also thank the team in the Biostatistics, Bioinformatics & Epidemiology Program at the Fred Hutchinson Cancer Research Center for supporting this work.

Dr. Matrajt is a research associate at the Fred Hutchinson Cancer Research Center. Her research interests include using quantitative tools to understand infectious disease dynamics and to optimize public health interventions.

Dr. Leung is a postdoctoral research fellow at the Fred Hutchinson Cancer Research Center. Her research interests include using mathematics to understand infectious disease transmission.

References

1. Li Q, Guan X, Wu P, Wang X, Zhou L, Tong Y, et al. Early transmission dynamics in Wuhan, China, of novel coronavirus-infected pneumonia. N Engl J Med. 2020;382:1199–207. https://doi.org/10.1056/NEJMoa2001316
2. World Health Organization. WHO Director-General's opening remarks at the media briefing on COVID-19 11 March 2020 [cited 2020 Mar 15]. https://www.who.int/dg/

speeches/detail/who-director-general-s-opening-remarks-at-the-media-briefing-on-covid-19---11-march-2020
3. Johns Hopkins University and Medicine. Coronavirus resource center. COVID-19 global cases [cited 2020 Apr 2]. https://coronavirus.jhu.edu/map.html
4. Holshue ML, DeBolt C, Lindquist S, Lofy KH, Wiesman J, Bruce H, et al.; Washington State 2019-nCoV Case Investigation Team. Washington State 2019-nCoV Case Investigation Team. First case of 2019 novel coronavirus in the United States. N Engl J Med. 2020;382:929–36. https://doi.org/10.1056/NEJMoa2001191
5. Snohomoish County Washington. Local declaration of emergency Snohomish County 2020 Mar 4 [cited 2020 Mar 15]. https://snohomishcountywa.gov/CivicAlerts.aspx
6. Washington State Department of Health. 2019 novel coronavirus outbreak (COVID-19) [cited 2020 Mar 15]. https://www.doh.wa.gov/emergencies/coronavirus
7. Proclamation by the governor: amending proclamations 20–05 and 20–06; 20–07. Washington, USA. 2020 Mar 11 [cited 2020 Mar 15]. https://www.governor.wa.gov/sites/default/files/20-07%20Coronavirus%20%28tmp%29.pdf
8. Office of the Governor. Washington State. Inslee announces school closures in King, Snohomish and Pierce counties. 2020 Mar 12 [cited 2020 Mar 15]. https://www.governor.wa.gov/news-media/inslee-announces-school-closures-king-snohomish-and-pierce%C2%A0counties
9. Proclamation by the governor: amending proclamations 20–05; 20–25, stay home–stay healthy. Washington, USA. 2020 Mar 23 [cited 2020 Apr 2]. https://www.governor.wa.gov/sites/default/files/proclamations/20-25%20Coronovirus%20Stay%20Safe-Stay%20Healthy%20%28tmp%29%20%28002%29.pdf
10. CBS News. Coronavirus updates from March 20, 2020 2020 [cited 2020 Mar 20]. https://www.cbsnews.com/live-updates/coronavirus-disease-covid-19-latest-news-2020-03-20
11. Schnirring L. France orders lockdown to slow COVID-19 spread. CIDRAP News 2020 Mar 16. Center for Infectious Disease Research and Policy [cited 2020 Mar 16]. http://www.cidrap.umn.edu/news-perspective/2020/03/france-orders-lockdown-slow-covid-19-spread
12. Minder R, Peltier E. Spain, on lockdown, weighs liberties against containing coronavirus. The New York Times. 2020 Mar 15 [cited 2020 Mar 16]. https://www.nytimes.com/2020/03/15/world/europe/spain-coronavirus.html
13. United States Census Bureau. Seattle-Tacoma-Bellevue metro area, Washington [cited 2020 Mar 15]. https://data.census.gov/cedsci
14. Lauer SA, Grantz KH, Bi Q, Jones FK, Zheng Q, Meredith HR, et al. The incubation period of coronavirus disease 2019 (COVID-19) from publicly reported confirmed cases: estimation and application. Ann Intern Med. 2020; Epub ahead of print. https://doi.org/10.7326/M20-0504
15. Wu Z, McGoogan JM. Characteristics of and important lessons from the coronavirus disease (COVID-19) outbreak in China: summary of a report of 72,314 cases from the Chinese Center for Disease Control and Prevention. JAMA. 2020;323:1239–42. https://doi.org/10.1001/jama.2020.2648
16. Novel Coronavirus Pneumonia Emergency Response Epidemiology Team. Vital surveillances: the epidemiological characteristics of an outbreak of 2019 novel coronavirus diseases (COVID-19)–China, 2020. China CDC Wkly. 2020;2:113–22 [cited 2020 Mar 15]. http://weekly.chinacdc.cn/en/article/id/e53946e2-c6c4-41e9-9a9b-fea8db1a8f51
17. Li R, Pei S, Chen B, Song Y, Zhang T, Yang W, et al. Substantial undocumented infection facilitates the rapid dissemination of novel coronavirus (SARS-CoV2). Science. 2020;eabb3221; Epub ahead of print. https://doi.org/10.1126/science.abb3221
18. Ferguson NM, Laydon D, Nedjati-Gilani G, Imai N, Ainslie K, Baguelin M, et al. Impact of non-pharmaceutical interventions (NPIs) to reduce COVID-19 mortality and healthcare demand. Imperial College London. 2020 Mar 16 [cited 2020 Mar 17].
19. Wallinga J, Teunis P, Kretzschmar M. Using data on social contacts to estimate age-specific transmission parameters for respiratory-spread infectious agents. Am J Epidemiol. 2006;164:936–44. https://doi.org/10.1093/aje/kwj317
20. Bedford T. Cryptic transmission of novel coronavirus revealed by genomic epidemiology. Bedford Lab. 2020 Mar 2 [cited 2020 Mar 15]. https://bedford.io/blog
21. Office of the Governor. Washington State. Inslee announces statewide shutdown of restaurants, bars and expanded social gathering limits. 2020 Mar 16 [cited 2020 Mar 18]. https://www.governor.wa.gov/news-media/inslee-announces-statewide-shutdown-restaurants-bars-and-expanded-social-gathering-limits
22. Ellyat H. No lockdown here: Sweden defends its more relaxed coronavirus strategy. CNBC. 2020 Mar 30 [cited 2020 Apr 2]. https://www.cnbc.com/2020/03/30/sweden-coronavirus-approach-is-very-different-from-the-rest-of-europe.html
23. Qiu H, Wu J, Hong L, Luo Y, Song Q, Chen D. Clinical and epidemiological features of 36 children with coronavirus disease 2019 (COVID-19) in Zhejiang, China: an observational cohort study. Lancet Infect Dis. 2020;S1473-3099(20)30198-5; Epub ahead of print. https://doi.org/10.1016/S1473-3099(20)30198-5
24. Lempel H, Hammond RA, Epstein JM. Costs of school closure. The Brookings Institution. 2009 Sep 30 [cited 2020 Apr 2]. https://www.brookings.edu/wp-content/uploads/2016/06/0930_school_closure_presentation.pdf
25. Zhou F, Yu T, Du R, Fan G, Liu Y, Liu Z, et al. Clinical course and risk factors for mortality of adult inpatients with COVID-19 in Wuhan, China: a retrospective cohort study. Lancet. 2020;395:1054–62. https://doi.org/10.1016/S0140-6736(20)30566-3
26. US Centers for Disease Control and Prevention. Interim pre-pandemic planning guidance: community strategy for pandemic influenza mitigation in the United States: early, targeted, layered use of nonpharmaceutical interventions. Atlanta: The Centers; 2007. https://stacks.cdc.gov/view/cdc/11425
27. Hasell J, Ortiz-Ospina E, Mathieu E, Ritchie H, Beltekian D, Roser M. To understand the global pandemic, we need global testing—the Our World in Data COVID-19 Testing dataset, How many tests for COVID-19 are being performed around the world? Our World In Data [cited 2020 Mar 16]. https://ourworldindata.org/covid-testing
28. Zhao J, Yuan Q, Wang H, Liu W, Liao X, Su Y, et al. Antibody responses to SARS-CoV-2 in patients of novel coronavirus disease 2019. Clin Infect Dis. 2020;ciaa344; Epub ahead of print. https://doi.org/10.1093/cid/ciaa344
29. Klein D, Hagedorn B, Kerr C, Hu H, Bedford T, Famulare M, et al. Working paper–model-based estimates of COVID-19 burden in King and Snohomish counties through April 7, 2020 [cited 2020 Mar 16]. https://institutefordisease-modeling.github.io/COVID-public/reports/Working%20paper%20–%20model-based%20estimates%20of%20COVID-19%20burden%20in%20King%20and%20Snohomish%20counties%20through%20April%207.pdf
30. Prem K, Liu Y, Russell TW, Kucharski AJ, Eggo RM, Davies N, et al.; Centre for the Mathematical Modelling of

Infectious Diseases COVID-19 Working Group. The effect of control strategies to reduce social mixing on outcomes of the COVID-19 epidemic in Wuhan, China: a modelling study. Lancet Public Health. 2020;S2468-2667(20)30073-6; [Epub ahead of print].
31. Ferretti L, Wymant C, Kendall M, Zhao L, Nurtay A, Abeler-Dörner L, et al. Quantifying SARS-CoV-2 transmission suggests epidemic control with digital contact tracing. Science. 2020;eabb6936; Epub ahead of print. https://doi.org/10.1126/science.abb6936
32. World Health Organization. WHO Director-General's opening remarks at the media briefing on COVID-19–16 March 2020 [cited 2020 Mar 18]. https://www.who.int/dg/speeches/detail/who-director-general-s-opening-remarks-at-the-media-briefing-on-covid-19---16-march-2020
33. Weiss P, Murdoch DR. Clinical course and mortality risk of severe COVID-19. Lancet. 2020;395:1014–5. https://doi.org/10.1016/S0140-6736(20)30633-4
34. Wölfel R, Corman VM, Guggemos W, Seilmaier M, Zange S, Müller MA, et al. Virological assessment of hospitalized patients with COVID-2019. Nature. 2020; Epub ahead of print. https://doi.org/10.1038/s41586-020-2196-x
35. Wu JT, Leung K, Leung GM. Nowcasting and forecasting the potential domestic and international spread of the 2019-nCoV outbreak originating in Wuhan, China: a modelling study. Lancet. 2020;395:689–97. https://doi.org/10.1016/S0140-6736(20)30260-9
36. Kraemer MUG, Yang C-H, Gutierrez B, Wu C-H, Klein B, Pigott DM, et al.; Open COVID-19 Data Working Group. The effect of human mobility and control measures on the COVID-19 epidemic in China. Science. 2020;eabb4218; Epub ahead of print. https://doi.org/10.1126/science.abb4218
37. Flaxman S, Mishra S, Gandy A, Unwin HJT, Coupland H, Mellan TA, et al. Imperial College COVID-19 Response Team. Report 13: estimating the number of infections and the impact of non-pharmaceutical interventions on COVID-19 in 11 European countries. 2020 Mar 30. [cited 2020 Mar 20]. https://www.imperial.ac.uk/media/imperial-college/medicine/sph/ide/gida-fellowships/Imperial-College-COVID19-Europe-estimates-and-NPI-impact-30-03-2020.pdf
38. Tuite AR, Fisman DN, Greer AL. Mathematical modelling of COVID-19 transmission and mitigation strategies in the population of Ontario, Canada. CMAJ. 2020 Apr 8 [Epub ahead of print].

Address for correspondence: Laura Matrajt, Fred Hutchinson Cancer Research Center, 1100 Fairview Ave N, Mail Stop M2-C200, Seattle, WA 98109, USA; email: laurama@fredhutch.org

Population Genomic Structure and Recent Evolution of *Plasmodium knowlesi*, Peninsular Malaysia

Suzanne E. Hocking, Paul C.S. Divis, Khamisah A. Kadir, Balbir Singh, David J. Conway

Most malaria in Malaysia is caused by *Plasmodium knowlesi* parasites through zoonotic infection from macaque reservoir hosts. We obtained genome sequences from 28 clinical infections in Peninsular Malaysia to clarify the emerging parasite population structure and test for evidence of recent adaptation. The parasites all belonged to a major genetic population of *P. knowlesi* (cluster 3) with high genomewide divergence from populations occurring in Borneo (clusters 1 and 2). We also observed unexpected local genetic subdivision; most parasites belonged to 2 subpopulations sharing a high level of diversity except at particular genomic regions, the largest being a region of chromosome 12, which showed evidence of recent directional selection. Surprisingly, we observed a third subpopulation comprising *P. knowlesi* infections that were almost identical to each other throughout much of the genome, indicating separately maintained transmission and recent genetic isolation. Each subpopulation could evolve and present a broader health challenge in Asia.

All endemic human malaria parasite species originated as zoonotic crossover infections from nonhuman primates (*1*–*3*) and now cause approximately half a million human deaths annually (*4*). Until recently, zoonotic malaria was considered to be very rare, but original findings in Malaysia (*5*,*6*) and subsequent surveys elsewhere have revealed that many human malaria cases in Southeast Asia are caused by the macaque parasite *Plasmodium knowlesi* (*7*). This parasite species now causes almost all malaria in Malaysia (*4*) and is responsible for clinical cases throughout Southeast Asia, where the distributions of macaque reservoir hosts and mosquito vectors overlap with human populations (*8*). As several countries in Southeast Asia are working toward eliminating malaria, *P. knowlesi* represents a special public health challenge. Because of the presence of wild reservoir hosts, elimination of *P. knowlesi* is unlikely, and the problem will deepen if the parasite adapts or environments change to enable more effective transmission between humans (*9*). Of particular concern, numbers of cases each year are continuing to increase (*4*), and intensive surveillance in particular areas indicates this increase is not attributable to ascertainment bias (*10*).

Population genetic studies are essential to determining whether recent parasite adaptation has occurred, which might reflect ongoing evolution that is likely to affect the epidemiology. The *P. knowlesi* parasite has a ≈25 megabase genome of 14 chromosomes (*11*,*12*), haploid in blood stage infections and recombining in a brief diploid stage after male and female parasites mate in the mosquito vector, so informative studies require analysis of loci throughout the genome. Understanding of *P. knowlesi* population genetics has been gained by microsatellite genotyping (*13*,*14*) and whole-genome sequencing (*15*,*16*). In Malaysian Borneo, *P. knowlesi* consists of 2 genetically divergent populations (termed clusters 1 and 2) associated with different reservoir hosts: cluster 1 with long-tailed macaques (*Macaca fascicularis*) and cluster 2 with pig-tailed macaques (*M. nemestrina*) (*14*). In Peninsular Malaysia, on the mainland of Asia, a different genetic subpopulation of *P. knowlesi* exists. This subpopulation was initially indicated by comparing genome sequences of a few old laboratory isolates from Peninsular Malaysia with genome sequences of recent clinical samples from Borneo (*15*), and by comparing sequences of 2 genes in clinical samples from both areas (*17*). Subsequent multilocus microsatellite analysis of recent clinical cases of *P. knowlesi* infection from Peninsular Malaysia has confirmed that all cases are attributable to the cluster 3 type (*13*).

Author affiliations: London School of Hygiene and Tropical Medicine Department of Infection Biology, London, UK (S.E. Hocking, D.J. Conway); Universiti Sarawak Malaysia Malaria Research Centre, Kota Samarahan, Malaysia (P.C.S. Divis, K.A. Kadir, B. Singh, D.J. Conway)

DOI: https://doi.org/10.3201/eid2608.190864

Experimental studies have been conducted on only a few strains of *P. knowlesi*, isolated many years ago and maintained in laboratory monkeys (*18*). Genome sequencing has revealed these strains to be of the cluster 3 type (*13*,*15*), and one of them has been adapted to in vitro culture in human erythrocytes, using 2 independent approaches involving culture with mixtures of macaque and human erythrocytes before growth in human erythrocytes alone (*19*,*20*). The short-term adaptability of this single strain is further illustrated by selection for culture in long-tailed macaque erythrocytes, which was associated with the loss of a specific ligand gene needed for invading human erythrocytes (*21*). These examples from laboratory observations strongly suggest that highly diverse natural parasite populations are likely to adapt to changing conditions.

All of the separately occurring *P. knowlesi* populations might evolve and emerge to present an even more serious public health challenge than already realized. To determine the population genetic substructure within *P. knowlesi* locally, we analyzed recent clinical samples from patients with *P. knowlesi* infection in Peninsular Malaysia by using whole-genome sequencing.

Materials and Methods

We collected heparinized venous blood samples of up to 10 mL from 56 patients with *P. knowlesi* malaria at 5 hospitals in Peninsular Malaysia during February 2016–January 2018 (Figure 1; Appendix 1 Table, https://wwwnc.cdc.gov/EID/article/26/8/19-0864-App1.pdf), after obtaining written informed consent from each patient. The study was approved by the Medical Research and Ethics Committee of the Malaysia Ministry of Health and by the Ethics Committee of the London School of Hygiene and Tropical Medicine.

We depleted leukocytes by passing each blood sample through a CF11 cellulose column to increase the proportion of parasite compared with host DNA. We extracted genomic DNA by using QIAamp DNA Mini kits (QIAGEN, https://www.qiagen.com) and confirmed that all contained only *P. knowlesi* by using nested PCR assays, testing for all locally known malaria parasite species (*22*). We lyophilized genomic DNA before transport to the United Kingdom, then dissolved the DNA in 30 μL of nuclease-free water and quantified it on a spectrophotometer by using the Quant-iT PicoGreen dsDNA Assay Kit (Thermo Fisher Scientific, https://www.thermofisher.com). We processed samples containing ≥300 ng of DNA for sequencing. We performed paired-end short-read genome sequencing by using Illumina MiSeq version 3 kits on the MiSeq platform (Illumina, https://www.illumina.com) with a read length of 300 bp, and aligned reads to the *P. knowlesi* PKNH 2.0 reference genome sequence (Appendix 1). After assembly and quality filtering, data from 28 clinical case samples were available for downstream analysis, representing samples from 5 hospitals in Peninsular Malaysia (Figure 1). For comparison with samples from elsewhere, we retrieved Illumina short reads from previous studies (*15*,*16*,*23*) and assembled them by using the identical pipeline as we had for the newly sequenced samples.

We masked from analysis parts of the genome to which short reads are difficult to uniquely map, including the subtelomeres and the multicopy *kir* and *SICAvar* gene families (Appendix 1). We called single-nucleotide polymorphisms (SNPs) by using

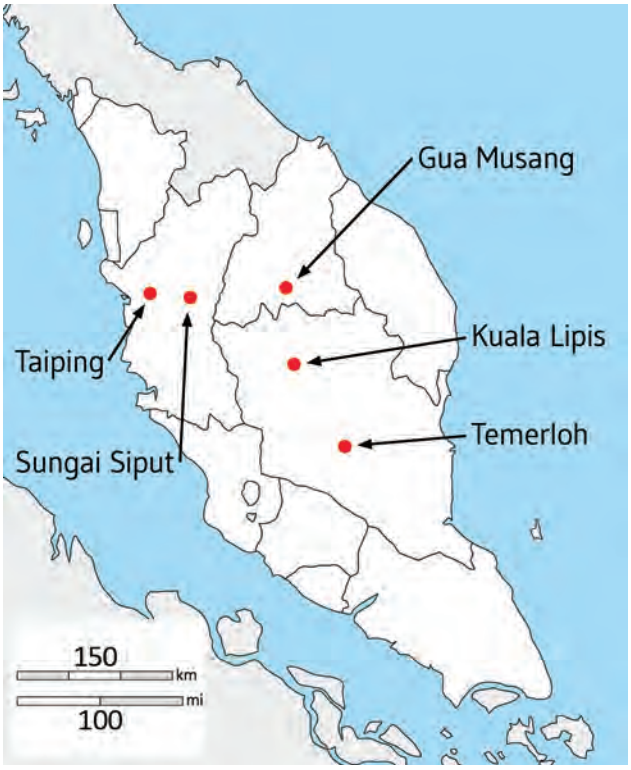

Figure 1. Locations of hospitals in peninsular Malaysia from which clinical *Plasmodium knowlesi* infections were sampled and sequenced in the states of Perak (Taiping and Sungai Siput), Kelantan (Gua Musang), and Pahang (Kuala Lipis and Temerloh). Of 56 infection samples processed through leukocyte depletion and subsequent DNA extraction, 32 had sufficient quantity and purity of *P. knowlesi* DNA for Illumina sequencing (https://www.illumina.com), of which 28 yielded high coverage genomewide sequence for population genomic analysis (sample and sequencing details listed in Appendix 1 Table, https://wwwnc.cdc.gov/EID/article/26/8/19-0864-App1.pdf).

a full repertoire of *P. knowlesi* genome sequences, including the 28 new sequenced infection samples from Peninsular Malaysia with high read coverage obtained in this study, as well as 74 previous samples from Malaysian Borneo (40 from cluster 1 and 34 from cluster 2) and 5 laboratory isolates (107 in total) (*15*,*16*,*23*). The procedures and parameters we used are comparable to those used for other original studies of *P. knowlesi* conducted previously (*15*,*16*) and to those used in population studies on endemic human malaria parasites, such as *P. falciparum*, that have much less diversity than *P. knowlesi* (*15*,*24*).

We used the packages adegenet (https://github.com/thibautjombart/adegenet/wiki) (*25*) and pegas (https://cran.r-project.org/web/packages/pegas/index.html) (*26*) in the R statistical framework to conduct principal component analysis and generate neighbor-joining trees by using an SNP-based pairwise genetic distance matrix. For population structure analysis, we used the package PopGenome (*27*) to calculate nucleotide diversity, within-population Tajima's D indices, and between-population fixation indices (F_{ST}). For sliding-window analysis genomewide, we calculated nucleotide diversity in nonoverlapping 50-kb windows. To scan for genes that might be under balancing selection, we calculated Tajima's D on a gene-by-gene basis and excluded genes with <3 SNPs from analysis. We calculated F_{ST} values between each of the major parasite clusters for all individual SNPs across the genome with a minor allele frequency of ≥10%, and we calculated mean values in all nonoverlapping sliding windows of 500 consecutive SNPs across the genome.

We performed a scan for loci under recent positive selection by identifying SNPs with an allele associated with extended haplotype homozygosity, using the R package rehh (*28*) and applying the default setting assumption that common alleles are more likely to be ancestral. We calculated the standardized integrated haplotype score (|iHS|) for biallelic SNPs with no missing calls and with a minor allele frequency of ≥10%. We set SNPs with |iHS| values in the top 0.01% as core SNPs, around which we identified putative windows of selection by using the extended haplotype homozygosity (EHH) score, plotted until the EHH signal declined to <0.05 on each side. We merged overlapping windows of EHH containing some of the same SNPs to produce a contiguous overall putative selection window for that region, and we considered any gaps of >20 kb between SNPs with elevated |iHS| values to break a putative window of selection.

Results

Genomic Diversity of Different *P. knowlesi* Subpopulations

We successfully obtained paired-end short read Illumina genome sequences with high-read depth mapping to the *P. knowlesi* reference sequence from 28 *P. knowlesi* clinical case samples (Appendix 1) gathered from hospitals at 5 locations in Peninsular Malaysia (Figure 1). Analysis of these new infection samples together with previous sequences from infections in Malaysian Borneo enabled 994,761 SNPs to be initially called, of which 40,934 SNPs were removed because they were in genomic regions with generally unreliable short-read mapping (*kir* and *SICAvar* genes and subtelomeres), resulting in a total of 953,827 SNPs throughout the rest of the genome. After filtering out SNPs that had missing data in >10% of individual infection samples, we included 474,109 high-quality SNPs in subsequent analysis (Appendix 2 Datasheet 1, https://wwwnc.cdc.gov/EID/article/26/8/19-0864-App2.xlsx).

We generated a neighbor-joining tree by using pairwise genetic distances among individual *P. knowlesi* infection samples, which considered most nucleotide calls for all SNPs within each infection sample (Figure 2, panel A). The tree showed that all of the 28 samples from Peninsular Malaysia belonged to a genetic population (cluster 3) divergent from those in Malaysian Borneo (clusters 1 and 2). These new clinical samples from Peninsular Malaysia clustered with the old laboratory isolates (mostly from Peninsular Malaysia) that were sequenced previously and had initially indicated the existence of a third major genetic population within this species (*15*). The overall genomewide nucleotide diversity (π) among the new cluster 3 samples was 4.13×10^{-3} (the allele frequency spectrum is shown in Appendix 1 Figure 1), broadly similar to that for cluster 1 and higher than for cluster 2 (Figure 2, panel B). Differences between clusters 1 and 2 have been examined in detail in original analysis of parasites from Malaysian Borneo (*16*), and higher population genomic diversity within *P. knowlesi* has been noted in comparison with endemic malaria parasite species *P. vivax* and *P. falciparum* (*15*).

Low Levels of Diversity within Individual Clinical Infections

Although all of the *P. knowlesi* clinical isolates were genotypically distinct from each other as indicated by considerable pairwise differences, most of them contained minimal within-infection sequence diversity, as indicated by the high values of the genomewide within-isolate fixation index F_{WS} (Figure 3). Of the 28

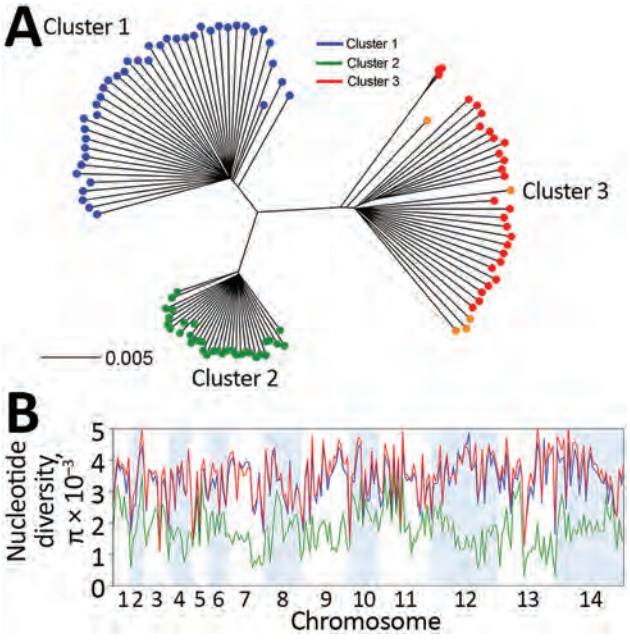

Figure 2. Genomewide analysis of diversity in *Plasmodium knowlesi* clinical samples from Peninsular Malaysia compared with samples from elsewhere. A) Neighbor-joining tree based on a pairwise genetic distance matrix between individual *P. knowlesi* infection samples for the 28 new clinical samples from Peninsular Malaysia (shown in red), 5 previously sequenced laboratory isolates (shown in orange), most of which were originally isolated from Peninsular Malaysia many years ago (*15*), and 74 samples from Malaysian Borneo that grouped into separate subpopulation clusters (cluster 1 shown in blue, cluster 2 in green) (*15*,*16*,*23*). All the clinical isolate samples from Peninsular Malaysia grouped into cluster 3 together with the laboratory isolates. The distance matrix is based on the proportion of all single-nucleotide polymorphisms (SNPs) showing differences between each infection sample (scale bar shows branch length for 0.5% of SNPs differing); most reads within each infection sample determine the allele scored for each SNP. B) Genomewide scan of nucleotide diversity (π) for *P. knowlesi* among the clinical isolates in Peninsular Malaysia (cluster 3, shown in red), compared with diversity observed in the subpopulations in Malaysian Borneo (clusters 1 and 2). The sliding window plot shows values of nucleotide diversity for nonoverlapping windows of 50 kb in each of the 14 chromosomes.

cluster 3 clinical isolates from Peninsular Malaysia in our study, only 4 were clearly mixed (with F_{WS} values <0.95). This low proportion of mixed genotype infections was similar to that observed for the different *P. knowlesi* subpopulations (clusters 1 and 2) in Malaysian Borneo (Figure 3).

Population Genetic Substructure of *P. knowlesi* in Peninsular Malaysia

Analysis of SNP allele frequencies genomewide confirmed that the *P. knowlesi* cluster 3 population in Peninsular Malaysia is highly divergent from each of the separate clusters 1 and 2 in Malaysian Borneo (Figure 4). Comparison of cluster 3 with cluster 1 reveals a genomewide mean F_{ST} values of 0.32 (with 3,713 SNPs being at complete fixation), whereas comparison of cluster 3 with cluster 2 reveals a genomewide mean F_{ST} value of 0.42, (with 6,738 SNPs being at complete fixation) (Figure 4; Appendix 1 Figure 2). We observed a high consistency across the genome in the level of divergence when comparing cluster 3 with cluster 1 (Figure 4, panel A), but more variation across the genome was apparent in the comparison between cluster 3 and cluster 2 (Figure 4, panel B). This finding is attributable to a previously described mosaic pattern of diversity across the genome of cluster 2 (*16*), which contributes to greater genomewide heterogeneity in divergence between clusters 1 and 2 in Malaysian Borneo (Figure 4, panel C) than between either of these and cluster 3 in Peninsular Malaysia.

The distance matrix-based neighbor-joining tree indicated internal branching of the *P. knowlesi* cluster 3 clinical samples from Peninsular Malaysia into 3 different subclusters (Figure 2, panel A). To examine this branching further, we focused the principal component analysis on the clinical samples from Peninsular Malaysia alone, which showed that they formed 3 groups (Figure 5, panel A). The smallest group contained 3 of the samples (GMK03, TPK03, and KLK12) separated from the rest along principal component 1 (which explained 10.5% of overall variation), whereas

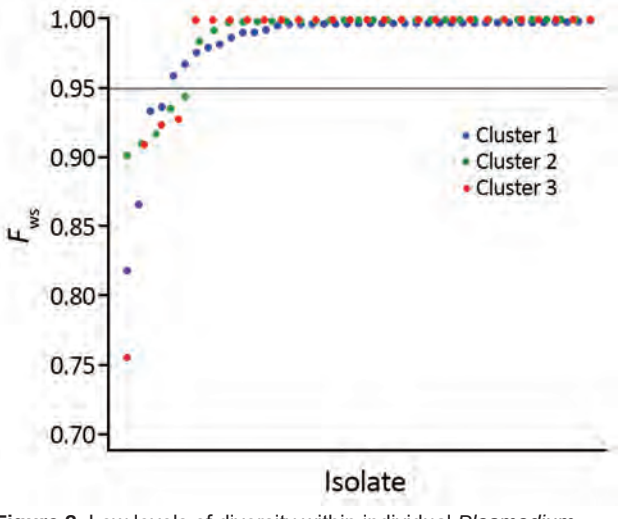

Figure 3. Low levels of diversity within individual *Plasmodium knowlesi* clinical infections from Malaysia as indicated by the high values of the genomewide within-isolate fixation index F_{WS} (potential range 0–1). A value of ≥0.95 is generally taken to indicate an infection dominated by a single genotype, whereas values <0.95 indicate infections that are clearly genotypically mixed. Each point shows the value for an individual infection sample; only 4 of the 28 cluster 3 clinical isolates from Peninsular Malaysia are clearly mixed (similar to the proportions observed in infections with the cluster 1 and 2 types in Malaysian Borneo).

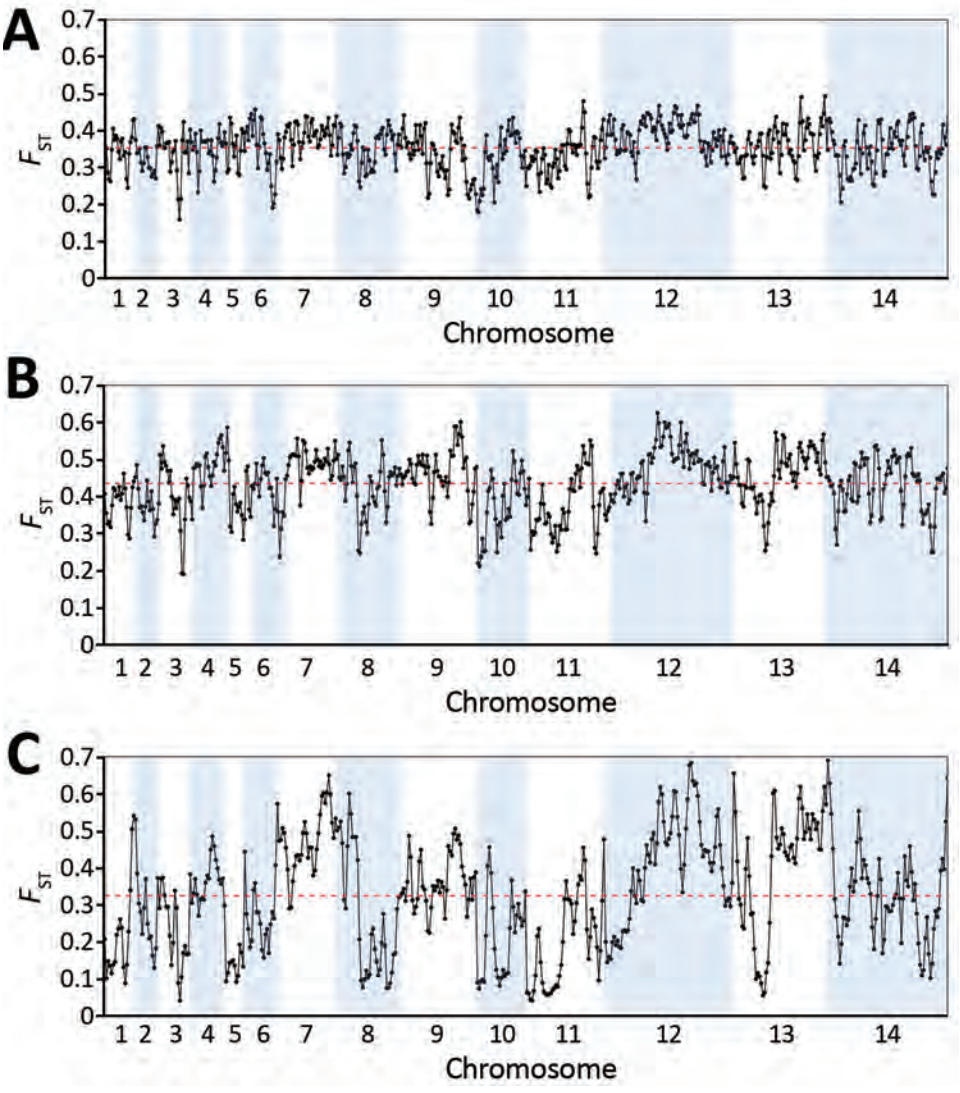

Figure 4. Genomewide between-population fixation index (F_{ST}) scan of divergence between *Plasmodium knowlesi* in Peninsular Malaysia sampled in this study (cluster 3) and the major subpopulations previously sampled in Malaysian Borneo (clusters 1 and 2). All single-nucleotide polymorphisms (SNPs) with overall allele frequencies ≥10% were included, and the solid points show values for analysis windows containing 500 consecutive SNPs, centered by the midpoint of each sequential window and overlapping by 250 SNPs. The red dashed line on each plot shows the genomewide mean value for all analyzed SNPs across the genome. A) The level of divergence between cluster 3 in Peninsular Malaysia and cluster 1 in Malaysian Borneo does not differ greatly throughout the genome (mean F_{ST} value 0.32). B) Divergence between cluster 3 in Peninsular Malaysia and cluster 2 in Malaysian Borneo is slightly higher (mean F_{ST} value 0.42) and shows more heterogeneity between genomic regions because of mosaic structure of diversity in cluster 2 (as explained by panel C). C) Divergence between clusters 1 and 2 in Malaysian Borneo, showing marked heterogeneity across the genome that explains most of the moderate heterogeneity shown in panel B, attributable to a mosaic structure of diversity within cluster 2, as previously reported (*16*).

the 2 other groups were less tightly separated along principal component 2 (which explained 6.5% of overall variation) (Figure 5, panel A). These 3 groups existing within *P. knowlesi* cluster 3 in Peninsular Malaysia are considered as subpopulations, designated in this article as subclusters A (15 of the infections), B (10 infections), and C (3 infections), which are also apparent in neighbor-joining analysis of the cluster 3 samples alone (Appendix 1 Figure 3). These different parasite genetic subclusters are not separated geographically within Peninsular Malaysia, each being detected from multiple sites (Figure 5, panel B), and the hospital with the largest sample size (in Kuala Lipis) had infections of all 3 subclusters. Moreover, infections of the different subcluster types were not temporally aggregated (Appendix 1 Table).

The most divergent of these types (subcluster C) consisted of infections that were highly related to each other, virtually identical in many parts of the genome (Figure 5, panel C). This finding is remarkable because each of these cases were sampled from different states within Peninsular Malaysia (Figure 4, panel B). Although subclusters A and B had similar levels of nucleotide diversity to each other, sliding-window analysis indicated a few genomic regions in which subcluster B has lower diversity than subcluster A (e.g., in a region covering half of chromosome 12) (Figure 5, panel C). Genomewide scan of differentiation between subclusters A and B by sliding-window F_{ST} analysis showed peaks of high differentiation against a background of low differentiation in most of the genome (Figure 5, panel D). The regions that

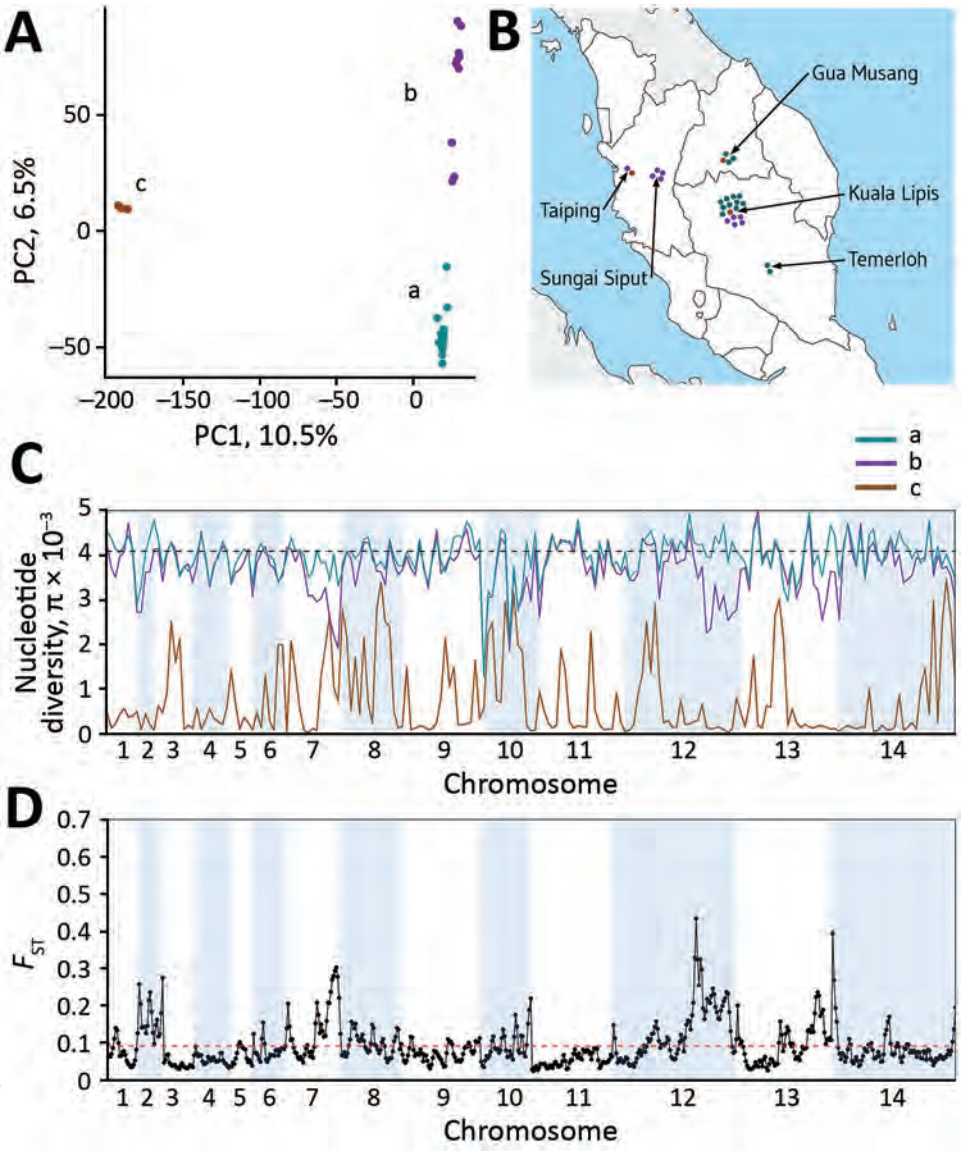

Figure 5. *Plasmodium knowlesi* cluster 3 clinical isolates forming genomic subpopulations that co-occur locally, Peninsular Malaysia. A) Principal component analysis of the 28 cluster 3 *P. knowlesi* clinical isolates from Peninsular Malaysia, showing clustering into 3 groups: subclusters A (15 isolates), B (10 isolates), and C (3 isolates). The assignment of all samples to these 3 subclusters is completely consistent with their placement in the within-cluster 3 branching of the neighbor-joining tree based on the pairwise distance matrix (Figure 2, panel A). The first principal component accounts for 10.5% of overall variation and separated subcluster 3 from the others, whereas the second principal component accounts for 6.5% of overall variation and separated subclusters A and B. B). Each of the cluster 3 *P. knowlesi* subclusters was detected at multiple sites within peninsular Malaysia (points shown at each of the 5 sampling sites show individual infections with colors for the different subclusters as in panel A). The site with most samples had all 3 subclusters co-occurring locally. C) Genomewide scan of diversity shows that the subcluster C samples are virtually identical in large parts of the genome, whereas subclusters A and B are both highly diverse throughout the genome, with only a few genomic regions showing lower diversity in subcluster B compared with A (in chromosomes 2, 7, 12, and 13). D) Genomewide scan of differentiation between subclusters A and B by sliding window between-population fixation index analysis shows peaks of differentiation corresponding to regions with differences in diversity. Most notable is a large region of chromosome 12 having many windows with between-population fixation index values >0.2 and containing some individual single-nucleotide polymorphisms with fixed differences (Appendix 1 Figure 2, https://wwwnc.cdc.gov/EID/article/26/8/19-0864-App1.pdf).

showed differences in levels of diversity are also the most differentiated between the subclusters, most notably the large region of chromosome 12, which has many windows with F_{ST} values exceeding 0.2 (Figure 5, panel D) and contains some individual SNPs with fixed differences (Appendix 1 Figure 4).

Identification of Genomic Loci under Recent Selection in Peninsular Malaysia

To scan for loci that might be under different selection pressures in *P. knowlesi* in Peninsular Malaysia, we summarized nucleotide site allele frequency spectra by calculating Tajima's D index for all 4,742 genes with ≥3 SNPs. Overall, values were negatively skewed (mean -0.86) (Figure 6, panel A); only 215 genes had values >0, of which only 8 had values >1.0 (Figure 6, panel B). This genomewide pattern is consistent with expectations if long-term population size expansion had occurred. Individual genes with unusually high Tajima's D values (Figure 6, panel B) might be under balancing selection and might be examined separately (Appendix 2 Datasheet 2).

Some genes with high values have orthologs in other malaria parasite species that are likely targets of immunity, including a tryptophan-rich protein (PKNH_1472400, D = 0.98), a 6-cysteine protein (PKNH_1254400, D = 0.61), an exported protein PHIST (PKNH_0808500, D = 0.57), and an MSP7-like protein (PKNH_1265900, D = 1.15). However, we found that some other genes with orthologs considered to be targets of immunity in other malaria parasite populations had negative Tajima's D values, including the circumsporozoite protein (*csp*) gene, which had the highest Tajima's D value genomewide in cluster 1 *P. knowlesi* in Malaysian Borneo (*15*), as well as the apical membrane antigen 1 gene (*ama1*, D = –1.35), the Duffy binding protein α (*DBPa*, D = –0.89), and the normocyte binding protein gene (NBPXa, D = –0.42). These findings indicate that the mode or strength of selection on orthologous targets is not uniform in all malaria parasite populations, including among different *P. knowlesi* subpopulations.

We used the standardized integrated haplotype score |iHS| index as a means of scanning for evidence of genomic regions that are likely to have been affected by recent positive directional selection. Analyzing the full population sample of clinical isolates from Peninsular Malaysia, we observed that 11 SNPs had standardized |iHS| values in the top 0.01%, and examination of the ranges of their extended haplotype homozygosity identified 4 distinct genomic windows of extended haplotypes (Figure 7; Appendix 2 Datasheet 3). Two of these (in chromosomes 1 and 9) spanned across genomic *SICAvar* and *kir* genes that had been masked from SNP calling and analysis. The other 2 windows of extended haplotype homozygosity did not include *SICAvar* or *kir* genes but covered ≈28 kb (11 genes) on chromosome 9 and ≈315 kb (81 genes) on chromosome 12. The large region of elevated |iHS| values on chromosome 12 coincides with the region having the highest genomic divergence between cluster 3 population subclusters A and B (Figure 5, panel D), indicating that recent selection on this region has affected part of the *P. knowlesi* population and contributed to the local genetic substructure in Peninsular Malaysia.

Discussion

Genomewide sequence analysis of new clinical isolates has revealed unexpected parasite population structure and evidence of recent selection in *P. knowlesi* in Peninsular Malaysia. On the basis of previous multilocus microsatellite analysis, we expected that genome sequencing of samples from Peninsular Malaysia would reveal a parasite population distinct from those previously described in Malaysian Borneo. This distinction was indeed clearly shown; all samples from Peninsular Malaysia belonged to a genetic population (cluster 3) that is highly divergent genomewide from both of the clusters 1 and 2 in Malaysian Borneo (mean F_{ST} values of 0.32 for cluster 1 and 0.42 for cluster 2). However, the cluster 3 clinical samples from Peninsular Malaysia themselves constituted 3 distinct subpopulations, and the cause of this local population genetic structure needs to be determined. No geographic separation is apparent; each of the three cluster 3 subpopulations was found in overlapping locations, and all were detected from among cases in the hospital that had most samples analyzed. The population structure might reflect >1

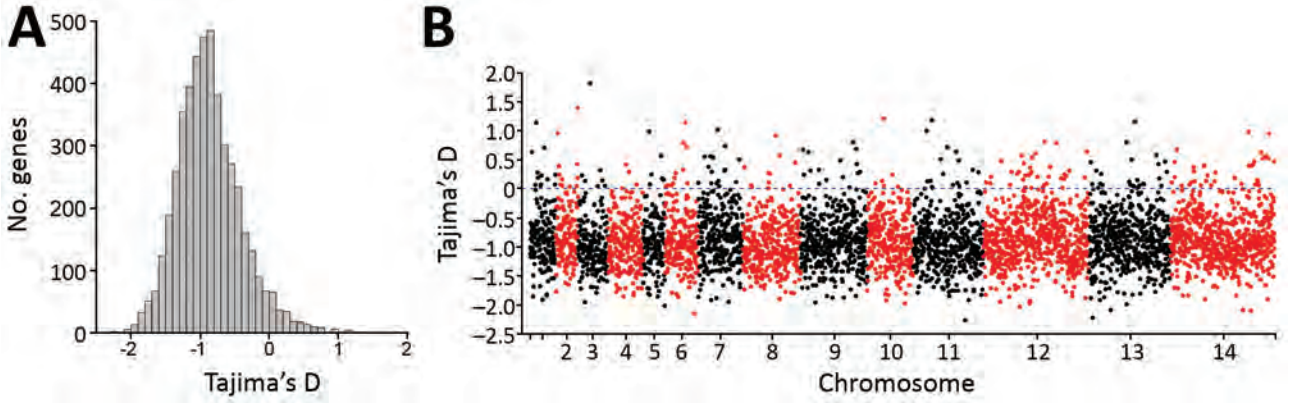

Figure 6. Summary of nucleotide site allele frequency distributions by Tajima's D indices for all 4,742 *Plasmodium knowlesi* genes with ≥3 SNPs among the 28 cluster 3 *P. knowlesi* infections in Peninsular Malaysia. A) Overall values were negatively skewed with a mean Tajima's D of –0.86, consistent with a pattern that would be caused by long-term population size expansion. B) Data for all individual genes show that those with high Tajima's D values are distributed throughout the genome. Some of these genes are likely to be underbalancing selection (individual values for all genes are shown in Appendix 2 Datasheet 2, https://wwwnc.cdc.gov/EID/article/26/8/19-0864-App2.xlsx).

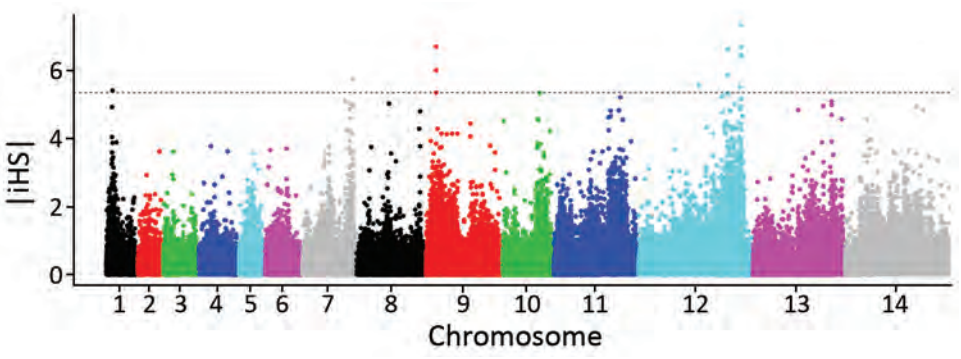

Figure 7. Scan for evidence of genomic regions affected by recent positive directional selection in *Plasmodium knowlesi* in Peninsular Malaysia, using the standardized integrated haplotype score |iHS| index. Examination of the ranges of extended haplotype homozygosity for individual single-nucleotide polymorphisms (SNPs) with high |iHS| values identified 4 distinct genomic windows of extended haplotypes (Appendix 2 Datasheet 3, https://wwwnc.cdc.gov/EID/article/26/8/19-0864-App2.xlsx). Two of these (in chromosomes 1 and 9) spanned across *SICAvar* and *kir* genes, which were masked from SNP calling, whereas the other 2 did not include *SICAvar* or *kir* genes but covered ≈28 kb on chromosome 7 and ≈315 kb on chromosome 12. The large region on chromosome 12 is a merged window, consisting of 4 high |iHS| core SNPs with overlapping windows of extended haplotype homozygosity, and coincides with the region of chromosome 12 that has the highest genomic divergence between cluster 3 population subclusters A and B (Figure 5, panel D, https://wwwnc.cdc.gov/EID/article/26/8/19-0864-F5.htm).

local zoonotic transmission cycle or could be a sign of recent selection and emergence of a subpopulation of *P. knowlesi* transmitted more effectively between humans.

In Malaysian Borneo, long-tailed macaques are reservoir hosts for the cluster 1 population of *P. knowlesi*, whereas pig-tailed macaques are reservoir hosts for the cluster 2 population (*13*,*14*), but whether different reservoir hosts contribute to the parasite population structure we have shown within Peninsular Malaysia is unknown. Microsatellite analysis of *P. knowlesi* in long-tailed macaques from Peninsular Malaysia has indicated that most of them belong to cluster 3, although some samples from long-tailed macaques had indeterminate cluster assignments (*13*). Our findings underscore the need to sample and genotype parasites from pig-tailed macaques in Peninsular Malaysia, as well as to analyze more samples from long-tailed macaques, to investigate whether the parasite subclusters have different reservoir host species locally.

Genetic subpopulations of *P. knowlesi* in Peninsular Malaysia might also be transmitted by different mosquito species. *P. knowlesi* is transmitted by the *Anopheles* Leucosphyrus group of mosquitoes, which contains a diverse array of species found throughout Southeast Asia (*29*), including *An. latens*, *An. cracens*, *An. introlatus*, and *An. hackeri*, in which *P. knowlesi* has been detected in Peninsular Malaysia, as well as other species that have been shown to be infected elsewhere (*30*). *Anopheles* Leucosphyrus group mosquitoes predominantly inhabit forested areas (*31*,*32*), so changes to forest areas and ongoing deforestation will affect human exposure. The potential vector species vary in relative abundance among different sampling sites in Peninsular Malaysia (*33*–*35*), but more surveys are required to determine the relative extent to which they transmit *P. knowlesi* and whether they transmit different populations of the parasite (*36*).

Genomewide scanning revealed discrete regions of divergence between subclusters A and B of *P. knowlesi* cluster 3, in particular a large region on chromosome 12. Interestingly, this region had the strongest evidence of recent directional selection, as indicated by the integrated haplotype score analysis. Moreover, this genomic region did not show evidence of recent selection in Malaysian Borneo (*15*), so the signature is specific to Peninsular Malaysia and indicates selection to be operating locally.

Even more unexpected is the observation of a separate *P. knowlesi* cluster 3 subpopulation (subcluster C), represented by 3 infections highly related to each other throughout most of the genome. Although less common, clinical cases with this parasite type were identified in different hospitals in 3 different states in Peninsular Malaysia. Population genetic substructure also has been observed in the endemic malaria parasites *P. falciparum* (*37*) and *P. vivax* (*38*) in Malaysia, although that observation has been interpreted as indicating fragmented populations that are close to being eliminated. Notable substructure of *P. falciparum* populations also has been observed in Cambodia, probably because of strong selection on locally emerging drug-resistant types in areas where transmission was low (*39*). Zoonotic *P. knowlesi* populations are probably substructured for other reasons, as previously observed in Malaysian Borneo, where the 2 divergent parasite genetic populations observed in human cases are associated with different reservoir host species (*13*,*14*).

Population genomic analysis of *P. knowlesi* so far has mainly focused on parasites from Malaysia, where most reported cases of *P. knowlesi* malaria have been identified. However, cases of *P. knowlesi* malaria in humans have now been reported from all Southeast Asia countries. Whether other local zoonotic subpopulations exist throughout the region or whether all parasites belong to the major genetic populations observed in Malaysia is unknown. Our findings highlight the importance of monitoring population genetic changes in Malaysia and conducting comparable analysis in other areas where *P. knowlesi* has only very recently been realized to occur in humans (*40*,*41*).

Acknowledgments

We thank the hospital directors for their cooperation, the medical and nursing staff for obtaining consent and blood samples from malaria patients, and the medical laboratory staff for processing the samples from the Malaysia Ministry of Health hospitals at Kuala Lipis, Gua Musang, Temerloh, Sungai Siput, and Taiping. We thank the Director General of Health in Malaysia for permission to publish this paper. We are grateful to Alfred Amambua-Ngwa for comments on the draft manuscript.

This study was supported by funds from Universiti Malaysia Sarawak (grant no. F05/SpTDG/1447/2016/4), European Research Council (grant no. AdG-2011-294428), and the Biotechnology and Biological Sciences Research Council (London Interdisciplinary Doctoral Training Programme PhD studentship support for S.E.H.).

About the Author

Dr. Hocking completed a PhD in the London Interdisciplinary Doctoral Training Programme (http://lido-dtp.ac.uk). Her thesis focuses on sequencing of genomes and transcriptomes to investigate population structure and biology of malaria parasites.

References

1. Liu W, Li Y, Learn GH, Rudicell RS, Robertson JD, Keele BF, et al. Origin of the human malaria parasite *Plasmodium falciparum* in gorillas. Nature. 2010;467:420–5. https://doi.org/10.1038/nature09442
2. Loy DE, Plenderleith LJ, Sundararaman SA, Liu W, Gruszczyk J, Chen YJ, et al. Evolutionary history of human *Plasmodium vivax* revealed by genomewide analyses of related ape parasites. Proc Natl Acad Sci U S A. 2018;115:E8450–9. https://doi.org/10.1073/pnas.1810053115
3. Rutledge GG, Böhme U, Sanders M, Reid AJ, Cotton JA, Maiga-Ascofare O, et al. *Plasmodium malariae* and *P. ovale* genomes provide insights into malaria parasite evolution. Nature. 2017;542:101–4. https://doi.org/10.1038/nature21038
4. WHO. World malaria report 2018 [cited 2019 Jun 13]. https://www.who.int/malaria/publications/world-malaria-report-2018
5. Cox-Singh J, Davis TM, Lee KS, Shamsul SS, Matusop A, Ratnam S, et al. *Plasmodium knowlesi* malaria in humans is widely distributed and potentially life threatening. Clin Infect Dis. 2008;46:165–71. https://doi.org/10.1086/524888
6. Singh B, Kim Sung L, Matusop A, Radhakrishnan A, Shamsul SS, Cox-Singh J, et al. A large focus of naturally acquired *Plasmodium knowlesi* infections in human beings. Lancet. 2004;363:1017–24. https://doi.org/10.1016/S0140-6736(04)15836-4
7. Shearer FM, Huang Z, Weiss DJ, Wiebe A, Gibson HS, Battle KE, et al. Estimating geographical variation in the risk of zoonotic *Plasmodium knowlesi* infection in countries eliminating malaria. PLoS Negl Trop Dis. 2016;10:e0004915. https://doi.org/10.1371/journal.pntd.0004915
8. Singh B, Daneshvar C. Human infections and detection of *Plasmodium knowlesi.* Clin Microbiol Rev. 2013;26:165–84. https://doi.org/10.1128/CMR.00079-12
9. William T, Jelip J, Menon J, Anderios F, Mohammad R, Awang Mohammad TA, et al. Changing epidemiology of malaria in Sabah, Malaysia: increasing incidence of *Plasmodium knowlesi.* Malar J. 2014;13:390. https://doi.org/10.1186/1475-2875-13-390
10. Cooper DJ, Rajahram GS, William T, Jelip J, Mohammad R, Benedict J, et al. *Plasmodium knowlesi* malaria in Sabah, Malaysia, 2015–2017: ongoing increase in incidence despite near-elimination of the human-only *Plasmodium* species. Clin Infect Dis. 2020;70:361–7.
11. Lapp SA, Geraldo JA, Chien JT, Ay F, Pakala SB, Batugedara G, et al. MaHPIC consortium. PacBiol assembly of a *Plasmodium knowlesi* genome sequence with Hi-C correction and manual annotation of the SICAvar gene family. Parasitology. 2018;145:71–84. https://doi.org/ 10.1017/S0031182017001329
12. Pain A, Böhme U, Berry AE, Mungall K, Finn RD, Jackson AP, et al. The genome of the simian and human malaria parasite *Plasmodium knowlesi.* Nature. 2008;455:799–803. https://doi.org/10.1038/nature07306
13. Divis PC, Lin LC, Rovie-Ryan JJ, Kadir KA, Anderios F, Hisam S, et al. Three divergent subpopulations of the malaria parasite *Plasmodium knowlesi.* Emerg Infect Dis. 2017;23:616–24. https://doi.org/10.3201/eid2304.161738
14. Divis PC, Singh B, Anderios F, Hisam S, Matusop A, Kocken CH, et al. Admixture in humans of two divergent *Plasmodium knowlesi* populations associated with different macaque host species. PLoS Pathog. 2015;11:e1004888. https://doi.org/10.1371/journal.ppat.1004888
15. Assefa S, Lim C, Preston MD, Duffy CW, Nair MB, Adroub SA, et al. Population genomic structure and adaptation in the zoonotic malaria parasite *Plasmodium knowlesi.* Proc Natl Acad Sci U S A. 2015;112:13027–32. https://doi.org/10.1073/pnas.1509534112
16. Divis PCS, Duffy CW, Kadir KA, Singh B, Conway DJ. Genome-wide mosaicism in divergence between zoonotic malaria parasite subpopulations with separate sympatric transmission cycles. Mol Ecol. 2018;27:860–70. https://doi.org/10.1111/mec.14477
17. Yusof R, Ahmed MA, Jelip J, Ngian HU, Mustakim S, Hussin HM, et al. Phylogeographic evidence for 2 genetically distinct zoonotic *Plasmodium knowlesi* parasites, Malaysia. Emerg Infect Dis. 2016;22:1371–80. https://doi.org/10.3201/eid2208.151885
18. Coatney GR, Collins WE, McWilson W, Contacos PG. The primate malarias. Atlanta: US Department of Health and Human Services; 1971.

19. Moon RW, Hall J, Rangkuti F, Ho YS, Almond N, Mitchell GH, et al. Adaptation of the genetically tractable malaria pathogen *Plasmodium knowlesi* to continuous culture in human erythrocytes. Proc Natl Acad Sci U S A. 2013;110:531–6. https://doi.org/10.1073/pnas.1216457110
20. Lim C, Hansen E, DeSimone TM, Moreno Y, Junker K, Bei A, et al. Expansion of host cellular niche can drive adaptation of a zoonotic malaria parasite to humans. Nat Commun. 2013;4:1638. https://doi.org/10.1038/ncomms2612
21. Moon RW, Sharaf H, Hastings CH, Ho YS, Nair MB, Rchiad Z, et al. Normocyte-binding protein required for human erythrocyte invasion by the zoonotic malaria parasite *Plasmodium knowlesi.* Proc Natl Acad Sci U S A. 2016;113:7231–6. https://doi.org/10.1073/pnas.1522469113
22. Lee KS, Divis PC, Zakaria SK, Matusop A, Julin RA, Conway DJ, et al. *Plasmodium knowlesi*: reservoir hosts and tracking the emergence in humans and macaques. PLoS Pathog. 2011;7:e1002015. https://doi.org/10.1371/journal.ppat.1002015
23. Pinheiro MM, Ahmed MA, Millar SB, Sanderson T, Otto TD, Lu WC, et al. *Plasmodium knowlesi* genome sequences from clinical isolates reveal extensive genomic dimorphism. PLoS One. 2015;10:e0121303. https://doi.org/10.1371/journal.pone.0121303
24. Duffy CW, Amambua-Ngwa A, Ahouidi AD, Diakite M, Awandare GA, Ba H, et al. Multi-population genomic analysis of malaria parasites indicates local selection and differentiation at the *gdv1* locus regulating sexual development. Sci Rep. 2018;8:15763. https://doi.org/10.1038/s41598-018-34078-3
25. Jombart T. adegenet: a R package for the multivariate analysis of genetic markers. Bioinformatics. 2008;24:1403–5. https://doi.org/10.1093/bioinformatics/btn129
26. Paradis E. pegas: an R package for population genetics with an integrated-modular approach. Bioinformatics. 2010;26:419–20. https://doi.org/10.1093/bioinformatics/btp696
27. Pfeifer B, Wittelsbürger U, Ramos-Onsins SE, Lercher MJ. PopGenome: an efficient Swiss army knife for population genomic analyses in R. Mol Biol Evol. 2014;31:1929–36. https://doi.org/10.1093/molbev/msu136
28. Gautier M, Vitalis R. rehh: an R package to detect footprints of selection in genome-wide SNP data from haplotype structure. Bioinformatics. 2012;28:1176–7. https://doi.org/10.1093/bioinformatics/bts115
29. Sallum MA, Peyton EL, Wilkerson RC. Six new species of the *Anopheles leucosphyrus* group, reinterpretation of *An. elegans* and vector implications. Med Vet Entomol. 2005;19:158–99. https://doi.org/10.1111/j.0269-283X.2005.00551.x
30. Vythilingam I, Wong ML, Wan-Yussof WS. Current status of *Plasmodium knowlesi* vectors: a public health concern? Parasitology. 2018;145:32–40. https://doi.org/10.1017/S0031182016000901
31. Moyes CL, Shearer FM, Huang Z, Wiebe A, Gibson HS, Nijman V, et al. Predicting the geographical distributions of the macaque hosts and mosquito vectors of *Plasmodium knowlesi* malaria in forested and non-forested areas. Parasit Vectors. 2016;9:242. https://doi.org/10.1186/s13071-016-1527-0
32. Sinka ME, Bangs MJ, Manguin S, Chareonviriyaphap T, Patil AP, Temperley WH, et al. The dominant *Anopheles* vectors of human malaria in the Asia-Pacific region: occurrence data, distribution maps and bionomic précis. Parasit Vectors. 2011;4:89. https://doi.org/10.1186/1756-3305-4-89
33. Jiram AI, Vythilingam I, NoorAzian YM, Yusof YM, Azahari AH, Fong MY. Entomologic investigation of *Plasmodium knowlesi* vectors in Kuala Lipis, Pahang, Malaysia. Malar J. 2012;11:213. https://doi.org/ 10.1186/1475-2875-11-213
34. Vythilingam I, Lim YA, Venugopalan B, Ngui R, Leong CS, Wong ML, et al. *Plasmodium knowlesi* malaria an emerging public health problem in Hulu Selangor, Selangor, Malaysia (2009–2013): epidemiologic and entomologic analysis. Parasit Vectors. 2014;7:436. https://doi.org/10.1186/1756-3305-7-436
35. Vythilingam I, Noorazian YM, Huat TC, Jiram AI, Yusri YM, Azahari AH, et al. *Plasmodium knowlesi* in humans, macaques and mosquitoes in peninsular Malaysia. Parasit Vectors. 2008;1:26. https://doi.org/10.1186/1756-3305-1-26
36. Wong ML, Ahmed MA, Sulaiman WYW, Manin BO, Leong CS, Quan FS, et al. Genetic diversity of zoonotic malaria parasites from mosquito vector and vertebrate hosts. Infect Genet Evol. 2019;73:26–32. https://doi.org/10.1016/j.meegid.2019.04.010
37. Anthony TG, Conway DJ, Cox-Singh J, Matusop A, Ratnam S, Shamsul S, et al. Fragmented population structure of *Plasmodium falciparum* in a region of declining endemicity. J Infect Dis. 2005;191:1558–64. https://doi.org/10.1086/429338
38. Auburn S, Benavente ED, Miotto O, Pearson RD, Amato R, Grigg MJ, et al. Genomic analysis of a pre-elimination Malaysian *Plasmodium vivax* population reveals selective pressures and changing transmission dynamics. Nat Commun. 2018;9:2585. https://doi.org/10.1038/s41467-018-04965-4
39. Miotto O, Almagro-Garcia J, Manske M, Macinnis B, Campino S, Rockett KA, et al. Multiple populations of artemisinin-resistant *Plasmodium falciparum* in Cambodia. Nat Genet. 2013;45:648–55. https://doi.org/10.1038/ng.2624
40. Herdiana H, Irnawati I, Coutrier FN, Munthe A, Mardiati M, Yuniarti T, et al. Two clusters of *Plasmodium knowlesi* cases in a malaria elimination area, Sabang Municipality, Aceh, Indonesia. Malar J. 2018;17:186. https://doi.org/10.1186/s12936-018-2334-1
41. Imwong M, Madmanee W, Suwannasin K, Kunasol C, Peto TJ, Tripura R, et al. Asymptomatic natural human infections with the simian malaria parasites *Plasmodium cynomolgi* and *Plasmodium knowlesi.* J Infect Dis. 2019;219:695–702. https://doi.org/10.1093/infdis/jiy519

Address for correspondence author: David J. Conway, Department of Infection Biology, Faculty of Infectious and Tropical Diseases, London School of Hygiene and Tropical Medicine, Keppel St, London WC1E 7HT, UK; email: david.conway@lshtm.ac.uk

Human Outbreak of Trichinellosis Caused by *Trichinella papuae* Nematodes, Central Kampong Thom Province, Cambodia

Yannick Caron, Sotharith Bory, Michel Pluot, Mary Nheb, Sarin Chan, Sang Houn Prum, Sun Bun Hong Lim, Mala Sim, Yi Sengdoeurn, Ly Sovann, Virak Khieu, Isabelle Vallée, Hélène Yera

In September 2017, a severe trichinellosis outbreak occurred in Cambodia after persons consumed raw wild pig meat; 33 persons were infected and 8 died. We collected and analyzed the medical records for 25 patients. Clinical signs and symptoms included myalgia, facial or peripheral edema, asthenia, and fever. We observed increased levels of creatine phosphokinase and aspartate aminotransferase, as well as eosinophilia. Histopathologic examination of muscle biopsy specimens showed nonencapsulated *Trichinella* larvae. A *Trichinella* excretory/secretory antigen ELISA identified *Trichinella* IgM and IgG. Biopsy samples were digested and larvae were isolated and counted. PCR for the 5S rDNA intergenic spacer region and a multiplex PCR, followed by sequencing identified the parasite as *Trichinella papuae*. This species was identified in Papua New Guinea during 1999 and in several outbreaks in humans in Thailand. Thus, we identified *T. papuae* nematodes in humans in Cambodia.

Trichinellosis is a parasitic disease caused by nematodes of the genus *Trichinella* and acquired by ingestion of raw or undercooked meat from infected animals (nonuminant mammals, birds, and reptiles). Approximately 11 million persons worldwide might be infected by *Trichinella* spp. (*1*). Numerous animals species (≈100), including humans, can be infected and the most common source of human trichinellosis is meat from pig or wild pig (*Sus scrofa*) (*2*). Therefore, this zoonotic disease is not only a public health hazard but also represents an economic problem in porcine animal production and food safety. Some countries in Europe implemented a *Trichinella* monitoring program (*3*,*4*), and a *Trichinella*-free pig production pilot program has also been set up in the United States (*5*). Nevertheless, estimation of the effect of trichinellosis in developing countries with reference to public health and social and economic costs is difficult.

Recent studies on the genetic diversity, zoogeographic, and epidemiologic features within this genus resulted in a revised *Trichinella* taxonomy comprising 10 species (13 genotypes): encapsulated (*T. spiralis*, *T. nativa*, *T. britovi*, *T. murrelli*, *T. nelsoni*, *T. patagoniensis*, and *T. chanchalensis*) and nonencapsulated (*T. pseudospiralis*, *T. papuae*, and *T. zimbabwensis*) (*2*,*6*,*7*). In Southeast Asia, relatively few human outbreaks were recorded, but it has been calculated that >40 million persons are at risk for *Trichinella* infection in China (*8*). The presence of *Trichinella* antibodies in asymptomatic persons in a rural population of Cambodia (unknown location) was described (*9*), and another study reported 24 cases of *Trichinella* spp. in Khmer immigrants living in the United States (*10*). In Vietnam (*11*) and Laos (*12*), several outbreaks were reported involving *T. spiralis* nematodes. However, in Thailand, several human outbreaks involving *T. spiralis*, *T. pseudospiralis*, and *T. papuae* nematodes were reported (*13*,*14*).

The *T. papuae* nematode (genotype T10) is one of the most recently discovered species and was first detected in sylvatic swine of Papua New Guinea in 1999 by using molecular tools (*15*). In addition to being a nonencapsulated species, *T. papuae* nematodes are known to use mammals and reptiles (mainly crocodiles but also to a lesser extent caimans, turtles, and

Author affiliations: Institut Pasteur, Phnom Penh, Cambodia (Y. Caron, M. Sim); Calmette Hospital, Phnom Penh (S. Bory, M. Pluot, M. Nheb, S. Chan); Preah Ket Mealea Hospital, Phnom Penh (S. H. Prum); Kampong Thom Province Hospital, Kampong Thom, Cambodia (S.B.H. Lim); Ministry of Health, Phnom Penh (Y. Sengdoeun, L. Sovann, V. Khieu); Agence Nationale Sécurité Sanitaire Alimentaire Nationale, Maisons-Alfort, France (I. Vallée); Paris University, Paris, France (H. Yera)

DOI: https://doi.org/10.3201/eid2608.191497

lizards) as hosts (*16*). Humans acquired the parasite by the consumption of raw meat from domestic animals, wild pigs, saltwater crocodiles, and turtles (*17*). This species was identified in Thailand in humans during outbreaks in 2006 (*14*) and 2007 (*13*) and in a patient returning from Malaysia in 2011 (*18*). The objective of this study was to report and describe a documented human outbreak of trichinellosis caused by *T. papuae* nematodes in Cambodia.

Materials and Methods

Study Area

At the end of September 2017, a trichinellosis outbreak occurred near Chak Tav village, Mean Rith commune, Sandan District in Kampong Thom Province, Cambodia. This location is situated in the Prey Lang Forest (13°07′N, 105°30′E), which is a nature reserve forest covering 3,600 km^2.

Data Sources and Ethics

During this outbreak, we collected medical and epidemiologic data from Kampong Thom Provincial Hospital and 2 hospitals (Preah Ket Mealea and Calmette) in Phnom Penh. The Pasteur Institute of Cambodia had an official agreement from the Communicable Disease Control Department of the Ministry of Health of Cambodia to study this outbreak, including collection of medical records of the patients, as well as remaining biologic samples. Because this retrospective study respected anonymity, did not involve any patient intervention, and was conducted in the frame of control and national epidemiologic surveillance, ethics agreement or informed consent was not necessary.

Serodiagnosis

Serodiagnosis was performed for most (11/12) patients hospitalized in Preah Ket Mealea Hospital by a laboratory in Vietnam (https://www.medic-lab.com). This laboratory used an excretory/secretory antigen–based ELISA for detection of IgM (negative result if optical density <1.0) and IgG (negative result if optical density <0.3).

Histopathologic Analysis

For all 13 patients at Calmette Hospital, we obtained 2 biopsy specimens from the deltoid and biceps or gastrocnemius muscles, preserved them in 10% phosphate-buffered formalin, and sent them to the Pathology Department of the hospital. Formalin-fixed samples were dissected, embedded in paraffin (at 56°C), cut with a rotary microtome preset for a thickness of 4 μm, and stained with hematoxylin phloxine saffron. Histopathologic preparations were then microscopically examined.

Detection of *Trichinella* larvae

Sections from slides, as well as remaining paraffin blocks for each of the sample were sent to the National Reference Laboratory for Human Trichinellosis at Cochin Hospital (Paris, France). Paraffin was eliminated from tissues after incubation in Histo-Clear (National Diagnostics, https://www.nationaldiagnostics.com) and then washed in ethanol and phosphate-buffered saline. We digested a total of 60–115 mg of muscle tissue by using pepsin/HCl solution for 30 min–1 hr at 45°C (*4*). Larvae were then collected, counted, and identified on the basis of morphologic characteristics (*19*).

Molecular Identification of Larvae

Molecular identification of larvae was also performed in the National Reference Laboratory for Human Trichinellosis. DNA was extracted from 30 mg of the deparaffinated samples by using the tissue QIA Amp DNA Mini Kit (QIAGEN, https://www.qiagen.com) and from larvae by using the NucliSens easyMAG Kit (bioMérieux, https://www.biomerieux.com) according to manufacturer's instruction. Pretreatment with proteinase K (>600 mAU/mL) was performed overnight at 56°C with shaking at 1,200 vibrations/min, and DNA was eluted in 100 μL of distilled water. DNA was also extracted from a *T. nativa* larval suspension and used as a positive control. A total of 200 μL of sterile water was used as a negative control.

Conventional PCR for *Trichinella* rDNA Intergenic Spacer Region

Primers and the protocol used to amplify the 5S rDNA intergenic spacer region of *Trichinella* were described (*20*). In brief, we used 0.5 μmol/L of each primer in a 50-μL reaction containing 1.5 mmol/L $MgCl_2$, 200 μM of each dNTP, 1.5 U of AmpliTaq Gold (Applied Biosystems, https://www.thermofisher.com) and 5 μL of extracted DNA. Reactions were run in a Perkin-Elmer Thermocycler (https://www.perkinelmer.com) under the following conditions: 95°C for 5 min for 1 cycle; 95°C for 30 s, 55°C for 30 s and 72°C for 40 s for 42 cycles; followed by a 15-min final extension step at 72°C. The PCR products were separated by 1% agarose gel electrophoresis at 90 mA and stained with ethidium bromide.

Multiplex PCR for *Trichinella* spp.

We used 5 primer pairs in a multiplex PCR as described (*21*,*22*): primer set I, expansion segment V (ESV) target locus; primer set II, internal transcribed

spacer region 1 (ITS1) target locus; primer set III, ITS1 target locus; primer set IV, ITS2 target locus; and primer set V, ITS2 target locus. Reactions were performed in 25 μL of 2XGOTaq HotStartGreen MasterMix (Promega, https://www.promega.com), 6.3 μL of nuclease-free water, 1.7 μL of total primers, and 17 μL of extracted DNA. We performed the PCR cycle as follows: a predenaturation and polymerase activation step at 95°C for 2 min, then 35 amplification cycles (denaturation at 95°C for 10 s, hybridization at 55°C for 30 s, and elongation at 72°C for 30 s), and a final elongation step at 72°C for 5 min. PCR products were isolated separated by using 2% agarose gel electrophoresis.

We sequenced PCR products by using appropriate primers (Eurofins-MWG, https://www.eurofins.fr) and aligned them by using BioEdit version 7.0.9 (https://www.biodeit.software.informer.com). We also performed a BLASTn (https://blast.ncbi.nlm.nih.gov) search. Sequences obtained in this study were deposited in GenBank, and accession numbers are listed in the Results.

Results

Course of the Outbreak

After consumption of raw meat from a wild pig during July–August 2017, a total of 33 persons (rangers, workers from the Ministry of Environment, and villagers) became infected by the nematode. The number and precise date of meal(s) were unknown. Eight persons died according to Khmer official sources (*23*) and others (*24*). On August 1, the first case-patient was hospitalized at Kampong Thom Provincial Hospital because of severe clinical signs and symptoms of trichinellosis (abdominal pain; fever; myalgia; swelling of the face, arms, and legs; joint pain; headache; and pruritus).

The Ministry of Health immediately sent a Rapid Response Team of the Department of Communicable Disease Control to the area and conducted a retrospective epidemiologic survey (results are not available) and a risk assessment (resulting in a moderate level of risk) (*23*). Nine patients were admitted to Kampong Thom Provincial Hospital, and 8 patients were transferred to Calmette Hospital. Seventeen other patients were admitted directly to Calmette Hospital (5) or Preah Ket Mealea Hospital (12).

Little information was available for the 8 persons who died: 6 had refused to be transferred to Phnom Penh and were given mainly traditional medicine, 1 died during transport from Kampong Thom to Phnom Penh, and 1 died in Calmette hospital. Several information sessions were held in Kampong Thom Province to warn the population and provide advice on sanitation. Furthermore, a workshop was also organized that involved national authorities and the World Health Organization in December 2017. Complete medical records of the 25 patients hospitalized in Phnom Penh hospitals were collected and analyzed.

Epidemiologic, Laboratory, and Clinical Features

We provide epidemiologic, laboratory, and clinical features for the 25 available case-patients (Table). The first patient hospitalized in Kampong Thom Provincial Hospital arrived on August 1, and most (25/33) patients were referred to Phnom Penh during September 6–October 17. The average age of the patients was 34.5 years (range 20–50 years), and the male:female ratio was 24:1.

According to the case definition criteria (*17*), a total of 23 cases could be classified as confirmed because of myalgia (or fever, edema, or diarrhea), eosinophilia (or increased level of muscle enzymes), positive serologic results, or muscle biopsy reports. Patient 15 was classified as having a suspected case because only myalgia, fever, and diarrhea were observed. Patient 16 was classified as having a highly probable case because he had myalgia, fever, edema, diarrhea, eosinophilia, and increased levels of muscle enzymes (creatine phosphokinase [CPK] and aspartate aminotransferase [AST]).

Every patient hospitalized in Phnom Penh reported muscle pain and swelling (25/25; 100%), followed by asthenia (18/25; 72%); fever (17/25; 68%), facial or periorbital edema (13/25; 52%); abdominal pain, diarrhea, and nausea (9/25; 36%); headache (8/25; 32%); dyspnea (7/25; 28%); and cough (3/25; 12%). All 25 patients had a history of consumption of wild pig meat. A total of 96% (24/25) of patients had leukocytosis (range 4–23 × 10^9 cells/L) and eosinophilia (range 1–10 × 10^9 cells/L). Patient 5 had no leukocytosis but did have eosinophilia.

Enzyme levels indicative of muscle damage were also increased in 96% (24/25) of the patients: CPK (range 110–1,499 U/L) and AST (range 30–310 U/L). CRP (range 6.3–310.3 mg/L) was increased for 68% (17/25) of the patients. Furthermore, levels of lactate dehydrogenase (range 137–2,300 U/L) was also increased for 62% (16/25) of the patients. All 13 biopsies performed in Calmette Hospital were positive for *Trichinella* larvae, and 91% (10/11) of serologic test results for patients at Preah Ket Mealea Hospital were positive for *Trichinella* IgG and IgM. In both hospitals in Phnom Penh, patients were hospitalized

Table. Characteristics for 25 patients during a human outbreak of trichinellosis caused by *Trichinella papuae* nematodes, Cambodia*

Pt no.	Age, y/sex	Clinical signs or symptoms	Length of hospital stay, d	Leu†	Eos†	Neu†	CPK†	LDH†	AST†	Biopsy result	IgM/IgG	PCR/PCR/ Seq‡
1	26/M	Mu, As, Oe, Dy	12	23	3	21	1,210	433	97	+	ND	–/+/ND
2	31/M	Mu, Fe, Hd, Oe, Dy	9	23	4	18	1,216	577	310	+	ND	–/+/ND
3	20/M	Mu, Fe, Cg, Dy	19	28	2	23	784	1,890	89	+	ND	+/+/+
4	34/M	Mu, As, Oe, Dy	14	21	2	19	1,499	469	59	+	ND	+/+/+
5	25/M	Mu, As	4	9	2	4	809	589	74	+	ND	+/+/+
6	26/M	Mu, Fe, Oe	14	20	2	19	340	584	51	+	ND	+/+/+
7	35/M	Mu, Hd, Gi, As, Oe	10	29	3	22	1,265	2,300	104	+	ND	–/–/ND
8	43/M	Mu, Fe, As, Oe	12	15	3	12	1,007	1,940	70	+	ND	–/+/ND
9	50/M	Mu, Oe	7	13	1	10	1,263	830	87	+	ND	–/+/ND
10	27/M	Mu, As, Oe	13	13	3	10	862	592	86	+	ND	–/+/ND
11	35//M	Mu, As, Oe	13	23	3	19	1,367	2,030	115	+	ND	-/+/ND
12	40/M	Mu, Fe, As, Oe, Cg, Dy	15	18	2	16	1,091	536	127	+	ND	–/+/ND
13	28/F	Mu, Fe, Gi, As, Oe, Dy, Cg	18	36	2	35	827	2,540	117	+	ND	–/+/+
14	46/M	Mu, Fe, Gi	17	22	3	20	1,521	248	100	ND	–/+	ND
15	22/M	Mu, Fe, Hd, As, Gi, Cg	8	16	1	11	110	137	30	ND	–/–	ND
16	40/M	Mu, Fe, Gi, As, Oe	18	18	10	12	1340	342	73	ND	ND	ND
17	42/M	Mu, Fe, Gi, As	16	25	5	20	260	162	44	ND	–/+	ND
18	36/M	Mu, Fe, Hd, As, Dy	16	17	2	12	899	ND	281	ND	–/+	ND
19	42/M	Mu, Fe, As	16	24	2	17	796	ND	161	ND	+/+	ND
20	26/M	Mu, Fe, As	16	21	8	17	340	ND	70	ND	+/+	ND
21	26/M	Mu, Hd, As Oe	25	18	1	16	1,073	291	94	ND	+/+	ND
22	34/M	Mu, Fe, As, Dy	25	21	4	20	622	303	89	ND	+/+	ND
23	41/M	Mu, Fe, Hd, Gi, As	15	16	1	13	866	246	170	ND	+/+	ND
24	42/M	Mu, Fe, Hd, Gi, As, Dy	15	18	1	15	524	ND	113	ND	–/+	ND
25	45/M	Mu, Fe, Hd, Gi	7	11	2	15	320	ND	154	ND	–/+	ND

*As, asthenia; AST, aspartate aminotransferase (reference range <37 U/L); Cg, cough; CPK, creatine phosphokinase (reference range 15–130 U/L); Dy, dyspnea; Eos, eosinophils (reference range 0.2–0.7 × 10^9 cells/L); Fe, fever; Gi, abdominal pain, diarrhea, and nausea; Hd, headache; Leu, leukocytes (reference range 4–9 × 10^9 cells/L); LDH, lactate dehydrogenase (reference range 225–450 U/L); Mu, muscle pain and swelling; ND, not determined; Neu, neutrophils; Oe, facial or periorbital edema; Pt, patient; Seq, sequencing; –, negative; +, positive.
†Values are the highest readings obtained during hospitalization.
‡Positive conventional PCR for *Trichinella* rDNA intergenic spacer region/multiplex PCR for *Trichinella* spp./sequencing.

for an average for 14 days (range 4–26 days). Hepatosplenomegaly was observed during abdominal ultrasound examination for 47% (9/19) of the patients. Chest radiography, electrocardiography, and echocardiography for all patients showed typical results. Patient 2 died from multiorgan failure (probably caused by septicemia), despite intensive care.

Identification and Confirmation of Larvae

Transverse sections of nonencapsulated larvae morphologically consistent with *Trichinella* sp. stage L1 larvae were identified by histopathologic analysis (Figure 1, panels A and B). A diffuse infiltration of larvae was visible in all slides, accompanied by abnormally clear cytoplasm, vacuolization, and disorganization of myofibrils or total necrosis of striated muscle. The interstitial connective tissue was edematous and had few inflammatory cells. There were no encysted larvae with a hyaline wall of a cyst or organized fibrosis. After digestion of the remaining biopsy sample with pepsin/HCl, *Trichinella* sp. larvae were found in 92% (12/13) of the patients. The mean ± SD number of larva in the 60-mg tissue sample was 17 ± 13 (minimum 4 and maximum 41). We also observed a nonencapsulated larvae of a *Trichinella* sp. after the pepsin/HCl digestion (Figure 1, panel C).

The 5S rDNA intergenic spacer region of *Trichinella* was amplified from 4/13 muscle biopsy specimens (for patients 3, 4, 5, and 6; GenBank accession numbers MN158145–8). The sequences alignment showed 10 positions of single-nucleotide polymorphisms on 794 nt between the isolates. The BLASTn matched with the highest percentage of identity (range 97.8%–98.0%) and the lowest E value (0.0) with the sequence of *T. papuae* nematodes (GenBank accession no. AY845861.1). Similarly, the multiplex PCR showed (Figure 2) a typical pattern for *T. papuae* nematodes (240-bp band) for 12/13 samples.

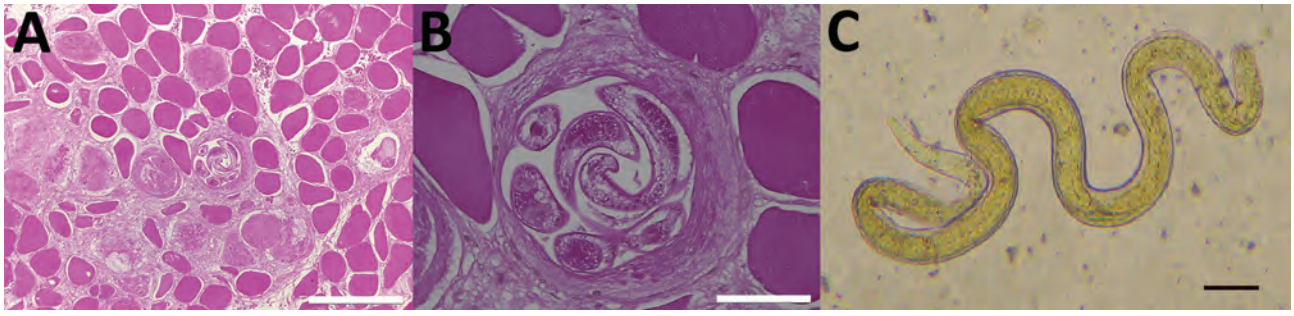

Figure 1. *Trichinella* larvae samples from patients in Cambodia. A) Transverse section of a muscle (bicep) biopsy specimen from patient 13 showing a nonencapsulated *T. papuae* stage 1 nematode larva in the center of the specimen (hematoxylin phloxine saffron stain; scale bar = 200 μm). B) Higher magnification view of the same biopsy specimen showing the coelomyarian muscle structure and stichosome of *Trichinella* larvae (scale bar = 50 μm). C) *T. papuae* stage 1 nematode larva after deparaffinization and artificial digestion of muscle biopsy specimen (scale bar = 50 μm).

The amplified ESV gene was sequenced (for patients 4, 6, and 13; GenBank accession nos. MN158365–7). Alignment showed 1 nt change over 238 nt between the isolates. The BLASTn matched with the highest percentage of identity (range 98.3%–100%) and the lowest E value (range 4.10×10^{-114} to 1.10×10^{-118}) for *T. papuae* nematodes from crocodiles in Papua New Guinea (GenBank accession nos. FJ493493.1 and FJ493494.1).

The ESV gene could not be amplified in 1 sample (patient 7). In addition, no larvae were observed in this sample after digestion with pepsin/HCl.

Treatment and Clinical Follow-up

All patients were given albendazole (800 mg or 15 mg/kg/d for a minimum of 10 days) and glucocorticosteroid (prednisolone) (60 mg or 1 mg/kg/d for 5 days). Supportive treatments such as painkillers for myalgia or intravenous fluid and electrolytes against hypovolemia and metabolic disorders were also administered. To our knowledge, 24 patients recovered, but it was not possible to obtain additional information from them.

Discussion

We report an outbreak of *T. papuae* nematode infection in Cambodia and provide epidemiologic, molecular, laboratory, and clinical data. The most probable mode of infection was consumption of wild pig meat, although the possibility of some infections being caused by consumption of reptile meat (e.g., Siamese crocodiles [*Crocodylus siamensis*] and lizards) present in the Prey Lang Forest, cannot be completely rule out (*14*). Several human outbreaks of trichinellosis (caused by nonencapsulated *Trichinella* species) through consumption of raw soft-shelled turtle (*Pelodiscus sinensis*) meat in South Korea (*25*) and Taiwan (*26*) have been described. *T. papuae* nematodes might have been the causative species in these infections because it is often found in reptile meat.

The central location of Kampong Thom Province in Cambodia (far from regions in Thailand that had previously described outbreaks) and the fact that a wild pig was the source of infection could indicate that Kampong Thom Province is a region to which *T. papuae* nematodes are endemic. Comparing the only 2 ESV sequences deposited in GenBank from *T. papuae* nematodes in Papua New Guinea (*27*) and those from this study showed an identity of 100%. Comparing of the only 5S rDNA intergenic spacer region sequence from *T. papuae* nematodes (GenBank accession no. AY845861.1) and those from this study showed an identity of ≈98%. A higher intraspecies variation was observed between the *T. papuae* sequences from Cambodia by using 5S rDNA intergenic spacer region analysis.

It is likely that outbreaks characterized by a low number of ingested larvae, few patients, or mild clinical signs and symptoms are not correctly diagnosed and consequently, public health services are not informed. This situation was also described in Papua New Guinea (*28*), Laos (*11*), and Vietnam (*12*). Therefore, trichinellosis is probably underdiagnosed, and the high number of deaths in this outbreak alerted authorities. Because no previous trichinellosis cases were recorded, we can hypothesize that sporadic cases are the rule.

The average yearly incidence of trichinellosis in humans worldwide is probably ≈10,000 cases, and the mortality rate is ≈0.2% (*29*). Complications can be life-threatening and affect mainly the elderly. Their frequency is variable and dependent on the epidemics; it can sometimes involve ≤30% of cases with neurologic complications and 5%–20% for cardiac and vascular complications. During this outbreak, the mortality rate was high (24%, 8/33). In comparison,

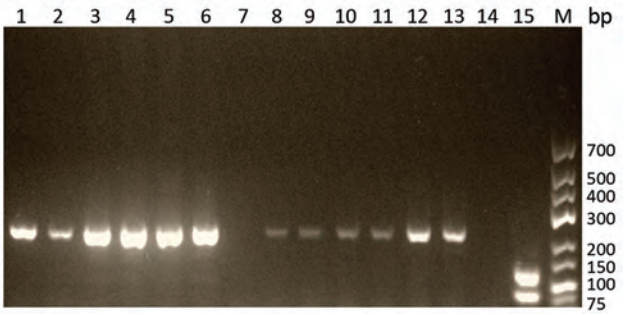

Figure 2. Gel electrophoresis (2% agarose) of products of *Trichinella* multiplex PCR using samples from patients in Cambodia. Lanes 1–6, patients 1–6: samples were extracted from muscle tissue and show the 240-bp band typical for *Trichinella papuae* nematodes. Lane 7, patient 7: sample was extracted from muscle tissue and showed no band. Lanes 8–13, patients 8–13: samples were extracted from larvae and show the 240-bp band typical for *T. papuae* nematodes. Lane 14, negative control; lane 15, positive control (*T. nativa* showing the expected 127-bp band); lane M, molecular mass ladder.

the observed mortality rate during the epidemic in France during 1985 was 5 deaths/1,000 persons (*30*). However, *T. spiralis* nematodes, not *T. papuae*, nematodes, were presumed to be the causative agent. Furthermore, to our knowledge, deaths caused by *T. papuae* nematodes have not been reported.

The quantity of ingested larvae (*2*), the quantity of alcohol (*31*,*32*) consumed during a meal, the nature of the host, and the species of *Trichinella* (*33*) are some of the parameters linked to virulence. However, the quantity of meat consumed (positively correlated with virulence) and the quantity of alcohol consumed (negatively correlated with virulence) was not known for our case-patients. Furthermore, little information was available for the patients who died. Infection with *Trichinella* species was not medically proven for 7 of the officially recorded fatal cases and this factor confounded accurate interpretation of the epidemiology of this outbreak. A high number of ingested larvae, a late diagnosis in the first hospital, or the choice of some patients to use traditional medicine instead of modern medicine could be a reason for this unusual high mortality rate. Moreover, access to medical care in Cambodia is limited and it was recently pointed out that the national healthcare system at the same time enables, encourages, and sanctions unregulated medical practice (*34*). In the case of fatal trichinellosis, cardiac or neural complications occurring in the first 2 weeks of infection are most common (*19*). Complications can be avoided by the early combined use of albendazole and prednisolone (*35*). These drugs were given to the 25 documented case-patients, even to the patient who eventually died.

Cultural factors, such as consumption of traditional dishes that contain raw or undercooked meat, play a major role in the transmission of *Trichinella* nematodes to humans. Because patients were referred to hospitals in Phnom Penh for a long period (78 days) after the first case, we can hypothesize that several contaminated meals could have been taken from the same meat source prepared in different ways (sun-dried meat is commonly eaten in Cambodia). However, samples from the meals were not available for examination. In Cambodia, common popular beliefs associated a strength transfer for man eating raw wild pig meat, but this type of food is widely rejected by woman because of its pronounced taste (M. Sim, Institut Pasteur, Phnom Penh, Cambodia, pers. comm., 2017 Dec 1) and can probably explain the observed unbalanced sex ratio. Other parasites, such as *Sarcocystis* spp. (*36*) or *Taenia* spp. (*37*), which are also transmitted by consumption of raw meat, are also endemic in Cambodia.

On the basis of clinical signs and symptoms, all patients arrived in Phnom Penh during the acute phase of trichinellosis because 100% had myalgia and swelling, 72% had asthenia, and 68% had fever. Furthermore 96% had moderate eosinophilia, and increased levels of muscle enzymes (AST, CPK, and lactate dehydrogenase) (*19*). Patients 15 and 16 could not be classified as having confirmed trichinellosis because of the absence of biopsy and serologic results. Nevertheless, albendazole-based treatment cured the patients. None of these patients had any complications. We hypothesize that most deaths occurred because of complications. The medical record of patient 2 showed that he underwent surgery (appendectomy) 2 weeks before his death (on September 21). It is likely that the course of the *Trichinella* infection and the surgery played a major role in fatal multiorgan failure. Moreover, the appendicitis symptoms could also have been related to trichinellosis.

ELISA is the recommended diagnostic technique for trichinellosis and is best used in combination with confirmatory immunoblotting (Western blot) (*19*). In this outbreak, ELISA was only performed for 44% (11/25) of the patients. Only 1 of these patients had a negative serologic result. Delayed seroconversion until 60 days postinfection has been described (*38*). The result of a second serology test would have been useful, but it was not possible to obtain a new blood sample from the patient. IgG and IgM can persist up to 1 year and occasionally even longer (11 years and 19 years have been reported) (*39*). Although a specific excretory/secretory antigen ELISA was used, we cannot eliminate the possibility of false-positive

results caused by cross-reactions with other endemic parasites (i.e., *Toxocara* spp., *Strongyloides stercoralis*, or *Toxoplasma* spp.) (*40*). Nevertheless, when considered in the context of consumption of raw wild pig meat, clinical symptoms and positive results for biopsies and molecular biology assays leave little doubt regarding the accuracy of serologic results.

Further investigations are needed to answer the questions raised by this outbreak and to identify the life cycle of *T. papuae* nematodes in Cambodia. It could be useful to determine the serologic status of inhabitants in the area of the outbreak and the prevalence of *Trichinella* infection in wild pigs and reptiles found in the nearby forest. The sylvatic and domestic life cycles of the parasite are probably linked, and it could be useful to investigate the spectrum of domestic hosts to avoid further outbreaks.

In Cambodia, a *Trichinella* species is now accurately identified as causing an outbreak. This finding should encourage authorities and involved sectors to implement measures to limit the effect of this major zoonotic parasite and its spreading to (domestic) pigs herds. Consumption of raw meat (particularly wild pig) must be avoided. Furthermore, this outbreak highlights that the *T. papuae* nematode should be reevaluated as a potential virulent species for humans.

Acknowledgment

We thank Cédric Rondot for providing technical support.

This study was supported by Institut Pasteur in Cambodia.

About the Author

Dr. Caron is a postdoctoral research scientist at the Institut Pasteur, Phnom Penh, Cambodia. His primary research interest is veterinary parasitology, particularly zoonoses.

References

1. Dupouy-Camet J. Trichinellosis: a worldwide zoonosis. Vet Parasitol. 2000;93:191–200. https://doi.org/10.1016/S0304-4017(00)00341-1
2. Gottstein B, Pozio E, Nöckler K. Epidemiology, diagnosis, treatment, and control of trichinellosis. Clin Microbiol Rev. 2009;22:127–45. https://doi.org/10.1128/CMR.00026-08
3. European Food Safety Authority. The community summary report on trends and sources of zoonoses, zoonotic agents, antimicrobial resistance and foodborne outbreaks in the European Union in 2006. European Food Safety Authority Journal. 2006;94:167–74.
4. The European Commission. Commission Implementing Regulation (EU) 2015/1375 of 10 August 2015 laying down specific rules on official controls for *Trichinella* in meat (text with EEA relevance); 2015 [cited 2019 May 10]. https://eur-lex.europa.eu/legal-content/EN/TXT/?uri=CELEX%3A32015R1375
5. Pyburn DG, Gamble HR, Wagstrom EA, Anderson LA, Miller LE. Trichinae certification in the United States pork industry. Vet Parasitol. 2005;132:179–83. https://doi.org/10.1016/j.vetpar.2005.05.051
6. Krivokapich SJ, Pozio E, Gatti GM, Prous CLG, Ribicich M, Marucci G, et al. *Trichinella patagoniensis* n. sp. (Nematoda), a new encapsulated species infecting carnivorous mammals in South America. Int J Parasitol. 2012;42:903–10. https://doi.org/10.1016/j.ijpara.2012.07.009
7. Sharma R, Thompson PC, Hoberg EP, Brad Scandrett W, Konecsni K, Harms NJ, et al. Hiding in plain sight: discovery and phylogeography of a cryptic species of Trichinella (Nematoda: Trichinellidae) in wolverine (*Gulo gulo*). Int J Parasitol. 2020;50:277–87. https://doi.org/10.1016/j.ijpara.2020.01.003
8. Bai X, Hu X, Liu X, Tang B, Liu M. Current research of trichinellosis in China. Front Microbiol. 2017;8:1472. https://doi.org/10.3389/fmicb.2017.01472
9. Pozio E. Taxonomy of *Trichinella* and the epidemiology of infection in the Southeast Asia and Australian regions. Southeast Asian J Trop Med Public Health. 2001;32 (Suppl 2):129–32.
10. Stehr-Green JK, Schantz PM. Trichinosis in Southeast Asian refugees in the United States. Am J Public Health. 1986;76:1238–9. https://doi.org/10.2105/AJPH.76.10.1238
11. Van D N, Thi Nga V, Dorny P, Vu Thrung N, Ngoc Minh P, Trung Dung BD, et al. Trichinellosis in Vietnam. Am J Trop Med Hyg. 2015;92:1265–7.
12. Barennes H, Sayasone S, Odermatt P, De Bruyne A, Hongsakhone S, Newton PN, et al. A major trichinellosis outbreak suggesting a high endemicity of *Trichinella* infection in northern Laos. Am J Trop Med Hyg. 2008;78:40–4. https://doi.org/10.4269/ajtmh.2008.78.40
13. Kusolsuk T, Kamonrattanakun S, Wesanonthawech A, Dekumyoy P, Thaenkham U, Yoonuan T, et al. The second outbreak of trichinellosis caused by *Trichinella papuae* in Thailand. Trans R Soc Trop Med Hyg. 2010;104:433–7. https://doi.org/10.1016/j.trstmh.2009.12.005
14. Khumjui C, Choomkasien P, Dekumyoy P, Kusolsuk T, Kongkaew W, Chalamaat M, et al. Outbreak of trichinellosis caused by *Trichinella papuae*, Thailand, 2006. Emerg Infect Dis. 2008;14:1913–5. https://doi.org/10.3201/eid1412.080800
15. Pozio E, Owen IL, La Rosa G, Sacchi L, Rossi P, Corona S. *Trichinella papuae* n.sp. (Nematoda), a new non-encapsulated species from domestic and sylvatic swine of Papua New Guinea. Int J Parasitol. 1999;29:1825–39. https://doi.org/10.1016/S0020-7519(99)00135-6
16. Pozio E. The broad spectrum of *Trichinella* hosts: from cold- to warm-blooded animals. Vet Parasitol. 2005;132:3–11. https://doi.org/10.1016/j.vetpar.2005.05.024
17. Pozio E, Zarlenga DS. New pieces of the *Trichinella* puzzle. Int J Parasitol. 2013;43:983–97. https://doi.org/10.1016/j.ijpara.2013.05.010
18. Intapan PM, Chotmongkol V, Tantrawatpan C, Sanpool O, Morakote N, Maleewong W. Molecular identification of *Trichinella papuae* from a Thai patient with imported trichinellosis. Am J Trop Med Hyg. 2011;84:994–7. https://doi.org/10.4269/ajtmh.2011.10-0675
19. Dupouy-Camet J, Murrell KD. FAO/WHO/OIE Guidelines for the surveillance, management, prevention and control of trichinellosis. Dupouy-Camet J, Murrell KD, editors. Paris: Food and Agriculture Organization of the United Nations, World Health Organization, World Organisation for Animal Health; 2007 [cited 2020 May 20]. http://www.trichinellosis.org/uploads/FAO-WHO-OIE_Guidelines.pdf

20. De Bruyne A, Yera H, Le Guerhier F, Boireau P, Dupouy-Camet J. Simple species identification of *Trichinella* isolates by amplification and sequencing of the 5S ribosomal DNA intergenic spacer region. Vet Parasitol. 2005;132:57–61. https://doi.org/10.1016/j.vetpar.2005.05.026
21. Zarlenga DS, Chute MB, Martin A, Kapel CM. A multiplex PCR for unequivocal differentiation of all encapsulated and non-encapsulated genotypes of *Trichinella.* Int J Parasitol. 1999; 29:1859–67. https://doi.org/10.1016/S0020-7519 (99)00107-1
22. Pozio E, La Rosa G. PCR-derived methods for the identification of *Trichinella* parasites from animal and human samples. Methods Mol Biol. 2003;216:299–309.
23. Ministry of Health. Cambodia. Cases of trichinellosis in Kampong Thom Province; 2017 [cited 2020 May 20]. http://www.cdcmoh.gov.kh/298-2017-09-26-02-39-19
24. Bo X. Cambodia confirms outbreak of trichinellosis in central Kampong Thom Province. Xinhua; September 26, 2017 [cited 2020 May 20]. http://www.xinhuanet.com/english/2017-09/26/c_136639855.htm
25. Jeong JT, Seo M, Hong S-T, Kim YK. An outbreak of trichinellosis by consumption of raw soft-shelled turtle meat in Korea. Korean J Parasitol. 2015;53:219–22. https://doi.org/10.3347/kjp.2015.53.2.219
26. Lo YC, Hung CC, Lai CS, Wu Z, Nagano I, Maeda T, et al. Human trichinosis after consumption of soft-shelled turtles, Taiwan. Emerg Infect Dis. 2009;15:2056–8. https://doi.org/10.3201/eid1512.090619
27. Pozio E, Owen IL, Marucci G, La Rosa G. Inappropriate feeding practice favors the transmission of *Trichinella papuae* from wild pigs to saltwater crocodiles in Papua New Guinea. Vet Parasitol. 2005;127:245–51. https://doi.org/10.1016/j.vetpar.2004.09.029
28. Owen IL, Gomez Morales MA, Pezzotti P, Pozio E. *Trichinella* infection in a hunting population of Papua New Guinea suggests an ancient relationship between *Trichinella* and human beings. Trans R Soc Trop Med Hyg. 2005;99:618–24. https://doi.org/10.1016/j.trstmh.2005.03.005
29. Pozio E. World distribution of *Trichinella* spp. infections in animals and humans. Vet Parasitol. 2007;149:3–21. https://doi.org/10.1016/j.vetpar.2007.07.002
30. Dupouy-Camet J, Talabani H, Ancelle T. Trichinellosis [in French]. Rev Prat. 2010;60:159–64.
31. Steven WM, Kumar SN, Stewart GL, Seelig LL Jr. The effects of ethanol consumption on the expression of immunity to *Trichinella spiralis* in rats. Alcohol Clin Exp Res. 1990; 14:87–91. https://doi.org/10.1111/j.1530-0277.1990.tb00452.x
32. Na HR, Zhu X, Stewart GL, Seelig LL Jr. Ethanol consumption suppresses cell-mediated inflammatory responses and increases T-helper type 2 cytokine secretion in *Trichinella spiralis*–infected rats. Alcohol Clin Exp Res. 1997;21:1179–85. https://doi.org/10.1111/j.1530-0277.1997.tb04435.x
33. Sadaow L, Intapan PM, Boonmars T, Morakote N, Maleewong W. Susceptibility of laboratory rodents to *Trichinella papuae*. Korean J Parasitol. 2013;51:629–32. https://doi.org/10.3347/kjp.2013.51.6.629
34. Gryseels C, Kuijpers LM, Jacobs J, Grietens KP. When "substandard" is the standard, who decides what is appropriate? Exploring healthcare provision in Cambodia. Critical Public Health. 2019;29:460–72. https://doi.org/10.1080/09581596.2019.1591614
35. Pozio E, Gomez Morales MA, Dupouy-Camet J. Clinical aspects, diagnosis and treatment of trichinellosis. Expert Rev Anti Infect Ther. 2003;1:471–82. https://doi.org/10.1586/14787210.1.3.471
36. Khieu V, Marti H, Chhay S, Char MC, Muth S, Odermatt P. First report of human intestinal sarcocystosis in Cambodia. Parasitol Int. 2017;66:560–2. https://doi.org/10.1016/j.parint.2017.04.010
37. Adenuga A, Mateus A, Ty C, Borin K, Holl D, San S, et al. Seroprevalence and awareness of porcine cysticercosis across different pig production systems in south-central Cambodia. Parasite Epidemiol Control. 2017;3:1–12. https://doi.org/10.1016/j.parepi.2017.10.003
38. Owen IL. Parasitic zoonoses in Papua New Guinea. J Helminthol. 2005;79:1–14. https://doi.org/10.1079/JOH2004266
39. Harms G, Binz P, Feldmeier H, Zwingenberger K, Schleehauf D, Dewes W, et al. Trichinosis: a prospective controlled study of patients ten years after acute infection. Clin Infect Dis. 1993;17:637–43. https://doi.org/10.1093/clinids/17.4.637
40. Gómez-Morales MA, Ludovisi A, Amati M, Cherchi S, Pezzotti P, Pozio E. Validation of an enzyme-linked immunosorbent assay for diagnosis of human trichinellosis. Clin Vaccine Immunol. 2008;15:1723–9. https://doi.org/10.1128/CVI.00257-08

Address for correspondence: Yannick Caron, Institut Pasteur, Phnom Penh, Cambodia; email: ycaron9@gmail.com or yannick.caron@qualyse.fr

Increased Sensitivity of *Plasmodium falciparum* to Artesunate/Amodiaquine Despite 14 Years as First-Line Malaria Treatment, Zanzibar

Mwinyi Msellem, Ulrika Morris, Aungpaing Soe, Faiza B. Abbas, Abdul-Wahid Ali, Rory Barnes, Paolo Frumento, Abdullah S. Ali, Andreas Mårtensson, Anders Björkman

Artemisinin-based combination therapies (ACTs) are first-line treatments for uncomplicated *Plasmodium falciparum* malaria. ACT resistance is spreading in Asia but not yet in Africa. Reduced effects of ACT partner drugs have been reported but with little information regarding widely used artesunate/amodiaquine (ASAQ). We studied its efficacy in Zanzibar after 14 years as first-line treatment directly by an in vivo, single-armed trial and indirectly by prevalences of different genotypes in the *P. falciparum* chloroquine-resistance transporter, multidrug-resistance 1, and Kelch 13 propeller domain genes. In vivo efficacy was higher during 2017 (100%; 95% CI 97.4%–100%) than during 2002–2005 (94.7%; 95% CI 91.9%–96.7%) (p = 0.003). Molecular findings showed no artemisinin resistance–associated genotypes and major increases in genotypes associated with high sensitivity/efficacy for amodiaquine than before ASAQ was introduced. Thus, the efficacy of ASAQ is maintained and appears to be increased after long-term use in contrast to what is observed for other ACTs used in Africa.

Artemisinin-based combination therapy (ACT) has been first-line treatment for uncomplicated *Plasmodium falciparum* malaria globally for the past 10–15 years and has contributed greatly to a reduction of malaria illnesses and deaths during 2005–2015 (*1*,*2*). However, artemisinin resistance emerged in Cambodia during 2008, where it then spread and even developed de novo throughout the Great Mekong Region (*3*,*4*). Possible resistance has been reported from eastern India (*5*) and, Guyana in South America (*6*) but not yet from Africa (*4*). However, ACT resistance represents a continuous threat in contexts such as Zanzibar, where numerous long-distance visitors represent a special risk for imported artemisinin-resistant malaria parasites. Chloroquine resistance entered eastern Africa most probably from India in late 1970s (*7*). In addition, selection of resistance/tolerance to the slowly eliminated long-acting partner drugs in ACT (e.g., amodiaquine) is expected, especially in highly malaria-endemic areas of Africa (*8*–*10*), which could result in relatively reduced ACT cure rates and reduced protection against artemisinin resistance (*11*). Currently, however, complete ACT resistance has developed and spread only in Asia (e.g., Cambodia) (*12*).

In Zanzibar, malaria transmission has been reduced substantially after new and reinforced malaria tools and interventions, including ACT for uncomplicated malaria (*2*), were implemented. The reduced parasite biomass on the islands of Zanzibar has resulted in an expected selection (bottleneck) of the parasite populations (*2*,*13*), which under strong drug exposure might select for drug resistance. The first-line ACT in Zanzibar has been artesunate/amodiaquine (ASAQ) since 2003, plus recently added single, low-dose primaquine. Artemether/lumefantrine was used as second-line treatment when ACT was first used, followed by quinine when treatment guidelines were revised in 2009 (*2*). Free access throughout the health systems has resulted in sustained high population coverage and compliance to ASAQ (*2*,*14*,*15*). The partner drug amodiaquine is relatively short-lived (half-life 2–8 hours) and is primarily metabolized to

Author affiliations: Mnazi Mmoja Hospital, Zanzibar, Tanzania (M. Msellem); Karolinska Institutet, Stockholm, Sweden (U. Morris, A. Soe, R. Barnes, P. Frumento, A. Bjorkman); Zanzibar Malaria Elimination Programme, Zanzibar, Tanzania (F.B. Abbas, A.-W. Ali, A.S. Ali); Uppsala University, Uppsala, Sweden (A. Mårtensson)

DOI: https://doi.org/10.3201/eid2608.191547

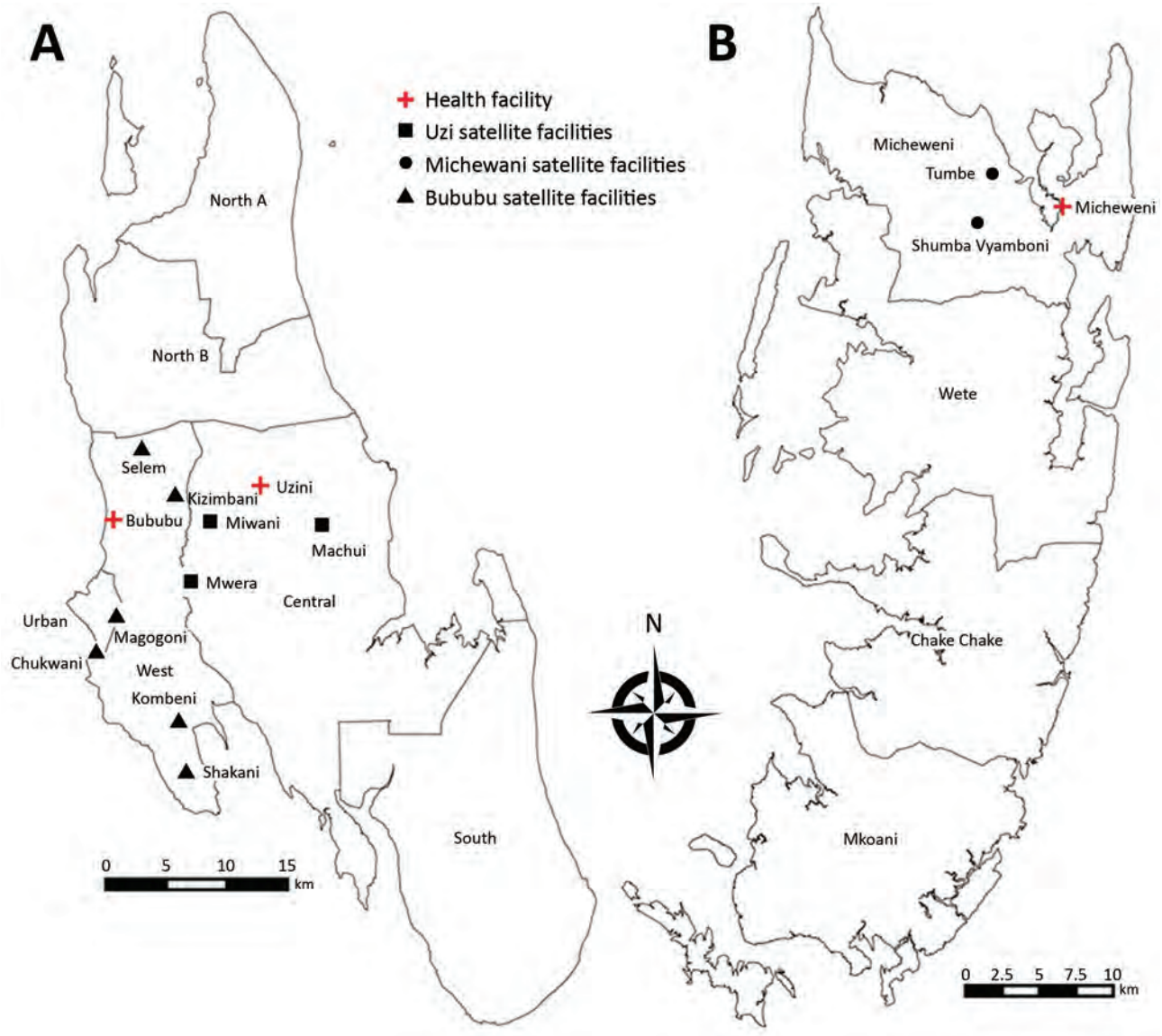

Figure 1. Locations of 14 study health centers, including 11 peripheral satellite health units and 3 referral health facilities for which increased sensitivity of *Plasmodium falciparum* to artesunate/amodiaquine despite 14 years as first-line malaria treatment was tested, Zanzibar. A) Unguja Island; B) Pemba Island.

its main biologically active metabolite desethyl-amodiaquine, which has a longer terminal elimination half-life (>7 days) (*16*).

Efficacy verses resistance to ACTs is primarily assessed by the in vivo response to standard treatment in which early clearance determines the effect of the artemisinin component, and the cure rate by days 28 or 42 after treatment determines the effect of the combination, especially that of the partner drug (*17*). Tolerance/resistance to the ACT components can also be estimated separately by genetic determination of different drug-resistance associated polymorphisms. A few longitudinal studies in Africa have examined tolerance/resistance trends to ACTs, especially to artemether/lumefantrine, suggesting largely maintained treatment efficacy but also higher prevalences of genotypes associated with tolerance to lumefantrine (*18*,*19*). However, there is a lack of combining longitudinal in vivo cure rates and molecular findings, particularly in relation to ASAQ, the second most widely used ACT in Africa.

In Zanzibar, 2 previous clinical trials in 2002–2003 (*20*) and 2005 (A. Bjorkman, unpub. data) showed high efficacy of ASAQ. A study of gene polymorphisms did not show any early trends of drug

Table 1. Characteristics of patients in 3 clinical trials testing increased sensitivity of *Plasmodium falciparum* to artesunate/amodiaquine despite 14 years as first-line malaria treatment, Zanzibar

Characteristic	Study group		
	2002–2003	2005	2017
No. screened*	2,097	2,076	9,062
No. enrolled	207	177	146
M:F ratio	104:103	82:95	101:45
Median age (range)	24 (5–73) mo	28 (4–60) mo	16 (2–60) y
Geometric mean parasite density per microliter (range)	19,731 (2,000–198,000)	20,890 (2,000–176,000)	7,886 (75–304,000)
Mean ± SD temperature, °C	38.7 ± 1.2	37.8 ± 1.2	37.8 ± 1.4
Mean ± SD hemoglobin level, g/dL	8.5 ± 1.6	9.2 ± 1.4	11.9 ± 2.2

*Febrile patients attending healthcare facilities with suspected uncomplicated *P. falciparum* malaria infections.

resistance selection after wide-scale ACT implementation (*21*). We conducted a new clinical trial and molecular survey of *P. falciparum* genes in 2017, after 14 years of large-scale use of ASAQ as first-line treatment. The objective of this study was to estimate the *P. falciparum* sensitivity to ASAQ, including both the in vivo treatment efficacy and the parasite profiles with regards to drug resistance–associated molecular characteristics (markers). The in vivo and molecular results were then compared with findings from previous studies conducted during 2002–2013.

Materials and Methods

Study Design and Area

We conducted a single-armed therapeutic efficacy trial of ASAQ (standard dose) and primaquine (single low-dose) treatment for uncomplicated *P. falciparum* malaria (ClinicalTrials.gov identification no. NCT03773536), in accordance with World Health Organization (*22*) and Worldwide Antimalarial Resistance Network guidelines (*23*), in the West and Central Districts (Unguja Island) and Micheweni District (Pemba Island) during May–September 2017. Study participants were recruited from 14 primary healthcare units, including 11 peripheral satellite facilities and 3 referral health facilities (Figure 1). We selected the facilities on the basis of relatively high malaria detection rates in 3 preceding months and proximity to 3 centrally located referral centers in the respective districts. The study was implemented in accordance with the Helsinki Declaration and approved by the Zanzibar Medical Research Ethical Committee, Zanzibar Food and Drug Board, and Regional Research Ethics Board in Stockholm, Sweden.

Study Participants

The participants (all ages) were recruited among febrile patients attending the 14 selected health facilities. They were screened by using malaria rapid diagnostic tests (mRDTs), and if positive results were found, they were referred to the closest referral center. Participants were considered eligible for study inclusion if they were confirmed to be febrile (axillary temperature ≥37.5°C) or had a history of fever (past 48 hours) and confirmed microscopically with any level of asexual *P. falciparum* parasitemia. They were finally enrolled if considered able to comply with the study protocol (e.g., residence <10 km from referral center) and if written informed consent was obtained from patient, parent, or guardian. Exclusion criteria were severe malaria signs, underlying disease, positive pregnancy test result, or suspected alternative reason for the febrile condition.

Study Procedure

The enrolled patients were given treatment and followed-up at the referral centers. They received the antimalarial standard treatment orally (i.e., fixed-dose combination of artesunate [4 mg/kg] plus amodiaquine [10 mg/kg]: ASAQ Winthrop; Sanofi Pharmaceuticals, https://www.sanofi.com) once a day for 3 consecutive days. A single low-dose (0.25 mg/kg) of primaquine (primaquine phosphate; Sanofi Pharmaceuticals) was co-administered on the first

Table 2. Characteristics of patients fulfilling study protocol in 2017, by age group and parasite density, Zanzibar

Characteristic	Study group				
	2017, all patients	2017, children ≤5 y of age	2017, children ≤10 y of age	2017, children ≤15 y of age	2017, parasite density >2,000/μL
Total	142	21	42	66	115
M:F ratio	99:43	13:8	28:14	45:21	81:34
Median age (range)	17 (2–60) y	48 (21–60) mo	5.5 (1.8–10) y	9 (1.8–15) y	16 (1.8–60) y
Geometric mean parasite density/μL (range)	7,899 (75–304,000)	15,773 (85–304,000)	11,847 (85–304,000)	10,618 (85–304,000)	14,305 (2,175–304,000)
Mean ± SD temperature, °C	37.8 ± 1.4	38.2 ± 1.2	38.1 ± 1.1	38.2 ± 1.2	37.9 ± 1.4
Mean ± SD hemoglobin level, g/dL	11.9 ± 2.2	9.1 ± 1.7	9.8 ± 1.9	10.6 ± 2.1	11.8 ± 2.3

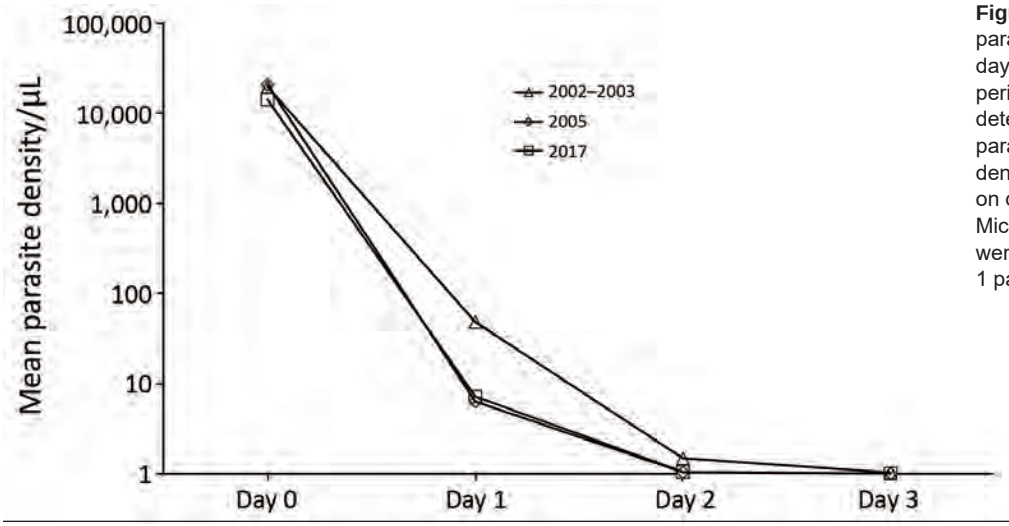

Figure 2. Comparison of parasite clearance rates until day 3 posttreatment for 3 study periods, Zanzibar. Microscopy determined geometrical mean parasite densities. Only parasite densities >2,000 parasites/µL on day 0 were included in 2017. Microscopy negative samples were given an arbitrary value of 1 parasite/µL.

day (D0). All doses were administered under direct supervision and observation for 30 min. If vomiting occurred, the patient was again given the same supervised dose and withdrawn from the study if a second vomiting occurred.

After the first 3 treatment days (D0, D1, and D2), the follow-up consisted of fixed appointments on D3, D7, D14, D21, and D28 and whenever the patient experienced any clinical symptoms. To ensure optimal compliance to the study protocol, an incentive of 5,000 Tanzanian shillings (US $2.20) was provided upon each visit, mainly to cover transportation costs.

At each follow-up visit, standard physical examination was performed and temperature was recorded. Finger-prick blood samples were collected for thick blood films and dried blood spots on filter paper (3MM; Whatman, https://www.cytivalifesciences.com). These filter papers were packaged in desiccated individual plastic bags and sent to the Karolinska Institutet (Stockholm, Sweden) for molecular analyses.

Microscopy reading of Giemsa-stained blood films was performed by 2 experienced microscopists at each visit. We quantified parasitemia by using the standard approximation method (40× parasites/200 leukocytes). A blood film was defined as positive if >1 asexual parasite was found per 1,000 leukocytes and the final parasite density was the average of 2 independent reads. An independent examination by a third microscopist was performed in case of discordant reads. We measured hemoglobin levels by using a HemoCue B-Hemoglobin Photometer (https://www.hemocue.com) on D0, D3, D7, D14, and D28, or any day of clinical suspicion of (hemolytic) anemia.

Molecular Analyses

We conducted PCR screening for all filter paper blood spots collected on D0, D3, D7, and D28 after DNA was extracted by using the Chelex-boiling method (*21*). A quantitative PCR specific for the rRNA genes of *Plasmodium* species was used to screen for parasite DNA and estimate parasite densities (*21*). Samples with cycle values <40 in duplicate runs were considered parasite positive. Single-nucleotide polymorphisms (SNPs) in the

Table 3. Parasite clearance determined by microscopy in *Plasmodium falciparum*–positive persons, Zanzibar*

Characteristic	Study group				
	2002–2003, n = 206	2005, n = 172	2017, all patients, n = 142	2017, age ≤5 y, n = 21	2017, parasite density >2,000/µL, n = 115
Parasite positivity by microscopy, no.; % (95% CI)					
Day 0	206; 100 (98–100)	172; 100 (98–100)	142; 100 (97–100)	21; 100 (84–100)	115; 100 (97–100)
Day 1	137; 67 (60–73)	64; 37 (30–45)	58; 41 (33–49)	12; 41 (34–78)	53; 46 (37–56)
Day 2	18; 9 (5–13)	1; 0.6 (0–3)	2; 1 (0–5)	0; 0 (0–16)	1; 1 (0–5)
Day 3	1; 0.5 (0–3)	0; 0 (0–2)	1; 0.7 (0–4)	0; 0 (0–16)	0; 0 (0–3)
Geometric mean parasite density/µL for parasite-positive persons (range)					
Day 0	19,858 (2,000–198,447)	20,822 (2,000–176,000)	7,899 (75–304,000)	15,773 (85–304,000)	14,305 (2,175–304,000)
Day 1	359 (9–173,882)	397 (12–25,000)	822 (30–13,700)	802 (64–4,970)	83 (30–13,700)
Day 2	89 (32–552)	560, NA	500 (250–1,000)	NA, NA	1,000, NA
Day 3	78, NA	NA, NA	120, NA	NA, NA	NA, NA

*Values are proportions of patients positive by microscopy and with geometric mean parasite densities on days 0, 1, 2, and 3 after treatment. NA, not applicable.

Table 4. Artesunate/amodiaquine treatment outcome with 28-day follow-up for increased sensitivity of *Plasmodium falciparum* to artesunate/amodiaquine despite 14 years as first-line malaria treatment, Zanzibar

Year of study, group	No patients*	No. (%) positive on day 3	No. (%) with parasite recrudescence†	No. (%) with recurrent new infection	p value‡
2002–2003, all patients§	206	1 (0.5)	13 (6)	44 (22)	Referent
2005, all patients§	172	0	7 (4)	16 (9)	Referent
2017, all patients	142	1 (1)	0	0	0.003
2017, children ≤5 y of age	21	0	0	0	0.614
2017, children ≤10 y of age	42	0	0	0	0.243
2017, children ≤15 y of age	66	0	0	0	0.055
2017, >2,000 parasites/μL	115	0	0	0	0.006

*Number fulfilling follow-up as per protocol.
†After PCR correction.
‡p value when compared with 2002–2003 and 2005 combined.
§All patients were ≤5 y of age and had parasite densities >2,000 parasites/μL in 2002–2003 and 2005.

P. falciparum multidrug-resistance 1 (*pfmdr1*) and *P. falciparum* chloroquine-resistance transporter (*pfcrt*) genes, associated with amodiaquine resistance (*8*,*9*) were analyzed in all D0 samples. SNPs at positions *pfcrt* K76T, *pfmdr1* N86Y, Y184F, and D1246Y were analyzed according to established nested PCR–restriction fragment length polymorphism protocols (*21*). In addition, polymorphisms in the 850-bp fragment of the *P. falciparum* Kelch13 propeller domain (*pfk13*), associated with artemisinin resistance were analyzed by using nested PCR amplification with Q5 high-fidelity polymerase (New England Biolabs, https://www.neb.uk.com), followed by direct Sanger sequencing of the PCR amplicon (*24*).

Study Outcomes

The primary outcome was PCR-corrected treatment failure rates assessed after 28 days. Secondary outcomes were parasite and fever clearance rates by D3, hemoglobin decrease by D7, residual PCR positivity, and D0 genotype profiles associated with parasite tolerance/resistance.

Comparator Studies

We compared the current clinical trial with 2 previous in vivo trials conducted in Zanzibar during 2002–2003 (*20*) and 2005 (A. Bjorkman, unpub. data) (ClinicalTrials.gov identifiers NCT03764527 and NCT03768908). Both studies were open-label, randomized, 2-armed studies comparing in vivo efficacy of ASAQ and artemether/lumefantrine in children (≤5 years of age) with uncomplicated *P. falciparum* malaria (range 2,000–20,0000 parasites/μL). Study procedures were similar to those in 2017. We performed paired PCR genotyping of the *P. falciparum* merozoite surface protein 2 gene in samples collected on D0 and for recurrent parasitemia days 14–28 (*20*) to differentiate reinfection from recrudescence.

We compared prevalences of molecular markers of drug resistance during 2002–2003, 2005, and 2017, as well as published data for 2010 and 2013 (*21*). Molecular genotyping of SNPs was conducted by using the same protocols (*21*) in all studies. *Pfk13* sequencing was only conducted in samples from 2017.

Samples Size

Sample size for the 2017 clinical trial was calculated for an estimated efficacy rate of 95% and a 95% CI within a total width of 10%. To achieve this power, 90 patients were required after attrition losses estimated to be 20%. However, we targeted 150 patients, a comparable number to those of previous trials (2002–2003 and 2005).

Statistical Analyses

We entered data into Microsoft Excel (https://www.microsoft.com) and cleaned data by using GSPro (https://www.dji.com). We performed statistical analyses by using Stata (https://www.stata.com). We calculated 95% CIs for proportions of patients cured by D28 by using the exact method described by Fagan (*25*); we compared proportions by using the Fisher exact test. We assessed associations between PCR positivity and patient characteristics at study baseline by using the Fisher exact test or Wilcoxon rank-sum (Mann-Whitney) test. We conducted trend analyses for genotypes by using logistic regression and year

Table 5. Parasite clearance determined by qPCR after treatment with ASAQ and single, low-dose primaquine, Zanzibar, 2017*

Day after treatment	Parasite positivity by PCR, no.; % (95% CI)	qPCR-determined geometric mean parasite density/μL (range)
Day 3	90; 63 (55–71)	2 (<1–796)
Day 7	42; 30 (22–37)	<1 (<1–18)
Day 28	9; 6 (2–10)	1 (<1–58)

*ASAQ, artesunate/amodiaquine; qPCR, quantitative PCR.

Table 6. Association between PCR positivity on days 3, 7, and 28 after treatment and patient characteristics at study baseline, Zanzibar*

Characteristic	PCR negative, day 3	PCR positive, day 3	p value,† day 3	PCR negative, day 7	PCR positive, day 7	p value,† day 7	PCR negative, day 28	PCR positive, day 28	p value,† day 28
Total (%)	52/142 (37)	90/142 (63)	NA	100/142 (70)	42/142 (30)	NA	133/142 (94)	9/142 (6)	
M:F ratio	33:19	65:25	0.35	70:30	28:14	0.70	91:42	72	0.72
Median age, y (range)	24 (2–57)	14 (2–60)	<0.001	19 (2–60)	12.5 (2–54)	0.01	17 (2–60)	14 (9–56)	0.54
Geometric mean parasite density/μL (range)	3,998 (75–120,955)	12,011 (78–304,269)	<0.001	6,185 (76–145,750)	14,940 (561–304,269)	0.01	7,847 (78–304,269)	11,259 (2,730–56,304)	0.61
Mean ± SD temperature, °C	37.2 ± 1.2	38.1 ± 1.3	<0.001	37.7 ± 1.4	38.0 ± 1.2	0.27	37.8 ± 1.4	38.0 ± 1.2	0.62
Mean ± SD hemoglobin level, g/dL	12.4 ± 2.2	11.7 ± 2.2	0.09	12.2 ± 2.2	11.3 ± 2.2	0.01	12.0 ± 2.3	11.4 ± 1.5	0.37

*NA, not applicable.
†Calculated by Fisher exact test (for sex) or Wilcoxon rank-sum (Mann-Whitney) test for continuous variables.

as a continuous variable. We performed analysis for the proportion of patients harboring mutant alleles (i.e., only mutant, or mixed with wild-type), as well as for the ratio of infections with mutants versus infections with the corresponding wild-types (mutants *pfcrt* 76T; *pfmdr1* 86Y, Y184, and 1246Y).

Results

Patients

The 14 health centers screened 9,062 febrile patients during May–September 2017; a total of 233 (2.6%) were positive by mRDT, and 146 satisfied all inclusion criteria and thus enrolled at the 3 referral centers. We provide demographic, clinical, and laboratory characteristics for patients (Table 1), along with data from the previous clinical trials during 2002–2003 and 2005. Despite different inclusion criteria regarding age and parasitemia, the geometrical mean parasite densities and ranges at study enrollment were similar (Table 2). A total of 142 (97%) of 146 patients in 2017 completed the study follow-up to D28. Four patients were excluded or did not complete follow-up because of vomiting on D1, itching on D3, too long travel distance to a referral center, and travel to mainland Tanzania.

Treatment Outcomes

Parasite clearance rates by microscopy up to D3 were similar in the 3 trials (Figure 2; Table 3). In 2017, one patient remained malaria positive at D3, after which all were microscopy negative up to D28 (Table 4). The cure rate of 100% (95% CI 97.4%–100.0%) in 2017 was higher when compared with the PCR-adjusted cure rate for 2002–2003 and 2005 combined (358/378, 94.7% [95% CI 91.9%–96.7%]; p = 0.003). Statistical significance was maintained after including only patients with >2,000 parasites/μL on day 0 in 2017 (p = 0.006), and near significance (p = 0.055) was achieved when adjusting for age ≤15 years (i.e., with <5 years of exposure to major malaria transmission. Numbers of recurrent parasitemias, defined as new infections during the 28 days of follow-up, were 44 (22%) in 2002–2003, 16 (9%) in 2005, and none (0%) in 2017, confirming higher malaria transmission rates in 2002–2005.

PCR positivity and parasite density estimates by quantitative PCR were analyzed only for the 2017 study (Table 5). Patients remained positive for much longer by PCR than by microscopy. PCR positivity on D3 and D7 were strongly associated with age, parasite density at study enrollment, baseline temperature, and hemoglobin value (Table 6). Associations were not significant for persons who were PCR positive on D28.

Fever clearance rates were similar: temperatures <37.5°C by D3 in 92.8% (95% CI 88.4%–95.9%) of patients in 2002–2003, 98.8% (95% CI 95.9%–99.9%) of patients in 2005, and 97.9% (95% CI 94.0%–99.6%) of patients in 2017. Hemoglobin levels at enrollment (D0) were higher in all patients in 2017 (Table 1) but similar in children ≤5 years of age when compared with 2002–2003 and 2005 (Table 2). The average decrease by D7 was –1.10 g/dL (range –6.1 g/dL to –3.3 g/dL) in 2017, when primaquine was added to ASAQ, and -0.20 g/dL (range –3.6 g/dL to –3.4 g/dL) in 2002–2003 after ASAQ alone (p<0.001). However, after adjusting for hemoglobin level at D0, the decrease was more pronounced in 2002–2003 (–0.60 g/dL) than in 2017 (–0.09 g/dL) (p = 0.003). There was no case of severe anemia (hemoglobin level <5 g/dL) at D0 or D7 in any study. No patient experienced any serious adverse event.

Polymorphisms in *pfcrt*, *pfmdr1*, and *pfk13* Genes

There was a significant reduction of *pfcrt* K76T prevalence from 98.0% in 2003 to 4.9% in 2017 (p<0.001) (Figure 3) and negative trends were also seen for *pfmdr1* 86Y, Y184, and 1246Y, all associated with reduced sensitivity to amodiaquine (*8*,*9*,*26*). *Pfmdr1* YYY and

YYD were the most frequent haplotypes in 2002–2003, and the NYD and NFD haplotypes were most frequent and the YYY totally absent in 2017 (Table 7). The decrease of YYY and YYD was highly significant between 2002–2003 and 2017 (p<0.001).

Regarding the *pfK13* gene, 139 (98%) of 142 samples collected 2017 were successfully sequenced. No nonsynonymous SNP was identified. Two synonymous mutations were found, the SNPs C469C (5 samples) and S477S (1 sample). Five samples were from patients at the Bububu health center, and 1 (C469C) was from a patient in Uzini who had traveled to mainland Tanzania.

Discussion

The high cure rate in 2017 (100%) was significantly higher than the combined cure rate in 2002–2003 and 2005 (94.7%) (p = 0.003). The microscopy-determined parasite clearance was as rapid as that in 2002–2003 and 2005 (≤3 days), and fever clearance was similar. These findings confirm maintained full efficacy of the artesunate compound (*17*) and suggest an increased cure rate by ASAQ. Compliance to the study protocol was high: only 4/146 patients were unable to complete follow-up despite logistical constraints of conducting the clinical trial in the low-transmission context in 2017. A large enough sample size was achieved by recruiting patients from 11 peripheral satellite health units and 3 referral health facilities (in which follow-up attendances were conducted) and by including patients of all ages and all parasite densities.

High in vivo efficacy is in agreement with previous findings from Madagascar (*27*) and Côte d'Ivoire (*28*) after 6 and 10 years of ASAQ use as first-line treatment, respectively. It might be argued that the observed higher cure rate in 2017 may be caused by a different study age group; added single low-dose primaquine; fixed-dose versus a loose combination of ASAQ compounds; or reduced malaria transmission compared with that in 2002–2003 and 2005. However, age-related protective immunity in the population in Zanzibar has decreased substantially (2) and thus is expected to have had little influence on cure rate, especially in children <15 years of age. Single low-dose primaquine is not expected to have had any major effect on the asexual P. falciparum stage (*29*), and whereas different efficacies by different ASAQ formulations have been reported in a large meta-analysis (*30*), no significant difference was found between a nonfixed loose combination of ASAQ with an amodiaquine dose of 30 mg/kg (used in the studies during 2002–2003 and 2005) compared with a fixed combination with same amodiaquine dose (used in our 2017 study). In addition, drug intake with the loose combination was highly supervised during 2002–2003 and 2005; some new infections might have been falsely misinterpreted as recrudescent during higher transmission in 2002–2003 and 2005, the opposite might also occur (*31*–*33*). A potential general limitation in the in vivo assessment of ASAQ efficacy, although according to World Health Organization recommendations (*22*), is that a 28-day follow-up might miss some late recrudescences (*20*). However, this possibility should not affect the comparative approach.

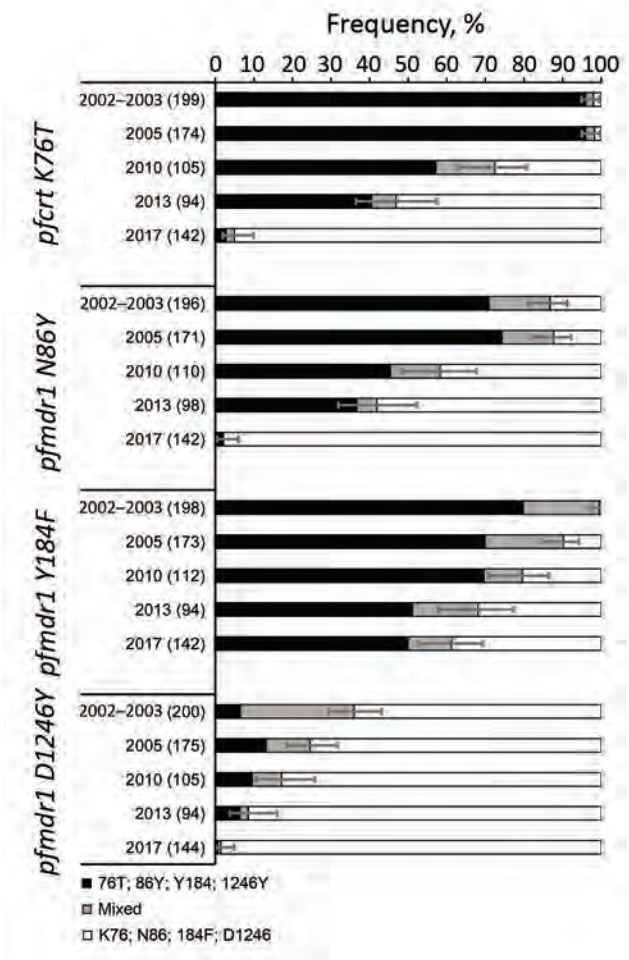

Figure 3. Frequency of polymorphisms associated with amodiaquine resistance in *Plasmodium falciparum* infections in Zanzibar, 2002–2017. Black bars indicate resistance alleles, gray bars indicate mixed infections, and white bars indicate wild-type alleles. Error bars indicate 95% CIs of proportions of infections harboring resistance alleles (either alone or mixed infections). Values in parentheses are the total number of genotyped samples shown next to the study year. Trend analysis: p<0.001 for *pfcrt* 76T + mixed, *pfmdr1* 86Y + mixed, *pfmdr1* Y184 + mixed, *pfmdr1* 1246Y + mixed; p<0.001 for *pfcrt* 76T, *pfmdr1* 86Y, *pfmdr1* Y184Y; and p = 0.016 for *pfmdr1* 1246Y. Pfcrt, *P. falciparum* chloroquine-resistance transporter gene; Pfmdr1, *P. falciparum* multidrug-resistance gene.

Table 7. *Plasmodium falciparum* multidrug-resistance 1 haplotype frequencies in clinical trials of increased sensitivity to artesunate/amodiaquine despite 14 years as first-line malaria treatment, Zanzibar*

Haplotype	Study group					p value†	p value‡
	2002–2003, n = 161	2005, n = 156	2010, n = 92	2013, n = 87	2017, n = 140		
YYY	31.1	20.5	12.0	8.0	0.0	<0.001	<0.001
YYD	57.1	63.5	38.0	31.0	2.1	<0.001	<0.001
YFD	0.0	4.5	7.6	0.0	0.0	<0.001	NA
NYD	11.2	7.1	26.1	27.6	58.6	<0.001	<0.001
NFY	0.0	0.0	0.0	1.1	0.7	0.25	0.46
NFD	0.6	4.5	16.3	32.2	38.6	<0.001	<0.001

*Values are percentages unless indicate otherwise. NA, not applicable.
†Comparing frequencies between all years by Fisher exact test.
‡Comparing frequencies between 2002–2003 and 2017 by Fisher exact test.

A minor reduction of hemoglobin levels from D0 to D7 was similarly observed in 2017 and 2002–2003 and 2005 and is consistent with common findings after ACT treatment (*34*). This reduction supports the safety of adding single low-dose primaquine in 2017 despite ≈10% prevalence of glucose-6-phosphate dehydrongenase deficiency in the population in Zanzibar.

Residual parasite positivity by PCR on D3 and several weeks posttreatment despite observed high ACT efficacy has been described and does not necessarily imply drug resistance (*35*–*37*). A key factor associated to such positivity was, as expected, high initial parasite density. What low-grade PCR positivity represents remains unclear, be it residual parasite DNA, gametocytes, or suppressed dormant and potentially surviving parasites (*37*,*38*).

Our study showed no sign of increased tolerance to artesunate because no resistance-associated mutations were detected in the *pfk13* gene, in accordance with several other studies in Africa (*4*). Moreover, prevalences of the SNPs *pfcrt* 76T and *pfmdr1* 86Y, Y184, and 1246Y associated with amodiaquine resistance (*8*,*9*,*26*) all decreased steadily during the observation period (Figure 3). Amodiaquine and chloroquine do generally select for similar mutations in the *Pfcrt* and *Pfmdr* genes. However, whereas chloroquine, used as first-line treatment up to 2003, did strongly select such mutations, this finding was reversed when amodiaquine combined with artesunate became first-line treatment. This finding is quite in contrast to longitudinal studies in areas that used other ACTs as first-line treatment. *P. falciparum* genotypes associated with tolerance/resistance to the ACT partner drugs lumefantrine (*18*,*39*), sulfadoxine/pyrimethamine (*40*,*41*) and piperaquine (*12*) have all been shown to consistently increase over time, after respective ACT use.

A major objective for combination therapy is for combined compounds to protect each other (i.e., preventing selection of resistance to either drug and both drugs combined). In Zanzibar, our in vivo and molecular findings suggest that *P. falciparum* has become increasingly sensitive to the combination ASAQ, despite its widescale use since 2003–2004. Although changes in allele frequencies in Zanzibar could be caused by genetic drift after rapid reduction in the parasite population in Zanzibar causing a genetic bottleneck, the temporal trends of *Pfcrt* and *Pfmdr1* alleles suggest a selection event as more likely. However, why are *pfcrt* and *pfmdr1* mutations associated with amodiaquine resistance selected against, in favor of the drug-sensitive wild-types over time despite being temporarily selected after each ASAQ treatment (*8*,*9*)?

Resistance mutations confer an advantage in the presence of the drug, although such mutations often come with fitness costs in the absence of the drug (*42*–*44*) (sometimes additional compensating mutations might also restore fitness in mutated parasites [*45*]). Thus, spread of drug resistance alleles might mostly be restricted when in competition with wild-type parasites in the absence of the drug (*46*,*47*). Such competition is expected in contexts such as Zanzibar, where decreasing transmission rates have led to a corresponding decrease in ASAQ use over time, especially because treatment is normally restricted to mRDT-positive patients only (*15*). In addition, a large proportion of infections are subpatent and thus represent a large reservoir of competing parasites unexposed to antimalarial drugs (*2*).

Potentially contributing to increased sensitivity to amodiaquine are infections imported from mainland Tanzania (*2*,*48*), where the first-line treatment is artemether/lumefantrine, which selects the opposite genotypes of those for amodiaquine (*8*–*10*). Another potential reason for less resistance selection by amodiaquine compared with lumefantrine might be different pharmacokinetic profiles and thus different selection windows after treatment with the respective ACTs. However, the immediate selection dynamics posttreatment have appeared rather similar for amodiaquine and lumefantrine (*8*–*10*). Accordingly,

elimination kinetics of desethyl-amodiaquine, (elimination half-life initially short but terminally >7 days) (*16*) and lumefantrine (elimination half-life ≈3 days) (*49*) are not highly different.

In areas of increased resistance to partner drugs, ACT cure rates have mostly remained relatively high as long as artemisinins remained highly effective (*11*), except for artesunate–sulfadoxine/pyrimethamine (*40*,*41*). When artemisinins were still effective in Southeast Asia, selection of mefloquine resistance after previous monotherapy was initially stopped and temporarily reversed when the ACT artesunate/mefloquine was introduced (*50*). However, reduced partner drug efficacy will always represent increased risk for development and selection of artemisinin resistance. When artemisinin starts to fail in addition to the failing partner drug, an accelerating and alarming development toward multidrug resistance to the combination is expected. This suggestion has occurred in the Greater Mekong Subregion for dihydroartemisinin/piperaquine (*12*).

Despite 14 years of widescale use of ASAQ as a first-line treatment for malaria in Zanzibar, there are no indications of increased tolerance/resistance to either drug. Our in vivo and molecular findings suggest an increased antimalarial activity by the partner drug amodiaquine. We believe that this finding might be primarily caused by fitness costs of the amodiaquine tolerance/resistance–related mutations in the *pfcrt* and *pfmdr1* genes in the low-transmission context with restricted and compliant use of ASAQ to parasitologically confirmed malaria cases only, and with relatively frequently imported parasites without chloroquine/amodiaquine resistance–associated mutations. ASAQ might have a comparative advantage, especially in low-transmission areas compared with other ACTs against development or spread of artemisinin- (and ACT-) resistant parasites.

Acknowledgments

We thank all patients and dedicated healthcare staff for participating in the study.

This study was supported by the Ministry of Health, Zanzibar, the Global Fund (grant QNB-M-MOH), the Erling-Persson Family Foundation, and the Swedish Research Council.

About the Author

Dr. Msellem is director of training and research at Mnazi Mmoja Hospital, Zanzibar, Tanzania. His primary research interests are malaria chemotherapy, antimicrobial drug resistance, and control/elimination.

References

1. World Health Organization. World malaria report, 2018 [cited 2020 May 26]. https://www.who.int/malaria/publications/world-malaria-report-2018/en
2. Björkman A, Shakely D, Ali AS, Morris U, Mkali H, Abbas AK, et al. From high to low malaria transmission in Zanzibar-challenges and opportunities to achieve elimination. BMC Med. 2019;17:14. https://doi.org/10.1186/s12916-018-1243-z
3. Takala-Harrison S, Jacob CG, Arze C, Cummings MP, Silva JC, Dondorp AM, et al. Independent emergence of artemisinin resistance mutations among *Plasmodium falciparum* in Southeast Asia. J Infect Dis. 2015;211:670–9. https://doi.org/10.1093/infdis/jiu491
4. WWARN K13 Genotype-Phenotype Study Group. Association of mutations in the *Plasmodium falciparum* Kelch13 gene (Pf3D7_1343700) with parasite clearance rates after artemisinin-based treatments-a WWARN individual patient data meta-analysis. BMC Med. 2019;17:1. https://doi.org/10.1186/s12916-018-1207-3
5. Das S, Saha B, Hati AK, Roy S. Evidence of artemisinin-resistant *Plasmodium falciparum* malaria in eastern India. N Engl J Med. 2018;379:1962–4. https://doi.org/10.1056/NEJMc1713777
6. Chenet SM, Akinyi Okoth S, Huber CS, Chandrabose J, Lucchi NW, Talundzic E, et al. Independent emergence of the *Plasmodium falciparum* Kelch propeller domain mutant allele C580Y in Guyana. J Infect Dis. 2016;213:1472–5. https://doi.org/10.1093/infdis/jiv752
7. Björkman A, Phillips-Howard PA. The epidemiology of drug-resistant malaria. Trans R Soc Trop Med Hyg. 1990; 84:177–80. https://doi.org/10.1016/0035-9203(90)90246-B
8. Holmgren G, Gil JP, Ferreira PM, Veiga MI, Obonyo CO, Björkman A. Amodiaquine resistant *Plasmodium falciparum* malaria in vivo is associated with selection of *pfcrt 76T* and *pfmdr1 86Y*. Infect Genet Evol. 2006;6:309–14. https://doi.org/10.1016/j.meegid.2005.09.001
9. Holmgren G, Hamrin J, Svärd J, Mårtensson A, Gil JP, Björkman A. Selection of *pfmdr1* mutations after amodiaquine monotherapy and amodiaquine plus artemisinin combination therapy in east Africa. Infect Genet Evol. 2007;7:562–9. https://doi.org/10.1016/j.meegid.2007.03.005
10. Sisowath C, Strömberg J, Mårtensson A, Msellem M, Obondo C, Björkman A, et al. In vivo selection of *Plasmodium falciparum* pfmdr1 86N coding alleles by artemether-lumefantrine (Coartem). J Infect Dis. 2005;191:1014–7. https://doi.org/10.1086/427997
11. Venkatesan M, Gadalla NB, Stepniewska K, Dahal P, Nsanzabana C, Moriera C, et al.; Asaq Molecular Marker Study Group. Polymorphisms in *Plasmodium falciparum* chloroquine resistance transporter and multidrug resistance 1 genes: parasite risk factors that affect treatment outcomes for *P. falciparum* malaria after artemether-lumefantrine and artesunate-amodiaquine. Am J Trop Med Hyg. 2014;91:833–43. https://doi.org/10.4269/ajtmh.14-0031
12. van der Pluijm RW, Imwong M, Chau NH, Hoa NT, Thuy-Nhien NT, Thanh NV, et al. Determinants of dihydroartemisinin-piperaquine treatment failure in *Plasmodium falciparum* malaria in Cambodia, Thailand, and Vietnam: a prospective clinical, pharmacological, and genetic study. Lancet Infect Dis. 2019;19:952–61. https://doi.org/10.1016/S1473-3099(19)30391-3
13. Björkman AB. Asymptomatic low-density malaria infections: a parasite survival strategy? Lancet Infect Dis. 2018;18:485–6. https://doi.org/10.1016/S1473-3099(18)30047-1

14. Beer N, Ali AS, Rotllant G, Abass AK, Omari RS, Al-mafazy AWH, et al. Adherence to artesunate-amodiaquine combination therapy for uncomplicated malaria in children in Zanzibar, Tanzania. Trop Med Int Health. 2009;14:766–74. https://doi.org/10.1111/j.1365-3156.2009.02289.x
15. Msellem MI, Mårtensson A, Rotllant G, Bhattarai A, Strömberg J, Kahigwa E, et al. Influence of rapid malaria diagnostic tests on treatment and health outcome in fever patients, Zanzibar: a crossover validation study. PLoS Med. 2009;6:e1000070. https://doi.org/10.1371/journal.pmed.1000070
16. Hietala SF, Bhattarai A, Msellem M, Röshammar D, Ali AS, Strömberg J, et al. Population pharmacokinetics of amodiaquine and desethylamodiaquine in pediatric patients with uncomplicated falciparum malaria. J Pharmacokinet Pharmacodyn. 2007;34:669–86. https://doi.org/10.1007/s10928-007-9064-2
17. Stepniewska K, Ashley E, Lee SJ, Anstey N, Barnes KI, Binh TQ, et al. In vivo parasitological measures of artemisinin susceptibility. J Infect Dis. 2010;201:570–9. https://doi.org/10.1086/650301
18. Malmberg M, Ngasala B, Ferreira PE, Larsson E, Jovel I, Hjalmarsson A, et al. Temporal trends of molecular markers associated with artemether-lumefantrine tolerance/resistance in Bagamoyo district, Tanzania. Malar J. 2013;12:103. https://doi.org/10.1186/1475-2875-12-103
19. Mwaiswelo R, Ngasala B, Gil JP, Malmberg M, Jovel I, Xu W, et al. Sustained high cure rate of artemether-lumefantrine against uncomplicated *Plasmodium falciparum* malaria after 8 years of its wide-scale use in Bagamoyo District, Tanzania. Am J Trop Med Hyg. 2017;97:526–32. https://doi.org/10.4269/ajtmh.16-0780
20. Mårtensson A, Strömberg J, Sisowath C, Msellem MI, Gil JP, Montgomery SM, et al. Efficacy of artesunate plus amodiaquine versus that of artemether-lumefantrine for the treatment of uncomplicated childhood *Plasmodium falciparum malaria* in Zanzibar, Tanzania. Clin Infect Dis. 2005;41:1079–86. https://doi.org/10.1086/444460
21. Morris U, Xu W, Msellem MI, Schwartz A, Abass A, Shakely D, et al. Characterising temporal trends in asymptomatic *Plasmodium* infections and transporter polymorphisms during transition from high to low transmission in Zanzibar, 2005–2013. Infect Genet Evol. 2015;33:110–7. https://doi.org/10.1016/j.meegid.2015.04.018
22. World Health Organization. Guidelines for the treatment of malaria, 3rd ed. Geneva: The Organization; 2015.
23. WWARN. Worldwide Antimalarial Resistance Network (WWARN) Explorer [cited 2019 Oct 15]. https://www.wwarn.org/tracking-resistance/wwarn-explorer
24. Ariey F, Witkowski B, Amaratunga C, Beghain J, Langlois AC, Khim N, et al. A molecular marker of artemisinin-resistant *Plasmodium falciparum* malaria. Nature. 2014;505:50–5. https://doi.org/10.1038/nature12876
25. Fagan T. Exact 95% confidence intervals for differences in binomial proportions. Comput Biol Med. 1999;29:83–7. https://doi.org/10.1016/S0010-4825(98)00047-X
26. Folarin OA, Bustamante C, Gbotosho GO, Sowunmi A, Zalis MG, Oduola AMJ, et al. In vitro amodiaquine resistance and its association with mutations in *pfcrt* and *pfmdr1* genes of *Plasmodium falciparum* isolates from Nigeria. Acta Trop. 2011;120:224–30. https://doi.org/10.1016/j.actatropica.2011.08.013
27. Raobela O, Andriantsoanirina V, Rajaonera DG, Rakotomanga TA, Rabearimanana S, Ralinoro F, et al. Efficacy of artesunate-amodiaquine in the treatment of falciparum uncomplicated malaria in Madagascar. Malar J. 2018;17:284. https://doi.org/10.1186/s12936-018-2440-0
28. Toure OA, Assi SB, N'Guessan TL, Adji GE, Ako AB, Brou MJ, et al. Open-label, randomized, non-inferiority clinical trial of artesunate-amodiaquine versus artemether-lumefantrine fixed-dose combinations in children and adults with uncomplicated falciparum malaria in Côte d'Ivoire. Malar J. 2014;13:439. https://doi.org/10.1186/1475-2875-13-439
29. Mwaiswelo R, Ngasala B, Jovel I, Aydin-Schmidt B, Gosling R, Premji Z, et al. Adding a single low-dose of primaquine (0.25 mg/kg) to artemether-lumefantrine did not compromise treatment outcome of uncomplicated *Plasmodium falciparum* malaria in Tanzania: a randomized, single-blinded clinical trial. Malar J. 2016;15:435. https://doi.org/10.1186/s12936-016-1430-3
30. Adjuik MA, Allan R, Anvikar AR, Ashley EA, Ba MS, Barennes H, et al.; WorldWide Antimalarial Resistance Network (WWARN) AS-AQ Study Group. The effect of dosing strategies on the therapeutic efficacy of artesunate-amodiaquine for uncomplicated malaria: a meta-analysis of individual patient data. BMC Med. 2015;13:66. https://doi.org/10.1186/s12916-015-0301-z
31. Juliano JJ, Gadalla N, Sutherland CJ, Meshnick SR. The perils of PCR: can we accurately 'correct' antimalarial trials? Trends Parasitol. 2010;26:119–24. https://doi.org/10.1016/j.pt.2009.12.007
32. Martensson A, Ngasala B, Ursing J, Isabel Veiga M, Wiklund L, Membi C, et al. Influence of consecutive-day blood sampling on polymerase chain reaction-adjusted parasitological cure rates in an antimalarial-drug trial conducted in Tanzania. J Infect Dis. 2007;195:597–601. https://doi.org/10.1086/510910
33. Messerli C, Hofmann NE, Beck H-P, Felger I. Critical evaluation of molecular monitoring in malaria drug efficacy trials and pitfalls of length-polymorphism markers. Antimicrob Agents Chemother. 2016;61:e01500–16.
34. Zwang J, D'Alessandro U, Ndiaye JL, Djimdé AA, Dorsey G, Mårtensson AA, et al. Haemoglobin changes and risk of anaemia following treatment for uncomplicated falciparum malaria in sub-Saharan Africa. BMC Infect Dis. 2017;17:443. https://doi.org/10.1186/s12879-017-2530-6
35. Beshir KB, Sutherland CJ, Sawa P, Drakeley CJ, Okell L, Mweresa CK, et al. Residual *Plasmodium falciparum* parasitemia in Kenyan children after artemisinin-combination therapy is associated with increased transmission to mosquitoes and parasite recurrence. J Infect Dis. 2013;208:2017–24. https://doi.org/10.1093/infdis/jit431
36. Vafa Homann M, Emami SN, Yman V, Stenström C, Sondén K, Ramström H, et al. Detection of malaria parasites after treatment in travelers: a 12-months longitudinal study and statistical modelling analysis. EBioMedicine. 2017;25:66–72. https://doi.org/10.1016/j.ebiom.2017.10.003
37. Chang HH, Meibalan E, Zelin J, Daniels R, Eziefula AC, Meyer EC, et al. Persistence of *Plasmodium falciparum* parasitemia after artemisinin combination therapy: evidence from a randomized trial in Uganda. Sci Rep. 2016;6:26330. https://doi.org/10.1038/srep26330
38. Cheng Q, Kyle DE, Gatton ML. Artemisinin resistance in *Plasmodium falciparum*: a process linked to dormancy? Int J Parasitol Drugs Drug Resist. 2012;2:249–55. https://doi.org/10.1016/j.ijpddr.2012.01.001
39. Otienoburu SD, Suay I, Garcia S, Thomas NV, Srisutham S, Björkman A, et al. An online mapping database of molecular markers of drug resistance in *Plasmodium*

falciparum: the ACT Partner Drug Molecular Surveyor. Malar J. 2019;18:12. https://doi.org/10.1186/s12936-019-2645-x
40. Mishra N, Kaitholia K, Srivastava B, Shah NK, Narayan JP, Dev V, et al. Declining efficacy of artesunate plus sulphadoxine-pyrimethamine in northeastern India. Malar J. 2014;13:284. https://doi.org/10.1186/1475-2875-13-284
41. Gadalla NB, Abdallah TM, Atwal S, Sutherland CJ, Adam I. Selection of *pfdhfr/pfdhps* alleles and declining artesunate/sulphadoxine-pyrimethamine efficacy against *Plasmodium falciparum* eight years after deployment in eastern Sudan. Malar J. 2013;12:255. https://doi.org/10.1186/1475-2875-12-255
42. Fröberg G, Ferreira PE, Mårtensson A, Ali A, Björkman A, Gil JP. Assessing the cost-benefit effect of a *Plasmodium falciparum* drug resistance mutation on parasite growth in vitro. Antimicrob Agents Chemother. 2013;57:887–92. https://doi.org/10.1128/AAC.00950-12
43. Bushman M, Morton L, Duah N, Quashie N, Abuaku B, Koram KA, et al. Within-host competition and drug resistance in the human malaria parasite *Plasmodium falciparum*. Proc Biol Sci. 2016;283:20153038. https://doi.org/10.1098/rspb.2015.3038
44. Dhingra SK, Gabryszewski SJ, Small-Saunders JL, Yeo T, Henrich PP, Mok S, et al. Global spread of mutant PfCRT and its pleiotropic impact on *Plasmodium falciparum* multidrug resistance and fitness. MBiol. 2019;10:e02731–18. https://doi.org/10.1128/mBio.02731-18
45. Straimer J, Gnädig NF, Stokes BH, Ehrenberger M, Crane AA, Fidock DA. *Plasmodium falciparum* K13 mutations differentially impact ozonide susceptibility and parasite fitness in vitro. MBio. 2017;8:e00172–17. https://doi.org/10.1128/mBio.00172-17
46. Laufer MK, Thesing PC, Eddington ND, Masonga R, Dzinjalamala FK, Takala SL, et al. Return of chloroquine antimalarial efficacy in Malawi. N Engl J Med. 2006;355:1959–66. https://doi.org/10.1056/NEJMoa062032
47. Mita T, Kaneko A, Lum JK, Bwijo B, Takechi M, Zungu IL, et al. Recovery of chloroquine sensitivity and low prevalence of the *Plasmodium falciparum* chloroquine resistance transporter gene mutation K76T following the discontinuance of chloroquine use in Malawi. Am J Trop Med Hyg. 2003;68:413–5. https://doi.org/10.4269/ajtmh.2003.68.413
48. Morgan AP, Brazeau NF, Ngasala B, Mhamilawa LE, Denton M, Msellem M, et al. Falciparum malaria from coastal Tanzania and Zanzibar remains highly connected despite effective control efforts on the archipelago. Malar J. 2020;19:47. https://doi.org/10.1186/s12936-020-3137-8
49. Hietala SF, Mårtensson A, Ngasala B, Dahlström S, Lindegårdh N, Annerberg A, et al. Population pharmacokinetics and pharmacodynamics of artemether and lumefantrine during combination treatment in children with uncomplicated falciparum malaria in Tanzania. Antimicrob Agents Chemother. 2010;54:4780–8. https://doi.org/10.1128/AAC.00252-10
50. Carrara VI, Zwang J, Ashley EA, Price RN, Stepniewska K, Barends M, et al. Changes in the treatment responses to artesunate-mefloquine on the northwestern border of Thailand during 13 years of continuous deployment. PLoS One. 2009;4:e4551. https://doi.org/10.1371/journal.pone.0004551

Address for correspondence: Anders Björkman, Department of Microbiology, Tumor and Cell Biology, Biomedicum quarter C9, Karolinska Institutet, Solnavägen 9, SE-171 77 Stockholm, Sweden; email: anders.bjorkman@ki.se

Factors Associated with Prescription of Antimicrobial Drugs for Dogs and Cats, United Kingdom, 2014–2016

David A. Singleton, Gina L. Pinchbeck, Alan D. Radford, Elena Arsevska, Susan Dawson, Philip H. Jones, Peter-John M. Noble, Nicola J. Williams, Fernando Sánchez-Vizcaíno

Antimicrobial stewardship is a cornerstone of efforts to curtail antimicrobial resistance. To determine factors potentially influencing likelihood of prescribing antimicrobials for animals, we analyzed electronic health records for unwell dogs (n = 155,732 unique dogs, 281,543 consultations) and cats (n = 69,236 unique cats, 111,139 consultations) voluntarily contributed by 173 UK veterinary practices. Using multivariable mixed effects logistic regression, we found that factors associated with decreased odds of systemic antimicrobial prescription were client decisions focused on preventive health: vaccination (dogs, odds ratio [OR] 0.93, 95% CI, 0.90–0.95; cats, OR 0.92, 95% CI 0.89–0.95), insurance (dogs, OR 0.87, 95% CI 0.84–0.90; cats, OR 0.82, 95% CI 0.79–0.86), neutering of dogs (OR 0.90, 95% CI 0.88–0.92), and practices accredited by the Royal College of Veterinary Surgeons (OR 0.79, 95% 95% CI 0.68–0.92). This large multicenter companion animal study demonstrates the potential of preventive healthcare and client engagement to encourage responsible antimicrobial drug use.

Antimicrobial drug use is a key driver of the promotion and transmission of antimicrobial resistance in humans, livestock, and companion animals (e.g., dogs, cats) (*1*–*5*). Of these groups, the role of companion animals in the development (*1*,*2*), carriage, (*6*) and transmission of antimicrobial-resistant bacteria among animal and human populations is being increasingly realized, partly because of the close proximity in which these animals reside with humans (*5*,*7*,*8*). Indeed, companion animals are now included in recent global action plans aimed at tackling the global health threat of antimicrobial resistance (*9*).

In human medicine, electronic health records (EHRs) and qualitative research techniques have been used extensively to identify practitioner- and patient-led factors associated with the likelihood of antimicrobial drug prescription (*10*–*13*). In veterinary medicine, studies investigating antimicrobial drug prescribing practices and related risk factors are more limited (*14*). Companion animal research has largely focused on postal surveys (*15*,*16*) and in-person interviews (*17*) to explore perceptions held by veterinary practitioners. However, recent advances in veterinary health informatics have provided opportunities for widescale use of veterinary EHRs to survey antimicrobial prescription (*18*,*19*).

Thus far, key insights into antimicrobial prescription frequency and variety have been demonstrated (*20*–*23*), including an apparent increased use of cefovecin in cats (*21*,*22*); the World Health Organization considers this third-generation cephalosporin to be a highest priority critically important antimicrobial (HPCIA) (*24*). Considerable interpractice (*20*,*22*), regional (*21*), and clinical presentation (*22*,*25*,*26*) variability in antimicrobial drug prescription frequency and choice has also been identified. Although previous studies have indicated divergence of veterinary opinion over when antimicrobial therapy is justified and which classes of antimicrobial drugs would be most appropriate (*15*–*17*), the reasons why such variation exists are unknown.

To identify factors potentially influencing antimicrobial prescribing in the clinical environment, we analyzed EHRs for a large, diverse population of dogs and cats, collected from a network of volunteer first-opinion (general) veterinary practices across Great Britain (England, Scotland, and Wales). We explored

Author affiliations: University of Liverpool Leahurst Campus, Neston, UK (D.A. Singleton, G.L. Pinchbeck, A.D. Radford, E. Arsevska, S. Dawson, P.H. Jones, P.-J.M. Noble, N.J. Williams); Animal and Plant Health Agency, Shrewsbury, UK (P.H. Jones); University of Bristol Langford Campus, Bristol, UK (F. Sánchez-Vizcaíno)

DOI: https://doi.org/10.3201/eid2608.191786

associations between antimicrobial prescription (including antimicrobials authorized for systemic administration, antimicrobials authorized for topical administration, and HPCIAs) and a range of veterinary practice, practitioner, client, and animal-related factors (including socioeconomic factors and preventive healthcare interventions) for animals presented primarily for investigation of disease.

Materials and Methods

Data Collection

For this cross-sectional study, we examined EHRs from 178 volunteer veterinary practices (386 unique sites) taking part in the Small Animal Veterinary Surveillance Network (SAVSNET; University of Liverpool, Liverpool, UK; ethical approval reference no. RETH000964), by using the Robovet practice management system (Covetrus, https://www.covetrus.com). We retrieved EHRs from booked consultations (*19*) from April 1, 2014, through March 31, 2016. Each consultation record included patient species, breed, sex, neuter status, insurance status, microchip status, vaccination history, date of birth, client's postal code, and any products dispensed at time of consultation. Every consultation record was further classified by the attending veterinary professional into 1 of 10 main presenting complaints (categorized as healthy, unhealthy, or postoperative), indicating the main reason the animal was presented to the veterinary practice, as previously described (*22*).

Data Management

General Data Management

Initially available were consultations for 762,648 dogs and 300,606 cats. We excluded animals for whom dates of birth were probably incorrectly recorded (i.e., 1,577 dogs recorded as >24.5 years and 2,467 cats as >26.0 years of age at consultation) and animals for whom a valid client postal code was lacking (23,705 dogs, 9,901 cats). We included only consultations in which animals were recorded as unhealthy (sick animal consultations) according to main presenting complaint (MPC) (282,263 of 737,366 remaining dog and 111,367 of 288,238 remaining cat consultations). We also excluded 5 veterinary practices that provided insufficient EHRs (<50 consultations) for adequate statistical analyses.

Using a semiautomated rule-based text-mining method as previously described (*22*), we identified antimicrobial prescription via the text-based product description and classified use as systemic (oral or injectable) or topical (topical, aural, ocular). All fluoroquinolones, macrolides, and third-generation cephalosporins were considered HPCIAs (*24*). We compiled a list of antimicrobials authorized for use in dogs or cats use in the United Kingdom (Appendix Table 1, https://wwwnc.cdc.gov/EID/article/26/8/19-1786-App1.pdf).

Animal Factors

Animals were considered vaccinated if the most recently recorded vaccination date (disregarding vaccine composition) was ≤3.5 years (broadly reflective of current vaccine interval guidelines) before the relevant consultation date (*27*). Breeds were summarized according to standardized breed terms (*28*) before being categorized into either genotypically similar breed groups (*29*), crossbreeds, breeds not yet genetically classified (unclassified), or breed not recorded/recognizable (unknown).

Client Factors

Using clients' home postal code, we assigned a measure of predicted deprivation to each client according to the most recent Indices of Multiple Deprivation (IMD): England 2015 (https://www.gov.uk/government/statistics/english-indices-of-deprivation-2015), Scotland 2012 (https://www2.gov.scot/Topics/Statistics/SIMD/DataAnalysis/Background-Data-2012), and Wales 2014 (https://statswales.gov.wales/Catalogue/Community-Safety-and-Social-Inclusion/Welsh-Index-of-Multiple-Deprivation/Archive/WIMD-2014). Because IMD measures between countries are not directly comparable, country was included in statistical models as a 3-level factor, and each country's complete set of IMD ranks was rescaled to the range of 0 to 1, with 1 corresponding to the least deprived area.

We determined country of residence and urban/rural status by referring to the National Statistics Postcode Look-up (https://geoportal.statistics.gov.uk/datasets/4f71f3e9806d4ff895996f832eb7aacf). The recorded centroid associated with each postal code was used to place each client within a 1-km^2 gridded cell, and each EHR was hence associated with an estimate of the number of dogs or cats within each 1-km^2 gridded cell as defined by Aegerter et al. (*30*). We then used postal code district to provide an estimate of the number of dogs or cats per household for each recorded postal code (*30*).

Veterinary Practice and Practitioner Factors

We used the Royal College of Veterinary Surgeons (RCVS) Practice Register (https://findavet.rcvs.org.

uk/home, accessed 2016 Oct 18) to summarize each veterinary practice into 4 categories of advertised species treated: companion animal; mixed (companion animal, large animal, and equine); companion and large animal; and companion animal and equine. Practices were considered accredited under the voluntary RCVS Practice Standards Scheme if ≥1 site was recorded as accredited (Core Standards, General Practice, or Veterinary Hospital), and as an RCVS Veterinary Hospital if the practice contained a veterinary hospital site. We also recorded practices listing referrals as an interest and practices employing ≥1 veterinary surgeon holding RCVS Advanced Veterinary Practitioner status or separate RCVS Specialist status in areas of relevance to companion animals.

Statistical Analyses

We used R (https://www.r-project.org) for all analyses. Descriptive proportions and 95% CIs were adjusted for clustering within sites (bootstrap method, n = 5,000 samples). Using the R package lme4 (https://cran.r-project.org/web/packages/lme4/index.html), we fitted univariable and multivariable mixed effects logistic regression models separately for dogs and cats. Because likelihood ratio tests (LRTs), the Akaike Information Criterion (AIC), the Bayesian Information Criterion (BIC), and evidence of interpractice antimicrobial prescription frequency variation (22) indicated that observations were clustered within veterinary practice, site, and animal, we therefore included all 3 factors as random intercepts in all models. We conducted separate analyses to assess the association between explanatory variables and 3 binary outcomes of interest: antimicrobial prescription authorized for systemic administration (systemic antimicrobial), topical administration (topical antimicrobial), and systemically administered HPCIAs.

Initial univariable screening included 15 categorical variables (sex, neutered status, microchip status, insurance status, vaccination status, genetic breed group, country of residence, client urban/rural status, main presenting complaint, treated species [practice type], RCVS accreditation, RCVS Veterinary Hospital, referral interest, RCVS Advanced Veterinary Practice, and RCVS specialist), and 4 continuous variables (age at consultation, rescaled IMD [rIMD] rank, dog or cat population per square kilometer, and mean number of dogs or cats per household at district of residence). For continuous explanatory variables, we included up to cubic polynomial terms if an LRT, AIC, and BIC indicated significantly improved fit, compared with linear and lesser polynomial terms. Explanatory variables were retained for multivariable analysis if an LRT indicated $p \leq 0.20$ against a null model.

To minimize AIC and BIC, we conducted manual stepwise backward elimination on multivariable models. A 2-way interaction between rIMD and the 3-level factor country was included in the initial multivariable model (and were deleted if AIC and BIC decreased); country alone was a false intercept. Confounding was accounted for by assessing effect variation upon removal of variables. Two-way interaction terms between other explanatory variables were assessed by using AIC, BIC, and an LRT. The variance inflation factor was used to assess multicollinearity (https://CRAN.R-project.org/package=car). For continuous variables, projected prescription probabilities and associated 95% CIs were calculated from log odds by using sjPlot (https://cran.r-project.org/web/packages/sjPlot/index.html). Statistical significance was defined as $p<0.05$.

Results

Analyzed data were from 281,543 consultations for sick dogs (155,732 unique dogs) and 111,139 sick cats (69,236 unique cats) from 173 veterinary practices (379 sites). A descriptive population summary is shown in Table 1, and a summary of genetic breed groups included in this study is shown in Appendix Table 2.

Dogs

Prescription of Antimicrobial Drugs

Systemic antimicrobial drugs were prescribed during 25.7% (95% CI 24.9%–26.6%) of consultations, topical antimicrobials during 14.2% (95% CI 13.9%–14.6%), and systemic HPCIAs during 1.4% (95% CI 1.2%–1.6%). The most commonly prescribed class of systemic HPCIAs was fluoroquinolones (0.9% of sick animal consultations, 95% CI 0.7%–1.0%), followed by third-generation cephalosporins (0.5%, 95% CI 0.4%–0.6%) and macrolides (0.1%, 95% CI 0.0%–0.2%). Antimicrobial prescription summarized according to common consultation by breed is shown in Appendix Table 3.

Prescription of Systemic Antimicrobial Drugs

Descriptive analyses and univariable model results are summarized in Appendix Table 4. Final multivariable model results are available in Table 2. Systemic antimicrobial drugs were less likely to be prescribed for vaccinated or neutered dogs than for nonvaccinated or non-neutered dogs. Systemic antimicrobial drugs were also less likely to be prescribed for insured dogs up to ≈12 years of age (Figure 1, panel

A). Odds for prescription of a systemic antimicrobial drug were greater for dogs with an MPC that was respiratory than for those with a gastroenteric MPC. Mixed practices were associated with significantly increased odds of this prescription compared with practices treating companion animals only. RCVS-accredited practices were less likely to prescribe a systemic antimicrobial.

Prescription of Systemic HPCIAs

Descriptive analyses and univariable model results are summarized in Appendix Table 5. Final multivariable model results are available in Table 3. Systemic HPCIAs were less likely to be prescribed for vaccinated or insured dogs; highest odds for prescription were for dogs with a respiratory MPC. Odds increased with age (Figure 2, panel A). In terms of genetic breed, the greatest odds of systemic HPCIA prescription were for the toy breed group, compared with retrievers.

Prescription of Topical Antimicrobial Drugs

Descriptive analyses and univariable model results are summarized in Appendix Table 6. Final multivariable model results are available in Table 4 (https://wwwnc.cdc.gov/EID/article/26/8/19-1786-T4.htm). Topical antimicrobial drugs were less likely to be prescribed for insured dogs, although odds increased significantly for male, microchipped, or vaccinated dogs. The effect of age varied according to MPC; an MPC of pruritus was generally associated with greatest odds of topical antimicrobial drug prescription throughout life, broadly decreasing with increased age (Figure 3, panel A). Odds of topical antimicrobial drug prescription were lowest for sight hounds compared with retrievers. Practices employing RCVS specialists were less likely to prescribe a topical antimicrobial.

Cats

Prescription of Antimicrobial Drugs

Systemic antimicrobial drugs were prescribed during 32.9% (95% CI 31.9–33.8) of consultations, topical antimicrobials during 6.1% (95% CI 5.9–6.3), and systemic HPCIAs during 17.3% (95% CI 16.2–18.4). The most commonly prescribed class of systemic HPCIA was third-generation cephalosporins (16.4% of consultations for sick cats, 95% CI 15.3–17.6), followed by fluoroquinolones (0.7%, 95% CI 0.4–0.9) and macrolides (0.03%, 95% CI 0.0–0.05). Antimicrobial prescription summarized according to common consultation by breed is shown in Appendix Table 7.

Prescription of Systemic Antimicrobial Drugs

Descriptive analyses and univariable model results are summarized in Appendix Table 8. Final multivariable model results are available in Table 5. Odds of systemic antimicrobial prescription were significantly reduced for vaccinated or insured cats. Odds were highest for cats with respiratory and trauma MPCs, although there was a significant interaction between sex and MPC; male cats presented for trauma were significantly more likely than female cats to receive an antimicrobial prescription. Systemic antimicrobial drugs were also less likely to be prescribed for female cats up to ≈15 years of age, when odds for female cats exceeded those for male cats (Figure 1, panel b). Mixed practices were more likely than practices treating companion animals only to prescribe a systemic antimicrobial drug.

Prescription of Systemic HPCIA Drugs

Descriptive analyses and univariable model results are summarized in Appendix Table 9. Final multivariable model results are available in Table 6. Systemic HPCIA drugs were less likely to be prescribed for vaccinated or insured cats. Although odds of prescription were greatest for cats with a respiratory MPC, RCVS-accredited practices were associated with increased odds for cats presented for trauma. Probability of prescription increased for cats up to 6–9 years of age, reduced until ≈18 years of age, and increased again thereafter; prescription was more likely for male cats 5–14 years of age (Figure 2, panel B). In terms of genetic breed, the greatest odds of systemic HPCIA prescription were for the Asian group compared with the West Europe group.

Prescription of Topical Antimicrobial Drugs

Descriptive analyses and univariable model results are summarized in Appendix Table 10. Final multivariable model results are available in Table 7. Topical antimicrobial drugs were less likely to be prescribed for insured cats. The effect of age at consultation varied according to MPC; probability of prescription decreased for pruritic cats until ≈7 years of age, before increasing again (Figure 3, panel B). In terms of genetic breed, odds were smallest for crossbreeds compared with those in the West Europe genetic breed group.

Discussion

We demonstrated frequent prescription of antimicrobial drugs, including systemic HPCIAs (particularly in cats), in veterinary practices in Great Britain. Considering the importance of HPCIAs in the context of antimicrobial resistance (*32*), we identified

a vital need to learn more about factors potentially driving such prescribing behaviors. We further augmented EHR data with a range of external data sources to identify key client, animal, and practice-related risk factors associated with prescription of systemic and topical antimicrobial and systemic HPCIA drugs; such factors potentially inform key antimicrobial stewardship targets of importance to companion animal practice.

Regarding client care decision-related factors, odds of prescription for systemic antimicrobial and HPCIA drugs were significantly lower for vaccinated dogs and cats, possibly reflecting perceived or actual reduced risk for antimicrobial drug–responsive disease in vaccinated animals. Although most companion animal vaccines target viruses, bacterial infection secondary to vaccine-preventable viral disease has been documented (*33*). Risk avoidance plays a major role in antimicrobial drug–prescribing practices (*12*), potentially prompting more frequent prescription for unwell, nonvaccinated animals. We speculate that previous engagement with preventive healthcare services might select for clients more likely to seek veterinary attention earlier or to pursue diagnostic options rather than empirical prescription. Regardless of what might be driving these trends, the O'Neill report recommends that promoting development and use of vaccines and alternatives to antibiotics should form a key component of efforts to curtail human dissemination of antimicrobial resistance (*34*); our

Table 1. Descriptive demographic summary of consultations for sick dogs and cats in study of factors associated with prescription of antimicrobial drugs for dogs and cats, United Kingdom, 2014–2016*

Category	Dogs, n = 281,543	Cats, n = 111,139
Categorical factors		
Country		
England	86.6 (81.4–91.9)	88.6 (83.8–93.5)
Scotland	6.1 (3.0–9.1)	4.5 (2.1–6.9)
Wales	7.4 (2.8–12.0)	7.0 (2.1–6.9)
Sex		
M	51.8 (51.3–52.3)	51.8 (51.3–52.4)
F	48.2 (47.7–48.7)	48.2 (47.6–48.7)
Neutered	64.6 (63.3–65.9)	82.8 (81.7–84.0)
Microchipped	54.4 (52.4–56.3)	37.8 (36.0–39.5)
Vaccinated	70.0 (68.6–71.3)	52.7 (51.2–54.1)
Insured	33.5 (31.1–35.9)	19.3 (17.3–21.3)
Urban	63.8 (59.5–68.1)	70.2 (66.2–74.2)
Main presenting complaint		
Gastroenteric	11.3 (11.0–11.6)	8.3 (8.0–8.7)
Respiratory	4.0 (3.8–4.1)	5.5 (5.2–5.8)
Pruritus	18.0 (17.3–18.6)	10.3 (9.9–10.7)
Trauma	16.8 (16.1–17.5)	17.0 (16.3–17.7)
Tumor	6.0 (5.8–6.3)	3.9 (3.6–4.1)
Kidney disease	0.7 (0.6–0.8)	2.9 (2.5–3.2)
Other unwell	43.3 (42.0–44.6)	52.1 (50.9–53.4)
Practice type		
Mixed	22.7 (15.1–30.3)	18.1 (11.6–24.6)
Companion animal	70.6 (62.4–78.8)	76.0 (68.9–83.1)
Companion and equine	2.4 (0.7–4.0)	2.3 (0.7–4.0)
Companion and large	4.3 (0.4–8.2)	3.5 (0.3–6.8)
Accredited	83.9 (77.1–90.6)	83.5 (76.5–90.5)
Hospital status	20.2 (14.4–26.0)	20.0 (14.5–25.5)
Referral interest	27.9 (20.9–34.9)	27.3 (20.3–34.2)
Employed RCVS AVP†	24.5 (17.2–31.7)	26.7 (19.2–34.2)
Employed RCVS specialist†	2.5 (0.8–4.2)	1.9 (0.6–3.1)
Continuous factors		
Age at consultation		
Mean	7.1 (7.1–7.2)	9.5 (9.5–9.6)
Median (min–max)	7.2 (0–22)	9.7 (0–25.9)
Rescaled indices of multiple, mean	0.59 (0.59–0.60)	0.60 (0.60–0.61)
rIMD deprivation rank, median (min–max)	0.62 (0.0–1.0)	0.63 (0.0–1.0)
Animals/household (*30*)		
Mean	0.59 (0.59–0.59)	0.50 (0.49–0.50)
Median (min–max)	0.47 (0–6.0)	0.39 (0–3.6)
Animals/km^2 (*30*)		
Mean	399.4 (397.8–401.0)	409.4 (407.0–411.8)
Median (min–max)	266 (0–4,360)	288 (0–5,363)

*Values are % consults (95% CI) except as indicated. AVP, Advanced Veterinary Practitioner; max, maximum; min, minimum; rIMD, rescaled Indices of Multiple Deprivation; RCVS, Royal College of Veterinary Surgeons;
†At least 1 employed veterinary surgeon holding RCVS AVP status, specialist status, or both.

Table 2. Results from a multivariable mixed effect logistic regression model assessing the association between a range of categorical animal, owner, practitioner and practice-related factors and the probability of prescribing a systemic antimicrobial for dogs, United Kingdom, 2014–2016*

Category	β	SE	OR (95% CI)	p value
Intercept				
England	−0.08	0.08	0.93 (0.80–1.08)	NA
Scotland	−0.06	0.09	0.94 (0.79–1.12)	NA
Wales	−0.13	0.09	0.88 (0.73–1.05)	NA
Categorical factors				
Initial complaint				
Gastroenteric	NA	NA	Referent	NA
Kidney disease	−0.38	0.06	0.68 (0.61–0.76)	**<0.01**
Other unwell	−0.94	0.02	0.39 (0.38–0.40)	**<0.01**
Pruritus	−0.68	0.02	0.51 (0.49–0.53)	**<0.01**
Respiratory	0.10	0.03	1.11 (1.06–1.17)	**<0.01**
Trauma	−0.89	0.02	0.41 (0.40–0.43)	**<0.01**
Tumor	−1.18	0.03	0.31 (0.29–0.32)	**<0.01**
Neuter status				
Not neutered	NA	NA	Referent	NA
Neutered	−0.11	0.01	0.90 (0.88–0.92)	**<0.01**
Sex				
F	NA	NA	Referent	NA
M	−0.03	0.01	0.97 (0.95–0.99)	**0.01**
Vaccination status				
Not vaccinated	NA	NA	Referent	NA
Vaccinated	−0.08	0.01	0.93 (0.90–0.95)	**<0.01**
Insurance status				
Not insured	NA	NA	Referent	NA
Insured	−0.14	0.02	0.87 (0.84–0.90)	**<0.01**
Genetic breed group (*29*)				
Retriever	NA	NA	Referent	NA
Ancient/spitz	0.25	0.05	1.28 (1.17–1.40)	**<0.01**
Crossbreed	0.06	0.02	1.06 (1.03–1.10)	**<0.01**
Herding	0.14	0.03	1.15 (1.09–1.22)	**<0.01**
Mastiff-like	0.15	0.02	1.16 (1.11–1.21)	**<0.01**
Scent hound	0.10	0.04	1.11 (1.03–1.19)	**<0.01**
Sight hound	0.31	0.04	1.36 (1.25–1.48)	**<0.01**
Small terrier	0.16	0.02	1.18 (1.13–1.22)	**<0.01**
Spaniel	0.16	0.02	1.17 (1.13–1.22)	**<0.01**
Toy	−0.00	0.03	1.00 (0.94–1.05)	0.92
Unclassified	0.11	0.02	1.12 (1.07–1.16)	**<0.01**
Unknown	0.09	0.05	1.09 (0.99–1.21)	0.075
Working dog	0.19	0.03	1.21 (1.15–1.27)	**<0.01**
Practice type				
Companion animal	NA	NA	Referent	NA
Mixed	0.14	0.07	1.15 (1.01–1.30)	**0.04**
Companion and equine	−0.05	0.15	0.95 (0.71–1.27)	0.73
Companion and large	0.13	0.14	1.14 (0.86–1.50)	0.37
Accreditation status				
None	NA	NA	Referent	NA
≥1 accredited site	−0.24	0.08	0.79 (0.68–0.92)	**<0.01**
Referral interest				
No	NA	NA	Referent	NA
Yes	−0.10	0.05	0.91 (0.82–1.00)	0.06
Continuous factors				
Age				
Linear	−1.12	0.01	0.89 (0.87–0.91)	**<0.01**
Quadratic	−0.09	0.01	0.92 (0.90–0.93)	**<0.01**
Cubic	0.05	0.01	1.05 (1.04–1.07)	**<0.01**
Interaction terms				
Insurance status (insured) and age				
Linear age interaction	0.08	0.02	1.09 (1.04–1.14)	**<0.01**
Quadratic age interaction	0.03	0.01	1.03 (1.00–1.06)	**0.03**
Cubic age interaction	−0.03	0.01	0.97 (0.95–1.00)	**0.02**

*n = 72,436/281,543 sick consultations. Random effect variance (± SD): animal 0.57 (± 0.76), site 0.05 (0.23), practice 0.06 (0.24). Boldface indicates significance (p<0.05). NA, not applicable; OR, odds ratio.

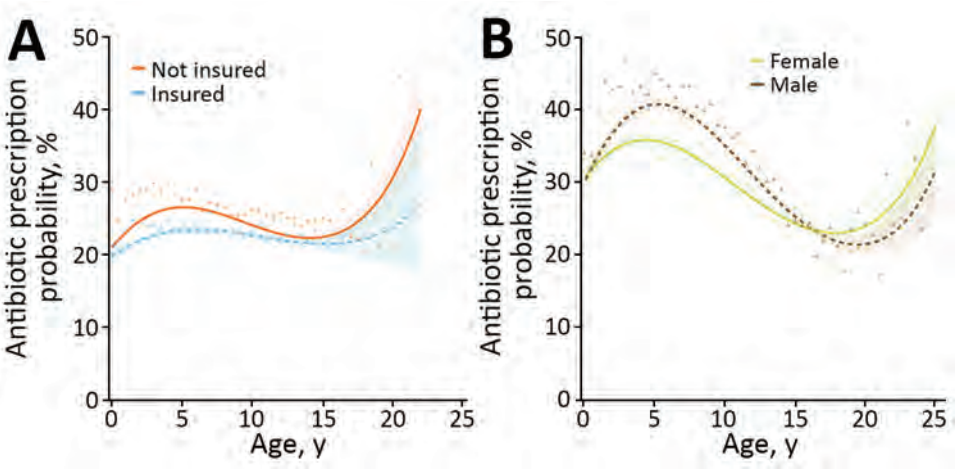

Figure 1. Results from 2 multivariable mixed effect logistic regression models predicting probability of systemic antimicrobial prescription in study of factors associated with prescription of antimicrobial drugs for dogs and cats, United Kingdom, 2014–2016. Modeling is shown for sick dogs (A) and cats (B) against age of the animal at time of consultation, in years. For dogs, an interaction term considering current insurance status has been included; for cats, an interaction term considering sex has been included. Lines refer to predicted probability; shading relates to 95% CIs for such predictions. Points and triangles are plotted to show original data points expressing the percentage of animals of each relevant age group (rounded to 0.5-year groups) for which a systemic antimicrobial was prescribed, according to the dataset analyzed.

findings suggest that such recommendations should also be considered for companion animals.

Insurance coverage was associated with decreased odds of prescription of systemic and topical antimicrobial drugs, potentially highlighting veterinary practitioners being more likely to seek a wider range of diagnostic options in preference to empirical antibiosis for insured animals. However, insured dogs were also associated with increased odds of prescription of systemic HPCIA drugs. Cost of therapy has been shown to influence choice of antimicrobial agent for companion animals (*17*), and HPCIA drugs are anecdotally considered a more expensive option than other antimicrobial drugs. Hence, our findings might reflect increased willingness to prescribe relatively expensive antimicrobial drugs for insured dogs.

Although HPCIA drug classification remains under debate, use of HPCIA drugs has formed a focus for antimicrobial resistance–related policy (*34*). Although several classes of HPCIA drugs (e.g., glycopeptides, which are not authorized for use in animals) are very rarely prescribed for companion animals in the United Kingdom (*22*), prescription of fluoroquinolones and third-generation cephalosporins (particularly for cats) is relatively common, although current antimicrobial drug prescribing guidance strongly discourages such practices (*35*).

With regard to animal-intrinsic factors, odds for prescription of systemic antimicrobial drugs were increased for younger male cats, although the opposite was found for dogs. Sex-based variation in risk for bacterial infection has been identified (*36*–*38*), and cat fight–related injuries are a frequently recorded clinical complaint (*39*), more commonly associated with young outdoor-ranging male cats (*40*). Indeed, we found that systemic antimicrobial drugs were more commonly prescribed for male cats presented for trauma. Furthermore, time of injury is less likely to be known for outdoor-ranging cats than for dogs; such uncertainty might prompt a more cautious approach to prescription of antimicrobial drugs (*41*).

Other studies have also identified age- or sex-related variation in risk for antimicrobial resistance (*36*–*38*). For instance, Radford et al. demonstrated decreased probability of systemic antimicrobial prescription with increased patient age (*20*), potentially reflecting increased actual or perceived incidence of noncommunicable disease as animals age. This interpretation might partly explain our findings, although we noted an exception with prescription of systemic HPCIA drugs. For cats, an easy-to-administer (injectable) long-acting third-generation cephalosporin formulation is widely used (*21*–*23*). Although not completely explanatory, our findings may suggest that as an animal ages, the client or veterinarian perceives an increased probability of an animal being refractory to an intervention (e.g., oral administration of tablets), increasing the likelihood of a prescriber choosing easy-to-administer formulations. A previously identified key influencer of antimicrobial agent choice was administration of inappropriate dosages as a result of noncompliance (*17*). Whether the risk for antimicrobial resistance posed by a possible underdose of a first-line antimicrobial outweighs the risk posed by the labeled dose of a third-line HPCIA drug remains unanswered.

As with humans (*10*,*11*,*13*), prescription of systemic antimicrobial drugs for dogs and cats was most

commonly associated with respiratory clinical signs. Humans having respiratory conditions are often inappropriately prescribed antimicrobial drugs; most respiratory conditions are viral or noninfectious in origin (*10*). The same has also been shown for companion animals, although bacterial infection secondary to primary viral disease has been documented (*42*). Considering these shared patterns, although prescribing guidance is available (*43*), we suggest respiratory disease as a pertinent area for further investigation of One Health antimicrobial stewardship intervention methods.

Increased odds of prescription of topical antimicrobial drugs was commonly associated with the retriever group of dogs, which contains several breeds commonly associated with dermatologic disease (*44*). This finding and interpretation is plausible, suggesting that the breed summarization technique used here to combat the modeling issues posed by the >250 dog and >50 cat breeds recorded in this dataset was useful. However, genetic linkage does not necessarily imply phenotypic similarity. As such, individual breed-level phenotypes might be responsible for conferring variant bacterial infection risk in ways not explored, and indeed potentially masked. In future analyses, we will aim to identify additional means by which breeds can be effectively summarized according to shared genotype and phenotype.

Although the individual animal accounted for most of the random effect variance seen in this study, veterinary-led factors might well yield more readily accessible routes toward stewardship. For site accreditation, the voluntary RCVS Practice Standards Scheme requires antimicrobial drug use policies,

Table 3. Results from a multivariable mixed effect logistic regression model assessing the association between a range of categorical animal, owner, practitioner and practice-related factors and the probability of prescribing a systemic highest priority critically important antimicrobial drug for dogs, United Kingdom, 2014–2016*

Category	β	SE	OR (95% CI)	p value
Intercept				
England	−4.77	0.11	0.01 (0.01–0.01)	NA
Scotland	−4.91	0.21	0.01 (0.01–0.01)	NA
Wales	−4.88	0.22	0.01 (0.01–001)	NA
Categorical factors				
Main presenting complaint				
Gastroenteric	NA	NA	Referent	NA
Kidney disease	0.11	0.18	1.12 (0.78–1.60)	0.55
Other unwell	−0.33	0.06	0.72 (0.64–0.80)	**<0.01**
Pruritus	−0.23	0.07	0.79 (0.70–0.90)	**<0.01**
Respiratory	0.29	0.09	1.33 (1.13–1.57)	**<0.01**
Trauma	−1.16	0.08	0.31 (0.27–0.37)	**<0.01**
Tumor	−0.92	0.11	0.40 (0.32–0.49)	**<0.01**
Vaccination status				
Not vaccinated	NA	NA	Referent	NA
Vaccinated	−0.10	0.04	0.91 (0.83–0.99)	**0.03**
Insurance status				
Not insured	NA	NA	Referent	NA
Insured	0.15	0.05	1.16 (1.07–1.27)	**<0.01**
Genetic breed group (*29*)				
Retriever	NA	NA	Referent	NA
Ancient/spitz	0.12	0.22	1.13 (0.73–1.74)	0.60
Crossbreed	0.24	0.08	1.27 (1.09–1.48)	**<0.01**
Herding	0.04	0.12	1.04 (0.82–1.32)	0.73
Mastiff-like	0.16	0.10	1.17 (0.97–1.43)	0.11
Scent hound	0.67	0.13	1.96 (1.52–2.52)	**<0.01**
Sight hound	0.43	0.17	1.54 (1.10–2.15)	**0.01**
Small terrier	0.67	0.08	1.96 (1.67–2.29)	**<0.01**
Spaniel	0.45	0.08	1.57 (1.33–1.84)	**<0.01**
Toy	0.94	0.10	2.56 (2.10–3.12)	**<0.01**
Unclassified	0.39	0.09	1.47 (1.24–1.74)	**<0.01**
Unknown	0.23	0.22	1.25 (0.81–1.94)	0.31
Working dog	0.45	0.11	1.56 (1.27–1.93)	**<0.01**
Continuous factors				
Age				
Linear	0.19	0.04	1.21 (1.12–1.31)	**<0.01**
Quadratic	−0.06	0.03	0.95 (0.90–0.99)	**0.03**
Cubic	0.04	0.02	1.04 (1.01–1.08)	**0.01**

*n = 3,971/281,543 sick consultations. Random effect variance (± SD): animal 3.04 (1.74), site 0.13 (0.36), practice 0.44 (0.66). Significant (p<0.05) results are displayed in boldface. NA, not applicable; OR, odds ratio.

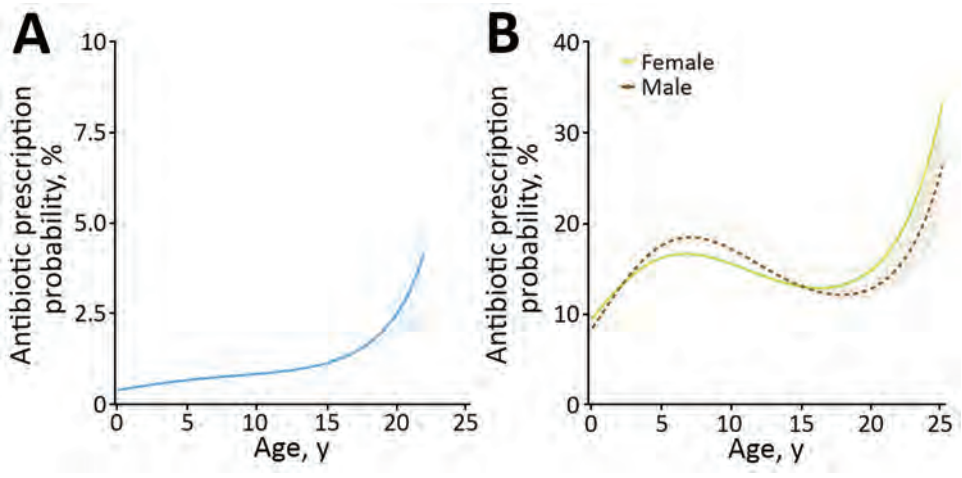

Figure 2. Results from 2 multivariable mixed effect logistic regression models predicting probability of systemic highest priority critically important antimicrobial (HPCIA) prescription in study of factors associated with prescription of antimicrobial drugs for dogs and cats, United Kingdom, 2014–2016. Modeling is shown for sick dogs (A) and cats (B) against age of the animal at time of consultation, in years. For cats, an interaction term considering sex has been included. Lines refer to predicted probability; shading relates to 95% CIs for such predictions. Points and triangles are plotted to show original data points expressing the percentage of animals of each relevant age group (rounded to 0.5-year groups) for which a systemic HPCIA was prescribed, according to the dataset analyzed.

infection control plans, and established clinical audits (*45*), and we observed reduced systemic antimicrobial prescription odds for dogs in accredited practices. Although practices seeking accreditation might already be more engaged with quality improvement, we nevertheless recommend further consideration as to whether the RCVS Practice Standards Scheme could play a more central role for encouraging stewardship in general and referral practices.

Compared with practices that treat companion animals only, mixed species practices were associated with increased odds of prescription of systemic antimicrobial drugs. Veterinary surgeons employed in different sectors expressed varied attitudes toward antimicrobial resistance (*16*), a finding perhaps demonstrated on a wide scale in this study. Practices employing RCVS specialists were also associated with reduced odds of prescription of topical antimicrobial drugs for dogs, potentially reflecting varied case management approaches (*46*) or caseloads compared with general practices.

Considering limitations of this study, although we successfully augmented EHRs with a variety of data sources, no dataset is infallible. For instance, the veterinary surgeon employment record of the RCVS Practice Register is updated only on an ad hoc basis. It is thus possible that the surveyed veterinary surgeon population varied over the 2-year study period in ways not captured here. Veterinary practices participating in SAVSNET are recruited by convenience and might not be representative of the wider UK population. Although we found no clear associations between IMD or pet population density and prescription, the complexities of summarizing IMD across the

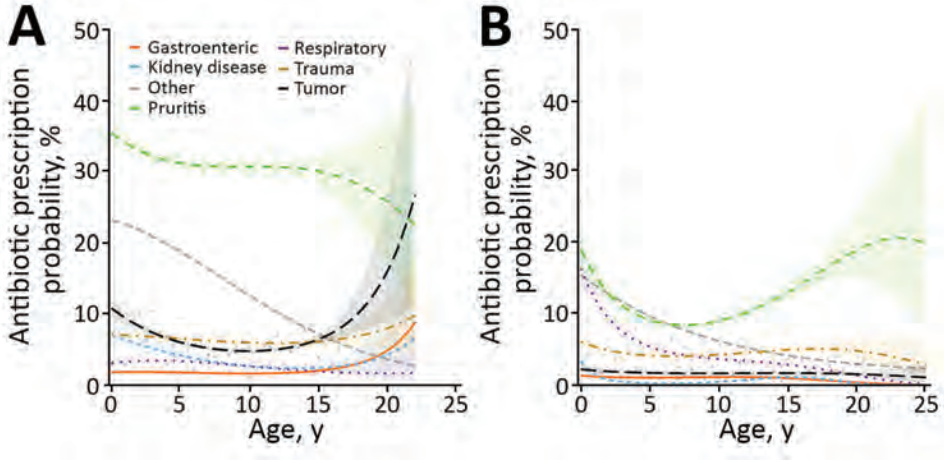

Figure 3. Results from 2 multivariable mixed effect logistic regression models predicting probability of topical antimicrobial prescription in study of factors associated with prescription of antimicrobial drugs for dogs and cats, United Kingdom, 2014–2016. Modeling is shown for sick dogs (A) and cats (B) against age of the animal at time of consultation, in years. For both species, an interaction term considering main reason for visit (main presenting complaint) has been included. Lines refer to predicted probability; shading relates to 95% CIs for such predictions. Points are plotted to show original data points expressing the percentage of animals of each relevant age group (rounded to 0.5-year groups) for which a topical antimicrobial was prescribed, according to the dataset analyzed.

Table 5. Results from a multivariable mixed effect logistic regression model assessing the association between a range of categorical animal, owner, practitioner and practice-related factors and the probability of prescribing a systemic antimicrobial in cats, United Kingdom, 2014–2016*

Category	β	SE	OR (95% CI)	p value
Intercept				
England	−0.81	0.06	0.45 (0.39–0.50)	NA
Scotland	−0.77	0.10	0.46 (0.38–0.57)	NA
Wales	−0.55	0.12	0.58 (0.46–0.72)	NA
Categorical factors				
Main presenting complaint				
Gastroenteric	NA	NA	Referent	NA
Kidney disease	−0.20	0.07	0.82 (0.71–0.94)	**0.01**
Other unwell	−0.23	0.04	0.79 (0.73–0.85)	**<0.01**
Pruritus	−0.37	0.05	0.69 (0.63–0.76)	**<0.01**
Respiratory	0.91	0.06	2.48 (2.23–2.77)	**<0.01**
Trauma	0.59	0.04	1.80 (1.65–1.97)	**<0.01**
Tumor	−0.56	0.07	0.57 (0.50–0.65)	**<0.01**
Sex				
F	NA	NA	Referent	NA
M	0.03	0.05	1.03 (0.93–1.14)	0.59
Vaccination status				
Not vaccinated	NA	NA	Referent	NA
Vaccinated	−0.09	0.02	0.92 (0.89–0.95)	**<0.01**
Insurance status				
Not insured	NA	NA	Referent	NA
Insured	−0.19	0.02	0.82 (0.79–0.86)	**<0.01**
Genetic breed group (*31*)				
West Europe	NA	NA	Referent	NA
Asian	0.20	0.05	1.22 (1.10–1.36)	**<0.01**
Crossbreed	0.14	0.03	1.16 (1.08–1.23)	**<0.01**
Mediterranean	0.36	0.26	1.43 (0.86–2.38)	0.17
Unclassified	0.11	0.06	1.11 (0.99–1.24)	0.07
Unknown	0.13	0.05	1.14 (1.03–1.26)	**0.01**
Practice type				
Companion animal	NA	NA	Referent	NA
Mixed	0.18	0.08	1.20 (1.03–1.39)	**0.02**
Companion and equine	−0.01	0.18	1.00 (0.70–1.41)	0.98
Companion and large	0.10	0.17	1.10 (0.80–1.53)	0.56
Referral interest				
No	NA	NA	Referent	NA
Yes	−0.08	0.06	0.92 (0.82–1.04)	0.18
Employed RCVS AVP†				
None	NA	NA	Referent	NA
≥1 AVP	−0.10	0.07	0.90 (0.79–1.04)	0.16
Continuous factors				
Age				
Linear	−0.38	0.02	0.69 (0.66–0.72)	**<0.01**
Quadratic	−0.08	0.01	0.90 (0.90–0.95)	**<0.01**
Cubic	0.10	0.01	1.08 (1.08–1.12)	**<0.01**
Cats per km^2 (*30*)				
Linear	−0.02	0.01	0.98 (0.97–1.00)	**0.02**
Interaction terms				
Male sex and age				
Linear age interaction	−0.10	0.03	0.91 (0.85–0.97)	**<0.01**
Quadratic age interaction	−0.10	0.02	0.91 (0.88–0.94)	**<0.01**
Cubic age interaction	0.03	0.02	1.03 (1.00–1.06)	0.11
Male sex and main presenting complaint				
Kidney disease	−0.26	0.11	0.77 (0.62–0.96)	**0.02**
Other unwell	0.17	0.05	1.19 (1.07–1.32)	**<0.01**
Pruritus	0.10	0.07	1.10 (0.96–1.26)	0.16
Respiratory	0.06	0.08	1.06 (0.91–1.23)	0.44
Trauma	0.48	0.06	1.62 (1.44–1.82)	**<0.01**
Tumor	0.15	0.10	1.16 (0.96–1.40)	0.12

*n = 36,521/111,139 sick consultations. Random effect variance (± SD): animal 0.50 (0.70), site 0.06 (0.25), practice 0.08 (0.28). Significant (p<0.05) results are displayed in boldface. NA, not applicable; OR, odds ratio;
RCVS, Royal College of Veterinary Surgeons.
†RCVS Advanced Veterinary Practitioner and/or specialist status.

Table 6. Results from a multivariable mixed effect logistic regression model assessing the association between a range of categorical animal, owner, practitioner and practice-related factors and the probability of prescribing a systemic highest priority critically important antimicrobial drug for cats, United Kingdom, 2014–2016*

Category	β	SE	OR (95% CI)	p value
Intercept				
England	–2.79	0.21	0.06 (0.04–0.09)	NA
Scotland	–2.74	0.24	0.07 (0.04–0.10)	NA
Wales	–2.55	0.24	0.08 (0.05–0.12)	NA
Categorical factors				
Main presenting complaint	NA	NA	Referent	NA
Gastroenteric	0.55	0.25	1.74 (1.08–2.82)	**0.02**
Kidney disease	0.59	0.12	1.80 (1.43–2.26)	**<0.01**
Other unwell	1.08	0.13	2.95 (2.28–3.81)	**<0.01**
Pruritus	1.50	0.14	4.47 (3.41–5.85)	**<0.01**
Respiratory	1.06	0.12	2.89 (2.27–3.67)	**<0.01**
Trauma	0.38	0.18	1.46 (1.04–2.03)	**0.03**
Tumor	NA	NA	Referent	NA
Sex	0.12	0.03	1.13 (1.07–1.19)	**<0.01**
F	NA	NA	Referent	NA
M	–0.06	0.02	0.95 (0.91–0.98)	**<0.01**
Vaccination status	NA	NA	Referent	NA
Not vaccinated	–0.14	0.03	0.87 (0.83–0.92)	**<0.01**
Vaccinated	NA	NA	Referent	NA
Insurance status	0.05	0.03	1.05 (1.00–1.11)	0.06
Not insured	NA	NA	Referent	NA
Insured	0.21	0.07	1.23 (1.08–1.40)	**<0.01**
Genetic breed group (*31*)	0.14	0.04	1.16 (1.06–1.26)	**<0.01**
West Europe	0.11	0.32	1.12 (0.59–2.11)	0.73
Asian	0.14	0.07	1.15 (1.00–1.33)	0.06
Crossbreed	0.12	0.06	1.12 (0.99–1.27)	0.07
Accreditation status				
Not accredited	NA	NA	Referent	NA
≥1 accredited site	0.10	0.22	1.10 (0.72–1.69)	0.65
Continuous factors				
Age				
Linear	–0.23	0.03	0.80 (0.76–0.85)	**<0.01**
Quadratic	–0.13	0.02	0.88 (0.85–0.90)	**<0.01**
Cubic	0.13	0.01	1.14 (1.11–1.17)	**<0.01**
Interaction terms				
Main presenting complaint and accreditation (accredited site)				
Kidney disease	0.23	0.26	1.26 (0.76–2.08)	0.37
Other unwell	0.21	0.13	1.23 (0.96–1.58)	0.10
Pruritus	0.00	0.14	1.00 (0.76–1.32)	1.00
Respiratory	0.23	0.15	1.26 (0.94–1.69)	0.12
Trauma	0.64	0.13	1.90 (1.46–2.47)	**<0.01**
Tumor	0.19	0.19	1.21 (0.83–1.75)	0.32
Male sex and age				
Linear age interaction	–0.06	0.04	0.95 (0.87–1.02)	0.17
Quadratic age interaction	–0.09	0.02	0.91 (0.87–0.95)	**<0.01**
Cubic age interaction	0.02	0.02	1.02 (0.98–1.06)	0.32

*n = 19,018/111,139 sick consultations. Random effect variance (± SD): animal 0.68 (0.82, site 0.13 (0.36), practice 0.44 (0.66). Significant (p<0.05) results are displayed in boldface. NA, not applicable; OR, odds ratio.

constituent countries of the United Kingdom (*47*), coupled with the relative infancy of pet population demographic studies (*30*), lead us to recommend re-evaluation as research methods further mature. The analyzed population was relatively skewed toward less deprived areas; to ascertain whether this finding is reflective of the wider UK pet-owning community, including the charity and low-income veterinary sectors in future analyses would be warranted. We advise caution for inferring causal relationships between factors and outcome variables explored in this cross-sectional study; similarly, group-level observations might have limited relevance to individual animals. More generalized SAVSNET limitations have been previously discussed; in brief, quantification of antimicrobial drug prescription depends on practitioners charging for antimicrobial drugs, and analyzed practices were recruited by convenience (*22*,*30*).

In conclusion, we demonstrated the value of using veterinary EHRs collected from a cohort of

Table 7. Results from a multivariable mixed effect logistic regression model assessing the association between a range of categorical animal, owner, practitioner and practice-related factors and the probability of prescribing a topical antimicrobial in cats, United Kingdom, 2014–2016*

Category	β	SE	OR (95% CI)	p value
Intercept				
England	–3.98	0.17	0.02 (0.01–0.03)	-NA
Scotland	–3.94	0.19	0.02 (0.01–0.03)	NA
Wales	–3.91	0.19	0.02 (0.01–0.03)	NA
Categorical factors				
Main presenting complaint				
Gastroenteric	NA	NA	Referent	NA
Kidney disease	–0.98	0.50	0.38 (0.14–1.00)	0.05
Other unwell	1.79	0.16	5.96 (4.37–8.12)	**<0.01**
Pruritus	2.13	0.16	8.37 (6.09–11.51)	**<0.01**
Respiratory	1.21	0.18	3.36 (2.35–4.82)	**<0.01**
Trauma	1.34	0.17	3.82 (2.76–5.28)	**<0.01**
Tumor	0.38	0.25	1.46 (0.90–2.36)	0.12
Sex				
F	NA	NA	Referent	NA
M	0.05	0.03	1.05 (1.00–1.11)	0.06
Neutered status				
Not neutered	NA	NA	Referent	NA
Neutered	–0.06	0.04	0.94 (0.88–1.01)	0.09
Insurance status				
Not insured	NA	NA	Referent	NA
Insured	–0.13	0.04	0.88 (0.82–0.95)	**<0.01**
Genetic breed group (*31*)				
West Europe	NA	NA	Referent	NA
Asian	–0.14	0.09	0.87 (0.73–1.03)	0.09
Crossbreed	–0.50	0.05	0.61 (0.55–0.67)	**<0.01**
Mediterranean	–0.40	0.50	0.67 (0.25–1.78)	0.42
Unclassified	–0.24	0.09	0.79 (0.66–0.95)	**0.01**
Unknown	–0.43	0.08	0.65 (0.56–0.77)	**<0.01**
Referral interest				
No	NA	NA	Referent	NA
Yes	0.08	0.05	1.08 (0.98–1.19)	0.11
Continuous factors				
Age				
Linear	0.08	0.26	1.09 (0.65–1.82)	0.75
Quadratic	–0.12	0.14	0.89 (0.68–1.17)	0.40
Cubic	–0.14	0.14	0.87 (0.66–1.15)	0.34
Interaction terms				
Main presenting complaint and age				
Linear age interaction				
Kidney disease	1.14	0.68	3.11 (0.82–11.84)	0.10
Other unwell	–0.61	0.27	0.54 (0.32–0.91)	**0.02**
Pruritus	0.18	0.27	1.19 (0.70–2.03)	0.52
Respiratory	–0.34	0.31	0.71 (0.39–1.29)	0.26
Trauma	0.07	0.28	1.07 (0.62–1.85)	0.81
Tumor	–0.07	0.38	0.93 (0.44–1.95)	0.85
Quadratic age interaction				
Kidney disease	0.52	0.32	1.69 (0.89–3.18)	0.11
Other unwell	0.16	0.14	1.17 (0.89–1.53)	0.26
Pruritus	0.42	0.14	1.52 (1.15–2.02)	**<0.01**
Respiratory	0.26	0.16	1.29 (0.95–1.77)	0.11
Trauma	0.22	0.15	1.24 (0.93–1.65)	0.14
Tumor	0.16	0.20	1.18 (0.80–1.73)	0.41
Cubic age interaction				
Kidney disease	–0.51	0.33	0.60 (0.31–1.16)	0.13
Other unwell	0.14	0.14	1.15 (0.87–1.52)	0.33
Pruritus	0.04	0.15	1.04 (0.78–1.38)	0.81
Respiratory	–0.03	0.16	0.97 (0.70–1.33)	0.84
Trauma	0.06	0.15	1.06 (0.79–1.42)	0.70
Tumor	0.10	0.19	1.10 (0.75–1.61)	0.62

*n = 6,769/111,139 sick consultations. Random effect variance (± SD): animal 0.82 (0.90,) site 0.02 (0.15), practice 0.03 (0.16). Significant (p<0.05) results are displayed in boldface. OR, odds ratio; RCVS, Royal College of Veterinary Surgeons.

veterinary practices to identify a range of factors associated with prescription of antimicrobial drugs for dogs and cats. Although factors influencing decision-making remain multifactorial and complex, our findings suggest that gathering clinical evidence surrounding respiratory disease might be of value to stewardship. Preventive healthcare could also play a role in stewardship and should form the basis of client-targeted health messaging, as should the RCVS Practice Standards Scheme for veterinary practitioners.

Acknowledgments

We thank data providers in veterinary practice (VetSolutions, Teleos, CVS, and other practitioners) and in veterinary diagnostics, without whose support and participation this research would not have been possible. We are especially grateful for the help and support provided by SAVSNET team members Susan Bolan, Bethaney Brant, and Steven Smyth.

This work was funded by The Veterinary Medicines Directorate (VM0520), the University of Liverpool, and SAVSNET. We are grateful for the support and major funding from the Biotechnology and Biological Sciences Research Council and the British Small Animal Veterinary Association, as well as for sponsorship from the Animal Welfare Foundation.

About the Author

Dr. Singleton is a veterinary surgeon working as a postdoctoral research associate at the University of Liverpool. His research interests are observational and interventional epidemiology, health informatics, and antimicrobial resistance within a One Health framework. Much of his work has used electronic health record data collated by SAVSNET.

References

1. Rantala M, Lahti E, Kuhalampil J, Pesonen S, Järvinen AK, Saijonmaa-Koulumies, et al. Antimicrobial resistance in *Staphylococcus* spp., *Escherichia coli* and *Enterococcus* spp. in dogs given antibiotics for chronic dermatological disorders, compared with non-treated control dogs. Acta Vet Scand. 2004;45:37–45. https://doi.org/10.1186/1751-0147-45-37
2. Trott DJ, Filippich LJ, Bensink JC, Downs MT, McKenzie SE, Townsend KM, et al. Canine model for investigating the impact of oral enrofloxacin on commensal coliforms and colonization with multidrug-resistant *Escherichia coli*. J Med Microbiol. 2004;53:439–43. https://doi.org/10.1099/jmm.0.05473-0
3. Cantón R, Bryan J. Global antimicrobial resistance: from surveillance to stewardship. Part 1: surveillance and risk factors for resistance. Expert Rev Anti Infect Ther Actions. 2012;10:1269–71. https://doi.org/10.1586/eri.12.120
4. Cuny C, Wieler LH, Witte W. Livestock-associated MRSA: the impact on humans. Antibiotics (Basel). 2015;4:521–43. https://doi.org/10.3390/antibiotics4040521
5. Zhang X-F, Doi Y, Huang X, Li HY, Zhong LL, Zeng KJ, et al. Possible transmission of *mcr-1*-harboring *Escherichia coli* between companion animals and human. Emerg Infect Dis. 2016;22:1679–81. https://doi.org/10.3201/eid2209.160464
6. Guardabassi L, Schwarz S, Lloyd DH. Pet animals as reservoirs of antimicrobial-resistant bacteria. J Antimicrob Chemother. 2004;54:321–32. https://doi.org/10.1093/jac/dkh332
7. Guardabassi L, Loeber ME, Jacobson A. Transmission of multiple antimicrobial-resistant *Staphylococcus intermedius* between dogs affected by deep pyoderma and their owners. Vet Microbiol. 2004;98:23–7. https://doi.org/10.1016/j.vetmic.2003.09.021
8. Johnson JR, Johnston B, Clabots CR, Kuskowski MA, Roberts E, DebRoy C. Virulence genotypes and phylogenetic background of *Escherichia coli* serogroup O6 isolates from humans, dogs, and cats. J Clin Microbiol. 2008;46:417–22. https://doi.org/10.1128/JCM.00674-07
9. World Health Organization. Global action plan on antimicrobial resistance [cited 2001 Jun 16]. http://apps.who.int/iris/bitstream/handle/10665/193736/9789241509763_eng.pdf
10. Altiner A, Wilm S, Wegscheider K, Sielk M, Brockmann S, Fuchs A, et al. Fluoroquinolones to treat uncomplicated acute cough in primary care: predictors for unjustified prescribing of antibiotics. J Antimicrob Chemother. 2010;65:1521–5. https://doi.org/10.1093/jac/dkq151
11. Hawker JI, Smith S, Smith GE, Morbey R, Johnson AP, Fleming DM, et al. Trends in antibiotic prescribing in primary care for clinical syndromes subject to national recommendations to reduce antibiotic resistance, UK 1995–2011: analysis of a large database of primary care consultations. J Antimicrob Chemother. 2014;69:3423–30. https://doi.org/10.1093/jac/dku291
12. McCullough AR, Rathbone J, Parekh S, Hoffmann TC, Del Mar CB. Not in my backyard: a systematic review of clinicians' knowledge and beliefs about antibiotic resistance. J Antimicrob Chemother. 2015;70:2465–73. https://doi.org/10.1093/jac/dkv164
13. McKay R, Mah A, Law MR, McGrail K, Patrick DM. Systematic review of factors associated with antibiotic prescribing for respiratory tract infections. Antimicrob Agents Chemother. 2016;60:4106–18. https://doi.org/10.1128/AAC.00209-16
14. Welsh CE, Parkin TDH, Marshall JF. Use of large-scale veterinary data for the investigation of antimicrobial prescribing practices in equine medicine. Equine Vet J. 2017;49:425–32. https://doi.org/10.1111/evj.12638
15. Hughes LA, Williams N, Clegg P, Callaby R, Nuttall T, Coyne K, et al. Cross-sectional survey of antimicrobial prescribing patterns in UK small animal veterinary practice. Prev Vet Med. 2012;104:309–16. https://doi.org/10.1016/j.prevetmed.2011.12.003
16. De Briyne N, Atkinson J, Pokludová L, Borriello SP, Price S. Factors influencing antibiotic prescribing habits and use of sensitivity testing amongst veterinarians in Europe. Vet Rec. 2013;173:475. https://doi.org/10.1136/vr.101454
17. Mateus AL, Brodbelt DC, Barber N, Stärk KD. Qualitative study of factors associated with antimicrobial usage in seven small animal veterinary practices in the UK. Prev Vet Med. 2014;117:68–78. https://doi.org/10.1016/j.prevetmed.2014.05.007
18. O'Neill DG, Church DB, McGreevy PD, Thomson PC, Brodbelt DC. Approaches to canine health surveillance.

Canine Genet Epidemiol. 2014;1:2. https://doi.org/10.1186/2052-6687-1-2
19. Sánchez-Vizcaíno F, Jones PH, Menacere T, Heayns B, Wardeh M, Newman J, et al. Small animal disease surveillance. Vet Rec. 2015;177:591–4. https://doi.org/10.1136/vr.h6174
20. Radford AD, Noble PJ, Coyne KP, Gaskell RM, Jones PH, Bryan JG, et al. Antibacterial prescribing patterns in small animal veterinary practice identified via SAVSNET: the Small Animal Veterinary Surveillance Network. Vet Rec. 2011;169:310. https://doi.org/10.1136/vr.d5062
21. Buckland EL, O'Neill D, Summers J, Mateus A, Church D, Redmond L, et al. Characterisation of antimicrobial usage in cats and dogs attending UK primary care companion animal veterinary practices. Vet Rec. 2016;179:489. https://doi.org/10.1136/vr.103830
22. Singleton DA, Sánchez-Vizcaíno F, Dawson S, Jones PH, Noble PJM, Pinchbeck GL, et al. Patterns of antimicrobial agent prescription in a sentinel population of canine and feline veterinary practices in the United Kingdom. Vet J. 2017;224:18–24. https://doi.org/10.1016/j.tvjl.2017.03.010
23. Burke S, Black V, Sánchez-Vizcaíno F, Radford A, Hibbert A, Tasker S. Use of cefovecin in a UK population of cats attending first-opinion practices as recorded in electronic health records. J Feline Med Surg. 2017;19:687–92. https://doi.org/10.1177/1098612X16656706
24. World Health Organization. WHO list of critically important antimicrobials (WHO CIA list) [cited 2001 Jun 19]. https://www.who.int/foodsafety/areas_work/antimicrobial-resistance/cia
25. German AJ, Halladay LJ, Noble PJ. First-choice therapy for dogs presenting with diarrhoea in clinical practice. Vet Rec. 2010;167:810–4. https://doi.org/10.1136/vr.c4090
26. Jones PH, Dawson S, Gaskell RM, Coyne KP, Tierney A, Setzkorn C, et al. Surveillance of diarrhoea in small animal practice through the Small Animal Veterinary Surveillance Network (SAVSNET). Vet J. 2014;201:412–8. https://doi.org/10.1016/j.tvjl.2014.05.044
27. Day MJ, Horzinek MC, Schultz RD, Squires RA; Vaccination Guidelines Group (VGG) of the World Small Animal Veterinary Association (WSAVA). WSAVA guidelines for the vaccination of dogs and cats. J Small Anim Pract. 2016;57:E1–45. https://doi.org/10.1111/jsap.2_12431
28. Sánchez-Vizcaíno F, Noble PM, Jones PH, Menacere T, Buchan I, Reynolds S, et al. Demographics of dogs, cats, and rabbits attending veterinary practices in Great Britain as recorded in their electronic health records. BMC Vet Res. 2017;13:218. https://doi.org/10.1186/s12917-017-1138-9
29. vonholdt BM, Pollinger JP, Lohmueller KE, Han E, Parker HG, Quignon P, et al. Genome-wide SNP and haplotype analyses reveal a rich history underlying dog domestication. Nature. 2010;464:898–902. https://doi.org/10.1038/nature08837
30. Aegerter J, Fouracre D, Smith GC. A first estimate of the structure and density of the populations of pet cats and dogs across Great Britain. PLoS One. 2017;12:e0174709. https://doi.org/10.1371/journal.pone.0174709
31. Lipinski MJ, Froenicke L, Baysac KC, Billings NC, Leutenegger C, Levy AM, et al. The ascent of cat breeds: genetic evaluations of breeds and worldwide random-bred populations. Genomics. 2008;91:12–1. https://doi.org/10.1016/j.ygeno.2007.10.009
32. World Health Organization. Critically important antimicrobials for human medicine: 5th revision 2016 [cited 2001 Apr 16]. http://apps.who.int/iris/bitstream/handle/10665/255027/9789241512220-eng.pdf
33. Goddard A, Leisewitz AL. Canine parvovirus. Vet Clin North Am Small Anim Pract. 2010;40:1041–53. https://doi.org/10.1016/j.cvsm.2010.07.007
34. O'Neill J. Review on antimicrobial resistance: tackling drug-resistant infections globally [cited 2015 Dec 15]. http://amr-review.org/home
35. British Small Animal Veterinary Association. BSAVA/SAMSoc guide to responsible use of antibacterials: PROTECT ME [cited 2011 Nov 18]. https://www.bsavalibrary.com/content/book/10.22233/9781910443644
36. Hall JL, Holmes MA, Baines SJ. Prevalence and antimicrobial resistance of canine urinary tract pathogens. Vet Rec. 2013;173:549. https://doi.org/10.1136/vr.101482
37. Hernandez J, Bota D, Farbos M, Bernardin F, Ragetly G, Médaille C. Risk factors for urinary tract infection with multiple drug-resistant *Escherichia coli* in cats. J Feline Med Surg. 2014;16:75–81. https://doi.org/10.1177/1098612X13504407
38. Huerta B, Maldonado A, Ginel PJ, Tarradas C, Gómez-Gascón L, Astorga RJ, et al. Risk factors associated with the antimicrobial resistance of staphylococci in canine pyoderma. Vet Microbiol. 2011;150:302–8. https://doi.org/10.1016/j.vetmic.2011.02.002
39. O'Neill DG, Church DB, McGreevy PD, Thomson PC, Brodbelt DC. Prevalence of disorders recorded in cats attending primary-care veterinary practices in England. Vet J. 2014;202:286–91. https://doi.org/10.1016/j.tvjl.2014.08.004
40. Chhetri BK, Berke O, Pearl DL, Bienzle D. Comparison of risk factors for seropositivity to feline immunodeficiency virus and feline leukemia virus among cats: a case-case study. BMC Vet Res. 2015;11:30. https://doi.org/10.1186/s12917-015-0339-3
41. Quinn JV, Polevoi SK, Kohn MA. Traumatic lacerations: what are the risks for infection and has the 'golden period' of laceration care disappeared? Emerg Med J. 2014;31:96–100. https://doi.org/10.1136/emermed-2012-202143
42. Feline bordetellosis: challenge and vaccine studies. Vet Rec. 1993;133:260–3. https://doi.org/10.1136/vr.133.11.260
43. Lappin MR, Blondeau J, Boothe D, Breitschwerdt EB, Guardabassi L, Lloyd DH, et al. Antimicrobial use guidelines for treatment of respiratory tract disease in dogs and cats: Antimicrobial Guidelines Working Group of the International Society for Companion Animal Infectious Diseases. J Vet Intern Med. 2017;31:279–94. https://doi.org/10.1111/jvim.14627
44. Nuttall T, Uri M, Halliwell R. Canine atopic dermatitis - what have we learned? Vet Rec. 2013;172:201–7. https://doi.org/10.1136/vr.f1134
45. Royal College of Veterinary Surgeons. Practice Standards Scheme [cited 2001 Dec 17]. https://www.rcvs.org.uk/setting-standards/practice-standards-scheme
46. Pleydell EJ, Souphavanh K, Hill KE, French NP, Prattley DJ. Descriptive epidemiological study of the use of antimicrobial drugs by companion animal veterinarians in New Zealand. N Z Vet J. 2012;60:115–22. https://doi.org/10.1080/00480169.2011.643733
47. Abel GA, Barclay ME, Payne RA. Adjusted indices of multiple deprivation to enable comparisons within and between constituent countries of the UK including an illustration using mortality rates. BMJ Open. 2016;6:e012750. https://doi.org/10.1136/bmjopen-2016-012750

Address for correspondence: David A. Singleton, University of Liverpool, Epidemiology and Population Health, Chester High Rd, Neston CH64 7TE, UK; email: D.A.Singleton@liverpool.ac.uk

Linezolid-Associated Neurologic Adverse Events in Patients with Multidrug-Resistant Tuberculosis, France

Marie Jaspard, Nathalie Butel, Najoua El Helali, Dhiba Marigot-Outtandy, Helene Guillot, Gilles Peytavin, Nicolas Veziris, Bahram Bodaghi, Philippe Flandre, Gregoire Petitjean, Eric Caumes, Valerie Pourcher

Linezolid is one of the most effective drugs for treating multidrug-resistant tuberculosis (MDR TB), but adverse effects remain problematic. We evaluated 57 MDR TB patients who had received ≥1 dose of linezolid during 2011–2016. Overall, patients received 600 mg/day of linezolid for a median of 13 months. In 33 (58%) patients, neurologic or ophthalmologic signs developed, and 18 (32%) had confirmed peripheral neuropathy, which for 78% was irreversible at 12 months after the end of TB treatment despite linezolid withdrawal. Among the 19 patients who underwent ophthalmologic evaluation, 14 patients had optic neuropathy that fully reversed for 2. A total of 16 (33%) of 49 patients had a linezolid trough concentration >2 mg/L, and among these, 14 (88%) experienced adverse effects. No significant association was found between trough concentration and neurologic toxicity. These findings suggest the need to closely monitor patients for neurologic signs and discuss optimal duration of linezolid treatment.

Worldwide, tuberculosis (TB) affects 10 million persons every year. Among them, multidrug-resistant TB (MDR TB) is diagnosed for 484,000 (*1*); and among MDR TB cases, 10% are caused by extensively drug-resistant (XDR) strains of *Mycobacterium tuberculosis*. Outcomes for patients in TB-endemic countries are very poor, particularly for those with XDR TB; cure rates are <20% (*2*). However, even in TB-endemic countries, individualized treatment adapted to drug susceptibility achieves cure rates of only 60% in patients with XDR TB (*3*,*4*). Similarly, a meta-analysis of 50 studies performed in 25 countries and including 12,030 patients receiving individualized treatment for MDR TB found a pooled success rate of 61% for combination therapy regimens containing linezolid (*5*). At Pitié-Salpêtrière Hospital in Paris, France, the survival rate for XDR TB patients for whom highly effective drugs (e.g., linezolid, bedaquiline, or both) were prescribed was 80% (*6*–*8*). Overall, an 80% cure rate can be achieved for patients with MDR TB treated with a drug regimen that includes linezolid (*9*–*12*).

The 2014 World Health Organization (WHO) guidelines promote using highly active drugs for MDR TB, especially that caused by XDR TB strains (*13*). In 2016 and 2018, these recommendations were updated, and linezolid, along with bedaquiline and levofloxacin/moxifloxacin, were upgraded to group A drugs that should be offered to all patients (*14*,*15*).

Although linezolid is highly effective, its long-term use in patients with MDR TB is impaired by its adverse effects. Myelosuppression occurs in ≈30% of patients, particularly those receiving high doses (>600 mg/d) (*9*,*12*), and neurotoxicity with peripheral neuropathy is experienced by 30% of patients after 2 to 4 months of receiving low doses (<600 mg/d) (*12*). Furthermore, linezolid-associated optic neuropathy appears after 5 to 10 months of treatment for 30% of patients (*11*,*16*). It is still debated whether linezolid trough concentrations >2 mg/L (*17*) or long-term exposure could predict the occurrence of adverse

Author affiliations: Sorbonne Université, Paris, France (M. Jaspard, H. Guillot, N. Veziris, B. Bodaghi, E. Caumes, V. Pourcher); Assistance Publique–Hôpitaux de Paris, Hôpitaux Universitaires Pitié-Salpêtrière Charles Foix, Paris (M. Jaspard, H. Guillot, E. Caumes, V. Pourcher); Assistance Publique – Hôpitaux de Paris, Groupe Hospitalier Pitié-Salpêtrière, Paris (N. Butel, B. Bodaghi); Groupe Hospitalier Paris Saint Joseph, Paris (N. El Helali, G. Petitjean); Bligny Medical Center, Briis sous Forges, France (D. Marigot-Outtandy); Assistance Publique–Hôpitaux de Paris, Hôpital Bichat-Claude Bernard, Paris (G. Peytavin); Université Paris Diderot, Sorbonne Paris Cité, Paris (G. Peytavin); Assistance Publique–Hôpitaux de Paris, Hôpitaux Universitaires de l'Est Parisien, Paris (N. Veziris); Institut Pierre Louis Institute d'Épidémiologie et de Santé Publique, Paris (P. Flandre, E. Caumes, V. Pourcher)

DOI: https://doi.org/10.3201/eid2608.191499

effects (*18*,*19*). We therefore evaluated the occurrence and management of neurologic and ophthalmologic adverse effects among MDR TB patients receiving a linezolid-based treatment regimen.

Methods

We retrospectively studied all patients with confirmed MDR TB who had received ≥1 dose of linezolid during January 2011–December 2016 and had been followed up for ≥12 months after the end of treatment. All patients had been admitted to Pitié-Salpêtrière Hospital, Paris, France, and most were discharged to Bligny Sanatorium and then followed up as outpatients. The TB drug regimen was adapted for each patient according to the results of drug susceptibility testing and discussion with the French Consilium team (*20*) in keeping with recommendations from the WHO and the Haut Conseil de la Santé Publique (*14*,*21*).

To monitor adverse effects of treatment, physicians performed daily neurologic and ophthalmologic examinations of hospitalized patients and monthly examinations of outpatients. Neurologic adverse effects included motor and sensory deficits, tendon reflex abnormalities, cranial nerve abnormalities, and pallesthesia. Ophthalmologic adverse effects included visual acuity loss, visual color abnormalities, or scotoma. If peripheral neuropathy was suspected, electromyography (EMG) was performed, including nerve conduction velocity (NCV) testing, to assess motor and sensory injuries to confirm the diagnosis. If a patient reported visual impairment indicating optic neuropathy, an ophthalmologist performed a specific clinical examination including Snellen best-corrected visual acuity measurement, relative afferent pupillary defect assessment, slit lamp examination, funduscopic examination, and color vision (Farnsworth D-15 Hue Test) and visual fields (Humphrey 24–2 SITA [Swedish Interactive Threshold Algorithm] standard or Goldmann) assessments. Nerve fiber layer thickness was evaluated by using optical coherence tomography for optic nerve abnormalities. If indicated, electrophysiologic measurement of visual evoked potential was also performed by an ophthalmologist. If an adverse effect was identified, follow-up frequency was determined by the physician, depending on severity of the effect. Neurologic and ophthalmologic adverse effect severity was classified by using the Common Terminology Criteria for Adverse Events (CTCAE) criteria (*22*).

Therapeutic drug monitoring for linezolid was performed at least once at the beginning of treatment (within the first month) for all patients except a few hospitalized at the beginning of 2011 when this analysis was not yet available at Pitié-Salpêtrière Hospital. If adverse effects occurred or if the dosage of linezolid was modified, serum concentration of linezolid was measured by using accredited ultra high–performance liquid chromatography–electrospray ionization/high-resolution mass spectrometry (European Medicines Agency, https://www.ema.europa.eu) and using stable isotope-labeled linezolid as an internal standard and a calibration range of 0.01–10.00 mg/L. We were able to follow patients for 12 months after end of treatment. Hence, we defined irreversibility of signs/symptoms as the persistence of signs/symptoms 12 months after the end of treatment.

We collected epidemiologic, clinical, and biological information from patients' medical files. We investigated whether some variables were associated with neurologic toxicities by using a logistic regression model. Linezolid trough concentration was considered high if it was >2 mg/L at least once at baseline or during treatment. The data fulfilled the confidentiality criteria of the French National Data Protection "Commission Nationale de l'Informatique et des Libertés" (CNIL 2085894).

Results

Patient Characteristics

During January 2011–December 2016, MDR TB was diagnosed for 65 patients at Pitié-Salpêtrière Hospital. Four patients did not receive linezolid, 2 with severe pulmonary TB died within 2 months after initiation of treatment, and 2 were unavailable for follow-up within the first 3 months. We included in our study the remaining 57 patients for whom at least 12 months of follow-up information after the end of TB treatment was available (Figure 1; Tables 1, 2).

Among the 57 patients, 11 (19%) were infected with an MDR strain of *M. tuberculosis*, 20 (35%) with a pre-XDR strain (resistance to isoniazid and rifampicin and either a fluoroquinolone or a second-line injectable agent but not both), and 26 (46%) with an XDR strain. A total of 55 patients had pulmonary TB, 2 had extrapulmonary TB (bone), and 11 had both (bone, lymph node, genital, or laryngeal). Of the 55 with pulmonary TB, the lesions involved both lungs for 42 (76%) patients, and cavitation was found in 39 (71%) patients.

Median duration of TB treatment was 19.4 months (interquartile range [IQR] 17.3–24.0 months). The linezolid dose was 600 mg once daily for all patients; no patient received >600 mg/day. The median duration of linezolid treatment was 12.8 months (IQR 6.0– 19.2 months).

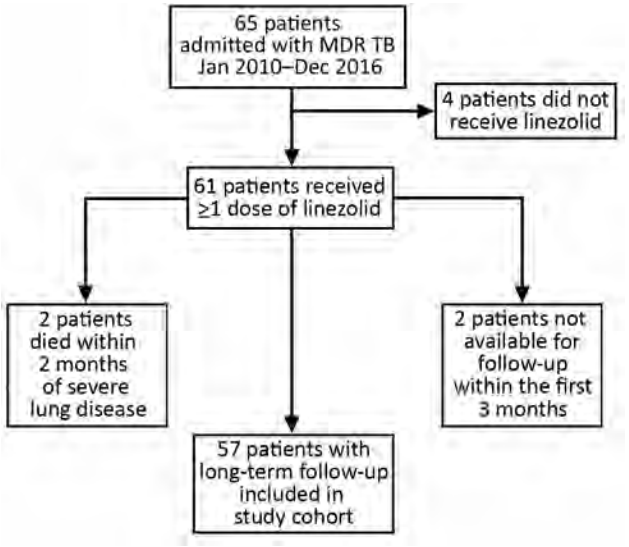

Figure 1. Outcomes for 65 patients with multidrug-resistant tuberculosis (MDR TB) admitted to Pitié-Salpêtrière Hospital, Paris, France, and included in study of linezolid-associated neurologic adverse events.

Among the 57 patients, treatment was successful, according to the WHO outcome definition (*23*), for 52 (91%); 3 were unavailable for follow-up, and 2 died with severe neurologic signs suggestive of serotonin syndrome. However, we cannot formally link these deaths to linezolid because of doubts about the degree of attribution.

One of the patients who died had arrived in France from Georgia in 2012 with XDR TB, hepatitis C virus co-infection, and a history of diabetes mellitus and high blood pressure. While in Georgia, he had received treatment for relapsing MDR TB for several years and received several drugs (para-aminosalicylic acid [PAS], cycloserine, ethionamide, moxifloxacin, clofazimine, clarithromycin, and capreomycin). When he arrived at the infectious disease department at Pitié Salpêtrière Hospital, and based on the French Consilium recommendations for patients with XDR TB, we initiated treatment with cycloserine, PAS, bedaquiline, meropenem/clavulanate, and linezolid. Treatment for diabetes (insulin) and high blood pressure (perindopril) was also started. Eleven months later, peripheral neuropathy appeared (confirmed by EMG), as well as orthostatic hypotension and mental confusion. We were reticent to change the TB treatment because of the highly resistant strain and severe lung disease (right upper lung lobectomy was performed after 10 months of TB treatment). Fifteen months after starting TB treatment, the patient suddenly experienced dysphagia, laryngeal hypoesthesia, dysarthria, bilateral myosis, myoclonus, hearing impairment, and visual impairment. Magnetic resonance imaging, electroencephalography, and cerebrospinal fluid analysis findings were unremarkable. TB treatment was immediately stopped, but the patient died; no cause was identified during autopsy. The patient's linezolid concentration was 0.2 mg/L 1 month after treatment start and 0.6 mg/L on the last day of treatment.

For the other patient who died, XDR TB was diagnosed and treatment began when he arrived in France from Armenia; initial treatment was PAS, bedaquiline, amikacin, meropenem/clavulanate, and linezolid, which was stopped rapidly because of poor tolerance. Previous TB treatment history in Armenia was unavailable. He also underwent a left upper lung lobectomy because of the absence of sputum culture conversion; was co-infected with the hepatitis C virus; and was addicted to tobacco, alcohol, and intravenous drugs. Five months after TB treatment was initiated, peripheral neuropathy developed (confirmed by EMG), although trough linezolid concentration was only 0.6 mg/L. During month 7 of treatment, trough linezolid concentration increased to 2.6 mg/L but otherwise remained <2 mg/L. After 12 months of TB treatment, the patient experienced a psychological disorder;

Table 1. Sociodemographic and medical characteristics of 57 patients who received linezolid for multidrug-resistant tuberculosis, Pitié-Salpêtrière Hospital, Paris, France, 2011–2016*

Characteristic	Value
Age, y, median (IQR)	35 (26–39)
Sex	
M	39 (68)
F	18 (32)
Country or region of origin	
Georgia	36 (63)
Other Eastern Europe and Russia	8 (14)
Africa†	5 (9)
Asia‡	5 (9)
France	3 (5)
History of treated TB	37 (65)
History of isoniazid-based regimen	23 (40)
History of linezolid-based regimen	0
HIV infection	5 (9)
Hepatitis B surface antigen–positive	1 (2)
Hepatitis C	24 (42)
Diabetes mellitus	2 (4)
History of intravenous drug use	20 (35)
Opioid substitution therapy, methadone or buprenorphine	12 (21)
Alcohol consumption	8 (14)
Body mass index at first visit, median (IQR), kg/m^2	20.1 (17.9–22.4)
Albumin level at first visit, median (IQR), g/L	34 (30–38)

*Values are no. (%) unless otherwise indicated. IQR, interquartile range; TB, tuberculosis.
†One from Algeria, 1 from Cameroon, 1 from Democratic Republic of the Congo, 2 from Côte d'Ivoire.
‡Three from China, 2 from Tibet.

sequential treatment consisted of loxapine, amitriptyline, mianserin, or oxazepam. Peripheral neuropathy worsened, causing severe leg pain requiring analgesia (opioids, pregabalin, clonazepam, gabapentin). At 15 months, linezolid was discontinued, and at 18 months, the remaining TB treatment was discontinued. A few days later, the patient was transferred to intensive care with dysphagia, loss of cough and tendon reflexes, distended bladder, sensory neuropathy, motor deficits, and pneumonia. All these signs and symptoms suggested brainstem injury or diffuse neuropathy. He died suddenly a few hours later. No autopsy was performed.

Table 2. Tuberculosis drugs prescribed for ≥1 mo included in linezolid-based regimen for 57 patients with multidrug-resistant tuberculosis, Pitié-Salpêtrière Hospital, Paris, France, 2011–2016*

Drug	No. (%) patients
Cycloserine	49 (86)
Para-aminosalicylic acid	49 (86)
Amikacin	41 (72)
Bedaquiline	40 (70)
Pyrazinamide	37 (65)
Moxifloxacin	33 (58)
Ethambutol	17 (30)
Ethionamide	13 (23)
Levofloxacin	6 (11)
Capreomycin	3 (5)
Delamanid	3 (5)
Meropenem/clavulanate	2 (4)

Adverse Effects

Overall, 33 (58%) patients reported ophthalmologic or neurologic signs/symptoms, possibly linked to linezolid exposure: 24 patients had peripheral neuropathologic signs/symptoms only, 2 patients had ophthalmologic signs/symptoms only, and 7 patients had both (Figure 2). Moreover, linezolid was stopped because of neurologic adverse effects for 23 patients (18 for peripheral neuropathy, 1 for optical neuropathy, and 4 for both neuropathies) after a median duration of linezolid exposure of 8.6 months (IQR 5.6–15.3 months).

Among the 57 patients, 31 reported peripheral neurologic signs/symptoms (24 peripheral only and 7 both peripheral and optical), peripheral sensory or motor neuropathy signs were detected during clinical examination for 25, and neuropathy was confirmed by EMG or NCV for 18 (32%) of the 57 (Figure 2). Among the 31 with neuropathy signs/symptoms, 12 were CTCAE classification grade 1, 18 were grade 2, and 1 was grade 4. Among the 18 patients with peripheral neuropathy confirmed by EMG/NCV, 14 (78%) had persistent signs/symptoms for at least 12 months after discontinuation of TB treatment. However, language barriers and precarious situations faced by these patients made evaluating sequelae severity difficult. Although all patients were ambulatory, 16 required long-term (until the end of the 12 months of follow-up) analgesic therapy such as pregabalin for 12 (75%) and paracetamol, levetiracetam, or opioids for the others.

Ophthalmologic testing was performed for 19 patients, of which 13 were routinely tested at the discretion of the treating physician, for fear of sides effects resulting from long-term exposure to linezolid, and 6 were tested after reporting optical signs/symptoms. Of the 19 patients tested, 14 (9 without complaints and 5 with complaints) had optic neuropathy (Table 3) attributed to linezolid after exclusion of other etiologies. Among these patients, CTCAE severity was grade 1 for 10 patients, grade 2 for 2 patients, and grade 4 for 2 patients.

After linezolid withdrawal, a second ophthalmologic examination for 9 patients indicated that 2 had fully recovered, 3 had improved visual acuity with residual impaired vision, and 4 showed no improvement. Five patients did not undergo a second examination, possibly because they had clinical improvement and did not report optical signs/symptoms.

The median delay between linezolid initiation and occurrence of neurologic adverse effects was 8.3 (IQR 4–11) months and of ophthalmologic adverse effects was 9.3 (IQR 1.6 –15.1) months. Overall, 27 (47%) of the 57 patients had neurologic side effects confirmed by EMG/NCV or specific ophthalmologic examination, 13 (23%) had peripheral neuropathy only, 9 (16%) had ophthalmologic neuropathy only, and 5 (9%) had both. Linezolid treatment duration was 15.1 (IQR 7.2–19.1) months for patients with confirmed neurologic adverse effects and 12.3 (IQR 5.5–21.1) months for those without (p = 0.9148).

Linezolid Trough Concentrations and Neuropathy

Linezolid trough concentrations were available for 49 patients and were analyzed in association with neuropathy (Table 4). Among the 16 (33%) patients with trough concentrations >2 mg/L (median 3 [IQR 2.4–3.7] mg/L) at least once at baseline or during treatment, 14 (88%) experienced linezolid-associated adverse effects: 9 had a peripheral neuropathy and 5 had optical neuropathy. Among the 33 (67%) patients with all trough concentrations ≤2 mg/L (median 0.4 [IQR 0.19–1] mg/L), 27 (82%) experienced linezolid-associated adverse effects: 17 had peripheral neuropathy and 10 had optical neuropathy. Among the 8 patients for whom linezolid concentration was not evaluated, linezolid-associated adverse effects developed in 6 (75%)

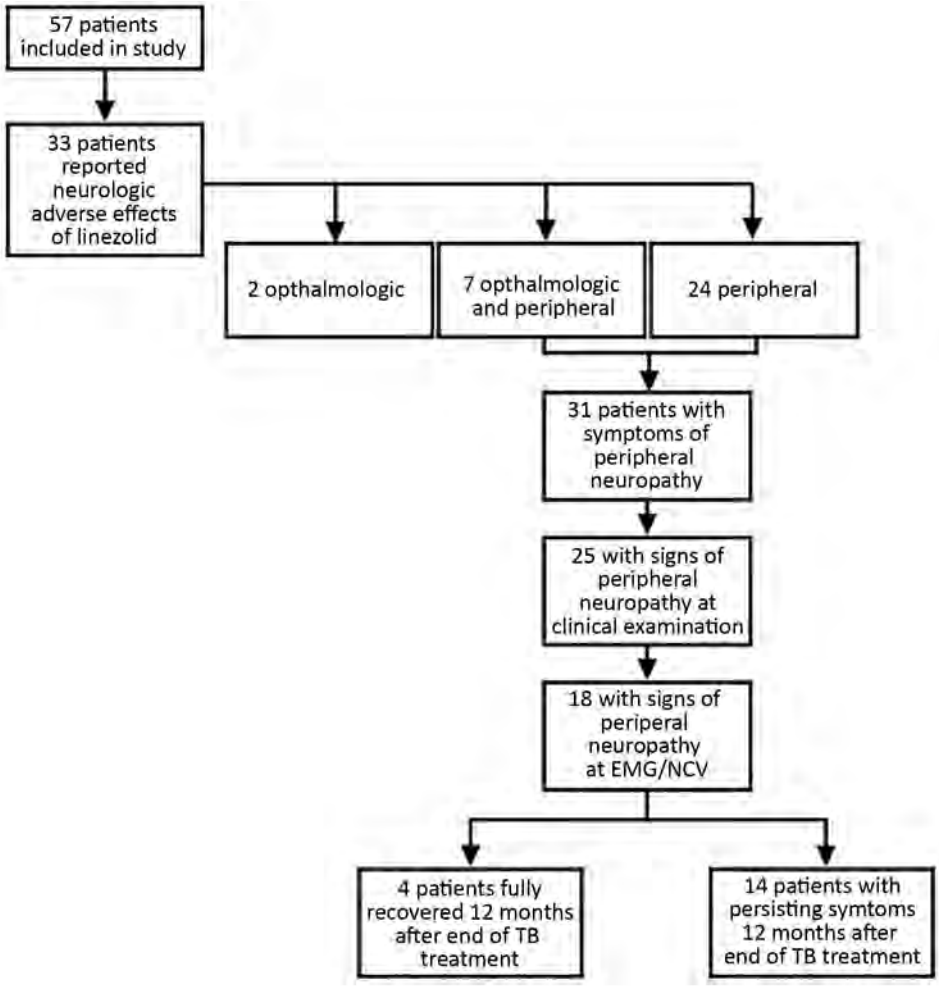

Figure 2. Peripheral neuropathy occurrence and evolution among the 57 patients who received linezolid for multidrug-resistant tuberculosis during 2011 and 2016, France. EMG, electromyelogram; NCV, nerve-conduction velocity testing; TB, tuberculosis.

patients: 5 had peripheral neuropathy and 1 had optic neuropathy. We found no association between development of neuropathy and demographic characteristics, trough concentration, or linezolid treatment duration (p>0.05) (Table 5).

Discussion

In our study, 58% of MDR/XDR TB patients reported a neurologic or ophthalmologic disorder possibly associated with linezolid exposure; neuropathies were confirmed for 47%. Linezolid-related peripheral neuropathy was confirmed (by EMG/NCV) for almost 32%. Neuropathy and demographic characteristics did not seem to be associated with trough concentration, or linezolid duration.

Linezolid-related optic neuropathies in patients receiving treatment for *Staphylococcus aureus* infections have been described (*24*) and can be asymptomatic or lead to reduced visual acuity, blurred vision, central scotoma, and dyschromatopsia (*19*,*25*). We found a high prevalence of confirmed optic neuropathy (25% of our cohort) that was fully reversible (meaning complete recovery of ophthalmologic disorder 12 months after the end of TB treatment) for only 2 of our patients after treatment withdrawal. We therefore suggest testing visual acuity and performing a sensory color vision test and a Goldmann visual field test before initiating linezolid with monthly checkups, as has been recently recommended (*19*).

Our finding of a peripheral neuropathy rate of 32% is similar to the neuropathy rate of 30% reported in a recent meta-analysis (*12*). In our study, peripheral neuropathy diagnosis was confirmed after a median duration of 8 months of treatment. In contrast, a study in China found that peripheral neuropathy occurred 2 to 4 months after treatment start (*11*). This difference can be explained by the high daily doses of linezolid received by patients in that study (1,200 mg/d loading dose for 6 weeks, then 600 mg/d) compared with the 600 mg/day received by all patients in our study. Various studies report irreversible neuropathy (*10*,*12*,*26*,*27*). In our study, 78% of patients

with confirmed peripheral neuropathy did not fully recover despite linezolid withdrawal. Those patients were followed up for 12 months after the end of their TB treatment. Some may have recovered after that follow-up period. Thus, this result should encourage closer monitoring of neurologic complaints with detailed and regular clinical neurologic examinations. Linezolid should also be immediately discontinued at the onset of neurologic signs/symptoms.

Questions persist about the 2 patients who died. First, both patients had concurrent conditions known to increase the risk for neurologic disorders. One patient had hepatitis C, diabetes, and high blood pressure; the other had hepatitis C and a history of substance abuse. Second, linezolid treatment was continued for both patients despite development of neurologic signs/symptoms. At that time, in 2013, TB treatment was continued in the context of a highly resistant strain of *M. tuberculosis*, lack of an effective drug (e.g., delamanid) for treatment, and severe disease, despite daily in-patient monitoring. In hindsight, stopping any neurotoxic treatments as soon as neurologic signs/symptoms occurred may have been wise. Third, the second patient received several psychotropic drugs, which can potentiate the linezolid effect and induce serotonin syndrome. Linezolid-associated serotonin syndrome has been described in association with use of various drugs such as metoclopramide, paroxetine, or amitriptyline (*28*,*29*). Hence, when long-term use of linezolid is unavoidable because of highly resistant TB, drugs that induce serotonin syndrome must not be prescribed.

Another way to monitor adverse effects of antimicrobial drugs is to systematically measure serum trough concentrations. The role of linezolid dosage, treatment duration, and cumulative dose on neuropathy occurrence is still debated. Bolhuis et al. stated that the linezolid area under the curve over 24 hours does not affect adverse effect occurrence but that long exposure duration and cumulative doses do (*18*). Song et al. demonstrated a direct correlation between linezolid dose, trough concentrations, and development of clinical toxicity. They found that adverse effects developed in all patients for whom mean linezolid trough was >2 mg/L, whereas they developed in >50% of those for whom mean linezolid trough was <2 mg/L (*17*). In our study, linezolid trough concentration was not associated with development of neurologic side effects. The fact that our study was retrospective could explain why our findings were not consistent with those of Song et al. (*17*).

Table 3. Characteristics of 14 patients who experienced optic neuropathy after linezolid treatment for multidrug-resistant tuberculosis, Pitié-Salpêtrière Hospital, Paris, France, 2011–2016*

Patient age, y/sex,	Fundus examination	Visual color†	Visual field	Involvement	Other	Linezolid duration, mo	Months from start of linezolid to onset of optic neuropathy	Reversibility after linezolid withdrawal
37/M	Papillary edema	Tritanopia	BSE	B	None	3.4	0.0	No
42/M	WNL	Tritanopia	Aciform scotoma	B	None	13.5	1.4	No
20/M	WNL	Tritanopia	WNL	B	None	18.5	1.6	Yes
40/M	WNL	Tritanopia	BSE	B	Optic neuropathy confirmed by VEP	15.3	14.6	Yes
48/M	WNL	Tritan	BSE	B	None	5.7	9.3	No
43/M	WNL	Tritanopia	NA	U	None	11.6	17.9	Yes
40/M	WNL	Tritanopia	BSE	U	None	18	NA	Yes
39/M	WNL	Tritanopia	BSE	B	None	23.1	15.4	Yes
42/M	WNL	Tritanopia	BSE	B	None	19.4	5.2	Yes
40/M	WNL	Tritanopia	NA	B		4.4	1.0	No
34/M	Papillary edema	Tritanopia	BSE	B	Optic neuropathy confirmed by VEP	16.6	15.1	Yes
21/M	Papillary edema	Tritanopia	Scotoma	B	Optic neuropathy confirmed by VEP	7.1	8.2	Yes
23/F	Hyperemia of optical nerve	Tritanopia	BSE	B	None	NA	10.2	Yes
30/M	Hyperemia of optical nerve	Tritan	BSE	B	None	19.1	16.2	Yes

*B, bilateral; BSE, blind spot enlargement; NA, not available; U, unilateral, VEP, visual evoked potential; WNL, within normal limits.
†Tritan, common blue–yellow color blindness.; tritarnopia, blue–yellow confusion typical in patients with optic neuropathies.

Table 4. Neuropathy according to linezolid trough concentration among of 57 patients with multidrug-resistant tuberculosis, Pitié-Salpêtrière Hospital, Paris, France, 2011–2016

Neuropathy	No. patients	Linezolid trough concentration		
		>2 mg/L, n = 16	≤2 mg/L, n = 33	Not available, n = 8
Clinical peripheral	31	9	17	5
Confirmed peripheral	18	5	10	3
Clinical optical	9	5	3	1
Confirmed optical	14	4	10	0
Peripheral + optical	10	3	6	1

When we compared patients with and without clinical or confirmed peripheral or optical neuropathy, we found no demographic characteristics associated with neuropathy occurrence (Table 5). However, in a study of MDR TB patients in India, the high rate of neuropathy was explained by a higher proportion of malnourished patients (*27*). For specific TB parameters, we found no association between the onset of neurologic adverse effects and trough concentration or linezolid treatment duration. Neuropathy seems to be independent of linezolid trough concentration (88% for >2 mg/L, 82% for ≤2 mg/L, 75% for those without measurement) or linezolid treatment duration. In addition, linezolid treatment duration was shorter among patients who did not experience neurologic adverse effects than among patients who did, but this finding was not statistically significant, probably because of small sample size.

Although the 2018 WHO recommendations state that linezolid should be offered to all patients, the optimal treatment duration has not yet been established (*15*). The high prevalence of linezolid toxicity in our cohort, together with the lack of reversibility for more than half of the patients, is not in favor of long linezolid treatment durations for MDR TB patients. Furthermore, recent findings regarding the short duration of treatment regimens for MDR TB (*30*–*32*) have led the WHO to recommend 9–12 months of therapy if particular patient criteria apply (*33*). Hence, because of the high level of linezolid neurotoxicity and a general trend to decrease MDR TB treatment duration, we suggest that exposure to linezolid should be as short as possible to avoid development of irreversible side effects (*34*). Close monitoring should also be offered to all patients receiving linezolid. In our study, 72% of patients with signs of neuropathy at clinical examination were found to have EMG/NCV abnormalities. Using clinical examination to screen for peripheral neuropathy is therefore effective, even if EMG/NCV is unavailable. Ophthalmologic examination is more complicated. Ophthalmologic abnormalities were found in 9 of 13 patients without signs/symptoms and in 5 of 6 patients with signs/symptoms. We are unable to make clear recommendations regarding ophthalmologic testing for this patient population. However, we felt it necessary to raise awareness about linezolid toxicity and highlight the need to evaluate visual acuity as often as possible for patients receiving long-term linezolid.

Our monocentric study is limited by its retrospective design. The data were incomplete for several key variables, such as pharmacokinetics and pharmacodynamics, which could explain the difference between our findings and those of the study by Song et al. (*17*). The overall sample size in each patient group was small and may have been insufficiently powered to show differences between groups. The fact that 42% (24/57) of patients had hepatitis C and 14% (8/57) had alcohol dependency might increase the risk for peripheral neuropathy, independent of linezolid exposure. Moreover, among the 17 patients who received concomitant ethambutol, 8 had confirmed optic neuropathy. Although the ophthalmologic injuries resulting from linezolid differ from those resulting from ethambutol, completely excluding ethambutol toxicity in our findings is

Table 5. Association between clinical and confirmed peripheral and optical neuropathy and patient characteristics among 57 patients with multidrug-resistant tuberculosis, Pitié-Salpêtrière Hospital, Paris, France, 2011–2016*

Characteristic	Clinical neuropathy		Confirmed neuropathy	
	Value	p value*	Value	p value*
Age, OR (95% CI)†	1.83 (0.9–3.7)	0.09	1.66 (0.8–3.3)	0.14
Immunosuppression treatment, OR (95% CI)	0.91 (0.3–2.7)	0.98	2.1 (0.7–6.2)	0.18
History of intravenous drug use, OR (95% CI)	0.43 (0.5–4.9)	0.43	1.79 (0.6–5.4)	0.30
Opioid substitution therapy, OR (95% CI)	1.6 (0.4–6.1)	0.49	1.92 (0.5–7)	0.32
Albumin, g/L	0.81 (0.4–1.8)	0.61	1.01 (0.5–2.2)	0.98
Linezolid treatment duration, mo	0.47 (0.2–1.2)	0.10	1.11 (0.5–2.7)	0.82
Culture conversion, d	0.93 (0.8–1.1)	0.35	1.15 (0.9–1.4)	0.21
Trough linezolid concentration >2 mg/L	2.07 (0.6–7.3)	0.26	0.83 (0.3–2.7)	0.76

*p values from univariate logistic models. OR, odds ratio.
†Risk based on age increase by 10-y intervals.

difficult. Thus, whenever possible, ethambutol use in a linezolid-based regimen must be avoided. Last, clinical examinations regarding ophthalmologic adverse effects were performed according to physician discretion without a systematic algorithm for recording adverse effects, which can bias the exact number of patients affected. This limitation, linked to the retrospective nature of the study, raises the issue of systematic ophthalmologic monitoring for patients receiving linezolid. One minor limitation is that only patients followed up for 12 months were included in the study. Two patients stopped coming to follow-up visits, possibly because of adverse linezolid events; thus, adverse events may have been underreported. However, these patients left during the first 3 months, probably before any neurologic adverse effects had developed.

Our study does, however, reflect the real difficulties of medical care and treatment surveillance of patients with highly resistant TB and serves to warn clinicians about long-term linezolid adverse effects. It also raises the crucial question of linezolid treatment duration for MDR TB patients. The patients in our study were in precarious economic and social situations; language barriers might explain the high rate of neurologic complications because patients might not have been able to explain their symptoms soon enough or might not have been sufficiently aware of the potential adverse effects of linezolid despite detailed explanations delivered by translators (by phone or internet). Overall, management was challenging for those patients, a situation that may occur elsewhere.

In conclusion, our study illustrates that MDR TB patients receiving linezolid should be monitored because neurologic adverse effects are severe, frequent, and often irreversible (at least at 12 months after treatment termination). Further studies are needed to evaluate the risk factors associated with linezolid toxicity and to evaluate the best treatment duration to decrease the rate of neurologic adverse effects without affecting MDR TB outcomes. However, systematic clinical examination should be implemented for all patients before treatment and monthly thereafter so that linezolid withdrawal can be discussed if neuropathy develops.

Acknowledgments

We thank all patients who contributed to this work. We also thank all the physicians involved in the management of our patients, particularly the Bligny Sanatorium team (M. Jachym, D. Le Du). We also thank Amanda Whereat for helping us with the manuscript.

About the Author

Dr. Jaspard is an infectious disease physician working in the infectious disease department at Pitié Salpetrière Hospital. She is also a PhD student in epidemiology. Her research interests include infectious diseases, including emerging diseases such as Ebola virus disease, Lassa fever, and coronavirus disease.

References

1. World Health Organization. Global tuberculosis report 2018 [cited 2020 Jun 10]. https://apps.who.int/iris/handle/10665/274453
2. Kim H-R, Hwang SS, Kim HJ, Lee SM, Yoo C-G, Kim YW, et al. Impact of extensive drug resistance on treatment outcomes in non-HIV-infected patients with multidrug-resistant tuberculosis. Clin Infect Dis. 2007;45:1290–5. https://doi.org/10.1086/522537
3. Velásquez GE, Becerra MC, Gelmanova IY, Pasechnikov AD, Yedilbayev A, Shin SS, et al. Improving outcomes for multidrug-resistant tuberculosis: aggressive regimens prevent treatment failure and death. Clin Infect Dis. 2014;59:9–15. https://doi.org/10.1093/cid/ciu209
4. Mitnick CD, Shin SS, Seung KJ, Rich ML, Atwood SS, Furin JJ, et al. Comprehensive treatment of extensively drug-resistant tuberculosis. N Engl J Med. 2008;359:563–74. https://doi.org/10.1056/NEJMoa0800106
5. Collaborative Group for the Meta-Analysis of Individual Patient Data in MDR-TB Treatment–2017; Ahmad N, Ahuja SD, Akkerman OW, Alffenaar J-WC, Anderson LF, Baghaei P, et al. Treatment correlates of successful outcomes in pulmonary multidrug-resistant tuberculosis: an individual patient data meta-analysis. Lancet. 2018 392:821–34. https://doi.org/10.1016/S0140-6736(18)31644-1
6. Guglielmetti L, Jaspard M, Le Dû D, Lachâtre M, Marigot-Outtandy D, Bernard C, et al. Long-term outcome and safety of prolonged bedaquiline treatment for multidrug-resistant tuberculosis. Eur Respir J. 2016. https://doi.org/10.1183/13993003.00411-2016
7. Henry B, Revest M, Dournon N, Epelboin L, Mellon G, Bellaud G, et al. Preliminary favorable outcome for medically and surgically managed extensively drug-resistant tuberculosis, France, 2009-2014. Emerg Infect Dis. 2016;22:518–21. https://doi.org/10.3201/eid2203.151130
8. Guglielmetti L, Le Dû D, Jachym M, Henry B, Martin D, Caumes E, et al.; MDR-TB Management Group of the French National Reference Center for Mycobacteria and the Physicians of the French MDR-TB Cohort. Compassionate use of bedaquiline for the treatment of multidrug-resistant and extensively drug-resistant tuberculosis: interim analysis of a French cohort. Clin Infect Dis. 2015;60:188–94. https://doi.org/10.1093/cid/ciu786
9. Zhang X, Falagas ME, Vardakas KZ, Wang R, Qin R, Wang J, et al. Systematic review and meta-analysis of the efficacy and safety of therapy with linezolid containing regimens in the treatment of multidrug-resistant and extensively drug-resistant tuberculosis. J Thorac Dis. 2015;7:603–15.
10. Lee M, Lee J, Carroll MW, Choi H, Min S, Song T, et al. Linezolid for treatment of chronic extensively drug-resistant tuberculosis. N Engl J Med. 2012;367:1508–18. https://doi.org/10.1056/NEJMoa1201964
11. Tang S, Yao L, Hao X, Zhang X, Liu G, Liu X, et al. Efficacy, safety and tolerability of linezolid for the treatment of

XDR-TB: a study in China. Eur Respir J. 2015;45:161–70. https://doi.org/10.1183/09031936.00035114
12. Agyeman AA, Ofori-Asenso R. Efficacy and safety profile of linezolid in the treatment of multidrug-resistant (MDR) and extensively drug-resistant (XDR) tuberculosis: a systematic review and meta-analysis. Ann Clin Microbiol Antimicrob. 2016;15:41. https://doi.org/10.1186/s12941-016-0156-y
13. World Health Organization. Companion handbook to the WHO guidelines for the programmatic management of drug-resistant tuberculosis [cited 2020 Jun 10]. http://www.who.int/tb/publications/pmdt_companionhandbook
14. World Health Organization. WHO treatment guidelines for drug-resistant tuberculosis; 2016 update [cited 2017 Jul 10]. http://www.who.int/tb/areas-of-work/drug-resistant-tb/MDRTBguidelines2016.pdf
15. World Health Organization. Rapid communication: key changes to treatment of multidrug- and rifampicin-resistant tuberculosis (MDR/RR-TB) [cited 2020 Jun 10]. http://www.who.int/tb/publications/2018/rapid_communications_MDR
16. Mehta S, Das M, Laxmeshwar C, Jonckheere S, Thi SS, Isaakidis P. Linezolid-associated optic neuropathy in drug-resistant tuberculosis patients in Mumbai, India. PLoS One. 2016;11:e0162138. https://doi.org/10.1371/journal.pone.0162138
17. Song T, Lee M, Jeon H-S, Park Y, Dodd LE, Dartois V, et al. Linezolid trough concentrations correlate with mitochondrial toxicity-related adverse events in the treatment of chronic extensively drug-resistant tuberculosis. EBioMedicine. 2015;2:1627–33. https://doi.org/10.1016/j.ebiom.2015.09.051
18. Bolhuis MS, Tiberi S, Sotgiu G, De Lorenzo S, Kosterink JGW, van der Werf TS, et al. Linezolid tolerability in multidrug-resistant tuberculosis: a retrospective study. Eur Respir J. 2015;46:1205–7. https://doi.org/10.1183/13993003.00606-2015
19. Dempsey SP, Sickman A, Slagle WS. Case report: linezolid optic neuropathy and proposed evidenced-based screening recommendation. Optom Vis Sci. 2018;95:468–74. https://doi.org/10.1097/OPX.0000000000001216
20. Guglielmetti L, Jaffre J, Bernard C, Brossier F. Multidisciplinary advisory teams to manage multidrug-resistant tuberculosis: the example of the French Consilium. Int J Tuberc Lung Dis 2019 ;1;23:1050–4. https://doi.org/10.5588/ijtld.18.0779
21. Haut Conseil de la Santé Publique. Tuberculose à bacilles résistants: diagnostic et prise en charge. Lignes directices. 2014 [cited 2020 Jun 10]. https://www.hcsp.fr/explore.cgi/avisrapportsdomaine?clefr=483
22. National Institutes of Health, National Cancer Institute. Common terminology criteria for adverse events (CTCAE) version 5.0 [cited 2020 Jun 10]. https://ctep.cancer.gov/protocolDevelopment/electronic_applications/ctc.htm
23. Laserson KF, Thorpe LE, Leimane V, Weyer K, Mitnick CD, Riekstina V, et al. Speaking the same language: treatment outcome definitions for multidrug-resistant tuberculosis. Int J Tuberc Lung Dis. 2005;9:640–5.
24. Lee E, Burger S, Shah J, Melton C, Mullen M, Warren F, et al. Linezolid-associated toxic optic neuropathy: a report of 2 cases. Clin Infect Dis. 2003;37:1389–91. https://doi.org/10.1086/379012
25. Karuppannasamy D, Raghuram A, Sundar D. Linezolid-induced optic neuropathy. Indian J Ophthalmol. 2014;62:497–500. https://doi.org/10.4103/0301-4738.118451
26. Xu H-B, Jiang R-H, Li L, Xiao H-P. Linezolid in the treatment of MDR-TB: a retrospective clinical study. Int J Tuberc Lung Dis. 2012;16:358–63. https://doi.org/10.5588/ijtld.11.0493
27. Udwadia ZF, Sen T, Moharil G. Assessment of linezolid efficacy and safety in MDR- and XDR-TB: an Indian perspective. Eur Respir J. 2010;35:936–8, author reply 938–40. https://doi.org/10.1183/09031936.00132009
28. Lalondriz Bueno YM, Monereo Muñoz M-B, Ripper C-J, Santolaria F. Serotoninergic syndrome due to linezolid and metoclopramide [in Spanish]. Enferm Infecc Microbiol Clin. 2014;32:690–1. https://doi.org/10.1016/j.eimc.2014.03.013
29. Morales-Molina JA, Mateu-de Antonio J, Grau Cerrato S, Marín Casino M. Likely serotoninergic syndrome from an interaction between amitriptyline, paroxetine, and linezolid [in Spanish]. Farm Hosp. 2005;29:292–3.
30. Aung KJM, Van Deun A, Declercq E, Sarker MR, Das PK, Hossain MA, et al. Successful '9-month Bangladesh regimen' for multidrug-resistant tuberculosis among over 500 consecutive patients. Int J Tuberc Lung Dis. 2014;18:1180–7. https://doi.org/10.5588/ijtld.14.0100
31. Van Deun A, Maug AKJ, Salim MAH, Das PK, Sarker MR, Daru P, et al. Short, highly effective, and inexpensive standardized treatment of multidrug-resistant tuberculosis. Am J Respir Crit Care Med. 2010;182:684–92. https://doi.org/10.1164/rccm.201001-0077OC
32. Nunn AJ, Phillips PPJ, Meredith SK, Chiang C-Y, Conradie F, Dalai D, et al. A trial of a shorter regimen for rifampin-resistant tuberculosis. N Engl J Med. 2019;380:1201–13. https://doi.org/10.1056/NEJMoa1811867
33. World Health Organization. Rapid communication: key changes to the treatment of drug-resistant tuberculosis. 2019 Dec [cited 2020 Jun 10]. http://www.who.int/tb/publications/2019/rapid_communications_MDR
34. Conradie F, Diacon AH, Everitt D, Mendel C, Van Niekerk C, Howell P, et al. The NIX-TB trial of pretomanid, bedaquiline and linezolid to treat XDR-TB. Abstract 80-LB. Presented at: Conference on Retroviruses and Opportunistic Infections. 2017 Feb 13–16; Seattle, WA, USA.

Address for correspondence: Marie Jaspard, Groupe Hospitalier Pitié-Salpêtrière, Service de Maladies Infectieuses, 47-83 Boulevard de l'Hôpital, Paris 75651, France; email: mariejaspard@hotmail.com

Naturally Acquired Human *Plasmodium cynomolgi* and *P. knowlesi* Infections, Malaysian Borneo

Thamayanthi Nada Raja, Ting Huey Hu, Khamisah Abdul Kadir, Dayang Shuaisah Awang Mohamad, Nawal Rosli, Lolita Lin Wong, King Ching Hii, Paul Cliff Simon Divis, Balbir Singh

To monitor the incidence of *Plasmodium knowlesi* infections and determine whether other simian malaria parasites are being transmitted to humans, we examined 1,047 blood samples from patients with malaria at Kapit Hospital in Kapit, Malaysia, during June 24, 2013–December 31, 2017. Using nested PCR assays, we found 845 (80.6%) patients had either *P. knowlesi* monoinfection (n = 815) or co-infection with other *Plasmodium* species (n = 30). We noted the annual number of these zoonotic infections increased greatly in 2017 (n = 284). We identified 6 patients, 17–65 years of age, with *P. cynomolgi* and *P. knowlesi* co-infections, confirmed by phylogenetic analyses of the *Plasmodium* cytochrome c oxidase subunit 1 gene sequences. *P. knowlesi* continues to be a public health concern in the Kapit Division of Sarawak, Malaysian Borneo. In addition, another simian malaria parasite, *P. cynomolgi*, also is an emerging cause of malaria in humans.

Plasmodium spp. were identified in the late 1800s, and ≥30 species have been described in primates, including humans, apes, and monkeys (*1*,*2*). Of these, humans are natural hosts to 4 species: *P. falciparum*, *P. malariae*, *P. vivax*, and *P. ovale*. Human infections with simian malaria parasites were thought to be extremely rare until *P. knowlesi* was identified as a major cause of malaria in humans in Kapit, Malaysian Borneo (*3*). Subsequent human cases of infection with *P. knowlesi* have been reported across Southeast Asia (*4*–*9*). Most cases are reported in the Malaysian Borneo states of Sarawak and Sabah (*4*,*10*,*11*). The zoonotic capability of this parasite was confirmed with the aid of molecular techniques because *P. knowlesi* is morphologically similar to *P. malariae* (*12*). Molecular detection methods also were used to identify other zoonotic malaria parasites infecting humans, such as *P. simium* (*13*,*14*) and *P. brasilianum* (*15*) in South America and *P. cynomolgi* (*16*,*17*) in Southeast Asia.

After the large focus on human *P. knowlesi* infections in the Kapit Division of Sarawak state in 2004 (*3*), extended studies on wild long-tailed macaques (*Macaca fascicularis*) and pig-tailed macaques (*M. nemestrina)* in the area found these species harbor 6 simian malaria parasites: *P. inui*, *P. knowlesi*, *P. cynomolgi*, *P. coatneyi*, *P. fieldi*, and *P. simiovale* (*12*,*18*). Among 108 macaques examined, *P. inui* was the most prevalent parasite (82%), along with *P. knowlesi* (78%) and *P. cynomolgi* (56%). Besides *P. knowlesi*, 2 other simian parasites, *P. inui* and *P. cynomolgi*, have zoonotic capabilities that have been proven through accidental and experimental infections (*1*,*19*–*21*). *P. inui* was experimentally reported to infect humans in 1938, with a subsequent report in 1966 (*20*,*21*). *P. cynomolgi* was reported to infect humans during an accidental transmission in a laboratory in the United States in 1956 and later by experimental trials (*1*,*19*). A single infection of naturally acquired *P. cynomolgi* in a human was described in Peninsular Malaysia in 2014 (*16*) and was confirmed through molecular characterization.

Successful transmission of zoonotic malaria is highly dependent on the bionomics and distribution of competent vectors (*22*). After the 2004 report on human *P. knowlesi* cases in Kapit, *Anopheles latens* mosquitoes were incriminated as the only vector for *P. knowlesi* in the area and were found to harbor sporozoites of other species of simian malaria parasites (*23*). Because wild macaques in Kapit harbored potentially zoonotic malaria parasites and vectors were transmitting *P. knowlesi* to humans, we aimed to

Author affiliations: Malaria Research Centre, Universiti Malaysia Sarawak, Kota Samarahan, Malaysia (T. Nada Raja, T.H. Hu, K.A. Kadir, D.S.A. Mohamad, N. Rosli, L.L. Wong, P.C.S. Divis, B. Singh); Kapit Hospital, Kapit, Malaysia (K.C. Hii)

DOI: https://doi.org/10.3201/eid2608.200343

determine whether human infections with *P. cynomolgi* and *P. inui* also occurred in the Kapit Division of Sarawak, Malaysian Borneo.

Materials and Methods

Study Area, Participants, and Detection of *Plasmodium* spp.

Kapit is the largest administrative division in Sarawak and has an area of 38,934 km^2. Most residents in Kapit belong to indigenous ethnic groups living in longhouses close to the forests. Inhabitants who are ill travel to Kapit Hospital for diagnosis and treatment. We enrolled 1,047 patients who had malaria from the Kapit and Song districts who were admitted to Kapit Hospital during June 24, 2013–December 31, 2017.

Malaria was diagnosed at Kapit Hospital by using blood film examination. Approximately 2 mL of venous blood was collected from each patient. Blood spots on filter paper and thick and thin films were prepared, and 500 µL aliquots of blood were stored frozen. We received samples at the Malaria Research Centre, Universiti Malaysia Sarawak, for further analyses. We extracted *Plasmodium* DNA from dried blood spots by using Instagene Matrix (BioRad Laboratories, https://www.bio-rad.com). We used nested PCR assays to test for the presence of different *Plasmodium* species by using primers specific for *P. falciparum*, *P. vivax*, *P. malariae*, *P. ovale*, *P. knowlesi*, *P. inui*, *P. cynomolgi*, *P. fieldi*, and *P. coatneyi* as described previously (*3*,*24*). We extracted genomic DNA from frozen blood samples by using the QIAamp DNA Mini Kit (QIAGEN, https://www.qiagen.com) and used it for molecular characterization of malaria parasites.

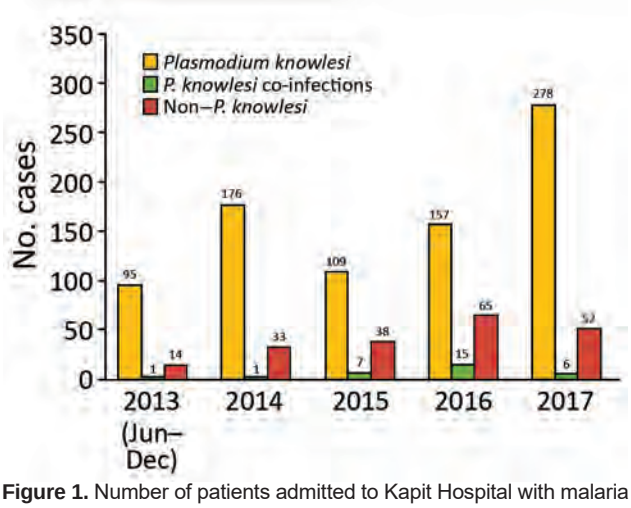

Figure 1. Number of patients admitted to Kapit Hospital with malaria during June 24, 2013–December 31, 2017, Malaysian Borneo. Non–*P. knowlesi* includes *P. falciparum*, *P. malariae*, *P. ovale*, and *P. vivax*. Infections with *Plasmodium* spp. other than *P. knowlesi* each year included the following. In 2013, *P. knowlesi* coinfections included 1 *P. cynomolgi* co-infection; non–*P. knowlesi* included 9 *P. falciparum*, 4 *P. vivax*, and 1 *P. ovale*. In 2014, *P. knowlesi* mixed included 1 *P. falciparum* coinfection; non–*P. knowlesi* included 14 *P. falciparum*, 4 *P. malariae*, 12 *P. vivax*, 3 *P. ovale*. In 2015, *P. knowlesi* co-infections included 3 *P. falciparum* and 4 *P. vivax* co-infections; non–*P. knowlesi* included 16 *P. falciparum*, 16 *P. vivax*, 1 *P. malariae*, 3 *P. falciparum*/*P. vivax* co-infections, 1 *P. falciparum*/*P. ovale* co-infection, and 1 *P. vivax*/*P. ovale* co-infection. In 2016, *P. knowlesi* co-infections included 8 *P. falciparum*, 6 *P. vivax*, and 1 *P. cynomolgi* co-infections; non–*P. knowlesi* included 41 *P. falciparum*, 14 *P. vivax*, 1 *P. ovale*, 3 *P. falciparum*/*P. vivax* co-infections, 1 *P. falciparum*/*P. malariae* co-infection, 4 *P. falciparum*/*P. ovale* co-infections, and 1 *P. vivax*/*P. ovale* co-infection. In 2017, *P. knowlesi* co-infections included 4 *P. cynomolgi*, and 2 *P. vivax* co-infections; non–*P. knowlesi* included 26 *P. falciparum*, 19 *P. vivax*, 3 *P. malariae*, 2 *P. ovale*, 1 *P. falciparum*/*P. vivax* co-infection, and 1 *P. falciparum*/*P. malariae* co-infection.

We obtained written consent from all enrolled patients or their parents or guardians for patients <17 years of age. Ethics clearance for this study was obtained from the medical research ethics committee of Universiti Malaysia Sarawak (approval nos. UNIMAS/TNC(AA)-03.02/06-Jld.2[24] and UNIMAS/NC-21.02/03-02 Jld.2[19]) and from the medical research and ethics committee of the Ministry of Health Malaysia (approval nos. NMRR-12-1086-13607[IIR] and NMRR-16-943-31224[IIR]).

PCR Amplification and Sequencing of Partial Cytochrome c Oxidase Subunit 1 Gene

Sequencing of the partial cytochrome c oxidase subunit 1 (COXI) gene of *P. cynomolgi* involved a 3-step PCR rather than the 2-step PCR used for *P. knowlesi*. First, we amplified the complete mitochondrial genome by PCR using *Plasmodium*-specific primers Pkmt F1 and Pkmt R1 (*24*). We performed PCR amplification for each sample in a 25-µL reaction mixture containing 1× PCR buffer for KOD FX Neo, 0.4 mmol dNTP mix (Toyobo, https://www.toyobo-global.com), 0.3 µmol of each primer (Pkmt F1 and Pkmt R1), 1 U/25 µL KOD FX Neo polymerase (Toyobo), and 3 µL of purified genomic DNA under the following conditions: 98°C for 30 s for first denaturation; 35 cycles at 98°C for 30 s, 55°C for 30 s, and 72°C for 5 min; then a final extension for 10 min at 72°C. We used S.N.A.P UV Gel Purification Kit (Invitrogen, https://www.thermofisher.com) to perform gel purification of the PCR amplified mitochondrial DNA (mtDNA) whole genome.

We then used the purified mtDNA amplicons as a template for the heminested touchdown PCR (TD-PCR) with *P. cynomolgi*-specific primers: cox1_F1 (5′-CCAAGCCTCACTTATTGTTAAT-3′), cox1_R1 (5′-ACCAAATAAAGTCATTGTTGATCC-3′), and cox1_R3 (5′-ATGGAAATGAGCAATTACATAG-3′). The heminested 1 (N1) TD-PCR amplification for each

sample was performed in an 11-μL reaction mixture containing 1× colorless PCR buffer, 2 mmol $MgCl_2$, 0.2 mmol dNTP mix, 0.25 μmol of each primer (cox1_F1 and cox1_R1), 0.275 U GoTaq G2 Flexi DNA Polymerase (Promega, https://www.promega.com), and 0.5 μL of purified mtDNA template under the following conditions: 94°C for 3 min for first denaturation; 10 cycles at 94°C for 30 s, 62°C for 45 s, and 72°C for 85 s; 25 cycles at 94°C for 30 s, 53°C for 45 s, and 72°C for 85 s; then a final extension for 5 min at 72°C. After N1 TD-PCR, we performed a heminested 2 (N2) TD-PCR amplification for each of the PCR products in a 22 μL reaction mixture containing similar concentration of PCR master-mix recipe with cox1_F1 and cox1_R1 primers and 1 μL of purified mtDNA template under the following conditions: 94°C for 3 min for first denaturation, 10 cycles at 94°C for 30 s, 59°C for 45 s, and 72°C for 85 s; 25 cycles at 94°C for 30 s, 53°C for 45 s, and 72°C for 85 s; then a final extension for 5 min at 72°C. We used the S.N.A.P UV Gel Purification Kit (Invitrogen) to gel purify the amplicon.

We performed TD-PCR amplification of the *P. knowlesi* COXI fragment by using *P. knowlesi*–specific primers: cox1_Pk_F1 (5′-CATATCCAAGCCTCATTTATGA-3′) and cox1_Pk_R1 (5′-GTGAAAATGAGCAATTACATAA-3′). Amplification was performed in a 22 μL reaction mixture containing similar concentration of PCR master-mix recipe with cox1_F1 and cox1_R1 primers and 1 μL of purified mtDNA template. We used the following thermal cycling parameters: 94°C for 3 min for first denaturation; 10 cycles at 94°C for 30 s, 62°C for 45 s, and 72°C for 85 s; 25 cycles at 94°C for 30 s, 56°C for 45 s, and 72°C for 85 s; then a final extension for 5 min at 72°C. We purified the amplicon as we mentioned in the previous step.

We cloned the purified COXI fragments into TOPO TA Cloning Kit with pCR2.1-TOPO vector (Invitrogen) according to the manufacturer's protocol. We purified the recombinant plasmids containing the COXI fragment by using the S.N.A.P. Plasmid DNA MiniPrep Kit (Invitrogen) and sent these to a commercial facility for DNA sequencing. For all samples, ≥3 clones each for *P. cynomolgi* and *P. knowlesi* were sequenced and both forward and reverse strands were sequenced for each clone.

Computational Analyses of COXI of *Plasmodium* spp.

We used ClustalX version 2 to align the COXI sequences (*25*). We inferred phylogenetic relationships by using the neighbor-joining method in MEGA7 (*26*) then by Bayesian Markov chain Monte Carlo (MCMC) method in the BEAST package version 1.7.5 (*27*). We confirmed the convergence of the chain by inspecting the MCMC samples using Tracer version 1.5 (https://tracer-1-5.software.informer.com), discarded the first 10% sampling of the MCMC chains as burn-in, and conformed the sample size to ≥200 for all continuous parameters. We used Tree Annotator to annotate the tree generated by BEAST and visualized the maximum clade credibility tree by using FigTree version 1.3.1 (https://figtree-1-3-1.software.informer.com). We deposited *Plasmodium* COXI sequences generated in this study in GenBank under accession nos. MN372324–61 (Appendix, https://wwwnc.cdc.gov/EID/article/26/8/20-0343.xlsx).

Microscopy

We stained thick and thin blood films with Giemsa by using pH 7.2 buffer and examined films under an Olympus BX53 microscope (Olympus, https://www.olympus-lifescience.com). We estimated parasitemia by examining thick blood films and counting parasites associated with ≤500 leukocytes by 2 independent microscopists. We converted the parasite count to a count per microliter of blood by using the actual leukocyte count of each patient measured with a Sysmex KX-21N Kobe hematology analyzer (Sysmex Corporation, https://www.sysmex.com). We used a light microscope to observe the morphologic characteristics of the parasites in thin blood films.

Results

Patient Demographics and Identification of Malaria Parasites

Of the 1,047 patients, 845 (80.7%) had *P. knowlesi* monoinfections or co-infections with other species of *Plasmodium*, based on nested PCR assays (Figure 1; Table 1). Most (730; 86.3%) patients were ≥20 years of age, 91 (11%) were 12–19 years of age, and 24 (3%) were <12 years of age; 540 (51.5%) were female and 507 (48.5%) were male. Six patients (codes K07, KT46, K199, K221, K222, and K229) had co-infections with *P. knowlesi* and *P. cynomolgi* (Table 2) without prior history of malaria, and Kapit Hospital initially diagnosed *P. knowlesi* by microscopy. Throughout the 5-year study, we observed a remarkable increase in *Plasmodium knowlesi* malaria cases. In 2017 alone, 284 cases were identified, >2 times that of the highest annual number of cases, 122, admitted during a previous clinical study at Kapit Hospital during 2006–2008 (*28*).

Despite the high number of *P. knowlesi* malaria cases, 19% (202) of malaria cases in Kapit Hospital were infected by human *Plasmodium* species (non–simian *Plasmodium* parasites). During 2013–2016, 2–3

Table 1. Comparison of microscopy and PCR for identifying *Plasmodia* spp. among patients with malaria during June 24, 2013–December 31, 2017, Kapit Hospital, Kapit, Malaysian Borneo*

	PCR												
Microscopy	Pf	Pk	Pm	Pv	Po	Pf + Pv	Pf + Pm	Pf + Po	Pk + Pf	Pk + Pv	Pk + Pcy	Pv + Po	Total
P. falciparum	93	4	0	2	0	3	0	1	0	0	0	0	103
P. knowlesi	7	810	1	12	2	2	1	1	12	11	6	0	865
P. malariae	6	1	7	2	0	1	1	1	0	0	0	0	19
P. ovale	0	0	0	1	2	0	0	1	0	0	0	1	5
P. vivax	0	0	0	48	3	1	0	1	0	1	0	1	55
Total	106	815	8	65	7	7	2	5	12	12	6	2	1,047

* Pcy, *Plasmodium cynomolgi*; Pf, *P. falciparum*; Pk, *P. knowlesi*; Pm, *P. malariae*; Po, *P. ovale*; Pv, *P. vivax*.

indigenous infections were reported annually, but no indigenous infections were recorded in 2017. Based on travel history, 95% (192/202) of patients infected with nonsimian *Plasmodium* species were timber camp workers who had returned to Sarawak after working in Africa, Papua New Guinea, Brazil, and the Solomon Islands.

Molecular Characterization of *P. cynomolgi* and *P. knowlesi* Coinfections

To confirm the *P. cynomolgi* and *P. knowlesi* coinfections, we obtained *Plasmodium* DNA sequences of 38 partial COXI genes (1,088–1,144 bp) from the 6 patients. The Bayesian phylogenetic inference of these DNA sequences showed 20 sequences formed a monophyletic clade with *P. cynomolgi* referral sequences and was distinct from the *P. vivax* clade. The remaining 18 sequences, however, formed 2 distinct subclades with the *P. knowlesi* referral sequences (Figure 2), confirming the presence of *P. knowlesi* and *P. cynomolgi* parasites in these patients.

Morphological Characterization of *P. cynomolgi* and *P. knowlesi* Co-infections

Parasitemia in the 6 patients with *P. cynomolgi* and *P. knowlesi* co-infections ranged from 213 to 84,299 parasites/μL blood (Table 2). Only patients K07 and K199 had blood films of high enough quality for morphologic characterization of *Plasmodium* species. On examination, we noted *P. cynomolgi*–infected erythrocytes constituted a small proportion of the malaria-infected erythrocytes, consisting of ≈1.5% of infected erythrocytes for patients K07 and 4.7% for patient K199. We estimated the percentage of *P. cynomolgi*–infected erythrocytes by using the number of early trophozoite stages with Schüffner's stippling because we only observed the trophozoite stage for *P. cynomolgi* in these 2 patients. We distinguished *P. cynomolgi* from *P. knowlesi* parasites based on morphologic characteristics of infected erythrocytes, as previously described (*1*). We observed Schüffner's stippling in early trophozoite-infected erythrocytes, which were enlarged and distorted at times (Figures 3, 4). The trophozoites of *P. cynomolgi* also had either single, double, or triple chromatin dots. The growing trophozoites of *P. knowlesi* did not cause erythrocyte enlargement and we did not observe Schüffner's stippling (Figure 4, panels K, L). Furthermore, we observed band-form trophozoites of *P. knowlesi* in certain erythrocytes (Figure 3, panel I; Figure 4, panel M), and we noted 16 merozoites in 1 schizont (Figure 3, panel J). For patient K07, we examined 4,154 erythrocytes; 12 (0.3%) had prominent Schüffner's stippling, but we did not observe malaria parasites within these erythrocytes (Figure 5).

Table 2. Parasitemia and characteristics of patients with diagnosed *Plasmodium cynomolgi and P. knowlesi* coinfections, Malaysian Borneo

Case no.	Year detected	Age, y/sex	Parasites/μL blood
K222	2017	36/F	213
KT46	2013	18/M	334
K229	2017	63/F	1,386
K221	2017	50/F	13,661
K199	2017	17/M	17,072
K07	2016	65/M	84,299

Discussion

The increasing number of patients admitted to Kapit Hospital with *P. knowlesi* infections represents a true increase in infections, not increased awareness, because we used nested PCR to examine *Plasmodium* DNA from blood spots on filter paper from all patients during the study period. The increasing incidence of *P. knowlesi* in the Kapit Division, particularly in 2017; the few patients infected with human malaria parasites, *P. falciparum, P. vivax, P. ovale*, and *P. malariae*, during June 2013–December 2016; and the lack of indigenous cases in Kapit in 2017 reflect the recent malaria situation in Malaysian Borneo and Peninsular Malaysia (*11*). The Ministry of Health, Malaysia, reported 7,745 cases of *P. knowlesi* malaria in Malaysia in 2017 and 2018, and 87% (6,743) occurred in the Malaysian Borneo states of Sarawak and Sabah (*29*). In 2017, only 85 cases of indigenous malaria caused by the human malaria parasites, *P. falciparum, P. vivax, P. ovale*, or *P. malariae* were reported, and none were reported in 2018 (*30*).

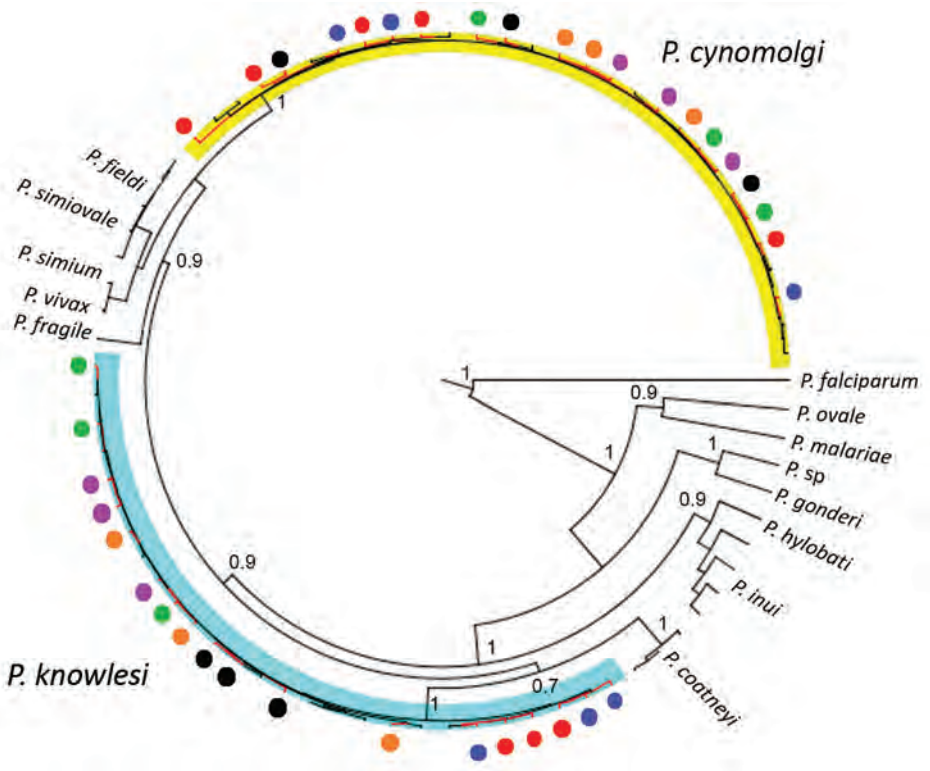

Figure 2. Maximum clade credibility tree for *Plasmodium* cytochrome c oxidase subunit 1 (COXI) sequences from samples from patients admitted to Kapit Hospital with malaria during June 24, 2013–December 31, 2017, Malaysian Borneo. Tree was generated by using strict clock model and Bayesian skyline coalescent tree prior. Circles indicate COXI sequences derived from patients: red indicates patient KT46; black indicates patient K07; orange indicates patient K199; purple indicates patient K221; blue indicates patient K222; and green indicates patient K229.

The increase in *P. knowlesi* malaria cases, particularly in Malaysian Borneo, is multifactorial and driven partly by anthropogenic land-use factors leading to changes in the transmission pattern of the parasite between humans, vectors, and macaque reservoirs (*31*). Both states in Malaysian Borneo have undergone substantial deforestation, primarily for palm oil plantations; the total area used for palm oil plantations in Sarawak and Sabah in 2018 was 3.12 million hectares (*32*) compared with just 2.3 million hectares in 2010 (*33*). Such extensive forest clearing activities result in loss of natural habitat for macaques and could have caused them to move closer to human settlements. In Sabah, an association between deforestation and increased incidence of human cases of *P. knowlesi* malaria has been demonstrated (*34*). Furthermore, predictive spatial scale analysis of data from a case-controlled study, a cross-sectional survey, and satellite

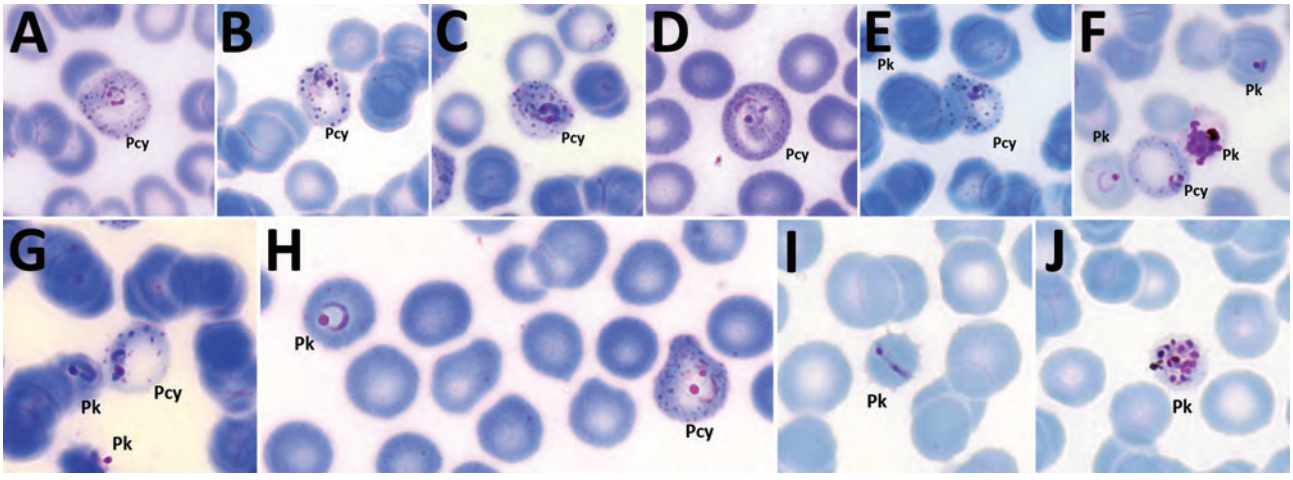

Figure 3. *Plasmodium cynomolgi* and *P. knowlesi* parasites in patient K07, admitted to Kapit Hospital, Kapit, Malaysia, with malaria in 2016. A–G) Early trophozoites of *P. cynomolgi* in enlarged and, at times, distorted erythrocytes, with Schüffner's stippling and either single, double, or triple chromatin dots. E–H) *P. knowlesi* and *P. cynomolgi* early trophozoites. I) Band form trophozoite of *P. knowlesi*. J) Schizont of *P. knowlesi*. Pcy, *P. cynomolgi*; Pk, *P. knowlesi*. Original magnification ×100.

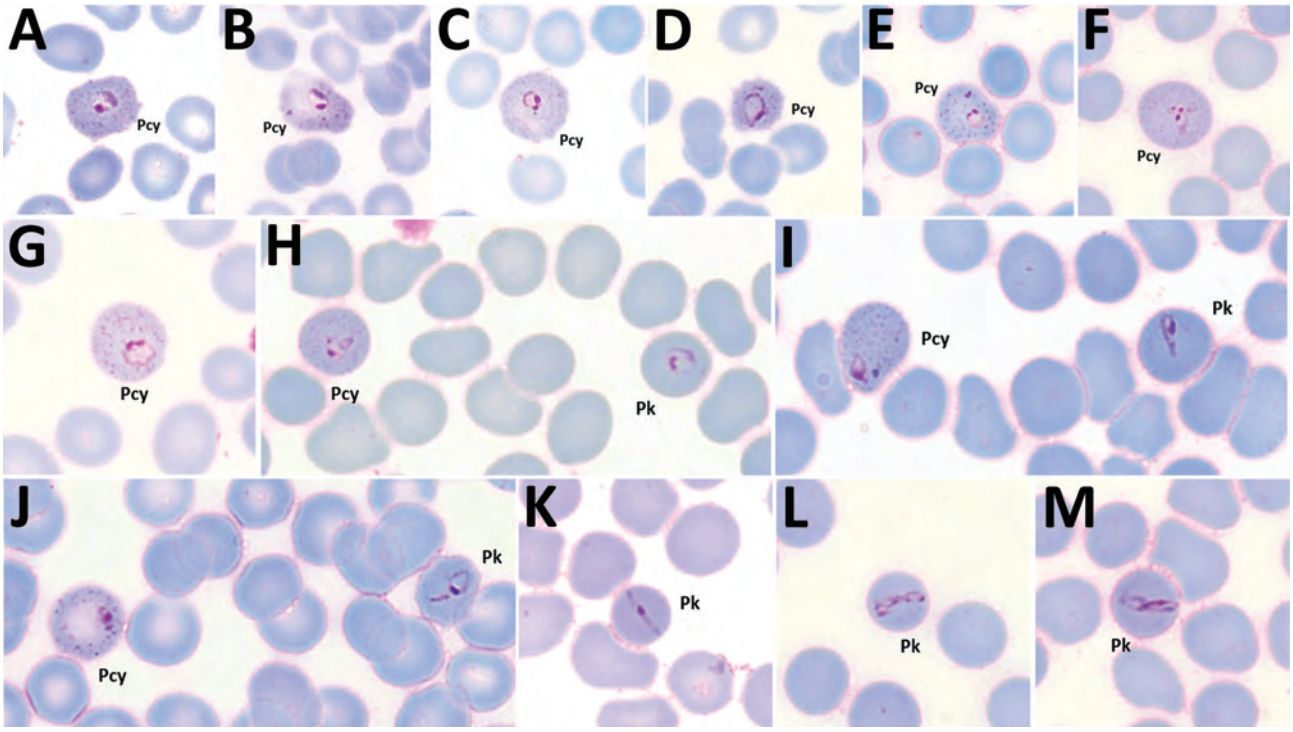

Figure 4. *Plasmodium cynomolgi* and *P. knowlesi* parasites in patient K199, admitted to Kapit Hospital in Kapit, Malaysia, with malaria in 2017. A–G) Early trophozoites of *P. cynomolgi* within enlarged and, at times, distorted erythrocytes, with Schüffner's stippling and single, double, or triple chromatin dots. H–J) Early trophozoites of *P. knowlesi* and *P. cynomolgi*. K–M) Band form trophozoites of *P. knowlesi*. Pcy, *P. cynomolgi*; Pk, *P. knowlesi*. Magnification ×100.

imagery showed that landscape fragmentation influences *P. knowlesi* transmission to humans (*35*). However, similar studies need to be undertaken in Sarawak to determine whether a direct relationship between land change use and number of *P. knowlesi* malaria cases exists because the vectors in Sarawak are different from those in Sabah.

Entomologic studies also need to be undertaken because vector bionomics is influenced by landscape factors, and abrupt land use conversion or modifications can change vector distribution, invasion, and behavior (*36*,*37*). One such study conducted in the Kinabatangan area of Sabah in Malaysian Borneo demonstrated that, in a 2-year period *Anopheles donaldi* mosquitoes displaced *An. balabacensis* mosquitoes, the previously dominant vector in that area (*38*). Changes in host preference, biting behavior, and adaptation of the mosquitoes to habitat changes could affect the transmission of zoonotic malaria in Malaysian Borneo. However, determining whether there have been changes in mosquito bionomics in Sarawak is difficult because only 1 study on vector bionomics was conducted in Kapit District in 2004. New detailed entomologic studies at various locations clearly are necessary.

In the 2 patients whose blood films we examined, *P. cynomolgi* parasites comprised ≈1.5% and 4.7% of the total malaria parasites, which explains why microscopy only detected single *P. knowlesi* infections in these patients. The dominance of *P. knowlesi* over *P. cynomolgi* is probably due to the differences in the period of development in the liver and the duration of the erythrocytic cycle between the 2 species. Studies undertaken on the Mulligan (M) strain, and the B strain of *P. cynomolgi* indicated that the incubation period in the liver varied from 15 to 20 days for the B strain and 16 to 37 days for the M strain (*1*), which is much longer than the estimated incubation period for *P. knowlesi* of 9–12 days (*1*). Furthermore, the asexual erythrocytic cycle of *P. knowlesi* is only 24 hours but is 48 hours for *P. cynomolgi* (*1*,*4*). Hence, if *P. knowlesi* and *P. cynomolgi* co-infection occur simultaneously through a single mosquito bite, *P. knowlesi* parasites would emerge from the liver before *P. cynomolgi* and replicate rapidly to become the dominant species infecting the person.

Unlike *P. knowlesi* infections, which can be severe and sometimes fatal (*4*), *P. cynomolgi* infections in humans are mild or even asymptomatic (*1*). In a series of experiments conducted in the United States in the

1960s, volunteers infected with *P. cynomolgi* had mild infections, and for 1 participant the infection persisted for 58 days (*1*,*39*,*40*). A natural infection was reported in a woman with fever in Peninsular Malaysia (*16*), and a tourist from Denmark also had a mild infection with *P. cynomolgi* after returning home from travels in Southeast Asia (*41*). Recently, naturally acquired *P. cynomolgi* and *P. knowlesi* co-infections in Cambodia (*17*) and *P. cynomolgi* monoinfections in Sabah, Malaysian Borneo (*42*), were all asymptomatic. However, our study is hospital-based, so all patients who had *P. cynomolgi* with *P. knowlesi* co-infections were symptomatic.

A recent study described the morphologic characteristics of young to near-mature trophozoites of *P. cynomolgi* in a naturally acquired human host (*41*). We observed only young trophozoites of *P. cynomolgi* in enlarged and at times distorted erythrocytes with Schüffner's stippling. We observed erythrocytes with stippling without malaria parasites in 1 of the patients. This phenomenon, termed pitting, was initially described for *P. knowlesi* in the 1960s during animal experiments (*43*,*44*). Pitting is a process by which the malaria parasite is expelled from an infected erythrocyte as it passes through the spleen. Once deparasitized through pitting, the erythrocytes return to circulation in the blood. The presence of pitting also was discovered in acute *P. falciparum* infections in which erythrocytes with ring-infected erythrocyte surface antigen and no intracellular parasites in circulation were observed (*45*–*47*). The presence of enlarged deparasitized erythrocytes with Schüffner's stippling from patient K07 suggests *P. cynomolgi* parasites might have been pitted, leaving the once-infected erythrocytes circulating in the patient's blood.

The morphologic similarities between *P. cynomolgi* and *P. vivax* have been described previously (*1*,*16*), highlighting the difficulty in correctly identifying *P. cynomolgi* by microscopy. In our study and recent reports of naturally acquired human *P. cynomolgi* infections in Cambodia, Malaysia, and Southeast Asia, molecular methods were necessary to identify *P. cynomolgi* (*17*,*41*,*42*). Microscopy, or rapid diagnostic tests, which are the main methods used in malaria surveys, would have identified the *P. cynomolgi* monoinfections in our study as *P. vivax*. Therefore, the incidence of *P. cynomolgi* in Asia, the natural habitat for several monkey hosts (*1*), is probably much higher than what has been reported so far. Continued surveillance by

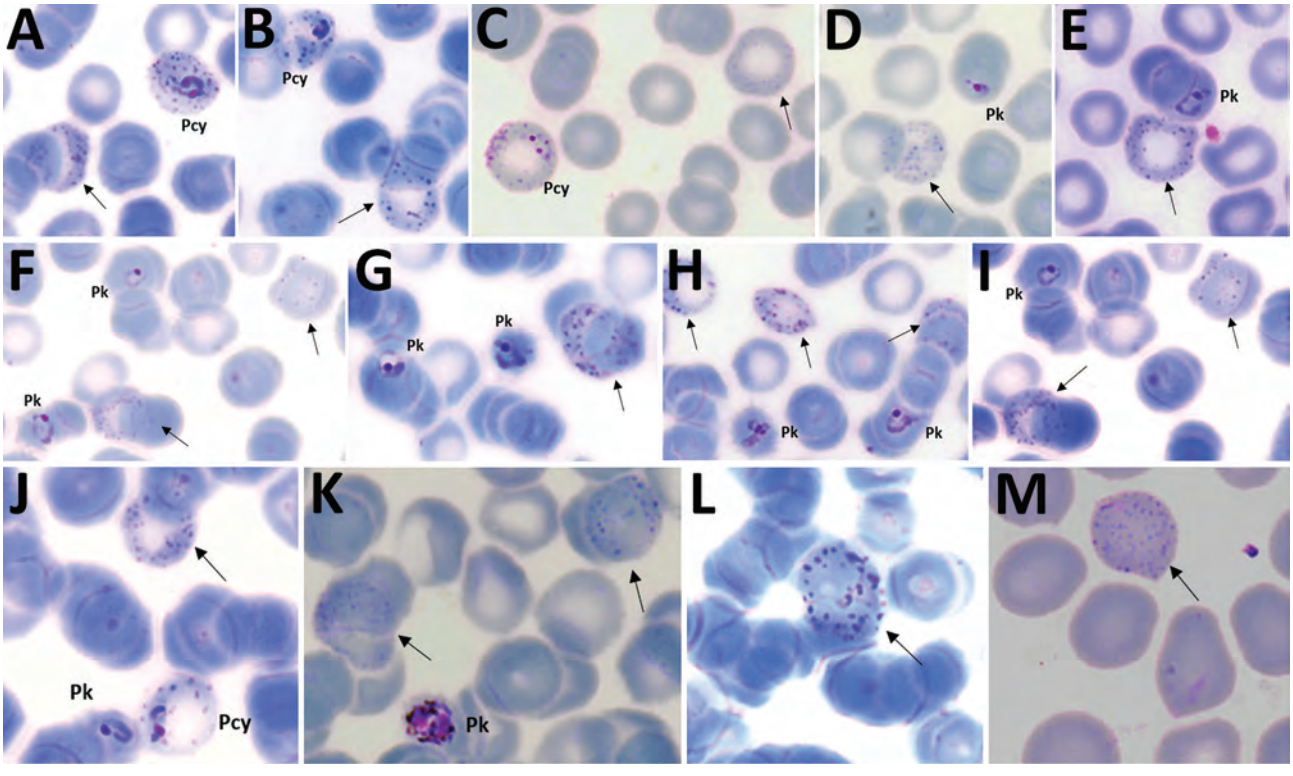

Figure 5. *Plasmodium cynomolgi* and *P. knowlesi* parasites in patient K07, admitted to Kapit Hospital in Kapit, Malaysia, with malaria in 2016. Arrows indicate Schüffner's stippling in erythrocytes without parasites. A–C) Early trophozoites of *P. cynomolgi*; D–I) early trophozoites of *P. knowlesi;* J) early trophozoites of *P. knowlesi* and *P. cynomolgi*; K) gametocyte of *P. knowlesi*. Pcy, *P. cynomolgi*; Pk, *P. knowlesi*. Magnification ×100.

using molecular methods is needed to obtain accurate data for the incidence of not only *P. cynomolgi*, but also *P. knowlesi*.

In conclusion, we observed that *P. knowlesi* continues to be of public health concern in the Kapit Division of Sarawak, Malaysian Borneo, and that another simian malaria parasite, *P. cynomolgi*, also is an emerging cause of malaria in humans. Further epidemiologic and entomologic studies using molecular tools and a multidisciplinary approach need to be undertaken in Southeast Asia to determine the incidence of *P. cynomolgi* and *P. knowlesi*. Such studies also will assist in determining whether these parasites continue to cause zoonotic infections or whether the loss of natural habitat of macaques, coupled with changes in mosquito composition, abundance, and feeding behavior and an increase in the human population, result in their switch to humans as the preferred hosts.

Acknowledgments

We thank colleagues at the Malaria Research Centre, UNIMAS, and the medical laboratory technologists, doctors, and nurses at Kapit Hospital for assistance, and the Director-General of Health in Malaysia for permission to publish this paper.

This study was supported by a postgraduate scholarship from the Ministry of Higher Education in Malaysia to T.H.H., and grants from UNIMAS (nos. 05-FA052000-0606-0002, F05/DPD/1793/2019, and F05/DPP/1505/2016).

About the Author

Dr. Nada Raja is a post-doctoral researcher at the Malaria Research Centre in UNIMAS, Malaysia. Her research interests include molecular evolution, population genetics, and genomics of malaria parasites.

References

1. Coatney GR, Collins WE, Warren M, Contacos PG. The primate malarias. Washington (DC): US National Institute of Allergy and Infectious Diseases; 1971.
2. Ramasamy R. Zoonotic malaria—global overview and research and policy needs. Front Public Health. 2014;2:123. https://doi.org/10.3389/fpubh.2014.00123
3. Singh B, Sung LK, Matusop A, Radhakrishnan A, Shamsul SS, Cox-Singh J, et al. A large focus of naturally acquired *Plasmodium knowlesi* infections in human beings. Lancet. 2004;363:1017–24. https://doi.org/10.1016/S0140-6736(04)15836-4
4. Singh B, Daneshvar C. Human infections and detection of *Plasmodium knowlesi*. Clin Microbiol Rev. 2013;26:165–84. https://doi.org/10.1128/CMR.00079-12
5. Zaw MT, Lin Z. Human *Plasmodium knowlesi* infections in South-East Asian countries. J Microbiol Immunol Infect. 2019;52:679–84. https://doi.org/10.1016/j.jmii.2019.05.012
6. Maeno Y, Culleton R, Quang NT, Kawai S, Marchand RP, Nakazawa S. *Plasmodium knowlesi* and human malaria parasites in Khan Phu, Vietnam: gametocyte production in humans and frequent co-infection of mosquitoes. Parasitology. 2017;144:527–35. https://doi.org/10.1017/S0031182016002110
7. Iwagami M, Nakatsu M, Khattignavong P, Soundala P, Lorphachan L, Keomalaphet S, et al. First case of human infection with *Plasmodium knowlesi* in Laos. PLoS Negl Trop Dis. 2018;12:e0006244. https://doi.org/10.1371/journal.pntd.0006244
8. Pongvongsa T, Culleton R, Ha H, Thanh L, Phongmany P, Marchand RP, et al. Human infection with *Plasmodium knowlesi* on the Laos-Vietnam border. Trop Med Health. 2018;46:33. https://doi.org/10.1186/s41182-018-0116-7
9. Lubis IND, Wijaya H, Lubis M, Lubis CP, Divis PCS, Beshir KB, et al. Contribution of *Plasmodium knowlesi* to multispecies human malaria infections in North Sumatera, Indonesia. J Infect Dis. 2017;215:1148–55. https://doi.org/10.1093/infdis/jix091
10. Cox-Singh J, Davis TME, Lee KS, Shamsul SSG, Matusop A, Ratnam S, et al. *Plasmodium knowlesi* malaria in humans is widely distributed and potentially life threatening. Clin Infect Dis. 2008;46:165–71. https://doi.org/ 10.1086/524888
11. Hussin N, Lim YAL, Goh PP, William T, Jelip J, Mudin RN. Updates on malaria incidence and profile in Malaysia from 2013 to 2017. Malar J. 2020;19:55. https://doi.org/10.1186/s12936-020-3135-x
12. Lee KS, Cox-Singh J, Singh B. Morphological features and differential counts of *Plasmodium knowlesi* parasites in naturally acquired human infections. Malar J. 2009;8:73. https://doi.org/10.1186/1475-2875-8-73
13. Brasil P, Zalis MG, de Pina-Costa A, Siqueira AM, Júnior CB, Silva S, et al. Outbreak of human malaria caused by *Plasmodium simium* in the Atlantic Forest in Rio de Janeiro: a molecular epidemiological investigation. Lancet Glob Health. 2017;5:e1038–46. https://doi.org/10.1016/S2214-109X(17)30333-9
14. de Alvarenga DAM, Culleton R, de Pina-Costa A, Rodrigues DF, Bianco C Jr, Silva S, et al. An assay for the identification of *Plasmodium simium* infection for diagnosis of zoonotic malaria in the Brazilian Atlantic Forest. Sci Rep. 2018;8:86. https://doi.org/10.1038/s41598-017-18216-x
15. Lalremruata A, Magris M, Vivas-Martínez S, Koehler M, Esen M, Kempaiah P, et al. Natural infection of *Plasmodium brasilianum* in humans: man and monkey share quartan malaria parasites in the Venezuelan Amazon. EBioMedicine. 2015;2:1186–92. https://doi.org/10.1016/j.ebiom.2015.07.033
16. Ta TH, Hisam S, Lanza M, Jiram AI, Ismail N, Rubio JM. First case of a naturally acquired human infection with *Plasmodium cynomolgi*. Malar J. 2014;13:68. https://doi.org/10.1186/1475-2875-13-68
17. Imwong M, Madmanee W, Suwannasin K, Kunasol C, Peto TJ, Tripura R, et al. Asymptomatic natural human infections with simian malaria parasites *Plasmodium cynomolgi* and *Plasmodium knowlesi*. J Infect Dis. 2019;219:695–702. https://doi.org/10.1093/infdis/jiy519
18. Nada Raja T, Hu TH, Zainudin R, Lee KS, Perkins SL, Singh B. Malaria parasites of long-tailed macaques in Sarawak, Malaysian Borneo: a novel species and demographic and evolutionary histories. BMC Evol Biol. 2018;18:49. https://doi.org/10.1186/s12862-018-1170-9
19. Cheong WH, Coombs GL. Transmission of *Plasmodium cynomolgi* (Perlis strain) to man. Southeast Asian J Trop Med Public Health. 1970;1:302.

20. Gupta JMD. Transmission of *Plasmodium inui* to man. Proc Natl Inst Sci India. 1938;4:241–4.
21. Coatney GR, Chin W, Contacos PG, King HK. *Plasmodium inui*, a quartan-type malaria parasite of Old World monkeys transmissible to man. J Parasitol. 1966;52:660–3. https://doi.org/10.2307/3276423
22. Garamszegi LZ. Patterns of co-speciation and host switching in primate malaria parasites. Malar J. 2009;8:110. https://doi.org/10.1186/1475-2875-8-110
23. Tan CH, Vythilingam I, Matusop A, Chan ST, Singh B. Bionomics of *Anopheles latens* in Kapit, Sarawak, Malaysian Borneo in relation to the transmission of zoonotic simian malaria parasite *Plasmodium knowlesi.* Malar J. 2008;7:52. https://doi.org/10.1186/1475-2875-7-52
24. Lee KS, Divis PCS, Zakaria SK, Matusop A, Julin RA, Conway DJ, et al. *Plasmodium knowlesi*: reservoir hosts and tracking the emergence in humans and macaques. PLoS Pathog. 2011;7:e1002015. https://doi.org/10.1371/journal.ppat.1002015
25. Larkin MA, Blackshields G, Brown NP, Chenna R, McGettigan PA, McWilliam H, et al. Clustal W and Clustal X version 2.0. Bioinformatics. 2007;23:2947–8. https://doi.org/10.1093/bioinformatics/btm404
26. Kumar S, Stecher G, Tamura K. MEGA7: Molecular Evolutionary Genetics Analysis version 7.0 for bigger datasets. Mol Biol Evol. 2016;33:1870–4 https://doi.org/10.1093/molbev/msw054
27. Drummond AJ, Suchard MA, Xie D, Rambaut A. Bayesian phylogenetics with BEAUti and the BEAST 1.7. Mol Biol Evol. 2012;29:1969–73. https://doi.org/10.1093/molbev/mss075
28. Daneshvar C, Davis TME, Cox-Singh J, Rafa'ee MZ, Zakaria SK, Divis PCS, et al. Clinical and laboratory features of human *Plasmodium knowlesi* infection. Clin Infect Dis. 2009;49:852–60. https://doi.org/10.1086/605439
29. Ministry of Health Malaysia. Annual report of malaria elimination progress and activities 2018. Kuala Lumpur: the Ministry; 2018.
30. World Health Organization. World malaria report 2018. Geneva: The Organization; 2018 [cited 2020 Jan 28]. https://www.who.int/malaria/publications/world-malaria-report-2018/report
31. Davidson G, Chua TH, Cook A, Speldewinde P, Weinstein P. The role of ecological linkage mechanisms in *Plasmodium knowlesi* transmission and spread. EcoHealth. 2019;16:594–610. https://doi.org/10.1007/s10393-019-01395-6
32. Malaysian Palm Oil Board: Economic and Industry Development Division. Overview of Malaysian palm oil industry 2018. Bangi, Malaysia: The Board; 2018 [cited 2020 Jan 16]. http://bepi.mpob.gov.my/images/overview/Overview_of_Industry_2018.pdf
33. Malaysian Palm Oil Board: Economic and Industry Development Division. Overview of Malaysian palm oil industry 2010. Bangi, Malaysia: The Board; 2010 [cited 2020 Jan 16]. http://bepi.mpob.gov.my/images/overview/Overview_of_Industry_2010.pdf
34. Fornace KM, Herman LS, Abidin TR, Chua TH, Daim S, Lorenzo PJ, et al. Exposure and infection to *Plasmodium knowlesi* in case study communities in Northern Sabah, Malaysia and Palawan, The Philippines. PLoS Negl Trop Dis. 2018;12:e0006432. https://doi.org/10.1371/journal.pntd.0006432
35. Brock PM, Fornace KM, Grigg MJ, Anstey NM, William T, Cox J, et al. Predictive analysis across spatial scales links zoonotic malaria to deforestation. Proc Biol Sci. 2019;286:20182351. https://doi.org/10.1098/rspb.2018.2351
36. Guerra CA, Snow RW, Hay SI. A global assessment of closed forests, deforestation and malaria risk. Ann Trop Med Parasitol. 2006;100:189–204. https://doi.org/10.1179/136485906X91512
37. Lambin EF, Tran A, Vanwambeke SO, Linard C, Soti V. Pathogenic landscapes: interactions between land, people, disease vectors, and their animal hosts. Int J Health Geogr. 2010;9:54. https://doi.org/10.1186/1476-072X-9-54
38. Vythilingam I, Chan ST, Shanmugratnam C, Tanrang H, Chooi KH. The impact of development and malaria control activities on its vectors in the Kinabatangan area of Sabah, East Malaysia. Acta Trop. 2005;96:24–30. https://doi.org/10.1016/j.actatropica.2005.06.022
39. Kuvin SFK, Beye HK, Stohlman F Jr, Contacos PG, Coatney GR. Clinical and physiological responses in sporozoite-induced B strain *Plasmodium cynomolgi* and *Plasmodium vivax* infections in normal volunteers. Trans R Soc Trop Med Hyg. 1962;56:371–8. https://doi.org/10.1016/0035-9203(62)90007-X
40. Coatney GR, Elder HA, Contacos PG, Getz ME, Greenland R, Rossan RN, et al. Transmission of the M strain of *Plasmodium cynomolgi* to man. Am J Trop Med Hyg. 1961;10:673–8. https://doi.org/10.4269/ajtmh.1961.10.673
41. Hartmeyer GN, Stensvold CR, Fabricius T, Marmolin ES, Hoegh SV, Nielsen HV, et al. *Plasmodium cynomolgi* as cause of malaria in tourist to Southeast Asia, 2018. Emerg Infect Dis. 2019;25:1936–9. https://doi.org/10.3201/eid2510.190448
42. Grignard L, Shah S, Chua TH, William T, Drakeley CJ, Fornace KM. Natural human infections with *Plasmodium cynomolgi* and other malaria species in an elimination setting in Sabah, Malaysia. J Infect Dis. 2019;220:1946–9. https://doi.org/10.1093/infdis/jiz397
43. Conrad ME, Dennis LH. Splenic function in experimental malaria. Am J Trop Med Hyg. 1968;17:170–2. https://doi.org/10.4269/ajtmh.1968.17.170
44. Schnitzer B, Sodeman T, Mead ML, Contacos PG. Pitting function of the spleen in malaria: ultrastructural observations. Science. 1972;177:175–7. https://doi.org/10.1126/science.177.4044.175
45. Angus BJ, Chotivanich K, Udomsangpetch R, White NJ. In vivo removal of malaria parasites from red blood cells without their destruction in acute falciparum malaria. Blood. 1997;90:2037–40. https://doi.org/10.1182/blood.V90.5.2037
46. Newton PN, Chotivanich K, Chierakul W, Ruangveerayuth R, Teerapong P, Silamut K, et al. A comparison of the *in vivo* kinetics of *Plasmodium falciparum* ring-infected erythrocyte surface antigen-positive and -negative erythrocytes. Blood. 2001;98:450–7. https://doi.org/10.1182/blood.V98.2.450
47. Buffet PA, Safeukui I, Deplaine G, Brousse V, Prendki V, Thellier M, et al. The pathogenesis of *Plasmodium falciparum* malaria in humans: insights from splenic physiology. Blood. 2011;117:381–92. https://doi.org/10.1182/blood-2010-04-202911

Address for correspondence: Balbir Singh, Malaria Research Centre, Universiti Malaysia Sarawak, 94300 Kota Samarahan, Sarawak, Malaysia; email: bsingh@unimas.my

Presence of Segmented Flavivirus Infections in North America

Kurt J. Vandegrift,[1] Arvind Kumar,[1] Himanshu Sharma, Satyapramod Murthy, Laura D. Kramer, Richard S. Ostfeld, Peter J. Hudson, Amit Kapoor

Identifying viruses in synanthropic animals is necessary for understanding the origin of many viruses that can infect humans and developing strategies to prevent new zoonotic infections. The white-footed mouse, *Peromyscus leucopus*, is one of the most abundant rodent species in the northeastern United States. We characterized the serum virome of 978 free-ranging *P. leucopus* mice caught in Pennsylvania. We identified many new viruses belonging to 26 different virus families. Among these viruses was a highly divergent segmented flavivirus whose genetic relatives were recently identified in ticks, mosquitoes, and vertebrates, including febrile humans. This novel flavi-like segmented virus was found in rodents and shares <70% aa identity with known viruses in the highly conserved region of the viral polymerase. Our data will enable researchers to develop molecular reagents to further characterize this virus and its relatives infecting other hosts and to curtail their spread, if necessary.

Most human infectious diseases have a zoonotic origin (*1*). RNA viruses are remarkable in their ability to evolve and infect a wide range of hosts, primarily due to their error-prone replication, small genome size, and ability to adapt (*2*). Recent studies describing human infections with animal coronaviruses and paramyxoviruses illustrate well the high zoonotic potential of animal RNA viruses (*3*). Not all viruses at the human–animal interface can breach the species barrier, and successful cross-species transmission often requires repeated introduction coupled with favorable circumstances (*3*). These multiple exposures provide increased opportunity for viral adaptation, and because humans are frequently exposed to viruses from synanthropic hosts, this channel becomes a likely route of infection. As such, we need to identify and characterize viruses from synanthropic animals to understand the origins of many human viruses and obtain insights into the emergence of potential zoonotic infections (*1*).

Rodents and bats are common sources of potential zoonotic viruses (*4*). In the northeastern United States, the white-footed mouse (*Peromyscus leucopus*) is one of the most widespread and abundant rodent species. These mice are highly adaptable, commonly become synanthropic, and invade human domiciles. Humans are exposed to a wide range of viruses from these mice, either directly as is the case with hantaviruses or indirectly through vectors such as ticks. These rodents are also known to harbor a range of zoonotic pathogens, including the tickborne *Borrelia burgdorferi*, which causes Lyme disease, and *Anaplasma phagocytilium*, which causes anaplasmosis (*5*). White-footed mice can also act as reservoirs for bacteria that are causative agents of Rocky Mountain spotted fever, tularemia, plague, and bartonellosis and for protozoans responsible for babesiosis, giardiasis, toxoplasmosis, and cryptosporidiosis (*6*). Infectious viruses reported in *P. leucopus* include lymphocytic choriomeningitis virus, Powassan or deer tick encephalitis virus, and hantaviruses (*7*,*8*).

The genome of flaviviruses is composed of a single-stranded positive-sense RNA that codes for a single polyprotein. The genome of Jingmen tick virus (JMTV), which was first identified in 2014 from ticks in the Jingmen province of China (*9*), is composed of 4 single-stranded positive-sense RNA

Author affiliations: Center for Infectious Disease Dynamics, Pennsylvania State University, University Park, Pennsylvania, USA (K.J. Vandegrift, P.J. Hudson); Center for Vaccines and Immunity, The Research Institute at Nationwide Children's Hospital, Columbus, Ohio, USA (A. Kumar, H. Sharma, S. Murthy, A. Kapoor); Wadsworth Center, New York State Department of Health, Albany, New York, USA (L.D. Kramer); University of Albany-SUNY School of Public Health, Albany (L.D. Kramer); The Cary Institute of Ecosystem Studies, Millbrook, New York, USA (R.S. Ostfeld); Ohio State University College of Medicine and Public Health, Columbus (A. Kapoor)

DOI: https://doi.org/10.3201/eid2608.190986

[1]These authors contributed equally to this article.

segments, 2 of which encode a polymerase protein (NS5) and a helicase protein (NS3) that show close phylogenetic relatedness with the corresponding proteins of classical flaviviruses (*9*). Later, several genetically diverse relatives of JMTV were found in several species of ticks, insects, and mammals (*9*–*13*). Together, these JMTV-like viruses are highly diverse and show differences in the number of genomic segments as well as protein coding strategies (*9*,*10*,*12*). In 2018, a metagenomics study revealed the presence of JMTV-like sequences in serum samples from human patients with Crimean-Congo hemorrhagic fever in Kosovo (*14*). Two studies published in 2019 reported the presence of JMTV sequences in humans in China with febrile illness and a history of recent tick bites (*15*,*16*). To date, no information is available on the presence of JMTV infections in insects, ticks, or vertebrates in North America.

Knowledge about viruses infecting *P. leucopus* and the levels to which humans are being exposed is limited. Although several studies have examined the prevalence of hantaviruses (*17*) and highly diverse hepaciviruses (*18*), there has been no attempt to characterize the blood virome of these common rodents. We used an unbiased, metaviromics approach to identify all viruses in the serum samples of 978 free-ranging white-footed mice captured over a period of 7 years from suburban and wild areas of Pennsylvania.

Materials and Methods

Origin and Details of White-Footed Mouse Samples

We collected serum samples from *P. leucopus* mice each spring and autumn during 2011–2017 from 4 sites in central Pennsylvania. We selected these sites because they provided gradient levels of human activity and so exposure to rodents; site 1 had the highest level of exposure and site 4 had the lowest. At site 1 (Deer Pens), mouse infestation is reported in residences, workplaces, and the surrounding area, providing a potentially high level of exposure to rodents. Site 2 (Spray Fields) is a disturbed forest where treated wastewater is sprayed; it is frequented daily by maintenance employees and dog walkers, but there are no residences on site. Site 3 (Scotia) is on Pennsylvania state game lands that border housing communities and has mostly seasonal visitors, such as hikers, hunters, and trappers. Site 4 (Stone Valley) is in a large contiguous forest that has very few people or residences. Additional details about the sites have been described previously (*19*).

Whole blood was obtained from the retro-orbital sinus of the anesthetized mice. These blood samples were centrifuged at 8,000 × *g* for 10 min and the serum was then collected with a micropipette. Samples were stored at –80°C. All procedures were approved by Penn State's Institutional Animal Care and Use Committee (IACUC #46246).

Metagenomics, Metaviromics, and Bioinformatics

We used serum samples from 978 wild free-ranging *P. leucopus* mice to generate the high-throughput sequence data to characterize the virome of these rodents. We used a 10-μL subsample of serum from each individual mouse to create 9 pools. We assigned individual mice to pools by bodyweight (as a proxy for age) and study site. We centrifuged serum pools at 8,000 × *g* for 10 min to remove particulate matter. The supernatants were treated with DNase (100 U), RNase (20 U), and Benzonase (250 U) to enrich samples for particle-protected (virion) nucleic acids. We used the QIAamp Viral RNA Mini Kit (QIAGEN Inc., https://www.qiagen.com) to extract nucleic acid from the serum pools and eluted it in 60 μL of elution buffer supplemented with 40 U of ribonuclease inhibitor, then stored at it –80°C before library preparation. We used a unique 20-nt barcoded oligonucleotide primer for each sample pool during reverse transcription PCR (RT-PCR) and second-strand DNA synthesis, as previously described (*20*). We prepared libraries for Illumina sequencing as previously described (*21*) and performed sequencing on a HiSeq 4000 platform (Illumina Inc., https://www.illumina.com) for 2×150 cycles in the Biomedicine Genomics Core at the Research Institute of Nationwide Children's Hospital (Columbus, Ohio, USA).

We used the 20-nt unique barcodes included in the primers to make libraries to demultiplex the sequence data. After removing low-complexity regions and low-quality bases, we aligned paired-end reads to the *P. leucopus* genomes with Bowtie2 mapper version 2.0.6 (SourceForge, https://sourceforge.net) to remove the host-derived sequences. We used MIRA version 4.0 (SourceForge) (22) for de novo assembly of remaining sequences. Finally, we analyzed all contigs and unique reads using MegaBLAST https://blast.ncbi.nlm.nih.gov/Blast.cgi) against the GenBank nonredundant nucleotide database. Next, we used BLASTX to analyze sequences that showed poor or no homology (e-score >0.001) against the viral GenBank protein database, followed by BLASTX against the nonredundant protein database. We then used reference genomes of known viruses available in GenBank to extract related sequences present in the 9 serum pools. Finally, we used specific PCR assays and traditional dideoxy

sequencing of amplicons to confirm bioinformatics-based assembly of virus reads.

Presence and Prevalence of Flavi-Like Segmented Virus and South Bay Virus

We selected 2 viruses recently identified in ticks for further characterization: a highly divergent JMTV-like virus, provisionally named flavi-like segmented virus (FLSV or FLSV-US); and South Bay virus (SBV), a tick virus that belongs to the family *Nairoviridae*, order *Bunyavirales* (*23*,*24*). We extracted individual serum samples from the 72 *P. leucopus* mice that made up the pool with the maximum number of unique FLSV-US sequence reads and screened for the presence of FLSV-US RNA by using a nested RT-PCR targeting the conserved NS5 polymerase region. We used the primers FLSV-US-F1 (5′-GGWGCYATGGGYTACCAGAT-3′) and FLSV-US-R1 (5′-TCCARGGTGAGTARTCCTTTCG-3′) in the first round of PCR, and FLSV-US-F2 (5′-GGWGCYATGGGYTACCAGATGGA-3′) and FLSV-US-R2 (5′-CCARGGTGAGTARTCCTTTCGARATC-3′) in the second round. The first-round PCR cycle included 8 min of initial denaturation at 95°C; 10 cycles of 95°C for 40 s, 56°C for 1 min, and 72°C for 1 min; 30 cycles of 95°C for 30 s, 54°C for 30 s, and 72°C for 1 min; and a final extension at 72°C for 5 min. In the first 10 cycles, the annealing temperature was ramped down by 0.5°C each cycle to enable nucleotide mismatch tolerance during primer hybridization. The second-round PCR conditions included 8 min of initial denaturation at 95°C; 10 cycles of 95°C for 40 s, 60°C for 1 min, and 72°C for 1 min; 30 cycles of 95°C for 30 s, 58°C for 30 s, and 72°C for 1 min; and a final extension at 72°C for 5 min.

We used a heminested RT-PCR targeting the viral polymerase gene to screen serum samples from the same 72 mice for the presence of SBV. We used the primers SBV-F1 (5′-AYCCAGATTGGAARCACTTCATAATG-3′) and SBV-R1 (5′-CCATATGTDGTAATMACYTTWGCATA-3′) for first round of PCR, and SBV-F2 (5′-GTTATGTTGAAGGACCTTAACAAAG-3′) and SBV-R1 for the second round. The PCR cycle for both rounds of PCR included 8 min of initial denaturation at 95°C; 10 cycles of 95°C for 30 s, 55°C for 2 min, and 72°C for 1 min; 30 cycles of 95°C for 25 s, 54°C for 30 s, and 72°C for 30 s; and a final extension at 72°C for 5 min. In the first 10 cycles, the annealing temperature was ramped down by 0.5°C each cycle to enable nucleotide mismatch tolerance during primer hybridization step.

Phylogenetic Analysis and Genome Organization of FLSV-US

We aligned sequences that showed substantial similarity with JMTV NS5 proteins with reference sequence YP_009029999.1 (GenBank accession no. MN811583) to design PCR primers for direct amplification of 2,568-nt FLSV-US sequences. After we confirmed the FLSV-US assembled sequence by Sanger sequencing, we aligned the translated protein sequence with the sequence of known JMTV-like viruses (aa 55 to 913 of NS5 protein) using BLOSUM protein weight matrix, using default parameters in MEGA 7.1 (*25*). We constructed a phylogenetic tree using the maximum-likelihood method and the best pattern substitution model with the lowest Bayesian information criterion score, LG+G+I model (Le Gascuel, Gamma distribution with 5 rate categories and evolutionary invariable sites) (*26*). To confirm that the FLSV-US genome is segmented, we used FLSV-US reads showing substantial similarity to JMTV NS3 protein for acquiring the 3′ end of FLSV-US NS3 coding segment using a poly-T oligonucleotide-primed cDNA synthesis followed by specific PCR, as previously described (*27*). The 3′ end sequence of FLSV-US NS3 coding segment and the complete 3′ untranslated region (UTR) is available in GenBank (accession no. MN811584).

Results

Serum Virome of *P. Leucopus*

A total of 242 million paired-end sequences were generated from the 9 pools representing the serum samples of 978 *P. leucopus*. Of these, 148 million (61%) were derived from the host genome. Of the remaining 94 million sequences, 65.6% of reads showed substantial similarity to known viruses (E-value <0.001). Further analysis classified these sequences into 26 known RNA and DNA virus families (Figure 1).

DNA Virome

We found parvoviruses, circoviruses, Torque teno viruses (TTV), polyomaviruses, and papillomaviruses in all 9 serum pools, and these were the most abundant DNA viruses. Among parvoviruses, bocaparvovirus (BocPV) sequences shared up to 90% aa identity with the nonstructural protein of a rodent BocPV identified in Brazil (*28*), and adeno-associated viruses (AAV) shared up to 65% aa identity with the nonstructural protein of a caprine AAV (*29*). The identified TTV sequences were genetically equidistant from rodent TTV (GenBank accession no. AEF5869) and mosquito TTV (GenBank accession no. AEF58766) (*30*); the sequences shared up to 60% aa identity with these 2 species of the genus *Omegatorquevirus* (*31*). The polyomavirus sequences shared up to 79% aa identity with the large T antigen of a polyomavirus isolated from the Montane grass mouse (*Akodon montensis*)

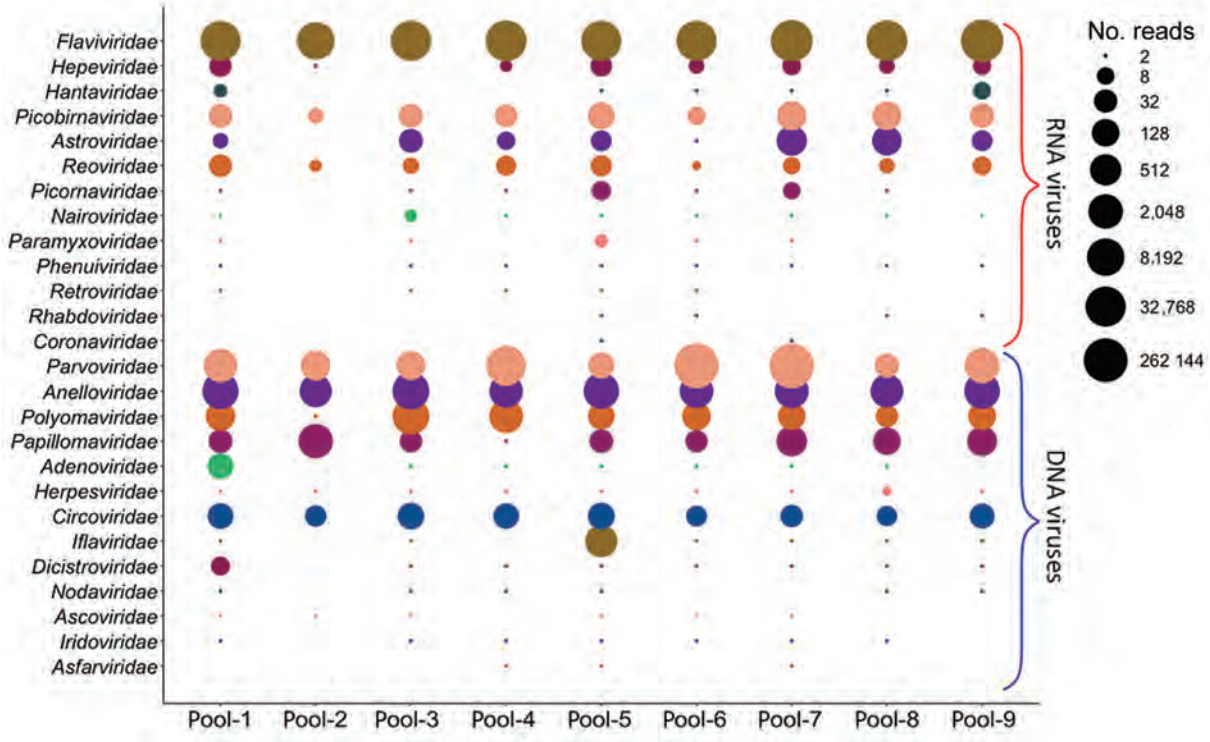

Figure 1. Bubble plot showing the abundance of different viruses in the serum virome of the white-footed mouse. Sequence reads showing the highest sequence similarity to known viruses were normalized as reads per million and were grouped into RNA and DNA virus families. Read numbers were transformed to log2, where the cutoff is ≥2 reads, represented by the smallest circle.

(*32*). These papillomavirus sequences belong to a tentatively identified new virus species within the genus *Iotapapillomavirus* that shares up to 79% aa identity with the papillomavirus found in *P. maniculatus* (GenBank accession no. NC_039039) (*33*).

RNA Virome

The most abundant RNA viruses present in the *P. leucopus* serum pools were the genetically diverged variants of hepaciviruses and pegiviruses (*34*). Phylogenetic analyses of these sequences indicated that the *P. leucopus* hepaciviruses form a distinct new genetic cluster (*35*). We found sequence reads of a novel hepevirus in 8 of the 9 serum pools. Genetic analysis of these *P. leucopus* hepevirus sequences suggest it is a new member of the genus *Orthohepevirus* because it shares <75% aa identity with the capsid proteins of hepevirus isolated from the common kestrel, *Falco tinnunculus* (*36*), and from rodents (*37*). Astrovirus-like sequences found in 8 serum pools shared up to 64% aa identity in the capsid protein and up to 73% aa identity in the nonstructural protein with the known species of the genus *Mamastrovirus*. Three of the 9 serum pools had sequences that were genetically closest to bat astroviruses (*38*) but shared up to 61% aa identity in the nonstructural protein. Sequences sharing up to 97% aa identity with hantaviruses recently found in *Peromyscus* sp. were also present in 6 serum pools (*39*). Coronavirus-related sequences were found in 2 serum pools and shared 98% aa identity with the porcine hemagglutinating encephalomyelitis virus (GenBank accession no. ACH72649). Paramyxovirus sequences were present in 5 serum pools and shared up to 90% nt identity with paramyxoviruses isolated from 3 rodent species: *Apodemus peninsulae* (accession no. KY370098), *Rattus norvegicus* (accession no. KX940961), and *R. andamanensis* (accession no. JN689227).

Rotavirus sequences were present in all serum pools and shared up to 78% nt identity in the NS3 gene with bovine rotavirus (GenBank accession no. JX442794) and human rotavirus (accession no. AB748601); <74% nt identity in the VP2 gene with avian rotavirus (accession no. FJ169854), human rotavirus (accession no. KF035108), and canine rotavirus (accession no. LC326510); and <45% aa identity in the VP6 gene to that of human rotavirus (accession no. AHK24897) and canine rotavirus (accession no. ACH97443). Picornavirus sequences were detected in 7 serum pools; these sequences shared up to 65% aa identity with marmot cardiovirus (accession no. AVX29481), <48% aa identity with rodent enterovirus

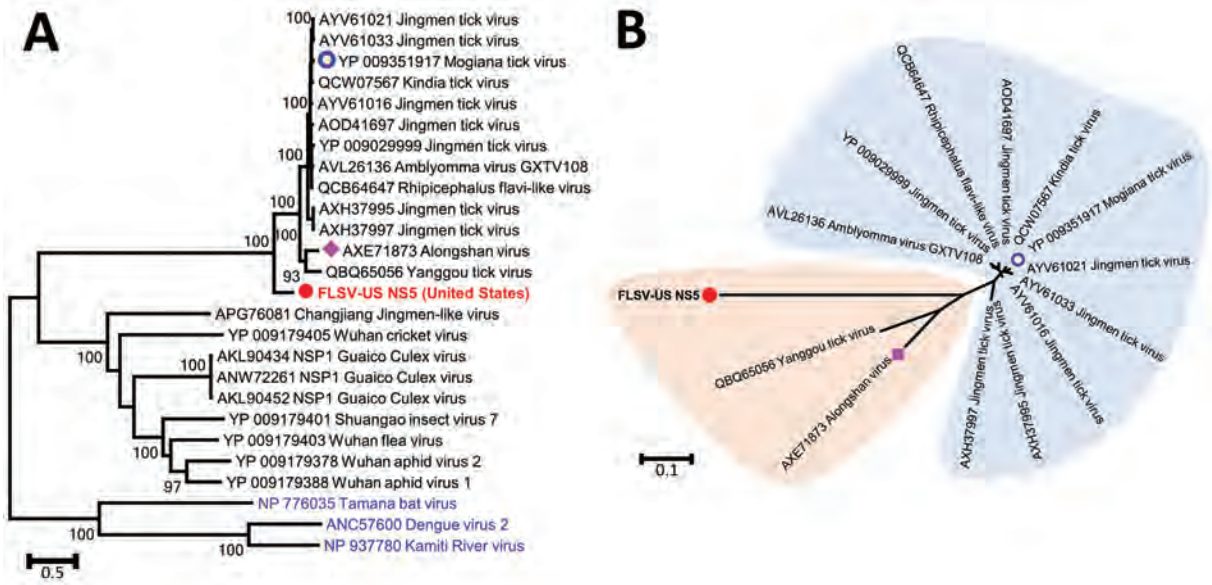

Figure 2. Phylogenetic analyses of FLSV-US (red) on the basis of NS5 proteins corresponding to amino acid positions 55 to 913 on Jingmen tick virus reference sequence YP_009029999.1. The trees are drawn to scale, with branch lengths measured in the number of substitutions per site. A) Phylogenetic analysis of conventional flaviviruses (blue) and recently identified segmented flavi-like viruses from ticks, mosquitoes, and other arthropods. B) Phylogenetic analysis of viruses closely related to FLSV-US. Alongshan virus was found in patients from China (purple diamond), Mogiana tick virus was found in ticks from Brazil (blue shading), and all other viruses were found in ticks collected in China. FLSV, flavi-like segmented virus.

(accession no. YP_009508417), <67% aa identity with *Rattus tanezumi* hunnivirus (accession no. AWK02689), and <87% aa identity with rodent hepatovirus (accession no. ALL35326).

SBV

Analysis of virome data showed the presence of SBV sequences in 8 of the 9 *P. leucopus* serum pools. Because SBV is not known to infect vertebrates, we used RT-PCR to screen serum samples of 72 individual mice; 5 samples were positive for SBV. Subsequent sequencing of PCR products showed that the SBV variants present in mice serum samples share 99%–100% nt identity with the SBV variants identified in *Ixodes scapularis* black-legged ticks (*24*,*40*).

FLSV

We found 370 sequence reads that showed the highest sequence similarity with the NS5 proteins of JMTV-like viruses. Similarly, we found 42 sequence reads that showed the highest sequence similarity with the NS3 proteins of JMTV-like viruses (*9*,*11*,*12*,*15*). These FLSV-US sequences were genetically equidistant from the 3 prototypic virus members of the JMTV-like virus group, namely JMTV, Mogiana tick virus, and Alongshan virus (*15*,*16*,*24*). Considering the potential consequentiality of a divergent JMTV-like virus infection in a widely distributed mammalian species in North America, we developed a broadly reactive PCR assay to confirm our results and to define infection prevalence of FLSV-US in *P. leucopus* mice.

PCR screening and amplicon sequencing confirmed the presence of FLSV-US nucleic acids in serum samples from 8 of the 72 mice in this pool, indicating an infection prevalence of 11%. Comparative sequence analysis determined ≈3.8% nt divergence in the NS5 region among FLSV-US variants infecting these mice (data not shown); all of these mutations were synonymous. Next, we acquired the near-complete coding region for a FLSV-US NS5 polymerase segment and used it for phylogenetic analysis (Figure 2). We determined that FLSV-US is more genetically diverse than the previously identified JMTV variants and Alongshan virus and shared <70% aa identity with these viruses (Table). We used a poly-T oligonucleotide primed cDNA synthesis to acquire the 3′ end of FLSV-US NS3 coding segment. Sequencing of the amplicon revealed the presence of a 388-nt 3′ untranslated region preceded by 96-aa NS3 protein coding region that showed highest sequence similarity with the carboxy terminal of JMTV NS3 protein. These results confirm that the FLSV-US genome is segmented like other known JMTV-like viruses and that the FLSV-US NS3 protein coding segment is polyadenylated.

Table. Percentages of pairwise amino acid distances between NS5 protein of FLSV-US and known JMTV-like viruses on the basis of the NS5 protein region corresponding to aa positions 55 to 913 on JMTV reference sequence YP_009029999.1

Sequence	ID*	A†	B	C	D	E	F	G	H	I	J	K	L	M	N
FLSV-US NS5†	A														
AOD41697 JMTV	B	31.2													
AVL26136 AMBV	C	31.8	2.8												
AXE71873 ALSV	D	34.7	19.6	19.8											
AXH37995 JMTV	E	34.7	7	7.3	19.4										
AXH37997 JMTV	F	32.2	6.9	7.2	19.4	0.1									
AYV61016 JMTV	G	31.5	2.8	2.9	19	6.8	6.6								
AYV61021 JMTV	H	31.8	4	4.3	19.4	7.3	7.2	3.1							
AYV61033 JMTV	I	31.9	4.1	4.4	19.3	7.2	7.1	3.3	0.6						
QBQ65056 YTV	J	33.4	20.4	20.5	18.3	20.1	20.1	20.1	20	19.9					
QCB64647 RFLV	K	31.5	2.4	1.5	19.1	6.4	6.3	2.3	3.4	3.5	19.9				
QCW07567 KTV	L	31.7	3.5	3.6	19.4	7.2	7.1	2.6	2.9	3	20.4	3			
YP_009029999 JMTV	M	31.8	3.7	2.3	19.6	7.2	7.1	3.4	4.4	4.4	20.4	2.2	3.7		
YP_009351917 MTV	N	30.8	3.7	3.8	19.7	6.9	6.8	2.4	2.7	2.8	20.4	3.5	2.7	4.2	

ALSV, Alongshan virus; AMBV, Amblyomma virus; ID, sequence identifier; JMTV, Jingmen tick virus; KYV, Kindia tick virus; MTV, Mogiana tick virus; RFLV, Rhipicephalus flavi-like virus; YTV, Yanggou tick virus.
†Virus identified in Pennsylvania, USA, as part of this study.
*Identifiers A–N in the top row represent the corresponding A-Z sequences in the left-hand column.

Discussion

Synanthropic small mammals serve as reservoirs for many zoonotic infections (*41*–*46*). Mice of the genus *Peromyscus* are highly adaptable and thrive in human-modified landscapes. In particular, *P. leucopus* and *P. maniculatus* are closely related and very abundant in North America, with *P. leucopus* most common in the eastern two thirds of the United States, plus Canada and northern Mexico, and *P. maniculatus* present in the central and western United States. These rodents have been recognized as reservoirs of highly pathogenic hantaviruses, but the diversity of viruses infecting them has remained largely unknown. A recent study (*18*) showed the presence of highly diverse hepaciviruses and pegiviruses in these rodents, and a study published in 2011 by Phan et al. identified several other viruses in fecal samples of 20 *P. leucopus* mice (*47*). Our study expands the host range of the recently identified tick virus SBV and identifies a highly diverse virus, FLSV-US, whose genetic relatives were recently shown to be pathogenic in humans (*15*,*16*).

Our results show high genetic diversity among viruses infecting these rodents. We not only confirmed infections of hantaviruses, hepaciviruses, and pegiviruses but also found viruses representing homologs of almost all viruses commonly present in human serum samples: anelloviruses, parvoviruses, polyomaviruses, papillomaviruses, and hepatitis E virus. We also found several viruses not commonly present in human or animal serum samples, such as coronaviruses, paramyxoviruses, astroviruses, enteroviruses, and rotaviruses. It is plausible that some mice, when captured, had transient viremia of these otherwise respiratory or gastroenteric infections. It would also be worthwhile to further investigate other samples including feces, skin, urine, saliva, and tissue or organs to identify additional viral diversity. This may also aid in determining the tissue tropism of these viruses and provide clues to potential routes of transmission.

Recently, several novel viruses have been identified in ticks from the United States (*24*). However, the host range and public health relevance of most of these new tick viruses remains unknown (*24*). We found 1 of these newly identified and highly prevalent tick viruses, SBV, in *P. leucopus* serum samples. To the best of our knowledge, SBV has not been detected in a vertebrate host; thus, our study indicates that this new tick virus can infect mammals and may have a wider host range than was previously known. Comparative sequence analyses indicate that the SBV variants detected in *P. leucopus* serum samples share 99%–100% nt identity with the SBV variants identified in ticks, indicating their common origin.

Several recent studies to characterize the viromes of ticks and mosquitoes in North America showed an absence of JMTV-like viruses (*24*,*40*,*48*). The presence of FLSV infections in a rodent species that is also a common host of ticks and mosquitoes is therefore intriguing and raises questions about the source of FLSV- infection in these mice. It is plausible that FLSV-US transmits through an arthropod vector other than ticks or mosquitoes because some distantly related viruses were found in pools of insects and arachnids (*10*).

In conclusion, we detected FLSV infections in a widespread mammalian species in North America, which is important because distant genetic relatives of FLSV-US have been shown to be transmitted by ticks and mosquitoes (*9*,*13*) and readily able to infect

humans (*15*,*16*). Until recently, these unusual flavi-like viruses had only been found in ticks, mosquitoes, and animals from China, Kosovo, and Brazil (*11*,*14*,*16*). However, in 2019, Wang et al. reported JMTV viremia in 86 of 374 humans with febrile illness, headache, and history of tick exposure (*16*). In addition, JMTV was shown to replicate in several cell lines of human and animal origin (*15*,*16*). Taken together, these studies indicate that FLSV-US and related viruses have the potential to infect a wide range of mammals, including humans. Finally, FLSV-US is genetically distinct from all known viruses; therefore, its sequence data will help in the identification of FLSV-US and its related variants infecting animals and humans in North America.

Funding was provided by the National Science Foundation's (NSF) Ecology and Evolution of Infectious Diseases program (grant number 1619072), the National Institute of Health awards R01 HL119485 and R21 HL140269, as well as The Research Institute of Nationwide Children's Hospital and The Institutes for Energy and the Environment of Pennsylvania State University

Dr. Vandegrift is a research associate professor in the Center for Infectious Disease Dynamics and Department of Biology at Penn State University. His primary research interests include disease ecology, zoonotic parasites, and emerging infectious diseases. Dr. Kumar is a postdoctoral fellow at the Center of Vaccine and Immunity, Nationwide Children's Hospital, Columbus, Ohio. His primary research interests include emerging virus discovery using next-generation sequencing and serologic approaches.

References:

1. Woolhouse MEJ, Gowtage-Sequeria S. Host range and emerging and reemerging pathogens. Emerg Infect Dis. 2005;11:1842–7. https://doi.org/10.3201/eid1112.050997
2. Holmes EC. The evolution and emergence of RNA viruses. Oxford: Oxford University Press; 2009.
3. Plowright RK, Parrish CR, McCallum H, Hudson PJ, Ko AI, Graham AL, et al. Pathways to zoonotic spillover. Nat Rev Microbiol. 2017;15:502–10. https://doi.org/10.1038/nrmicro.2017.45
4. Luis AD, Hayman DTS, O'Shea TJ, Cryan PM, Gilbert AT, Pulliam JRC, et al. A comparison of bats and rodents as reservoirs of zoonotic viruses: are bats special? Proc Biol Sci. 2013;280:20122753. https://doi.org/10.1098/rspb.2012.2753
5. Hersh MH, Ostfeld RS, McHenry DJ, Tibbetts M, Brunner JL, Killilea ME, et al. Co-infection of blacklegged ticks with *Babesia microti* and *Borrelia burgdorferi* is higher than expected and acquired from small mammal hosts. PLoS One. 2014;9:e99348. https://doi.org/10.1371/journal.pone.0099348
6. Barbour AG. Infection resistance and tolerance in *Peromyscus* spp., natural reservoirs of microbes that are virulent for humans. Semin Cell Dev Biol. 2017;61:115–22. https://doi.org/10.1016/j.semcdb.2016.07.002
7. Gage KL, Ostfeld RS, Olson JG. Nonviral vector-borne zoonoses associated with mammals in the United States. J Mammal. 1995;76:695–715. https://doi.org/10.2307/1382741
8. Childs JE, Ksiazek TG, Spiropoulou CF, Krebs JW, Morzunov S, Maupin GO, et al. Serologic and genetic identification of *Peromyscus maniculatus* as the primary rodent reservoir for a new hantavirus in the southwestern United States. J Infect Dis. 1994;169:1271–80. https://doi.org/10.1093/infdis/169.6.1271
9. Qin XC, Shi M, Tian JH, Lin XD, Gao DY, He JR, et al. A tick-borne segmented RNA virus contains genome segments derived from unsegmented viral ancestors. Proc Natl Acad Sci U S A. 2014;111:6744–9. https://doi.org/10.1073/pnas.1324194111
10. Shi M, Lin XD, Vasilakis N, Tian JH, Li CX, Chen LJ, et al. Divergent viruses discovered in arthropods and vertebrates revise the evolutionary history of the *Flaviviridae* and related viruses. J Virol. 2015;90:659–69. https://doi.org/10.1128/JVI.02036-15
11. Villa EC, Maruyama SR, de Miranda-Santos IKF, Palacios G, Ladner JT. Complete coding genome sequence for Mogiana tick virus, a Jingmenvirus isolated from ticks in Brazil. Genome Announc. 2017;5:e00232-17. https://doi.org/10.1128/genomeA.00232-17
12. Ladner JT, Wiley MR, Beitzel B, Auguste AJ, Dupuis AP II, Lindquist ME, et al. A multicomponent animal virus isolated from mosquitoes. Cell Host Microbe. 2016;20:357–67. https://doi.org/10.1016/j.chom.2016.07.011
13. Souza WM, Fumagalli MJ, Torres Carrasco AO, Romeiro MF, Modha S, Seki MC, et al. Viral diversity of *Rhipicephalus microplus* parasitizing cattle in southern Brazil. Sci Rep. 2018;8:16315. https://doi.org/10.1038/s41598-018-34630-1
14. Emmerich P, Jakupi X, von Possel R, Berisha L, Halili B, Günther S, et al. Viral metagenomics, genetic and evolutionary characteristics of Crimean-Congo hemorrhagic fever orthonairovirus in humans, Kosovo. Infect Genet Evol. 2018;65:6–11. https://doi.org/10.1016/j.meegid.2018. 07.010
15. Jia N, Liu HB, Ni XB, Bell-Sakyi L, Zheng YC, Song JL, et al. Emergence of human infection with Jingmen tick virus in China: a retrospective study. EBioMedicine. 2019;43:317–24. https://doi.org/10.1016/j.ebiom.2019.04.004
16. Wang ZD, Wang B, Wei F, Han SZ, Zhang L, Yang ZT, et al. A new segmented virus associated with human febrile illness in China. N Engl J Med. 2019;380:2116–25. https://doi.org/10.1056/NEJMoa1805068
17. Song JW, Baek LJ, Nagle JW, Schlitter D, Yanagihara R. Genetic and phylogenetic analyses of hantaviral sequences amplified from archival tissues of deer mice (*Peromyscus maniculatus nubiterrae*) captured in the eastern United States. Arch Virol. 1996;141:959–67. https://doi.org/10.1007/BF01718170
18. Kapoor A, Simmonds P, Scheel TKH, Hjelle B, Cullen JM, Burbelo PD, et al. Identification of rodent homologs of hepatitis C virus and pegiviruses. MBio. 2013;4:e00216–13. https://doi.org/10.1128/mBio.00216-13
19. Vandegrift KJ, Hudson PJ. Could parasites destabilize mouse populations? The potential role of *Pterygodermatites peromysci* in the population dynamics of free-living mice, *Peromyscus leucopus*. Int J Parasitol. 2009;39:1253–62. https://doi.org/10.1016/j.ijpara.2009.02.025
20. Moser LA, Ramirez-Carvajal L, Puri V, Pauszek SJ, Matthews K, Dilley KA, et al. A universal next-generation sequencing protocol to generate noninfectious barcoded cDNA libraries from high-containment RNA viruses. mSystems. 2016;1:e00039-15. https://doi.org/10.1128/mSystems.00039-15

21. Kapoor A, Kumar A, Simmonds P, Bhuva N, Singh Chauhan L, Lee B, et al. Virome analysis of transfusion recipients reveals a novel human virus that shares genomic features with hepaciviruses and pegiviruses. MBio. 2015;6:e01466–15. https://doi.org/10.1128/mBio.01466-15
22. Chevreux B, Pfisterer T, Drescher B, Driesel AJ, Müller WEG, Wetter T, et al. Using the miraEST assembler for reliable and automated mRNA transcript assembly and SNP detection in sequenced ESTs. Genome Res. 2004;14:1147–59. https://doi.org/10.1101/gr.1917404
23. Tokarz R, Williams SH, Sameroff S, Sanchez Leon M, Jain K, Lipkin WI. Virome analysis of *Amblyomma americanum*, *Dermacentor variabilis*, and *Ixodes scapularis* ticks reveals novel highly divergent vertebrate and invertebrate viruses. J Virol. 2014;88:11480–92. https://doi.org/10.1128/JVI.01858-14
24. Vandegrift KJ, Kapoor A. The ecology of new constituents of the tick virome and their relevance to public health. Viruses. 2019;11:E529. https://doi.org/10.3390/v11060529
25. Kumar S, Stecher G, Tamura K. MEGA7: molecular evolutionary genetics analysis, version 7.0 for bigger datasets. Mol Biol Evol. 2016;33:1870–4. https://doi.org/10.1093/molbev/msw054
26. Le SQ, Gascuel O. An improved general amino acid replacement matrix. Mol Biol Evol. 2008;25:1307–20. https://doi.org/10.1093/molbev/msn067
27. Kapoor A, Li L, Victoria J, Oderinde B, Mason C, Pandey P, et al. Multiple novel astrovirus species in human stool. J Gen Virol. 2009;90:2965–72. https://doi.org/10.1099/vir.0.014449-0
28. de Souza WM, Dennis T, Fumagalli MJ, Araujo J, Sabino-Santos G Jr, Maia FGM, et al. Novel parvoviruses from wild and domestic animals in Brazil provide new insights into parvovirus distribution and diversity. Viruses. 2018;10:E143. https://doi.org/10.3390/v10040143
29. Arbetman AE, Lochrie M, Zhou S, Wellman J, Scallan C, Doroudchi MM, et al. Novel caprine adeno-associated virus (AAV) capsid (AAV-Go.1) is closely related to the primate AAV-5 and has unique tropism and neutralization properties. J Virol. 2005;79:15238–45. https://doi.org/10.1128/JVI.79.24.15238-15245.2005
30. Ng TFF, Willner DL, Lim YW, Schmieder R, Chau B, Nilsson C, et al. Broad surveys of DNA viral diversity obtained through viral metagenomics of mosquitoes. PLoS One. 2011;6:e20579. https://doi.org/10.1371/journal.pone.0020579
31. de Souza WM, Fumagalli MJ, de Araujo J, Sabino-Santos G Jr, Maia FGM, Romeiro MF, et al. Discovery of novel anelloviruses in small mammals expands the host range and diversity of the *Anelloviridae*. Virology. 2018;514:9–17. https://doi.org/10.1016/j.virol.2017.11.001
32. Maia FGM, de Souza WM, Sabino-Santos G Jr, Fumagalli MJ, Modha S, Murcia PR, et al. A novel polyomavirus in sigmodontine rodents from São Paulo State, Brazil. Arch Virol. 2018;163:2913–5. https://doi.org/10.1007/s00705-018-3913-8
33. Hansen TA, Fridholm H, Frøslev TG, Kjartansdóttir KR, Willerslev E, Nielsen LP, et al. New type of papillomavirus and novel circular single stranded DNA virus discovered in urban *Rattus norvegicus* using circular DNA enrichment and metagenomics. PLoS One. 2015;10:e0141952. https://doi.org/ 10.1371/journal.pone.0141952
34. Kapoor A, Simmonds P, Scheel TK, Hjelle B, Cullen JM, Burbelo PD, et al. Identification of rodent homologs of hepatitis C virus and pegiviruses. MBio. 2013;4:e00216–13. https://doi.org/10.1128/mBio.00216-13
35. Smith DB, Becher P, Bukh J, Gould EA, Meyers G, Monath T, et al. Proposed update to the taxonomy of the genera *Hepacivirus* and *Pegivirus* within the *Flaviviridae* family. J Gen Virol. 2016;97:2894–907. https://doi.org/10.1099/jgv.0.000612 sss
36. Reuter G, Boros Á, Mátics R, Kapusinszky B, Delwart E, Pankovics P. Divergent hepatitis E virus in birds of prey, common kestrel (*Falco tinnunculus*) and red-footed falcon (*F. vespertinus*), Hungary. Infect Genet Evol. 2016;43:343–6. https://doi.org/10.1016/j.meegid.2016.06.013
37. Wu Z, Lu L, Du J, Yang L, Ren X, Liu B, et al. Comparative analysis of rodent and small mammal viromes to better understand the wildlife origin of emerging infectious diseases. Microbiome. 2018;6:178. https://doi.org/10.1186/s40168-018-0554-9
38. Yinda CK, Ghogomu SM, Conceição-Neto N, Beller L, Deboutte W, Vanhulle E, et al. Cameroonian fruit bats harbor divergent viruses, including rotavirus H, bastroviruses, and picobirnaviruses using an alternative genetic code. Virus Evol. 2018;4:vey008. https://doi.org/10.1093/ve/vey008
39. McMullan LK, Albariño CG, Ksiazek TG, Nichol ST, Spiropoulou CF. Complete genome sequences of a hantavirus isolate from New York. Genome Announc. 2018;6:e00188-18. https://doi.org/10.1128/genomeA.00188-18
40. Sakamoto JM, Ng TFF, Suzuki Y, Tsujimoto H, Deng X, Delwart E, et al. Bunyaviruses are common in male and female *Ixodes scapularis* ticks in central Pennsylvania. PeerJ. 2016;4:e2324. https://doi.org/10.7717/peerj.2324
41. Peters CJ. Emerging infections: lessons from the viral hemorrhagic fevers. Trans Am Clin Climatol Assoc. 2006;117:189–96, discussion 196–7.
42. Fernando R, Capone D, Elrich S, Mantovani R, Quarles L III, D'Amato A, et al. Infection with New York orthohantavirus and associated respiratory failure and multiple cerebral complications. Emerg Infect Dis. 2019;25:1241–3. https://doi.org/10.3201/eid2506.181966
43. Kreuder Johnson C, Hitchens PL, Smiley Evans T, Goldstein T, Thomas K, Clements A, et al. Spillover and pandemic properties of zoonotic viruses with high host plasticity. Sci Rep. 2015;5:14830. https://doi.org/10.1038/srep14830
44. Pandit PS, Doyle MM, Smart KM, Young CCW, Drape GW, Johnson CK. Predicting wildlife reservoirs and global vulnerability to zoonotic *Flaviviruses*. Nat Commun. 2018;9:5425. https://doi.org/10.1038/s41467-018-07896-2
45. Alexander KA, Lewis BL, Marathe M, Eubank S, Blackburn JK. Modeling of wildlife-associated zoonoses: applications and caveats. Vector Borne Zoonotic Dis. 2012;12:1005–18. https://doi.org/10.1089/vbz.2012.0987
46. Ostfeld RS, Brisson D, Oggenfuss K, Devine J, Levy MZ, Keesing F. Effects of a zoonotic pathogen, *Borrelia burgdorferi*, on the behavior of a key reservoir host. Ecol Evol. 2018;8:4074–83. https://doi.org/10.1002/ece3.3961
47. Phan TG, Kapusinszky B, Wang C, Rose RK, Lipton HL, Delwart EL. The fecal viral flora of wild rodents. PLoS Pathog. 2011;7:e1002218. https://doi.org/10.1371/journal.ppat.1002218
48. Sadeghi M, Altan E, Deng X, Barker CM, Fang Y, Coffey LL, et al. Virome of > 12 thousand *Culex* mosquitoes from throughout California. Virology. 2018;523:74–88. https://doi.org/10.1016/j.virol.2018.07.029

Address for correspondence: Amit Kapoor, Abigail Wexner The Research Institute at Nationwide Children's Hospital, 700 Children's Dr, Columbus, OH 43205, USA; email: amit.kapoor@nationwidechildrens.org

Characterizing Norovirus Transmission from Outbreak Data, United States

Molly K. Steele, Mary E. Wikswo, Aron J. Hall, Katia Koelle, Andreas Handel, Karen Levy, Lance A. Waller, Ben A. Lopman

Norovirus is the leading cause of acute gastroenteritis outbreaks in the United States. We estimated the basic (R_0) and effective (R_e) reproduction numbers for 7,094 norovirus outbreaks reported to the National Outbreak Reporting System (NORS) during 2009–2017 and used regression models to assess whether transmission varied by outbreak setting. The median R_0 was 2.75 (interquartile range [IQR] 2.38–3.65), and median R_e was 1.29 (IQR 1.12–1.74). Long-term care and assisted living facilities had an R_0 of 3.35 (95% CI 3.26–3.45), but R_0 did not differ substantially for outbreaks in other settings, except for outbreaks in schools, colleges, and universities, which had an R_0 of 2.92 (95% CI 2.82–3.03). Seasonally, R_0 was lowest (3.11 [95% CI 2.97–3.25]) in summer and peaked in fall and winter. Overall, we saw little variability in transmission across different outbreaks settings in the United States.

Norovirus is the most common cause of outbreaks of acute gastroenteritis (AGE) in the United States (*1*,*2*). The Centers for Disease Control and Prevention (CDC) collects data on AGE outbreaks through the National Outbreak Reporting System (NORS). During 2009–2017, norovirus was the suspected or confirmed etiology of 47% of AGE outbreaks reported to NORS (*3*). The size and severity of outbreaks varies across different settings, times of year, and genotypes, suggesting norovirus transmissibility is variable across different outbreak settings and contexts (*4*). Generally, the transmission potential of infectious diseases is influenced by the infectiousness of the pathogen, the duration of infectiousness, and the number of susceptible contacts exposed during the infectious period (*5*).

Author affiliations: Emory University, Atlanta, Georgia, USA (M.K. Steele, A.J. Hall, K. Koelle, K. Levy, L.A. Waller, B.A. Lopman); Centers for Disease Control and Prevention, Atlanta (M.E. Wikswo, A.J. Hall); University of Georgia, Athens, Georgia, USA (A. Handel)

DOI: https://doi.org/10.3201/eid2608.191537

The reproduction number is a metric for quantifying transmissibility of a pathogen. The basic reproduction number (R_0) is the average number of secondary cases that arise from a primary case in a completely susceptible population. The effective reproduction number (R_e) quantifies the average number of secondary cases that arise from a primary case in a population that is not completely susceptible. R_e varies over the course of an outbreak as the proportion of the susceptible population changes (*6*,*7*). R_0 and R_e are not just metrics of the biologic properties of pathogens but also measures of the transmissibility of a pathogen within a specific population or setting (*8*,*9*).

Several transmission modeling studies in different settings have estimated R_0 and R_e of norovirus, but a large variation in these estimates occurs and R_0 ranges from 1.1–7.2 (*10*). Much of the R_0 variation likely is due to differences in the structures, population mixing assumptions, and data between transmission models in different settings (*10*). Generally, model estimates from community surveillance data result in an R_0 of ≈2, but estimates from outbreak data tend to be higher and more variable. The variability of estimates from models that use outbreak data likely are driven by context; outbreaks might occur in populations that are not representative of the population as a whole and transmission likely is higher in these settings than in the community (*4*).

We estimated R_0 and R_e for thousands of norovirus outbreaks in the United States. We evaluated whether R_0 was associated with setting, season, year, or geographic region. In addition, we assessed whether norovirus was suspected or confirmed as the cause of the outbreak.

Methods

Data

We obtained data on all norovirus outbreaks during 2009–2017 from NORS and CaliciNet (*11*). We defined

an outbreak as ≥2 epidemiologically linked cases of suspected or laboratory-confirmed norovirus. NORS data consist of web-based reports of all foodborne, waterborne, and enteric disease outbreaks transmitted by contact with environmental sources, infected persons or animals, or unknown modes of transmission reported by state, local, and territorial public health agencies. This web-based reporting system collects epidemiologic information, including the dates; settings, such as long-term care facilities, child daycare facilities, hospitals, and schools; geographic location of the outbreak; the estimated total number of cases; and exposed population (*2*). For settings that report staff and guest case numbers, we included these data in the estimated total number of cases and exposed population. CaliciNet data consists of sequence-derived genotypes and epidemiologic data from norovirus outbreaks submitted from local, state, and federal public health laboratories. We obtained CaliciNet genotypes that were linked to outbreak data we acquired from NORS.

For all outbreaks reported to NORS, data are collected on the total estimated primary cases, including all laboratory-confirmed and suspected primary cases. These data exclude cases associated with secondary illnesses, such as person-to-person norovirus transmission in households after a restaurant-based outbreak. However, data for calculating attack rates, specifically the number of exposed persons and the subset of the exposed persons who became ill, are only collected for outbreaks with person-to-person, environmental, or unknown transmission modes. In addition, data collected from outbreaks might not be documented consistently across a report. For example, outbreaks for which setting-specific information on the total number of guests and staff that are reported to be ill, referred to as total ill, might not match the reported total estimated primary cases. During 2009–2017, a total of 17,822 suspected and confirmed norovirus outbreaks were reported to NORS. We excluded 10,728 outbreaks based on the following criteria, which we imposed hierarchically: transmission was not person-to-person (n = 3,866); the outbreak exposure occurred in multiple states (n = 8); the outbreak occurred in Puerto Rico (n = 3), which we excluded because of small sample size; the size of total exposed population or major setting were not reported (n = 5,573); the total estimated primary cases and the total ill among the exposed population were not equal (n = 1,231); or the total estimated primary cases or the total ill among the exposed population were reported to be greater than the total exposed population size (n = 47) (Appendix Figure 1, https://wwwnc.cdc.gov/EID/article/26/8/19-1537-App1.pdf). In all, 7,094 norovirus outbreaks met our inclusion criteria in subsequent analyses (Appendix Table 1). We did not use imputation techniques to infer values for missing data because no good proxy variables inferred missing data for major settings and exposed population size.

Estimating R_0 and R_e

We used the final size method to calculate R_0, R_e, and associated SEs (*12*; Appendix). The final size method calculates R_0 and R_e based on 3 variables: the total population size of the outbreak (*N*), the total number of cases in the outbreak (*C*), and the number of susceptible persons at the start of the outbreak (*S*). In our calculations, *C* was informed by NORS outbreak data for the estimated total number ill and *N* by the exposed population. NORS data does not include nor can it inform the number of susceptible persons at the start of an outbreak. Therefore, to estimate *S*, we used norovirus challenge study data on the percent of persons that become infected and develop AGE after challenge with virus. Across all published studies, the weighted average of participants in whom gastroenteritis developed after challenge is 47% (range 27%–80%; Appendix Table 1) (*13*–*19*). We assumed *S* is the number of persons susceptible to disease, as opposed to infection. To calculate *S*, we multiplied 47% by *N* and rounded to the nearest integer. For 890 outbreaks, the total number of cases, *C*, was greater than our estimated *S*; for these outbreaks we set *S* equal to *C*, corresponding to a 100% attack rate. We also calculated *S* assuming 27% and 80% of *N* were susceptible to assess the sensitivity of our model results to this parameter.

Regression Analysis

After estimating R_0, R_e, and associated SEs for each norovirus outbreak, we fit a linear regression model to the log-transformed estimated reproduction numbers to assess whether outbreak setting, census region, season, year, suspected or confirmed norovirus, or genotype were associated with transmissibility. All variables were categorical, where the reference was assigned as the group with the most outbreaks reported, except for the suspected or confirmed variable, for which we set the referent to outbreaks with confirmed norovirus etiology. We used weighted least squares combined with estimated standard errors to produce robust estimates accounting for heteroscedasticity and non–normally distributed model residuals by using the estimatr package in R version 3.4.2 (*20*,*21*). We included the following variables in our models: outbreak setting; census region;

meteorological season, defined as spring (March 1–May 31), summer (June 1–August 31), fall (September 1–November 30), or winter (December 1–February 28); year, defined as July–June; whether norovirus was suspected or confirmed; and norovirus genotype, categorized as GI, GII.4, or GII.non4.

For outbreaks for which we calculated R_0 and R_e, we had norovirus genotype data for only 22% (1,571). In a preliminary analysis, we fit a univariate linear regression model to estimate R_0 by norovirus genotype alone and by norovirus genotype and year and found no evidence for variation (Appendix). Given these results and the small sample size, we did not include norovirus genotype in our models and performed model selection on the remaining variables. To determine which variables to include, we used a forward selection process and selected the model with the lowest Akaike information criterion and Bayes information criterion values.

Sensitivity Analysis

We tested the sensitivity of our regression model results to different modeling approaches and different assumptions of the percent susceptible at the start of an outbreak. We also fit a logistic regression model of binary transmission and a negative binomial regression of the final outbreak size by using the log-transformed exposed population size as a measure of the attack rate of an outbreak. Thus, we could make comparisons between the models to see if the results from modeling continuous transmission were consistent with the results of modeling binary transmission and attack rates. In addition, we ran all the regression models again using the assumption that 27% and 80% susceptible at the start of an outbreak, which corresponds to the minimum and maximum percent susceptible to AGE from published challenge studies (Appendix Table 2).

Results

Of the 7,094 norovirus outbreaks included in our final dataset, 75% (5,335) occurred in long-term care and assisted living facilities and 57% (4,016) occurred in winter. The median outbreak size was 28 cases (interquartile range [IQR] 16–47) and the median attack rate was 22% (IQR 11%–36%) (Table 1). The median R_0 was 2.75 (IQR 2.38–3.65) and the median R_e was 1.29 (IQR 1.12–1.74).

Model Selection and Regression Analysis

The final selected model included the following variables: major setting, census region, season, year, and whether norovirus was suspected or confirmed (Akaike information criterion = 5,803; Bayes information criterion = 5,968) (Appendix Table 3). For long-term care and assisted living facilities, R_0 was 3.35 (95% CI 3.26–3.45). R_0 for outbreaks in all other settings did not differ substantially, except for outbreaks in schools, colleges, and universities, in which R_0 was slightly reduced, 2.92 (95% CI 2.82–3.03) (Table 2; Appendix Figure 2). We found that R_0 differed substantially by outbreak status; suspected norovirus outbreaks had a lower R_0, 3.02 (95% CI 2.94–3.10), than that for confirmed outbreaks (R_0 = 3.35 [95% CI 3.26–3.45]).

Estimated R_0 varied only slightly by census region and was lowest in the northeast (R_0 = 3.00 [95% CI 2.92–3.08]). Season and year also contributed to changes in the R_0. Estimated R_0 was highest in winter (3.35 [95% CI 3.26–3.45]) and fall (3.37 [95% CI 3.24–3.50]) and lowest during the summer months (3.11 [95% CI 2.97–3.25]). Outbreaks reported during January 2009–June 2012 all had higher estimated R_0 (range for individual seasonal years 3.77–3.93) than the reference period, July 2016–June 2017 (Table 2; Appendix Figure 2). Our findings were generally robust to assumptions about the proportion susceptible at the start of the outbreak and whether we modeled the outcome of R_0, R_e, or final outbreak size (Appendix Tables 4–6, Figure 3).

Discussion

By using a large national outbreak dataset, we investigated transmission patterns of norovirus outbreaks. Our analysis led to several key findings. First, reported norovirus outbreaks in the United States have modest R_0 (2.75 [IQR 2.38–3.65]) and R_e (1.29 [IQR 1.12–1.74]) values. Second, we found that R_0 and R_e did not vary across most settings, except for outbreaks in schools, colleges, and universities, which had lower estimated transmission values. Third, we found higher transmission in laboratory-confirmed outbreaks relative to suspected outbreaks and higher transmission for outbreaks occurring in the winter months relative to summer months.

Our finding that norovirus outbreaks in the United States have modest transmission values is somewhat surprising. In a recent review of norovirus modeling studies, Gaythorpe et al. (*10*) found R_0 estimates for norovirus were 1.1–7.2. Of note, R_0 and R_e estimates from transmission modeling studies that analyzed data from norovirus outbreaks were high, but variability between studies was high; R_e estimates were ≈1–14 (*22*–*24*). Our estimates are within the reproduction numbers estimated by using transmission models of norovirus based on outbreak data (*22*,*25*).

Table 1. Norovirus outbreaks with exposed population size reported to the National Outbreak Reporting System, United States, 2009–2017*

Characteristics	No. (%)	Median attack rate, % (IQR)	Median final size, % (IQR)	Median R_0 (IQR)
All outbreaks	7,094 (100)	22 (11–36)	28 (16–47)	2.75 (2.38–3.65)
Major setting				
Child day care	272 (4)	21 (13–36)	18 (11–29)	2.67 (2.39–3.60)
Hospital or healthcare facility	271 (4)	22 (11–38)	19 (11–34)	2.70 (2.33–3.59)
Long-term care or assisted living facility	5,335 (75)	23 (13–36)	30 (17–47)	2.81 (2.42–3.76)
Other	350 (5)	20 (10–36)	24 (15–40)	2.66 (2.35–3.60)
Private home or residence	42 (1)	66 (50–91)	9 (6–16)	3.80 (2.26–4.92)
Restaurant	77 (1)	50 (27–64)	10 (6–16)	3.12 (2.53–4.31)
School, college, or university	747 (11)	12 (6–24)	42 (19–80)	2.41 (2.24–2.92)
Season				
Winter	4,016 (57)	22 (12–36)	30 (17–51)	2.80 (2.40–3.77)
Fall	808 (11)	21 (11–37)	26 (15–47)	2.72 (2.36–3.63)
Spring	1,964 (28)	20 (11–35)	27 (15–44)	2.69 (2.37–3.57)
Summer	306 (4)	17 (9–33)	19 (11–32)	2.57 (2.29–3.33)
Outbreak status				
Confirmed	3,114 (44)	26 (15–40)	35 (20–55)	2.99 (2.51–4.22)
Suspected	3,980 (56)	18 (9–31)	24 (14–40)	2.59 (2.32–3.27)
Census region				
Northeast	1,898 (27)	17 (9–29)	31 (17–53)	2.58 (2.30–3.23)
Midwest	2,205 (31)	25 (13–39)	26 (15–44)	2.87 (2.44–3.98)
South	2,224 (31)	23 (12–38)	29 (17–47)	2.81 (2.39–3.93)
West	767 (11)	21 (13–34)	28 (16–44)	2.75 (2.42–3.57)
Year				
2009 Jan–Jun†	243 (3)	28 (15–42)	35 (20–55)	3.09 (2.50-4.56)
2009 Jul–2010 Jun	275 (4)	29 (15–45)	35 (19–57)	3.17 (2.51–4.77)
2010 Jul–2011 Jun	592 (8)	29 (16–44)	32 (19–54)	3.12 (2.54–4.58)
2011 Jul–2012 Jun	679 (10)	27 (15–40)	35 (19–59)	3.01 (2.52–4.29)
2012 Jul–2013 Jun	967 (14)	21 (12–36)	28 (16–46)	2.73 (2.38–3.61)
2013 Jul–2014 Jun	913 (13)	20 (11–33)	29 (18–51)	2.68 (2.38–3.45)
2014 Jul–2015 Jun	941 (13)	21 (11–35)	28 (16–46)	2.74 (2.3–3.61)
2015 Jul–2016 Jun	1,007 (14)	17 (9–32)	25 (14–42)	2.57 (2.31–3.29)
2016 Jul–2017 Jun	1,070 (15)	19 (10–31)	26 (14–42)	2.63 (2.33–3.24)
2017 Jul–Dec†	407 (6)	20 (10–34)	22 (14–38)	2.66 (2.33–3.55)

*IQR, interquartile range.
†Partial norovirus years included in this analysis. The National Outbreak Reporting System was established in January 2009, and the first year of this analysis is 2009 January–June. At the time of analysis, we received data through December 2017.

However, our estimates are higher than those from several studies that estimated reproduction numbers by using population-level transmission models (*26*–*29*), suggesting that transmission of norovirus in outbreak settings is higher than sporadic transmission in the community.

From our main analysis, we found that outbreaks in schools, colleges, and universities had lower estimated transmission, but transmission varied little across all other settings. Relative to outbreaks in long-term care and assisted living facilities, outbreaks that occurred in private homes or residences and restaurants had higher final sizes, and schools, colleges, and universities had lower estimated attack rates. Our finding that outbreaks in the winter had higher estimated transmissibility than outbreaks that occurred in summer is likely a factor of the strong wintertime seasonality of noroviruses in the United States (*30*,*31*). Consistent with this finding are the observations that norovirus case and outbreak reports are inversely correlated with temperature (*30*,*31*) and that survival of norovirus surrogate viruses, such as murine norovirus and feline calicivirus, declines with increasing temperatures (*32*,*33*).

Several differences we found might be driven by surveillance biases rather than differences in norovirus transmission. Suspected norovirus outbreaks without a laboratory-confirmed outbreak etiology had lower transmission than laboratory-confirmed norovirus outbreaks, perhaps because suspected outbreaks are not investigated as well as confirmed outbreaks and have lower rates of case ascertainment. Outbreaks reported in the south had higher estimated R_0 and R_e relative to outbreaks in the northeast, which might be related to differences in the quality of reporting between these regions. For example, if surveillance in certain regions only captured larger, more easily detectable outbreaks with higher attack rates, this could bias our estimates of transmissibility upwards. Tremendous variability exists in outbreak reporting between states, ≈100-fold difference between the highest and lowest reporting states, which

likely affects the observed outbreak characteristics we included (*34*). Similarly, NORS has been collecting outbreak reports since January 2009, but in August 2012 CDC began a concerted effort to improve norovirus outbreak reporting to NORS and CaliciNet with the introduction of NoroSTAT (*35*,*36*). Thus, our finding that norovirus outbreaks reported before August 2012 were larger and had higher estimated R_0 and R_e values might be related to CDC's efforts to capture outbreaks that previously would not have been reported, such as smaller outbreaks. Further, because the transmission mode can be difficult to identify for norovirus outbreaks, our analysis might have included outbreaks for which the mode of transmission was misclassified as person-to-person. Larger outbreaks with higher transmission are more likely to be reported, and our results might not reflect transmission in smaller outbreaks. In addition, the exposed population size is difficult to quantify and is not consistently reported to NORS. Thus, the differences we found in estimated attack rates across different settings could be due to true variability in the exposed population size across settings or variability in the reliable reporting of the exposed population size. However, our analysis restricted to outbreaks in long-term care and assisted living facilities found the same trends among the variables for outbreak status, census region, season, and year as our analysis of all outbreaks, which suggests the results are robust.

Table 2. Estimated log-linear change in R_0 from the intercept for linear regression of log transformed R_0 for norovirus outbreaks reported to the National Outbreak Reporting System, United States, 2009–2017

Category	Estimated log-linear change in R_0 (95% CI)
Intercept	3.35 (3.26–3.45)
Major setting	
Long-term care or assisted living facility	Referent
Child day care	0.99 (0.95–1.03)
Hospital or healthcare facility	0.93 (0.90–0.97)
Other	0.97 (0.93–1.01)
Private home or residence	0.99 (0.82–1.19)
Restaurant	1.01 (0.91–1.11)
School, college, or university	0.87 (0.85–0.89)
Season	
Winter	Referent
Fall	1.00 (0.98–1.03)
Spring	0.98 (0.96–1.00)
Summer	0.93 (0.89–0.96)
Outbreak status	
Confirmed	Referent
Suspected	0.90 (0.88–0.92)
Census region	
South	Referent
Northeast	0.89 (0.87–0.91)
Midwest	1.00 (0.97–1.02)
West	0.98 (0.95–1.01)
Year	
2009 Jan–Jun	1.16 (1.10–1.23)
2009 Jul–2010 Jun	1.17 (1.11–1.23)
2010 Jul–2011 Jun	1.16 (1.12–1.21)
2011 Jul–2012 Jun	1.12 (1.08–1.16)
2012 Jul–2013 Jun	1.04 (1.01–1.07)
2013 Jul–2014 Jun	1.02 (0.99–1.06)
2014 Jul–2015 Jun	1.05 (1.02–1.08)
2015 Jul–2016 Jun	1.02 (0.99–1.05)
2016 Jul–2017 Jun	Referent
2017 Jul–Dec	1.04 (1.00–1.09)

Our study has several additional limitations. First, our process of data selection might have introduced bias into our analyses. We excluded outbreaks that occurred in multiple states, which are likely to have higher transmissibility given the larger geographic range involved; however, only 8 multistate outbreaks occurred during the study period, thus the bias is likely negligible. A substantial proportion of the dataset, 5,573 (31%) outbreaks, had to be excluded because the exposed population size was not reported. Excluding these outbreaks could introduce bias if the exposed population size is more likely to be reported for outbreaks with smaller, or larger, exposed population sizes. We only included outbreaks with person-to-person transmission; thus, our estimates of transmissibility are not generalizable to norovirus outbreaks where transmission occurs via other modes, such as foodborne, waterborne, or environmental transmission.

A second set of limitations relates to the final size method. This method assumes a susceptible-infected-recovered type infection in a homogenously mixing population (*12*), but this simplification likely does not reflect true mixing patterns. In addition, we might observe different mixing patterns in each of the different outbreak settings, such as older persons in long-term care facilities versus young children in childcare. The final size method also underestimates reproduction numbers for outbreaks with high attack rates. For example, in private homes, attack rates are high, but exposed population sizes are small. If everyone in the household is infected, then no additional infections can occur in the home. Thus, the final size method cannot capture any additional transmission that could have happened if the exposed population size had been larger, such as a higher number of persons in the household. Becker termed this limitation the "wasted infection potential" (*37*). Further, the final size method does not account for the effect of control measures. For some of the outbreaks represented in our dataset, control measures were most likely implemented, such as isolating ill persons and cleaning contamination. Such interventions likely would reduce the number ill, and the estimated R_0 would be lower than the R_0 in the absence of control measures.

In addition, the final size method assumes that the proportion of susceptible persons is known at the start of an outbreak; however, the level of susceptibility to norovirus is not well known. Certain host genetic factors are associated with the ability of norovirus to establish an infection within a human host (*38*–*41*), leading to variable susceptibility to norovirus infection (*42*–*44*). Secretor-negative persons have nonfunctional fucosyltransferase-2 genes, causing infection failure for norovirus genogroups I and II type 4 (*38*,*40*,*41*,*45*,*46*). Our estimates of R_0 and R_e assume that 47% of the population in our dataset is susceptible at the start of all outbreaks. However, the proportion susceptible varies among outbreaks and potentially over time and age as the distribution of circulating norovirus genotypes change. Further, our regression model estimates were sensitive to our assumption of the percent susceptible at the start of an outbreak. When we assumed 47% and 80% of the population was susceptible, the estimated transmissibility of norovirus in private homes or residences and restaurants was higher than transmissibility in long-term care and assisted living facilities. However, when we assumed 27% of the population was susceptible at the start of an outbreak, the association between private homes or residences and restaurants reversed. These settings then had lower estimated transmission relative to outbreaks in long-term care and assisted living facilities because the population size that can be infected is much lower, thus reducing the estimates of R_0 and R_e. For example, if a household had 15 persons, the maximum possible R_0 assuming 27% susceptibility is 4, which is lower than the average predicted R_0 for outbreaks in the reference group. Therefore, the results for private homes or residences and restaurants, where exposed population sizes are lower, should be interpreted with caution because transmission values in these settings might be underestimated. We also assumed that only symptomatic persons contribute to transmission in our calculation; persons with asymptomatic norovirus infections can contribute to transmission, but they likely are not as infectious as persons with symptomatic infections (*22*,*47*).

Finally, our main analysis does not account for norovirus genotype. Because of the limited data available on outbreak genotype we were not able to fully assess whether certain genotypes were more transmissible. As more genotyping data become available, future studies should investigate transmissibility.

We estimated reproduction numbers by using the final size method for >7,000 outbreaks from a national outbreak reporting system, then used these estimates to examine factors associated with norovirus transmission. Our analyses suggest that norovirus transmission rates are modest. Such modest rates of R_e suggest there are opportunities for effective control measures to curtail transmission of norovirus. However, challenges remain. Transmission by asymptomatic persons, which we did not account for in this analysis and generally goes undetected in surveillance, can limit the effectiveness of traditional control methods focused on ill persons, even for pathogens with modest transmission (*48*).

Overall, we found limited variation in R_0 and R_e for reported norovirus outbreaks in the United States, particularly across different settings. Our findings highlight the need for better data on the total exposed population sizes in outbreaks, which heavily influence estimates of attack rates, R_0, and R_e, to further refine estimates of these outbreak factors.

This work was supported by funding from the Norovirus Vaccine Modeling (NoVaMod) project (grant no. R01 GM124280), the National Institutes of Health, Agency for Healthcare Research Quality (grant no. R01 HS025987), and the National Institutes of Health graduate and postdoctoral training grant in environmental health science and toxicology (grant no. T32 ES012870).

The findings and conclusions in this report are those of the authors and do not necessarily represent the official position of the Centers for Disease Control and Prevention or the US Department of Health and Human Services.

About the Author

Dr. Steele is an epidemiologist in the Influenza Division, National Center for Immunization and Respiratory Diseases, Centers for Disease Control and Prevention. Her research interests include infectious disease dynamics and predicting public health impacts of vaccination.

References

1. Hall AJ, Wikswo ME, Manikonda K, Roberts VA, Yoder JS, Gould LH. Acute gastroenteritis surveillance through the National Outbreak Reporting System, United States. Emerg Infect Dis. 2013;19:1305–9. https://doi.org/10.3201/eid1908.130482
2. Wikswo ME, Kambhampati A, Shioda K, Walsh KA, Bowen AB, Hall AJ. Outbreaks of acute gastroenteritis transmitted by person-to-person contact, environmental contamination, and unknown modes of transmission–United States, 2009–2013. MMWR Surveill Summ. 2015;64:1–16 https://doi.org/10.15585/mmwr.mm6412a1
3. U.S. Centers for Disease Control and Prevention. National Outbreak Reporting System (NORS) [cited 2018 Oct 22]. https://www.cdc.gov/nors/data.html
4. Burke RM, Shah MP, Wikswo ME, Barclay L, Kambhampati A, Marsh Z, et al. The norovirus epidemiologic

triad: predictors of severe outcomes in US norovirus outbreaks, 2009–2016. J Infect Dis. 2019;219:1364–1372. https://doi.org/10.1093/infdis/jiy569
5. Rothman K, Greenland S, Lash T. Modern epidemiology. Philadelphia: Lippincott Williams & Wilkins; 2008.
6. Keeling MJ, Rohani P. Modeling infectious diseases in humans and animals. Boston: Princeton University Press; 2007.
7. Diekmann O, Heesterbeeck JAP. Mathematical epidemiology of infectious diseases: model building, analysis and interpretation, 1st edition. West Essex, England: John Wiley & Sons; 2000.
8. Guerra FM, Bolotin S, Lim G, Heffernan J, Deeks SL, Li Y, et al. The basic reproduction number (R_0) of measles: a systematic review. Lancet Infect Dis. 2017;17:e420–8. https://doi.org/10.1016/S1473-3099(17)30307-9
9. Ridenhour B, Kowalik JM, Shay DK. Unraveling R_0: considerations for public health applications. Am J Public Health. 2014;104:e32–41. https://doi.org/10.2105/AJPH.2013.301704
10. Gaythorpe KAM, Trotter CL, Lopman B, Steele M, Conlan AJK. Norovirus transmission dynamics: a modelling review. Epidemiol Infect. 2018;146:147–58. https://doi.org/10.1017/S0950268817002692
11. U.S. Centers for Disease Control and Prevention. CaliciNet [cited 2020 Mar 18]. https://www.cdc.gov/norovirus/reporting/calicinet/data.html
12. Becker NG. Analysis of infectious disease data. London: Chapman and Hall/CRC; 1989.
13. Ajami NJ, Barry MA, Carrillo B, Muhaxhiri Z, Neill FH, Prasad BVV, et al. Antibody responses to norovirus genogroup GI.1 and GII.4 proteases in volunteers administered Norwalk virus. Clin Vaccine Immunol. 2012;19:1980–3. https://doi.org/10.1128/CVI.00411-12
14. Lindesmith L, Moe C, Lependu J, Frelinger JA, Treanor J, Baric RS. Cellular and humoral immunity following Snow Mountain virus challenge. J Virol. 2005;79:2900–9. https://doi.org/10.1128/JVI.79.5.2900-2909.2005
15. Bernstein DI, Atmar RL, Lyon GM, Treanor JJ, Chen WH, Jiang X, et al. Norovirus vaccine against experimental human GII.4 virus illness: a challenge study in healthy adults. J Infect Dis. 2015;211:870–8. https://doi.org/10.1093/infdis/jiu497
16. Treanor JJ, Madore HP, Dolin R. Development of an enzyme immunoassay for the Hawaii agent of viral gastroenteritis. J Virol Methods. 1988;22:207–14. https://doi.org/10.1016/0166-0934(88)90103-6
17. Frenck R, Bernstein DI, Xia M, Huang P, Zhong W, Parker S, et al. Predicting susceptibility to norovirus GII.4 by use of a challenge model involving humans. J Infect Dis. 2012;206:1386–93. https://doi.org/10.1093/infdis/jis514
18. Atmar RL, Opekun AR, Gilger MA, Estes MK, Crawford SE, Neill FH, et al. Norwalk virus shedding after experimental human infection. Emerg Infect Dis. 2008;14:1553–7. https://doi.org/0.3201/eid1410.080117
19. Leon JS, Kingsley DH, Montes JS, Richards GP, Lyon GM, Abdulhafid GM, et al. Randomized, double-blinded clinical trial for human norovirus inactivation in oysters by high hydrostatic pressure processing. Appl Environ Microbiol. 2011;77:5476–82. https://doi.org/10.1128/AEM.02801-10
20. R Core Team. R: A language and environment for statistical computing. Vienna: R Foundation for Statistical Computing; 2018 [cited 2018 Oct 22]. http://www.r-project.org
21. Blair G, Cooper J, Coppock A, Humphreys M, Sonnet L, Fultz N, et al. Package "estimatr". 2019 [cited 2019 Nov 12]. https://cran.r-project.org/web/packages/estimatr/estimatr.pdf
22. Sukhrie FH, Teunis P, Vennema H, Copra C, Thijs Beersma MFC, Bogerman J, et al. Nosocomial transmission of norovirus is mainly caused by symptomatic cases. Clin Infect Dis. 2012;54:931–7. https://doi.org/10.1093/cid/cir971
23. Vanderpas J, Louis J, Reynders M, Mascart G, Vandenberg O. Mathematical model for the control of nosocomial norovirus. J Hosp Infect. 2009;71:214–22. https://doi.org/10.1016/j.jhin.2008.11.024
24. Heijne JCM, Rondy M, Verhoef L, Wallinga J, Kretzschmar M, Low N, et al. Quantifying transmission of norovirus during an outbreak. Source Epidemiol. 2012;23:277–84. https://doi.org/10.1097/EDE.0b013e3182456ee6
25. O'Dea EB, Pepin KM, Lopman BA, Wilke CO. Fitting outbreak models to data from many small norovirus outbreaks. Epidemics. 2014;6:18–29. https://doi.org/10.1016/j.epidem.2013.12.002
26. Simmons K, Gambhir M, Leon J, Lopman B. Duration of immunity to norovirus gastroenteritis. Emerg Infect Dis. 2013;19:1260–7. https://doi.org/10.3201/eid1908.130472
27. Steele MK, Remais JV, Gambhir M, Glasser JW, Handel A, Parashar UD, et al. Targeting pediatric versus elderly populations for norovirus vaccines: a model-based analysis of mass vaccination options. Epidemics. 2016;17:42–9. https://doi.org/10.1016/j.epidem.2016.10.006
28. Milbrath MO, Spicknall IH, Zelner JL, Moe CL, Eisenberg JNS. Heterogeneity in norovirus shedding duration affects community risk. Epidemiol Infect. 2013;141:1572–84. https://doi.org/10.1017/S0950268813000496
29. Lawrence L, Kerrod E, Gani R, Leach S. Microbiological risk assessment for norovirus infection contribution to the overall burden afforded by foodborne infections. London: Food Standards Agency; 2004.
30. Ahmed SM, Lopman BA, Levy K. A systematic review and meta-analysis of the global seasonality of norovirus. PLoS One. 2013;8:e75922. https://doi.org/10.1371/journal.pone.0075922
31. Lopman B, Armstrong B, Atchison C, Gray JJ. Host, weather and virological factors drive norovirus epidemiology: time-series analysis of laboratory surveillance data in England and Wales. PLoS One. 2009;4:e6671. https://doi.org/10.1371/journal.pone.0006671
32. Duizer E, Bijkerk P, Rockx B, De Groot A, Twisk F, Koopmans M. Inactivation of caliciviruses. Appl Environ Microbiol. 2004;70:4538–43. https://doi.org/10.1128/AEM.70.8.4538-4543.2004
33 Doultree JC, Druce JD, Birch CJ, Bowden DS, Marshall JA. Inactivation of feline calicivirus, a Norwalk virus surrogate. J Hosp Infect. 1999;41:51–7. https://doi.org/10.1016/S0195-6701(99)90037-3
34. Hall AJ, Wikswo ME, Pringle K, Gould LH, Parashar UD; Division of Viral Diseases, National Center for Immunization and Respiratory Diseases, CDC. Vital signs: foodborne norovirus outbreaks—United States, 2009–2012. MMWR Morb Mortal Wkly Rep. 2014;63:491–5.
35. Shah MP, Wikswo ME, Barclay L, Kambhampati A, Shioda K, Parashar UD, et al. Near real-time surveillance of U.S. norovirus outbreaks by the norovirus sentinel testing and tracking network—United States, August 2009–July 2015. MMWR Morb Mortal Wkly Rep. 2017;66:185.
36. U.S. Centers for Disease Control and Prevention. Reporting and Surveillance for Norovirus. NoroSTAT [cited 2018 Oct 22]. https://www.cdc.gov/norovirus/reporting/noroSTAT/index.html
37. Becker NG. Martingale methods for the analysis of epidemic data. Stat Methods Med Res. 1993;2:93–112. https://doi.org/10.1177/096228029300200106

38. Hutson AM, Atmar RL, Marcus DM, Estes MK. Norwalk virus-like particle hemagglutination by binding to histo-blood group antigens. J Virol. 2003;77:405–15. https://doi.org/10.1128/jvi.77.1.405-415.2003
39. Hutson AM, Airaud F, Lependu J, Estes MK, Atmar RL. Norwalk virus infection associates with secretor status genotyped from sera. J Med Virol. 2005;77:116–20. https://doi.org/10.1128/jvi.77.1.405-415.2003
40. Hutson AM, Atmar RL, Graham DY, Estes MK. Norwalk virus infection and disease is associated with ABO histo–blood group type. J Infect Dis. 2002;185:1335–7. https://doi.org/10.1086/339883
41. Lindesmith L, Moe C, Marionneau S, Ruvoen N, Jiang X, Lindblad L, et al. Human susceptibility and resistance to Norwalk virus infection. Nat Med. 2003;9:548–53. https://doi.org/10.1038/nm860
42. Wyatt RG, Dolin R, Blacklow NR, DuPont HL, Buscho RF, Thornhill TS, et al. Comparison of three agents of acute infectious nonbacterial gastroenteritis by cross-challenge in volunteers. J Infect Dis. 1974;129:709–14. https://doi.org/10.1093/infdis/129.6.709
43. Parrino TA, Schreiber DS, Trier JS, Kapikian AZ, Blacklow NR. Clinical immunity in acute gastroenteritis caused by Norwalk agent. N Engl J Med. 1977;297:86–9. https://doi.org/10.1056/NEJM197707142970204
44. Graham DY, Jiang X, Tanaka T, Opekun AR, Madore HP, Estes MK. Norwalk virus infection of volunteers: new insights based on improved assays. J Infect Dis. 1994;170:34–43. https://doi.org/10.1093/infdis/170.1.34
45. Marionneau S, Airaud F, Bovin NV, Pendu JL, Ruvoën-Clouet N. Influence of the combined ABO, FUT2, and FUT3 polymorphism on susceptibility to Norwalk virus attachment. J Infect Dis. 2005;192:1071–7. https://doi.org/10.1086/432546
46. Marionneau S, Ruvoën N. BeatriceLe Moullac–Vaidye, Monique Clement, Anne Cailleau–Thomas, Guillermo Ruiz–Palacois, et al. Norwalk virus binds to histo-blood group antigens present on gastroduodenal epithelial cells of secretor individuals. Gastroenterology. 2002;122:1967–77. https://doi.org/10.1053/gast.2002.33661
47. Sukhrie FH, Siebenga JJ, Beersma MFC, Koopmans M. Chronic shedders as reservoir for nosocomial transmission of norovirus. J Clin Microbiol. 2010;48:4303–5. https://doi.org/10.1128/JCM.01308-10
48. Ferguson NM, Cummings DAT, Fraser C, Cajka JC, Cooley PC, Burke DS. Strategies for mitigating an influenza pandemic. Nature. 2016;442:448–52. https://doi.org/10.1038/nature04795

Address for correspondence: Molly Steele, Centers for Disease Control and Prevention, 1600 Clifton Rd NE, Mailstop H24-7; Atlanta, GA 30329-4027, USA; email: MSteele@cdc.gov

Imported Monkeypox, Singapore

Sarah Ee Fang Yong, Oon Tek Ng, Zheng Jie Marc Ho, Tze Minn Mak, Kalisvar Marimuthu, Shawn Vasoo, Tsin Wen Yeo, Yi Kai Ng, Lin Cui, Zannatul Ferdous, Po Ying Chia, Bryan Jun Wei Aw, Charmaine Malenab Manauis, Constance Khia Ki Low, Guanhao Chan, Xinyi Peh, Poh Lian Lim, Li Ping Angela Chow, Monica Chan, Vernon Jian Ming Lee, Raymond Tzer Pin Lin, Mok Kwee Derrick Heng, Yee Sin Leo

In May 2019, we investigated monkeypox in a traveler from Nigeria to Singapore. The public health response included rapid identification of contacts, use of quarantine, and postexposure smallpox vaccination. No secondary cases were identified. Countries should develop surveillance systems to detect emerging infectious diseases globally.

Monkeypox is a zoonosis endemic to West and Central Africa; human cases were first reported in 1970 (*1*). An outbreak ongoing in Nigeria since 2017 is the largest documented (*2*). Exported cases in the United Kingdom and Israel were reported from travelers infected in Nigeria in 2018 (*3*,*4*). An earlier outbreak of human cases in the United States in 2003 was linked to contact with prairie dogs infected by rodents from Ghana (*5*).

Singapore is a globally connected city-state in Southeast Asia, placing it at risk for importation of emerging infectious diseases. For this reason, the Singapore Ministry of Health informed frontline medical practitioners in 2018 of the risk for monkeypox. Seven months later, a case of travel-associated monkeypox was diagnosed in Singapore. We present case details and public health management for this case, together with lessons learned and implications for control.

Author affiliations: Ministry of Health Singapore, Singapore (S.E.F. Yong, Z.J.M. Ho, C.K.K. Low, G. Chan, X. Peh, V.J.M. Lee, M.K.D. Heng); National Centre for Infectious Diseases, Singapore (O.T. Ng, T.M. Mak, K. Marimuthu, S. Vasoo, T.W. Yeo, Y.K. Ng, L. Cui, Z. Ferdous, P.Y. Chia, B.J.W. Aw, C.M. Manauis, P.L. Lim, L.P.A. Chow, M. Chan, R.T.P. Lin, Y.S. Leo); National Public Health Laboratory, Singapore (T.M. Mak, Y.K. Ng, L. Cui, R.T.P. Lin); Tan Tock Seng Hospital, Singapore (O.T. Ng, K. Marimuthu, S. Vasoo, T.W. Yeo, Z. Ferdous, P.Y. Chia, B.J.W. Aw, C.M. Manauis, P.L. Lim, L.P.A. Chow, Y.S. Leo); National University Health System, Singapore (S.E.F. Yong); Nanyang Technological University, Singapore (O.T. Ng, P.Y. Chia, P.L. Lim, Y.S. Leo); National University of Singapore, Singapore (K. Marimuthu, P.L. Lim, Y.S. Leo)

DOI: https://doi.org/10.3201/eid2608.191387

The Case

On May 8, 2019, monkeypox was laboratory-confirmed in a 38-year-old man from Nigeria who had traveled to Singapore. The man resided in Delta State, Nigeria, but had attended a wedding in Ebonyi State during April 21–23, where he reported ingestion of barbecued bushmeat that might have been contaminated. He did not handle raw meat and had no exposure to wild animals or their products. He held an administrative job and reported no contact with rodents or with persons with pox-like illnesses.

The man arrived in Singapore on April 28 and attended a business workshop on April 29–30. Fever, chills, and myalgia developed on April 30, and a vesicular rash on his face developed on May 1 and progressed cephalocaudally. After symptoms developed, he remained in his hotel room most of the time. He sought medical attention on May 7; an ambulance transported him to the Tan Tock Seng Hospital emergency department, and he was transferred to the adjacent National Centre for Infectious Diseases. The same day, the treating physician notified the Ministry of Health about the suspected monkeypox case.

At examination in the emergency department, the patient had a fever of 37.7°C. He had multiple pustular lesions of varying stages over his face, trunk, and limbs (Figure 1, panel A), including palms and soles, penile shaft, and glans penis. There was no oral involvement. Cervical and inguinal lymphadenopathy were present.

In view of his travel history and symptoms, differential diagnoses considered included monkeypox and other poxvirus infections. Whole blood and swab specimens of the lesions and vesicle fluid were sent to the National Public Health Laboratory, where tests for orthopoxvirus were positive at 2 hours and monkeypox virus at 6 hours after specimen receipt. Serum and swab specimens tested positive for orthopoxvirus

Figure 1. Dermatologic features of monkeypox in a 38-year-old man, Singapore, 2019. A) Pustular lesions on the hand at the start of hospitalization. B, C) Resolving lesions with shedding of scabs of the hands (B) and feet (C) toward end of hospitalization (day 17). D, E) Crusting of right fourth finger lesion (D) and lesions at varying stages (vesicles and scabbing) on the left chest (E) on day 15 of hospitalization.

but negative for variola virus on the BioFire FilmArray Biothreat Panel version 2.5 (https://www.biofiredx.com). We confirmed orthopoxvirus from swab specimen using a panorthopoxvirus PCR targeting E9L (DNA polymerase) (*6*) and by direct visualization of virus particles using transmission electron microscopy, which showed features characteristic of orthopoxviruses (Figure 2, panels A, B) (*7*).

Detailed molecular analysis using PCR for monkeypox was positive for 2 monkeypox genes (B6R and B7R) (*8*). We further confirmed monkeypox by next-generation sequencing using the Illumina MiSeq platform (https://www.illumina.com). Sequencing read analysis showed alignment with monkeypox virus. The assembled sequence covered 98% of the closest genome reference on GenBank (accession no. KJ642617.1, a strain from Nigeria), with 99.96% identity. We aligned the consensus sequence with selected representative archived sequences with multiple alignment using Fast Fourier Transform (*9*) and created a maximum-likelihood tree using RAxML (*10*) with γ-distributed rate differences and 1,000 bootstrap validation. The virus belonged to the West African clade and clustered with strains from Nigeria with 100% bootstrap support (Figure 2, panel C).

The patient was isolated in a negative-pressure room and remained well throughout admission. He was examined daily for new pustules and evolution of scabs (Figure 1, panels B–E). By May 24, all scabs had shed, and he was de-isolated and discharged.

Within 24 hours after notification of the suspected monkeypox case, the Ministry of Health contact tracing team established the patient's activities, identified contacts, and determined risk categories. These activities were performed through interviews with the patient and with his contacts. Close contacts were defined as persons who were within 2 meters of the patient for ≥30 minutes or had physical contact with him or had physical contact with surfaces or materials contaminated by secretions from him from April 30 on (*11*).

We identified 23 close contacts (19 workshop attendees and 4 hotel staff) and 8 lower risk contacts.

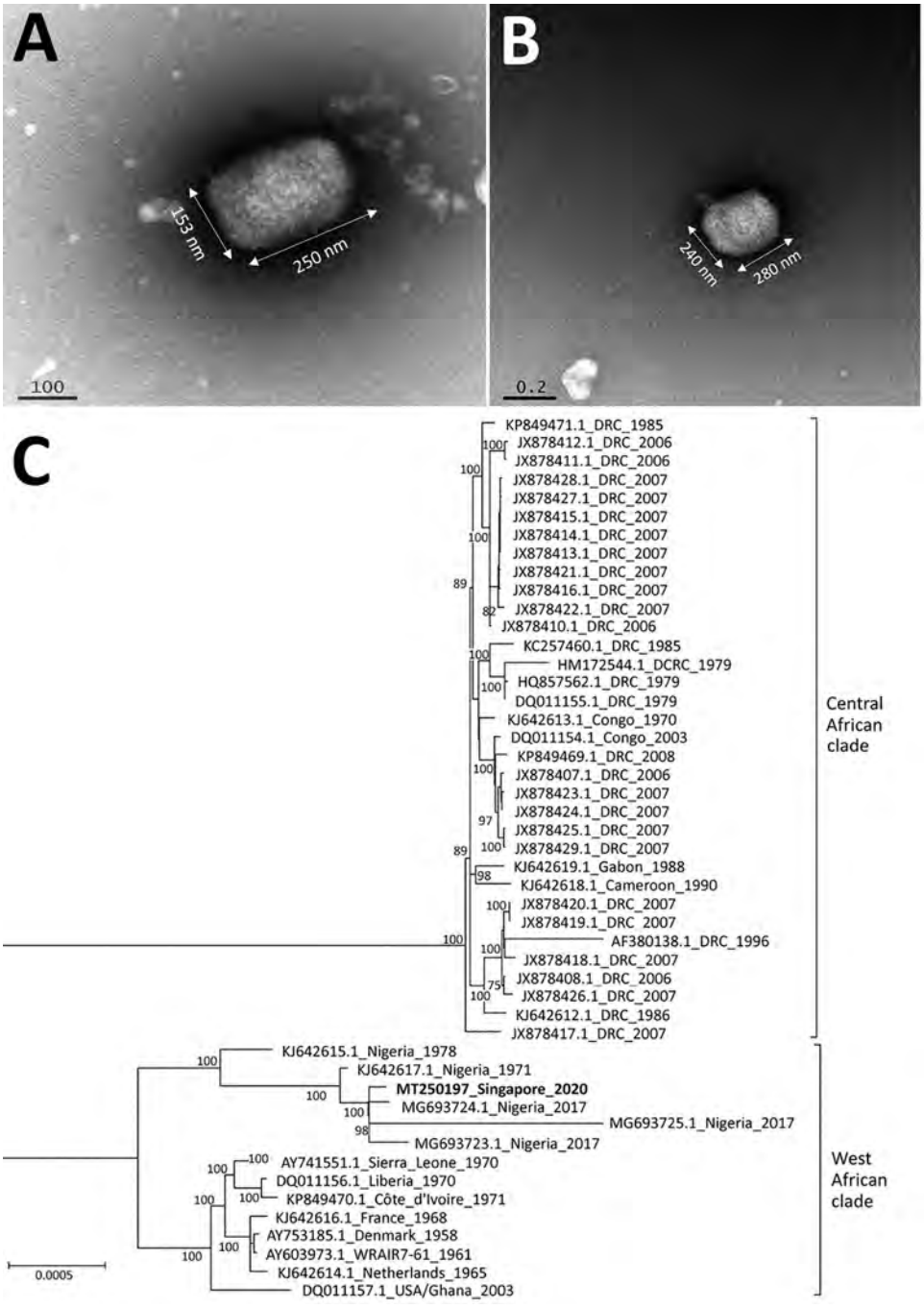

Figure 2. Transmission electron microscopy and maximum-likelihood phylogenetic tree of monkeypox virus in 38-year-old man, Singapore, 2019. A, B) Multiple brick-shaped particles, ranging from 230–290 nm by 130–240 nm, were observed from vesicle fluid under transmission electron microscopy. Tubular structures were observed with phosphotungstic acid stain (A), and a central ring-like depression was observed with gadolinium acetate stain (B). C) Phylogeny of monkeypox sequences, with the patient's monkeypox strain in bold. All strains are identified by GenBank accession number, location, and year. The evolutionary relationships between monkeypox strains was determined based on 184,338 bases within the central core region of the monkeypox genome. The maximum-likelihood tree was created using RAxML (*10*) with γ-distributed rate differences and 1,000 bootstrap validation. Only bootstrap values >70% are displayed on the internal branches. Central African and West African clades are indicated. Scale bar indicates genetic distance between sequences.

Quarantine orders were issued to 22 close contacts on May 9; they were required to remain at home or at a government quarantine facility for the duration of the remaining incubation period (21 days). They were not allowed to come into physical contact with others on the same premises and were monitored for fever and rash ≥3 times each day through video calls. One close contact, who was well, had left Singapore for Nigeria on May 5; we provided details to the Nigerian International Health Regulations National Focal Point.

Close contacts were offered smallpox vaccination (ACAM2000; Sanofi Pasteur Biologics Co, https://www.sanofi.com) as postexposure prophylaxis. Of the 22 close contacts, 14 received the vaccination, 2 had contraindications, and 6 declined. All vaccinated persons had a scab or ulcer at day 6–8 of review. Side effects included slight fever and mild swelling at the vaccination site; no serious adverse events were reported. Lower risk contacts were placed on phone surveillance twice a day for the remaining incubation period.

Because of the early suspicion of an infectious disease, all healthcare workers who interacted with the patient used personal protective equipment. Ambulance paramedics and Tan Tock Seng Hospital emergency staff had worn N95 masks and disposable gowns and gloves. At the National Centre for Infectious Disease, healthcare workers donned full personal protective equipment (N95 mask, eye protection, disposable headgear, gloves, and sterile disposable gowns). Thus, no healthcare workers were quarantined or removed from work, but they were monitored for symptoms as an added precaution.

We followed up all contacts for 21 days after exposure. Monkeypox did not develop in any contacts, and we found no evidence of secondary transmission in Singapore.

Conclusions

The patient's clinical manifestations of a vesiculopustular rash and uncomplicated illness was similar to monkeypox cases in the United Kingdom and Israel, which were also linked to travel from Nigeria (*3*,*4*,*12*). All exported cases were of the West African clade, which is thought to be milder and less transmissible than the Congo Basin clade (*13*). Nevertheless, human-to-human transmission had been also demonstrated in Nigeria and the United Kingdom.

Singapore's experience with monkeypox highlights the critical role frontline clinicians play in surveillance of emerging infectious diseases. This situation was similar to the 2016 Zika outbreak in Singapore, when a general practitioner contacted the Ministry of Health about an unusual increase in persons with fever, rash, and joint pains (*14*). In both instances, the Ministry of Health had informed physicians about the evolving global situation. Public health agencies should prioritize regular communication with healthcare workers as integral to preparedness for emerging infectious diseases.

Unlike previous monkeypox outbreaks, the outbreak in Nigeria affected predominantly urban dwellers and resulted in exported cases to geographically disparate countries (*1*). Increasing urbanization and better connectivity can lead to the emergence and spread of infections to new areas (*15*). Our experience with monkeypox highlights the importance of countries investing in preparedness, including maintaining surveillance systems suited to detecting the emergence of infectious diseases globally.

Acknowledgments

We thank Nataline Tang and Pei Ling Loh for their assistance in the National Public Health Laboratory, Shi Ling Chen for processing and preparation of the sample for electron microscopy examination, Bei Bei Chen for help with the sequencing reactions, and Vithia Gunalan for advice on the sequence assembly.

About the Author

Dr. Yong is a preventive medicine resident at the National University Health System, Singapore. Her primary research interest is public health policy, including the development of health systems.

References

1. Yinka-Ogunleye A, Aruna O, Dalhat M, Ogoina D, McCollum A, Disu Y, et al.; CDC Monkeypox Outbreak Team. Outbreak of human monkeypox in Nigeria in 2017–18: a clinical and epidemiological report. Lancet Infect Dis. 2019;19:872–9. https://doi.org/10.1016/S1473-3099(19)30294-4
2. Centers for Disease Control and Prevention. Monkeypox in Nigeria. 2019 [cited 2019 Sep 15]. https://wwwnc.cdc.gov/travel/notices/watch/monkeypox-nigeria
3. Vaughan A, Aarons E, Astbury J, Balasegaram S, Beadsworth M, Beck CR, et al. Two cases of monkeypox imported to the United Kingdom, September 2018. Euro Surveill. 2018;23:23. https://doi.org/10.2807/1560-7917.ES.2018.23.38.1800509
4. Erez N, Achdout H, Milrot E, Schwartz Y, Wiener-Well Y, Paran N, et al. Diagnosis of imported monkeypox, Israel, 2018. Emerg Infect Dis. 2019;25:980–3. https://doi.org/10.3201/eid2505.190076
5. Centers for Disease Control and Prevention. 2003 United States outbreak of monkeypox. 2018 [cited 2019 Aug 17]. https://www.cdc.gov/poxvirus/monkeypox/outbreak.html
6. Kulesh DA, Baker RO, Loveless BM, Norwood D, Zwiers SH, Mucker E, et al. Smallpox and pan-orthopox virus detection

by real-time 3′-minor groove binder TaqMan assays on the roche LightCycler and the Cepheid smart Cycler platforms. J Clin Microbiol. 2004;42:601–9. https://doi.org/10.1128/JCM.42.2.601-609.2004
7. Gelderblom HR, Madeley D. Rapid viral diagnosis of orthopoxviruses by electron microscopy: optional or a must? Viruses. 2018;10:E142. https://doi.org/10.3390/v10040142
8. Li Y, Olson VA, Laue T, Laker MT, Damon IK. Detection of monkeypox virus with real-time PCR assays. J Clin Virol. 2006;36:194–203. https://doi.org/10.1016/j.jcv.2006.03.012
9. Katoh K, Standley DM. MAFFT: iterative refinement and additional methods. Methods Mol Biol. 2014;1079:131–46. https://doi.org/10.1007/978-1-62703-646-7_8
10. Stamatakis A. RAxML version 8: a tool for phylogenetic analysis and post-analysis of large phylogenies. Bioinformatics. 2014;30:1312–3. https://doi.org/10.1093/bioinformatics/btu033
11. Centers for Disease Control and Prevention. Monkeypox—transmission. 2015 [cited 2019 Sep 3]. https://www.cdc.gov/poxvirus/monkeypox/transmission.html
12. Vaughan A, Aarons E, Astbury J, Brooks T, Chand M, Flegg P, et al. Human-to-human transmission of monkeypox virus, United Kingdom, October 2018. Emerg Infect Dis. 2020;26:782–5. https://doi.org/10.3201/eid2604.191164
13. Brown K, Leggat PA. Human monkeypox: current state of knowledge and implications for the future. Trop Med Infect Dis. 2016;1:8. https://doi.org/10.3390/tropicalmed1010008
14. Ho ZJM, Hapuarachchi HC, Barkham T, Chow A, Ng LC, Lee JMV, et al.; Singapore Zika Study Group. Outbreak of Zika virus infection in Singapore: an epidemiological, entomological, virological, and clinical analysis. Lancet Infect Dis. 2017;17:813–21. https://doi.org/10.1016/S1473-3099(17)30249-9
15. Alirol E, Getaz L, Stoll B, Chappuis F, Loutan L. Urbanisation and infectious diseases in a globalised world. Lancet Infect Dis. 2011;11:131–41. https://doi.org/10.1016/S1473-3099(10)70223-1

Address for correspondence: Yee Sin Leo, National Centre for Infectious Diseases, 16 Jalan Tan Tock Seng, Singapore 308442; email: Yee_Sin_Leo@ncid.sg; Mok Kwee Derrick Heng, Ministry of Health Singapore, 16 College Rd., College of Medicine Building, Singapore 169854, Singapore; email: Derrick_HENG@moh.gov.sg

Population-Based Estimates of Chronic Conditions Affecting Risk for Complications from Coronavirus Disease, United States

Mary L. Adams, David L. Katz, Joseph Grandpre

We estimated that 45.4% of US adults are at increased risk for complications from coronavirus disease because of cardiovascular disease, diabetes, respiratory disease, hypertension, or cancer. Rates increased by age, from 19.8% for persons 18–29 years of age to 80.7% for persons ≥80 years of age, and varied by state, race/ethnicity, health insurance status, and employment.

Data for China indicate that 81% of coronavirus disease (COVID-19) patients had mild cases, 14% had severe cases, and 5% had critical cases (*1*,*2*). The overall case-fatality rate (CFR) in China was 3.8% (*3*), but CFRs were higher for adults with chronic conditions of cardiovascular disease (CVD; CFR 13.2%), diabetes (9.2%), chronic respiratory disease (8.0%), hypertension (8.4%), and cancer (7.6%), compared with 1.4% for patients with none of these conditions (*3*). Our objective for this study was to use population-based US data to estimate the fraction of adults in the community who might be at increased risk for complications from COVID-19 because they reported any of the chronic conditions with a high CFR in China.

The Study

We used publicly available 2017 Behavioral Risk Factor Surveillance System (BRFSS) data (*4*) from telephone surveys of 444,649 randomly selected adults ≥18 years of age in the 50 states and the District of Columbia (DC). Because the BRFSS includes only noninstitutionalized adults, residents of nursing homes and assisted living facilities are among those not surveyed. We chose to use 2017 data to include hypertension, which was not addressed in 2018. Data were adjusted for the probability of selection and weighted to be representative of the adult population in each state by age, sex, race/ethnicity, marital status, education, home ownership, and telephone type. Weights and stratum variables needed for analysis were included.

We did not age-adjust results to reflect the age distribution of each state rather than a standard population. The median response rate for cell phone and landline surveys combined was 47.2%, ranging from 33.9% in California to 61.1% in Utah (*5*). Reliability and validity of the BRFSS have been found to be moderate to high for many survey measures, in particular those used here, which can be checked versus medical records (*6*).

The key variable was a composite measure including adults reporting that they were ever told they had CVD (heart attack, angina, coronary heart disease, or stroke), diabetes, asthma, chronic obstructive pulmonary disease, hypertension, or cancer other than skin. We counted the number of chronic conditions for each respondent and adults who reported ≥1 condition and were considered to be at heightened risk for complications from COVID-19. A secondary measure was receipt of a seasonal influenza vaccination in the past year as a rough estimate of potential demand for a COVID-19 vaccine when available.

Demographic measures included age group (18–29, 30–39, 40–49, 50–59, 60–69, 70–79, and ≥80 years of age; we created these measures by combining 5-year age groups provided in the dataset); self-reported race/ethnicity (non-Hispanic White, Black or African American, Hispanic of any race, American Indian/Alaska native, Asian/Pacific Islander, and other); health insurance coverage (any kind of healthcare coverage, including health insurance, prepaid plans such as health maintenance organizations, or government plans such as Medicare, or Indian Health Service); employment status (employed or self-employed, out

Author affiliations: On Target Health Data LLC, Suffield, Connecticut, USA (M.L. Adams); True Health Initiative, Derby, Connecticut, USA (D.L. Katz); Wyoming Department of Health, Cheyenne, Wyoming, USA; (J. Grandpre)

DOI: https://doi.org/10.3201/eid2608.200679

of work, homemaker, student, retired, or unable to work); and state of residence, which included DC.

We used Stata version 14.1 (StataCorp LP, https://www.stata.com) for analysis to account for the complex sample design of the BRFSS. We report point estimates and 95% CIs or population estimates by using weights, stratum, and primary sampling unit variables supplied in the dataset (*4*). Missing values were excluded from analysis.

Among 444,649 survey respondents, 48.7% were male, 13.9% were ≥70 years of age, 63.3% were white, 18.2% were retired, and 12.1% were uninsured. We obtained similar results for the study sample when 11,508 records that had missing values were removed. Overall, 45.4% (95% CI 45.1%–45.7%) of respondents fit the description of being at heightened risk for complications from COVID-19.

Among all adults, 26.7% (95% CI 26.5%–27.0%) reported 1 chronic condition, 12.0% (95% CI 11.8%–12.2%) reported 2 chronic conditions, 4.7% (95% CI 4.6%–4.8%) reported 3 chronic conditions, and 2.0% (95% CI 1.9%–2.1%) reported ≥4 chronic conditions. Prevalence rates of separate chronic conditions were 8.5% for CVD, 6.6% for chronic obstructive pulmonary disease, 9.1% for asthma (active condition), 10.8% for diabetes, 32.4% for hypertension, and 6.8% for cancer. Although the percentage of adults with any of the chronic conditions increased with age (Table 1, https://wwwnc.cdc.gov/EID/article/26/8/20-0679-T1.htm), more than half (53.4%) of the total were 18–59 years of age. Rates also varied by state, race/ethnicity, insurance status, and employment, but not by sex (Table 1).

State results obtained directly from Stata (Table 2) list the number of adults in each state at increased risk for complications and the percentage that number represents among all states. Results for reporting a seasonal influenza vaccination in the past year were 40.3% (95% CI 40.0%–40.6%) for all adults, including 33.7% (95% CI 33.3%–34.2%) for adults who had none of the chronic conditions and 48.0% (95% CI 47.5%–48.5%) for persons who had any of the 6 chronic conditions.

Conclusions

We estimated that 45.4% of US adults, with a wide range across age groups and states, might be at increased risks for complications from COVID-19 because of existing chronic conditions. The 18.7% who reported ≥2 chronic conditions might be at even greater risk on the basis of other studies (*7*). Although complication rates increased with increasing age, 53% of those at greater risk for complications were <60 years of age. Preliminary data suggest that some of these same chronic conditions increase risk for COVID-19 complications in the United States (*8*). Another BRFSS study that omitted hypertension and used a different definition of risk estimated that 37.6% of US adults were at risk for complications (*9*).

Table 2. Number of adults with any of 6 chronic conditions increasing risk for coronavirus disease complications and percentage of total in each state, 2017 Behavioral Risk Factor Surveillance System, United States*

State	No. adults at risk	% Adults at risk†
AL	1,997,864	1.78
AK	237,208	0.21
AZ	2,351,799	2.10
AR	1,181,105	1.06
CA	12,240,142	10.93
CO	1,701,776	1.52
CT	1,239,597	1.11
DE	357,530	0.32
DC	213,357	0.19
FL	7,696,749	6.88
GA	3,541,358	3.16
HI	486,156	0.43
ID	534,533	0.48
IL	4,404,556	3.93
IN	2,428,188	2.17
IA	1,067,133	0.95
KS	983,323	0.88
KY	1,789,444	1.60
LA	1,806,330	1.61
ME	530,809	0.47
MD	2,054,758	1.84
MA	2,302,809	2.06
MI	3,749,235	3.35
MN	1,625,778	1.45
MS	1,150,036	1.03
MO	2,137,650	1.91
MT	356,113	0.32
NE	616,905	0.55
NV	1,048,591	0.94
NH	485,340	0.43
NJ	3,106,880	2.78
NM	701,585	0.63
NY	6,419,321	5.73
NC	3,713,582	3.32
ND	243,096	0.22
OH	4,268,748	3.81
OK	1,461,941	1.31
OR	1,418,689	1.27
PA	4,738,414	4.23
RI	393,069	0.35
SC	1,912,134	1.71
SD	281,110	0.25
TN	2,610,800	2.33
TX	8,977,387	8.02
UT	796,721	0.71
VT	226,397	0.20
VA	2,921,171	2.61
WA	2,464,452	2.20
WV	827,193	0.74
WI	1,949,872	1.74
WY	194,544	0.17
Total	111,943,278	100

*Chronic conditions: cardiovascular disease, diabetes, chronic obstructive pulmonary disease, asthma, hypertension, or cancer other than skin.
†Values were obtained directly from state and will not agree with calculations made from raw data.

The list of chronic conditions used in our analysis is similar to groups at increased risk for seasonal influenza complications (*10*), except that the influenza group includes obese adults. Obesity is much lower in China than in the United States (*11*), which might account for that difference. Both lists include persons with chronic diseases for which behavioral risk factors have been well identified (*12*,*13*). In particular, the 7 risk factors of smoking, sedentary lifestyle, obesity, diabetes, hypertension, high cholesterol, and inadequate fruit and vegetable consumption together contributed to an average of 41.4% of the burden of 5 of the 6 chronic conditions used in our study (all except cancer); obesity and smoking contributed the most to the burden (*12*). Results showing seasonal influenza vaccination rates <50% are concerning. Although a vaccine specific for this coronavirus is currently unavailable, results for seasonal influenza vaccination suggest that it might not be widely used.

Our study does not address possible differences in contracting the disease, only the risk for development of complications among persons who have COVID-19 on the basis of results for China (*1*–*3*). Because we surveyed only noninstitutionalized adults, we excluded 1.3 million adults in nursing homes (*14*), which almost certainly underestimates risk. Data are self-reported, and reliability and validity can vary for different measures tested (*6*). However, as long as a respondent was told they had a chronic condition, validity was high. Age groups used for analysis did not match those used for weighting data, but that limitation should have a minimal effect on results. Low response rates could introduce bias but, as noted, validity appears high for the measures used in this study.

We estimated that 45.4% of US adults are potentially at increased risk for complications from COVID-19 because of chronic conditions that are, in turn, associated with common modifiable risk factors. Such estimates will vary depending on exact criteria used and the prevalence of the risk factors associated with the chronic conditions, along with age, state of residence, and other demographic factors.

Data collection, analysis, and interpretation for this study were supported by the Centers for Disease Control and Prevention (Grant/Cooperative Agreement no. 1U58DP006069-01).

About the Author

Ms. Adams is a consultant at On Target Health Data LLC, Suffield, CT. Her primary research interest is chronic diseases (including dementia) and their risk factors.

References

1. Wu Z, McGoogan JM. Characteristics of and important lessons from the coronavirus disease 2019 (COVID-19) outbreak in China: summary of a report of 72 314 cases from the Chinese Center for Disease Control and Prevention. JAMA. 2020;323:1239 [Epub ahead of print]. https://doi.org/10.1001/jama.2020.2648
2. The epidemiological characteristics of an outbreak of 2019 novel coronavirus diseases (COVID-19) in China [in Chinese]. Zhonghua Liu Xing Bing Xue Za Zhi. 2020;41:145–51.
3. World Health Organization. Report of the WHO–China joint mission on coronavirus disease 2019 (COVID-19), February 28, 2020 [cited 2020 Apr 17]. https://www.who.int/docs/default-source/coronaviruse/who-china-joint-mission-on-covid-19-final-report.pdf
4. Behavioral Risk Factor Surveillance System (BRFSS) Survey Data and Documentation [cited 2020 Mar 3]. https://www.cdc.gov/brfss/data_documentation/index.htm
5. Centers for Disease Control and Prevention. Behavioral Risk Factor Surveillance System 2017 Summary Data Quality Report, June 13, 2018 [cited 2018 Nov 16]. https://www.cdc.gov/brfss/annual_data/2015/pdf/2015-sdqr.pdfhttps://www.cdc.gov/brfss/annual_data/2017/pdf/2017-sdqr-508.pdf
6. Pierannunzi C, Hu SS, Balluz L. A systematic review of publications assessing reliability and validity of the Behavioral Risk Factor Surveillance System (BRFSS), 2004-2011. BMC Med Res Methodol. 2013;13:49. https://doi.org/10.1186/1471-2288-13-49
7. Sambamoorthi U, Tan X, Deb A. Multiple chronic conditions and healthcare costs among adults. Expert Rev Pharmacoecon Outcomes Res. 2015;15:823–32. https://doi.org/10.1586/14737167.2015.1091730
8. Chow N, Fleming-Dutra K, Gierke R, Hall A, Hughes M, Pilishvili T, et al.; CDC COVID-19 Response Team. Preliminary estimates of the prevalence of selected underlying health conditions among patients with coronavirus disease 2019 United States, February 12–March 28, 2020. MMWR Morb Mortal Wkly Rep. 2020;69:382–6. https://doi.org/10.15585/mmwr.mm6913e2
9. Koma W, Neuman T, Claxton G, Rae M, Kates J, Michaud J. How many adults are at risk of serious illness if infected with coronavirus? Kaiser Family Foundation, Washington, DC. March 2020 [cited 2020 Apr 17]. https://www.kff.org/global-health-policy/issue-brief/how-many-adults-are-at-risk-of-serious-illness-if-infected-with-coronavirus/
10. Centers for Disease Control and Prevention. Influenza (flu): people at high risk for flu complications [cited 2020 Apr 17]. https://www.cdc.gov/flu/highrisk/index.htm
11. Wu Y. Overweight and obesity in China. BMJ. 2006;333:362–3. https://doi.org/10.1136/bmj.333.7564.362
12. Adams ML, Grandpre J, Katz DL, Shenson D. The impact of key modifiable risk factors on leading chronic conditions. Prev Med. 2019;120:113–8. https://doi.org/10.1016/j.ypmed.2019.01.006
13. Adams ML, Grandpre J, Katz DL, Shenson D. Linear association between number of modifiable risk factors and multiple chronic conditions: Results from the Behavioral Risk Factor Surveillance System. Prev Med. 2017;105:169–75. https://doi.org/10.1016/j.ypmed.2017.09.013
14. Centers for Disease Control and Prevention. National Center for Health Statistics. Nursing home care [cited 2020 Apr 17]. https://www.cdc.gov/nchs/fastats/nursing-home-care.htm

Address for correspondence: Mary L. Adams, On Target Health Data LLC, 247 N Stone St, West Suffield, CT 06093, USA; email: madams.ontargethealthdata@gmail.com

Prolonged Persistence of SARS-CoV-2 RNA in Body Fluids

Jiufeng Sun,[1] Jianpeng Xiao,[1] Ruilin Sun,[1] Xi Tang,[1] Chumin Liang, Huifang Lin, Lilian Zeng, Jianxiong Hu, Runyu Yuan, Pingping Zhou, Jinju Peng, Qianlin Xiong, Fengfu Cui, Zhe Liu, Jing Lu, Junzhang Tian, Wenjun Ma, Changwen Ke

We prospectively assessed 49 coronavirus disease cases in Guangdong, China, to estimate the frequency and duration of detectable severe acute respiratory syndrome coronavirus 2 RNA in human body fluids. The prolonged persistence of virus RNA in various body fluids may guide the clinical diagnosis and prevention of onward virus transmission.

In December 2019, coronavirus disease (COVID-19) caused by a novel coronavirus, severe acute respiratory syndrome coronavirus 2 (SARS-CoV-2), emerged in Wuhan, China (*1*,*2*). As of April 1, 2020, the virus had expanded to 195 countries, and >820,000 confirmed cases with >40,000 deaths had been recorded (*3*–*6*).

Clinically, the confirmation of SARS-CoV-2 infection relies on detection of virus RNA in various body fluids. The World Health Organization recommends taking upper and lower respiratory samples simultaneously during the acute phase of infection to detect virus RNA. Recent studies reported a persistent shedding of SARS-CoV-2 in upper respiratory and intestinal samples (*7*,*8*). However, the frequency with which SARS-CoV-2 RNA can be detected in body fluids and the period during which it remains detectable are not well understood. A detailed understanding of the dynamics of the early stages of SARS-CoV-2 infection is needed to inform diagnostic testing and prevention interventions, because existing evidence is based only on observations from case reports. We recruited hospitalized patients with COVID-19 from 2 designated provincial emergency hospitals for e merging infectious diseases in Guangdong, China, and tested specimens by real-time reverse transcription PCR (rRT-PCR) to estimate the duration of the detection of SARS-CoV-2 RNA in various body fluids, using an accelerated failure time (AFT)–based modeling study.

The Study

We recruited 43 patients with mild cases of COVID-19 (22 male, 21 female; median age 43, range 1–70 years) and 6 patients with severe cases (6 male; median age 67, range 46–76 years) for this study. We obtained throat swab, nasopharyngeal swab, sputum, and feces specimens every 3 days for 4 weeks. We tested all specimens by rRT-PCR (Appendix, https://wwwnc.cdc.gov/EID/article/26/8/20-1097-App1.pdf). We used parametric Weibull regression models (AFT) to estimate the time until the loss of SARS-CoV-2 RNA detection in each body fluid and reported findings in medians and 95th percentiles using R software version 3.6.1 with flexsurv, survival, and survminer packages (*9*). We used Lnorm and gamma models as comparisons to evaluate the sensitivity and stability of Weibull regression models. We defined the time until loss of SARS-CoV-2 RNA detection in each fluid as the number of days between the day after illness onset and the day of the first negative rRT-PCR result. For the cases that involved intermittent shedding of SARS-CoV-2, we used the date of the first negative result after the final recorded positive rRT-PCR results. Of the 49 case-patients, 15 were discharged from the hospital after <4 weeks of observation time.

We obtained a total of 490 specimens (32.75% of the designated number of samples, 1,006 missing samples), including 88 throat swab samples (23.53%, 198 missing samples), 62 sputum samples (16.58%,

Author affiliations: Guangdong Provincial Center for Disease Control and Prevention, Guangzhou, China (J. Sun, J. Xiao, C. Liang, H. Lin, L. Zeng, J. Hu, R. Yuan, P. Zhou, J. Peng, Q. Xiong, F. Cui, Z. Liu, J. Lu, W. Ma, C. Ke); Guangdong Second Provincial General Hospital, Guangzhou (R. Sun, J. Tian); First People's Hospital of Foshan, Foshan, China (X. Tang)

DOI: https://doi.org/10.3201/eid2608.201097

[1]These authors contributed equally to this work.

Table. Prolonged persistence of SARS-CoV-2 RNA in body fluids from hospitalized patients with coronavirus disease, Guangdong, China*

	Mild cases, n = 43		Severe cases, n = 6	
Specimens	Median (95% CI)	95th percentile (95% CI)	Median (95% CI)	95th percentile (95% CI)
Throat swab	15.6 (11.8–20.7)	32.8 (25.9–42.3)	33.9 (24.2–47.3)	53.9 (39.4–81.7)
Sputum	20.0 (14.1–27.0)	43.7 (33.6–60.4)	30.9 (23.5–39.1)	44.7 (36.3–58.0)
Nasopharyngeal swab	22.7 (18.8–27.5)	46.3 (39.0–55.2)	33.5 (25.7–42.7)	49.4 (38.4–68.5)
Feces	24.5 (21.2–28.3)	45.6 (40.0–52.8)	32.5 (26.3–39.1)	48.9 (41.3–59.7)

*The time until the loss of SARS-CoV-2 RNA detection in each body fluid was estimated by using parametric Weibull regression models. Data are presented as medians and 95th percentiles in days after illness onset. SARS-CoV-2, severe acute respiratory syndrome coronavirus 2.

312 missing samples), 175 nasopharyngeal swab samples (46.79%, 199 missing samples), and 165 fecal samples (44.12%, 209 missing samples). Of these, 171 specimens tested positive for SARS-CoV-2 RNA by rRT-PCR, including 16 throat swab samples, 38 sputum samples, 89 nasopharyngeal swab samples, and 28 feces samples (Appendix Figure 1). We used Weibull models to estimate the median and the 95th percentile for the time until the loss of SARS-CoV-2 RNA detection in swab, sputum, and fecal samples (Table; Figures 1, 2). The sensitivity and stability evaluation of the Weibull, Lnorm, and gamma models showed no differences among them ($p<0.05$) (Appendix Table, Figures 2, 3).

Conclusions

In this study, we estimated the time for COVID-19 case-patients to clear SARS-CoV-2 RNA in the acute phase of infection through an AFT-based modeling study. We found persistent shedding of virus RNA in nasopharyngeal swab and feces samples. The estimated time until loss of virus RNA detection ranged from 45.6 days for nasopharyngeal swab samples to 46.3 days for feces samples in mild cases and from 48.9 days for nasopharyngeal swab samples to 49.4 days for feces samples in severe cases, which was longer than those of SARS-CoV and MERS-CoV (*10*,*11*). Lan et al. reported positive rRT-PCR results in throat swab sampless from patients who recovered from mild COVID-19 for 50 days at maximum (*8*). Wu et al. found prolonged presence of SARS-CoV-2 viral RNA in fecal samples (*7*). However, we found that the median time for throat samples from mild cases was 15.6 days (95% CI 11.8–20.7 days) and the 95th percentile was 32.8 days (95% CI 25.9–42.3 days). Therefore, detection of virus RNA for mild cases in throat swab samples at the 50th day after illness onset should be a low-probability event, beyond the 95th percentile limit. Similarly, the detection of virus RNA in fecal samples from mild cases was also close to the 95th percentile limit we estimated (45.6 days, 95% CI 40.0-52.8 days).

We found differences in median time until loss of virus RNA detection among respiratory specimen types in mild cases but not in severe cases (Table). We do not believe this finding was linked to the severity of COVID-19, but we had a limited sample size of severe cases in this study. The additional test using Lnorm or gamma models addressed similar phenomena. Nevertheless, the estimated time until the loss of RNA detection in various body fluids in this study was reasonable and was consistent with previous findings in case reports.

Challenges have been raised recently in the molecular diagnosis of COVID-19. Upper respiratory samples show lower positive rates and instable states of confirmation of SARS-CoV-2, whereas lower respiratory samples, such as bronchoalveolar lavage fluid, are suitable specimens for detection of virus RNA (*12*). The probable explanation of discrepant results with our estimates was the irregular operation of sampling in upper respiratory samples in clinics, rather than short-term shedding of virus RNA. In addition, the median duration in archived publications in China was 12.0 days (mean 12.8 days) (*13*), which was shorter than, but close to, our estimate in throat swab samples. This finding was in line with throat swab samples being suggested as a clinical sample for diagnosis of COVID-19 at the early stages of the outbreak in China (National Health Commission of the People's Republic of China, unpub. data, 2020 Jan 15).

Our study has limitations. First, we did not test serum specimens to address RNAemia or serologic trends. The reasons are the findings of extreme low positive rates of RNAemia in our initial study (1 of 49 cases), which does not yield any estimated conclusion. The serologic test was not conducted because reliable IgM/IgG kits were unavailable. Second, virus isolation and tests of specimens' infectivity were not conducted. We focused on estimating the duration of the detection of SARS-CoV-2 RNA in various body fluids among COVID-19 cases but did not imply the existence of infectious virus particles. Third, the number of missing specimens was higher than the initial study designed, attributed mainly to low proportions of purulent sputum production in viral pneumonia cases, as well as low compliance of patients. Fourth, this study may pose selection bias because

modest-sized groups of cases were included. Finally, the prerequisite we assumed was that all COVID-19 cases had SARS-CoV-2 RNA in all sampling specimens at symptom onset, which means that the median and 95th percentile we estimated were shorter than expected because of the uncertainty of incubation time. The time estimated in this study through hospitalized COVID-19 cases may not be generalizable to all infections with SARS-CoV-2, such as asymptomatic cases.

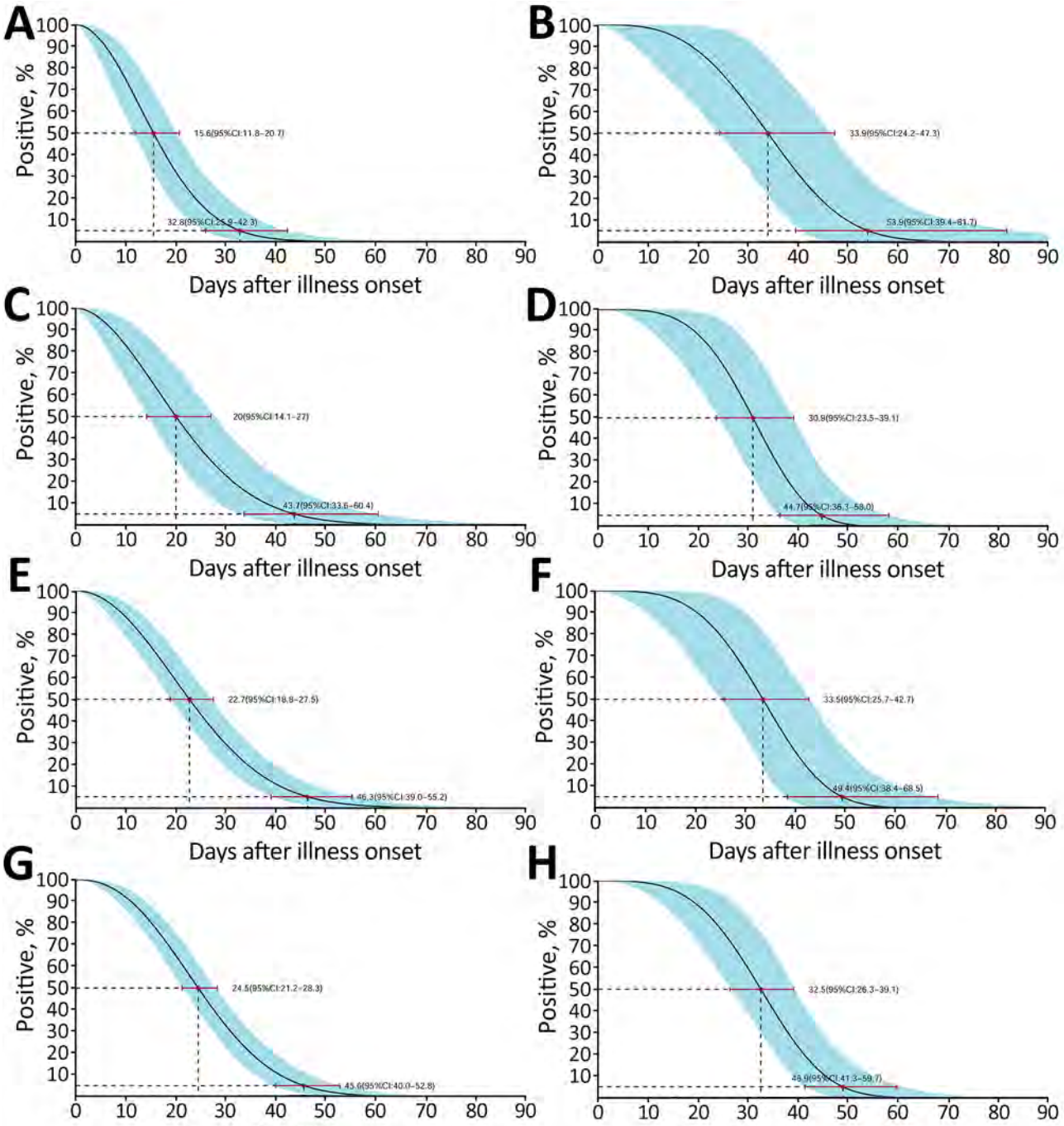

Figure 1. Time until clearance of severe acute respiratory syndrome coronavirus 2 RNA in throat swab, sputum, nasopharyngeal, and feces samples among hospitalized patients with coronavirus disease, as estimated with the use of Weibull regression, Guangdong, China. A, B) Throat swab specimens from patients with mild (A) and severe (B) cases; C, D) sputum samples from patients with mild (C) and severe (D) cases; nasopharyngeal swab samples from patients with mild (E) and severe (F) cases; G, H) feces samples from patients with mild (G) and severe (H) cases. A total of 43 patients with mild and 6 with severe cases were tested. The medians and 95th percentiles of the time until the loss of detection are indicated; error bars and shading indicate 95% CIs.

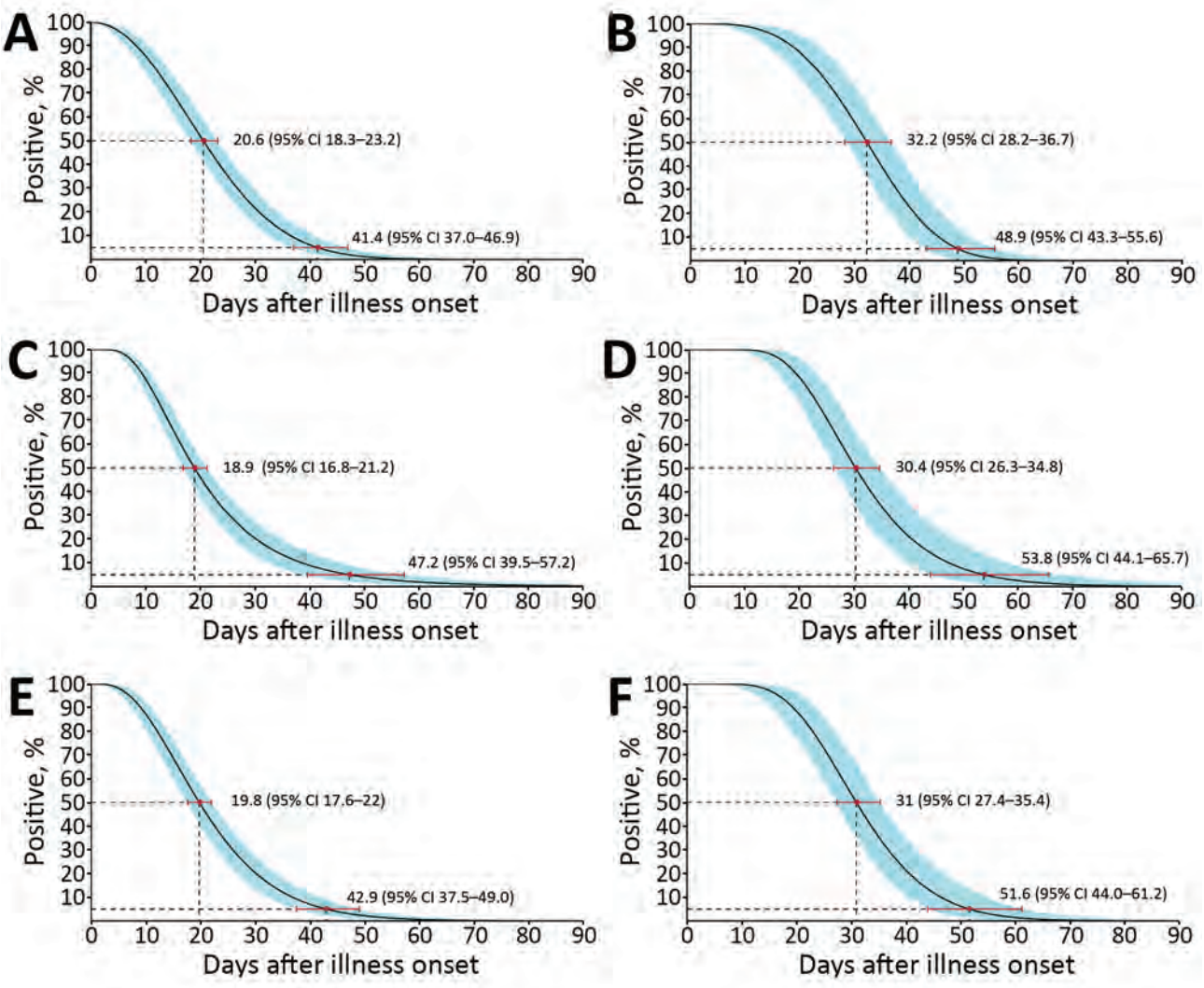

Figure 2. Time until clearance of severe acute respiratory syndrome coronavirus 2 RNA in any clinical specimens of throat swab, sputum, nasopharyngeal swab, or feces samples among hospitalized patients with coronavirus disease, as estimated with the use of Weibull, Lnorm, and gamma regression, Guangdong, China. A, B) Weibull regression for mild (A) and severe (B) cases; C, D) Lnorm regression for mild (C) and severe cases (D); E, F) gamma regression for mild (E) and severe (F) cases. A total of 43 patients with mild and 6 with severe cases were tested. The medians and 95th percentiles of the time until the loss of detection are indicated; error bars and shading indicate 95% CIs.

In conclusion, our results show prolonged persistence of SARS-CoV-2 RNA in hospitalized patients with COVID-19. Health professionals should consider these findings in diagnostic recommendations and prevention measures for COVID-19.

Acknowledgments

We thank the laboratory and administrative personnel at Guangdong Provincial Center for Disease Control for their contribution to the follow-up investigation.

This project was supported by grants from the Guangzhou Science and Technology Program (no. 201904010012), Guangdong Provincial Science and Technology Program (no. 2018B020207006), and Guangdong Provincial Novel Coronavirus Scientific and Technological Project (no. 2020111107001).

About the Author

Dr. Jiufeng Sun is a research scientist at the Guangdong Center for Disease Control and Prevention, Guangdong, China. His research interests are epidemiology of emerging infectious diseases and evolution of associated viruses.

References

1. Wu F, Zhao S, Yu B, Chen YM, Wang W, Song ZG, et al. A new coronavirus associated with human respiratory disease in China. Nature. 2020;579:265–9. https://doi.org/10.1038/s41586-020-2008-3
2. Zhou P, Yang XL, Wang XG, Hu B, Zhang L, Zhang W, et al. A pneumonia outbreak associated with a new coronavirus of probable bat origin. Nature. 2020;579:270–3. https://doi.org/10.1038/s41586-020-2012-7
3. Li Q, Guan X, Wu P, Wang X, Zhou L, Tong Y, et al. Early transmission dynamics in Wuhan, China, of novel coronavirus-infected pneumonia. N Engl J Med. 2020;382:1199–207. https://doi.org/10.1056/NEJMoa2001316
4. Holshue ML, DeBolt C, Lindquist S, Lofy KH, Wiesman J, Bruce H, et al.; Washington State 2019-nCoV Case Investigation Team. First case of 2019 novel coronavirus in the United States. N Engl J Med. 2020;382:929–36. https://doi.org/10.1056/NEJMoa2001191
5. Rothe C, Schunk M, Sothmann P, Bretzel G, Froeschl G, Wallrauch C, et al. Transmission of 2019-nCoV infection from an asymptomatic contact in Germany. N Engl J Med. 2020;382:970–1. https://doi.org/10.1056/NEJMc2001468
6. Wu JT, Leung K, Leung GM. Nowcasting and forecasting the potential domestic and international spread of the 2019-nCoV outbreak originating in Wuhan, China: a modelling study. Lancet. 2020;395:689–97. https://doi.org/10.1016/S0140-6736(20)30260-9
7. Wu Y, Guo C, Tang L, Hong Z, Zhou L, Dong X, et al. Prolonged presence of SARS-CoV-2 viral RNA in faecal samples. Lancet Gastroenterol Hepatol. 2020;5:434–5. https://doi.org/10.1016/S2468-1253(20)30083-2
8. Lan L, Xu D, Ye G, Xia C, Wang S, Li Y, et al. Positive RT-PCR test results in patients recovered from COVID-19. JAMA. 2020;2020:27. https://doi.org/10.1001/jama.2020.2783
9. Paz-Bailey G, Rosenberg ES, Doyle K, Munoz-Jordan J, Santiago GA, Klein L, et al. Persistence of Zika virus in body fluids—final report. N Engl J Med. 2018;379:1234–43. https://doi.org/10.1056/NEJMoa1613108
10. Oh MD, Park WB, Choe PG, Choi SJ, Kim JI, Chae J, et al. Viral load kinetics of MERS coronavirus infection. N Engl J Med. 2016;375:1303–5. https://doi.org/10.1056/NEJMc1511695
11. Corman VM, Albarrak AM, Omrani AS, Albarrak MM, Farah ME, Almasri M, et al. Viral shedding and antibody response in 37 patients with Middle East respiratory syndrome coronavirus infection. Clin Infect Dis. 2016;62:477–83. https://doi.org/10.1093/cid/civ951
12. Zhang W, Du RH, Li B, Zheng XS, Yang XL, Hu B, et al. Molecular and serological investigation of 2019-nCoV infected patients: implication of multiple shedding routes. Emerg Microbes Infect. 2020;9:386–9. https://doi.org/10.1080/22221751.2020.1729071
13. Guan WJ, Ni ZY, Hu Y, Liang WH, Ou CQ, He JX, et al.; China Medical Treatment Expert Group for Covid-19. Clinical characteristics of coronavirus disease 2019 in China. N Engl J Med. 2020 Feb 28 [Epub ahead of print] https://doi.org/10.1056/NEJMoa2002032

Addresses for correspondence: Changwen Ke, Guangdong Provincial Center for Disease Control and Prevention, Guangzhou 510300, China; email: kecw1965@aliyun.com; Junzhang Tian, Guangdong Seconded Provincial General Hospital, Guangzhou 510317, China; email: jz.tian@163.com

Prognostic Value of Leukocytosis and Lymphopenia for Coronavirus Disease Severity

Glen Huang[1], Alex J. Kovalic[1], Christopher J. Graber[1]

To evaluate lymphopenia as a marker for coronavirus disease severity, we conducted a meta-analysis of 10 studies. Severe illness was associated with lower lymphocyte and higher leukocyte counts. Using these markers for early identification of patients with severe disease may help healthcare providers prioritize the need to obtain therapy.

The incidence of coronavirus disease (COVID-19), caused by severe acute respiratory syndrome coronavirus-2 (SARS-CoV-2), has spread rapidly globally; as of March 29, 2020, ≈670,000 cases had been confirmed worldwide (*1*). COVID-19 is typically a pulmonary infection that can range from mild illness to acute respiratory distress syndrome and multiple organ failure; however, other symptoms such as myalgias and anorexia have been noted (*2*). Although many ongoing studies are investigating measurement of proinflammatory cytokines and other biomarkers as a way to prognosticate infection severity, we investigated use of 2 easily obtained predictors: lymphopenia and leukocytosis (*3*).

The Study

We searched 3 major databases—MEDLINE/PubMed, EMBASE, and CENTRAL (Cochrane Central Register of Controlled Trials)—for clinical studies published December 1, 2019, through March 28, 2020. To broadly identify studies detailing lymphocyte and leukocyte testing among patients with COVID-19, we used the following search criteria: "(COVID-19 OR SARS-CoV-2 OR 2019-NCoV OR HCov-19 OR novel coronavirus) AND (laboratory OR WBC OR lymphocyte)." We prioritized studies that measured lymphocyte and leukocyte counts among patients who had severe or critical cases versus those with mild cases. Severe cases were defined as significant respiratory distress (acute hypoxic respiratory failure, acute respiratory distress syndrome, need for mechanical ventilation, or intensive care unit admission) caused by COVID-19.

Our meta-analysis included articles about studies and clinical trials that met the following 4 inclusion criteria: 1) involved adult, human patients; 2) written in English; 3) reported lymphocyte and leukocyte counts for patients; and 4) compared patients with severe versus mild illness. Our meta-analysis excluded articles about studies with the following 9 characteristics: 1) involved nonhuman subjects; 2) written in a language other than English; 3) were not a clinical trial, such as a review paper or letter; 4) were out of the scope of the study question detailed above; 5) did not provide raw data to perform quantitative meta-analysis; 6) involved pediatric patients; 7) did not have the full article available; 8) were duplicates; and 9) were ongoing or not completed.

We performed the meta-analysis by using Review Manager software version 5.3 (The Cochrane Collaboration, https://training.cochrane.org). We calculated mean differences (MDs) between groups for continuous variables and reported 95% CIs for both severe and nonsevere cases. If the included studies provided medians and interquartile ranges instead of MDs and SDs, we imputed the MDs and SDs as described previously (*4*–*6*) and additionally described in the Cochrane Handbook for Systematic Reviews (*7*). We considered results statistically insignificant if $p>0.05$ or if the MD included zero. We assessed statistical heterogeneity by using the I^2 statistic and awarded the following values: 0%–24%, homogeneity; 25%–49%, mild heterogeneity; 50%–74%, moderate heterogeneity; and ≥75%, high

Author affiliations: David Geffen School of Medicine at University of California Los Angeles, Los Angeles, California, USA (G. Huang, C.J. Graber); Novant Forsyth Medical Center, Winston Salem, North Carolina, USA (A.J. Kovalic); VA Greater Los Angeles Healthcare System, Los Angeles (C.J. Graber)

DOI: https://doi.org/10.3201/eid2608.201160

[1]All authors contributed equally to this article.

heterogeneity. If moderate to high heterogeneity was present (I^2>50%), then we used the random effects model to pool the effect sizes of included studies and subgroup analyses.

We identified 959 articles; among them, 318 were duplicates. We then screened the remaining 641 by title, abstract, or both. We assessed 59 articles as eligible (included patient-level clinical data) and identified 8 studies (included lymphocyte counts and stratification of illness severity) for the quantitative synthesis (Appendix Table, https://wwwnc.cdc.gov/EID/article/26/8/20-1160-App1.pdf). These studies described 1,289 cases of COVID-19, of which 592 (45.9%) were classified as severe.

We compared lymphocyte and leukocyte counts in patients with severe/critical versus mild cases of COIVD-19 (Appendix Figure). All laboratory data were captured at the time of patient admission. Overall, patients categorized as having severe illness tended to have lower lymphocyte counts (pooled MD -0.36, 95% CI -0.50 to -0.22; p<0.00001) and higher leukocyte counts (pooled MD 1.32, 95% CI 0.62 to 2.02; p<0.00001). Fan et al. reported an absolute lymphocyte count of >1.0 × 10^9 cells/L for 39/58 (69.6%) patients in the nonsevere group and 2/9 (22.2%) patients in the severe group (*8*). Huang et al. reported an absolute lymphocyte count of <1 × 10^9 cells/L in 15/28 (54%) patients in the nonsevere group and 11/13 (83%) in the severe group (*9*). Wan et al. reported an absolute lymphocyte count of <1.0 × 10^9 cells/L for 36/95 (38%) patients in the nonsevere group and 32/40 (80%) in the severe group (*10*). Zhang et al. reported a decreased lymphocyte count for 28/82 (70.7%) patients in the nonsevere group and 46/56 (82.1%) in the severe group (*11*).

Conclusions

Pooled data across early studies validate a significant correlation between elevated leukocyte count and decreased lymphocyte count among patients with severe cases of COVID-19 compared with those with mild cases. Why lymphopenia is associated with severe illness remains unclear. It has been hypothesized that this association could result from direct lymphocyte infection, destruction of lymphatic tissue, inflammation leading to lymphocyte apoptosis, or inhibition of lymphocytes by metabolic disorders such as lactic acidosis (*12*). Lymphopenia as a marker of severity does not seem to be specific to COVID-19; it has been used to prognosticate other viral pneumonias such as influenza (*13*). Neutrophilia may be more specific to severe disease than leukocytosis, but neutrophil count was not uniformly reported across the studies included in our analysis.

Despite our findings regarding clinical characteristics of severe COVID-19, our study had several limitations. First, our literature search found an expected paucity of data surrounding this topic because published characterizations of patients with COVID-19 remain minimal. More COVID-19 data from other nations and patient populations will aid in the comparison and validation of our clinical findings. Second, we noted significant heterogeneity in both the leukocyte and lymphocyte analyses. This phenomenon probably resulted from the small sample size, limited and early data, and skewed representation of the patient population. Third, the definitions of severe cases were somewhat inconsistent across these studies, varying from acute hypoxic respiratory failure to requiring mechanical ventilation. This variability could further compound the heterogeneity found across these studies. Last, only a minority of the manuscripts reported the proportion of patients with lymphopenia, and variable cutoffs based on the articles' reference ranges made it difficult to ascertain a cutoff for severe disease.

With the rising cases of COVID-19 and limited resources (*14*), being able to prioritize patients with severe disease is crucial. Some therapeutic agents are being investigated (*15*); however, supplies are often low and procurement may be delayed. The sooner patients with severe disease can be identified, the sooner the process of obtaining therapy can be initiated.

About the Author

Dr. Huang is a first-year infectious diseases fellow at the University of California, Los Angeles. His research interests include infective endocarditis and transplant infectious diseases.

References

1. Coronavirus COVID-19 Global Cases by the Center for Systems Science and Engineering (CSSE) at Johns Hopkins University [cited 2020 Mar 29]. https://gisanddata.maps.arcgis.com/apps/opsdashboard/index.html#/bda7594740fd40299423467b48e9ecf6
2. Chen N, Zhou M, Dong X, Qu J, Gong F, Han Y, et al. Epidemiological and clinical characteristics of 99 cases of 2019 novel coronavirus pneumonia in Wuhan, China: a descriptive study. Lancet. 2020;395:507–13. https://doi.org/10.1016/S0140-6736(20)30211-7
3. Conti P, Ronconi G, Caraffa A, Gallenga CE, Ross R, Frydas I, et al. Induction of pro-inflammatory cytokines (IL-1 and IL-6) and lung inflammation by coronavirus-19 (COVI-19 or SARS-CoV-2): anti-inflammatory strategies. J Biol Regul Homeost Agents. 2020;34:1.

4. Hozo SP, Djulbegovic B, Hozo I. Estimating the mean and variance from the median, range, and the size of a sample. BMC Med Res Methodol. 2005;5:13. https://doi.org/10.1186/1471-2288-5-13
5. Luo D, Wan X, Liu J, Tong T. Optimally estimating the sample mean from the sample size, median, mid-range, and/or mid-quartile range. Stat Methods Med Res. 2018; 27:1785–805. https://doi.org/10.1177/0962280216669183
6. Wan X, Wang W, Liu J, Tong T. Estimating the sample mean and standard deviation from the sample size, median, range and/or interquartile range. BMC Med Res Methodol. 2014;14:135. https://doi.org/10.1186/1471-2288-14-135
7. Higgins JPT, Thomas J, Chandler J, Cumpston M, Li T, Page MJ, et al., editors. Cochrane Handbook for Systematic Reviews of Interventions version 6.0 (updated July 2019) [cited 2020 Mar 29]. http://www.training.cochrane.org/handbook
8. Fan BE, Chong VCL, Chan SSW, Lim GH, Lim KGE, Tan GB, et al. Hematologic parameters in patients with COVID-19 infection. Am J Hematol. 2020 Mar 4 [Epub ahead of print]. https://doi.org/10.1002/ajh.25847
9. Huang C, Wang Y, Li X, Ren L, Zhao J, Hu Y, et al. Clinical features of patients infected with 2019 novel coronavirus in Wuhan, China. Lancet. 2020;395:497–506. https://doi.org/10.1016/S0140-6736(20)30183-5
10. Wan S, Xiang Y, Fang W, Zheng Y, Li B, Hu Y, et al. Clinical features and treatment of COVID-19 patients in northeast Chongqing. J Med Virol. 2020. https://doi.org/10.1002/jmv.25783
11. Zhang JJ, Dong X, Cao YY, Yuan YD, Yang YB, Yan YQ, et al. Clinical characteristics of 140 patients infected with SARS-CoV-2 in Wuhan, China. Allergy. 2020 Feb 19 [Epub ahead of print]. https://doi.org/10.1111/all.14238
12. Tan L, Wang Q, Zhang D, Ding J, Huang Q, Tang Y-Q, et al. Lymphopenia predicts disease severity of COVID-19: a descriptive and predictive study. Signal Transduct Target Ther. 2020;5:33. https://doi.org/10.1038/s41392-020-0148-4
13. Bellelli V, d'Ettorre G, Celani L, Borrazzo C, Ceccarelli G, Venditti M. Clinical significance of lymphocytopenia in patients hospitalized with pneumonia caused by influenza virus. Crit Care. 2019;23:330. https://doi.org/10.1186/s13054-019-2608-1
14. White DB, Lo B. A framework for rationing ventilators and critical care beds during the COVID-19 pandemic. JAMA. 2020 Mar 27 [Epub ahead of print]. https://doi.org/10.1001/jama.2020.5046
15. McCreary EK, Pogue JM. on behalf of the Society of Infectious Diseases Pharmacists. Coronavirus 2019 treatment: a review of early and emerging options. Open Forum Infect Dis. 2020 Mar 23 [Epub ahead of print]. https://doi.org/10.1093/ofid/ofaa105

Address for correspondence: Glen Huang, Rm 37-121CHS, UCLA, 10833 Le Conte Ave, Los Angeles, CA 90095-1688, USA; email: glenhuang@mednet.ucla.edu

SARS-CoV-2 Phylogenetic Analysis, Lazio Region, Italy, February–March 2020

Barbara Bartolini, Martina Rueca, Cesare Ernesto Maria Gruber, Francesco Messina, Fabrizio Carletti, Emanuela Giombini, Eleonora Lalle, Licia Bordi, Giulia Matusali, Francesca Colavita, Concetta Castilletti, Francesco Vairo, Giuseppe Ippolito, Maria Rosaria Capobianchi, Antonino Di Caro

We report phylogenetic and mutational analysis of severe acute respiratory syndrome coronavirus 2 virus strains from the Lazio region of Italy and provide information about the dynamics of virus spread. Data suggest effective containment of clade V strains, but subsequently, multiple waves of clade G strains were circulating widely in Europe.

Severe acute respiratory syndrome coronavirus 2 (SARS-CoV-2) has raised serious concerns because of its rapid dissemination worldwide. Italy is one of the countries with the highest number of coronavirus disease (COVID-19) cases (*1*,*2*). Nevertheless, the information about the molecular epidemiology of SARS-CoV-2 strains circulating in Italy is still limited. The analysis of sequence data shown in GISAID (https://www.gisaid.org) indicates that the initial introduction of SARS-CoV-2 in Italy through 2 infected tourists in January was effectively contained (*3*), and no further circulation of similar clade V strains has been so far detected. An intense wave of infections occurred afterwards, initially affecting Lombardy and Veneto and later on all the other regions of Italy. The strains detected in Italy since February 20 belonged only to clade G. This clade, apparently originating in Shanghai, has been widely circulating in the European Union (EU) countries before reaching Italy (*3*–*5*).

Preliminary data suggested that multiple introductions of clade G strains have occurred in Italy, giving rise to contemporary circulation of different strains also detected in other EU countries; this pattern suggests that, after partially undetected introduction of the virus in EU from China, the circulation of travelers within EU ignited virus spread in Europe.

Affiliation: National Institute for Infectious Diseases "Lazzaro Spallanzani" IRCCS, Rome, Italy

DOI: https://doi.org/10.3201/eid2608.201525

We report the phylogenetic and mutational analysis of SARS-CoV-2 strains detected in the Lazio region of Italy, providing additional information on the dynamics of virus dissemination in this country.

The Study

We analyzed nasopharyngeal swab (n = 6) and bronchoalveolar lavage (n = 3) samples from 9 patients with COVID-19 to perform SARS-CoV-2 whole-genome reconstruction and mutational analysis. We collected samples in late February and early March, 2020 (Table 1). At sampling time, all patients reported symptoms such as fever, sore throat, cough, or other respiratory symptoms. Two sequences were identical, so we included only 1 of them in the analysis, resulting in 8 total sequences. We named the sequences INMI3–INMI10 for their detection at National Institute for Infectious Diseases and analyzed them together with the previously published INMI1 and INMI2 (*6*), along with all the sequences from Italy posted to GISAID database by April 11, 2020.

We performed next-generation sequencing (SARS-CoV-2 Panel) on Ion Torrent platform (Thermo Fisher Scientific, https://www.thermofisher.com) using shotgun approach for INMI3–4 and amplicon approach for INMI5–10. After quality control, we generated a median number of 4.3×10^7 reads for each shotgun sample and 1.5×10^6 for each amplicon sample (ranging from 7.5×10^5 to 4.8×10^7). The sequencing mean depth of SARS-CoV-2 ranged from 367-fold in INMI3 to 16,661-fold in INMI5.

We submitted consensus sequences to GISAID. We used the proposed phylogenetic lineage classification (A. Rambaut et al., unpub. data, https://doi.org/10.1101/2020.04.17.046086) in phylogenetic analysis; for comparison to previously published reports, we maintained references to clades reported in GISAID. INMI1 and INMI2 are included in clade V

Table 1. Demographic and epidemiologic data for patients with severe acute respiratory syndrome coronavirus 2, Italy, 2020

Characteristic	INMI3	INMI4	INMI4bis	INMI5	INMI6	INMI7	INMI8	INMI9	INMI10
Sample type*	NPS	NPS	NPS	NPS	NPS	BAL	NPS	BAL	BAL
Sex	M	M	F	M	M	F	F	M	M
Age, y	32	41	38	53	60	70	65	33	56
Region	Emilia Romagna	Lombardy	Lombardy	Lazio	Lazio	Lazio	Lazio	Lazio	Lazio
Collection date	Mar 1	Feb 28	Feb 27	Mar 4	Mar 23	Mar 23	Mar 7	Mar 23	Mar 4

*BAL, bronchoalveolar lavage; NPS, nasopharyngeal swab.

according to GISAID phylogenetics, as reported (*6*), and clade B2; the clade includes other sequences from EU countries, but no additional sequences from Italy. All other INMI sequences cluster with the GISAID G clade, and with the B1 clade; we focused subsequent analysis on clade B1 (Figure).

The clade B1 INMI sequences are distributed in 2 main clusters, one including most of the northern Italy strains and the other including sequences mainly from central Italy. In particular, INMI4, which was epidemiologically linked to Bergamo (Lombardy region), clusters with sequences from central Italy (Abruzzo region). The other INMI sequences cluster with strains from northern Italy. Of note, in both clusters the sequences from Italy are intermixed with sequences from other EU countries, which can also be seen in the broader phylogenetic analysis on GISAID, in which more EU sequences are analyzed. We have identified 5 synonymous and 9 nonsynonymous substitutions distributed along the whole genome (Table 2).

Each patient showed several amino acid substitutions ranging from 4 to 7. The G clade–specific single-nucleotide polymorphism A23403G led the amino acid change D614G in the S protein. We observed one additional mutation in this protein, that of C21575T (L5F) in INMI7, which is detected in few other sequences in GISAID, interspersed among different non-G clades (M. Chiara et al., unpub. data, https://doi.org/10.1101/2020.03.30.016790). Its location in a marginal region of the gene and the sporadic distribution in different clades indicates repeated occurrence not followed by fixation, consistent with no evolutionary advantage.

The S protein in the SARS-CoV-2 virus is a chief determinant of the host range and pathogenicity. The virion attaches to the cell membrane by binding the S protein with the host ACE2 receptor (*7*). The D614G mutation, located in the putative S1–S2 junction region near the furin polybasic cleavage site (RRAR), might have an effect on priming by host cell proteases; however, the real impact of this high-frequency mutation is unclear.

The variants C241T, C3037T (located in the noncoding region) and C14408T (in open reading frame1ab, orf1ab) were present in all INMI3–INMI10 sequences. These mutations have been detected in several SARS-CoV-2 isolates throughout Europe and are characteristic of clade G (C. Yin, unpub. data). A nonsynonymous substitution D3G in membrane glycoprotein was detected in 1 INMI9 sequence.

We detected 3 nucleotide changes in INMI4, located in a high variable region of the gene, in 2 adjacent codons of the nucleocapsid (N) gene, two 2-amino acid changes, R203K and G204R. N protein, responsible for the formation of helical nucleocapsid, can elicit humoral and cell mediated immune response and has potential value in vaccine development. However, none of the observed mutations has been so far associated with changes in viral pathogenicity or transmissibility.

Conclusions

The phylogenetic reconstruction we report suggests possible multiple introduction of SARS-CoV-2 virus in Italy, supporting previously reported analysis conducted on a more limited number of sequences (*3*–*5*).

The analysis consistently places the strains described in this study in 2 distinct clusters in B1 clade. No other sequence from Italy clusters in B2 (or GISAID V) clade, indicating the positive effect of containment measures established by health authorities in both Italy and China to limit viral transmission directly from China. The same measures were unable to contain a wave of subsequent multiple introductions in Italy of strains that were widely circulating in Europe, all clustering with clade B1.

The inclusion of the viral sequences from infections occurring in the Lazio region helps to demonstrate the dynamics of virus circulation in Italy. In particular, a small number of mutations have been detected in these strains, but the real impact and role that these mutations may have on the pathogenicity and transmissibility of SARS-CoV-2 remains to be determined.

A limitation of our research is that only a portion of viral sequences, including the sequences from Italy, have been published as of April 10, 2020; phylogenetic analysis could substantially change when more sequences are made available. Continued genomic surveillance strategies are needed to improve monitoring and understanding of current SARS-CoV-2 epidemics, which might help to lessen the public health impact of COVID-19. Furthermore, increased

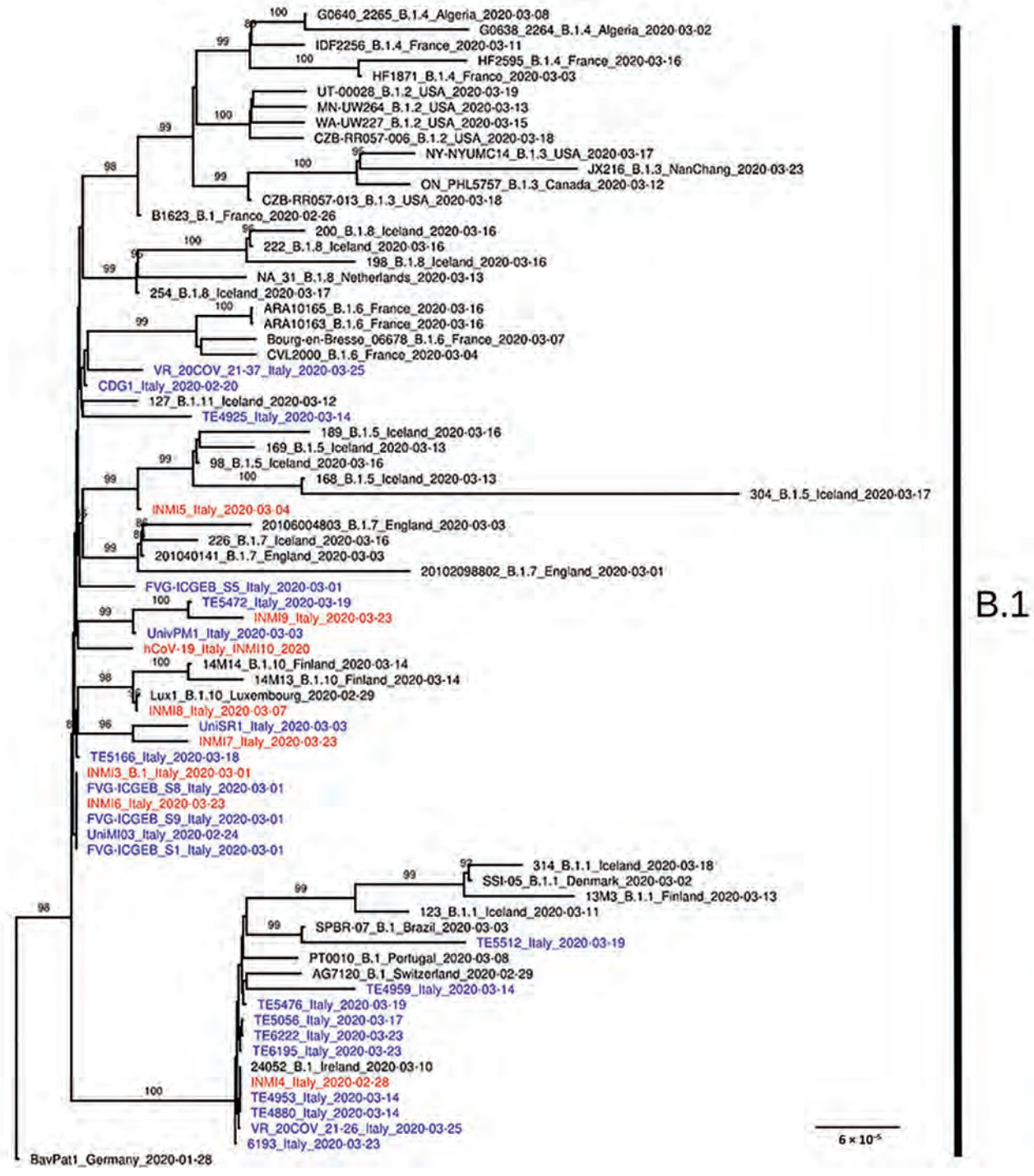

Figure. Phylogenetic analysis of 150 severe acute respiratory syndrome coronavirus 2 representative genome sequences from lineage B1, including genomes collected in Italy (blue) and sequences identified for this study at the National Institute for Infectious Diseases (red). Available genomes were retrieved from GISAID (https://www.gisaid.org) on April 10, 2020; we discarded sequences with low coverage depth (low amount of read sequenced) or low coverage length (not complete genome sequences). Representative sequences from every B lineage (A. Rambaut et al., unpub. data, https://doi.org/10.1101/2020.04.17.046086v1), together with all genome sequences collected in Italy so far, were selected for further analysis. Multiple sequence alignment was obtained with MAFFT version 7.271 (https://mafft.cbrc.jp/alignment/software). Phylogenetic analysis was performed with IQ-TREE (http://www.iqtree.org): transition model with empirical base frequencies and invariable sites was selected with ModelFinder, and the best tree was found performing 1,000 bootstrap ultrafast replicates. Bootstrap values of ≥80% are reported on each branch. Scale bar represents number of substitutions per site. An expanded tree showing more comparison sequences is available online (https://wwwnc.cdc.gov/EID/article/26/8/20-1525-F1.htm).

Table 2. Consensus sequences of severe acute respiratory syndrome coronavirus 2 samples, Italy, 2020*

Wuhan-Hu-1 strain	Nucleotide position	INMI3	INMI4	INMI5	INMI6	INMI7	INMI8	INMI9	INMI10	Amino acid	Region
A	187					G				Noncoding	UTR
C	241	T	T	T	T	T	T	T	T	Noncoding	UTR
C	2062								T	Noncoding	UTR
C	3037	T	T	T	T	T	T	T	T	Syn	Orf1ab
G	4255							T		Syn	Orf1ab
C	14408	T	T	T	T	T	T	T	T	P4715L	Orf1ab
T	16456							G		S5398A	Orf1ab
A	20268			G						Syn	Orf1ab
C	21575					T				L5F	Spike glycoprotein
A	23403	G	G	G	G	G	G	G	G	D614G	Spike glycoprotein
C	23575						T			Syn	Spike glycoprotein
A	26530							G		D3G	Membrane glycoprotein
C	28881		A							R203K	Nucleocapsid protein
G	28882		A							R203K	Nucleocapsid protein
G	28883		C							G204R	Nucleocapsid protein

*Nucleotide positions refer to the Wuhan-Hu-1 reference genome (GenBank accession no. MN908947). Orf, open reading frame; Syn, synonymous substitution; UTR, untranslated region.

sequencing capacity is necessary for contact tracing and enhanced surveillance activity.

Acknowledgments

We thank the contributors of genome sequences of the newly emerging coronavirus (the originating and submitting laboratories) for sharing their sequences and other metadata through the GISAID Initiative, on which this research is based. We thank Salvatore Conti and Alessandro Albiero for their support in NGS sequencing and analysis.

The INMI sequences have been deposited in GISAID with accession IDs as follows: INMI3: EPI_ISL_ 417921; INMI4: EPI_ISL_417922; INMI5: EPI_ISL_ 417923; INMI6: EPI_ISL_ 419254; INMI7: EPI_ISL_ 419255; INMI 8: EPI_ISL_424342; INMI 9: EPI_ISL_424343; INMI 10: EPI_ISL_424344.

This research was supported by funds to National Institute for Infectious Diseases "Lazzaro Spallanzani" IRCCS from Ministero della Salute, Ricerca Corrente, linea1; European Commission–Horizon 2020 (EU project 653316-EVAg; EU project no. 101003544–CoNVat; EU project no. 101003551–EXSCALATE4CoV).

B.B. coordinated the experiments and wrote the manuscript; B.B. and M.R. performed the NGS experiment; G.M., F.C., F.Ca., E.L., L.B., C.C. performed SARS-CoV-2 diagnosis; F.V. performed the epidemiological analysis; C.E.M.G., F.M. and E.G. performed bioinformatic and phylogenetic analysis; M.R.C. and A.D.C. supervised the study design; G.I. read and revised the manuscript. All the authors read and approved the manuscript.

About the Author

Dr. Bartolini is a senior scientist at Microbiology Laboratory and Infectious Diseases Biorepository at the National Institute for Infectious Diseases "L. Spallanzani." Her primary research interests are next-generation sequencing and emerging and reemerging infections.

References

1. World Health Organization (WHO). Coronavirus disease 2019 (COVID-19) situation report—81. 2020 Apr 10 [cited 2020 May 14]. https://www.who.int/docs/default-source/coronaviruse/situation-reports/20200410-sitrep-81-covid-19.pdf?sfvrsn=ca96eb84_2
2. European Centre for Disease Control and Prevention (ECDC). COVID-19 situation update worldwide, as of 10 April 2020. 2020 Apr 10 [cited 2020 May 14]. https://www.ecdc.europa.eu/en/geographical-distribution-2019-ncov-cases
3. Giovanetti M, Angeletti S, Benvenuto D, Ciccozzi M. A doubt of multiple introduction of SARS-CoV-2 in Italy: a preliminary overview. J Med Virol. 2020;1–3. https://doi.org/10.1002/jmv.25773
4. Stefanelli P, Faggioni G, Lo Presti A, Fiore S, Marchi A, Benedetti E, et al.; on behalf of ISS COVID-19 Study Group. Whole-genome and phylogenetic analysis of two SARS-CoV-2 strains isolated in Italy in January and February 2020: additional clues on multiple introductions and further circulation in Europe. Euro Surveill. 2020;25. https://doi.org/10.2807/1560-7917.ES.2020.25.13.2000305
5. Zehender G, Lai A, Bergna A, Meroni L, Riva A, Balotta C, et al. Genomic characterization and phylogenetic analysis of SARS-COV-2 in Italy. J Med Virol. 2020;1–4. PubMed
6. Capobianchi MR, Rueca M, Messina F, Giombini E, Carletti F, Colavita F, et al. Molecular characterization of SARS-CoV-2 from the first case of COVID-19 in Italy. Clin Microbiol Infect. 2020 Mar 27 [Epub ahead of print]. https://doi.org/10.1016/j.cmi.2020.03.025
7. Ou X, Liu Y, Lei X, Li P, Mi D, Ren L, et al. Characterization of spike glycoprotein of SARS-CoV-2 on virus entry and its immune cross-reactivity with SARS-CoV. Nat Commun. 2020;11:1620. https://doi.org/10.1038/s41467-020-15562-9

Address for correspondence: Antonino Di Caro, National Institute for Infectious Diseases "Lazzaro Spallanzani," IRCCS Via Portuense 292, 00149 Rome, Italy; email: antonino.dicaro@inmi.it

Plasma-Derived Extracellular Vesicles as Potential Biomarkers in Heart Transplant Patient with Chronic Chagas Disease

Nuria Cortes-Serra, Maria Tays Mendes, Clara Mazagatos,[1] Joan Segui-Barber, Cameron C. Ellis, Cristina Ballart, Ana Garcia-Alvarez, Montserrat Gállego, Joaquim Gascon, Igor C. Almeida, María Jesús Pinazo, Carmen Fernandez-Becerra

Chagas disease is emerging in countries to which it is not endemic. Biomarkers for earlier therapeutic response assessment in patients with chronic Chagas disease are needed. We profiled plasma-derived extracellular vesicles from a heart transplant patient with chronic Chagas disease and showed the potential of this approach for discovering such biomarkers.

Chagas disease, caused by *Trypanosoma cruzi* parasite, is one of the most prevalent parasitic infections in Latin America and is responsible for millions of clinical cases. However, mainly because of migratory movements, the epidemiology of Chagas disease has changed in recent decades; cases have increased substantially in North America, Europe, and Asia, where it is not endemic (*1*). Thus, raising awareness of this debilitating or deadly neglected tropical disease and promoting the creation of global strategies for its accurate diagnosis, treatment, and control are of paramount importance.

Detection of *T. cruzi*–specific antibodies in serologic assays is the current standard technique for diagnosing chronic Chagas disease. However, this so-called conventional serology is not a valid indicator of chemotherapeutic outcomes because most patients remain seropositive for 10–20 years after treatment (*2*). Therefore, validated biomarkers are lacking for early assessment of therapeutic responses for testing current and new drugs or treatment regimens.

Extracellular vesicles (EVs) are cell-derived membranous nanoparticles present in most biologic fluids. Biofluid-derived EVs are minimally invasive molecular tools for diagnosing and screening diseases (*3*). They can be released by various mammalian cells and pathogens, and their use as predictive biomarkers for disease progression and treatment outcomes has been reported for different pathologic conditions, including parasitic diseases (*3*,*4*).

The Study

The Ethical Committee of Clinical Research of Hospital Clinic (Barcelona, Spain; reference no. Reg. HCB/2015/0616) approved this project. The patient provided written informed consent before sample collection.

In 2009, a 51-year-old patient from Bolivia with a history of chronic Chagas disease, exhibiting severe organ involvement (chronic cardiomyopathy Kuschnir III and megacolon and megaesophagus degree IV) (*5*), was admitted to the International Health Department (Hospital Clinic, Barcelona). Serologic diagnosis for chronic Chagas disease was performed using 2 ELISA kits (Ortho-Clinical Diagnostics, https://www.orthoclinicaldiagnostics.com) and BioELISA Chagas

Author affiliations: Barcelona Institute for Global Health (ISGlobal), Universitat de Barcelona, Barcelona, Spain (N. Cortes-Serra, C. Mazagatos, J. Segui-Barber, C. Ballart, M. Gállego, J. Gascon, M.J. Pinazo, C. Fernandez-Becerra); Border Biomedical Research Center, The University of Texas at El Paso, El Paso, Texas USA (M.T. Mendes, C.C. Ellis, I.C. Almeida); Secció de Parasitologia, Departament de Biologia, Sanitat i Medi Ambient, Facultat de Farmàcia i Ciències de l'Alimentació, Universitat de Barcelona, Barcelona, Spain (C. Ballart, M. Gállego); Arrhythmias Unit, Hospital Clinic, University of Barcelona, Barcelona, Spain (A. Garcia-Alvarez); Institut d'Investigació en Ciències de la Salut Germans Trias i Pujol, Badalona, Spain (C. Fernandez-Becerra)

DOI: https://doi.org/10.3201/eid2608.191042

[1]Current affiliation: CIBER Epidemiología y Salud Pública (CIBERESP); Centro Nacional de Epidemiología, Instituto de Salud Carlos III, Madrid, Spain.

Table 1. Timeline of heart transplant patient with chronic Chagas disease from initial diagnosis to last follow-up and death*

Date	Infection	Observation, treatment, outcome
2015 Aug	Cytomegalovirus, detected by serology	Diagnosed only by positive IgG serology, no active infection (no positive IgM serology). No treatment.
2015 Aug	Toxoplasmosis, detected by serology	Diagnosed only by positive IgG serology, no active infection (no positive IgM serology). No treatment.
2015 Nov		Heart transplantation on Nov. 28. Patient started with immunosuppressive therapy (tacrolimus, azathioprine, prednisone) until the end of follow-up.
2016 Jan	Chagas disease reactivation, detection by qPCR	Pretreatment sample collected on Jan 28. Patient started BZN treatment (2.5 mg/kg, twice a day, 60 d) on Feb 3.
2016 Mar	Bronchopulmonary aspergillosis, detected by serology and CT	BZN course interrupted on Mar 21. Completed 80% of the prescribed treatment.
2016 Mar	Bronchopulmonary aspergillosis	Aspergillosis treatment started on Mar 22. Initially with voriconazole and amphotericin B liposomal. Treatment was changed to posaconazole until the end of the follow-up.†
2016 Apr	Chagas disease reactivation, detected by qPCR	On Apr 14, patient started second round of BZN treatment until May 5, completing 100% of the prescribed treatment.
2016 May		Posttreatment sample collected on May 11.
2016 Aug		Late organ rejection. Patient died.

*BZN, benznidazole; CT, computed tomographic scan; qPCR, quantitative PCR.
†Parasite clearance could be related to the prolonged used of posaconazole, as previously reported (*6*), and/or the combined use of posaconazole and benznidazole because a second round of the latter was started in April 2016.

(Biokit, https://www.biokit.com). Together with clinical management of dysphagia and constipation, a pacemaker in the context of third-degree atrioventricular block was implanted. In July 2015, an echocardiogram revealed iterative cardiac failure and severe ventricular dysfunction (ejection fraction 15%–20%). On November 28, 2015, the patient underwent heart transplantation without incident, and results of follow-up endomyocardial biopsies showed no early signs of transplant rejection.

After transplantation and in the context of immunosuppression therapy (Table 1), quantitative PCR (qPCR) was performed weekly to detect *T. cruzi* in the blood (*Tc*-qPCR) (*7*). First benznidazole treatment was started when several consecutive and positive *Tc*-qPCRs confirmed Chagas disease reactivation. Three weeks after benznidazole treatment, the *Tc*-qPCR became negative. After completion of 80% of the treatment, bronchopulmonary aspergillosis developed, and the benznidazole course was interrupted. The *Tc*-qPCR became positive and a second benznidazole course was initiated; this time the patient completed the initial prescribed dose without evidence of therapeutic failure based on *Tc*-qPCR results. Plasma samples for purification and characterization of EVs were collected before the first benznidazole treatment and just after the second course (Table 1). Unexpectedly, the patient died in August 2016 because of a late organ rejection. Therefore, samples at 6 and 12 months posttreatment, already included in the approved protocol, were not collected.

To determine whether circulating EVs from this patient could have been used as predictive biomarkers to evaluate therapeutic response and disease outcome in the Chagas disease context, we collected pretreatment and posttreatment plasma samples, and EVs were enriched by size-exclusion chromatography (SEC) and characterized as described (*8*) (Figure 1, panel A). As negative controls, plasma samples from 2 healthy donors were also subjected to SEC. We characterized eluting EVs by bead-based assay and Nanoparticle Tracking Analysis (Figure 1, panels B, C). We pooled aliquots (100 μL) from SEC fractions 7–10 and determined protein composition using 2D-liquid chromatography–tandem mass spectrometry (2D-LC-MS/MS). In brief, samples were digested with trypsin and resulting peptides were resolved by high-pH reversed-phase peptide fractionation (*9*), followed by C18 reversed-phase nanoflow ultrahigh-performance liquid chromatography coupled to a Q Exactive Plus Hybrid Quadrupole-Orbitrap Mass Spectrometer (QE Plus MS; Thermo Fisher Scientific, https://www.thermofisher.com), as described (*10*). Raw 2D-LC-MS/MS data were analyzed using Proteome Discoverer version 2.1.1.21 software (Thermo Fisher Scientific), followed by Scaffold perSPECtives version 4.8.7 (Proteome Software; http://www.proteomesoftware.com). A protein database with combined human, *T. cruzi*, and potential contaminants was generated from UniProt (https://www.uniprot.org). Using a false-discovery rate <1% and 1 unique peptide per protein, we identified 12 *T. cruzi* proteins and 338 human proteins (Appendix, https://wwwnc.cdc.gov/EID/article/26/8/19-1042-App1.xlsx). However, when we applied the more stringent criterion of ≥2 unique peptides per protein, we detected only 1 *T. cruzi* protein (i.e., pyruvate phosphate dikinase [PPDK]), and 288 human proteins, of which we identified 19 only in pretreatment samples (Table 2). PPDK has been identified by proteomic

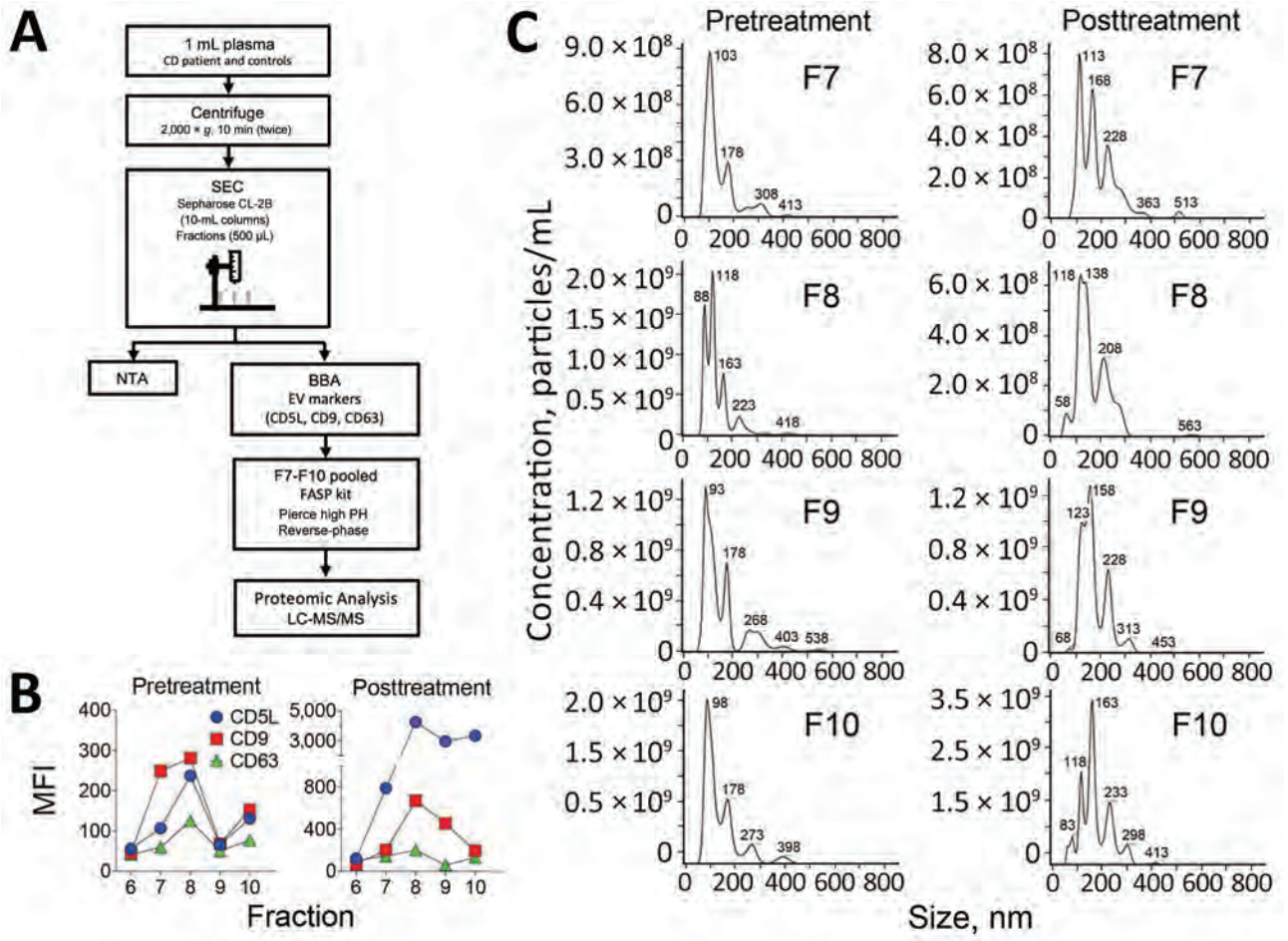

Figure 1. Isolation and characterization of plasma-derived EVs. A) Schematic diagram of the isolation and characterization of EVs derived from plasma samples. The details of each step are explained in The Study section. B) EVs were characterized by BBA using the classical EV markers CD5L, CD9, and CD63. C) NTA of SEC fractions F7–10. BBA, bead-based assay; EV, extracellular vesicle; LC-MS/MS, liquid chromatography–tandem mass spectrometry; MFI, median fluorescence intensity; NTA, nanoparticle tracking analysis; SEC, size-exclusion chromatography.

analysis of *T. cruzi* total secretome and EVs (*10*–*12*). This protein plays a central role in the metabolism of *T. cruzi* glycosomes and has been shown to be upregulated when trypomastigote forms are incubated with the extracellular matrix, an obligatory step before host-cell invasion and differentiation of trypomastigote into amastigote forms (*13*). The specific role of PPDK in EVs secreted by this patient remains to be determined.

Among the 19 human proteins uniquely identified in EVs from the patient with chronic Chagas disease before treatment, the mannan binding lectin serine protease 2 (MASP2) is worth highlighting. A recent study with human samples showed that *MASP2* gene polymorphisms and MASP2 levels are associated with high risk for chronic Chagas disease cardiomyopathy (*14*). Furthermore, mannose-binding lectin, which activates complement on *T. cruzi* through MASP2, has been related to a decrease in blood and tissue parasite load and in myocarditis and cardiac fibrosis in experimental *T. cruzi* infection (*15*). In this study, mRNA levels of collagen-1 and -6 increased in the infected animals' hearts (*15*). These results could support our findings because collagen α-1 is one of the proteins identified exclusively in EVs before patient treatment (Table 2).

Another important observation is the identification of a higher number of human proteins in patient-derived EVs than in the 2 healthy donor–derived EV samples (Figure 2; Appendix). Of the total proteins identified, in which statistical analysis was feasible, 4 were significantly upregulated in patient-derived EVs before treatment, particularly for the proteins complement C1s subcomponent, isoform CRA_b, FLJ00385 protein, and cDNA FLJ75416 (Appendix). Complement C1s subcomponent recently

was identified among the 6 upregulated EV biomarkers with potential for clinical applications in myocardial infarction (*3*).

Conclusions

Proteins associated with EVs secreted by *T. cruzi* have been identified in the conditioned medium of different parasite stages (*11*–*13*) but not in biofluids from Chagas disease patients. We described the proteomic profiling of plasma-derived EVs purified directly from a heart transplant patient with chronic Chagas disease who exhibited reactivation after immunosuppression. We identified human and parasite proteins present or upregulated in plasma-derived EVs from a chronic Chagas disease patient before chemotherapy and that are absent or downregulated after treatment. We thus hypothesize that EV proteins released by the host or parasite during infection might be potential biomarker candidates for evaluating therapeutic response and disease outcome in chronic Chagas disease, independently of the immunologic status of patients.

Table 2. *Trypanosoma cruzi* and human proteins identified in plasma-derived EVs from a heart transplant patient with chronic Chagas disease before benznidazole chemotherapy but absent after treatment and in healthy donors

Protein name†	UniProt accession no.	Unique peptides			
		ChD Pre-BZN‡	ChD Post-BZN	Healthy 1	Healthy 2
T. cruzi					
Pyruvate. phosphate dikinase OS = Trypanosoma cruzi marinkellei GN = MOQ_000480 PE = 3 SV = 1	K2MVM1_TRYCR	2 (0.96)	0	0	0
Homo sapiens					
Collagen α-1(VI) chain OS = Homo sapiens GN = COL6A1 PE = 1 SV = 3	CO6A1_HUMAN	3 (1.44)	0	0	0
Group of Angiopoietin-related protein 6 OS = Homo sapiens GN = ANGPTL6 PE = 1 SV = 1+1	ANGL6_HUMAN (+1)	3 (1.44)	0	0	0
sp|PPIA_HUMAN|	sp|PPIA_HUMAN|	3 (1.44)	0	0	0
Mannan binding lectin serine protease 2 OS = Homo sapiens GN = MASP2 PE = 1 SV = 4	MASP2_HUMAN	2 (1.92)	0	0	0
Myosin regulatory light chain 12B OS = Homo sapiens GN = MYL12B PE = 1 SV = 2	ML12B_HUMAN	2 (1.92)	0	0	0
Collagen α-2(VI) chain OS = Homo sapiens GN = COL6A2 PE = 1 SV = 4	CO6A2_HUMAN	2 (1.44)	0	0	0
Collectin subfamily member 10 (C-type lectin). isoform CRA_a OS = Homo sapiens GN = COLEC10 PE = 4 SV = 1	tr|A0A024R9J3|A0A024R9J3_HUMAN	2 (1.44)	0	0	0
Group of Coagulation factor XIII A chain OS = Homo sapiens GN = F13A1 PE = 1 SV = 4+2	F13A_HUMAN (+2)	2 (1.44)	0	0	0
Tyrosine 3-monooxygenase/tryptophan 5-monooxygenase activation protein. eta polypeptide. isoform CRA_b OS = Homo sapiens GN = YWHAH PE = 3 SV = 1	tr|A0A024R1K7|A0A024R1K7_HUMAN	2 (1.44)	0	0	0
Fibrinogen-like protein 1 OS = Homo sapiens GN = FGL1 PE = 1 SV = 3	FGL1_HUMAN	2 (0.96)	0	0	0
Group of L-lactate dehydrogenase A chain OS = Homo sapiens GN = LDHA PE = 1 SV = 2+1	LDHA_HUMAN (+1)	2 (0.96)	0	0	0
Group of Laminin subunit α-2 OS = Homo sapiens GN = LAMA2 PE = 1 SV = 1+1	A0A087WX80_HUMAN (+1)	2 (0.96)	0	0	0
Group of MHC class I antigen (Fragment) OS = Homo sapiens GN = HLA-A PE = 3 SV = 1+3	tr|D2KZ27|D2KZ27_HUMAN (+3)	2 (0.96)	0	0	0
Group of Serum amyloid A protein OS = Homo sapiens GN = SAA1 PE = 1 SV = 1+2	E9PQD6_HUMAN (+2)	2 (0.96)	0	0	0
Group of Transforming growth factor β-induced 68kDa isoform 2 (Fragment) OS = Homo sapiens GN = TGFBI PE = 2 SV = 1+1	tr|A0A0S2Z4K6|A0A0S2Z4K6_HUMAN (+1)	2 (0.96)	0	0	0
Heparan sulfate proteoglycan 2 (Perlecan). isoform CRA_b OS = Homo sapiens GN = HSPG2 PE = 4 SV = 1	tr|A0A024RAB6|A0A024RAB6_HUMAN	2 (0.96)	0	0	0
Neurogenic locus notch homologue protein 3 OS = Homo sapiens GN = NOTCH3 PE = 1 SV = 2	NOTC3_HUMAN	2 (0.96)	0	0	0
V1–16 protein (Fragment) OS = Homo sapiens GN = V1–16 PE = 4 SV = 1	tr|Q5NV81|Q5NV81_HUMAN	2 (2.88)	0	0	0
Rheumatoid factor RF-ET6 (Fragment) OS = Homo sapiens PE = 2 SV = 1	tr|A2J1N5|A2J1N5_HUMAN	2 (5.29)	0	0	0

*BZN, benznidazole; ChD, Chagas disease.
†All proteins were identified by at least 2 unique peptides. A unique peptide is defined as a peptide found only in ≥1 protein members of the same protein family of a certain proteome.
‡Normalized total spectrum count values are indicated in parenthesis. Complete mass spectrometry proteomic data have been deposited to the ProteomeXchange Consortium (http://proteomecentral.proteomexchange.org) via the PRoteomics IDEntifications Database (PRIDE, https://www.ebi.ac.uk/pride/) partner repository, with the dataset identifier PXD014668 and 10.6019/PXD014668.

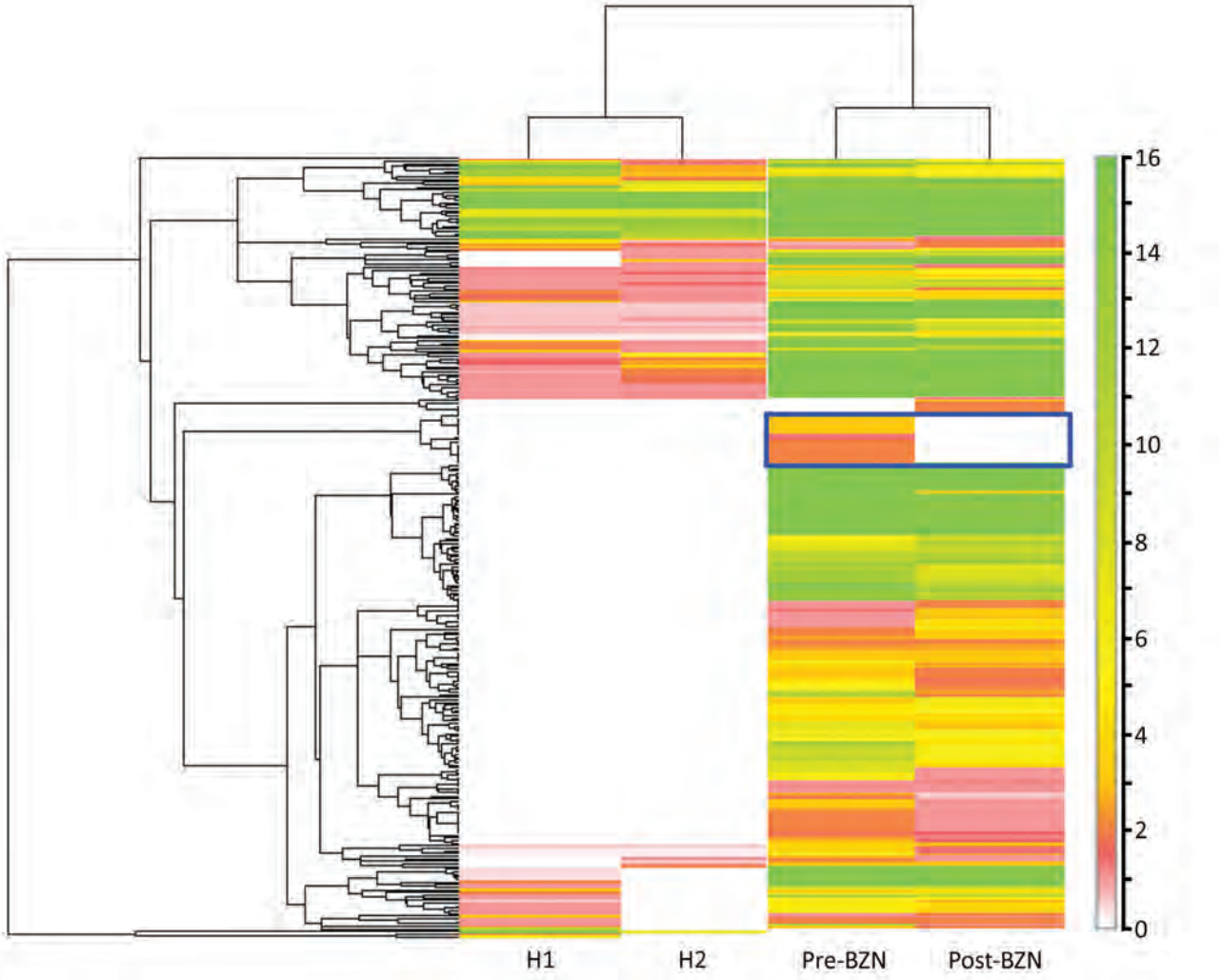

Figure 2. Human proteomic profile of plasma-derived EVs from a heart transplant patient with chronic Chagas disease before and after BZN treatment and from 2 healthy donors. Heatmap of the identified human EV-derived proteins. Heatmap was generated from proteomic data by the Scaffold perSPECtives software (Proteome Software; http://www.proteomesoftware.com). Hierarchical clustering (on the left), using single-linkage clustering with a Euclidean distance metric, was performed based on the normalized weighted spectrum counts of the identified proteins. Color gradient scale bar (Y-axis) indicates normalized spectrum counts (numerical matrix) translated into a color image, as described in the Scaffold perSPECtives version 3.0 User's Manual (http://www.proteomesoftware.com/pdf/scaffold_perspectives_users_guide.pdf?v=232de555). More human proteins were found in EVs isolated from the patient, before and after BZN treatment than from EVs derived from the 2 healthy donors (H1, H2). BZN, benznidazole; EV, extracellular vesicle.

However, our results should be interpreted with caution because they represent a single clinical case. Further research is needed to validate and provide stronger evidence that circulating EVs in patients with chronic Chagas disease can serve as biomarkers in disease progression and early assessment of therapeutic outcomes. Moreover, the future incorporation of such validated biomarkers in a point-of-care device could help in the detection of very low parasites in circulation, particularly when concentrations are below the PCR detection level (*2*).

Acknowledgments

We thank the patient and healthy donors who participated in this study. We are particularly grateful to Hernando A. del Portillo for helpful discussions and support throughout this project and to Marc Nicolau for technical assistance.

Barcelona Institute for Global Health (ISGlobal) receives support from the Spanish Ministry of Science, Innovation and Universities through the Centro de Excelencia Severo Ochoa 2019–2023 Program (CEX2018-000806-S). ISGlobal and Institut d'Investigació en Ciències de la Salut Germans Trias i Pujol (IGTP) are members of the Centres de Recerca de Catalunya (CERCA

Program), Generalitat de Catalunya. Work in the laboratory of C.F.B. is funded by Fundació La Marató de TV3 (reference 566/U/2018) and Fundación Mundo Sano. This project was co-financed by the European Union through the European Regional Development Fund with the support of Secretaria d'Universitats i Recerca del Departament d'Empresa i Coneixement de la Generalitat de Catalunya. N.C., M.G., J.G., and M.J.P. receive funds from the Redes temáticas de investigación cooperativa en salud (RETICS), Spanish Tropical Diseases Network "RD12/0018/0010" and from the Agencia de Gestió d'Ajuts Universitaris i de Recerca, Generalitat de Catalunya; grant "2017 SGR 00924." M.G., C.B., J.G., M.J.P., and I.C.A. belong to the Ibero-American Nuevas Herramientas para el Diagnóstico y la Evaluación del Paciente con Enfermedad de Chagas network. I.C.A. is partially supported by grants no. 2G12MD007592 and 5U54MD007592 from the National Institute on Minority Health and Health Disparities of the US National Institutes of Health. We are grateful to the Biomolecule Analysis Core Facility at University of Texas at El Paso, Border Biomedical Research Center, funded by National Institute on Minority Health and Health Disparities grants 2G12MD007592 and 5U54MD007592. M.T.M. received a PhD fellowship from the Science Without Borders Program, Coordenação de Aperfeiçoamento de Pessoal de Nível Superior, Brazil.

About the Author

Ms. Cortes-Serra is a PhD student in ISGlobal, Hospital Clinic–Universitat de Barcelona, Barcelona, Spain. Her research interests include extracellular vesicles and neglected infectious diseases, especially Chagas disease.

References

1. Pinazo MJ, Gascon J. The importance of the multidisciplinary approach to deal with the new epidemiological scenario of Chagas disease (global health). Acta Trop. 2015;151:16–20. https://doi.org/10.1016/j.actatropica.2015.06.013
2. Pinazo MJ, Thomas MC, Bustamante J, Almeida IC, Lopez MC, Gascon J. Biomarkers of therapeutic responses in chronic Chagas disease: state of the art and future perspectives. Mem Inst Oswaldo Cruz. 2015;110:422–32. https://doi.org/10.1590/0074-02760140435
3. Cheow ES, Cheng WC, Lee CN, de Kleijn D, Sorokin V, Sze SK. Plasma-derived extracellular vesicles contain predictive biomarkers and potential therapeutic targets for myocardial ischemic (MI) injury. Mol Cell Proteomics. 2016;15:2628–40. https://doi.org/10.1074/mcp.M115.055731
4. Marcilla A, Martin-Jaular L, Trelis M, de Menezes-Neto A, Osuna A, Bernal D, et al. Extracellular vesicles in parasitic diseases. J Extracell Vesicles. 2014;3:25040. https://doi.org/10.3402/jev.v3.25040
5. Rassi A Jr, Rassi A, Marin-Neto JA. Chagas disease. Lancet. 2010;375:1388–402. https://doi.org/10.1016/S0140-6736(10)60061-X
6. Pinazo MJ, Espinosa G, Gállego M, López-Chejade PL, Urbina JA, Gascón J. Successful treatment with posaconazole of a patient with chronic Chagas disease and systemic lupus erythematosus. Am J Trop Med Hyg. 2010;82:583–7. https://doi.org/10.4269/ajtmh.2010.09-0620
7. Abras A, Ballart C, Llovet T, Roig C, Gutiérrez C, Tebar S, et al. Introducing automation to the molecular diagnosis of *Trypanosoma cruzi* infection: a comparative study of sample treatments, DNA extraction methods and real-time PCR assays. PLoS One. 2018;13:e0195738. https://doi.org/10.1371/journal.pone.0195738
8. de Menezes-Neto A, Sáez MJ, Lozano-Ramos I, Segui-Barber J, Martin-Jaular L, Ullate JM, et al. Size-exclusion chromatography as a stand-alone methodology identifies novel markers in mass spectrometry analyses of plasma-derived vesicles from healthy individuals. J Extracell Vesicles. 2015;4:27378. https://doi.org/10.3402/jev.v4.27378
9. Yang F, Shen Y, Camp DG II, Smith RD. High-pH reversed-phase chromatography with fraction concatenation for 2D proteomic analysis. Expert Rev Proteomics. 2012;9:129–34. https://doi.org/10.1586/epr.12.15
10. Ribeiro KS, Vasconcellos CI, Soares RP, Mendes MT, Ellis CC, Aguilera-Flores M, et al. Proteomic analysis reveals different composition of extracellular vesicles released by two *Trypanosoma cruzi* strains associated with their distinct interaction with host cells. J Extracell Vesicles. 2018;7:1463779. https://doi.org/10.1080/20013078.2018.1463779
11. Bayer-Santos E, Aguilar-Bonavides C, Rodrigues SP, Cordero EM, Marques AF, Varela-Ramirez A, et al. Proteomic analysis of *Trypanosoma cruzi* secretome: characterization of two populations of extracellular vesicles and soluble proteins. J Proteome Res. 2013;12:883–97. https://doi.org/10.1021/pr300947g
12. Bautista-López NL, Ndao M, Camargo FV, Nara T, Annoura T, Hardie DB, et al. Characterization and diagnostic application of *Trypanosoma cruzi* trypomastigote excreted-secreted antigens shed in extracellular vesicles released from infected mammalian cells. J Clin Microbiol. 2017;55:744–58. https://doi.org/10.1128/JCM.01649-16
13. Mattos EC, Canuto G, Manchola NC, Magalhães RDM, Crozier TWM, Lamont DJ, et al. Reprogramming of *Trypanosoma cruzi* metabolism triggered by parasite interaction with the host cell extracellular matrix. PLoS Negl Trop Dis. 2019;13:e0007103. https://doi.org/10.1371/journal.pntd.0007103
14. Boldt AB, Luz PR, Messias-Reason IJ. MASP2 haplotypes are associated with high risk of cardiomyopathy in chronic Chagas disease. Clin Immunol. 2011;140:63–70. https://doi.org/10.1016/j.clim.2011.03.008
15. Rothfuchs AG, Roffê E, Gibson A, Cheever AW, Ezekowitz RA, Takahashi K, et al. Mannose-binding lectin regulates host resistance and pathology during experimental infection with *Trypanosoma cruzi*. PLoS One. 2012;7:e47835. https://doi.org/10.1371/journal.pone.0047835

Address for correspondence: Carmen Fernandez-Becerra or María Jesús Pinazo, ISGlobal, Hospital Clinic–Universitat de Barcelona, Carrer Rosselló, 132, 6º E-08036, Barcelona, Spain; email: carmen.fernandez@isglobal.org or mariajesus.pinazo@isglobal.org

Increasing Malaria Parasite Clearance Time after Chloroquine Therapy, South Korea, 2000–2016

Seong Yeon Park, Yoon Soo Park, Yoonseon Park, Yee Gyung Kwak, Je Eun Song, Kkot Sil Lee, Shin-Hyeong Cho, Sang-Eun Lee, Hyun-Il Shin, Joon-Sup Yeom

We reviewed the clinical efficacy of chloroquine for *Plasmodium vivax* malaria, the changing trend of parasite clearance time, and fever clearance time during 2000–2016 in South Korea. Median parasite clearance time and fever clearance time increased significantly over the study period. Chloroquine was mostly underdosed when used to treat *P. vivax* malaria.

Plasmodium vivax is the only form of malaria indigenous to South Korea (*1*); combination chloroquine and primaquine therapy has been the mainstay of vivax malaria treatment. After *P. vivax* reemerged after being eliminated in South Korea in the late 1970s, it mainly occurred in soldiers or veterans stationed in the demilitarized zone between North Korea and South Korea. Because of this focus, mass chloroquine chemoprophylaxis has been administered in place for soldiers working in high-risk areas since 1997 (*2*,*3*). However, there is concern that mass chemoprophylaxis might lead to reduced chloroquine susceptibility (*2*). In addition, soldiers were often given lower doses than that recommended by the World Health Organization (WHO); Commons et al. reported that underdosing of chloroquine was associated with recurrence and increased parasite clearance time (PCT) (*4*). We studied the trends in South Korea during 2000–2016 for treatment efficacy on the basis of PCT and fever clearance time (FCT).

Author affiliations: Dongguk University Ilsan Hospital, Gyeonggi-do, South Korea (S.Y. Park); National Health Insurance Service Ilsan Hospital, Gyeonggi-do (Y.S. Park, Y. Park); Inje University Ilsan Paik Hospital, Gyeonggi-do (Y.G. Kwak, J.E. Song); Myongji Hospital, Gyeonggi-do (K.S. Lee); Korea Centers for Disease Control and Prevention, Chungcheongbuk-do, South Korea (S.-H. Cho, S.-E. Lee, H.-I. Shin); Yonsei University College of Medicine, Seodaemun-gu, Seoul, South Korea (J.-S. Yeom)

DOI: https://doi.org/10.3201/eid2608.190687

The Study

We conducted this study in 4 hospitals in Goyang, Gyeonggi Province, and 1 hospital in Seoul. The study population consisted of patients >18 years of age in whom *P. vivax* malaria had been diagnosed during 2000–2016 and who had been prescribed chloroquine alone or in combination with primaquine. We determined PCT, defined as the time in hours from chloroquine administration until the first blood smear negative for parasites after which the patient's follow-up smears were also negative, from malaria smears taken daily in routine treatment of patients. To determine FCT, defined as the time from chloroquine administration until the patient's body temperature decreased to <37.5°C for 48 consecutive hours (*5*), we checked for fever every 4–6 hours or whenever the patient felt febrile.

This study was approved by the local institutional review board. Statistical analyses were performed with SPSS Statistics 20 (IBM, https://www.ibm.com). For PCT and FCT, we reported median and interquartile ranges (IQR) because Shapiro-Wilk test results showed that outcome measures did not follow a normal distribution. We compared trend analyses for PCT and FCT by enrollment periods using a linear-by-linear association.

We analyzed included data from a total of 1,199 malaria cases over the 17-year study period. The mean (±SD) age of patients was 41.7 ±14.2 years. None of the patients died of malaria during the study period; 44 relapsed. We divided the years of the study period into 3 ranges. During 2000–2005, 404 malaria cases occurred; that number increased to 566 during 2006–2010, then decreased to 229 during 2011–2016. (Table 1).

Median PCT increased from 63.0 hours during 2000–2005 to 75.0 hours during 2011–2016 ($p<0.001$). The proportion of patients whose PCT

was >48 hours significantly increased over the 17 years from 76.3% during 2000–2005 to 86.6% during 2011–2016 (p = 0.03). In addition, the proportion of PCT at >72 hours also significantly increased from 30.5% during 2000–2005 to 52.4% during 2011–2016 (p = 0.005).

We found fever in 1,074 (89.6%) of 1,199 patients at the time *P. vivax* malaria was diagnosed. Among those patients, median FCT increased from 28.0 hours during 2000–2005 to 48.0 hours during 2011–2016 (p<0.001). The proportion of patients whose FCT was >48 hours increased from 17.6% during 2000–2005 to 48.1% during 2011–2016 (p<0.001). The proportion of patients whose FCT was >72 hours also increased significantly from 5.7% during 2000–2005 to 16.0% during 2011–2016 (p = 0.001).

All of the study patients were treated with either hydroxychloroquine or chloroquine phosphate. The mean total dose of chloroquine base administered was 23.0 mg/kg body weight in 838 patients (69.9%), which is less than the WHO-recommended target dose of 25 mg/kg. The trend of the mean of the total dose of chloroquine base decreased from 23.5 mg/kg during 2000–2005 to 22.1 mg/kg during 2011–2016 (p<0.001). In addition, the proportion of patients receiving less than the WHO-recommended dose increased from 68.8% during 2000–2005 to 77.3% during 2011–2016 (p = 0.02).

Comparing patients with mean total chloroquine doses of ≥25 mg/kg or <25 mg/kg, we found that men were more likely than women to be in the <25 mg/kg group (84.2% vs. 44.9%; p<0.001) (Table 2). Median FCT was longer in the <25 mg/kg group (65.0 h vs. 62.5 h; p = 0.02) and patients whose fever lasted >72 hours were more common in the <25 mg/kg group (12.1% vs. 7.8%; p = 0.03). Relapse was also more common in this group (4.7% vs. 1.4%; p = 0.003).

Conclusions

In this study, we made 2 important findings. First, the trend of increased PCT and FCT in South Korea might be ascribed to decreased *P. vivax* susceptibility to chloroquine that could be seen before the emergence of WHO-recognized drug resistance. Mass chemoprophylaxis of military personnel with hydroxychloroquine started in 1997 in South Korea (*3*,*6*). However, mass chemoprophylaxis with poor compliance to recommended dosing among the patients increased the possibility of chloroquine-resistant strains of *P. vivax* emerging. This finding may explain the failure of the prophylactic hydroxychloroquine treatment to widely protect South Korean army soldiers from *P. vivax* malaria by 2000, chloroquine-resistant cases occurring by the early to mid-2000s (*7*), and the increase in PCT after chloroquine treatment since the late 2000s (*2*).

Second, in areas with chloroquine-sensitive *P. vivax,* WHO recommends oral chloroquine at a total dose of 25 mg base/kg. Lower total doses are not recommended because they encourage the emergence of resistance (*8*). However, in the current study, ≈70% of patients received a suboptimal dose (<25 mg/kg) of chloroquine, partly because the total dose of chloroquine administered in South Korea was usually fixed at 1,500 mg base, as recommended by the US Centers for Disease Control and Prevention (*9*), rather than a weight-based dose. In our study, the average body weight of patients significantly

Table 1. Demographic and clinical data for patients with *Plasmodium vivax* malaria, by study period, South Korea, 2000–2016*

Variable	Years			p value
	2000–2005, n = 404	2006–2010, n = 566	2011–2016, n = 229	
Age, y, mean (±SD)	40.5 ±14.3	42.5 ±14.0	41.6 ±14.6	0.06
Sex				
M	279 (69.1)	410 (72.4)	179 (78.2)	0.045
F	125 (30.9)	156 (27.6)	50 (21.8)	
Weight, kg, mean (±SD)	66.3 ± 0.57	68.4 ± 0.53	70.5 ± 0.88	<0.001
Smear follow-up	131 (32.4)	168 (29.7)	82 (35.8)	0.23
Median PCT (IQR), h	63.0 (49.0–82.0)	66.0 (56.3–78.0)	75.0 (52.0–96.5)	<0.001
PCT >48 h	100/131 (76.3)	145/168 (86.3)	71/82 (86.6)	0.03
PCT >72 h	40/131 (30.5)	61/168 (36.3)	43/82 (52.4)	0.005
Fever	347 (85.9)	521 (92.0)	206 (90.0)	0.04
Median FCT (IQR), h	28.0 (14.0–42.0)	43.0 (29.0–59.0)	48.0 (28.0–66.0)	<0.001
FCT >48 h	49/279 (17.6)	198/477 (41.5)	87/181 (48.1)	<0.001
FCT >72 h	16/279 (5.7)	54/477 (11.3)	29/181 (16.0)	0.001
CQ, mg/kg, mean (±SD)	23.5 ±5.0	22.9 ±4.4	22.1 ±4.8	0.001
CQ <25 mg/kg	278 (68.8)	383 (67.7)	177 (77.3)	0.02
Primaquine, mg/kg, mean (±SD)	0.23 ± 0.06	0.24 ± 0.06	0.29 ± 0.12	<0.001
Primaquine <0.25	265/373 (71.0)	343/543 (63.2)	114/221 (51.6)	<0.001
Relapse	9/394 (2.3)	20/541 (3.7)	10/220 (4.5)	0.20

*Values are no. (%) patients/no. treated except as indicated. CQ, chloroquine; FCT, fever clearance time; IQR, interquartile range; PCT, parasite clearance time.

Table 2. Comparison of clinical features for patients with *Plasmodium vivax* malaria, according to the dosage of chloroquine, South Korea*

Variable	CQ ≥25 mg/kg, n = 361	CQ <25 mg/kg, n = 838	p value
Age, y, mean (±SD)	42.6 ± 16.2	41.2 ± 13.2	0.13
Sex			
M	162 (44.9)	706 (84.2)	<0.001
F	199 (55.1)	132 (15.8)	
Positive for underlying disease	66 (18.3)	144 (17.2)	0.35
Primaquine administration	350 (97.0)	831 (99.2)	0.006
Primaquine, mg/kg, mean (±SD)	0.27 (0.25–0.30)	0.21 (0.19–0.23)	<0.001
Smear follow-up	122 (33.8)	259 (30.9)	0.18
Median PCT (IQR), h	62.5 (51.8–81.8)	65.0 (52.0–81.0)	0.19
PCT >48 h	98/122 (80.3)	215/259 (83.0)	0.31
PCT >72 h	37/122 (30.3)	91/259 (35.1)	0.21
Fever	322 (89.2)	752 (89.7)	0.43
Median FCT (IQR), h	37.0 (23.0–54.0)	38.0 (24.0–48.0)	0.02
FCT >48 h	98/295 (33.2)	238/647 (36.8)	0.16
FCT >72 h	23/295 (7.8)	78/647 (12.1)	0.03
Relapse	5 (1.4)	39 (4.7)	0.003

*Values are no. (%) patients/no. treated except as indicated. CQ, chloroquine; FCT, fever clearance time; IQR, interquartile range; PCT, parasite clearance time.

increased, from 66 kg during 2000–2005 to 71 kg during 2011–2016 (p<0.001), but the recommended total fixed dose of chloroquine did not change. On the basis of the WHO recommendation of 25 mg/kg base, a total dose of chloroquine of 1,500 mg base would have been inadequate for patients whose body weight was >60 kg. In our study, we also found that relapse was more common in the <25 mg/kg chloroquine dose group (4.7% vs 1.4%; p = 0.003).

This study has several limitations. First, parasite clearance was identified in only one third of study patients, but malaria smears were taken once daily, so clearance of parasites could have occurred at any hour in the interval between slides being taken, which could have affected the calculation of PCT. Second, temperature measurements might have been affected by the use of antipyretics and patients were not checked for fever hourly during hospitalization, either of which could have affected the calculation of FCT. Third, due to the retrospective nature of the study, we could not obtain other information that might affect estimates of PCT, such as patient vomiting, which indicates that the medication may not have been absorbed normally, or FCT, such as duration of fever before malaria diagnosis. Prospective studies are needed to more accurately assess whether PCT or FCT has increased.

In summary, increased PCT and FCT might be ascribed to reduced parasite susceptibility to chloroquine that could be seen before emergence of drug resistance in South Korea. Therefore, a proactive and continuous surveillance system for PCT and FCT is needed. In addition, chloroquine is mostly underdosed in the treatment of *P. vivax* malaria in South Korea; thus, clinicians should adhere to weight-based treatment guidelines.

This study was supported by a grant from the Korea Centers for Disease Control and Prevention (grant no. 2016-E54004-00), South Korea.

About the Author

Dr. Seong Yeon Park is a professor in the department of infectious diseases, Dongguk University, South Korea. Her research interests include malaria and other viral diseases.

References

1. Feighner BH, Pak SI, Novakoski WL, Kelsey LL, Strickman D. Reemergence of *Plasmodium vivax* malaria in the republic of Korea. Emerg Infect Dis. 1998;4:295–7. https://dx.doi.org/10.3201/eid0402.980219
2. Yeom JS, Jun G, Kim JY, Lee WJ, Shin EH, Chang KS, et al. Status of *Plasmodium vivax* malaria in the Republic of Korea, 2008–2009: decrease followed by resurgence. Trans R Soc Trop Med Hyg. 2012;106:429–36. https://doi.org/10.1016/j.trstmh.2012.03.011
3. Im JH, Huh K, Yoon CG, Woo H, Lee JS, Chung MH, et al. Malaria control and chemoprophylaxis policy in the Republic of Korea Armed Forces for the previous 20 years (1997–2016). Malar J. 2018;17:295. https://doi.org/10.1186/s12936-018-2449-4
4. Commons RJ, Simpson JA, Thriemer K, Humphreys GS, Abreha T, Alemu SG, et al. The effect of chloroquine dose and primaquine on *Plasmodium vivax* recurrence: a WorldWide Antimalarial Resistance Network systematic review and individual patient pooled meta-analysis. Lancet Infect Dis. 2018;18:1025–34. https://doi.org/10.1016/S1473-3099(18)30348-7s
5. Subramony H, Tangpukdee N, Krudsood S, Poovorawan K, Muangnoicharoen S, Wilairatana P. Evaluation of efficacy of chloroquine for *Plasmodium vivax* infection using parasite clearance times: a 10-year study and systematic review. Ann Acad Med Singapore. 2016;45:303–14.
6. Yeom JS, Ryu SH, Oh S, Choi DH, Song KJ, Oh YH, et al. Evaluation of anti-malarial effects of mass chemoprophylaxis in the Republic of Korea army. J Korean Med Sci. 2005;20:707–12. https://doi.org/10.3346/jkms.2005.20.5.707

7. Lee KS, Kim TH, Kim ES, Lim HS, Yeom JS, Jun G, et al. Chloroquine-resistant *Plasmodium vivax* in the Republic of Korea. Am J Trop Med Hyg. 2009;80:215–7. https://doi.org/10.4269/ajtmh.2009.80.215
8. World Health Organization. Guidelines for the treatment of malaria. Geneva: World Health Organization; 2015.
9. CDC. Guidelines for treatment of malaria in the United States [updated 2019 April 1] [cited 2019 May 10]. https://www.cdc.gov/malaria/resources/pdf/Malaria_Treatment_Table.pdf

Address for correspondence: Joon-Sup Yeom, Department of Internal Medicine, Yonsei University College of Medicine, 50-1, Yonsei-ro, Seodaemun-gu, Seoul, South Korea; email: joonsup.yeom@gmail.com

etymologia

Acanthamoeba [ə¸kæn.Θə'mi.bə]

Nitika Pradhan

From the Greek *akantha* (spike/thorn), which was added before amoeba (change) to describe this organism as having a spine-like structure (acanthopodia). This organism is now well-known as *Acanthamoeba*, an amphizoic, opportunistic, and nonopportunistic protozoan protist widely distributed in the environment.

In 1930, it was reported by Castellani in yeast (*Cryptococcus pararoseus*) culture, and was later (1931) classified as the genus *Acanthamoeba* by Volkonsky. It was later found to be the etiologic agent of *Acanthamoeba* granulomatous encephalitis and keratitis in humans. This organism can also cause cutaneous acanthamebiasis in debilitated and immunocompromised patients.

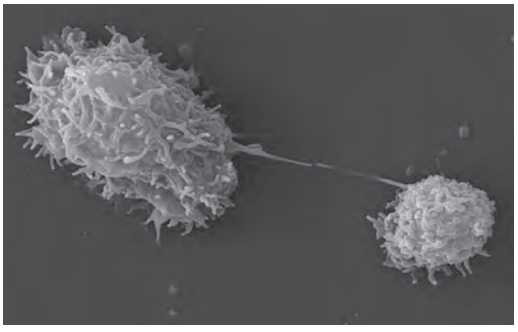

This scanning electron microscopic image shows an *Acanthamoeba polyphaga* protozoa about to complete the process of cell division known as mitosis, thereby becoming 2 distinct organisms. Note the numerous pseudopodia projecting from the surfaces of these organisms. These pseudopodia enable the amoebae to move about and grasp objects in their environment. Source: Centers for Disease Control and Prevention/ Catherine Armbruster, Margaret William; photograph, Janice Haney Carr, 2009.

Sources

1. Castellani A. An amoeba found in culture of yeast: preliminary note. J Trop Med Hyg. 1930;33:160.
2. De Jonckheere JF. Ecology of *Acanthamoeba*. Rev Infect Dis. 1991;13(Suppl 5):385–7. https://doi.org/10.1093/clind/13.Supplement_5.S385
3. Khan NA. *Acanthamoeba*: biology and increasing importance in human health. FEMS Microbiol Rev. 2003;16:273–307.

Author affiliation: Kalinga Institute of Industrial Technology, Bhubaneswar, India

Address for correspondence: Nitika Pradhan, Kalinga Institute of Industrial Technology, Bhubaneswar, India; email: nitikapradhan32@gmail.com

DOI: https://doi.org/10.3201/eid2608.ET2608

Disseminated *Echinococcus multilocularis* Infection without Liver Involvement in Child, Canada, 2018

Joanna Joyce,[1] Xiao-Ou He,[1] Katya Rozovsky,[1] Camelia Stefanovici,[1] Sergio Fanella[1]

An immunocompetent child in Canada received a diagnosis of disseminated alveolar *Echinococcus multilocularis* infection. The case lacked typical features of liver involvement and was possibly related to a rare congenital portosystemic shunt. We summarize the rapidly evolving epidemiology of *E. multilocularis* parasites in Canada.

Alveolar echinococcosis (AE) is a zoonosis caused by the metacestode of *Echinococcus multilocularis* parasites. The definitive hosts include foxes and canines; humans become infected through accidental ingestion of ova dispersed in the environment from feces. AE affects mainly adults, by the formation of irregular lesions within various organs, primarily the liver (*1*,*2*). In Canada, the incidence of human cases of *E. multilocularis* is low (*3*). We describe a case of disseminated AE without hepatic involvement in a child from Manitoba with a congenital portosystemic shunt, in the context of emerging epidemiology of AE in Canada.

The Study

A 12-year-old boy from a remote community who had a history of latent tuberculosis treated 10 years previously was brought for care of 2 months of painless gross hematuria. His only other exposure history was occasionally playing with local stray dogs. He denied other symptoms. Results of his physical examination were unremarkable aside from a BMI of 35.4 kg/m^2.

Laboratory studies were notable for an erythrocyte sedimentation rate of 55 mm/h (reference <10 mm/h) and detection of erythrocytes and leukocyte esterase in the urine. Serology for HIV was negative, and lymphocyte subset values were within reference ranges. An ultrasound showed a large irregular echogenic lesion within the left kidney measuring ≈10 cm. A computed tomography (CT) scan of the abdomen showed an irregular cystoid mass measuring 8.2 × 8.7 × 12.3 cm, occupying the upper and interpolar regions of the left kidney. Magnetic resonance imaging (MRI) of the abdomen showed a heterogenous centrally necrotic renal mass exhibiting no notable central enhancement. Mild peripheral enhancement of the renal lesion was seen on MRI, likely corresponding to fibroinflammatory components (Figure 1).

CT of the chest and brain demonstrated numerous bilateral pulmonary nodules measuring ≤1.2 cm and a few small clustered ring-enhancing lesions in the left frontal lobe measuring ≤8 mm. These lesions were further characterized on brain MRI and again demonstrated ring enhancement, along with associated vasogenic edema (Appendix Figure, https://wwwnc.cdc.gov/EID/article/26/8/19-1644-App1.pdf). The patient underwent a biopsy of the renal lesion. CT of the abdomen also demonstrated a rare vascular anomaly of his portal system. The portal veins were diminutive in caliber, and a large caliber portosystemic shunt arose from the superior mesenteric vein, which drained into the right common iliac vein. This anomaly is consistent with a type II congenital portosystemic shunt (Abernethy malformation) (*4*).

The working diagnosis was tuberculosis. Samples from sputum, feces, urine, bronchoalveolar lavage, and renal biopsy did not show the presence of acid-fast bacilli on staining. Results of *Mycobacterium tuberculosis* PCR performed on the renal tissue and bronchoalveolar lavage sample were negative. The patient was initiated on antimycobacterial therapy while awaiting results from cultures, which were negative after 6 weeks of incubation.

Author affiliations: Memorial University, St. John's, Newfoundland, Canada (J. Joyce); University of Manitoba, Winnipeg, Manitoba, Canada (X.-O. He, K. Rozovsky, C. Stefanovici, S. Fanella)

DOI: https://doi.org/10.3201/eid2608.191644

[1]All authors contributed equally to the preparation of this article.

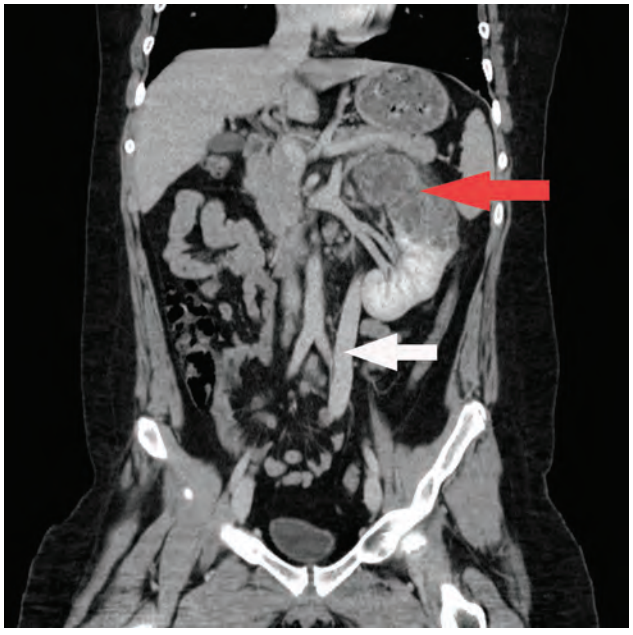

Figure 1. Coronal contrast enhanced CT (computed tomography) of the abdomen of a child with disseminated *Echinococcus multilocularis* infection without liver involvement, Canada, 2018. There is a large irregular hypodense left renal lesion (red arrow). A large porto-systemic shunt is partially visualized (white arrow).

Under ultrasound, sections of core biopsies showed a predominantly solid lesion composed of dense fibroconnective tissue and containing macrophages, myofibroblasts, occasional multinucleated giant cells, and epithelioid histiocytes (Figure 2). In a few cores, there was evidence of variable-sized cystic structures encircled by a thin laminated layer with a thickness of 17–39.6 μm, as measured on Masson trichrome special stain (Figure 2). The luminal side of the cysts contained abundant dystrophic calcifications. A scolex was identified, which is uncommon (Figure 2) (*5*) and suggestive of a multicystic parasitic mass with associated periparasitic granulomatous inflammation, most supportive of *E. multilocularis* species. Echinococcal species serology using *E. granulosus* cyst soluble antigens was strongly positive.

We sent tissue samples to the National Reference Centre for Parasitology, where a PCR-based assay was positive for *E. multilocularis* infection (*6*). Treatment with albendazole was initiated, and tuberculosis medications were discontinued. We decided to proceed with medical therapy and defer any surgical intervention, given the exceedingly difficult surgical approach to perform a total nephrectomy while avoiding rupture of cyst contents. The BMI and the shunt also made surgery challenging, as did the location and numbers of other lesions.

Two years later, the patient is asymptomatic, and tolerating albendazole. Regular MRI imaging has shown no notable changes in the extent of the lesions.

Conclusions

This case of disseminated AE has notable aspects. Cases of human AE are rare in Canada and in children. This case-patient had multisystem disease without

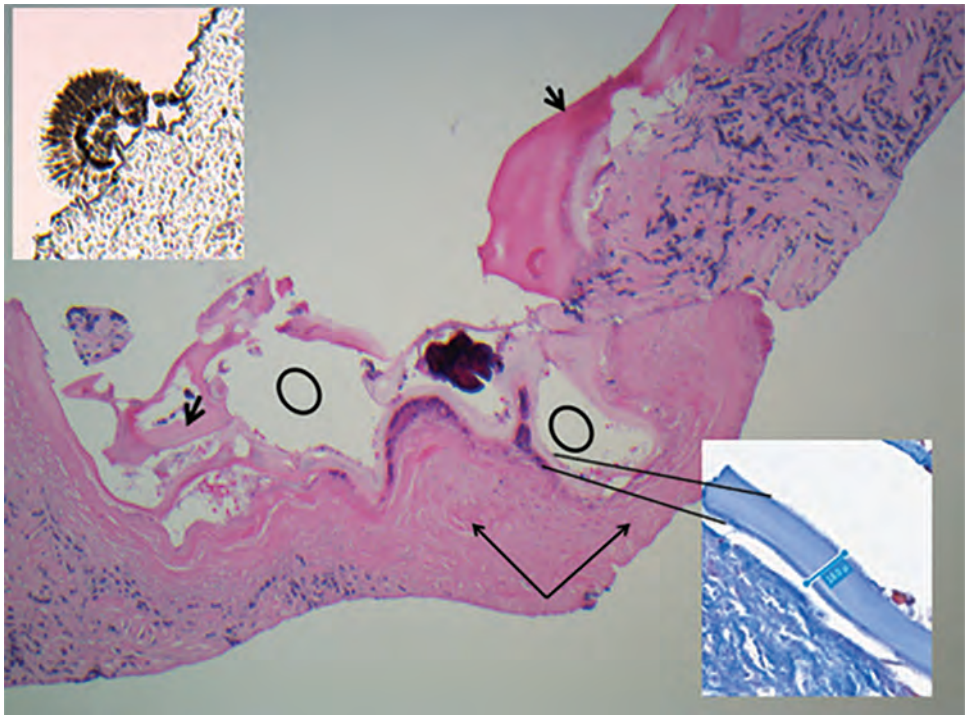

Figure 2. Kidney core biopsy of a child with disseminated *Echinococcus multilocularis* infection without liver involvement, Canada, 2018. Shown are folded laminated membrane (short black arrows) encircling variable-sized cystic structures (black circles) containing calcified and necrotic debris and dense periparasitic fibrosis (long black arrows), in a background of chronic inflammation and fibrosis. No residual normal kidney parenchyma was seen (hematoxylin and eosin stain, original magnification ×40). Inset at lower right shows laminar membrane, 18–19.4 μm in thickness in a background of fibrosis (Masson trichrome, original magnification ×40). Insert at upper left shows scolex attached to the paraffin edge of the block (original magnification ×40).

evidence of hepatic involvement in the setting of a rare congenital portosystemic shunt.

The epidemiology of *E. multilocularis* parasites in Canada has been rapidly evolving over the past decade. Recent reports have identified additional areas of endemicity in wildlife, as well as human cases. Historically, affected wildlife were predominantly from the Arctic and far north or in the northern regions of central Canada, including Manitoba, Saskatchewan, and Alberta (*3, 7–9*). Identification in wildlife from periurban environments is increasing. *E. multilocularis* parasites were detected in 23 of 91 canid carcasses collected within the Calgary and Edmonton metropolitan areas during 2009–2011 (*10*). Positive isolates from coyotes and deer mice in an urban region in Saskatchewan, as well as positive isolates from periurban areas of northern British Columbia, demonstrated a haplotype that was similar to some isolates from Europe (*7*,*11*). In an older study, 23% of coyotes tested in a rural national park in Manitoba were positive for *E. multilocularis* parasites (*9*). Recently, scat samples from 10 of 169 domestic dogs and wild canids from suburban parks around Winnipeg were positive (*12*). After a small cluster of domestic dogs that had diagnoses of *E. multilocularis* infection in Ontario, a survey of wild canid carcasses was conducted across southern Ontario. Of 460 fecal samples, 23% were positive by PCR for *E. multilocularis* DNA (*13*). Of the 18 affected public health units, 10 had clustering with higher prevalence and were in regions with human population densities of up to 1,700 persons/km^2. Risk for human transmission clearly exists around several large urban centers in Canada.

Human AE, especially pediatric AE, has rarely been reported in Canada. Using hospital discharge data, we found no cases of AE documented in Manitoba during 2002–2012 and only 16 reported nationally (*14*). Alarmingly, during 2013–2020, a total of 7 human cases have been confirmed through the Alberta Public Health Laboratory, with 6 confirmed after 2016 (*15*). All were in adults, and all had hepatic lesions. In contrast, our patient was a child with no evidence of liver involvement despite extensive extrahepatic disease. In previous large case series, both aspects were unusual (*16*). A European registry of 559 patients had only 4 reported as children (*17*). Only 13 of the 559 patients lacked any liver involvement.

Factors favoring liver involvement are poorly understood. Our case illustrates an additional mechanism for extrahepatic AE involvement. We suggest that having a congenitally hypoplastic or absent portal vein can be a contributor for extrahepatic AE. In our case, the oncosphere released by ova invaded the small intestine and traveled through the superior mesenteric veins and into the large portosystemic shunt by path of least resistance. The portosystemic shunt drains directly into the right common iliac vein, providing a route for spread to different organs, including the kidneys, lungs, and brain in our case.

In summary, we describe a challenging case of AE and emphasize the difficulty in establishing the diagnosis given the lack of liver involvement, age of the patient, and context of local epidemiology. When viewed in the scope of the recent literature, the epidemiology of AE in Canada is evolving, including our understanding of trends involving suburban regions with large human populations. Surveillance using a One Health approach would help in planning for the future.

Acknowledgments

The authors acknowledge the diagnostic support of the National Reference Centre for Parasitology (NRCP) in the J.D. MacLean Centre for Tropical Diseases at McGill University.

About the Author

Dr. Joyce is a clinical assistant professor in the Faculty of Medicine at Memorial University of Newfoundland, Canada. Her current clinical and research interests include outpatient management of infectious diseases, tropical medicine, and antimicrobial stewardship.

References

1. McManus DP, Zhang W, Li J, Bartley PB. Echinococcosis. Lancet. 2003;362:1295–304. https://doi.org/10.1016/S0140-6736(03)14573-4
2. Jenkins EJ, Peregrine AS, Hill JE, Somers C, Gesy K, Barnes B, et al. Detection of European strain of *Echinococcus multilocularis* in North America. Emerg Infect Dis. 2012;18:1010–2. https://doi.org/10.3201/eid1806.111420
3. Massolo A, Liccioli S, Budke C, Klein C. *Echinococcus multilocularis* in North America: the great unknown. Parasite. 2014;21:73. https://doi.org/10.1051/parasite/2014069
4. Uller W, Alomari AI. Abernethy malformation. Radiographics. 2015;35:1623–4. https://doi.org/10.1148/rg.2015150089
5. Reinehr M, Micheloud C, Grimm F, Kronenberg PA, Grimm J, Beck A, et al. Pathology of echinococcosis: a morphologic and immunohistochemical study on 138 specimens with focus on the differential diagnosis between cystic and alveolar echinococcosis. Am J Surg Pathol. 2020;44:43–54. https://doi.org/10.1097/PAS.0000000000001374
6. Schneider R, Gollackner B, Edel B, Schmid K, Wrba F, Tucek G, et al. Development of a new PCR protocol for the detection of species and genotypes (strains) of *Echinococcus* in formalin-fixed, paraffin-embedded tissues. Int J Parasitol. 2008;38:1065–71. https://doi.org/10.1016/j.ijpara.2007.11.008
7. Gesy KM, Schurer JM, Massolo A, Liccioli S, Elkin BT, Alisauskas R, et al. Unexpected diversity of the cestode

Echinococcus multilocularis in wildlife in Canada. J Parasitol Parasites Wildl. 2014;3:81–7. https://doi.org/10.1016/j.ijppaw.2014.03.002
8. Cerda JR, Buttke DE, Ballweber LR. *Echinococcus* spp. tapeworms in North America. Emerg Infect Dis. 2018;24:230–5. https://doi.org/10.3201/eid2402.161126
9. Samuel WM, Ramalingam S, Carbyn LN. Helminths in coyotes (*Canis latrans* Say), wolves (*Canis lupus* L.), and red foxes (*Vulpes vulpes* L.) of southwestern Manitoba. Can J Zool. 1978;56:2614–7. https://doi.org/10.1139/z78-351
10. Catalano S, Lejeune M, Liccioli S, Verocai GG, Gesy KM, Jenkins EJ, et al. *Echinococcus multilocularis* in urban coyotes, Alberta, Canada. Emerg Infect Dis. 2012;18:1625–8. https://doi.org/10.3201/eid1810.120119
11. Gesy KM, Jenkins EJ. Introduced and native haplotypes of *Echinococcus multilocularis* in wildlife in Saskatchewan, Canada. J Wildl Dis. 2015;51:743–8. https://doi.org/10.7589/2014-08-214
12. Tse C, Bullard J, Rusk R, Douma D, Plourde PJ. Surveillance of *Echinococcus* tapeworm in coyotes and domestic dogs in Winnipeg, Manitoba: abstract. Can Commun Dis Rep. 2019;45:171–6. https://doi.org/10.14745/ccdr.v45i78a01
13. Kotwa JD, Isaksson M, Jardine CM, Campbell GD, Berke O, Pearl DL, et al. *Echinococcus multilocularis* infection, Southern Ontario, Canada. Emerg Infect Dis. 2019;25:265–72. https://doi.org/10.3201/eid2502.180299
14. Schurer JM, Rafferty E, Farag M, Zeng W, Jenkins EJ. Echinococcosis: an economic evaluation of a veterinary public health intervention in rural Canada. PLoS Negl Trop Dis. 2015;9:e0003883. https://doi.org/10.1371/journal.pntd.0003883
15. Massolo A, Klein C, Kowalewska-Grochowska K, Belga S, MacDonald C, Vaughan S, et al. European *Echinococcus multilocularis* identified in patients in Canada. N Engl J Med. 2019;381:384–5. https://doi.org/10.1056/NEJMc1814975
16. James E, Boyd W. *Echinococcus alveolaris*: (with the report of a case). Can Med Assoc J. 1937;36:354–6.
17. Kern P, Bardonnet K, Renner E, Auer H, Pawlowski Z, Ammann RW, et al.; European Echinococcosis Registry. European Echinococcosis Registry: human alveolar echinococcosis, Europe, 1982–2000. Emerg Infect Dis. 2003;9:343–9. https://doi.org/10.3201/eid0903.020341

Address for correspondence: Sergio Fanella, Rm 530 Basic Medical Sciences Building, 745 Bannatyne Ave, Winnipeg, Manitoba R3E 0J9, Canada; email: Sergio.Fanella@umanitoba.ca

Canine *Dracunculus* Nematode Infection, Toledo, Spain

Irina Diekmann, Alaa Aldin Alnassan, Majda Globokar, Nikola Pantchev, Lina Kurzrock, Leticia Hernandez, Javier Lopez, Ricardo Ruano, Silvia Herrero, Georg von Samson-Himmelstjerna, Jürgen Krücken

A fragment of a *Dracunculus*-like worm was extracted from the hind limb of a 2-year-old dog from Toledo, Spain. Cytochrome oxidase I and rRNA sequences confirmed an autochthonous mammalian *Dracunculus* worm infection in Europe. Sequence analyses suggest close relation to a parasite obtained from a North American opossum.

The nematode genus *Dracunculus* contains 14 accepted species, 10 of which parasitize reptiles. The mammalian parasites include *D. fuelleborni*, *D. lutrae*, *D. insignis* and the human pathogen *D. medinensis*. Adult female *Dracunculus* worms are located in the host subcutaneous tissue, especially at the distal extremities (*1*). Human dracunculosis was an important neglected tropical disease, but successful eradication programs have eliminated the parasites from most endemic countries, with the exception of Chad, Ethiopia, South Sudan, Mali, and Angola. In 2019, only 53 human cases but 1,991 animal infections, predominantly in dogs, were reported worldwide (*2*). Infection occurs by ingestion of copepods containing third-stage larvae through drinking water or by feeding on paratenic hosts such as frogs, tadpoles, or fish (*3*,*4*). No genetic differences can be observed between worms infecting humans and dogs, which now appear to be important reservoir hosts (*5*). In addition, *D. lutrae* (host: North American river otter *Lontra canadensis*) and *D. insignis* (wide host range, including raccoons, several mustelids, and canids) worms infect predominantly carnivores in North America (*6*,*7*).

The taxonomy of *Dracunculus* is based on morphologic characteristics of male worms, which are rarely available. Therefore, identification based on 18S rRNA has been used for phylogenetic analysis, and identification based on mitochondrial marker cytochrome oxidase C subunit I (COI) has been used for phylogeny, barcoding and intraspecific variation analyses (*6*).

Author affiliations: Freie Universität Berlin, Berlin, Germany (I. Diekmann, G. von Samson-Himmelstjerna, J. Krücken); IDEXX Laboratories, Ludwigsburg, Germany (A.A. Alnassan, M. Globokar, N. Pantchev, L. Kurzrock); IDEXX Laboratories, Barcelona, Spain (L. Hernandez, J. Lopez); Clínica Mediterráneo, Madrid, Spain (R. Ruano, S. Herrero)

DOI: https://doi.org/10.3201/eid2608.201661

The Study

In summer 2018, a 2-year-old dog resembling a podenco (a local breed in Spain) was brought to a veterinarian in Madrid, Spain, with an oozing ulcer laterally in the tarsal region on the left hind limb. The dog had been in the owner's possession for 1 year at the time. Before that, the dog lived on a pig farm in Toledo, Spain, where the previous owner did not take care of the animal and the dog had access to the food and water supplied for the pigs. Because of a case of abuse, the dog was rescued from the farm.

A 12-cm-long front end of a nematode was extracted from the ulcer (Figure 1, panel A). In the preceding year, the dog had been regularly dewormed, wore a collar to protect against fleas and ticks, and was treated with allopurinol against leishmaniosis; the animal had not traveled abroad. After the removal of the nematode fragment by the veterinarian, the nematode was fixed in 70% ethanol and submitted to IDEXX Laboratories (Ludwigshaven, Germany) for diagnosis. Morphologic examination of the nematode excluded a filarioid species, and a female *Dracunculus* worm was suspected on the basis of the structure of the papillae around the mouth capsule and the worm size (Figure 1, panel B) (*9*). For female specimens, species identification is impossible. No larval stages were found in the specimen because only the anterior end of the worm was collected and the uterus was probably lost.

We amplified and sequenced partial nuclear 18S and 28S rRNA and mitochondrial COI fragments (*10*–*12*; Appendix, https://wwwnc.cdc.gov/EID/article/26/8/20-1661-App1.pdf). From the aligned sequences, we constructed maximum-likelihood phylogenetic trees by using IQtree 1.6.12 (*13*). Partial 18S rRNA sequences (832 bp, GenBank accession no. MT311138.1)

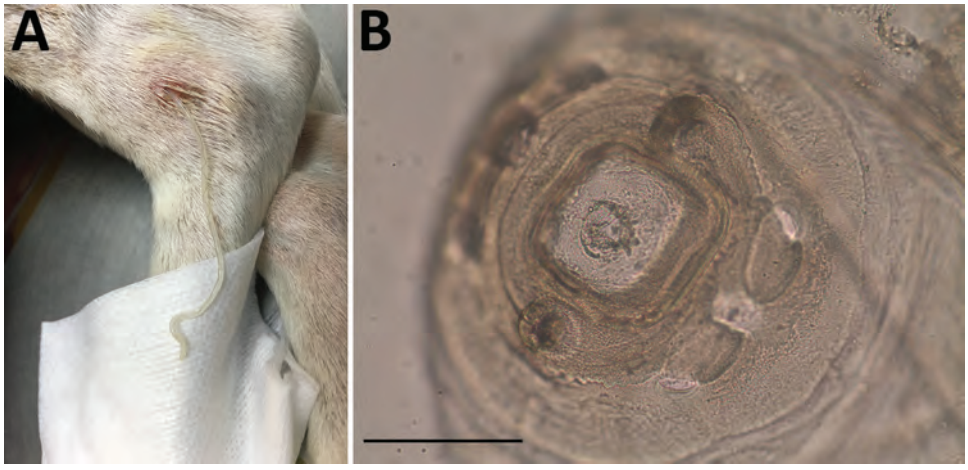

Figure 1. *Dracunculus* worm extracted from a dog in Toledo, Spain, 2018. A) Nematode extracted from the subcutaneous tissue of tarsal region on the left hind limb of naturally infected dog. B) Microphotograph of the anterior end with characteristic papillae. Scale bar represents 50 µm.

showed 99.6% identity to *D. lutrae* (GenBank accession no. JF934737.1), *Dracunculus* sp. V3104 (GenBank accession no. DQ503457.1), and *D. insignis* (GenBank accession no. AY947719.1) and 99.5% identity to *D. medinensis* (GenBank accession no. MK881307.1). Comparison with *D. oesophageus*, the only reptile parasite currently listed in GenBank, shared 96.7% identity (GenBank accession no. AY852269.1).

For the 28S rRNA fragment (231 bp, GenBank accession no. MT311140.1), only 1 homologous sequence from *Dracunculus* sp. HMM2018 isolate SAN-7590 sequence was available (GenBank accession no. KY990016.1) and showed an identity of 97.8%. Phylogenetic analysis using 18S rRNA data confirmed assignment to the genus *Dracunculus* and placed the specimen from Spain in a highly supported cluster containing the mammalian parasites *D. medinensis* and *D. insignis* but not the snake parasite *D. oesophageus* (Appendix Figure). Thus, morphologic and rRNA sequence data agreed in the assignment

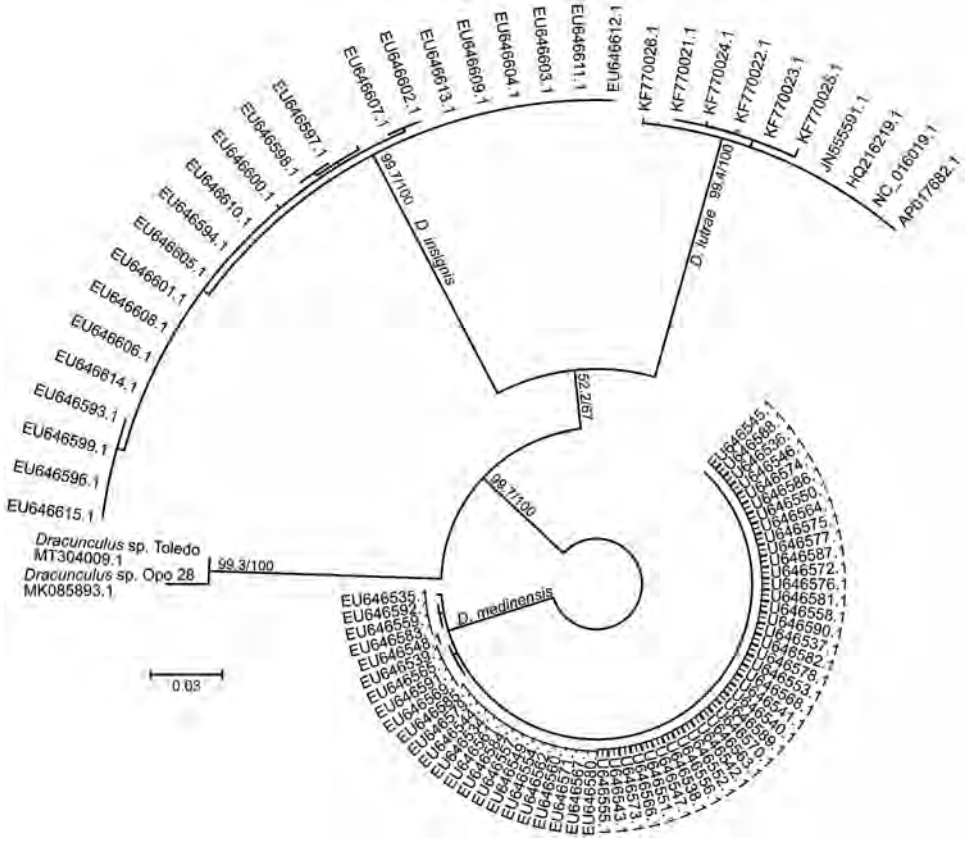

Figure 2. Unrooted maximum-likelihood phylogenetic tree based on *Dracunculus* spp. mitochondrial marker cytochrome oxidase C subunit I sequences from a dog in Toledo, Spain, 2018, and reference sequences. Node support values represent results of ultrafast bootstrapping before and the Shimodaira-Hasegawa approximate likelihood ratio test after the slash. Labels at end nodes represent GenBank accession numbers. Scale bar indicates substitutions per site.

of the specimen to the genus *Dracunculus*, but no species identification was possible.

The partial COI sequence (654bp, GenBank accession no. MT304009.1) showed that the nematode shared 98.3% identity with *Dracunculus* sp. Opo28 (GenBank accession no. MK085893.1), a species found in an opossum (*Didelphis virginiana*) from Georgia, USA; 92.5% with *D. insignis* (GenBank accession no. MK085896.1); 90.7% with *D. lutrae* (GenBank accession no. EU646603.1); and 89.3% identity with *D. medinensis* (GenBank accession no. AP017682.1). The phylogenetic analysis based on COI sequences positioned the nematode in a cluster together with *Dracunculus* sp. Opo28, clearly separated from the 3 other *Dracunculus* species known to infect mammals (Figure 2). The species was designated *Dracunculus* sp. Toledo.

Conclusions

Today, the distribution of known *Dracunculus* worm species infecting mammals is limited to only a few areas endemic for *D. medinensis* worms in Africa, for *D. lutrae* worms in Canada, and for *D. insignis* worms in North America (*6*,*7*). *D. fuelleborni* worms were identified only once in an opossum in Brazil in 1934 (*8*). Canine *Dracunculus* worm infections can be caused by *D. insignis* worms in North America and *D. medinensis* worms in Africa and Asia. Rarely, canine *Dracunculus* infections have been reported from nonendemic countries such as Kazakhstan (*14*); however, because these countries have never been endemic for *D. medinensis* worms, such reports might represent infections with other species. The case in Spain represents an autochthonous mammalian case in Europe, which was considered to be free of such parasites, and manifests a knowledge gap regarding the distribution of *Dracunculus* spp. worms in mammals (*6*,*7*). Although *Dracunculus* worms had not been reported in mammals in Europe until now, unreported cases might have occurred (e.g., cases in which misidentification resulted in diagnosis of other subcutaneous nematodes, such as *Dirofilaria repens*).

The close relationship of the worm extracted in Spain to *Dracunculus* sp. Opo 28 suggests that both specimens belong to the same (or 2 closely related) species. Because *Dracunculus* sp. Opo 28 was obtained from an opossum, the possibility that both specimens represent the species *D. fuelleborni* cannot be excluded. Given that *Dracunculus* sp. Opo28 and *Dracunculus* sp. Toledo worms were found in hosts not closely related to each other as well as on different continents, North America and Europe, the species might have a wide host and geographic range. Opossums are not among the wildlife of Europe, and reservoir hosts for *Dracunculus* sp. Toledo worms need to be identified. Because *Dracunculus* sp. Opo28 and *Dracunculus* sp. Toledo worms are closely related to *D. insignis*, which frequently parasitizes raccoons, importation of this *Dracunculus* species to Europe with this invasive host species is conceivable and should be further investigated. Although the worm extracted in Spain is not *D. oesophageus*, we cannot exclude entirely the possibility that the nematode is not one of the other reptile parasites that have been described so far only morphologically. Currently, nothing is known about the presence of *Dracunculus* spp. in copepod intermediate hosts, fish and amphibian paratenic hosts, and mammalian wildlife reservoir hosts in Spain. Because the *Dracunculus* sp. Toledo worm extracted in Spain had not been reported from dogs previously, canines are probably not epidemiologically relevant hosts. Feeding on infected fish entrails was shown to be a major transmission route to dogs in Chad (*15*), and infection of the dog in Spain also likely occurred through this route. Obtaining life cycle and prevalence data will require systematic sampling of wildlife and domestic carnivores during necropsies, combined with PCR screening of copepods.

Acknowledgments

The authors thank the research training group GRK 2046 (Graduierten-Kolleg 2046) for stimulating discussions that substantially improved the manuscript.

I.D. was funded by the Deutsche Forschungsgemeinschaft (German Research Foundation) under project number 251133687/GRK 2046.

About the Author

Irina Diekmann is a PhD student in the Research Training Group 2046 (Parasite Infections: From Experimental Models to Natural Systems) at the Institute for Parasitology and Tropical Veterinary Medicine, Freie Universität Berlin. Her research interests are molecular characterization of nematodes, parasite life cycles, and parasite–host interactions.

References

1. Cleveland CA, Garrett KB, Cozad RA, Williams BM, Murray MH, Yabsley MJ. The wild world of Guinea worms: a review of the genus *Dracunculus* in wildlife. Int J Parasitol Parasites Wildl. 2018;7:289–300. https://doi.org/10.1016/j.ijppaw.2018.07.002
2. WHO Collaborating Center for Research Training and Eradication of Dracunculiasis, CDC. Guinea worm wrap-up #265. 2020 [cited 2020 May 4]. https://www.cartercenter.org/resources/pdfs/news/health_publications/guinea_worm/wrap-up/265.pdf

3. Cleveland CA, Eberhard ML, Thompson AT, Garrett KB, Swanepoel L, Zirimwabagabo H, et al. A search for tiny dragons (*Dracunculus medinensis* third-stage larvae) in aquatic animals in Chad, Africa. Sci Rep. 2019;9:375. https://doi.org/10.1038/s41598-018-37567-7
4. Cleveland CA, Eberhard ML, Thompson AT, Smith SJ, Zirimwabagabo H, Bringolf R, et al. Possible role of fish as transport hosts for *Dracunculus* spp. larvae. Emerg Infect Dis. 2017;23:1590–2. https://doi.org/10.3201/eid2309.161931
5. Thiele EA, Eberhard ML, Cotton JA, Durrant C, Berg J, Hamm K, et al. Population genetic analysis of Chadian Guinea worms reveals that human and non-human hosts share common parasite populations. PLoS Negl Trop Dis. 2018;12:e0006747. https://doi.org/10.1371/journal.pntd.0006747
6. Elsasser SC, Floyd R, Hebert PD, Schulte-Hostedde AI. Species identification of North American guinea worms (Nematoda: *Dracunculus*) with DNA barcoding. Mol Ecol Resour. 2009;9:707–12. https://doi.org/10.1111/j.1755-0998.2008.02393.x
7. Williams BM, Cleveland CA, Verocai GG, Swanepoel L, Niedringhaus KD, Paras KL, et al. *Dracunculus* infections in domestic dogs and cats in North America; an under-recognized parasite? Vet Parasitol Reg Stud Rep. 2018;13:148–55. https://doi.org/10.1016/j.vprsr.2018.05.005
8. Travassos L. *Dracunculus fuelleborni* n. sp., parasito de *Didelphis aurita* Wied [in Portuguese]. Mem Inst Oswaldo Cruz. 1934;28:235–7. https://doi.org/10.1590/S0074-02761934000200003
9. Chabaud AG. Spirurida. Camallanoidea, Dracunculoidea, Gnathostomatoidea, Physalopteroidea, Rictularoidea and Thelazioidea. In: Anderson RC, Chabaud AG, Willmott S, editors. Keys to the nematode parasites of vertebrates: archival volume. Wallingford (UK): CABI; 2009. p. 334–60.
10. Blaxter ML, De Ley P, Garey JR, Liu LX, Scheldeman P, Vierstraete A, et al. A molecular evolutionary framework for the phylum Nematoda. Nature. 1998;392:71–5. https://doi.org/10.1038/32160
11. Demeler J, Ramünke S, Wolken S, Ianiello D, Rinaldi L, Gahutu JB, et al. Discrimination of gastrointestinal nematode eggs from crude fecal egg preparations by inhibitor-resistant conventional and real-time PCR. PLoS One. 2013;8:e61285. https://doi.org/10.1371/journal.pone.0061285
12. Duscher GG, Harl J, Fuehrer HP. Evidence of *Troglotrema acutum* and *Skrjabingylus* sp coinfection in a polecat from Lower Austria. Helminthologia. 2015;52:63–6. https://doi.org/10.1515/helmin-2015-0011
13. Trifinopoulos J, Nguyen LT, von Haeseler A, Minh BQ. W-IQ-TREE: a fast online phylogenetic tool for maximum likelihood analysis. Nucleic Acids Res. 2016;44(W1):W232-5. https://doi.org/10.1093/nar/gkw256
14. Chun-Syun F. *Dracunculus* infection in dogs in Kazakhstan [in Russian]. Med Parazitol (Mosk). 1958;27:219–20.
15. McDonald RA, Wilson-Aggarwal JK, Swan GJF, Goodwin CED, Moundai T, Sankara D, et al. Ecology of domestic dogs *Canis familiaris* as an emerging reservoir of Guinea worm *Dracunculus medinensis* infection. PLoS Negl Trop Dis. 2020;14:e0008170. https://doi.org/10.1371/journal.pntd.0008170

Address for correspondence: Jürgen Krücken, Freie Universität Berlin, Institute for Parasitology and Tropical Veterinary Medicine, Robert-von-Ostertag Str. 7-13, 14163 Berlin, Germany; email: juergen.kruecken@fu-berlin.de

Leishmania donovani Infection with Atypical Cutaneous Manifestations, Himachal Pradesh, India, 2014–2018

Lovlesh Thakur, Kiran K. Singh, Hemant R. Kushwaha, Sudarshan K. Sharma, Vinay Shankar, Ajeet Negi, Ghanshyam Verma, Sandhya Kumari, Aklank Jain, Manju Jain

We conducted a molecular study of parasite sequences from a cohort of cutaneous leishmaniasis patients in Himachal Pradesh, India. Results revealed atypical cutaneous disease caused by *Leishmania donovani* parasites. *L. donovani* variants causing cutaneous manifestations in this region are different from those causing visceral leishmaniasis in northeastern India.

Leishmaniasis is a complex disease with cutaneous, mucocutaneous, or visceral manifestations depending on the parasite species and host immunity. Despite continued elimination efforts, leishmaniasis continues to afflict known and newer endemic regions, where 0.5–0.9 million new cases of visceral leishmaniasis (VL) and 0.6–1.0 million new cases of cutaneous leishmaniasis (CL) occur every year (*1*). An increase in VL and CL cases from newer foci and atypical disease manifestation pose a challenge to leishmaniasis control programs (*2*–*7*). Unlike the known species-specific disease phenotype, parasite variants can cause atypical disease, so that *Leishmania* species generally associated with VL can cause CL and vice versa.

In India, VL caused by *L. donovani* parasites in the northeastern region and CL caused by *L. tropica* in the western Thar Desert represent the prevalent forms of the disease (*2*). Himachal Pradesh is a more recently leishmaniasis-endemic state in northwest where VL and CL coexist; CL incidence is higher than VL incidence and most cases are attributable to *L. donovani* instead of *L. tropica* infection (*8*,*9*). Sharma et al. conducted limited molecular analysis of a few CL cases and reported preliminary findings (*8*). For an in-depth study on the involvement of *L. donovani* parasites in CL cases, we conducted a comprehensive molecular analysis of CL cases in Himachal Pradesh.

Author affiliations: Central University of Punjab, Bathinda, India (L. Thakur, K.K. Singh, A. Jain, M. Jain); Jawaharlal Nehru University, New Delhi, India (H.R. Kushwaha); Indira Gandhi Medical College, Shimla, India (S.K. Sharma, A. Negi, G. Verma, S. Kumari); Maharishi Markandeshwar Medical College and Hospital, Kumarhatti-Solan, India (V. Shankar)

DOI: https://doi.org/10.3201/eid2608.191761

The Study

During 2014–2018, an increase in CL cases occurred in Himachal Pradesh; case reports came from different tehsils (i.e., townships) in Kinnaur, Shimla, and Kullu and the previously nonendemic districts of Mandi and Solan (Appendix Table 1, Figure 1, https://wwwnc.cdc.gov/EID/article/26/8/19-1761-App1.pdf). We confirmed 60 CL cases indigenous to the state with detailed patient information, demonstration of the presence of Leishman-Donovan bodies and CL-specific histopathologic changes in skin lesional specimens, and PCR detection of parasitic infection (Appendix).

We conducted PCR and restriction fragment-length polymorphism (RFLP) analysis of parasite species–specific internal transcribed spacer 1 (ITS1) sequences by using appropriate standard controls. We detected the expected ≈320-bp product with a *Hae*III RFLP pattern specific to *L. donovani* complex in all patient biopsy specimens, indicating *L. donovani*, *L. infantum*, or both as the causative agent of infection (Appendix Figure 4) (*10*).

BLAST analysis (https://blast.ncbi.nlm.nih.gov/Blast.cgi) of 44 ITS1 test sequences showed all the samples to be closest to *L. donovani*, having maximum identity to *L. donovani* isolates from Bhutan (GenBank accession nos. JQ730001–2) and possibly *L. infantum*. None of the CL cases were consistent with *L. tropica* infection, unlike in a previous report (*8*). To distinguish whether HP isolates were *L. donovani*, *L. infantum*, or both and to infer genetic and geographic relatedness between

these isolates and standard reference strains, we performed ITS1 microsatellite repeat analysis and phylogenetic classification (*11*–*13*). The 4 ITS1 polymorphic microsatellite repeat analysis indicate HP isolates different from *L. infantum* and closest to the *L. donovani* isolates from Bhutan (Table 1; Figure 1, panel A). We detected a polymorphism in the third poly (TA) microsatellite locus with 5 repeats and

Table 1. Standard *Leishmania* strains used in ITS1-based microsatellite polymorphism and phylogenetic analysis of cutaneous leishmaniasis isolates, Himachal Pradesh, India, 2014–2018*

Standard *Leishmania* strains (place of origin)	WHO code	Genbank accession no.	Zymodeme	Disease form	Strain type†	ITS1 polymorphic microsatellite stretches (nucleotide position, bp)			
						Poly C (24–39)	Poly A (24–39)	Poly TA (61–76)	Poly A (124–134)
VL- and CL-causing *L. infantum* and *L. donovani* parasite strains									
L. infantum (Tunisia)	MHOM/TN/80/IPT1	AJ000289	MON-1	VL	A	3	6	4	8
L. donovani (India)	MHOM/IN/00/DEVI	AJ634376	MON-2	VL	H	2	8	5	7
L. donovani (Sri Lanka)	MHOM/LK/2002/ L60c	AM901447	MON-37	CL	ND	2	8	5	7
L. donovani (Bangladesh)	ND	KT921417	ND	VL	ND	2	8	5	7
L. donovani (Kenya)	MHOM/KE/85/ NLB323	AJ000297	MON-37	VL	G	2	8	5	7
L. donovani (Sudan)	MHOM/SD/75/ LV139	AJ000291	ND	CL	E	2	8	6	8
	MHOM/SD/93/9S	AJ634372	MON-18	VL	F	2	9	5	7
L. donovani (Ethiopia)	MHOM/ET/67/HU3	AJ634373	MON-18	VL	F	2	9	5	7
L. donovani (China)	MHOM/CN/00/ Wangjie1	AJ000294	MON-35	VL	C	3	6	4	7
L. donovani (HP, India)	MHOM/IN/83/ CHANDIGARH	AM901449	MON-37	VL	ND	2	8	2, TAA, 3	7
L. donovani (Bhutan)	Trashigang1	JQ730001	ND	VL	ND	2	8	2, TAA, 3	8
	Samtse1	JQ730002	ND	VL	ND	2	9	2, TAA, 3	8
CL-causing *L. donovani* isolates from Himachal Pradesh‡									
HPCL22	–	MG982955	ND	CL	ND	Heterogeneous		2, TAA, 3	8
HPCL27	–	MG982958	ND	CL	ND	Heterogeneous		2, TAA, 3	8
HPCL28	–	MG982959	ND	CL	ND	Heterogeneous		2, TAA, 3	8
HPCL32	–	MG982963	ND	CL	ND	Heterogeneous		2, TAA, 3	8
HPCL42	–	MG982972	ND	CL	ND	Heterogeneous		2, TAA, 3	8
HPCL45	–	MG982975	ND	CL	ND	Heterogeneous		2, TAA, 3	8
HPCL47	–	MG982977	ND	CL	ND	Heterogeneous		2, TAA, 3	8
HPCL49	–	MG982978	ND	CL	ND	Heterogeneous		2, TAA, 3	8
HPCL52	–	MG982981	ND	CL	ND	Heterogeneous		2, TAA, 3	8
HPCL55	–	MG982983	ND	CL	ND	Heterogeneous		2, TAA, 3	8
CL-causing standard WHO *Leishmania* species									
L. major	MHOM/SU/73/ 5ASKH	AJ000310	MON-4	CL	ND	4	6	6	6
L. tropica	MHOM/SU/60/OD	EU326226	LON-7	CL	ND	4	9	1, TTA, 2	3,C,4A
L. mexicana	MHOM/MX/85/ SOLIS	AJ000313	MON-152	CL	ND	2	8	1,	3,C,7A
L. braziliensis	MHOM/BR/00/ LTB300	FN398338	MON-166	CL	ND	2	6	1	5
L. amazonensis	MHOM/BR/73/ M2269	HG512964	MON-132	CL	ND	2	7	1	3,C,6A

*CL, cutaneous leishmaniasis; HP, Himachal Pradesh; ITS1, internal transcribed spacer 1; ND, not determined; VL, visceral leishmaniasis; WHO, World Health Organization.
†ITS sequences strain type according to Kuhls et al. (*13*).
‡These species represent 10/44 samples used in polymorphic microsatellite analysis.

an atypical insert of TAA and the fourth poly (A) microsatellite tract with 8 repeats; these polymorphisms were identical to the VL-causing *L. donovani* isolates from Bhutan. An *L. donovani* Chandigarh isolate originally from HP is reported to be closest to the Bhutan isolates and matched with HP isolates at

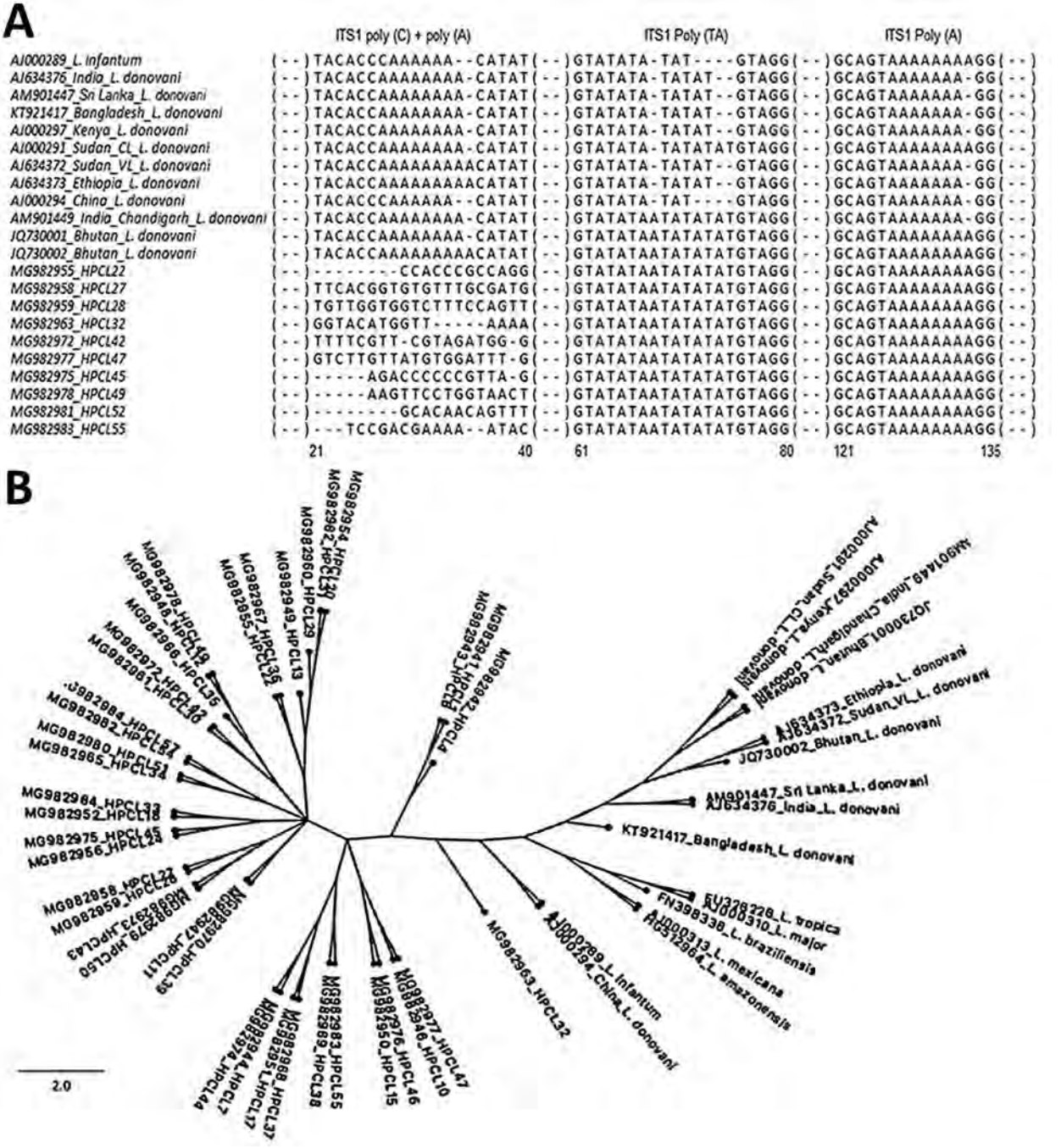

Figure 1. ITS1-based molecular analysis of clinical isolates from cutaneous leishmaniasis (CL) patients, Himachal Pradesh, India, 2014–2018. A) Multiple sequence alignment of ITS1 microsatellite repeat sequences of representative parasite isolates from CL patients with those of L. donovani complex reference strains from different geographic regions. Sequences were aligned by using BioEdit sequence alignment program (https://bioedit.software.informer.com/7.2). B) Phylogenetic tree of ITS1 sequences from CL test isolates (designated as HPCL, numbered in order of their collection) and standard Leishmania strains. Tree constructed by using maximum-likelihood method with 5,000 bootstraps in the dnaml program of PHYLIP package (http://evolution.genetics.washington.edu/phylip/doc/main.html). GenBank accession numbers are indicated. Scale bar indicates the nucleotide substitution per site. ITS1, internal transcribed spacer 1; RFLP, restriction fragment length polymorphism.

Table 2. Standard *Leishmania* strains used in partial 6PGDH amino acid–based phylogenetic analysis of cutaneous leishmaniasis isolates, Himachal Pradesh, India, 2014–2018*

Species (place of origin)	WHO code	Zymodeme	GenBank accession no.	Pathology
WHO standards				
L. donovani (India)	MHOM/IN/0000/DEVI	MON-2	AM157147	VL
L. major (Turkmenistan)	MHOM/TM/1973/5ASKH	ND	AY706107	CL
L. infantum	ND	ND	XM_001469106	ND
L. mexicana	MHOM/BZ/82/BEL21	ND	AY386372	CL
L. tropica	ND	ND	AY045763	CL
L. amazonensis	ND	ND	AY168562	CL
Regional standards				
L. donovani (China)	MHOM/CN/90/9044	ND	JX021389	VL
L. donovani (Kenya)	IMAR/KE/1962/LRC–L57	MON-37	AJ888902	ND
L. donovani (Sri Lanka)	MHOM/LK/2010/OVN3	MON-37	JX481773	VL
L. donovani (Sri Lanka)	MHOM/LK/2002/L59	MON-37	AJ888888	CL
L. donovani (Bangladesh)	MHOM/BD/1997/BG1	ND	AJ888899	VL
L. donovani (Brazil)	ND	ND	AY168567	ND
L. donovani (Kerala, India)	ND	ND	KJ461872	CL

*6PGDH, 6-phosphogluconate dehydrogenase gene; CL, cutaneous leishmaniasis; ND, not determined; VL, visceral leishmaniasis; WHO, World Health Organization.

the third poly (TA) stretch (*12*). However, Himachal Pradesh isolates were distinct at the first poly C and the second poly A microsatellite tracts and had heterogeneous base sequences. Thus, these isolates represent *L. donovani* genetic variants; none showed the ITS1 sequence type previously assigned to the referred *L. donovani* isolates by Kuhls et al. (*13*). Our phylogenetic analysis of 44 ITS1 test sequences and ITS1 reference sequences placed all the CL-causing *L. donovani* isolates from Himachal Pradesh into a discrete cluster different from the VL-causing *L. donovani* from India and elsewhere and the CL-causing *L. donovani* isolates from Sri Lanka. The Himachal Pradesh CL isolates within the cluster exhibited considerable heterogeneity (Table 1; Figure 1, panel B; Appendix Table 4).

Sequences of the 6-phosphogluconate dehydrogenase gene (6PGDH) exhibit a high degree of polymorphism and have been used to identify *Leishmania* species and differentiate region-specific zymodemes (*14*). We performed multiple sequence alignment of the representative partial 6PGDH amino acid sequences from Himachal Pradesh isolates by using the homologous 6PGDH protein sequences of the reference *Leishmania* isolates to determine their genetic and geographic relatedness (Table 2; Figure 2, panel A; Appendix Table 4, Figure 5). Himachal Pradesh isolates exhibited a 6PGDH sequence specific to Mon-37 and different from Mon-2 (having aspartic acid in place of asparagine) at position 326 (Figure 2, panel A). Thus, CL-causing *L. donovani* from Himachal Pradesh were distinct from the most common VL-causing India Mon-2 *L. donovani* and the Bangladesh *L. donovani* isolate, whereas they were similar to the CL-causing *L. donovani* isolate from Kerala and CL- and VL-causing Mon-37 isolates from Sri Lanka and the isolates from Kenya, Brazil, and China.

Phylogenetic analysis of 6PGDH amino acid sequences of CL isolates grouped them into a heterogeneous cluster; variants were closer to a viserotropic *L. donovani* isolate from Sri Lanka and distinct from the VL-causing *L. donovani* isolates from India and Bangladesh and CL-causing isolates from Kerala and Sri Lanka (Figure 2, panel B). However, the HPCL55 isolate (GenBank accession no. MH208450) grouped differently. The HPCL49 isolate (GenBank accession no. MH208446) showed relatedness to the standard *L. infantum* strain, although ITS1 analysis using BLAST and microsatellite repeat sequences showed regions of similarity with *L. donovani*. ITS1 and 6PGDH sequence analysis suggest that Himachal Pradesh isolates from CL patients consist of heterogenous *L. donovani* variants and possibly represent hybrid genotypes.

None of the CL patients had VL-specific symptoms or VL history. Ten of 43 patient blood samples tested positive for rK39 antibody, and 37 of 51 samples were positive for the circulating parasite DNA with *L. donovani*–specific ITS1 (Appendix Figure 6, panel A, B). The result suggests asymptomatic systemic *L. donovani* infection in a fraction of CL patients.

Conclusions

The presence of leishmaniasis in Himachal Pradesh is not yet well known in India and globally (*15*). Our epidemiologic study shows newer CL pockets during 2014–2018; thus, the state needs to be recognized as leishmaniasis-endemic by public health authorities (Appendix Figure 1). We conclude that CL cases in Himachal Pradesh are caused by *L. donovani* variants

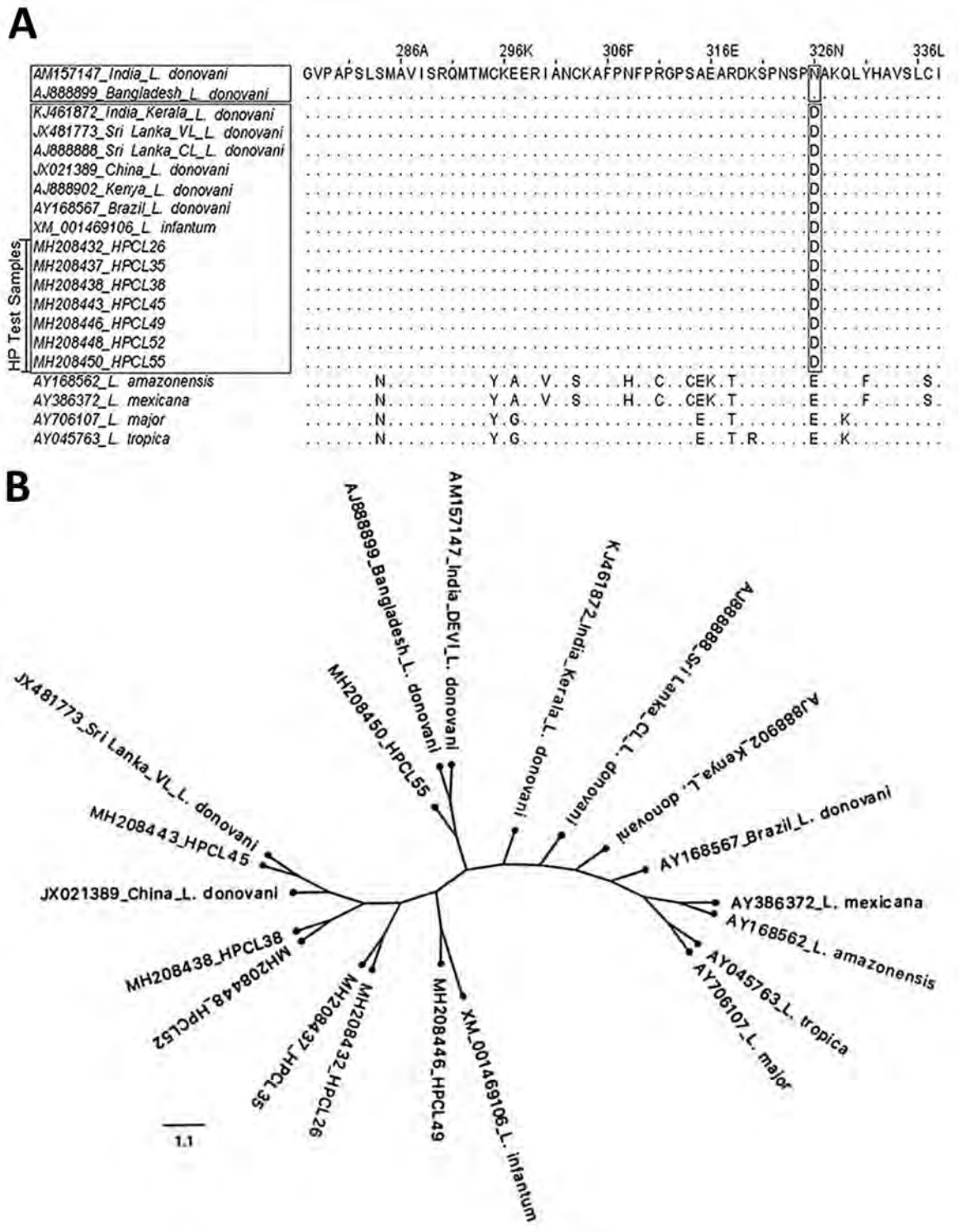

Figure 2. 6PGDH-based molecular analysis of clinical isolates from cutaneous leishmaniasis (CL) patients, Himachal Pradesh, India, 2014–2018. A) Sequence alignment of partial 6PGDH amino acid of CL isolates exhibit replacement of asparagine (N) with aspartic acid (D) at position 326 analogous to visceral leishmaniasis–causing and CL-causing isolates from Sri Lanka. B) Phylogenetic tree for 6PGDH sequences from CL test isolates (designated as HPCL, numbered in order of their collection) and standard *Leishmania* strains. Tree constructed by using maximum-likelihood method with 5,000 bootstraps in the *dnaml* program of PHYLIP package (http://evolution.genetics.washington.edu/phylip/doc/main.html). GenBank accession numbers are indicated. Scale bar indicates the amino acid substitution per site. 6PGDH, 6-phosphogluconate dehydrogenase gene; HP, Himachal Pradesh.

distinct from the viscerotropic *L. donovani* strain from northeast India. The CL isolates in Himachal Pradesh exhibit considerable heterogeneity and indicate the possible existence of genetic hybrids. The scenario appears somewhat similar to Sri Lanka and Kerala, where *L. donovani* parasites cause cutaneous disease, albeit with differences in the region-specific *L. donovani* variants. In lieu of the coexistence of VL and CL in Himachal Pradesh, parasite isolates from VL patients also need to be characterized. To understand the biology of atypical *L. donovani* variants with cutaneous manifestations and to genetically differentiate the dermotropic versus viscerotropic potential of *L. donovani* variants, comparison of CL- and VL-causing isolates in Himachal Pradesh using whole-genome sequence analysis is required.

L. donovani parasites in the blood of some CL patients represent human reservoirs similar to asymptomatic VL carriers, and the parasite variants have the potential to cause full-blown VL manifestations. An elaborate surveillance program dedicated to the Himachal Pradesh region is urgently required for better diagnosis, treatment, prediction of parasite variants in different afflicted pockets, and prevention of transmission of the disease to other regions.

Acknowledgments

We thank Greg Matlashewski for his helpful suggestions and comments to improve the manuscript, Wen Wei Zhang for technical suggestions, and Rentala Madhubala for generously gifting *Leishmania donovani* and *L. major* standard cultures.

About the Author

Ms. Thakur is a PhD student in the Department of Zoology at the Central University of Punjab, Bathinda, Punjab, India. Her primary research interests include the epidemiology and pathogenesis of infectious and parasitic diseases.

References

1. World Health Organization. Leishmaniasis. 2019 [cited 2019 Sep 1]. https://www.who.int/en/news-room/fact-sheets/detail/leishmaniasis
2. Thakur L, Singh KK, Shanker V, Negi A, Jain A, Matlashewski G, et al. Atypical leishmaniasis: a global perspective with emphasis on the Indian subcontinent. PLoS Negl Trop Dis. 2018;12:e0006659. https://doi.org/10.1371/journal.pntd.0006659
3. Sandhya R, Rakesh P, Dev S. Emergence of visceral leishmaniasis in Kollam District, Kerala, southern India. Int J Community Med Public Health. 2019;6:1350–2. https://doi.org/10.18203/2394-6040.ijcmph20190639
4. Kumar NP, Srinivasan R, Anish TS, Nandakumar G, Jambulingam P. Cutaneous leishmaniasis caused by *Leishmania donovani* in the tribal population of the Agasthyamala Biosphere Reserve Forest, Western Ghats, Kerala, India. J Med Microbiol. 2015;64:157–63. https://doi.org/10.1099/jmm.0.076695-0
5. Siriwardana Y, Zhou G, Deepachandi B, Akarawita J, Wickremarathne C, Warnasuriya W, et al. Trends in recently emerged *Leishmania donovani* induced cutaneous leishmaniasis, Sri Lanka, for the first 13 Years. BioMed Res Int. 2019;2019:4093603. https://doi.org/10.1155/2019/4093603
6. Sharma NL, Mahajan VK, Negi AK. Epidemiology of a new focus of localized cutaneous leishmaniasis in Himachal Pradesh. J Commun Dis. 2005;37:275–9. PubMed
7. Kumari S, Garg A. Lip leishmaniasis: a new emerging clinical form of cutaneous leishmaniasis from sub-Himalayan Region. Journal of Medical Science and Clinical Research. 2018;06:62–9.
8. Sharma NL, Mahajan VK, Kanga A, Sood A, Katoch VM, Mauricio I, et al. Localized cutaneous leishmaniasis due to *Leishmania donovani* and *Leishmania tropica*: preliminary findings of the study of 161 new cases from a new endemic focus in Himachal Pradesh, India. Am J Trop Med Hyg. 2005;72:819–24. https://doi.org/10.4269/ajtmh.2005.72.819
9. Sharma NL, Sood A, Arora S, Kanga A, Mahajan V, Negi A, et al. Characteristics of *Leishmania* spp. isolated from a mixed focus of cutaneous and visceral leishmaniasis in Himachal Pradesh (India). Internet J Third World Med. 2009;7(8).
10. el Tai NO, Osman OF, el Fari M, Presber W, Schönian G. Genetic heterogeneity of ribosomal internal transcribed spacer in clinical samples of *Leishmania donovani* spotted on filter paper as revealed by single-strand conformation polymorphisms and sequencing. Trans R Soc Trop Med Hyg. 2000;94:575–9. https://doi.org/10.1016/S0035-9203(00)90093-2
11. Dávila AM, Momen H. Internal-transcribed-spacer (ITS) sequences used to explore phylogenetic relationships within *Leishmania*. Ann Trop Med Parasitol. 2000;94:651–4. https://doi.org/10.1080/00034983.2000.11813588
12. Yangzom T, Cruz I, Bern C, Argaw D, den Boer M, Vélez ID, et al. Endemic transmission of visceral leishmaniasis in Bhutan. Am J Trop Med Hyg. 2012;87:1028–37. https://doi.org/10.4269/ajtmh.2012.12-0211
13. Kuhls K, Mauricio IL, Pratlong F, Presber W, Schönian G. Analysis of ribosomal DNA internal transcribed spacer sequences of the *Leishmania donovani* complex. Microbes Infect. 2005;7:1224–34. https://doi.org/10.1016/j.micinf.2005.04.009
14. Ranasinghe S, Zhang W-W, Wickremasinghe R, Abeygunasekera P, Chandrasekharan V, Athauda S, et al. *Leishmania donovani* zymodeme MON-37 isolated from an autochthonous visceral leishmaniasis patient in Sri Lanka. Pathog Glob Health. 2012;106:421–4. https://doi.org/10.1179/2047773212Y.0000000054
15. World Health Organization. Leishmaniasis country profile–2015, India. 2017 [cited 2019 Sep 1]. https://www.who.int/leishmaniasis/burden/India_2015-hl.pdf?ua=1

Address for correspondence: Manju Jain, Department of Biochemistry, Central University of Punjab, City Campus, Mansa Rd, Bathinda, Punjab, 151001, India, email: manjujainmda@gmail.com

Doxycycline and Sitafloxacin Combination Therapy for Treating Highly Resistant *Mycoplasma genitalium*

Duygu Durukan, Michelle Doyle, Gerald Murray, Kaveesha Bodiyabadu, Lenka Vodstrcil, Eric P.F. Chow, Jorgen S. Jensen, Christopher K. Fairley, Ivette Aguirre, Catriona S. Bradshaw

Antimicrobial-resistant *Mycoplasma genitalium* is becoming increasingly common and creating major treatment challenges. We present early data on combination therapy with doxycycline and sitafloxacin to treat highly resistant *M. genitalium*. We found the regimen was well tolerated and cured 11/12 infections that had failed prior regimens with moxifloxacin and pristinamycin.

Mycoplasma genitalium is a sexually transmitted bacterium with marked capacity for developing antimicrobial resistance (*1*). Macrolides and 4th-generation fluroquinolones, such as moxifloxacin, have been the main agents displaying efficacy against *M. genitalium*. However, macrolide resistance has increased to >50% in many nations, and quinolone resistance is increasing (*2*–*6*). In Australia, 16% of *M. genitalium* strains are reported to have dual-class resistance (*5*), and Japan reports dual-class resistance of up to 25% (*2*), resulting in infections that often cannot be cured with current recommended therapies.

Sequential monotherapy with doxycycline followed by moxifloxacin (*7*–*9*) is currently first-line therapy for macrolide-resistant *M. genitalium* in guidelines in Australia and the United Kingdom and achieves cure in 92% of cases (95% CI 88.1%–94.6%) at our service (*7*). When the doxycycline/moxifloxacin sequential regimen fails, we use a pristinamycin-based regimen, which achieves 75% cure (95% CI 66%–82%) (*10*). Since August 2017, for patients in whom both regimens failed, we administered a combination of 100 mg doxycycline and 100 mg sitafloxacin 2 times/day for 7 days.

Access to sitafloxacin is limited in many countries, but it is available in the Asia-Pacific region. Most publications on sitafloxacin are from Japan, where its use as a monotherapy is reported to cure ≈90% of *M. genitalium* infections (*11*). However, combination therapies can optimize cure and prevent further resistance in bacteria prone to developing resistance, such as *M. genitalium*. In vitro, a combination of doxycycline and sitafloxacin (doxycycline+sitafloxacin) shows synergy for quinolone-susceptible *M. genitalium* strains but has not been evaluated for highly resistant strains (J.S. Jensen, unpub. data). We provide early data on the efficacy and tolerability of a 7-day doxycycline+sitafloxacin combination therapy for treatment-resistant *M. genitalium*. The ethics committee of Alfred Hospital (Melbourne) approved this study (approval no. 232/16).

The Study

The study included 12 cases of macrolide-resistant *M. genitalium* detected among all patients assessed with the clinical protocol at Melbourne Sexual Health Centre (MSHC), Carlton, Victoria, Australia, for routine *M. genitalium* testing (*7*,*9*) during August 2017–April 2019 (Figure). During the study period, 96 (8%) of *M. genitalium* cases failed to respond to doxycycline/moxifloxacin; we subsequently treated 56 with pristinamycin, which failed in 15 (27%) patients. All 15 opted for combination therapy; 11 provided a test of cure, and the other 4 did not complete follow up. One

Author affiliations: Alfred Health, Carlton, Victoria, Australia (D. Durukan, M. Doyle, L. Vodstrcil, E.P.F. Chow, C.K. Fairley, I. Aguirre, C.S. Bradshaw); Monash University, Clayton, Victoria, Australia (D. Durukan, L. Vodstrcil, E.P.F. Chow, C.K. Fairley, C.S. Bradshaw); Royal Children's Hospital, Parkville, Victoria, Australia (G. Murray, K. Bodiyabadu); The Royal Women's Hospital, Parkville (G. Murray, K. Bodiyabadu); Statens Serum Institut, Copenhagen, Denmark (J.S. Jensen)

DOI: https://doi.org/10.3201/eid2608.191806

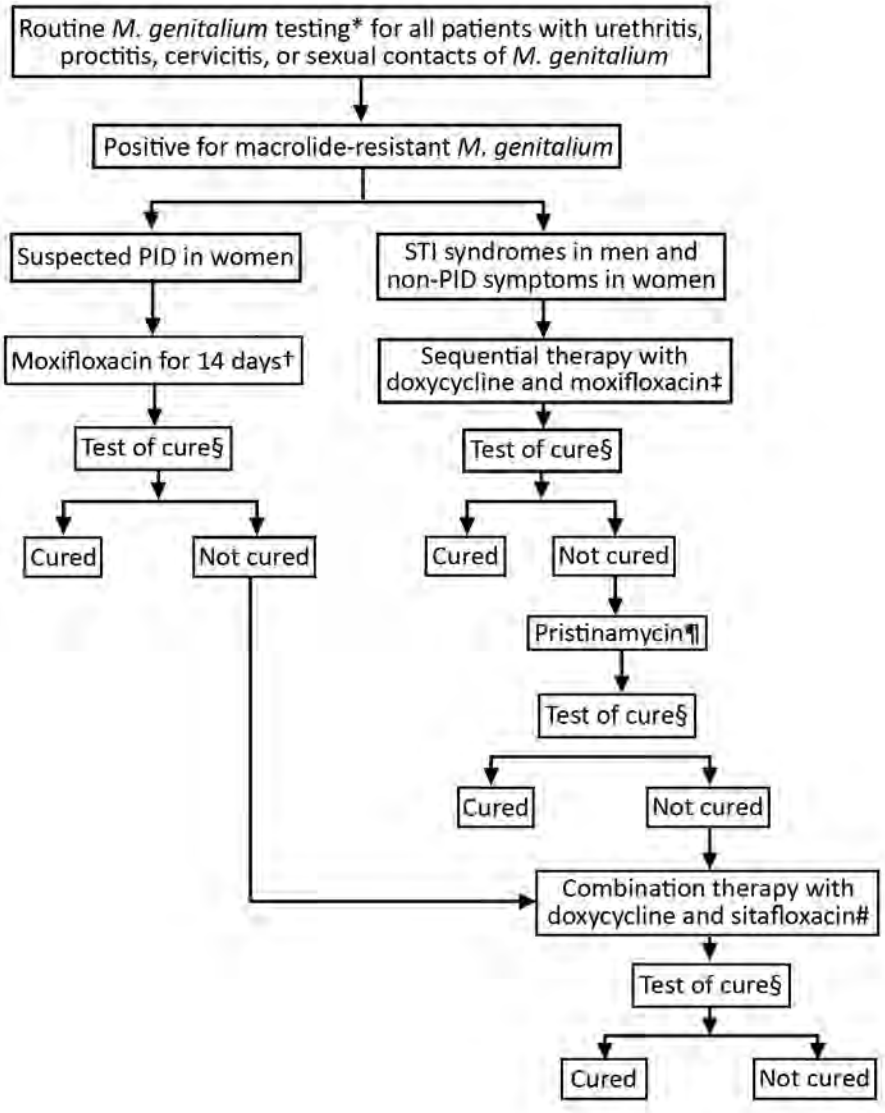

Figure. Clinical approach and treatment for patients with diagnosed macrolide-resistant *Mycoplasma genitalium* at Melbourne Sexual Health Centre, Australia. PID, pelvic inflammatory disease; STI, sexually transmitted infection. *Routine testing with the ResistancePlus MG assay (SpeeDx, https://plexpcr.com). †Moxifloxacin 400 mg/day for 14 days. ‡Doxycycline 100 mg 2 times/day for 7 days, then moxifloxacin 400 mg/d for 7 days. §Test of cure was recommended 14–28 days after completing antimicrobial treatment and all patients received a reminder. ResistancePlus MG Assay was used for all tests of cure. ¶When sequential therapy failed, patients were given a pristinamycin-based regimen for 10 days, either 1 g 4 times/day alone or 1 g 3 times/day in combination with doxycycline 100 mg 2 times/day. Doxycycline pretreatment also was given to some patients. #Doxycycline 100 mg and sitafloxacin 100 mg taken together 2 times/day for 7 days.

additional patient also received combination therapy because her pelvic inflammatory disease (PID) did not respond to moxifloxacin. Our final analysis included 12 patients.

Among study participants, 9 sought treatment for urogenital symptoms and 1 for PID; 2 were asymptomatic contacts of persons with *M. genitalium*. Median age was 29 years (interquartile range [IQR] 27–32 years). All men (10/12) had urethral infections; the 2 women had cervicovaginal infections.

We tested patient samples using the ResistancePlus MG Assay (SpeeDx, https://plexpcr.com). We defined treatment-resistant *M. genitalium* as microbiological failure and persistent symptoms after first-line and second-line therapies failed. We classified microbial cure as *M. genitalium* not detected and microbial failure as a positive result on test of cure 14–28 days after completing antimicrobial drug therapy.

At MSHC, we often give doxycycline before the main regimen to reduce *M. genitalium* load and optimize cure (*12*). We term moxifloxacin-containing regimens as first-line, pristinamycin-containing regimens as second-line, and combination therapy as third-line (Table 1). All 12 patients received a moxifloxacin-based regimen; 9 had sequential doxycycline/moxifloxacin in keeping with clinical guidelines (*9*). The other 3 had moxifloxacin alone, 1 for PID, and 2 received treatments prior to coming to MSHC (1 was treated for 10 days and the other for 30 days, but we do not know the physician's rationale for treatment duration). Moxifloxacin-based regimens failed in all patients; 11 were then treated with pristinamycin, which also failed. We administered combination

Table 1. Antimicrobial regimens and test of cure data for patients treated for *Mycoplasma genitalium* with doxycycline and sitafloxacin combination therapy, Melbourne Sexual Health Centre, Carleton, Victoria, Australia*

		First-line therapy, sequential; d			Second-line therapy, sequential; d			Third-line therapy, combination; d		
Case no.	Baseline test	Doxy†	Moxi	TOC	Doxy†	Pris	TOC	Doxy†	Combination‡	TOC
1§	+	7	7	+	7	10	+	21	7	Cured
2	+	7	7	+	7	10	+	28	7	Cured
3	+	7	7	+	7	10	+	21	7	Cured
4§	+	None	10¶	+	7	10	+	None	7	Cured
5	+	7	7	+	7	10	+	None	7	Cured
6§	+	None	30¶	+	21	10	+	14	7	Cured
7	+	7	7	+	None	10	+	7	7	Cured
8	+	7	7	+	None	10	+	7	7	Cured
9	+	7	7	+	7	10	+	7	7	Failed
10§	+	7	7¶	+	None	10	+	3	7	Cured
11§	+	None	14#	+	None**	None	None	5	7	Cured
12	+	7	7	+	10††	10	+	3	7	Cured

*Doxy, doxycycline; Moxi, moxifloxacin; Pris, pristinamycin; TOC, test of cure; +, macrolide-resistant *M. genitalium* detected.
†Doxycycline 100 mg 2 times/day commonly was given first as monotherapy in first, second, and third drug regimens; duration is specified for each case.
‡Sitafloxacin 100 mg 2 times/day and doxycycline 100 mg 2 times/day were given concurrently for 7 days.
§Patients who had prior failed antimicrobial therapy for *M. genitalium* infection before coming to Melbourne Sexual Health Centre (MSHC). Case no. 1 received 1 g azithromycin before coming to MSHC and this regimen failed. Case no. 4 received moxifloxacin 400 mg/d for 10 days before coming to MSHC and this regimen failed. Case no. 6 received 3 1-g doses of azithromycin given on separate occasions and this regimen failed, then received 2 courses of doxycycline 100 mg 2 times/day for 14 d each which also failed; then received a 30-day course of moxifloxacin 400 mg/d which also failed, before coming to MSHC. Case no. 10 received doxycycline 100 mg 2 times/day for 7 d then 1 g azithromycin which failed; then received doxycycline 100 mg 2 times/day for 7 d which failed, after which the patient received moxifloxacin 400 mg/d for 7 d, which also failed before coming to MSHC. Case no. 11 received doxycycline and azithromycin at unspecified doses or duration before coming to MSHC.
¶Moxifloxacin-containing regimen given to a patient in the community before they came to MSHC. This regimen often varied from firstline therapy given at MSHC.
#Moxifloxacin 400 mg/d × 14 d was given as a first regimen to this patient because of diagnosed pelvic inflammatory disease.
**Patient was diagnosed with possible *M. genitalium*–related pelvic inflammatory disease and did not receive a pristinamycin–containing regimen (*14*).
††Patient was given 1 g pristinamycin 3 times/day in combination with doxycycline 100 mg 2 times/day rather than 1 g 4 times/day because both regimens have shown equivalent efficacy at our service (*10*).

therapy without preceding pristinamycin to 1 patient because of concerns regarding her PID.

All patients received doxycycline+sitafloxacin combination therapy for 7 days; 9 had preceding doxycycline for varying durations (Table 1). Among 12 patients, 11 (91.7%; 95% CI 64.9%–98.5%) were cured and achieved complete symptom resolution after combination therapy. Combination therapy failed in 1 patient who experienced persistent dysuria. Median time to test of cure after combination therapy was 20 (IQR 14–24) days. Median duration from first *M. genitalium* diagnosis to cure was 125 (IQR 106–144) days. Before test of cure, all patients were classified as no- or low-risk for reinfection by the treating clinician on the basis of no sex or 100% condom use with any partner or sex with a fully treated partner in the interval between treatment and test of cure (*7*,*12*).

All patients whose first-line and second-line therapies failed were symptomatic, including the 2 who initially were asymptomatic contacts. All 10 men reported persistent fluctuating dysuria, 6 reported urethral discharge, 2 urethral irritation or itching, and 1 meatal inflammation. Both women reported fluctuating abnormal vaginal discharge, 1 reported intermittent dysuria, and the patient with PID reported persistent dyspareunia. Men typically experienced a stepwise reduction in urethral symptoms after commencing antimicrobial drugs, but dysuria reemerged during follow-up.

Among 10 patients for whom adherence and adverse effects are available, 9 (90.0%; 95% CI 60.0%–99.5%) reported taking all doses of both drugs, including the patient whose treatment failed; 1 reported missing 1 tablet of sitafloxacin. Six (60.0%; 95% CI 31.3%–83.2%) patients reported no adverse effects. Among the other 4, adverse effects were mild and resolved spontaneously (1 each of diarrhea, arthralgia, tendon pain, and possible blurred vision).

Sanger sequencing of the quinolone resistance–determining regions of the *parC* and *gyrA* genes revealed single nucleotide polymorphisms for *parC* in all cases and for *gyrA* in 5/12 cases before combination therapy (Table 2). The *parC* mutations corresponded to amino acid changes S83I (G248T; n = 11) and D87N (G259A; n = 1). The *gyrA* mutations corresponded to amino acid changes M95I (G285A; n = 3), A79S (G235T; n = 1), and D99N (G295A; n = 1). In 1 case, a *gyrA* mutation appeared to develop after moxifloxacin failure (case 9; Table 2). The patient in whom combination therapy failed had a single *parC* S83I change detected (Table 2).

Conclusions

Combination therapy with doxycycline+sitafloxacin was well tolerated and effective against treatment-

Table 2. Amino acid changes in the quinolone resistance–determining regions of *parC* and *gyrA* genes of macrolide-resistant *Mycoplasma genitalium* in patients treated with combination therapy, Melbourne Sexual Health Centre, Carlton, Victoria, Australia*

Case no.	Sexual orientation	Baseline test		TOC after first-line therapy		TOC after second-line therapy		TOC after third-line therapy	
		parC	*gyrA*	*parC*	*gyrA*	*parC*	*gyrA*	*parC*	*gyrA*
1	MSM	NA	NA	S83I	n/A	S83I	D99N	Cured	
2	MSM	S83I	M95I	S83I	M95I	S83I	M95I	Cured	
3	MSM	S83I	WT	S83I	WT	S83I	WT	Cured	
4	MSW	NA	NA	NA	NA	S83I	A79S	Cured	
5	MSW	D87N	WT	D87N	WT	D87N	WT	Cured	
6	MSW	NA	NA	S83I	WT	S83I	WT	Cured	
7	MSW	S83I	WT	S83I	WT	S83I	WT	Cured	
8	MSM	S83I	WT	S83I	WT	S83I	WT	Cured	
9	MSW	S83I	WT	S83I	WT	S83I	WT	S83I	WT
10	MSM	NA	NA	S83I	WT	S83I	WT	Cured	
11	W	S83I	WT	S83I	M95I	ND	ND	Cured	
12	W	S83I	M95I	S83I	M95I	S83I	M95I	Cured	

*MSM, men who have sex with men; MSW, men who have sex with women only; NA, sample was not available for sequencing; ND, not done; W, heterosexual woman; WT, wild type.

resistant *M. genitalium*. The regimen was acceptable to clinicians and is now used as our third-line regimen.

Moxifloxacin failure has been associated with specific polymorphisms in the quinolone resistance–determining regions of *parC* (*2*,*5*). The *parC* G248T mutation, which causes amino acid change S83I, is the most common mutation associated with moxifloxacin failure (*5*). The less common G259A(D87N) mutation has been associated with higher moxifloxacin MICs in 3 *M. genitalium* strains (J.S. Jensen, unpub. data). S83I contributes to both sitafloxacin and moxifloxacin failure (*5*). Although sitafloxacin is more likely than moxifloxacin to cure an infection carrying an S83I mutation, we previously found concurrent *gyrA* mutations, particularly M95I, increased the risk for sitafloxacin failure (*5*). In this study, moxifloxacin failed in all 12 cases with a *parC* mutation and 5 had a concurrent *gyrA* mutation. However, 11/12 cases were cured with the doxycycline+sitafloxacin combination. Of note, the 1 treatment failure occurred in a case with only the *parC* G248T/S83I mutation, no concurrent *gyrA* mutation, and no more detectable resistance than cured cases.

Of note, sitafloxacin alone might have cured some or all infections. Further studies comparing sequential and combination therapy with doxycyline+sitafloxacin in highly resistant *M. genitalium* are needed. However, treatment failures, particularly in cases with concurrent *parC* and *gyrA* mutations, would be expected. Moreover, the variable duration of preceding doxycycline may have improved cure.

In conclusion, our results provide important early data on the efficacy and tolerability of doxycycline+sitafloxacin combination therapy to cure highly resistant *M. genitalium* infections. This approach could become part of a broader stewardship strategy to evaluate combination therapy, which might be needed to further prevent development of antimicrobial-resistant *M. genitalium*.

Acknowledgments

We thank the staff at Melbourne Sexual Health Centre for collecting the clinical data for this study, Afrizal Afrizal and Jun Kit Sze for their help with maintaining our electronic patient database, and the laboratory staff at the Royal Women's Hospital for handling the specimens.

This work was supported by Monash University Central Clinical School departmental scholarship to D.D. and the National Health and Medical Research Council Early Career Fellowship to E.P.F.C. (no. 1091226).

G.M. reports holding joint grants with SpeeDx Pty. Ltd (https://plexpcr.com) outside the submitted work. Melbourne Sexual Health Centre receives institutional funding from Speedx Pty Ltd for support in other research projects on *Mycoplasma genitalium*, in which C.S.B., M.D., and C.K.F. are involved. E.P.F.C. reports grants from Merck & Co. (https://www.merck.com) and Seqirus Australia (https://www.seqirus.com) outside the submitted work. C.K.F. reports grants from SpeeDx Pty. Ltd. during the study. C.S.B. reports grants from SpeeDx Pty. Ltd. outside the submitted work. All other authors report no potential conflicts.

About the Author

Ms. Durukan is an MD-PhD candidate at Monash University, Clayton, Victoria, Australia. Her primary research interests are sexually transmitted infections and epidemiology.

References

1. Bradshaw CS, Jensen JS, Waites KB. New horizons in *Mycoplasma genitalium* treatment. J Infect Dis. 2017; 216(suppl_2):S412–S9. https://doi.org/10.1093/infdis/jix132
2. Hamasuna R, Le PT, Kutsuna S, Furubayashi K, Matsumoto M, Ohmagari N, et al. Mutations in *ParC* and *GyrA* of moxifloxacin-resistant and susceptible *Mycoplasma genitalium* strains. PLoS One. 2018;13:e0198355. https://doi.org/10.1371/journal.pone.0198355
3. Braam JF, van Dommelen L, Henquet CJM, van de Bovenkamp JHB, Kusters JG. Multidrug-resistant *Mycoplasma genitalium* infections in Europe. Eur J Clin Microbiol Infect Dis. 2017;36:1565–7. https://doi.org/10.1007/s10096-017-2969-9
4. Xiao L, Waites KB, Van Der Pol B, Aaron KJ, Hook EW III, Geisler WM. *Mycoplasma genitalium* infections with macrolide and fluoroquinolone resistance-associated mutations in heterosexual African American couples in Alabama. Sex Transm Dis. 2019;46:18–24. https://doi.org/10.1097/OLQ.0000000000000891
5. Murray GL, Bodiyabadu K, Danielewski J, Garland SM, Machalek DA, Fairley CK, et al. Moxifloxacin and sitafloxacin treatment failure in *Mycoplasma genitalium* infection: sssociation with *parC* mutation G248T (S83I) and concurrent *gyrA* mutations. J Infect Dis. 2020;221:1017–1024. PubMed https://doi.org/10.1093/infdis/jiz550
6. Machalek D, Tao Y, Shilling H, Jensen J, Unemo M, Murray G, et al. P601 Macrolide and fluoroquinolone resistance-associated mutations in *Mycoplasma genitalium*: a systematic review and meta-analysis. Sex Transm Infect. 2019;95(Suppl 1):A266. https://doi.org/10.1136/sextrans-2019-sti.669
7. Durukan D, Read TRH, Murray G, Doyle M, Chow EPF, Vodstrcil LA, et al. Resistance-guided antimicrobial therapy using doxycycline-moxifloxacin and doxycycline-2.5g azithromycin for the treatment of *Mycoplasma genitalium* infection: efficacy and tolerability. Clin Infect Dis. 2019 Oct 20 [Epub ahead of print]. https://doi.org/10.1093/cid/ciz10312019
8. Soni S, Horner P, Rayment M, Pinto-Sander N, Naous N, Parkhouse A, et al. British Association for Sexual Health and HIV national guideline for the management of infection with *Mycoplasma genitalium* (2018). Int J STD AIDS. 2019;30:938–50. https://doi.org/10.1177/0956462419825948
9. Australia Sexual Health Alliance. Australian STI management guidelines for use in primary care. Sydney, Australia: The Alliance; 2018 [cited 2019 Dec 3]. http://www.sti.guidelines.org.au
10. Read TRH, Jensen JS, Fairley CK, Grant M, Danielewski JA, Su J, et al. Use of pristinamycin for macrolide-resistant *Mycoplasma genitalium* infection. Emerg Infect Dis. 2018;24:328–35. https://doi.org/10.3201/eid2402.170902
11. Takahashi S, Hamasuna R, Yasuda M, Ito S, Ito K, Kawai S, et al. Clinical efficacy of sitafloxacin 100 mg twice daily for 7 days for patients with non-gonococcal urethritis. J Infect Chemother. 2013;19:941–5. https://doi.org/10.1007/s10156-013-0620-y
12. Read TRH, Fairley CK, Murray GL, Jensen JS, Danielewski J, Worthington K, et al. Outcomes of resistance-guided sequential treatment of *Mycoplasma genitalium* infections: a prospective evaluation. Clin Infect Dis. 2019;68:554–60. https://doi.org/10.1093/cid/ciy477

Address for correspondence: Duygu Durukan, Melbourne Sexual Health Centre, 580 Swanston St, Carlton 3053, VIC, Australia; email: duygu.durukan@monash.edu

Autochthonous Gnathostomiasis in Madagascar

Annie Raharisoa,[1] Arezki Izri,[1] Romain Lovanirina Andrianjafy, Ranto Andriantsilavina Rajaona, Anthony Marteau, Remy Durand, Mohammad Akhoundi

We used molecular tools to identify an autochthonous case of gnathostomiasis in Madagascar. This severe ocular infection, caused by *Gnathostoma spinigerum* nematodes, led to vision loss in the patient's left eye. Clinicians should be aware of this parasitosis in Madagascar and other countries in Africa.

Human gnathostomiasis is a foodborne parasitic zoonosis caused by spiruroid nematodes of the genus *Gnathostoma* (*1*). There are 13 species of *Gnathostoma*, including 6 from Asia and 7 from the Americas. Of these species, 4 (*G. spinigerum*, *G. hispidum*, *G. doloresi*, and *G. nipponicum*) in Asia and 1 (*G. binucleatum*) in Latin America are pathogenic to humans (*2*). The life cycle of the parasite requires ≥3 hosts, some of which might be paratenic. Host species vary depending on the *Gnathostoma* species; for most *Gnathostoma* species, humans are accidental dead-end hosts. Ingestion of the third larval stage of *Gnathostoma* spp. in raw or undercooked freshwater fish, eels, frogs, reptiles, or birds results in cutaneous, and sometimes visceral, larva migrans. Other proposed routes of infection include drinking water contaminated with infected *Cyclops* spp. crustaceans and transcutaneous penetration during the preparation of contaminated food (*3*). Clinical signs and symptoms of infection depend on the affected organ(s) (*3*,*4*), which might include the skin; gastrointestinal or genitourinary tracts; lungs; and, more rarely, the central nervous system and the eyes (*5*). Infection results in nonspecific signs and symptoms, such as fever, urticaria, anorexia, nausea, vomiting, and diarrhea, accompanied by larval migration; in the case of central nervous system involvement, infection can be fatal (*3*). Painful or pruritic migratory subcutaneous edema is the most common symptom of *Gnathostoma* infection. Physicians diagnose gnathostomiasis on the basis of eosinophilia, migratory lesions, and the patient's history of geographic and dietary exposures (*6*).

Author affiliations: Avicenne Hospital, Bobigny, France (A. Raharisoa, A. Izri, A. Marteau, R. Durand, M. Akhoundi); Centre Hospitalier Universitaire Joseph Ravoahangy Andrianavalona, Antananarivo, Madagascar (A. Raharisoa, R.L. Andrianjafy, R.A. Rajaona); IHU Méditerranée Infection, Marseille, France (A. Izri); Université Paris-Saclay, Châtenay-Malabry, France (R. Durand)

DOI: https://doi.org/10.3201/eid2608.200383

The Study

In November 2016, a 24-year-old female farmer noticed an ecchymotic edema in the upper and lower eyelids of her right eye. She lived with her family in a village next to Anjozorobe, a city located 90 km northwest of Antananarivo, Madagascer, and had no history of travel abroad. She had no history of ocular problems or allergic reactions.

In the following days, the development of conjunctivitis and reduction in visual acuity prompted her to visit the general practitioner. The physician prescribed her a 3-week treatment including several antimicrobial medications. This regimen did not result in clinical improvement. In December 2016, the physician referred her to the Hospital Centre of Joseph Ravoahangy Andrianavalona Ampefiloha (Antananarivo) as a result of her worsening condition.

The interview and clinical examination revealed ptosis, preseptal cellulitis with an abscess, and decreased visual acuity of the right eye. She also had a unilateral headache on the same side (subjective pain rating 4/10). Blood measurements including erythrocyte sedimentation rate, neutrophilic leukocyte count, eosinophil count, and hepatic aminotransferases (aspartate aminotransferase, alanine aminotransferase) were within reference limits. Leukoconcentration and parasitological analysis by microscopy of a thick blood smear did not indicate microfilaria infection. Abdominal ultrasound examination revealed no hepatic or splenic abnormalities. We drained the abscess and prescribed a first-line empirical treatment of gentamicin, metronidazole, and levofloxacin. On the 7th day of hospitalization, the patient reported a sudden pain in the other eye. We conducted a slit-lamp examination,

[1]These first authors contributed equally to this article.

Figure 1. Anterior view of the third-stage larva of *Gnathostoma spinigerum* isolated from left eye of a woman in Madagascar, 2016. Scale bar indicates 1 mm.

which revealed a worm in the anterior chamber of the left eye. We removed the mobile worm from the left eye through a small sclerocorneal tunnel.

Ocular ultrasound analysis showed a thickened retina. Doppler analysis revealed a hypervascularisation with an inflammatory appearance associated with a retinal detachment or an echodetectable foreign body. Ophthalmologic evaluation of the left eye by funduscopic examination revealed preretinal and vitreous hemorrhages. We prescribed mebendazole (100 mg 2×/d for 21 days) to treat further probable infection by *Gnathostoma* parasites. Unfortunately, the long delay to correct diagnosis and treatment led to blindness in the patient's left eye.

Macroscopic examination of the extracted parasite revealed a white cylindrical body 12 mm long and 4 mm wide. Microscopic analysis showed an organism with a bulbous head, a cephalic region covered by transverse rows of cuticular spines, a body curved at the middle, and a shortened anterior end (Figure 1). These morphologic criteria (i.e., body shape, number of rows of hooks at the cephalic end, the spines covering the body) enabled us to identify the worm as a member of a *Gnathostoma* sp. (*3*).

For further identification, we extracted the DNA of the worm using Chelex 10% (Bio-Rad, https://www.bio-rad.com). We then performed a conventional PCR selective for an 800-bp fragment of the cytochrome oxidase I gene (*7*). BLAST analysis (http://blast.ncbi.nlm.nih.gov/Blast.cgi) identified the specimen as *G. spinigerum* because it shared ≥99% identity with an isolate from GenBank (accession no. MK033968). We deposited the corresponding sequence in GenBank (accession no. LC505621). We constructed an inferred phylogenetic tree of *G. spinigerum* with GenBank sequences using MEGA version 5.0 software (*8*). Our MEGA analysis used the neighbor-joining method with bootstrap values determined by 1,000 replicates (Figure 2). All sequences, including the one originating from Madagascar, clustered in the same species group. This grouping occurred despite the absence of sequences from other African *Gnathostoma* species.

Conclusions

Gnathostomiasis is endemic to Southeast Asia, Central America, and South America. A few cases have also been reported from nonendemic regions such as Australia (*9*). Until 2003, this disease was not thought to be endemic in Africa. However, reports of imported cases from Zambia, South Africa, and Botswana ruled out this hypothesis (*5*,*10*–*13*). Furthermore, zoonotic *Gnathostoma* infection has been reported from Zambia (*10*). In 2000, a case of clinical gnathostomiasis was reported in a 43-year-old traveler returning to Italy from Madagascar (*14*).

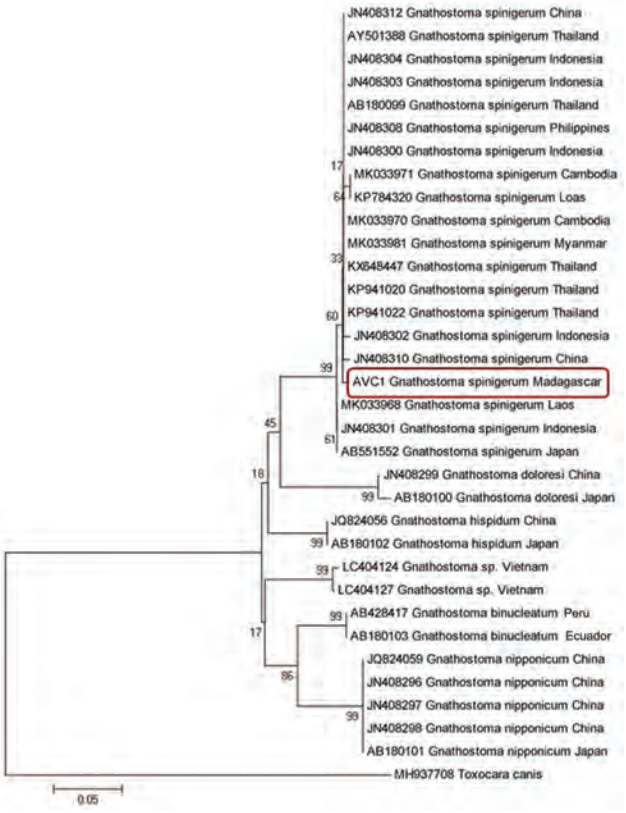

Figure 2. Neighbor-joining phylogenetic tree of *Gnathostoma spinigerum* isolated from a woman in Madagascar, 2016 (red box), and reference sequences from GenBank. The tree was constructed using MEGA (*8*) with bootstrap values determined by 1,000 replicates and compares the cytochrome oxidase I gene sequences.

G. spinigerum nematodes, whose primary hosts are cats and dogs, are widely distributed in tropical and subtropical areas, especially in Asia. Consumption of raw meat or freshwater fish in endemic areas is the major risk factor for infection. Consequently, we believe this infection was acquired through eating raw fish or drinking water contaminated by copepods. After being ingested, the larvae probably passed through the gastrointestinal barrier and migrated through the bloodstream to the ocular system. Our patient regularly used the freshwater river near her house for drinking and sanitary purposes. This practice leads us to consider contaminated freshwater, rather than the ingestion of raw fish, as a probable source of her infection. The habit of eating raw meat or fish may explain the higher incidence of *Gnathostoma* infection in some regions of the world, such as Southeast Asia (*7*).

Diagnosing gnathostomiasis can be difficult for physicians who are unfamiliar with this nematode, especially in nonendemic regions. This lack of physician awareness might lead to missed or delayed diagnosis. Physicians should also screen family members of affected patients because many families share eating habits. In this case, we evaluated the patient's relatives with clinical (checks for painful migratory skin lesions or skin nodules, eye damage) and biological (eosinophil count, erythrocyte sedimentation rate) examinations. We did not observe any signs of infection.

Albendazole and ivermectin are usually considered the best treatments for gnathostomiasis (*12*,*13*). In this case, we prescribed mebendazole according to a local protocol used to cure a wide spectrum of nematode infections.

In conclusion, we used molecular tools to identify a case of *G. spinigerum* in Madagascar. Previous studies in Africa have relied only on morphology for species confirmation. Clinicians should be aware of the existence of gnathostomiasis in Madagascar and other countries in Africa and also of the potentially severe complications associated with ocular gnathostomiasis.

About the Author

Dr. Annie Raharisoa is a medical parasitologist in the department of Parasitology-Mycology at University-Hospital Centre of Joseph Ravoahangy Andrianavalona Ampefiloha, Antananarivo. Her primary research interests include tropical parasitic infections and helminthology.

References

1. Bravo F, Gontijo B. Gnathostomiasis: an emerging infectious disease relevant to all dermatologists. An Bras Dermatol. 2018; 93:172–80. https://doi.org/10.1590/abd1806-4841.20187498
2. Jongthawin J, Intapan PM, Sanpool O, Sadaow L, Janwan P, Thanchomnang T, et al. Three human gnathostomiasis cases in Thailand with molecular identification of causative parasite species. Am J Trop Med Hyg. 2015;93:615–8. https://doi.org/10.4269/ajtmh.15-0284
3. Herman JS, Chiodini PL. Gnathostomiasis, another emerging imported disease. Clin Microbiol Rev. 2009;22:484–92. https://doi.org/10.1128/CMR.00003-09
4. Katchanov J, Sawanyawisuth K, Chotmongkol V, Nawa Y. Neurognathostomiasis, a neglected parasitosis of the central nervous system. Emerg Infect Dis. 2011;17:1174–80. https://doi.org/10.3201/eid1707.101433
5. Nawa Y, Katchanov J, Yoshikawa M, Rojekittikhun W, Dekumyoy P, Kusolusuk T, et al. Ocular gnathostomiasis: a comprehensive review. The Journal of Tropical Medicine and Parasitology. 2010;33:77–86.
6. Herman JS, Wall EC, van Tulleken C, Godfrey-Faussett P, Bailey RL, Chiodini PL. Gnathostomiasis acquired by British tourists in Botswana. Emerg Infect Dis. 2009;15:594–7. https://doi.org/10.3201/1504.081646
7. Boonroumkaew P, Sanpool O, Rodpai R, Sadaow L, Somboonpatarakun C, Laymanivong S, et al. Molecular identification and genetic diversity of Gnathostoma spinigerum larvae in freshwater fishes in southern Lao PDR, Cambodia, and Myanmar. Parasitol Res. 2019;118:1465–72. https://doi.org/10.1007/s00436-019-06292-z
8. Tamura K, Peterson D, Peterson N, Stecher G, Nei M, Kumar S. MEGA5: molecular evolutionary genetics analysis using maximum likelihood, evolutionary distance, and maximum parsimony methods. Mol Biol Evol. 2011;28:2731–9. https://doi.org/10.1093/molbev/msr121
9. Jeremiah CJ, Harangozo CS, Fuller AJ. Gnathostomiasis in remote northern Western Australia: the first confirmed cases acquired in Australia. Med J Aust. 2011;195:42–4. https://doi.org/10.5694/j.1326-5377.2011.tb03188.x
10. Hale DC, Blumberg L, Frean J. Case report: gnathostomiasis in two travelers to Zambia. Am J Trop Med Hyg. 2003;68:707–9. https://doi.org/10.4269/ajtmh.2003.68.707
11. Müller-Stöver I, Richter J, Häussinger D. Infection with Gnathostoma spinigerum as a cause of eosinophilic oesophagitis [in German]. Dtsch Med Wochenschr. 2004;129:1973–5. https://doi.org/10.1055/s-2004-831835
12. Frean J. Gnathostomiasis acquired by visitors to the Okavango Delta, Botswana. Trop Med Infect Dis. 2020;5:39. https://doi.org/10.3390/tropicalmed5010039
13. Moore DA, McCroddan J, Dekumyoy P, Chiodini PL. Gnathostomiasis: an emerging imported disease. Emerg Infect Dis. 2003;9:647–50. https://doi.org/10.3201/eid0906.020625
14. Veraldi S, Carrera C, Pravettoni C, Alessi E. A case of suspected cutaneous gnathostomiasis. G Ital Dermatol Venereol. 2000;135:363–5.

Address for correspondence: Mohammad Akhoundi, Parasitology-Mycology Department, Avicenne Hospital, AP-HP, Sorbonne Paris Nord University, 125 route de Stalingrad, 93009 Bobigny CEDEX, France; email: m.akhoundi@yahoo.com

Genotypic Heterogeneity of *Orientia tsutsugamushi* in Scrub Typhus Patients and Thrombocytopenia Syndrome Co-infection, Myanmar

Aye Marlar Win,[1] Yen Thi Hai Nguyen,[1] Yuri Kim,[1] Na-Young Ha, Jun-Gu Kang, Hongil Kim, Bo San, Okkar Kyaw, Wah Win Htike, Dong-Ok Choi, Keun-Hwa Lee,[2] Nam-Hyuk Cho[2]

Serologic and molecular surveillance of serum collected from 152 suspected scrub typhus patients in Myanmar revealed *Orientia tsutsugamushi* of genotypic heterogeneity. In addition, potential co-infection with severe fever with thrombocytopenia syndrome virus was observed in 5 (3.3%) patients. Both scrub typhus and severe fever with thrombocytopenia syndrome are endemic in Myanmar.

Scrub typhus is a miteborne febrile illness caused by the bacterium *Orientia tsutsugamushi*, which is endemic in the Asia-Pacific region and a major cause of undifferentiated febrile disease (*1*). *O. tsutsugamushi* infections were documented in Myanmar during the 1940s (*2*). Since then, however, no report has described the prevalence and genetics of scrub typhus in Myanmar, although 2 studies, including 1 from 2017, identified scrub typhus as one of the primary infections causing acute febrile illness on the Thailand–Myanmar border (*3*,*4*). These results underscore the need for research on this vectorborne infection in Myanmar, including studies defining the genotypic diversity of *O. tsutsugamushi*. Lack of this information has been a serious obstacle to developing effective diagnostic methods and a vaccine for scrub typhus (*1*).

The tickborne virus severe fever with thrombocytopenia syndrome virus (SFTSV), of the genus *Banyangvirus*, can cause hemorrhagic fever with a mortality rate of up to 40% (*5*). SFTSV infections are endemic in eastern Asia, and retrospective studies have confirmed its presence in China in 1996 (*6*), South Korea in 2000 (*7*), Japan in 2005 (*8*), and Vietnam in 2017 (*9*). In addition, mixed infection with SFTSV and *O. tsutsugamushi* has been detected in patients in South Korea, where both pathogens are endemic (*7*,*10*). These results further emphasize the urgent need for epidemiologic studies of vectorborne diseases in areas of endemicity to improve our ability to accurately differentiate febrile infectious diseases with atypical signs and symptoms during the initial stages so they can be promptly treated. Here, we used blood samples from suspected scrub typhus patients in Myanmar to investigate the serologic prevalence and genotypic diversity of *O. tsutsugamushi*. We also examined these patients for possible co-infection with SFTSV, which has been an emerging threat to public health in eastern Asia.

The Study

To investigate the genotypic diversity of *O. tsutsugamushi* and potential co-infection with SFTSV in Myanmar, we collected whole blood samples from 152 clinically suspected scrub typhus patients (Table; Appendix Table 1, https://wwwnc.cdc.gov/EID/article/26/8/20-0135-App1.pdf) in Sagaing and Magway Provinces (Figure 1) during February 2018–January 2019. Mean age of the suspected scrub typhus patients was 27 ± 19.8 years (range of 2–73 years). We observed eschar, a selection criteria for scrub typhus, in 144 (94.7%) of the 152 patients. Mean fever duration was 6 days (SD ± 2.9 days).

Author affiliations: University of Medicine 1, Yangon, Myanmar (A.M. Win, O. Kyaw, W.W. Htike); Seoul National University College of Medicine, Seoul, South Korea (Y.T.H. Nguyen, Y. Kim, N.-Y. Ha, J.-G. Kang, H. Kim, N.-H. Cho); Private practitioner, Sagaing, Myanmar (B. San); Bore Da Biotech, Seongnam, South Korea (D.-O. Choi); Hanyang University College of Medicine, Seoul (K.-H. Lee); Seoul National University Medical Research Center and Bundang Hospital, Seoul (N.-H. Cho)

DOI: https://doi.org/10.3201/eid2608.200135

[1]These first authors contributed equally to this article.

[2]These authors were co–principal investigators.

Table. Baseline characteristics and summary of serologic and molecular diagnosis of suspected scrub typhus patients enrolled in study of genotypic heterogeneity of *Orientia tsutsugamushi*, Myanmar

Category	Value
Age	
Age, y mean ± SD	27.0 ± 19.8
Age distribution, y	
≤10	38 (25.0)
11–20	38 (25.0)
21–30	23 (15.1)
31–40	10 (6.6)
41–50	17 (11.0)
51–60	16 (10.5)
≥61	10 (6.6)
Sex ratio, M:F (% male)	93/59 (61.2)
Clinical variables	
Fever duration, d, mean ±SD	6.1 ± 2.9
Eschar	144 (94.7)
Rash	3 (2.0)
Myalgia	25 (20)
Method of diagnosis of scrub typhus	
ICT	41/128 (32.0)
TSA56 IgG	36/128 (28.1)
ScaA IgG	25/128 (19.5)
IFA	138/152 (90.8)
O. tsutsugamushi IgG	119/152 (78.3)
O. tsutsugamushi IgM	90/152 (59.2)
PCR (*tsa56*)	9/152 (5.9)
Method of diagnosis of SFTSV	
RT-PCR	5/152 (3.3)

*Values are no. (%) patients or no. patients/no. tested (%) except as indicated. ICT, immunochromatography test; IFA, indirect immunofluorescence assay; RT-PCR, reverse transcription PCR; SFTSV, severe fever with thrombosis syndrome virus.

For initial serologic diagnosis of 128 serum samples, we used immunochromatography test strips coated with TSA56 and ScaA antigens, which revealed respective positive rates of 28.1% (36/128) and 19.5% (25/128); the overall positive rate was 32.0% (41/128). Of the 128 samples, 20 (15.6%) reacted with both antigens and 5 of 36 (13.9%) were positive for ScaA antigen only (Table; Appendix Figure 1), suggesting a potential applicability of ScaA antigen, when used simultaneously with TSA56 antigen, for the diagnosis of scrub typhus during the acute phase (*11*). To confirm serologic positivity against the bacterial antigen, we also conducted an indirect immunofluorescence assay using cells infected with *O. tsutsugamushi*, the standard method for diagnosing scrub typhus (*12*). Among the 152 serum samples we tested, results were positive (≥1:40) for 119 (78.3%) for specific IgG and for 90 (59.2%) for IgM (Table; Appendix Table 1). Median titers of the positive serum samples were 1:640 for both IgG and IgM. Among the suspected scrub typhus patients, test results for 13 (8.6%) serum samples were negative for both IgG and IgM against *O. tsutsugamushi*.

For molecular diagnosis of scrub typhus, we examined all the serum samples by PCR to confirm infection and identify the genotypes of *O. tsutsugamushi* in the patients in Myanmar. From the 152 serum samples, we detected specific PCR products in 9 (5.9%) and sequenced them for genotyping. We compared results of phylogenetic analysis of the 9 *tsa56* gene sequences with sequences from 17 protogenotypes (*1*), which revealed ≥5 genotypes, including Karp_A (4/9, 44.4%), Karp_B (1/9, 11.1%), Kato_B (2/9, 22.2%), Gilliam (1/9, 11.1%), and JG_C (1/9, 11.1%) (Figure 2).

Figure 1. Locations in Sagaing and Magway Provinces in Myanmar, where suspected scrub typhus patients' serum samples were collected for study of genotypic heterogeneity of *Orientia tsutsugamushi*.

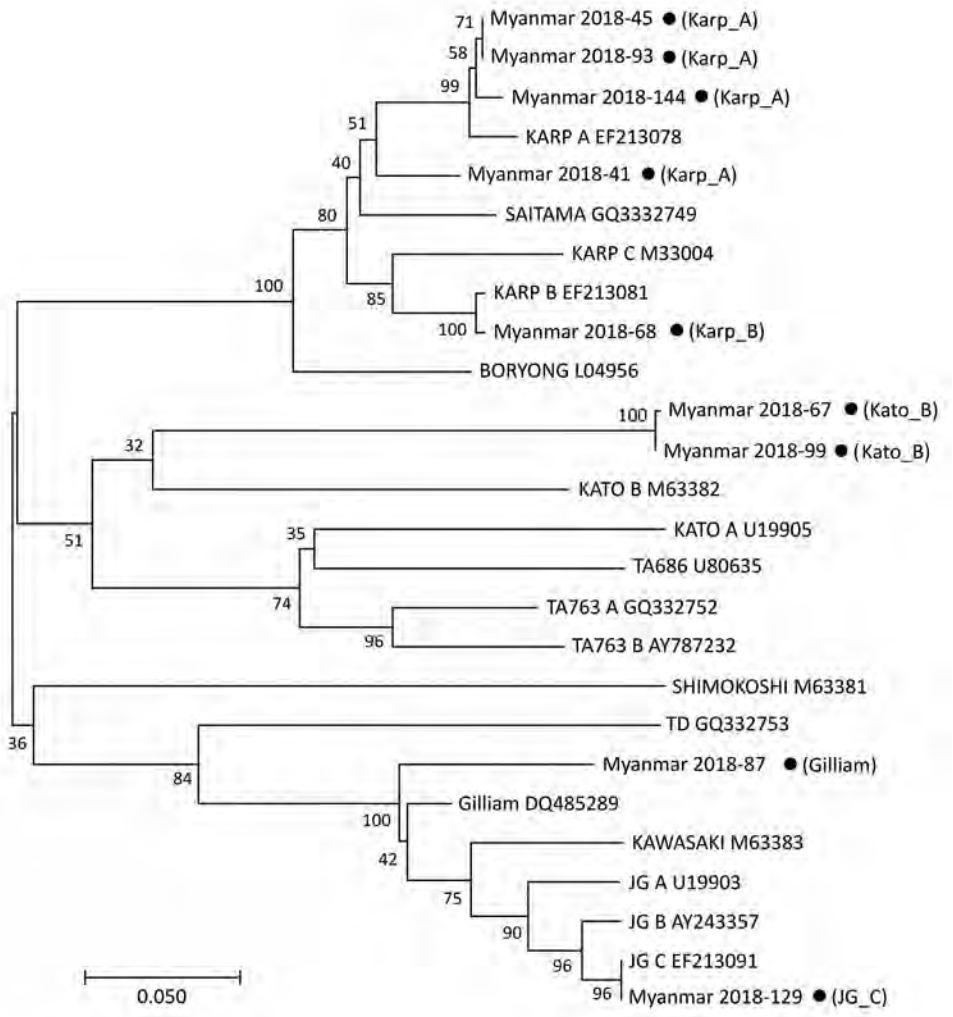

Figure 2. Phylogenetic tree constructed on the basis of *Orientia tsutsugamushi tsa56* gene sequences for scrub typhus patients in Myanmar (black dots) and reference sequences. The tree was constructed using the maximum likelihood method with MEGA7 (http://www.megasoftware.net). The *tsa56* gene sequences identified in this study are indicated by black circles and compared with 17 representative genotype sequences reported by a previous study (*1*). The percentage of replicate trees in which the associated genotypes clustered together in the bootstrap test (1,000 replicates) is shown next to the branches.

Finally, we used reverse transcription PCR analysis to investigate possible SFTSV infection in the patients (*7*,*9*,*13*). Among 152 patients' serum samples, 5 (3.3%) were positive for the partial small (S) segment of the SFTSV RNA genome, indicating SFTSV infection. Results from phylogenetic analysis of the partial S segment sequences showed that 4 isolates were the same as those previously reported from Vietnam (*9*); 1 isolate differed by 1 base from the other 4 isolates (Appendix Figure 2), suggesting genetic homogeneity of SFTSV in southern Asia. Of note, 4 out of the 5 SFTSV-positive patients had eschar, and 4 were <15 years of age (Appendix Figure 2). Furthermore, 3 of them carried high titers (≥1:2560) of IgG, IgM, or both specific to *O. tsutsugamushi*, as measured by indirect immunofluorescence assay (Appendix Table 1), suggesting co-infection with scrub typhus. All patients were successfully treated and recovered, including the SFTSV-positive febrile patients, after 5–7 days of fever.

Conclusions

We observed a high prevalence of antibodies against *O. tsutsugamushi* in suspected scrub typhus patients in Myanmar, suggesting that scrub typhus, previously reported in the 1940s, remains prevalent in this country (*2*). Of note, a high prevalence of scrub typhus in children was confirmed (*4*); therefore, young children with febrile illness should be carefully observed for early diagnosis and treatment of scrub typhus. Because we were only able to examine serum samples collected from patients during the acute phase of infection and could not assess the rise of antibody titers in paired samples collected in convalescent phases, we were not able to confirm the exact rate of prevalence of scrub typhus in the suspected patients. The baseline levels of antibody titers against *O. tsutsugamushi* in healthy persons need to be assessed to determine the cutoff titer levels for diagnosing acute scrub typhus in the endemic region (*14*).

In addition, genotyping *O. tsutsugamushi* revealed that ≥5 different genotypes are currently present and showed genetic heterogeneity in Myanmar. Moreover, we detected possible co-infection with SFTSV and *O. tsutsugamushi* in 5 patients. None of these patients had a history of travel abroad, and all live in the same village in Sagaing Province, suggesting that there may be hot spots for SFTSV infection. Co-infection with *O. tsutsugamushi* and SFTSV might be mediated by either simultaneous transmission from 2 different vectors each carrying 1 pathogen or by a single tick or mite species carrying both pathogens (*10*). Four of 5 SFTSV-positive patients were <15 years of age, and all 5 recovered within a week. Given that the disease severity of SFTS is associated with host age and the viral genotype (*15*), milder clinical symptoms observed in these patients might have been because of exposure at a younger age or prevalence of less virulent genotypes of SFTSV in Myanmar. Therefore, continuous surveillance of SFTS patients needs to be conducted, reporting detailed clinical manifestations and associated viral genotypes prevalent in the local area. In addition, more reliable differential diagnosis techniques and prevention and control measures are required for better clinical practices and outcomes in the endemic regions of multiple tickborne and miteborne pathogens.

This work was supported by a grant from the National Research Foundation of Korea (grant number: 2017M3A9E4061998) and the Korean Health Technology R&D Project of the Ministry of Health & Welfare, Republic of Korea (grant number: HI15C2891). N.T.H.Y., Y.K., N.Y.H., J.G.K., and H.K. received a scholarship from the BK21-plus education program provided by the National Research Foundation of Korea.

About the Author

Dr. Win is a medical microbiologist working at the University of Medicine 1, Yangon, Myanmar. Her primary research interests are epidemiology and pathogenesis of various infectious diseases endemic in Myanmar.

References

1. Kim G, Ha NY, Min CK, Kim HI, Yen NTH, Lee KH, et al. Diversification of *Orientia tsutsugamushi* genotypes by intragenic recombination and their potential expansion in endemic areas. PLOS Neglect Trop Dis. 2017;11:e0005408. PubMed https://doi.org/10.1371/journal.pntd.0005408
2. Davis GE, Austrian RC, Bell EJ. Observations on tsutsugamushi disease (scrub typhus) in Assam and Burma: the recovery of strains of *Rickettsia orientalis*. Am J Hyg. 1947;46:268–86. https://doi.org/10.1093/oxfordjournals.aje.a119168
3. Parola P, Miller RS, McDaniel P, Telford SR III, Rolain JM, Wongsrichanalai C, et al. Emerging rickettsioses of the Thai-Myanmar border. Emerg Infect Dis. 2003;9:592–5. https://doi.org/10.3201/eid0905.020511
4. Brummaier T, Kittitrakul C, Choovichian V, Lawpoolsri S, Namaik-Larp C, Wattanagoon Y. Clinical manifestations and treatment outcomes of scrub typhus in a rural health care facility on the Thailand-Myanmar border. J Infect Dev Ctries. 2017;11:407–13. https://doi.org/10.3855/jidc.8912
5. Liu S, Chai C, Wang C, Amer S, Lv H, He H, et al. Systematic review of severe fever with thrombocytopenia syndrome: virology, epidemiology, and clinical characteristics. Rev Med Virol. 2014;24:90–102. https://doi.org/10.1002/rmv.1776
6. Hu J, Shi C, Li Z, Guo X, Qian Y, Tan W, et al. A cluster of cases of severe fever with thrombocytopenia syndrome bunyavirus infection in China, 1996: a retrospective serological study. PLoS Negl Trop Dis. 2018;12:e0006603. https://doi.org/10.1371/journal.pntd.0006603
7. Thi Hai Yen N, Kim C, Jeong S, Jeon K, Choi H, Ro HJ, et al. Severe fever with thrombocytopenia syndrome virus infection or mixed infection with scrub typhus in South Korea in 2000–2003. Am J Trop Med Hyg. 2019;101:1096–9. https://doi.org/10.4269/ajtmh.19-0392
8. Takahashi T, Maeda K, Suzuki T, Ishido A, Shigeoka T, Tominaga T, et al. The first identification and retrospective study of severe fever with thrombocytopenia syndrome in Japan. J Infect Dis. 2014;209:816–27. https://doi.org/10.1093/infdis/jit603
9. Tran XC, Yun Y, Van An L, Kim SH, Thao NTP, Man PKC, et al. Endemic severe fever with thrombocytopenia syndrome, Vietnam. Emerg Infect Dis. 2019;25:1029–31. https://doi.org/10.3201/eid2505.181463
10. Ra SH, Kim JY, Cha HH, Kwon JS, Lee HJ, Jeon NY, et al. Coinfection of severe fever with thrombocytopenia syndrome and scrub typhus in patients with tick-borne illness. Am J Trop Med Hyg. 2019;101:1259–62. https://doi.org/10.4269/ajtmh.19-0242
11. Watthanaworawit W, Turner P, Turner C, Tanganuchitcharnchai A, Jintaworn S, Hanboonkunupakarn B, et al. Diagnostic accuracy assessment of immunochromatographic tests for the rapid detection of antibodies against *Orientia tsutsugamushi* using paired acute and convalescent specimens. Am J Trop Med Hyg. 2015;93:1168–71. https://doi.org/10.4269/ajtmh.15-0435
12. Paris DH, Dumler JS. State of the art of diagnosis of rickettsial diseases: the use of blood specimens for diagnosis of scrub typhus, spotted fever group rickettsiosis, and murine typhus. Curr Opin Infect Dis. 2016;29:433–9. https://doi.org/10.1097/QCO.0000000000000298
13. Yoo JR, Heo ST, Kang JH, Park D, Kim JS, Bae JH, et al. Mixed infection with severe fever with thrombocytopenia syndrome virus and two genotypes of scrub typhus in a patient, South Korea, 2017. Am J Trop Med Hyg. 2018;99:287–90. https://doi.org/10.4269/ajtmh.18-0088
14. Kim DM, Lee YM, Back JH, Yang TY, Lee JH, Song HJ, et al. A serosurvey of *Orientia tsutsugamushi* from patients with scrub typhus. Clin Microbiol Infect. 2010;16:447–51. https://doi.org/10.1111/j.1469-0691.2009.02865.x
15. Yun SM, Park SJ, Kim YI, Park SW, Yu MA, Kwon HI, et al. Genetic and pathogenic-diversity of severe fever with thrombocytopenia syndrome (SFTSV) in South Korea. JCI Insight. 2020;5:e129531.

Addresses for correspondence: Nam-Hyuk Cho, Seoul National University College of Medicine, 103 Daehak-ro, Jongno-gu, Seoul 03080, South Korea; email: chonh@snu.ac.kr;
Keun-Hwa Lee, Hanyang University College of Medicine, Department of Microbiology, 222 Wangsimni-ro, Seongdong-gu, Seoul 04763, South Korea; email: yomust7@gmail.com

Leishmania infantum in US-Born Dog

Marcos E. de Almeida, Dennis R. Spann, Richard S. Bradbury

Leishmaniasis is a vectorborne disease that can infect humans, dogs, and other mammals. We identified one of its causative agents, *Leishmania infantum*, in a dog born in California, USA, demonstrating potential for autochthonous infections in this country. Our finding bolsters the need for improved leishmaniasis screening practices in the United States.

Leishmaniasis is a tropical and subtropical zoonosis affecting 0.9–1.6 million persons every year. Its manifestations range from self-healing cutaneous lesions to severe visceral leishmaniasis (VL) forms that can be fatal (*1*,*2*). In the Americas, VL is usually caused by *Leishmania infantum* parasites, which several species of blood-feeding sand fly vectors can transmit to humans and other reservoirs. In urban areas, dogs are the main domestic reservoirs of *L. infantum*, maintaining the parasitic life cycle and facilitating transmission of parasites to humans and other mammals (*3*). Alternative routes of *Leishmania* spp. transmission, such as vertical transmission and dog-to-dog transmission by biting, have been associated with autochthonous canine leishmaniasis (Can-VL) (*2*–*4*). In addition, biochemical abnormalities, such as genetic mutations of macrophage proteins, have been associated with increased susceptibility to VL in some breeds, including boxers (*5*).

The accurate differentiation between clinical and subclinical infections is critical in determining the appropriate course of treatment. However, correct diagnosis of Can-VL is challenging because an absence of amastigotes in samples, including blood and tissue, does not rule out infection. Furthermore, the sensitivity and specificity of diagnostic tests vary according to the protocol of the test used (*3*). The geospatial overlap of dogs and vectors infected with *L. infantum* might be linked with human disease. For instance, in focal areas of Brazil the prevalence of infected dogs was associated with the occurrence of clinical VL cases (*8*,*9*). However, in areas to which Can-VL is endemic, attempts to control and prevent Can-VL using controversial procedures, including culling infected dogs, have failed to reduce the spread of human VL cases (*6*,*7*). In North America, most cases of leishmaniasis are acquired during travel or military service in areas to which the disease is endemic. However, leishmaniasis can also be transmitted within the United States. Sylvatic reservoir animals and sand flies, including *Lutzomyia shannoni*, *L. longipalpis*, *L. anthophora*, and *L. diabolica*, are endemic to many US states (*2*). Outbreaks and isolated cases of autochthonous Can-VL affecting foxhounds and other breeds have been reported over the past 2 decades in the United States and Canada (*2*,*3*,*10*). In addition, our laboratory identified a strain of *Leishmania mexicana* in Texas that infected >50 persons, including a patient who shared the same strain with an *L. anthophora* sand fly found in the household (*11*). Here we describe an autochthonous case of Can-VL caused by *L. infantum* sand flies in a US-born dog.

Author affiliations: Centers for Disease Control and Prevention, Atlanta, Georgia, USA (M.E. de Almeida, R.S. Bradbury); Sacramento Area Veterinary Internal Medicine, Sacramento, California, USA (D.R. Spann)

DOI: https://doi.org/10.3201/eid2608.200149

Case Report

In September 2016, a 1.3-year-old male neutered California-born boxer with no overseas travel history was brought to Sacramento Area Veterinary Internal Medicine (Sacramento, California, USA) by his owner. The dog had granulomatous cutaneous lesions, hypercalcemia, hyperphosphatemia, and hyperglobulinemia, a set of signs that prompted our diagnosis of systemic histiocytosis. The dog was from an apparently healthy litter born to an apparently healthy female relocated from Spain, a country to which Can-VL is endemic. We initially suspected lymphoma but ruled it out on the basis of splenic, lymph node, and bone marrow aspirates and a parathyroid-related peptide test that all yielded negative results. We treated the dog's cutaneous lesions and biochemical abnormalities with a tapering dosage of oral prednisone. At the next appointment 17 months after the first visit, the dog had a mildly enlarged prescapular lymph node and anemia as well as biochemical abnormalities, including hyperglobulinemia and hypoalbuminemia. He had also lost ≈3.6 kg.

In February 2018, we used light microscopy to identify structures consistent with *Leishmania* spp.

amastigotes in an aspirate of the enlarged prescapular lymph node (Figure). We also performed a *Leishmania* indirect immunofluorescence assay serology evaluation with a serial 2-fold dilution of the dog serum. We determined positivity at dilutions of ≥1:64; the sample tested positive at a titer of 2,048. In March 2018, we confirmed infection with *L. infantum* using PCR followed by DNA sequencing analysis (GenBank accession no. MN991197) as previously described (*12*).

From March through July 2018, we treated the dog with 4 courses of marbofloxacin (100 mg orally every 24 hours) and allopurinol (265 mg orally every 12 hours). In August 2018, we briefly discontinued medications because of the development of neutropenia in the dog. From November 2018 through April 2019, we treated the dog with allopurinol (300 mg every 24 hours), and in April we increased the dose (to 300 mg every 12 hours). In May 2019, strabismus, anisocoria with progressive discomfort, and ataxia developed. A neurologist consult was declined by the dog's owner, and we resumed marbofloxacin treatment. In mid-May we prescribed antiinflammatory therapy with prednisone as a palliative measure. However, these treatments did not alleviate signs, and we humanely euthanized the dog in late May. We were unable to locate siblings from the same litter for leishmaniasis testing. The breeder reported that the mother died in 2017 of an unknown cause.

Conclusions

We diagnosed Can-VL in a US-born dog. Given the lack of other risk factors for Can-VL infection, we hypothesize that the dog probably acquired infection through vertical transmission. In countries to which Can-VL is endemic, veterinarians most likely would consider leishmaniasis as a potential diagnosis for fever, granulomatous skin lesions, and weight loss in a dog. However, in the United States, veterinarians often consider leishmaniasis to be a travel-acquired disease and might not suspect this infection in a dog with similar signs. Therefore, veterinarians should consider Can-VL as a potential diagnosis, depending on the dog's travel and breeding history. Dogs infected with *Leishmania* spp. are important reservoirs, especially in areas where competent vector sand flies are found. Dogs with Can-VL, clinical or subclinical, might contribute to parasite transmission and the occurrence of VL in humans (*7*–*9*,*13*). In areas where sand fly vectors are not prevalent, infectious dogs relocated or returning from areas to which the disease is endemic can still spread Can-VL through transmission routes such as biting, blood transfusion, and breeding (*10*). Current measures to control Can-VL include the regular use of topical sand fly repellents, canine vaccination, and treatment of infected dogs (*6*,*7*).

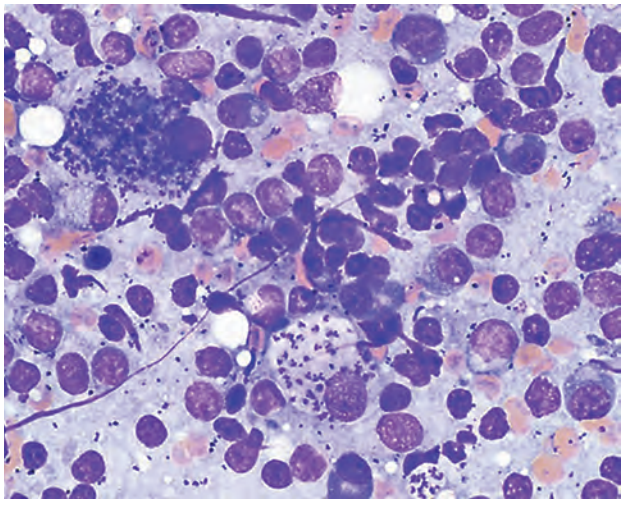

Figure. Structures resembling *Leishmania* spp. amastigotes in a lymph node sample from a 1.3-year-old male boxer, California, USA. Sample was prepared in slides stained with Giemsa and examined by light microscopy. Molecular analysis identified the species as *L. infantum*. Original magnification ×1,000.

Changing environmental factors may expand the geographic range of sand fly vectors in North America (*14*), increasing the exposure of humans and animals to the disease. The existence of competent vectors for *Leishmania* spp. in the United States has been demonstrated through a growing number of recently reported autochthonous human cases. For example, >50 human autochthonous cases of cutaneous leishmaniasis caused by *L. mexicana* have been reported in Texas and Oklahoma (*11*,*14*). Meanwhile, a possible autochthonous infection with an *Leishmania donovani* complex species in a 2-year-old boy was recently reported in North Dakota (*15*).

We hypothesize that this case of Can-VL was probably acquired through vertical transmission because of the lack of evidence supporting California as a leishmaniasis endemic region and the fact that this dog, who had no travel history, was born to a female dog relocated from Spain. Given the lack of surveillance and relative ease of dog-to-dog transmission, Can-VL is probably underreported in North America. The veterinary and public health community should be alert to the existence of autochthonous canine infections and competent vectors of *Leishmania* parasites in the United States, which might contribute to the occurrence of VL in humans. The risk for vertical transmission of Can-VL highlights the need to test all animals either relocated or retuning from areas to which the disease is endemic. This testing will be crucial to improving the surveillance and control of leishmaniasis in North America.

Acknowledgments

We thank Jacqueline Brady and Henry Bishop for the invaluable assistance on creating the tissue smears and image preparation.

About the Author

Dr. de Almeida is an associate service fellow in the Division of Parasitic Diseases and Malaria, Center for Global Health, Centers for Diseases Control and Prevention, Atlanta. His primary research interests include the development of molecular diagnostic tests for parasites.

References

1. Alvar J, Vélez ID, Bern C, Herrero M, Desjeux P, Cano J, et al.; WHO Leishmaniasis Control Team. Leishmaniasis worldwide and global estimates of its incidence. PLoS One. 2012;7:e35671. https://doi.org/10.1371/journal.pone.0035671
2. Duprey ZH, Steurer FJ, Rooney JA, Kirchhoff LV, Jackson JE, Rowton ED, et al. Canine visceral leishmaniasis, United States and Canada, 2000–2003. Emerg Infect Dis. 2006;12:440–6. https://doi.org/10.3201/eid1203.050811
3. Petersen CA, Barr SC. Canine leishmaniasis in North America: emerging or newly recognized? [vi.]. Vet Clin North Am Small Anim Pract. 2009;39:1065–74, vi. https://doi.org/10.1016/j.cvsm.2009.06.008
4. Boggiatto PM, Gibson-Corley KN, Metz K, Gallup JM, Hostetter JM, Mullin K, et al. Transplacental transmission of *Leishmania infantum* as a means for continued disease incidence in North America. PLoS Negl Trop Dis. 2011;5:e1019. https://doi.org/10.1371/journal.pntd.0001019
5. Sanchez-Robert E, Altet L, Utzet-Sadurni M, Giger U, Sanchez A, Francino O. Slc11a1 (formerly Nramp1) and susceptibility to canine visceral leishmaniasis. Vet Res. 2008;39:36. https://doi.org/10.1051/vetres:2008013
6. Dantas-Torres F, Miró G, Baneth G, Bourdeau P, Breitschwerdt E, Capelli G, et al. Canine leishmaniasis control in the context of One Health. Emerg Infect Dis. 2019;25:1–4. https://doi.org/10.3201/eid2512.190164
7. Otranto D, Dantas-Torres F. The prevention of canine leishmaniasis and its impact on public health. Trends Parasitol. 2013;29:339–45. https://doi.org/10.1016/j.pt.2013.05.003
8. Teixeira-Neto RG, da Silva ES, Nascimento RA, Belo VS, de Oliveira C, Pinheiro LC, et al. Canine visceral leishmaniasis in an urban setting of southeastern Brazil: an ecological study involving spatial analysis. Parasit Vectors. 2014;7:485. https://doi.org/10.1186/s13071-014-0485-7
9. Ursine RL, Dias JV, Morais HA, Pires HH. Human and canine visceral leishmaniasis in an emerging focus in Araçuaí, Minas Gerais: spatial distribution and socio-environmental factors. Mem Inst Oswaldo Cruz. 2016;111:505–11. https://doi.org/10.1590/0074-02760160133
10. Schaut RG, Robles-Murguia M, Juelsgaard R, Esch KJ, Bartholomay LC, Ramalho-Ortigao M, et al. Vectorborne transmission of *Leishmania infantum* from hounds, United States. Emerg Infect Dis. 2015;21:2209–12. https://doi.org/10.3201/eid2112.141167
11. Kipp EJ, de Almeida ME, Marcet P, Bradbury RS, Benedict T, Lin W, Dotson EM, Hergert M. An atypical case of autochthonous cutaneous leishmaniasis associated with naturally infected phlebotomine sand flies in Texas, United States. Am J Trop Med Hyg. In press 2020.
12. de Almeida ME, Steurer FJ, Koru O, Herwaldt BL, Pieniazek NJ, da Silva AJ. Identification of *Leishmania* spp. by molecular amplification and DNA sequencing analysis of a fragment of rRNA internal transcribed spacer 2. J Clin Microbiol. 2011;49:3143–9. https://doi.org/10.1128/JCM.01177-11
13. Courtenay O, Carson C, Calvo-Bado L, Garcez LM, Quinnell RJ. Heterogeneities in *Leishmania infantum* infection: using skin parasite burdens to identify highly infectious dogs. PLoS Negl Trop Dis. 2014;8:e2583. https://doi.org/10.1371/journal.pntd.0002583
14. McIlwee BE, Weis SE, Hosler GA. Incidence of endemic human cutaneous leishmaniasis in the United States. JAMA Dermatol. 2018;154:1032–9. https://doi.org/10.1001/jamadermatol.2018.2133
15. Douvoyiannis M, Khromachou T, Byers N, Hargreaves J, Murray HW. Cutaneous leishmaniasis in North Dakota. Clin Infect Dis. 2014;59:e73–5. https://doi.org/10.1093/cid/ciu386

Address for correspondence: Marcos de Almeida, Centers for Disease Control and Prevention, 1600 Clifton Rd NE, Mailstop H23-9, Atlanta, GA 30329-4027, USA; email: bnz0@cdc.gov

Mother-to-Child Transmission of Andes Virus through Breast Milk, Chile[1]

Marcela Ferrés, Constanza Martínez-Valdebenito, Jenniffer Angulo, Carolina Henríquez, Jorge Vera-Otárola, María José Vergara, Javier Pérez, Jorge Fernández, Viviana Sotomayor, María Francisca Valdés, Diego González-Candia, Nicole D. Tischler, Cecilia Vial, Pablo Vial, Gregory Mertz, Nicole Le Corre

Andes virus (ANDV) is the only hantavirus transmitted between humans through close contact. We detected the genome and proteins of ANDV in breast milk cells from an infected mother in Chile who transmitted the virus to her child, suggesting gastrointestinal infection through breast milk as a route of ANDV person-to-person transmission.

Andes virus (ANDV), a member of the *Orthohantavirus* genus in the *Hantaviridae* family, has a trisegmented, single-stranded RNA-genome and is the etiologic agent of hantavirus cardiopulmonary syndrome (HCPS) in Chile and Argentina (*1*). The main route of infection in humans is through the inhalation of aerosolized viral particles present in contaminated rodent excreta (*1*), but the virus can also be transmitted from person to person (*2*,*3*). During acute disease, ANDV RNA can be detected in patients' blood, respiratory secretions, saliva, gingival crevicular fluid, and urine (*2*). Epidemiologic data has suggested that person-to-person transmission mainly occurs through close contact with oral fluids during the prodromal and acute phases of infection (*2*). We report epidemiologic and virologic analyses of a mother in Chile with ANDV infection and apparent transmission to her newborn. The Ethical Review Board of Facultad de Medicina, Pontificia Universidad Católica de Chile, approved the study.

Author affiliations: Pontificia Universidad Católica de Chile, Santiago, Chile (M. Ferrés, C. Martinez-Valdebenito, J. Angulo, C. Henriquez, J. Vera-Otarola, M.J. Vergara, J. Perez, N. Le Corre); Instituto de Salud Pública de Chile, Santiago (J. Fernandez), Ministerio de Salud de Chile, Santiago (V. Sotomayor, M.F. Valdes); Fundación Ciencia & Vida, Santiago (D. Gonzalez-Candia, N. Tischler); Universidad San Sebastián, Santiago (N. Tischler); Universidad del Desarrollo, Santiago (C. Vial, P. Vial); University of New Mexico, Albuquerque, New Mexico, USA (G. Mertz)

DOI: https://doi.org/10.3201/eid2608.200204

The Study

Six days after delivery of a healthy girl, a 21-year-old woman from Parral, Chile, suffered lower-extremity myalgia and weakness. Subsequently, she noted fever of 39.5°C, severe headache, and diaphoresis; she was hospitalized 15 days after delivery. The diagnosis of ANDV infection was confirmed by real-time reverse transcription PCR for ANDV RNA in blood cells, as previously described (*4*). The patient did not report any activities with possible environmental exposure to rodent excreta. However, she had close contact with her father, who had HCPS, while caring for him during his prodromic phase, 12 days before her delivery (Figure 1). She breast-fed and took care of her newborn until day of life (DOL) 15. Although asymptomatic, the newborn was hospitalized for observation at DOL 17; at that time, ANDV IgM testing was negative (Reagenta, https://www.reagena.com). The newborn was screened several times for viral ANDV RNA in blood. On DOL 22, RT-PCR results were negative, but results were positive on DOL 30. Two days later, the baby was transferred to a pediatric intensive care unit with extracorporeal membrane oxygenation availability because of fever. However, severe HCPS developed in the newborn, and she died 4 days later.

Results of ELISA for ANDV-specific IgM/IgG in serum (Euroimmun, https://www.euroimmun.com) were positive for both the mother and the newborn. A breast milk sample tested positive for ANDV RNA on day 16 after the mother's first symptoms; previous samples of breast milk were not available. We also tested other body fluids from the newborn, including urine, saliva, and cerebrospinal fluid for ANDV RNA by real-time RT-PCR (Appendix Table, https://wwwnc.cdc.gov/EID/article/26/8/20-0204-App1.pdf).

[1]Preliminary results from this study were presented at 11th International Conference on Hantaviruses, September 1-4, 2019, Leuven, Belgium.

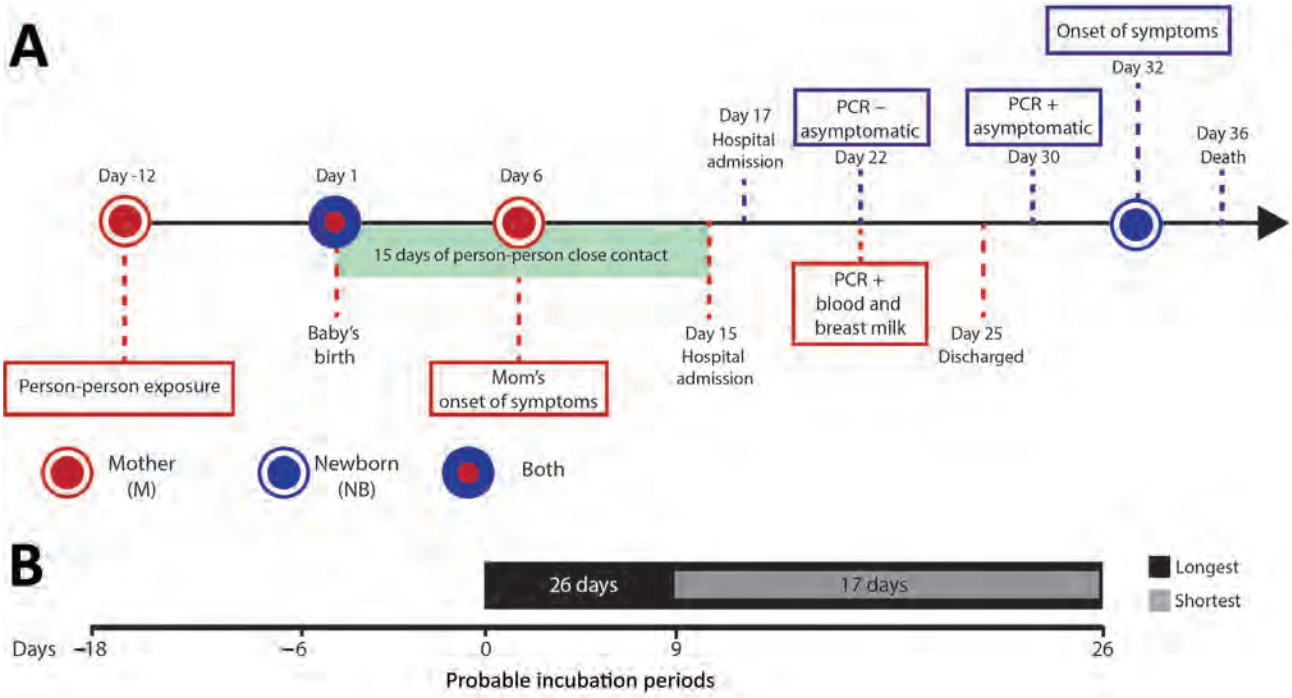

Figure 1. Epidemiologic timeline for mother-to-child transmission of Andes virus through breast milk, Chile. A) Key epidemiologic events related to the mother (represented by M, red circles and lines) and the newborn (NB, blue circle and lines). Blue-and-red circle represents the birth of the newborn; light green rectangle represents the 15 days of close contact that included breastfeeding. We show details for the baby above the time bar and details for the mother below the time bar. B) Longest (black bar) and shortest (light gray bar) probable person-to-person incubation period.

ANDV RNA has previously been detected in bodily fluids other than blood, such as saliva, respiratory secretions, and urine (*2*). Therefore, close contact with such fluids may explain additional cases for which high-risk environmental and rodent exposure is absent or improbable. In our study of the infected newborn, we ruled out environmental exposure; the only possible source was close contact to her mother during the incubation period and initial clinical disease. The mother maintained breast-feeding until the baby was hospitalized and confirmed to be viremic.

To evaluate the presence of ANDV particles in breast milk, we performed a culture in Huh-7 cells mock-infected and incubated with a breast milk pellet and, as a positive control, ANDV at a multiplicity of infection of 1 (*5*). After infection, we identified viral nucleoprotein (N) and glycoprotein (Gc) through immunofluorescence assay (Appendix). We detected N protein in the cytoplasmic compartment of ANDV-infected cells and cells incubated with breast milk but not in mock-infected cells (Figure 2, panel A). To verify detection specificity, we used 2 different ANDV N protein antibodies generated in mice and rabbits. Again, we identified N protein in ANDV-infected cells and incubated with breast milk but not in mock-infected cells (Figure 2, panel B). Moreover, N and Gc proteins were only detectable in ANDV-infected cells and cells incubated with breast milk (Figure 2, panel C). Of interest, we did not stain ANDV-infected cells from breast milk by 4′,6-diamidino-2- phenylindole (DAPI, Vectashield H1200; Vector Laboratories, Inc, https://vectorlabs.com) (Appendix Figures 1, 2); the nuclear compartment of mock-infected Huh-7 cells and ANDV positive control were stained by DAPI. ANDV-infected cells from breast milk (8 μm [SD ±1.2 μm] in diameter on the basis of 10 cells from different captured fields) were clearly smaller in size than the Huh-7 cells (27 μm [SD ± 4.3 μm]). Altogether, our results demonstrate the presence of ANDV in enucleated breast milk cells.

Breast milk contains a variety of blood cells (monocytes, T-cells, NK cells, B cells, and neutrophils) and hematopoietic stem cells (*6*). In this context, we know that ANDV can be present in buffy coat cells for up to 15 days before illness onset (*7*); is always present during the acute phase of the disease, including the febrile prodrome phase; and remains in a small proportion of cases during convalescence (*7*). Assuming that breast milk contained ANDV-infected cells, direct inoculation in Peyer's patches in the newborn may have resulted in

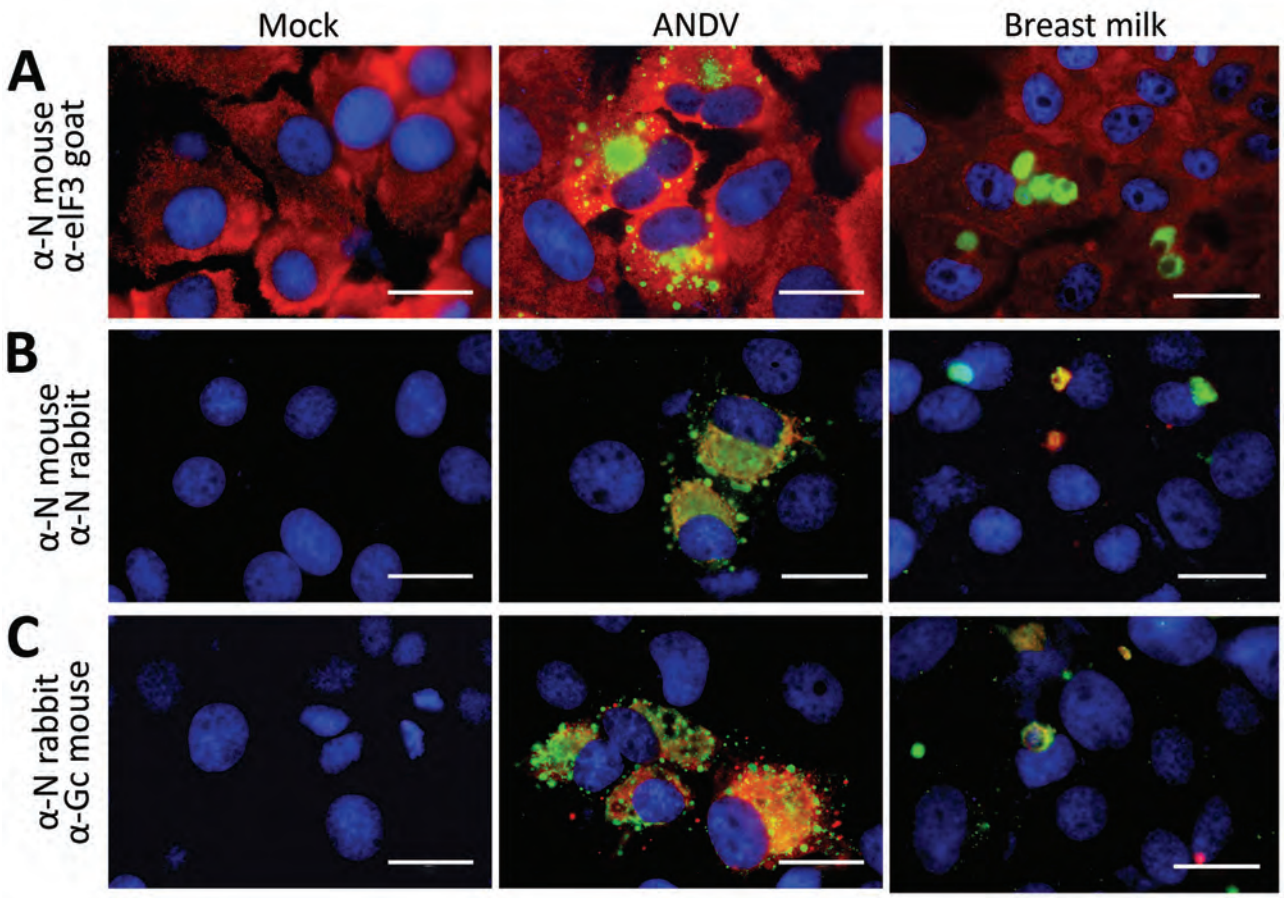

Figure 2. Detection of ANDV N and Gc proteins from enucleated cells from breast milk from a mother in Chile. A) Detection of N protein and the cytoplasmic marker eIF3. B) Detection of N protein with 2 different primary antibodies. C) Detection of N and Gc proteins. Huh-7 cells were mock-infected (mock column), ANDV infected (ANDV column), or incubated with a pellet from breast milk (breast milk column). Coverslips were incubated with mouse and rabbit antibodies. Scale bars indicate 20 μm. Complete methods are described in the Appendix (https://wwwnc.cdc.gov/EID/article/26/8/20-0204-App1.pdf). ANDV, Andes virus; Gc, glycoprotein; N, nucleoprotein.

virus entry (*8*). Another possible mode of transmission is close contact with respiratory secretions and saliva of the infected mother. However, because ANDV was present in breast milk and the newborn's exposure to breast milk was much greater than to other fluids, transmission by breast milk is very likely.

Another factor that may help explain oral infection in the neonatal period is the gastrointestinal characteristics in the first month of life, such as the adjustment of stomach pH, rapid gastric emptying time, and increased permeability of the intestine due to loosened intestinal intercellular spaces (*9*). Sin Nombre virus was detected in breast milk samples by RT-PCR, but the exposed child did not become infected (*10*). Similar results were found in 2 women infected with Puumala virus (*11*). Vertical transmission was excluded in 4 pregnant women infected with hantavirus species in Europe (*12*). Bellomo et al. reported a newborn infected with ANDV but did not report the presence of ANDV in breast milk (*13*). Our case provides further evidence for a gastrointestinal transmission of ANDV, which is consistent with previous reports of Puumala virus and ANDV infections in Syrian hamster models of hantavirus cardiopulmonary disease and in 1 newborn human case (*13*–*15*).

Conclusions

We describe mother-to-child transmission of ANDV infection in Chile. Our analyses proved the presence of ANDV in breast milk, proposing breast-feeding as an additional mechanism of transmission. In this context, we recommend that ANDV-infected mothers refrain from breast-feeding until ANDV RNA is undetectable in blood and breast milk. In addition, we advise strict clinical and virologic surveillance of children potentially exposed to family members with ANDV infection for early diagnosis and hospitalization for adequate intensive care.

Acknowledgments

We thank Irma Valenzuela, Johanna Acevedo, Mauricio Yañez, Catalina Infante, Analia Cuiza, Claudia Marco, Francisca Valdivieso, and the health personnel who cared for the patients at Hospital Regional de Talca. We thank the Microscopy Advanced Unit (UMA-MED) and Biosafety Level 3 facility at the Escuela de Medicina, Pontificia Universidad Católica de Chile. We also thank Thomas Weitzel for critical review of this manuscript. This work was supported by the National Institute of Allergy and Infectious Diseases of the National Institutes of Health (grant no. U01AI045452 to M.F, P.V., and G.M.); the Fondo Nacional de Desarrollo Científico y Tecnológico (FONDECYT no. 1161197 to M.F. and J.A., no. 1161447 to C.V., no. 11180167 to J.A., no. 1181799 to N.T.D. and no. 11150611 to J.V-O.); the Programa de Investigación Asociativa (no. ACT1408 to M.F, N.L.C.,.and J.V.-O.); and the Centro Científico y Tecnológico de Excelencia Basal (no. AFB 170004 to N.T.D.).

About the Author

Dr. Ferres is a professor of pediatrics and infectious disease specialist at Medical School of Pontificia Universidad Catolica de Chile. Her main research interests include emerging viral infectious diseases, particularly Andes virus epidemiology and diagnosis in humans.

References

1. Vaheri A, Strandin T, Hepojoki J, Sironen T, Henttonen H, Mäkelä S, et al. Uncovering the mysteries of hantavirus infections. Nat Rev Microbiol. 2013;11:539–50. https://doi.org/10.1038/nrmicro3066
2. Martinez-Valdebenito C, Calvo M, Vial C, Mansilla R, Marco C, Palma RE, et al. Person-to-person household and nosocomial transmission of Andes hantavirus, southern Chile, 2011. Emerg Infect Dis. 2014;20:1629–36. https://doi.org/10.3201/eid2010.140353
3. Padula PJ, Edelstein A, Miguel SD, López NM, Rossi CM, Rabinovich RD. Epidemic outbreak of hantavirus pulmonary syndrome in Argentina. Molecular evidence of person to person transmission of Andes virus [in Spanish]. Medicina (B Aires). 1998;58(Suppl 1):27–36.
4. Vial C, Martinez-Valdebenito C, Rios S, Martinez J, Vial PA, Ferres M, et al. Molecular method for the detection of Andes hantavirus infection: validation for clinical diagnostics. Diagn Microbiol Infect Dis. 2016;84:36–9. https://doi.org/10.1016/j.diagmicrobio.2015.07.019
5. Vera-Otarola J, Solis L, Soto-Rifo R, Ricci EP, Pino K, Tischler ND, et al. The Andes hantavirus NSs protein is expressed from the viral small mRNA by a leaky scanning mechanism. J Virol. 2012;86:2176–87. https://doi.org/10.1128/JVI.06223-11
6. Witkowska-Zimny M, Kaminska-El-Hassan E. Cells of human breast milk. Cell Mol Biol Lett. 2017;22:11. https://doi.org/10.1186/s11658-017-0042-4
7. Ferres M, Vial P, Marco C, Yanez L, Godoy P, Castillo C, et al.; Andes Virus Household Contacts Study Group. Prospective evaluation of household contacts of persons with hantavirus cardiopulmonary syndrome in Chile. J Infect Dis. 2007;195:1563–71. https://doi.org/10.1086/516786
8. Cabinian A, Sinsimer D, Tang M, Zumba O, Mehta H, Toma A, et al. Transfer of maternal immune cells by breastfeeding: maternal cytotoxic T lymphocytes present in breast milk localize in the Peyer's patches of the nursed infant. PLoS One. 2016;11:e0156762. https://doi.org/10.1371/journal.pone.0156762
9. Wilson CB, Nizet V, Maldonado Y, Remington JS, Klein JO. Remington and Klein's infectious diseases of the fetus and newborn infant. 8th ed. Philadelphia: Elsevier Saunders; 2015.
10. Pai RK, Bharadwaj M, Levy H, Overturf G, Goade D, Wortman IA, et al. Absence of infection in a neonate after possible exposure to Sin Nombre hantavirus in breast milk. Clin Infect Dis. 1999;29:1577–9. https://doi.org/10.1086/313523
11. Pettersson L, Boman J, Juto P, Evander M, Ahlm C. Outbreak of Puumala virus infection, Sweden. Emerg Infect Dis. 2008;14:808–10. https://doi.org/10.3201/eid1405.071124
12. Hofmann J, Führer A, Bolz M, Waldschläger-Terpe J, Meier M, Lüdders D, et al. Hantavirus infections by Puumala or Dobrava-Belgrade virus in pregnant women. J Clin Virol. 2012;55:266–9. https://doi.org/10.1016/j.jcv.2012.07.011
13. Bellomo C, Alonso D, Coelho R, Iglesias A, Periolo N, Martínez VP. A newborn infected by Andes virus suggests novel routes of hantavirus transmission: a case report. Clin Microbiol Infect. 2020;26:130–1. https://doi.org/10.1016/j.cmi.2019.09.012
14. Latus J, Tenner-Racz K, Racz P, Kitterer D, Cadar D, Ott G, et al. Detection of Puumala hantavirus antigen in human intestine during acute hantavirus infection. PLoS One. 2014;9:e98397. https://doi.org/10.1371/journal.pone.0098397
15. Witkowski PT, Perley CC, Brocato RL, Hooper JW, Jürgensen C, Schulzke JD, et al. Gastrointestinal tract as entry route for hantavirus infection. Front Microbiol. 2017;8:1721. https://doi.org/10.3389/fmicb.2017.01721

Address for correspondence: Marcela Ferrés, Escuela de Medicina, Pontificia Universidad Católica de Chile, Marcoleta 391, Santiago, Chile; email: mferres@med.puc.cl. Nicole Le Corre, Escuela de Medicina, Pontificia Universidad Católica de Chile, Marcoleta 391, Santiago, Chile; email: n.lecorre.p@gmail.com

Bertiella studeri Infection in Children, Sri Lanka

Anjalie Amarasinghe, Thanh H. Le, Susiji Wickramasinghe

We provide a detailed molecular and phylogenetic description of *Bertiella studeri* tapeworms infecting children in Sri Lanka. Our findings can be used to identify multiple species of *Bertiella* tapeworms that can infect human hosts in the Old World.

The genus *Bertiella*, which has 29 known tapeworm species, belongs to the subfamily *Anoplocephalinae* of the *Anoplocephalidae* family (*1*). These tapeworms are common parasites in the small intestine of primates (*2*). Of these species, only *B. studeri*, *B. mucronata*, and *B. satyri* (*3*), which was recently redescribed as a different species (*4*), can infect humans (*4*,*5*). Children acquire this infection usually by eating contaminated fruits or by ingesting contaminated soil. The earliest identified cases of human bertiellosis in Sri Lanka occurred in 1975; these cases and 1 further case were reported in 1976. Six cases were reported in the literature from 1988–2006 (*6*). The most recent report was in 2006 from Rathnapura, Sabaragamuwa Province, Sri Lanka (*7*).

The morphologic, taxonomic, and molecular analysis of several species classified in the family *Anoplocephalidae* are not well documented (*6*). A recent study has identified an unexpected genetic diversity that suggests the existence of several *Bertiella* species in primates and humans (*6*,*8*). Multiple species of *Bertiella* tapeworms may infect humans in the New World and the Old World. It is not certain whether the Old World and New World *Bertiella* infections, previously all identified as *B. studeri* or *B. mucronata*, actually represent multiple different species; the true taxonomic distinction and geographic distribution of these 2 species are not entirely clear (*6*). Furthermore, diagnosis entirely based on egg morphology, size, and geographic distribution is insufficient to discriminate *B. studeri* tapeworms from other *Bertiella* spp. infecting humans (*9*).

Author affiliations: University of Peradeniya, Peradeniya, Sri Lanka (A. Amarasinghe, S. Wickramasinghe); Vietnam Academy of Science and Technology, Hanoi, Vietnam (T.H. Le)

DOI: https://doi.org/10.3201/eid2608.200324

This study provides the molecular analysis of the *B. studeri* tapeworms infecting children in Sri Lanka and describes phylogenetic relationships for this species. The Ethics Review Committee in the Faculty of Medicine, University of Peradeniya, Sri Lanka approved this study (protocol no. 2019/EC/03).

The Study

We conducted a retrospective study using tapeworm proglottids (Appendix Figure 1, https://wwwnc.cdc.gov/EID/article/26/8/20-0324-App1.pdf) from 24 pediatric patients referred to the Department of Parasitology, Faculty of Medicine, University of Peradeniya, Peradeniya, Sri Lanka, during 2007–2017. Patients were all <10 years of age (range 3.5–9 years). No other epidemiologic data were available.

We extracted genomic DNA separately using a commercial DNA extraction kit (PureLink; Invitrogen, https://www.thermofisher.com). We amplified 2 mitochondrial markers, nicotinamide adenine dinucleotide hydrogenase subunit 1 gene (NAD1) and cytochrome c oxidase subunit 1 gene (COX1), and 3 nuclear ribosomal markers, the second internal transcribed spacer region (ITS2), 28S large subunit ribosomal region (28S), and 18S rRNA gene (18S), using the specified primers and PCR conditions (Appendix Table). We subjected the PCR products to Sanger sequencing; only the ethanol-preserved samples provided a sufficient amount of DNA for sequencing (Appendix). We inferred molecular phylogenetic analysis and evolutionary history using maximum-likelihood and Bayesian methods.

Phylogenetic analysis identified a monophyletic group of *Bertiella* species in all 5 maximum-likelihood trees. The NAD1 region revealed several clades within the *Bertiella* monophyletic group (Figure 1, panel A); sequence similarity search identified 90.19% match with *Bertiella* species (GenBank accession no. JQ771111). The COX1 sequence similarity search identified 95.10% match with *Bertiella* species (GenBank accession no. JQ771106); COX1 analysis identified 2 clades in the *Bertiella* monophyletic

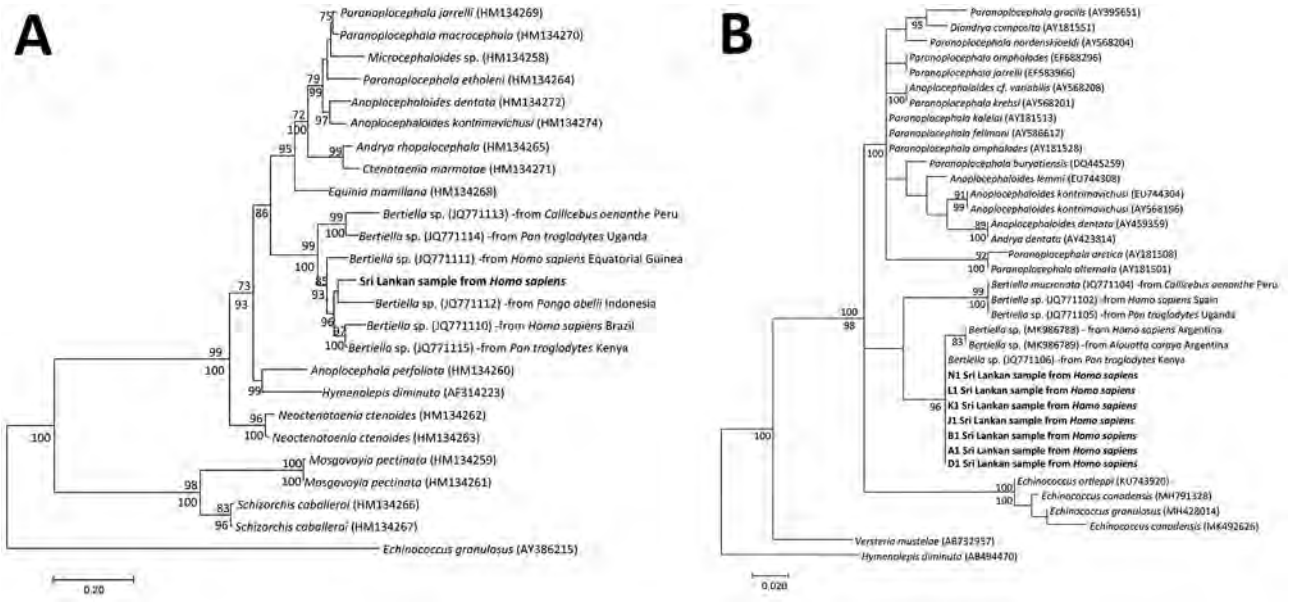

Figure 1. Molecular phylogeny of the mitochondrial markers in a study of *Bertiella* tapeworms in children in Sri Lanka. Bold text indicates *B. studeri* samples from Sri Lanka. A) Maximum-likelihood tree containing 25 taxa constructed by the analysis of partial NAD1 sequence alignment. B) Maximum-likelihood tree containing 37 taxa was constructed by the analysis of partial COX1 sequence alignment. Numbers above the nodes indicate the percentages of 1,000 nonparametric bootstrap pseudoreplicates (>70) and below the nodes the percentages of 1,000 Bayesian posterior probabilities (>70). GenBank accession numbers are provided for reference sequences. Scale bars represent nucleotide divergence.

group (Figure 1, panel B). *Bertiella* species from human hosts, acquired in Equatorial Guinea and Argentina, and *B. mucronata* (New World) from *Callicebus oenanthe* monkeys were separated from the Sri Lanka clade (Figure 1, panel B).

The ITS2 sequences showed 99.35% similarity with *B. studeri* (GenBank accession no. AB586129) and 100% similarity with *Bertiella* species (GenBank accession no. JQ771096). All the *B. studeri* sequences from Asia are in 1 clade. The second clade included 3 sequences from *Pan troglodytes* chimpanzee in Kenya, 1 from a human infection acquired in Equatorial Guinea, and 1 from a human host in Brazil (Figure 2, panel A). The 28S rRNA gene analysis revealed 2 clades for *Bertiella* from humans and nonhuman primates (Figure 2, panel B). The sequence similarity search revealed 94.66% similarity with *Bertiella* species (GenBank accession no. KJ888951). Furthermore, we identified a single-nucleotide polymorphism in 28S rRNA region (T to C) between the samples from Sri Lanka that suggest genetic diversity (Appendix Figure 2, panel A). In the ML tree for 18S rRNA region, Sri Lanka samples and *B. studeri* obtained from *Macaca fascicularis* macaque formed a single clade (Figure 2, panel C). The sequence similarity search for 18S rRNA region identified 99.84% match with *B. studeri* (GenBank accession no. GU323706). Furthermore, 18S rRNA region in the Sri Lanka samples have a single-nucleotide polymorphism (T to C) with the *Bertiella* sequence from *M. fascicularis* (Appendix Figure 2, panel B).

Records we examined showed patients had white, flat, motile worm segments in stools, and some patients had reported abdominal disturbances and intermittent diarrhea. Previous studies reported recurrent abdominal pain and continuous perianal itching, anorexia, weight loss, and intermittent diarrhea in infected patients (*6*); however, these symptoms are not unique to *Bertiella* infection, and so the correct diagnosis of bertiellosis is important. Treatment failure for *B. studeri* worms using niclosamide was reported in a 30-month-old patient in Sri Lanka in 2004 (*10*) and in a 5-year-old patient in Sabaragamuwa Province, Sri Lanka (*7*).

Conclusions

Our results suggest an intraspecific diversity of *Bertiella* tapeworms. Such diversity may occur according to the host and the geographic location. A previous study conducted by Doležalová et al. (*8*,*11*) has suggested a broad genetic diversity among the *Bertiella* species in primates and humans; further studies are required to support this suggestion. According to the available demographic data, most of the patients resided in Central

Province, Sri Lanka; the most likely reason that they comprised most patients is the *Bertiella* tapeworm reservoir hosts, particularly Ceylon torque monkey (*Macaca sinica*) and gray langur (*Presbytis entellus*), that inhabit this region (*12*,*13*). Over time, these monkey populations have lost their habitats due to deforestation and rapid urbanization in Sri Lanka; they are now regular visitors in suburban and urban areas scavenging for food near human settlements, which has increased human exposure to *B. studeri* infection (*14*,*15*).

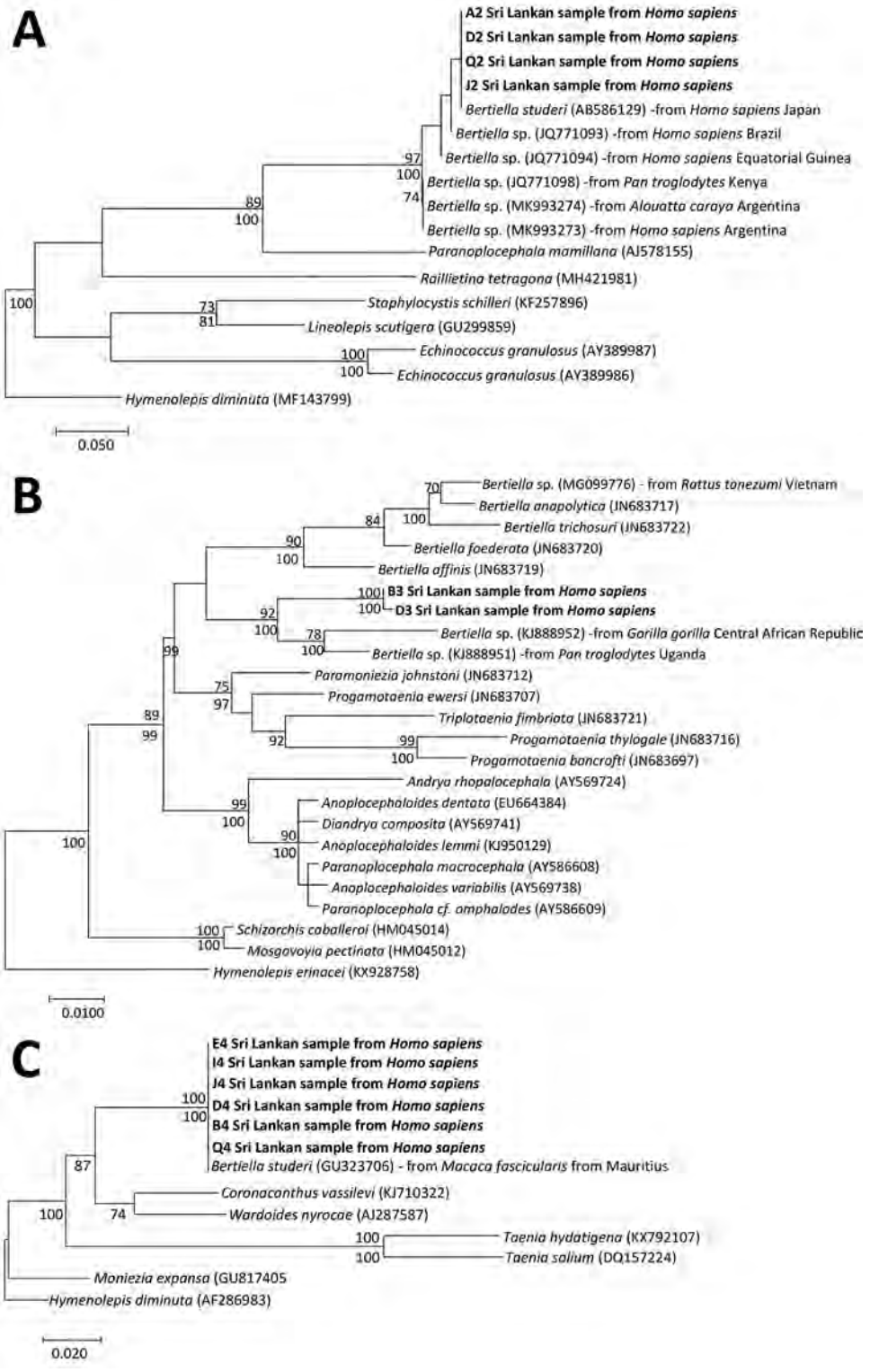

Figure 2. Molecular phylogeny of the nuclear ribosomal markers in study of *Bertiella* tapeworms in children in Sri Lanka. Bold text indicates *Bertiella studeri* samples from Sri Lanka. A) Maximum-likelihood tree containing 17 taxa, constructed by the analysis of partial ITS2 sequence alignment. B) Maximum likelihood tree containing 24 taxa, constructed by the analysis of partial 28S sequence alignment. C) Maximum-likelihood tree containing 13 taxa, constructed by the analysis of partial 18S sequence alignment. Numbers above the nodes indicate the percentages of 1,000 nonparametric bootstrap pseudoreplicates (>70) and below the nodes the percentages of 1,000 Bayesian posterior probabilities (>70). GenBank accession numbers are provided for reference sequences. Scale bars represent nucleotide divergence.

Unavailability of molecular data for *B. studeri* 28S, COX1, and NAD1 markers in GenBank was a constraint that we encountered during phylogenetic analysis. In our study, we generated molecular data for 2 mitochondrial markers (NAD1, COX1), and 3 nuclear ribosomal markers (28S, 18S, ITS2) and submitted them to GenBank (Appendix). The molecular data obtained can be used for further analysis in diagnostics, to discern phylogenetic relationships and evolutionary correlations, and to understand the transmission dynamics of *B. studeri* tapeworms. Our data may also be used to assist in elucidating if multiple species of *Bertiella* sp. tapeworms infect human hosts in the Old World.

This study was funded by the University Research Grant (no. URG/2018/31/M), University of Peradeniya, Sri Lanka.

A.A. carried out the laboratory work, sequence analysis, and wrote the manuscript with input from all authors. T.H.L. carried out DNA sequencing. S.W. performed sequence analysis, manuscript writing, and finalized the manuscript. S.W. had the final responsibility for the decision to submit for publication. All authors reviewed the draft and approved the decision to submit for publication.

About the Author

Ms. Amarasinghe is a research assistant in the Department of Parasitology, Faculty of Medicine, University of Peradeniya, Sri Lanka. She is particularly interested in parasitology research.

References

1. Beveridge I. Family Anoplocephalidae Cholodkovsky, In: Khalil LF, Jones A, Bray RA, editors. Keys to the cestode parasites of vertebrates. Cambridge: CAB International; 1994. p. 315–66.
2. Stiles CW, Hassall A. *Bertiella*, new name for the cestode genus Bertia Blanchard, 1891. Science. 1902;16:434. https://doi.org/10.1126/science.16.402.434
3. Blanchard R. On the helminths of anthropoid primates [in French]. Mem Soc Zool Fr. 1891;4:186–96.
4. Foitová I, Mašová S, Tenora F, Koubková B, Hodová I, Vyskočilová M, et al. Redescription and resurrection of *Bertiella satyri* (Cestoda, Anoplocephalidae) parasitizing the orangutan (*Pongo abelii*) in Indonesia. Parasitol Res. 2011;109:689–97. https://doi.org/10.1007/s00436-011-2300-0
5. Chandler AC. New records of *Bertiella satyri* (Cestoda) in man and apes. Parasitology. 1925;17:421–5. https://doi.org/10.1017/S0031182000004844</jrn>
6. Sapp SGH, Bradbury RS. The forgotten exotic tapeworms: a review of uncommon zoonotic Cyclophyllidea. Parasitology. 2020;147:533–58. https://doi.org/10.1017/S003118202000013X</jrn>
7. Morawakkorala RN, Senarathna AMRD, de Alwis ACD, Abeywardana SP. Two cases of monkey tapeworm (*Bertiella studeri*) infestation from Sabaragamuwa Province. Sri Lanka Journal of Child Health. 2006;35:34–5. https://doi.org/10.4038/sljch.v35i1.7</jrn>
8. Doležalová J, Vallo P, Petrželková KJ, Foitová I, Nurcahyo W, Mudakikwa A, et al. Molecular phylogeny of anoplocephalid tapeworms (Cestoda: Anoplocephalidae) infecting humans and non-human primates. Parasitology. 2015; 142:1278–89. https://doi.org/10.1017/S003118201500058X
9. Galán-Puchades MT, Fuentes MV, Mas-Coma S. Morphology of *Bertiella studeri* (Blanchard, 1891) sensu Stunkard (1940) (Cestoda: Anoplocephalidae) of human origin and a proposal of criteria for the specific diagnosis of bertiellosis. Folia Parasitol (Praha). 2000;47:23–8. https://doi.org/10.14411/fp.2000.005</jrn>
10. Gallella SD, Gunawardena GS, Karunaweera ND. *Bertiella studeri* infection: resistance to niclosamide. Ceylon Med J. 2004;49:65. https://doi.org/10.4038/cmj.v49i2.3267
11. Servián A, Zonta ML, Cociancic P, Falcone A, Ruybal P, Capasso S, et al. Morphological and molecular characterization of *Bertiella* sp. (Cestoda, Anoplocephalidae) infection in a human and howler monkeys in Argentina. Parasitol Res. 2020;119:1291–300. https://doi.org/10.1007/s00436-020-06615-5
12. Huffman MA, Nahallage CA, Hasegawa H, Ekanayake S, De Silva LG, Athauda IR. Preliminary survey of the distribution of four potentially zoonotic parasite species among primates in Sri Lanka. J Natl Sci Found Sri Lanka. 2013;41:319. https://doi.org/10.4038/jnsfsr.v41i4.6246
13. Dissanaike AS. Parasitic zoonoses in Sri Lanka: an update. Ceylon Med J. 2002;47:46–7. https://doi.org/10.4038/cmj.v47i2.3450
14. Furtado AP, Batista EJ, Gonçalves EC, Silva AM, Melo FT, Giese EG, et al. Human bertielliasis in Amazonia: case report and challenging diagnosis. PLoS Negl Trop Dis. 2012;6:e1580. https://doi.org/10.1371/journal.pntd.0001580
15. Paçô JM, Campos DM, Araújo JL. Human bertiellosis in Goiás, Brazil: a case report on human infection by *Bertiella* sp. (Cestoda: Anoplocephalidae). Rev Inst Med Trop São Paulo. 2003;45:159–61. https://doi.org/10.1590/S0036-46652003000300008

Address for correspondence: Susiji Wickramasinghe, Department of Parasitology, Faculty of Medicine, University of Peradeniya, Peradeniya, 20400, Sri Lanka; email: susijij@pdn.ac.lk or susijijp@yahoo.co.jp

Spread of Multidrug-Resistant Bacteria by Moth Flies from Hospital Waste Water System

Thomas Rupprecht,[1] Annette Moter, Alexandra Wiessener, Joerg Reutershan, Klaus Lang-Schwarz, Michael Vieth, Christian Rupprecht, Ruediger Wagner, Thomas Bollinger[1]

We documented and analyzed moth fly occurrence and spread of multidrug-resistant bacteria in a tertiary care hospital in Germany. The moth flies (*Clogmia albipunctata*) bred in the sewage system, then moved into the hospital, carrying biofilm and multidrug-resistant bacteria on their feet. Subsequently, the hospital developed a pest control protocol.

Hospital-acquired infections caused by multidrug-resistant (MDR) pathogens pose major challenges (*1*). Whereas the concept of transmission of pathogenic bacterial organisms through contact with medical staff is well established, other ways of spreading have not been sufficiently addressed. A tertiary care hospital in Germany observed sporadic outbreaks of MDR pathogens that could not be attributed to usual means of contamination. Concurrently, an increase in moth flies was observed.

Psychodidae, the family that encompasses moth flies, includes a few species that can cause severe health problems, including the species *Psychoda alternata* and *Clogmia albipunctata*. Both species occur in large numbers where poor hygienic conditions exist, such as in sewage treatment plants, hospital waste water systems, or other environments where microbial biofilms exists, and therefore are considered nuisance pests (*2*). Reports suggest that wounds attract adult moth flies (*3*) and larvae have even been reported in samples from tear ducts (*3*). *C. albipunctata* moth flies have become a severe source of insect infestations in hospitals. One report (*4*) provides a summary of the permanent distribution of the species throughout Europe.

Observations of both moth flies and outbreaks of MDR bacteria in the hospital were not initially linked. However, a newly constructed operating room (OR) could not be opened for use for >2 years due to occurrence of moth flies. The results of this study suggest that spreading of MDR bacteria by moth flies could explain these outbreaks.

The Study

We performed microbiologic analysis of all biofilm samples and moth flies by matrix-assisted laser desorption/ionization time-of-flight (MALDI-TOF) mass spectrometry (Bruker, https://www.bruker.com) and Phoenix automated microbiology system (Becton Dickinson, https://www.bd.com) according to European Committee on Antimicrobial Susceptibility Testing (EUCAST, https://eucast.org) guidelines. To visualize biofilms we used fluorescence in situ hybridization protocol on sections of embedded samples or moth flies (Appendix, https://wwwnc.cdc.gov/EID/article/26/8/19-0750-App1.pdf). We considered pathogens to be MDR if nonsusceptible to ≥1 agent in 3 of the defined categories, extensively-drug-resistant (XDR) if nonsusceptible to ≥1 agent in all but ≤2 of defined categories, and pan-drug resistant (PDR) if nonsusceptible to all listed antimicrobials (*5*).

We identified the moth flies as *C. albipunctata* (Figure 1, panel A) and found that they had entered the hospital room from a forgotten shunt between the drains and the waste air system (Appendix). To confirm that sewage pipes contained bacterial biofilms and moth fly eggs, samples were taken from the pipes, fixed, and stained. Psychodidae eggs were found in the biofilm (Figure 1, panel B). Infestation with moth flies seemed to increase with proximity to the central drain (Figure

Author affiliations: Klinikum Bayreuth, Bayreuth, Germany (T. Rupprecht, J. Reutershan, K. Lang-Schwarz, M. Vieth, T. Bollinger); Friedrich-Alexander University, Erlangen, Germany (T. Rupprecht, M. Vieth); Charité-Universitätsmedizin, Berlin, Germany (A. Moter, A. Wiessener); Eberhard Karls University, Tübingen, Germany (J. Reutershan); University of Oxford, Oxford, UK (C. Rupprecht); Universität Kassel, Kassel, Germany (R. Wagner); University Hospital Schleswig-Holstein, Lübeck, Germany (T. Bollinger)

DOI: https://doi.org/10.3201/eid2608.190750

[1]These authors were co–principal investigators.

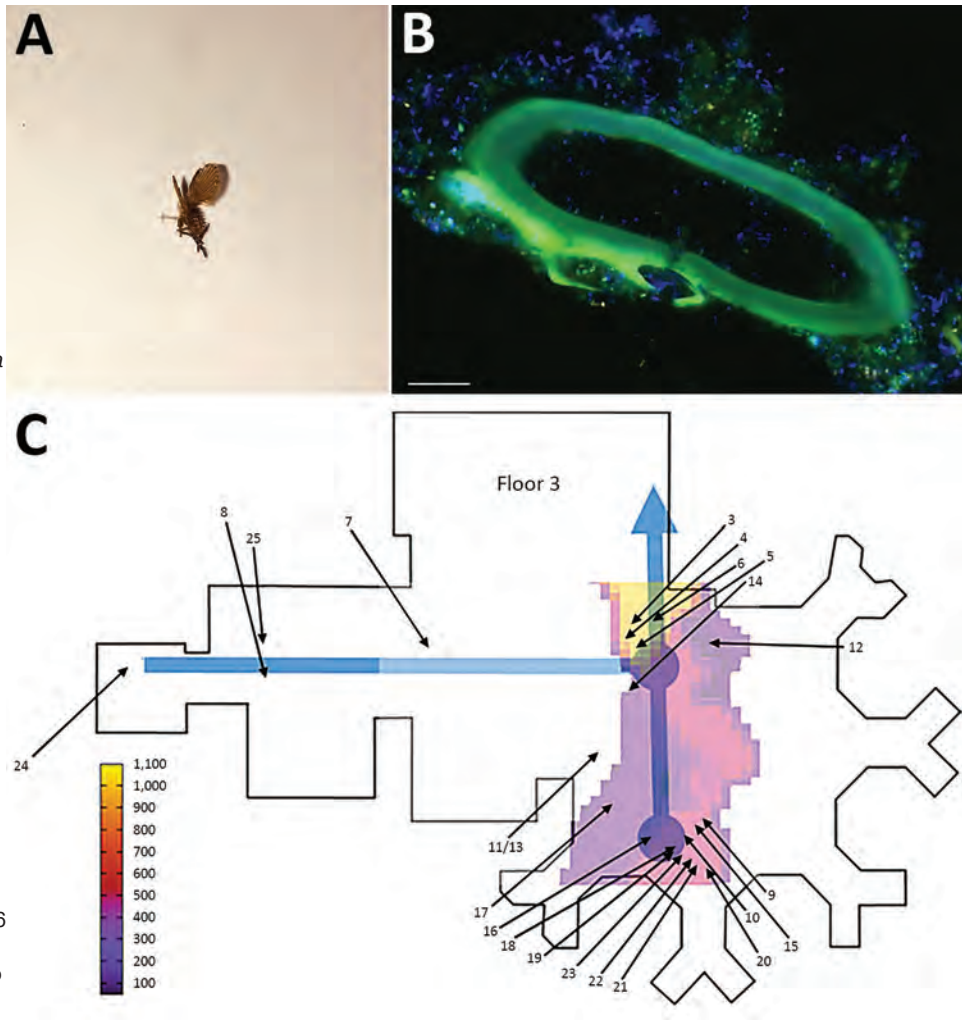

Figure 1. Investigation of multidrug-resistant bacteria spread by moth flies via biofilm in a hospital, Germany. A) Magnified *Clogmia albipunctata* moth fly. The length of the corpus is 2.5 mm. B) Fluorescence in situ hybridization (FISH) from biofilm of a sewage pipe with a blind end in the operating room (OR) using the pan-bacterial FISH-probe EUB338 labeled with fluorescein isothiocyanate (green), *Pseudomonas aeruginosa* specific probe labeled with Cy3 (orange), and nucleic acid stain DAPI (Thermo Fisher Scientific, https://www.thermofisher.com/) (blue). The oval structure seen is consistent with an eggshell of Psychodidae, which is colonized by bacteria. C) Schematic map of floor –3 (topographically representative of the hospital building). Blue lines represent the main sewage pipe; heat map shows the frequency of *C. albipunctata* occurrence merged from all floors of the building; blue arrow indicates sewage system discharge from the hospital; black arrows indicate where moth flies were captured on level –3. Arrow numbers correspond to the numbers in Tables 1, 2; arrows 3–6 indicate the position of the closed OR. The gradients in the heat map (summarized over all floors) point to the yellow region, which is 1 floor above the central sewage collection point of the hospital. The central sewage lines were inspected; we found biofilm and multiple moth flies at all investigated points.

1, panel C). Furthermore, we observed that moth flies were able to pass through the water-filled siphon of a bedpan washer (Video 1, https://wwwnc.cdc.gov/EID/article/26/8/19-0750-V1.htm) and we identified extensive biofilm in the drains (Video 2, https://wwwnc.cdc.gov/EID/article/26/8/19-0750-V2.htm).

Fluorescence in situ hybridization and fluorescence microscopy on sections of embedded moth flies showed the presence of biofilms and bacteria on their feet (Figure 2). Not every moth fly caught was tested; however, representative moth flies from each identified location were tested. Furthermore, biofilm in sewage pipes revealed a kind of ecosystem consisting of moth fly larvae, vermicular, fungi, and bacteria (Appendix Figure 1). Subsequently we collected and microbiologically analyzed *C. albipunctata* and biofilm from different parts of the hospital (Tables 1, 2). Of the moth flies we analyzed microbiologically, we found that 41.1% carried MDR or even XDR bacteria (Appendix). Overall, 43.9% of specimens were MDR or XDR.

We subsequently examined pest control options. Our first approach, removing biofilm from accessible pipes in the sewage system, did not successfully reduce or eliminate moth flies. Our second approach, mechanically and chemically cleaning all sinks and proximal sewage lines, also did not prevent periodic reoccurrence of moth flies. Our third approach was more successful. We flushed all sinks in the OR at the same time with 60°C hot water for 15 min/wk, daily during summer, which suppressed *C. albipunctata* moth flies in the OR but not in the rest of the hospital.

Conclusions

Infection with and colonization by MDR bacteria is an increasing challenge in health care (*6*). Psychodidae (moth flies) are small, 1–4 mm in size, and have been

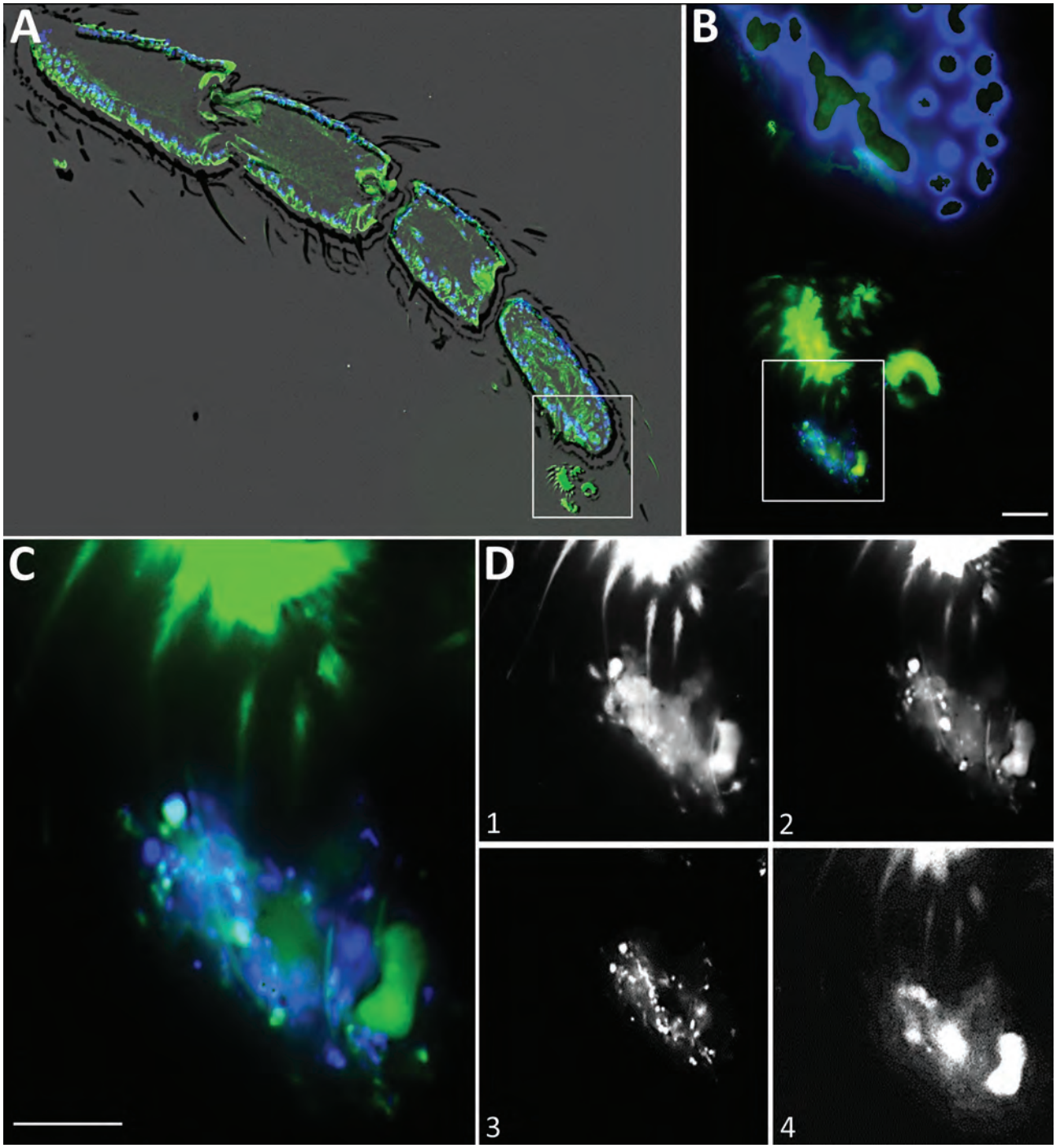

Figure 2. Fluorescence in situ hybridization (FISH) from a longitudinal section of a leg of a *Clogmia albipunctata* moth fly from a hospital in Germany. The fly was caught in the hospital, embedded, and stained (Appendix, https://wwwnc.cdc.gov/EID/article/26/8/19-0750-App1.pdf). A) Overview showing an overlay of the fluorescent images with a phase contrast to visualize the limbs of the legs. B) Higher magnification of the inset from panel A shows the anatomy of the tarsus and claws with an adjacent biofilm, which is stained by the bacterial probe (green) and DAPI (blue). C) Higher magnification of the inset from panel B shows the biofilm. Blue represents DAPI staining of DNA; bacteria were stained green with pan-bacterial FISH probe EUB338-FITC, *Enterobacterales* stained orange with an *Escherichia coli*–specific FISH probe (data not shown), and NONEUB (nonsense EUB) probe labeled with Cy5 was used to exclude unspecific probe binding. D) Overlay of the DAPI and fluorescein isothiocyanate channel shows the biofilm with different bacterial morphotypes. Different planes of the z-stack in the green channel (pan-bacterial probe) of the identical microscopic field depicts the different claws embracing the biofilm (D1 and D2). D3 shows the DAPI filter-set only with the DNA of the bacteria, whereas D4 shows the autofluorescence in the Cy5 filter-set NONEUB probe.

Table 1. Occurrence of moth flies in a hospital, Germany*

No.	Psychodidae larvae/eggs	Count†	Type of room (comment)	Floor‡
1	Adult	1	Sewage line service opening (under OR 1)	–4
2	Larvae and eggs	>100	Sewage line service opening (200 m distant from OR 1)	–4
3	Adult	>50	OR 7§	–3
4	Adult	>500	Washroom, OR 7	–3
5	Adult	>50	Corridor, OR 7	–3
6	Adult	>50	Supply rooms for OR 7	–3
7	Adult	3	Corridor connecting ORs 1–6	–3
8	Adult	1	Corridor to ICU 58	–3
9	Adult	>20	Toilet (A3–40)	–3
10	Adult	>5	Doctor's room (A3–43) St 35	–3
11	Adult	>10	Toilet (G3–58)	–3
12	Adult	>10	OR dermatology (B3–61)	–3
13	Adult	>500	Washing room G3–62	–3
14	Adult	>500	Toilet A3–06	–3
15	Adult	>5	Supply room (A3–41)	–3
16	Adult and eggs	>500 (>100 eggs)	Shower (F3–07) St 35	–3
17	Adult	>500	Shower floor 35 (F3–31), patient room and corridor	–3
18	Adult	>10	Bathroom floor 34 (E3–07)	–3
19	Adult	>10	Shower floor 34 (E3–08)	–3
20	Adult	>10	Clean supply room floor 34 (E3–01)	–3
21	Adult	>10	Kitchen floor 34 (E3–02)	–3
22	Adult	>10	Staff room floor 34 (E3–04)	–3
23	Adult	>10	Doctor's room floor 34 (E3–05)	–3
24	Adult	>5	ICU floor 58 W3001	–3
25	Adult	3	OR 12 heart surgery¶	–3
26	Adult	>500	Sluice to hospital kitchen (S2–20)	–2
27	Adult	>500	Hospital kitchen toilets (S2–20a, b)	–2
28	Adult	>10	Supply room emergency department (R1–52)	–1
29	Adult	>10	Kitchen emergency department (R1–57)	–1
30	Adult	>10	Toilet emergency department (R1–55)	–1
31	Adult	>10	Patient rooms emergency department	–1

Patient numbers correspond to the numbers in Table 2 and Figure 1, panel C. ICU, intensive care unit; OR, operating room; St, suite.
†Count of Psychodidae larvae and adult flies during June 2016–October 2018.
‡Floor numbers are negative because the hospital is in part built on a hill so that Floor 0 is the most top level (Floor 0 had no moth fly observations).
§OR 7 had been closed for years until we eliminated the source of moth flies.
¶In OR 12 only 1 moth fly was found even after an intense search. From all immediately reported occasions 1–2 moth flies were caught and analyzed microbiologically (see Table 2 for results).

regarded as unharmful vermin except in highly sterile areas. Therefore, they have often been overlooked or ignored and not considered a high-consequence problem.

The results of our study suggest a change in this point of view is needed. If generalized to other hospitals, our findings indicate that *C. albipunctata* moth flies in hospitals, combined with MDR, XDR, or PDR (pandrug-resistant) bacteria in biofilms, pose an underestimated threat. The danger from this symbiotic system between moth flies and these bacteria results from moth fly eggs and larvae living in biofilm that is contaminated by a patient's bacterial flora. Furthermore, biofilms can rapidly grow and spread over distances kilometers in length (*7*) and are almost impossible to eradicate. In the third and fourth stages of development, larvae living in the biofilm can begin to move, thus overcoming the water barriers in showers, bathtubs, toilets, and other washing units. At this point, adult moth flies can enter the hospital (Video 1) and transport drug-resistant bacteria from the microbial flora of the biofilm into the hospital.

We frequently found *Stenotrophomonas maltophilia* on *C. albipunctata* moth flies and also in clinical samples from deep respiratory material, wounds, blood culture, urine, and bile. In 1 patient, for example, we found hospital-acquired *S. maltophilia* and a genetically identical strain in drains in a ward ≈250 m away (data not shown). Even though this evidence is scant, it does support our hypothesis.

In addition, low doses of antimicrobials excreted by patients can result in the quick development and spread of plasmids (resistance genes) and virulence factors in biofilms (*8*). This process might result in resistance developing not only in a patient's microbiota but also in hospital biofilm. Our observations suggest that the adult *C. albipunctata* moth flies can move freely throughout sewage systems and that they carry bacterial biofilm on their feet. Many authors have suggested the existence of missing links in polyclonal outbreaks and in other hard-to-explain observations (*9,10*). We hypothesize that moth flies in symbiotic combination with biofilms could, in part, explain one such observed

transmission. However, the findings of this study are limited by the moderate number of moth flies, which should be addressed in future investigations.

Currently, there are no proven strategies, including chemical methods, to prevent or eradicate moth flies in sewage systems. However, weekly or, during summer, daily flushing with hot water (60°C) for 15 min was sufficient to suppress the moth flies in our study. We propose a prevention protocol including flushing weekly or daily with hot water (60°C), mechanical removal of biofilms; deconstruction of unused siphons or replacement by heatable siphons; and checking for unexpected outlets, such as drill holes, from drains into hospital rooms. These measures will not eliminate but might substantially suppress the problem. Once moth flies leave the drains, among the few available biofilms are patient wounds. Research has reported that adult moth flies are attracted to them, and *C. albipunctata* larvae have been found in wounds (*11*,*12*). Searching for moth flies and determining their microbial load might be advisable, especially if an unexpected bacterial outbreak occurs. Finally, our observations should be taken into account in the planning of hospital sewage systems in the future.

The authors declare no conflict of interest.

Table 2. Multidrug resistant bacteria on moth flies and biofilm in a hospital, Germany*

No.	Specimens tested	Location found	Species identified†	Can produce biofilm?	Resistance level‡	Macroscopic/ histologic findings
1	Biofilm	Sewage line	*Achromobacter xylosoxidans*	Yes	Not classified	Biofilm, *Candida*, mucin, eggs
2	Biofilm	Sewage line	*Pseudomonas* spp. *Escherichia coli* *Lysinibacillus fusiformis*	Yes	Potential XDR§ MDR	Biofilm, cocoons, eggs
3	Moth fly	OR 7	*Bacillus* spp., *Citrobacter freundii*	Yes	MDR	NA
4	Biofilm	Endoscopy of sewage lines in washroom, OR 7	*Advenella species* *Bacillus* spp. *Pseudomonas aeuginosa* *Stenotrophomonas maltophilia*	Yes Yes Yes	Potential XDR§	Extensive biofilm in all sewage lines, mucin, *Candida*
	Moth fly	Washroom OR 7	Sterile	NA	ND	NA
5	Moth fly	Corridor OR 7	*P. mosselii* *S. maltophilia*	Yes	Potential XDR§	NA
7	Moth fly	Corridor OR 1-6	*Bacillus* spp. *B. megatariume*	Yes Yes	ND	NA
8	Moth fly	Corridor ICU CS	*Bacillus* spp.	Yes		NA
9	Moth fly	Toilet (A3-40)	*S. maltophilia*		Potential XDR§	
	2 moth flies	Toilet (A3-40)	Sterile	NA	ND	NA
10	Moth fly	Doctors room (A3-43)	*Bacillus* spp. *P. nitroreducens*	Yes Yes	ND	NA
	Moth fly	Doctors room (A3-43)	*B. cereus* *B. thuringienses*	Yes Yes	ND	NA
14	Moth fly	Toilet (A3-06)	*Bacillus* spp. *B. cereus* *Chryseobacterium indologenses*	Yes	ND	NA
16	Biofilm	Shower drain	*B. cereus* *Bacillus* spp. *P. putida*	Yes	ND	Biofilm, eggs, *Candida albicans*
	Moth fly	Shower (F3-07)	*Bacillus cereus* *L. sphaericus* *Staphylococcus epidermidis*	Yes	ND	NA
	2 moth flies	Shower (F3-07)	*S. maltophilia* *B. thuringiensis*	Yes	Potential XDR	NA
17	Moth fly	Shower (F3-31)	*Enterococcus faecium (vanA)* *Bacillus* spp. *S. maltophilia*	Yes	Possible XDR¶ Potential XDR§	NA
	Moth fly	Shower (F3-31)	*E. faecium*	Yes	MDR	NA
24	Moth fly	ICU floor C	Sterile	NA	ND	NA

*Numbers at left are patient numbers, which correspond to the numbers in Table 1 and Figure 1, panel C. CS, cardiosurgery; C, cardiology; ICU, intensive care unit; MDR, multidrug resistant; OR, operating room; NA, not applicable; ND, not detected; XDR, extensively drug resistant.
†Microbiology, histology, and fluorescence in situ hybridization findings in the investigated specimens. Note that not every moth fly from the Table 1 count column was analyzed.
‡Resistance levels defined in Magiorakos et al. (*13*).
§Potential XDR means that the international standards have not been applied to the bacterium *S. maltophilia*. Additional details are available in the Appendix (https://wwwnc.cdc.gov/EID/article/26/8/19-0750-App1.pdf).
¶Possible XDR means that it could be XDR but not all antimicrobial categories were tested. Additional details are available in the Appendix.

About the Author

Dr. Thomas Rupprecht is a lecturer at the University Erlangen Nürnberg and medical director at the hospital Bayreuth. His research interests are complex human and environmental biosystems, their influence on disease occurrence and treatment, and mathematical modeling in both.

References

1. Gerlich MG, Piegsa J, Schäfer C, Hübner NO, Wilke F, Reuter S, et al. Improving hospital hygiene to reduce the impact of multidrug-resistant organisms in health care—a prospective controlled multicenter study. BMC Infect Dis. 2015;15:441. https://doi.org/10.1186/s12879-015-1184-5
2. Faulde M, Spiesberger M. Hospital infestations by the moth fly, *Clogmia albipunctata* (Diptera: Psychodinae), in Germany. J Hosp Infect. 2012;81:134–6. https://doi.org/10.1016/j.jhin.2012.04.006
3. El-Dib NA, El Wahab WMA, Hamdy DA, Ali MI. Case report of human urinary myiasis caused by *Clogmia albipunctata* (Diptera: Psychodidae) with morphological description of larva and pupa. J Arthropod Borne Dis. 2017;11:533–8.
4. Oboňa J, Balážovž L, Cáfal R, Dobránsky M, Filipovič P, Ivčič B, et al. Additions to the range expansion of the invasive moth midge *Clogmia albipunctata* (Williston, 1893) in Slovakia (Diptera Psychodidae). Folia faunistica Slovaca 17, 387–391.
5. Magiorakos A-P, Srinivasan A, Carey RB, Carmeli Y, Falagas ME, Giske CG, et al. Multidrug-resistant, extensively drug-resistant and pandrug-resistant bacteria: an international expert proposal for interim standard definitions for acquired resistance. Clin Microbiol Infect. 2012;18:268–81. https://doi.org/10.1111/j.1469-0691.2011.03570.x
6. Cassini A, Högberg LD, Plachouras D, Quattrocchi A, Hoxha A, Simonsen GS, et al. Attributable deaths and disability-adjusted life-years caused by infections with antibiotic-resistant bacteria in the EU and the European Economic Area in 2015: a population-level modelling analysis. Lancet Infect Dis. 2019;19:56–66. https://doi.org/10.1016/S1473-3099(18)30605-4
7. Vlamakis H, Chai Y, Beauregard P, Losick R, Kolter R. Sticking together: building a biofilm the *Bacillus subtilis* way. Nat Rev Microbiol. 2013;11:157–68. https://doi.org/10.1038/nrmicro2960
8. Madsen JS, Hylling O, Jacquiod S, Pécastaings S, Hansen LH, Riber L, et al. An intriguing relationship between the cyclic diguanylate signaling system and horizontal gene transfer. ISME J. 2018;12:2330–4. https://doi.org/10.1038/s41396-018-0183-0
9. Clarivet B, Grau D, Jumas-Bilak E, Jean-Pierre H, Pantel A, Parer S, et al. Persisting transmission of carbapenemase-producing Klebsiella pneumoniae due to an environmental reservoir in a university hospital, France, 2012 to 2014. Euro Surveill. 2016;21:30213. https://doi.org/10.2807/1560-7917.ES.2016.21.17.30213
10. McBain AJ, Bartolo RG, Catrenich CE, Charbonneau D, Ledder RG, Rickard AH, et al. Microbial characterization of biofilms in domestic drains and the establishment of stable biofilm microcosms. Appl Environ Microbiol. 2003;69:177–85. https://doi.org/10.1128/AEM.69.1.177-185.2003
11. Taylan-Ozkan A, Babur C, Kilic S, Nalbantoglu S, Dalkilic I, Mumcuoglu KY. Urogenital myiasis caused by *Psychoda albipennis* (Diptera: Nematocera) in Turkey. Int J Dermatol. 2004;43:904–5. https://doi.org/10.1111/j.1365-4632.2004.02051.x
12. Tu W-C, Chen H-C, Chen K-M, Tang L-C, Lai S-C. Intestinal myiasis caused by larvae of *Telmatoscopus albipunctatus* in a Taiwanese man. J Clin Gastroenterol. 2007;41:400–2. https://doi.org/10.1097/01.mcg.0000212615.66713.ba
13. Falagas ME, Koletsi PK, Bliziotis IA. The diversity of definitions of multidrug-resistant (MDR) and pandrug-resistant (PDR) *Acinetobacter baumannii* and *Pseudomonas aeruginosa*. J Med Microbiol. 2006;55:1619–29. https://doi.org/10.1099/jmm.0.46747-0

Address for correspondence: Thomas Bollinger, Klinikum Bayreuth, Preuschwitzer Str. 101, 95445 Bayreuth, Germany; e-mail: Thomas.Bollinger@klinikum-bayreuth.de

Atypical Pathogenicity of Avian Influenza (H3N1) Virus Involved in Outbreak, Belgium, 2019

Mieke Steensels, Philippe Gelaude, Steven Van Borm, Thierry Van Den Berg, Mickaël Cargnel, Virginie Roupie, Fabienne Rauw, Bénédicte Lambrecht

In 2019, an outbreak of avian influenza (H3N1) virus infection occurred among commercial poultry in Belgium. Full-genome phylogenetic analysis indicated a wild bird origin rather than recent circulation among poultry. Although classified as a nonnotifiable avian influenza virus, it was associated with reproductive tropism and substantial mortality in the field.

Avian influenza is a highly contagious viral disease of poultry, able to infect all species of birds (*1*). Of the 2 existing pathotypes, low pathogenicity avian influenza (LPAI) and highly pathogenic avian influenza (HPAI), infection with LPAI virus is mostly undetected in a flock but can cause some respiratory signs, egg drop, lethargy, and limited mortality (*2*,*3*). Avian influenza H5/H7 subtypes are all notifiable to the authorities in Europe because adaptive mutations can influence the polybasic nature of the hemagglutinin (HA) cleavage site, resulting in HPAI emergence (*4*). For all other avian influenza subtypes, only those with an intravenous pathogenicity index (IVPI) >1.2 must be reported (*5*).

The Study

In January 2019, H3N1 virus was isolated from an outdoor laying hens farm in Belgium. The affected flock was culled, but 3 months later (April), H3N1 virus was again detected on this farm (*5*–*8*), indicative of incomplete virus elimination. Since then, 82 holdings in northwestern Belgium were infected with H3N1 virus in a 16-week period, involving different poultry species and types of farms (Figure 1, panels A, B). In southern Belgium, only 1 farm was clinically affected, for which a direct link with a positive farm in northwestern Belgium was identified. Also, 5 farms with asymptomatic poultry tested positive for H3N1 virus (Figure 1, panel A), without a clear link to the category of farm or species (2 broiler, 1 outdoor laying, 1 ostrich, and 1 broiler breeder farm). In France, 3 farms were H3N1-positive; 2 showed a direct link with a company from the affected area of Belgium (*9*).

The clinical picture in the field started mostly with discolored eggs for laying hens and breeders, followed by an increased mortality rate of up to 60% in breeder hens and 40% in laying hens. In addition, a marked egg drop, up to 100%, was reported. Recovered animals never fully regained their laying potential. A second wave of mortality caused by secondary infection was detected later. During autopsy, specific lesions were detected (e.g., point bleeding in the proventriculus, trachea, and brain; congestion of the kidneys, ovary, and brain; and atrophy of the oviduct, resulting in egg yolk leakage and peritonitis).

For the virus strain isolated in April from poultry on the index farm (A/Gallus gallus/Belgium/3497_0001/2019), hereafter called the 3497_April isolate, the IVPI was 0.13 (Sciensano Bioethics Committee approval 20170117-01), indicating a low pathogenicity phenotype. The complete coding sequences of the HA and neuraminidase (NA) genes, identified by Sanger sequencing, of the strains isolated in January (A/Gallus gallus/Belgium/609/2019 [H3N1]; GenBank accession nos. MK972679 [H3]; MK972680 [N1]) and April (A/Gallus gallus/Belgium/3497_0001/2019 [H3N1]; GenBank accession nos. MK972681 [H3] and MK972682 [N1]) confirmed their relationship. These results demonstrated that the virus from January 2019 had evolved into a poultry-adapted strain by April 2019, with a deletion in the stalk of the NA gene, previously described as

Author affiliations: Sciensano, Brussels, Belgium (M. Steensels, S. Van Borm, T. Van Den Berg, M. Cargnel, V. Roupie, F. Rauw, B. Lambrecht); Animal Health Vlaanderen, Torhout, Belgium (P. Gelaude)

DOI: https://doi.org/10.3201/eid2608.191338

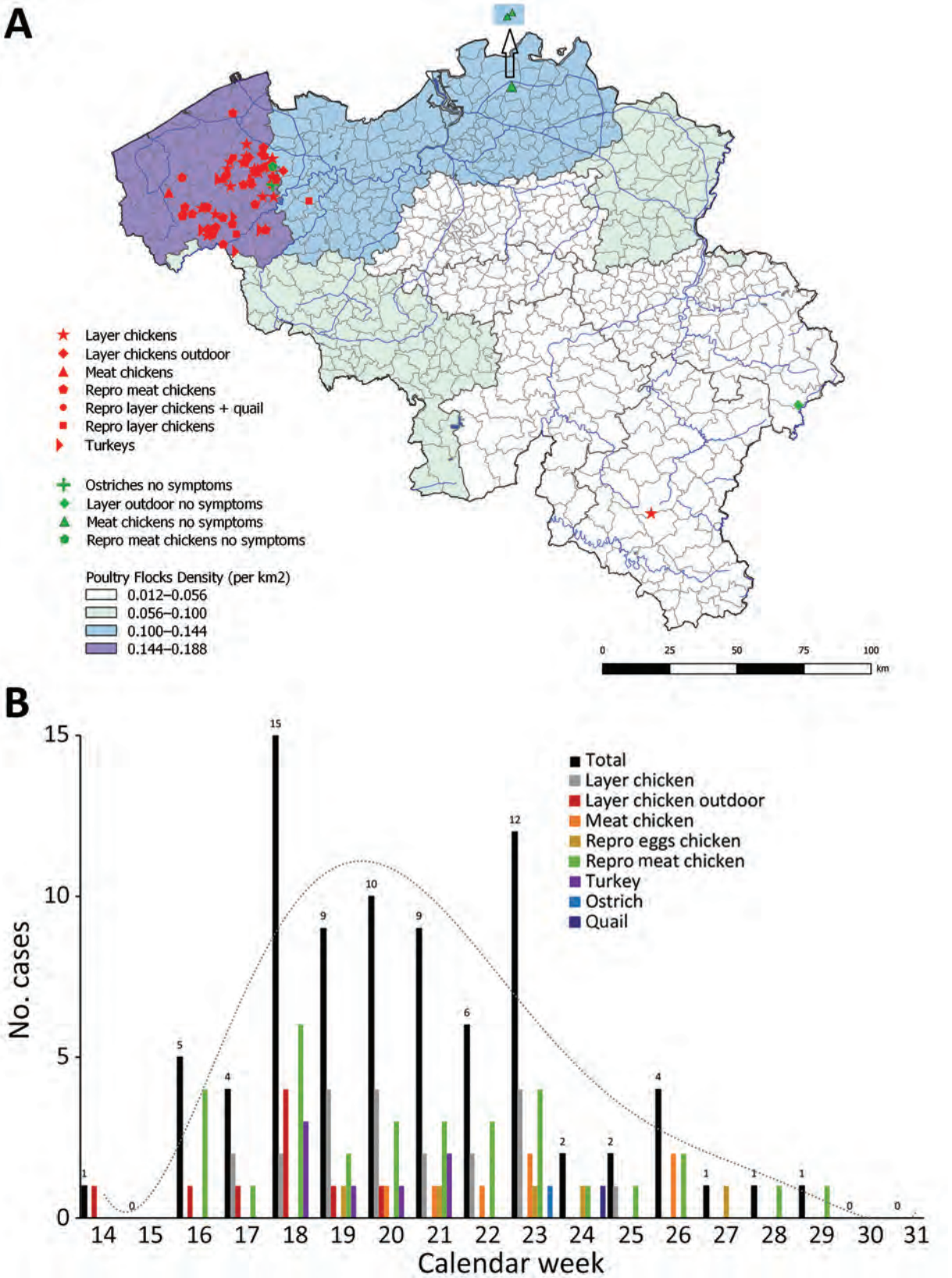

Figure 1. Outbreaks of avian influenza (H3N1) virus among poultry in Belgium, 2019. A) Geographic distribution; B) weekly number of newly identified farms with avian influenza (H3) and poultry species involved. Repro, reproduction.

crucial for adaptation from wild birds to poultry (*10,11*). Next-generation sequencing of the 3497_April isolate demonstrated that the most closely related publicly available sequence of all 8 complete genome segments (accession nos. MN006980–7) linked to avian influenza viruses from Eurasia that were circulating in wild birds with occasional spillover to poultry (Table 1). Using neighbor-joining and maximum-likelihood phylogenetic analyses, we were unable to clearly associate the 2019 outbreak virus with recent virus isolates from poultry (data not shown).

We performed in vivo infection studies (Sciensano Bioethics Committee approval 20180222-01) with the 3497_April isolate, obtained after inoculation of a lung/trachea homogenate into 9-day-old embryonated specific pathogen–free chicken eggs. First, we inoculated 11-week-old specific pathogen–free White Leghorn chickens oculonasally with 10^6 50% egg infectious dose (EID_{50}) of the 3497_April virus, but no clinical signs were noted over 14 days. At the end of the experiment, 100% (by nucleoprotein [NP] competition ELISA; IDVet, https://www.id-vet.com) and 90% (by standard hemagglutination inhibition [HI]) of the infected birds had seroconverted, confirming infection. Subsequently, to evaluate a possible synergistic effect of a potential bacterial cofactor, we inoculated a non–antibiotic treated lung/trachea homogenate from an H3N1 virus–confirmed animal simultaneously with the H3N1 isolate. At 6–11 days postinoculation (dpi), 40% of the birds exhibited clinical signs (lethargy, clouded eyes, and ruffled feathers) and some died (10% on 13 dpi). This co-infection did not reproduce the clinical picture observed in the field, indicating that a bacterial cofactor would not be necessary to produce the clinical signs seen in the field.

Because the clinical effect in the field was greater for layer hens in production, we performed a third in vivo evaluation in 24-week-old conventional Bovans Brown laying hens, avian influenza negative serologically (NP ELISA and HI [*5*]) and virologically (real-time reverse transcription PCR [*7*]) at arrival. Six chickens were infected with 10^6 EID_{50}/bird and 6 noninfected sentinel birds were added at 1 dpi. Of the 6 infected birds, 2 died at 6 and 7 dpi, showing either no or mild clinical signs at 5 dpi. Autopsy of each bird that died confirmed some of the lesions described for birds in the field (pronounced congestion in the brain, kidney, and intestine; and kidney enlargement). Among the sentinel birds, 1 bird died at 8 dpi without prior clinical signs or clear pathologic lesions during autopsy but demonstrated a higher amount of viral RNA (10^5) in the organs compared with the other sentinel birds at the end of the study (21 dpi) (Figure 2, panel B). Analysis of viral RNA excretion (Figure 2, panel A) demonstrated viral shedding from all infected and sentinel birds and a significant increase ($p<0.05$) from 2 dpi to 5 dpi in both groups (nonparametric Wilcoxon signed-rank test). Excretion did not differ between sentinel and infected chicken except at 5 dpi, when cloacal excretion by sentinel chickens was significantly higher ($p<0.05$) than that by infected chickens (nonparametric Mann-Whitney test). No significant difference was observed between oropharyngeal and

Table 1. Most homologous publicly available sequence for each gene segment of A/Gallus gallus/Belgium/3497_0001/2019 (H3N1) virus*

Gene	Closest BLAST hit (closest poultry BLAST hits)		
	Sequences	Accession no.	Nucleotide identity, %
PB2	A/tufted duck/Georgia/1/2012 (H2N3) (A/chicken/Hubei/ZYSJF15/2016[H9N2])	MF147767.1 (KY415880.1)	97.74 (96.66)
PB1	A/northern shoveler/Egypt/MB-D-695C/2016 (H7N3) (A/chicken/Sichuan/k141/2017[H5N6])	MN208053.1 (MH715337.1)	98.58 (98.24)
PA	A/mallard duck/Netherlands/56/2015 (H3N2) (A/pigeon/Anhui/08/2013[H3N8])	MF755261.1 (KJ579961.1)	98.68 (96.68)
HA	A/Mallard/Netherlands/37/2015 (H3N8) (A/chicken/Viet Nam/HN-1724/2014[mixed])	MK414733.1 (MK963734.1)	98.32 (96.68)
NP	A/duck/Mongolia/543/2015 (H4N6) (A/chicken/Italy/22A/1998[H5N9], A/chicken/Vietnam/HU1-976/2014[H9N2])	LC121413.1 (CY022624.1, LC069933.1)	98.50 (96.79, 96.64)
NA	A/mallard duck/Georgia/7/2015 (H6N1) (A/chicken/Vietnam/HU4-26/2015[H6N1], A/chicken/France/150169a/2015[H5N1])	MF694086.1 (LC339717.1, KU310449.1)	97.94 (96.78, 96.45)
M	A/mallard/Netherlands/89/2017 (H4N6) (A/domestic duck/Georgia/9/2016[H4N6])	MK192396.1 (MF694025.1)	98.91 (98.11)
NS	A/mallard duck/Netherlands/31/2013 (H10N7) (A/chicken/France/150169a/2015[H5N1], A/chicken/Korea/C47/2009(H9N2))	KX979173.1 (KU310451.1, KY785842.1)	99.19 (98.04, 97.46)

*Determined by BLASTn analysis (https://blast.ncbi.nlm.nih.gov/Blast.cgi). NA, neuraminidase; M, matrix; neuraminidase; HA, hemagglutinin; matrix; NS, nonstructural; PA, polymerase acidic; PB, polymerase basic.

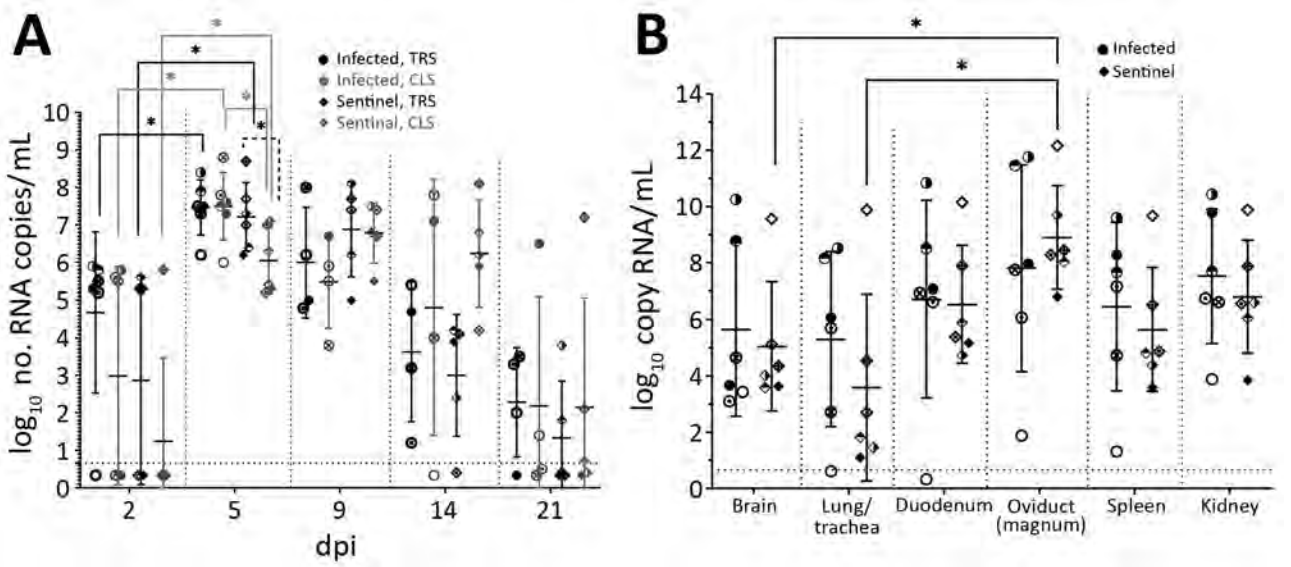

Figure 2. Viral presence in birds during experimental infection with avian influenza (H3N1) isolated from poultry in Belgium, 2019. The individual excretion values are shown (different patterns in circles and diamonds correspond to individual birds) in addition to the average group value ± SDs (error bars). Asterisks (*) indicate statistically relevant differences between time points, groups, or organs, p<0.05. Note: for diluted viral isolates the correspondence between log10 (no. copies/mL) and log10 (50% egg infectious dose/mL) is a difference of ≈1 log less in egg infectious dose. The exact link (by determining the titer of infectious virus in the samples) was considered beyond the scope of this article. A) Viral RNA excretion of infected and sentinel birds at different points after infection, by respiratory gastrointestinal tract samples. B) Viral presence in the organs of infected and sentinel birds at time of death or the end of the experiment (21 dpi), determined by real-time reverse transcription PCR. Viral RNA excretion or presence is expressed as the logarithm of the number of viral RNA copies/mL as quantification was performed relative to an external curve during real-time reverse transcription PCR analysis. CLS, cloacal samples; dpi, days postinfection; repro, reproduction; TRS, oropharyngeal swab samples.

cloacal excretions, except at 5 dpi oropharyngeal excretion by sentinel chickens was higher (p<0.05) (nonparametric Wilcoxon signed-rank test).

Conclusions

The viral RNA excretion period of the H3N1 virus under investigation demonstrates an extended period of virus excretion compared with that generally expected for LPAI viruses. LPAI virus excretion mostly starts 1–2 days after infection and continues for 7–10 days, peaking on day 5, then quickly declining because of immunity onset (*12,13*). In sentinel birds, the viral RNA concentration was significantly higher (p<0.05) in the oviduct than in the brain and lung/trachea

Table 2. Seroconversion of sentinel birds and birds infected with A/Gallus gallus/Belgium/3497_0001/2019 (H3N1) virus

Bird	9 dpi				14 dpi				21 dpi			
	ELISA-NP†		HI‡		ELISA-NP†		HI‡		ELISA-NP†		HI‡	
	S/N, %	IR	log 2	IR	S/N, %	IR	log 2	IR	S/N, %	IR	log 2	IR
Infected 1	4.3	+	6	+	4.8	+	10	+	5.5	+	8	+
Infected 2	5.0	+	6	+	5.6	+	9	+	4.7	+	9	+
Infected 3	5.8	+	6	+	4.8	+	9	+	4.3	+	9	+
Infected 4	10.2	+	3	–	9.0	+	3	–	12.6	+	3	–
Infected 5	NA	NA	NA	NA	NA	NA	NA		NA	NA	NA	NA
Infected 6	NA	NA	NA	NA	NA	NA	NA		NA	NA	NA	NA
Average (SD)	6.3 ±2.6		5.3 ±1.5		6.0 ±2.0		7.8 ±3.2		6.8 ±3.9		7.3 ±2.9	
Sentinel 1	17.6	+	2	–	5.3	+	7	+	4.8	+	9	+
Sentinel 2	5.9	+	2	–	4.9	+	7	+	4.8	+	7	+
Sentinel 3	7.7	+	2	–	4.9	+	6	+	4.6	+	8	+
Sentinel 4	NA	NA	NA	NA	NA	NA	NA		NA	NA	NA	NA
Sentinel 5	5.7	+	3	–	4.7	+	8	+	4.8	+	9	+
Sentinel 6	5.6	+	2	–	4.4	+	7	+	5.5	+	8	+
Average (SD)	8.5 ±5.1		2.2 ±0.4		4.8 ±0.3		7.0 ±0.7		4.9 ±0.4		8.2 ± 0.8	

*dpi, days postinfection; ELISA-NP, nucleoprotein competition ELISA; HI, hemagglutination inhibition; IR, immune response; NA, not applicable because of bird death; S/N, signal-to-noise ratio; +, positive immune response; –, negative immune response.
†(IDVet, https://www.id-vet.com/). ELISA data are presented as the percentage of competition detected, the S/N.
‡HI test with the homologous H3N1 antigen. HI data are presented as log2 of the HI titer.

(nonparametric Friedman test) (Figure 2, panel B); differences with other organs were not significant. In infected chickens, this trend was confirmed, albeit not significantly. The systemic distribution, although limited to chickens during laying, is a typical feature for HPAI and is not expected for LPAI. All birds had seroconverted at 9 dpi, as measured by NP competition ELISA, and all but 1 infected bird seroconverted at 9 dpi and all surviving sentinels had seroconverted at 14 dpi as measured by HI (Table 2).

No virus transmission to humans was reported. All 20 analyzed conjunctival swab specimens from farmers without clear influenza-like symptoms on the infected farms were negative for H3N1 virus by the Belgian National Reference Center of Influenza (I. Thomas, Sciensano, pers. comm., 2019 Jul 31).

Although this virus was classified as LPAI according to official definitions using IVPI or molecular criteria, it was more pathogenic in laying hens than expected for a non-notifiable LPAI. Increased pathogenicity was shown by systemic distribution, clinical signs, and increased transmissibility in poultry (especially laying hens) under field and experimental conditions.

Acknowledgments

We thank the technical staff of the reference laboratory for Avian Influenza/Newcastle Disease in Belgium for their work during this epidemic, specifically Catherine Rasseneur, Alexandre Ausloos, Victoria Duchatel, Gloria Villalba, and Vincent Van Hoof. We also thank Christophe Delgrange for his involvement in bird handling and sampling assistance for animal experiments and Isabelle Thomas and Cyril Barbezange for analyzing the human conjunctival swab samples and sharing the information.

Financing of diagnostic analysis was provided by the Federal Agency for the Safety of the Food Chain.

About the Author

Dr. Steensels is head of the Reference Laboratory for Avian Influenza and Newcastle Disease in Belgium, and has research interests in diagnostic testing as well as pathogenicity of and vaccination against avian influenza and Newcastle disease.

References

1. Alexander DJ. A review of avian influenza in different bird species. Vet Microbiol. 2000;74:3–13. https://doi.org/10.1016/S0378-1135(00)00160-7
2. Bonfante F, Patrono LV, Aiello R, Beato MS, Terregino C, Capua I. Susceptibility and intra-species transmission of the H9N2 G1 prototype lineage virus in Japanese quail and turkeys. Vet Microbiol. 2013;165:177-83. https://doi.org/10.1016/j.vetmic.2013.03.014 PMID: 23597652
3. Perdue ML, Suarez DL. Structural features of the avian influenza virus hemagglutinin that influence virulence. Vet Microbiol. 2000;74:77–86. https://doi.org/10.1016/s0378-1135(00)00168-1
4. Horimoto T, Kawaoka Y. Reverse genetics provides direct evidence for a correlation of hemagglutinin cleavability and virulence of an avian influenza A virus. J Virol. 1994; 68:3120–8. https://doi.org/10.1128/JVI.68.5.3120-3128.1994
5. World Organisation for Animal Health. Chapter 2.3.4. Avian influenza. In: Manual of diagnostic tests and vaccines for terrestrial animals 2015. Paris: The Organisation; 2015.
6. Van Borm S, Steensels M, Ferreira HL, Boschmans M, De Vriese J, Lambrecht B, et al. A universal avian endogenous real-time reverse transcriptase-polymerase chain reaction control and its application to avian influenza diagnosis and quantification. Avian Dis. 2007;51(Suppl): 213–20. https://doi.org/10.1637/7552-033106R.1
7. Spackman E, Senne DA, Myers TJ, Bulaga LL, Garber LP, Perdue ML, et al. Development of a real-time reverse transcriptase PCR assay for type A influenza virus and the avian H5 and H7 hemagglutinin subtypes. J Clin Microbiol. 2002;40:3256–60. https://doi.org/10.1128/JCM.40.9.3256-3260.2002
8. Hoffmann B, Hoffmann D, Henritzi D, Beer M, Harder TC. Riems influenza a typing array (RITA): an RT-qPCR-based low density array for subtyping avian and mammalian influenza a viruses. Sci Rep. 2016;6:27211. https://doi.org/10.1038/srep27211
9. Cauchard J, Briand FX, Cherbonnel M, Eterradossi N, Grasland B, Le Bouquin S, et al. Foyers H3N1 en France (nord) et en Belgique: situation au 14 juin 2019 [cited 2019 Jul 31]. https://www.plateforme-esa.fr/article/foyers-h3n1-en-france-nord-et-en-belgique-situation-au-14-juin-2019
10. Sorrell EM, Song H, Pena L, Perez DR. A 27-amino-acid deletion in the neuraminidase stalk supports replication of an avian H2N2 influenza A virus in the respiratory tract of chickens. J Virol. 2010;84:11831–40. https://doi.org/10.1128/JVI.01460-10
11. Munier S, Larcher T, Cormier-Aline F, Soubieux D, Su B, Guigand L, et al. A genetically engineered waterfowl influenza virus with a deletion in the stalk of the neuraminidase has increased virulence for chickens. J Virol. 2010;84:940–52. https://doi.org/10.1128/JVI.01581-09
12. Bergervoet SA, Germeraad EA, Alders M, Roose MM, Engelsma MY, Heutink R, et al. Susceptibility of chickens to low pathogenic avian influenza (LPAI) viruses of wild bird- and poultry-associated subtypes. Viruses. 2019;11:E1010. https://doi.org/10.3390/v11111010
13. Swayne DE. Epidemiology of avian influenza in agricultural and other man-made systems. In: Swayne DE, editor. Avian influenza, 1st edition. Hoboken (NJ): Wiley-Blackwell; 2008.

Address for correspondence: Mieke Steensels, Sciensano, Avian Virology and Immunology, Groeselenberg 99, Brussels 1180, Belgium; email: Mieke.Steensels@sciensano.be

In Vivo Observation of Trombiculosis with Fluorescence–Advanced Videodermatoscopy

Alice Ramondetta,[1] Simone Ribero,[1] Andrea Peano, Pietro Quaglino,[2] Paolo Broganelli[2]

Trombiculosis is a skin infestation by larvae of mites of the Trombiculidae family. We used fluorescence–advanced videodermatoscopy to diagnose trombiculosis in a woman in Italy with targetoid patches. This method might be useful for identifying atypical manifestations of trombiculosis.

Trombiculosis is a skin infestation by mites of the Trombiculidae family. Adult mites live and reproduce on the surface of the soil, whereas the larvae feed on warm-blooded vertebrates, including humans. These mites are also known as harvest mites or chiggers (*1*–*6*). Although trombiculid mites are endemic to most of the world, certain soil conditions limit common habitats to grassy fields, forests, parks, gardens, and the moist areas along lakes and streams (*1*).

Only the larvae (0.15–0.3 mm long), which are 6-legged and orange or bright red, are responsible for chigger bites. Infestation usually occurs when larvae are particularly abundant, throughout late summer and autumn (*7*). Trombiculid larvae do not burrow into the host's skin; instead, they use jaw-like structures to attach to hairless areas on the host, secrete digestive enzymes that liquify host epidermal cells, and feed on broken-down tissue and digested cutaneous cells for 2–10 days (*1*). The host response is mainly caused by sensitization to the injected saliva. Its intensity might vary from a slightly irritable erythema to papules or vesicles with intense itch (*3*).

Trombiculid mites are also vectors of infectious agents. For example, *Leptotrombidium* mites transmit scrub typhus in the Far East (*3*). We report a case of trombiculosis in a woman in Turin, Italy.

Case Report

In April 2019, a 48-year-old woman sought care at the Dermatology Clinic University Hospital of Turin, Turin, Italy, for onset of small roundish, targetoid patches, with peripheral erythematous halo and central lightening, on her trunk (Figure 1). The patient was otherwise in good health. A few days before the patches developed, she had gone on an excursion in the countryside near Turin.

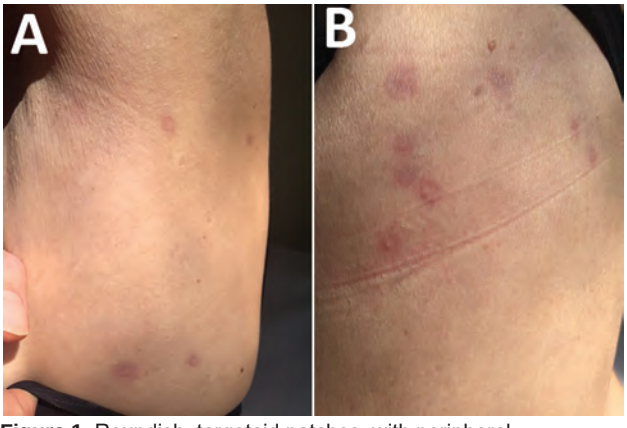

Figure 1. Roundish, targetoid patches, with peripheral erythematous halo and central lightening located on left abdomen (A) and on the back (B) of a 48-year-old woman with trombiculosis, Italy, April 2019.

We used fluorescence–advanced videodermatoscopy (FAV), an optical electronic system using a monochromatic light-emitting source with an λ of 405 nm (±5 nm) and a field of view of 340 μm, to examine the patient. FAV uses the ability of endogenous molecules to absorb specific wavelengths and emit fluorescence. The examination is conducted in vivo; the optical device is directly applied to the skin. The images are visualized in real time by using grayscale to indicate the levels of light absorption (i.e., black indicates no fluorescence, and white indicates highest fluorescence) (*8*).

By placing the probe on one of the patient's skin patches, we visualized an oval-shaped mite with 3

Author affiliation: Università degli Studi di Torino, Turin, Italy

DOI: https://doi.org/10.3201/eid2608.200077

[1]These first authors contributed equally to this article.

[2]These senior authors contributed equally to this article.

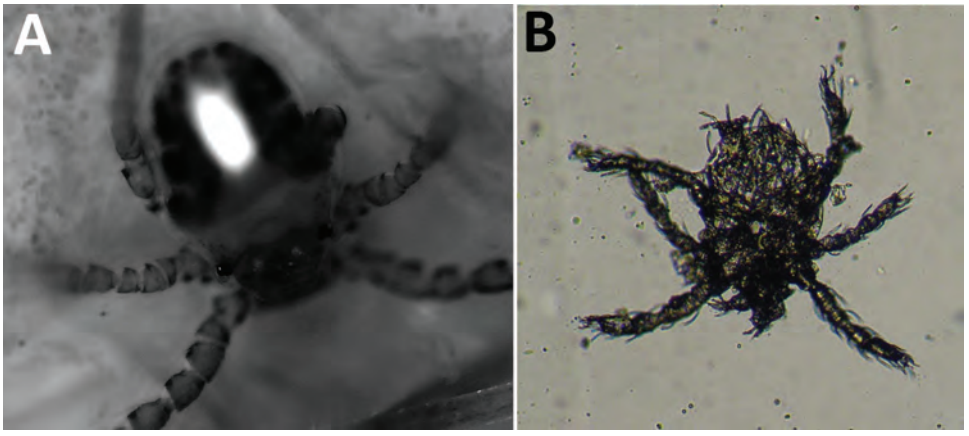

Figure 2. Images of trombiculid mites from infestation of a 48-year-old woman, Italy, April 2019. A) Fluorescence–advanced videodermatoscopy image shows oval body with 3 pairs of legs. Original magnification ×500. B) Optical microscope examination of 1 larva detected from a superficial skin scraping. Original magnification ×100.

pairs of legs (Figure 2, panel A). We identified this image as the larval stage of a trombiculid mite. We also detected 1 larva on direct examination from a superficial skin scraping (Figure 2, panel B). The patient was treated with topical ivermectin for 7 days, resulting in complete regression of the lesions.

Conclusions

FAV facilitated a real-time diagnosis of trombiculosis in this case. Without this technology, the diagnosis of trombiculosis might have been complicated by the atypical presentation (trombiculosis usually manifests with erythematous homogeneous macules) and seasonality of the case (in Italy, trombiculosis is more prevalent in autumn [*7*]). To our knowledge, the diagnosis of trombiculosis using videodermatoscopic findings has been reported in only 1 other case (*6*).

We suspect the agent responsible for this case was the *Neotrombicula autumnalis* mite, the most frequent causative agent of trombiculosis in Europe (*2*–*5*). However, because we could not collect larvae to perform morphologic or molecular studies, we could not definitively identify the mite. At least 4 other species of trombiculid mites might cause trombiculosis in Europe, namely *Kepkatrombicula desaleri*, *Blankaartia acuscutellaris*, *Trombicula toldti*, and *N. inopinata* (*9*). In addition, the number of cases caused by species other than *N. autumnalis* might be underestimated because, in most reports, the identification does not appear to have been attributed with sufficient taxonomic criteria (*9*).

About the Author

Dr. Ramondetta is a fourth-year resident in dermatology at the Dermatology Clinic of the University of Turin. Her primary research interests include pediatric dermatology and digital dermoscopy.

References

1. McClain D, Dana AN, Goldenberg G. Mite infestations. Dermatol Ther. 2009;22:327–46. https://doi.org/10.1111/j.1529-8019.2009.01245.x
2. Gasser R, Wyniger R. Distribution and control of Trombiculidae with special reference to *Trombicula autumnalis* [in German]. Acta Trop. 1955;12:308–26.
3. di Meo N, Fadel M, Trevisan G. Pushing the edge of dermoscopy in new directions: entomodermoscopy of *Trombicula autumnalis*. Acta Dermatovenerol Alp Panonica Adriat. 2017;26:45–6. https://doi.org/10.15570/actaapa.2017.14
4. Jones JG. Chiggers. Am Fam Physician. 1987;36:149–52.
5. Brennan JM, Goff ML. Keys to the genera of chiggers of the western hemisphere (acarina: trombiculidae). J Parasitol. 1977;63:554–66. https://doi.org/10.2307/3280021
6. Nasca MR, Lacarrubba F, Micali G. Diagnosis of trombiculosis by videodermatoscopy. Emerg Infect Dis. 2014;20:1059–60. https://doi.org/10.3201/eid2006.130767
7. Leone F, Di Bella A, Vercelli A, Cornegliani L. Feline trombiculosis: a retrospective study in 72 cats. Vet Dermatol. 2013;24:535–e126. https://doi.org/10.1111/vde.12053
8. Sanlorenzo M, Vujic I, De Giorgi V, Tomasini C, Deboli T, Quaglino P, et al. Fluorescence-advanced videodermatoscopy: a new method for in vivo skin evaluation. Br J Dermatol. 2017;177:e209–10. https://doi.org/10.1111/bjd.15594
9. Stekolnikov AA, Santibáñez P, Palomar AM, Oteo JA. Neotrombicula inopinata (Acari: Trombiculidae) - a possible causative agent of trombiculiasis in Europe. Parasit Vectors. 2014;7:90. https://doi.org/10.1186/1756-3305-7-90

Address for correspondence: Alice Ramondetta, Dermatology Clinic, Department of Medical Sciences, University of Turin, via Cherasco 23 Turin, Italy; email: ramondetta.alice@gmail.com

Evolution and Antigenic Drift of Influenza A(H7N9) Viruses, China, 2017–2019

Jiahao Zhang,[1] Hejia Ye,[1] Huanan Li,[1] Kaixiong Ma, Weihong Qiu, Yiqun Chen, Ziwen Qiu, Bo Li, Weixin Jia, Zhaoping Liang, Ming Liao, Wenbao Qi

After a sharp decrease of influenza A(H7N9) virus in China in 2018, highly pathogenic H7N9 viruses re-emerged in 2019. These H7N9 variants exhibited a new predominant subclade and had been cocirculating at a low level in eastern and northeastern China. Several immune escape mutations and antigenic drift were observed in H7N9 variants.

Since emerging in China in 2013, influenza A(H7N9) viruses have continued to circulate in mainland China, sporadically causing human infection (*1*–*3*). As of February 2020, a total of 1,568 laboratory-confirmed human cases and 616 related deaths had been reported, for a fatality rate of ≈40% (http://www.fao.org/ag/againfo/programmes/en/empres/H7N9/situation_update.html). In mid-2016, a highly pathogenic avian influenza (HPAI) virus of subtype H7N9 emerged, and the number of cases in humans began to rise sharply during a fifth wave (*4*,*5*). Animal studies indicated that these HPAI H7N9 viruses are highly virulent in chickens and have gained transmissibility among ferrets (*5*–*7*). Also, the cocirculation of HPAI (H7N9) viruses caused high genetic diversity and host adaption (*8*), posing public health concerns.

Although HPAI H7N9 viruses spread widely across China in 2017 (*8*,*9*), after an influenza H5/H7 bivalent vaccine for poultry was introduced in September 2017, the prevalence of the H7N9 viruses in birds and humans decreased dramatically (*6*,*10*). In early 2019, when the novel HPAI H7N9 viruses re-emerged, the isolation of HPAI H7N9 viruses from birds revealed them to be responsible for continuous epidemics in northeastern China (*11*). In March 2019, a human death in Gansu, China, was confirmed to have been caused by an H7N9 virus (*12*). To explore the prevalence and evolution of influenza A(H7N9) viruses, we sequenced 28 hemagglutinin (HA) and neuraminidase (NA) genes of poultry-origin H7N9 viruses circulating in China during 2019.

The Study

During January–December 2019, we conducted poultry surveillance for influenza virus at live poultry markets in 15 provinces of China (Appendix Figure 9, https://wwwnc.cdc.gov/EID/article/26/8/20-0244-App1.pdf). We isolated 28 H7N9 viruses from tracheal and cloacal swab samples of chickens in Shandong, Hebei, and Liaoning Provinces (Figure 1, panel C; Appendix Table 1). Vaccination of all chickens in China was compulsory according to the Ministry of Agriculture and Rural Affairs of the People's Republic of China. We sequenced the HA and NA genes of 28 H7N9 viruses and submitted the sequences to GISAID (https://www.gisaid.org) (Appendix Table 2). All H7N9 viruses had 4 continuous basic amino acids at cleavage sites (i.e., KRKRTAR/G and KRKRIAR/G), suggestive of high

Author affiliations: College of Veterinary Medicine, South China Agricultural University, Guangzhou, China (J. Zhang, H. Li, K. Ma, Y. Chen, Z. Qiu, B. Li, W. Jia, M. Liao, W. Qi); National Avian Influenza Para-Reference Laboratory, Ministry of Agriculture and Rural Affairs of the People's Republic of China, Guangzhou (J. Zhang, H. Li, W. Jia, M. Liao, W. Qi); Key Laboratory of Animal Vaccine Development, Ministry of Agriculture and Rural Affairs of the People's Republic of China, Guangzhou (J. Zhang, W. Jia, M. Liao, W. Qi); National and Regional Joint Engineering Laboratory for Medicament of Zoonoses Prevention and Control, National Development and Reform Commission, Guangzhou (J. Zhang, W. Jia, M. Liao, W. Qi); Key Laboratory of Zoonoses Prevention and Control of Guangdong Province, Guangzhou (J. Zhang, W. Jia, M. Liao, W. Qi); Guangzhou South China Biological Medicine Co., Ltd, Guangzhou (H. Ye, W. Qiu, Z. Liang); Guangdong Laboratory for Lingnan Modern Agriculture, Guangzhou (W. Jia, M. Liao, W. Qi)

DOI: https://doi.org/10.3201/eid2608.200244

[1]These authors contributed equally to this article.

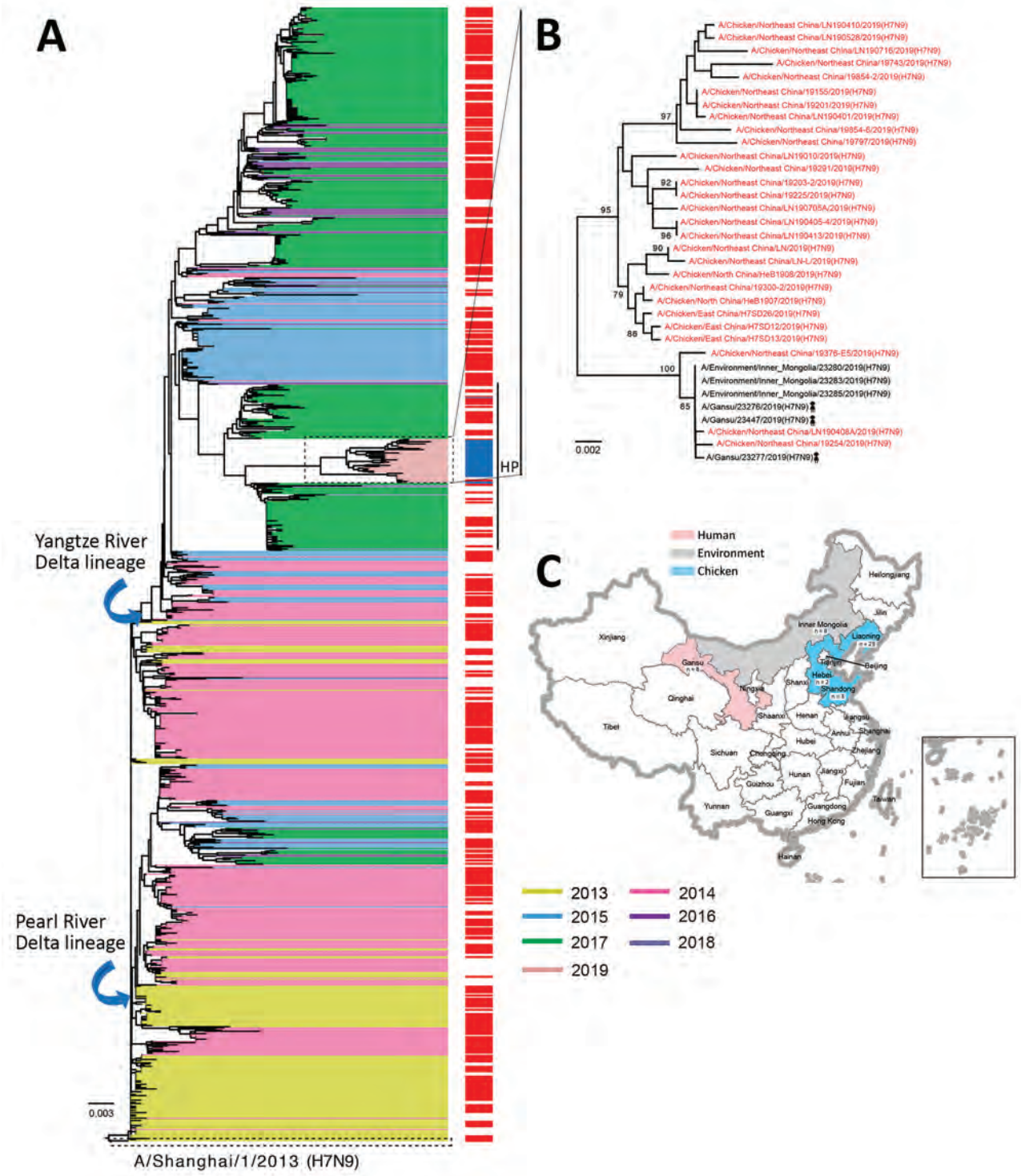

Figure 1. Evolutionary history of influenza A(H7N9) viruses, China, 2017–2019. A) Phylogenic tree of the hemagglutinin gene of H7N9 viruses. Colors indicate reference H7N9 viruses (n = 1,038) from each wave together with the H7N9 isolates from this study (panel B). Red on the right of the tree indicates isolates from humans. All branch lengths are scaled according to the numbers of substitutions per site. The tree was rooted by using A/Shanghai/1/2013(H7N9), which was collected in February 2013. B) Hemagglutinin gene tree revealing a single cluster of highly pathogenic H7N9 viruses circulating during 2019. Red indicates the H7N9 isolates from this study. Scale bar represents number of nucleotide substitutions per site. C) Distribution of highly pathogenic influenza A(H7N9) viruses during 2019. The backgrounds indicate the sampling spaces of highly pathogenic influenza A(H7N9) viruses during 2019 in humans (red), environment (gray), and chickens (blue). The map was designed by using ArcGIS Desktop 10.4 software (ESRI, http://www.esri.com).

pathogenicity. Phylogenic analysis demonstrated that the HA and NA genes of all of these HPAI H7N9 viruses belonged to the Yangtze River Delta lineage and formed a new subclade (Figure 1, panel A), which exhibited a long genetic distance to the HPAI H7N9 viruses that persisted during 2017–2018. In particular, the HA and NA genes of A/chicken/northeast China/19376-E5/2019(H7N9), A/chicken/northeast China/19254/2019(H7N9), and A/chicken/northeast China/LN190408A/2019(H7N9) were genetically closely related to the human-infecting influenza A(H7N9) viruses from Gansu (Figure 1, panel B; Appendix Figures 1–3), implying the potential risk for the reemerged HPAI H7N9 viruses to infect humans.

A root-to-tip regression analysis of temporal structure revealed aspects of the clock-like structure of 189 H7N9 viruses (correlation coefficient 0.89; R^2 0.95) during 2013–2019 (Figure 2, panel A). The epidemic HPAI H7N9 viruses had circulated in China since 2017 and can be classified into 2 sublineages, A and B. The HA and NA genes of the HPAI H7N9 viruses in 2019 belonged to a new sublineage B, whereas the HPAI H7N9 viruses circulating in 2017–2018 grouped into sublineage A (Figure 2, panel B; Appendix Figures 4, 5). Using the evolutionary rates of HA and NA, we estimated the times of origin (95% highest population density) of HPAI H7N9 viruses in sublineage B, which were September 2017–June 2018 for HA and April 2017–May 2018 for NA. Our HPAI H7N9 isolates exhibited traits of sublineages B-1 and B-2. We observed that the HPAI H7N9 viruses in eastern and northeastern China belonged to sublineage B-2 (Figure 2, panel B). However, in mid-2019, the HPAI H7N9 viruses continued to evolve and formed sublineage B-1, which suggested that the estimated times to the most recent common ancestors were May 2019 for HA genes and February 2019 for NA genes. Also, the human- and chicken-origin HPAI H7N9 viruses from Liaoning, Gansu, and Inner Mongolia clustered together in sublineage B-1. These results indicate that the poultry-origin H7N9 virus in sublineage B-1 emerged before the human spillover event in March 2019.

Although no substantial difference surfaced in the substitution rate of HA genes between H7N9 viruses during 2017–2018 and the viruses during 2019, the increased substitution rate occurred in the first and second codons of reemerged HPAI H7N9 viruses (Appendix Table 4). In a maximum clade credibility tree of the HA gene, 9 independently occurring mutations gave rise to the new sublineage-B circulating in 2019, including A9S, R22K, E71K, I78V, T116K, V125T, A151T, K301R, D439N (H7 numbering, https://www.fludb.org/brc/haNumbering.spg) (Figure 2, panel B), and only the V125T and A151T substitutions of the HA protein were reported as immune escape mutations (*13*). In addition, sublineage B-1 appeared to have acquired 3 parallel K184R, I499V, I520T (H7 numbering) mutations. The prevailing K184R substitutions of HPAI H7N9 viruses occurred during 2019. The K184R mutation was located in the antigenic site B and receptor binding region (Appendix Figure 6), suggesting that K184R was a potential mediator of viral antigenicity.

We used a hemagglutinin inhibition assay with an antigen of 15 H7N9 viruses circulating during 2017–2019, along with specific antiserum of 6 H7N9 viruses and 2 commonly used reassortant inactivated vaccines, H7N9-Re-2 and H7N9-rGD76, as controls. Antiserum from chickens vaccinated with H7N9-Re-2 strains showed high titers (9–10 $\log_2$) and with H7N9-rGD76 strains showed low titers (4–8 $\log_2$) to the HPAI H7N9 viruses circulating during 2018–2019 (Table 1). Moreover, the cross–hemagglutinin inhibition assay suggested statistically significant antigenic differences between the HPAI H7N9 viruses circulating during 2017 and during 2018–2019 (Table 2; Appendix Figure 7), indicative of antigenic drift of the reemerged HPAI H7N9 viruses. H7N9-Re-2 and H7N9-rGD76 inactivated vaccines have been widely used in chicken populations in mainland China since 2019 (*14*). Of note, we found that the virus shedding of chickens vaccinated with H7N9-Re-2 and H7N9-rGD76 against HPAI H7N9 viruses during 2019 ranged from 30% to 80% (Appendix Table 3); therefore, a timely update of H7N9 vaccine is needed.

Next, we evaluated the protective efficacy of the new candidate H7N9 inactivated vaccine (H71903)—that is, reverse genetic recombinant carrying HA and NA of A/chicken/east China/H7SD12/2019(H7N9) with internal genes of A/duck/Guangdong/D7/2007(H5N2)—in chickens against the challenge of 4 HPAI H7N9 viruses prevailing in sublineage B in 2019. All of the control chickens challenged with the H7N9 viruses died within 6 days of challenge (Appendix Figure 8). However, virus shedding was not detected from any of the vaccinated chickens challenged with H7N9 viruses (Appendix Table 3), indicating that the new candidate H7N9 vaccine could provide sound protection for chickens against challenge with these reemerged H7N9 variants.

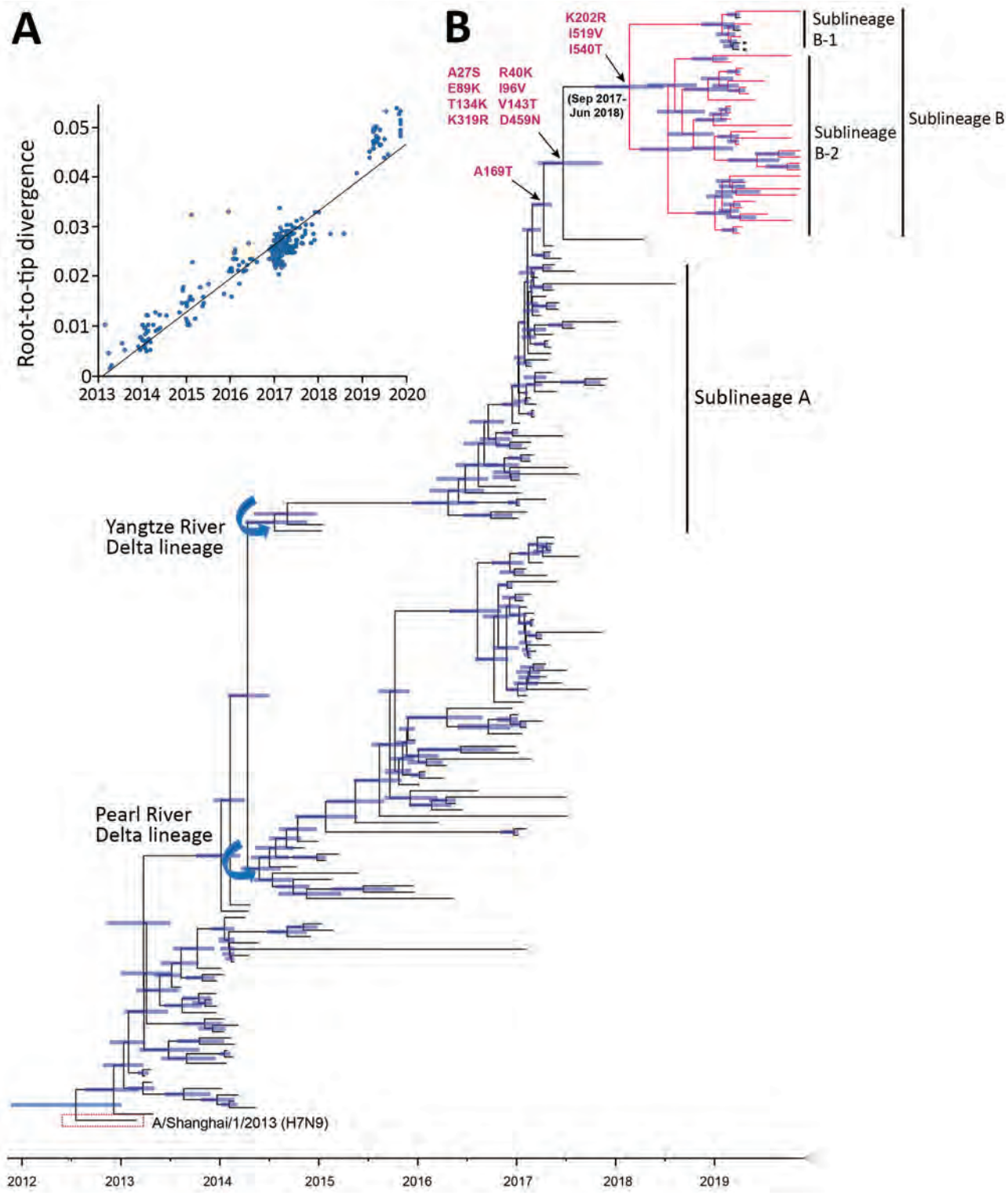

Figure 2. Time-scaled evolution of influenza A(H7N9) viruses, China. A) Analysis of root-to-tip divergence against sampling date for the hemagglutinin gene segment (n = 189). B) Maximum clade credibility tree of the hemagglutinin sequence of H7N9 viruses sampled in China (n = 189); the H7N9 viruses collected in this study are highlighted in red. Asterisk indicates viruses from a human with H7N9 infection within sublineage B during March 2019. Shaded bars represent the 95% highest probability distribution for the age of each node. Parallel amino acid changes along the trunk are indicated.

Table 1. Results of hemagglutinin inhibition assay in study of evolution and antigenic drift of influenza A(H7N9) viruses, China, 2019*

	Antiserum, titer							
Antigen	H7N9-Re-2†	H7N9-rGD76†	181115	H7SD12	H71903‡	LN19010	19225	19294
H7N9-Re-2	1,024	2,048	256	512	512	1,024	1,024	2,048
H7N9-rGD76	128	1,024	128	512	256	256	256	128
181115	64	256	1,024	256	256	256	128	128
H7SD12	64	256	256	1,024	1,024	2048	1,024	1,024
H71903	64	512	256	1,024	1,024	1,024	2048	1,024
LN19010	32	256	32	512	512	512	512	512
19225	32	256	64	1,024	512	1,024	512	1,024
19294	32	256	64	512	512	1,024	512	512
19300–1	32	256	64	1,024	512	1,024	512	512
19743	16	64	16	512	256	256	256	128
19797	16	32	16	256	128	128	64	128
19854–2	16	64	16	512	256	256	256	256
19854–6	16	64	16	256	256	512	256	256
LN191012	16	64	16	512	256	256	128	128
AH191005	32	128	32	1,024	512	256	256	256

*181115, A/chicken/northeast China/181115/2018(H7N9); H7SD12, A/chicken/east China/H7SD12/2019(H7N9); HeB1908, A/chicken/north China/HeB1908/2019(H7N9); LN19010, A/chicken/northeast China/LN19010/2019(H7N9); 19225, A/chicken/northeast China/19225/2019(H7N9); 19294, A/chicken/northeast China/19294/2019(H7N9); 19300–1, A/chicken/northeast China/19300–1/2019(H7N9); 19743, A/chicken/northeast China/19743/2019(H7N9); 19797, A/chicken/northeast China/197971/2019(H7N9); 19854–2, A/chicken/northeast China/19854–2/2019(H7N9); 19854–6, A/chicken/northeast China/19854–6/2019(H7N9); LN19010, A/chicken/northeast China/LN19010/2019(H7N9); LN191012, A/chicken/northeast China/LN191012/2019(H7N9); AH191005, A/chicken/east China/AH191005/2019(H7N9).
†H7N9-Re-2 and H7N9-rGD76 are vaccine strains widely used in China; both antigen and antiserum of H7N9-Re-2 were purchased from the Harbin Weike Biotechnology Development Company (www.hvriwk.com), the antigen of H7N9-Re-2 was available from reassortant avian influenza virus trivalent vaccine. The antigen and antiserum of H7N9-rGD76 were available from Guangzhou South China Biologic Medicine (http://www.gzscbm.com).
‡H71903 is candidate vaccine strain containing the hemagglutinin and neuraminidase genes from H7SD12 and 6 internal genes from A/duck/Guangdong/D7/2007(H5N2). H7SD12, 181115, HeB1908, LN19010, 19225, 19294, 19300–1, 19743, 19797, 19854–2, 19854–6, LN19010, LN191012, and AH191005 are highly pathogenic H7N9 strains in this study.

Conclusions

Our findings highlight that the HPAI H7N9 viruses that reemerged during 2019 had been cocirculating at a low level in eastern and northeastern China after the vaccination strategy was implemented. These HPAI H7N9 viruses continued to evolve and showed antigenic drift, posing a public health concern. Although vaccination can largely control the occurrence of H7N9 virus outbreaks, it can also accelerate the generation of novel variants. Therefore, comprehensive surveillance and enhancement of biosecurity precautions should be undertaken immediately to prevent the influenza virus epidemic from becoming a pandemic.

Acknowledgments

We acknowledge all contributors who submitted the sequence data on which this research is based to the GISAID EpiFlu Database. All submitters of data may be contacted directly through the GISAID website (http://www.gisaid.org).

This work was supported by the Key Research and Development Program of Guangdong Province (2019B020218004), the National Natural Science Foundation of China (31672586, 31830097, and 319410014), the Earmarked Fund for China Agriculture Research System (CARS-41-G16), the Guangdong Province Universities

Table 2. *r* values of cross-hemagglutinin inhibition assay in study of evolution and antigenic drift of influenza A(H7N9) viruses, China, 2019*

	Antiserum, *r* value							
Strain	H7N9-Re-2	H7N9-rGD76	181115	H7SD12	H71903	LN19010	19225	19294
H7N9-Re-2	1	0.5	0.25	0.18	0.18	0.25	0.25	0.35
H7N9-rGD76	0.5	1	0.18	0.35	0.35	0.35	0.35	0.25
181115	0.25	0.18	1	0.25	0.25	0.13	0.13	0.13
H7SD12	0.18	0.35	0.25	1	1	1.41	1.41	1
H71903	0.18	0.35	0.25	1	1	1	1.41	1
LN19010	0.25	0.35	0.13	1.41	1	1	1.41	1.41
19225	0.25	0.35	0.13	1.41	1.41	1.41	1	1.41
19294	0.35	0.25	0.13	1	1	1.41	1.41	1

*H7N9-Re-2 and H7N9-rGD76 are vaccine strains widely used in China; both antigen and antiserum of H7N9-Re-2 were purchased from the Harbin Weike Biotechnology Development Company (http://www.hvriwk.com). The antigen of H7N9-Re-2 was available from reassortant avian influenza virus trivalent vaccine. The antigen and antiserum of H7N9-rGD76 were available from Guangzhou South China Biologic Medicine (http://www.gzscbm.com). H71903 is candidate vaccine strain containing the hemagglutinin and neuraminidase genes from H7SD12 and 6 internal genes from A/duck/Guangdong/D7/2007(H5N2). 181115, H7SD12, LN19010, 19225, and 19294 are highly pathogenic H7N9 strains in this study. *r* values indicate antigenic relatedness. $r>1$ indicates no significant antigenic difference between the strains; $r = 1$ indicates the same antigenicity; $r<0.5$ indicates a statistically significant antigenic difference between the strains. 181115, A/chicken/northeast China/181115/2018(H7N9); H7SD12, A/chicken/east China/H7SD12/2019(H7N9); LN19010, A/chicken/northeast China/LN19010/2019(H7N9); 19225, A/chicken/northeast China/19225/2019(H7N9); 19294, A/chicken/northeast China/19294/2019(H7N9).

and Colleges Pearl River Scholar Funded Scheme (2018, to W.Q.), and the Young Scholars of Yangtze River Scholar Professor Program (2019, to W.Q.).

About the Author

Dr. Zhang is a PhD student at South China Agricultural University, Guangzhou, China. His research interests are the epidemiology and pathogenesis of emerging and re-emerging infectious diseases.

References

1. Kang M, Lau EHY, Guan W, Yang Y, Song T, Cowling BJ, et al. Epidemiology of human infections with highly pathogenic avian influenza A(H7N9) virus in Guangdong, 2016 to 2017. Euro Surveill. 2017;22:22. https://doi.org/10.2807/1560-7917.ES.2017.22.27.30568
2. Wang X, Jiang H, Wu P, Uyeki TM, Feng L, Lai S, et al. Epidemiology of avian influenza A H7N9 virus in human beings across five epidemics in mainland China, 2013-17: an epidemiological study of laboratory-confirmed case series. Lancet Infect Dis. 2017;17:822–32. https://doi.org/10.1016/S1473-3099(17)30323-7
3. Liu D, Shi W, Shi Y, Wang D, Xiao H, Li W, et al. Origin and diversity of novel avian influenza A H7N9 viruses causing human infection: phylogenetic, structural, and coalescent analyses. Lancet. 2013;381:1926–32. https://doi.org/10.1016/S0140-6736(13)60938-1
4. Shi J, Deng G, Kong H, Gu C, Ma S, Yin X, et al. H7N9 virulent mutants detected in chickens in China pose an increased threat to humans. Cell Res. 2017;27:1409–21. https://doi.org/10.1038/cr.2017.129
5. Qi W, Jia W, Liu D, Li J, Bi Y, Xie S, et al. Emergence and adaptation of a novel highly pathogenic H7N9 influenza virus in birds and humans from a 2013 human-infecting low-pathogenic ancestor. J Virol. 2018;92:92.
6. Shi J, Deng G, Ma S, Zeng X, Yin X, Li M, et al. Rapid evolution of H7N9 highly pathogenic viruses that emerged in China in 2017. Cell Host Microbe. 2018;24:558–68. https://doi.org/10.1016/j.chom.2018.08.006
7. Bao L, Bi Y, Wong G, Qi W, Li F, Lv Q, et al. Diverse biological characteristics and varied virulence of H7N9 from wave 5. Emerg Microbes Infect. 2019;8:94–102. https://doi.org/10.1080/22221751.2018.1560234
8. Quan C, Shi W, Yang Y, Yang Y, Liu X, Xu W, et al. New threats from H7N9 influenza virus: spread and evolution of high- and low-pathogenicity variants with high genomic diversity in wave five. J Virol. 2018;92:92. https://doi.org/10.1128/JVI.00301-18
9. Lu J, Raghwani J, Pryce R, Bowden TA, Thézé J, Huang S, et al. Molecular evolution, diversity, and adaptation of influenza A(H7N9) viruses in China. Emerg Infect Dis. 2018;24:1795–805. https://doi.org/10.3201/eid2410.171063
10. Wu J, Ke C, Lau EHY, Song Y, Cheng KL, Zou L, et al. Influenza H5/H7 virus vaccination in poultry and reduction of zoonotic infections, Guangdong Province, China, 2017–18. Emerg Infect Dis. 2019;25:116–8. https://doi.org/10.3201/eid2501.181259
11. Jiang W, Hou G, Li J, Peng C, Wang S, Liu S, et al. Antigenic variant of highly pathogenic avian influenza A(H7N9) virus, China, 2019. Emerg Infect Dis. 2020;26:26. https://doi.org/10.3201/eid2602.191105
12. Yu D, Xiang G, Zhu W, Lei X, Li B, Meng Y, et al. The re-emergence of highly pathogenic avian influenza H7N9 viruses in humans in mainland China, 2019. Euro Surveill. 2019;24:13–21. https://doi.org/10.2807/1560-7917.ES.2019.24.21.1900273
13. Henry Dunand CJ, Leon PE, Huang M, Choi A, Chromikova V, Ho IY, et al. Both neutralizing and non-neutralizing human H7N9 influenza vaccine-induced monoclonal antibodies confer protection. Cell Host Microbe. 2016;19:800–13. https://doi.org/10.1016/j.chom.2016.05.014
14. Ministry of Agricultural and Rural Affairs of the People's Republic of China. No. 99 announcement [in Chinese] [cited 2018 Dec 13]. http://www.moa.gov.cn/gk/tzgg_1/gg/201812/t20181213_6164848.htm

Address for correspondence: Ming Liao and Wenbao Qi, No.483, Wushan Rd, Tianhe District, Guangzhou, Guangdong, China; email: mliao@scau.edu.cn and qiwenbao@scau.edu.cn

Doubling Time of the COVID-19 Epidemic by Province, China

Kamalich Muniz-Rodriguez,[1] Gerardo Chowell,[1] Chi-Hin Cheung, Dongyu Jia, Po-Ying Lai, Yiseul Lee, Manyun Liu, Sylvia K. Ofori, Kimberlyn M. Roosa, Lone Simonsen, Cecile Viboud, Isaac Chun-Hai Fung

Author affiliations: Georgia Southern University, Statesboro, Georgia, USA (K. Muniz-Rodriguez, D. Jia, M. Liu, S.K. Ofori, I.C.-H. Fung); Georgia State University, Atlanta, Georgia, USA (G. Chowell, Y. Lee, K.M. Roosa); National Institutes of Health, Bethesda, Maryland, USA (G. Chowell, C. Viboud); Independent researcher, Hong Kong (C.-H. Cheung); Boston University, Boston, Massachusetts, USA (P.-Y. Lai); Roskilde University, Roskilde, Denmark (L. Simonsen)

DOI: https://doi.org/10.3201/eid2608.200219

In China, the doubling time of the coronavirus disease epidemic by province increased during January 20–February 9, 2020. Doubling time estimates ranged from 1.4 (95% CI 1.2–2.0) days for Hunan Province to 3.1 (95% CI 2.1–4.8) days for Xinjiang Province. The estimate for Hubei Province was 2.5 (95% CI 2.4–2.6) days.

Our ability to estimate the basic reproduction number (R_0) of emerging infectious diseases is often hindered by the paucity of information about the epidemiologic characteristics and transmission mechanisms of new pathogens (*1*). Alternative metrics could synthesize real-time information about the extent to which the epidemic is expanding over time. Such metrics would be particularly useful if they rely on minimal and routinely collected data that capture the trajectory of an outbreak (*2*).

Epidemic doubling times characterize the sequence of intervals at which the cumulative incidence doubles (*3*). If an epidemic is growing exponentially with a constant growth rate r, the doubling time remains constant and equals $(\ln 2)/r$. An increase in the doubling time indicates a slowdown in transmission if the underlying reporting rate remains unchanged (Appendix, https://wwwnc.cdc.gov/EID/article/26/8/20-0219-App1.pdf) (*4*).

We analyzed, by province, the number of times coronavirus disease (COVID-19) cumulative incidence doubled and the evolution of the doubling times in mainland China (*5*), from January 20 (when nationwide reporting began) through February 9, 2020. We retrieved province-level daily cumulative incidence data from provincial health commissions' websites and conducted 2 sensitivity analyses based on a longer and a shorter time period (Appendix). We excluded Tibet from further analysis because only 1 case was reported during the study period.

During January 20–February 9, the harmonic mean of the arithmetic means of the doubling times estimated from cumulative incidence ranged from 1.4 (95% CI 1.2–2.0) days in Hunan Province to 3.1 (95% CI 2.1–4.8) days in Xinjiang Province. We estimated doubling time as 2.5 (95% CI 2.4–2.6) days in Hubei Province. The cumulative incidence doubled 6 times in Hubei Province during the study period. The harmonic mean of the arithmetic means of doubling times for mainland China except Hubei Province was 1.8 (95% CI 1.5–2.3) days. Fujian, Guangxi, Hebei, Heilongjiang, Henan, Hunan, Jiangxi, Shandong, Sichuan, and Zhejiang provinces had a harmonic mean of the arithmetic means of doubling times <2 days (Figure; Appendix Figure 1).

As the epidemic progressed, it took longer for the cumulative incidence in mainland China (except Hubei) to double, which indicated an overall subexponential growth pattern outside Hubei Province (Appendix Figures 1, 2). In Hubei Province, the doubling time decreased and then increased. A gradual increase in the doubling time coincided with the social distancing measures and intraprovincial and interprovincial travel restrictions imposed across China since the implementation of the quarantine of Wuhan on January 23 (*6*).

Our estimates of doubling times are shorter than prior estimates. Li et al. covered cases reported by January 22 and found a doubling time estimate of 7.4 (95% CI 4.2–14) days (*5*). Wu et al. statistically inferred case counts in Wuhan by internationally exported cases as of January 25 and estimated doubling time as 6.4 (95% CI 5.8–7.1) days (*7*). Volz et al. identified a common viral ancestor on December 8, 2019, using Bayesian phylogenetic analysis and fitted an exponential growth model to provide the epidemic growth rate and estimated a doubling time of 7.1 (95% CI 3.0–20.5) days (*8*). Our estimates are based on cumulative confirmed case count by reporting date by province during January 20–February 9, 2020.

Our study is subject to several limitations, including underreporting of cases (*9*). One reason for underreporting is underdiagnosis, resulting from a lack of diagnostic tests, healthcare workers, and

[1]These authors contributed equally to this article.

other resources. Further, underreporting is likely heterogeneous across provinces. As long as reporting remains invariant over time within the same province, the calculation of doubling times remains reliable; however, this is a strong assumption. Growing awareness of the epidemic and increasing availability of diagnostic tests might have strengthened reporting over time, which could have artificially

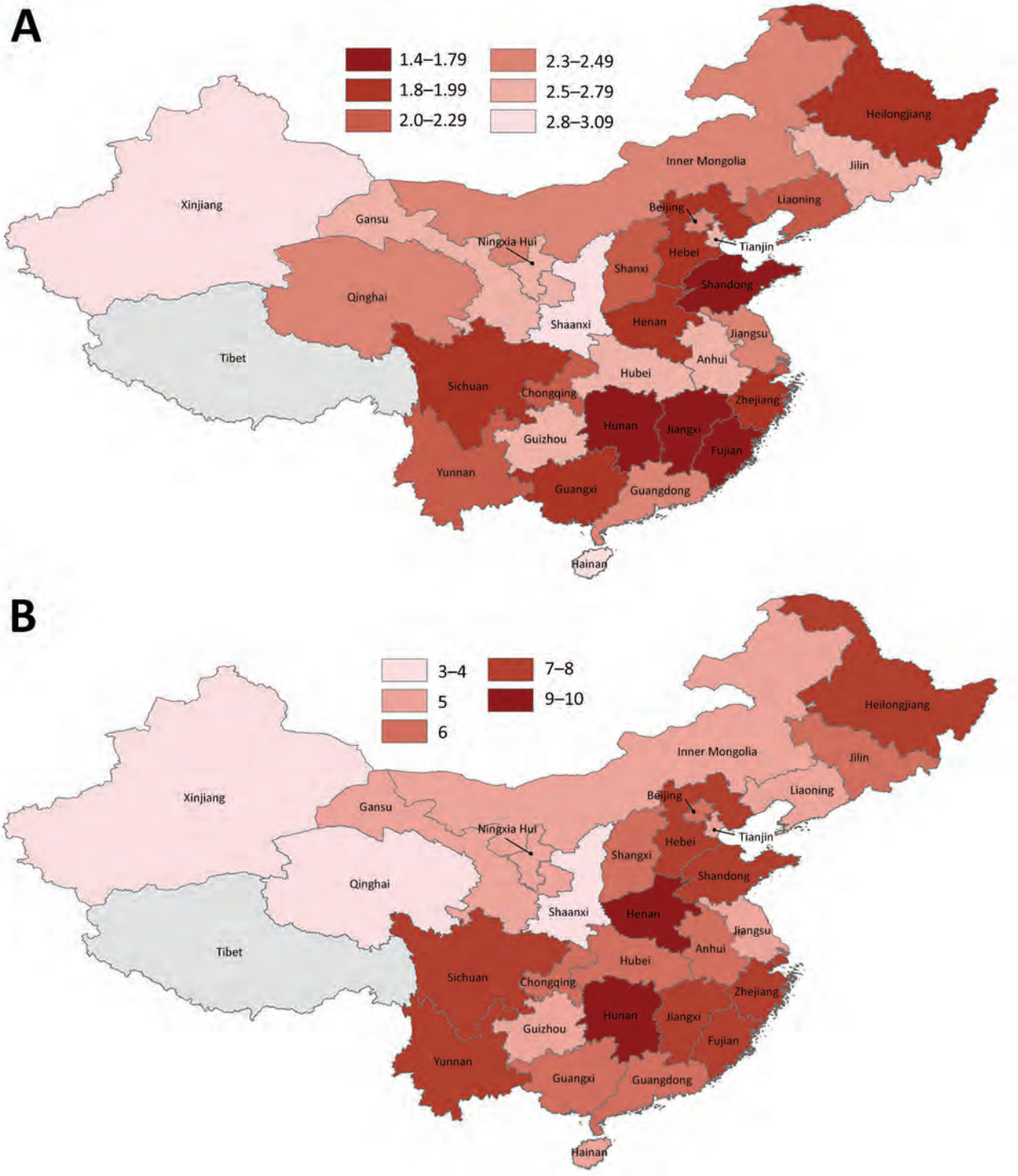

Figure. Doubling time estimates for coronavirus disease in mainland China, by province, January 20–February 9, 2020. A) Harmonic mean of the arithmetic means of doubling time estimates; B) number of times the cumulative incidence doubled during the study period.

shortened the doubling time. Nevertheless, apart from Hubei and Guangdong Provinces (first cases reported on January 19, 2020), nationwide reporting began only on January 20; at that point, authorities in China openly acknowledged the magnitude and severity of the epidemic.

Because of a lack of detailed case data describing incidence trends for imported and local cases, we focused our analysis on the overall trajectory of the epidemic without adjusting for the role of imported cases on the local transmission dynamics. It is likely that the proportion of imported cases could be large for provinces that reported only a few cases; their short doubling times in the study period could simply reflect rapid detection of imported cases. However, with the data through February 9, only 2 provinces had a cumulative case count <40 (Appendix Table 1). It would be worthwhile to investigate the evolution of the doubling time after accounting for case importations if more detailed data become available.

In summary, we observed an increasing trend in the epidemic doubling time of COVID-19 by province of China during January 20–February 9, 2020. The harmonic mean of the arithmetic means of doubling times of cumulative incidence during the study period in Hubei Province, where the outbreak was first recognized, was estimated at 2.5 (95% CI 2.4–2.6) days.

G.C. receives support from National Science Foundation grant no. 1414374 as part of the joint NSF-NIH-USDA Ecology and Evolution of Infectious Diseases program. I.C.-H.F. receives salary support from the National Center for Emerging and Zoonotic Infectious Diseases, Centers for Disease Control and Prevention (grant no. 19IPA1908208). This article is not part of I.C.-H.F.'s CDC-sponsored projects.

About the Authors

Ms. Muniz-Rodriguez is a doctoral student at the Jiann-Ping Hsu College of Public Health, Georgia Southern University, Statesboro, Georgia, USA. Her research interests include infectious disease epidemiology, digital epidemiology, and disaster epidemiology. Dr. Chowell is a professor of epidemiology and biostatistics and chair of the department of population health sciences at Georgia State University School of Public Health, Atlanta, Georgia. As a mathematical epidemiologist, he studies the transmission dynamics of emerging infectious diseases, such as Ebola, MERS, and SARS.

References

1. Anderson RM, May RM. Infectious diseases of humans. Oxford: Oxford University Press; 1991.
2. Drake JM, Bakach I, Just MR, O'Regan SM, Gambhir M, Fung IC-H. Transmission models of historical Ebola outbreaks. Emerg Infect Dis. 2015;21:1447–50. https://doi.org/10.3201/eid2108.141613
3. Vynnycky E, White RG. An introduction to infectious disease modelling. Oxford: Oxford University Press; 2010.
4. Muniz-Rodriguez K, Fung IC-H, Ferdosi SR, Ofori SK, Lee Y, Tariq A, et al. Severe acute respiratory syndrome coronavirus 2 transmission potential, Iran, 2020. Emerg Infect Dis. 2020 Apr 22 [Epub ahead of print]. https://doi.org/10.3201/eid2608.200536
5. Li Q, Guan X, Wu P, Wang X, Zhou L, Tong Y, et al. Early transmission dynamics in Wuhan, China, of novel coronavirus-infected pneumonia. N Engl J Med. 2020;382:1199–207. https://doi.org/10.1056/NEJMoa2001316
6. Du Z, Wang L, Cauchemez S, Xu X, Wang X, Cowling BJ, et al. Risk for transportation of 2019 novel coronavirus disease from Wuhan to other cities in China. Emerg Infect Dis. 2020;26:1049–52. https://doi.org/10.3201/eid2605.200146
7. Wu JT, Leung K, Leung GM. Nowcasting and forecasting the potential domestic and international spread of the 2019-nCoV outbreak originating in Wuhan, China: a modelling study. Lancet. 2020;395:689–97. https://doi.org/10.1016/S0140-6736(20)30260-9
8. Volz E, Baguelin M, Bhatia S, Boonyasiri A, Cori A, Cucunubá Z, et al. Report 5: phylogenetic analysis of SARS-CoV-2. 2020 [cited 2020 Apr 15]. https://www.imperial.ac.uk/media/imperial-college/medicine/sph/ide/gida-fellowships/Imperial-College-COVID19-phylogenetics-15-02-2020.pdf
9. Fang G, Li S, Liu Y, Xin N, Ma K. People beyond the statistics: died of "normal pneumonia"? [in Chinese]. Caijing Zachi [Finance and Economics Magazine]. 2020 [cited 2020 Feb 13]. https://web.archive.org/web/20200213190623/http://www.sohu.com/a/370032279_120094087

Address for correspondence: Isaac Chun-Hai Fung, Department of Biostatistics, Epidemiology, and Environmental Health Sciences, Jiann-Ping Hsu College of Public Health, Georgia Southern University, Statesboro, GA 30460, USA; email: cfung@georgiasouthern.edu

Severe Acute Respiratory Syndrome Coronavirus 2 Transmission Potential, Iran, 2020

Kamalich Muniz-Rodriguez,[1] Isaac Chun-Hai Fung,[1] Shayesteh R. Ferdosi, Sylvia K. Ofori, Yiseul Lee, Amna Tariq, Gerardo Chowell

Author affiliations: Georgia Southern University, Statesboro, Georgia, USA (K. Muniz-Rodriguez, I.C.-H. Fung, S.K. Ofori); The Translational Genomics Research Institute, Phoenix, Arizona, USA (S.R. Ferdosi); Georgia State University School of Public Health, Atlanta, Georgia, USA (Y. Lee, A. Tariq, G. Chowell)

DOI: https://doi.org/10.3201/eid2608.200536

To determine the transmission potential of severe acute respiratory syndrome coronavirus 2 in Iran in 2020, we estimated the reproduction number as 4.4 (95% CI 3.9–4.9) by using a generalized growth model and 3.5 (95% CI 1.3–8.1) by using epidemic doubling time. The reproduction number decreased to 1.55 after social distancing interventions were implemented.

Since early 2020, Iran has been experiencing a devastating epidemic of coronavirus disease (COVID-19) (*1*). To determine the transmission potential of severe acute respiratory syndrome coronavirus 2 and thereby guide outbreak response efforts, we calculated basic reproduction numbers (R_0). During the early transmission phase, R_0 quantifies the average number of secondary cases generated by a primary case in a completely susceptible population, absent interventions or behavioral changes. $R_0>1$ indicates the possibility of sustained transmission; $R_0<1$ implies that transmission chains cannot sustain epidemic growth. As the epidemic continues, the effective reproduction number (R_e) offers a time-dependent record of the average number of secondary cases per case as the number of susceptible persons becomes depleted and control interventions take effect. We used 2 methods to quantify the reproduction number by using the curve of reported COVID-19 cases in Iran and its 5 regions (Appendix Table 1, https://wwwnc.cdc.gov/EID/article/26/8/20-0536-App1.pdf). The Georgia Southern University Institutional Review Board made a non–human subjects determination for this project (H20364), under the G8 exemption category.

For method 1, we used a generalized growth model (*2*) with the growth rate and its scaling factor to characterize the daily reported incidence. Next, we simulated the calibrated generalized growth model by using a discretized probability distribution of the serial interval and assuming a Poisson error structure (Appendix).

We based method 2 on calculation of the epidemic's doubling times, which correspond to the times when the cumulative incidence doubles and are estimated by using the curve of cumulative daily reported cases. To quantify parameter uncertainty, we used parametric bootstrapping with a Poisson error structure around the number of new reported cases to derive 95% CIs (*3*–*5*). Assuming exponential growth, the epidemic growth rate is equal to ln(2)/doubling time. Assuming that the preinfectious and infectious periods follow an exponential distribution, $R_0 \approx (1 +$ growth rate × serial interval) (Appendix) (*6*).

For both methods, the serial interval was assumed to follow a gamma distribution; mean (± SD) = 4.41 (± 3.17) days (*7*; C. You et al., unpub. data, https://www.medrxiv.org/content/10.1101/2020.02.08.20021253v2). We used MATLAB version R2019b (https://www.mathworks.com) and R version 3.6.2 (https://www.r-project.org) for data analyses and creating figures. We determined that a priori $\alpha = 0.05$.

Using Wikipedia as a starting point, we double-checked the daily reported new cases during February 19–March 19, 2020 (the day before the Iranian New Year) against official Iran press releases and other credible news sources and corrected the data according to official data (Appendix Tables 2, 3, Figure 1). Incident cases for the 5 regions were missing for 2 days (March 2–3), which we excluded from our analysis. Because the reported national number of new cases did not match the sum of new cases reported in Iran's 5 regions on March 5, we treated each time series as independent and used the data as reported. Using method 1, we estimated R_0 data for February 19–March 1, 2020. Using method 2, we estimated R_0 from the early transmission phase (February 19–March 1, 2020) and R_e based on the growth rate estimated during March 6–19, 2020, when the epidemic slowed, probably reflecting the effect of social distancing.

Using method 1, we estimated an R_0 of 4.4 (95% CI 3.9–4.9) for COVID-19 in Iran. We estimated a growth rate of 0.65 (95% CI 0.56–0.75) and a scaling parameter of 0.96 (95% CI 0.93–1.00) (Appendix Table 4). The scaling parameter indicated near-exponential epidemic growth (Figure). Using method 2, we found

[1]These first authors contributed equally to this article.

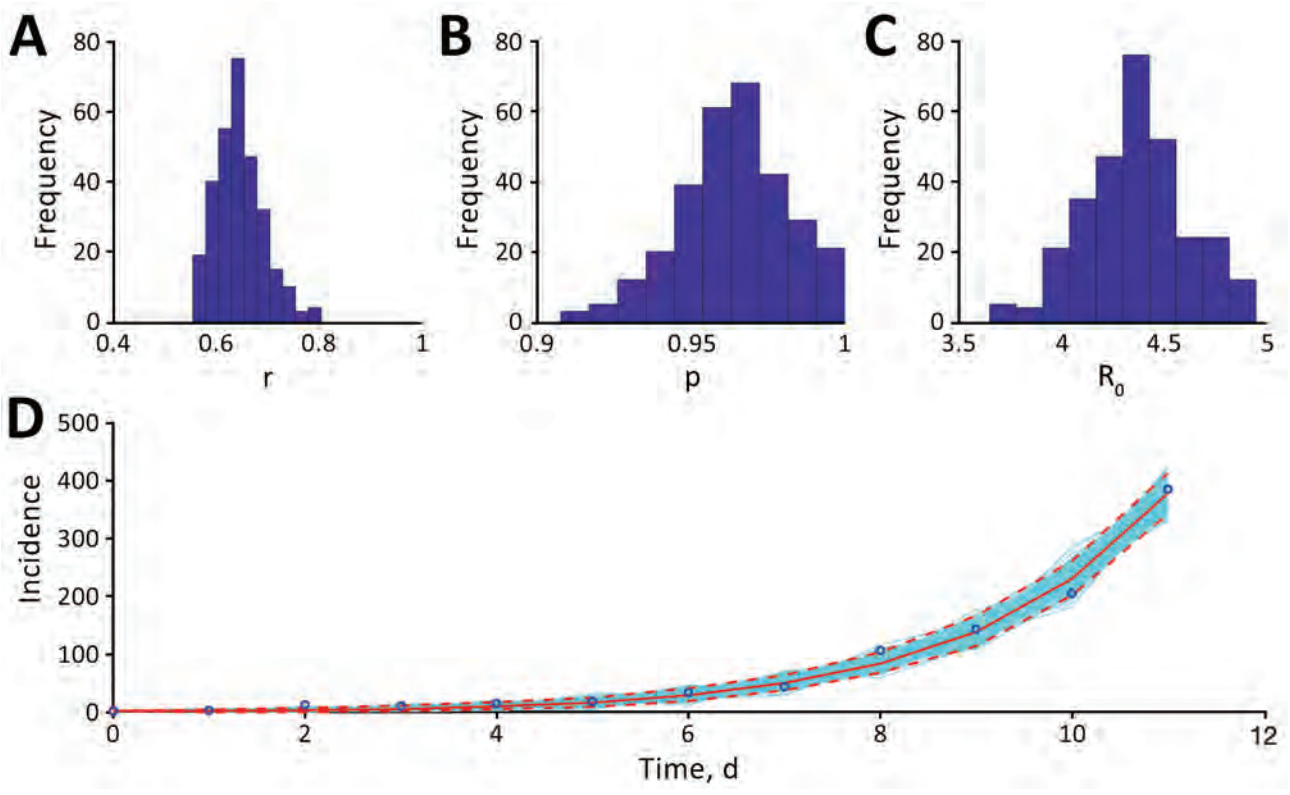

Figure. Estimates of transmission potential for severe acute respiratory syndrome coronavirus 2 in Iran, 2020. A) Growth rate, r; B) scaling of the growth rate parameter, p; C) mean basic reproduction number, R_0; and D) fit of the generalized growth model (method 1) to the Iran data, assuming Poisson error structure as of March 1, 2020. Dashed lines indicate 95% CIs.

that during February 19–March 1, the cumulative incidence of confirmed cases in Iran had doubled 8 times. The estimated epidemic doubling time was 1.20 (95% CI 1.05–1.45) days, and the corresponding R_0 estimate was 3.50 (95% CI 1.28–8.14). During March 6–19, the cumulative incidence of confirmed cases doubled 1 time; doubling time was 5.46 (95% CI 5.29–5.65) days. The corresponding R_e estimate was 1.55 (95% CI 1.06–2.57) (Appendix Table 5, Figures 7, 8). Our results are robust and consistent with Iran's COVID-19 R_0 estimates of 4.7 (A. Ahmadi et al., unpub. data, https://www.medrxiv.org/content/10.1101/2020.03.17.20037671v3) and 4.86 (E. Sahafizadeh, unpub. data, https://www.medrxiv.org/content/10.1101/2020.03.20.20038422v2) but higher than the R_0 of 2.72 estimated by N. Ghaffarzadegan and H. Rahmandad (unpub. data, https://www.medrxiv.org/content/10.1101/2020.03.22.20040956v1).

Our study has limitations. Our analysis is based on the number of daily reported cases, whereas it would be ideal to analyze case counts by dates of symptoms onset, which were not available. Case counts could be underreported because of underdiagnosis, given subclinical or asymptomatic cases or limited testing capacity to test persons with mild illness. The rapid increase in case counts might represent a belated realization of epidemic severity and rapid catching up and testing many persons with suspected cases. If the reporting ratio remains constant over the study period, and given the near-exponential growth of the epidemic's trajectory, our estimates would remain reliable. Although data are not stratified according to imported and local cases, we assumed that persons were infected locally because transmission has probably been ongoing in Iran for some time (*8*).

Although the COVID-19 epidemic in Iran has slowed substantially, the situation remains dire. Tighter social distancing interventions are needed to bring this epidemic under control.

G.C. received support from NSF grant 1414374 as part of the joint NSF-NIH-USDA Ecology and Evolution of Infectious Diseases program. I.C.-H.F. received salary support from the Centers for Disease Control and Prevention (CDC) (19IPA1908208). This article is not part of I.C.-H.F's CDC-sponsored projects.

About the Authors

Ms. Muniz-Rodriguez is a doctoral student in epidemiology and Dr. Fung is an associate professor of epidemiology at Jiann-Ping Hsu College of Public Health, Georgia Southern University. Their research interests include infectious disease epidemiology, digital health, and disaster emergency responses.

References

1. Wood G. Coronavirus could break Iranian society [cited 2020 Feb 29]. https://www.theatlantic.com/ideas/archive/2020/02/iran-cannot-handle-coronavirus/607150/
2. Viboud C, Simonsen L, Chowell G. A generalized-growth model to characterize the early ascending phase of infectious disease outbreaks. Epidemics. 2016;15:27–37. https://doi.org/10.1016/j.epidem.2016.01.002
3. Banks HT, Hu S, Thompson WC. Modeling and inverse problems in the presence of uncertainty: CRC Press; 2014.
4. Chowell G, Ammon CE, Hengartner NW, Hyman JM. Transmission dynamics of the great influenza pandemic of 1918 in Geneva, Switzerland: assessing the effects of hypothetical interventions. J Theor Biol. 2006;241:193–204. https://doi.org/10.1016/j.jtbi.2005.11.026
5. Chowell G, Shim E, Brauer F, Diaz-Dueñas P, Hyman JM, Castillo-Chavez C. Modelling the transmission dynamics of acute haemorrhagic conjunctivitis: application to the 2003 outbreak in Mexico. Stat Med. 2006;25:1840–57. https://doi.org/10.1002/sim.2352
6. Vynnycky E, White RG. An introduction to infectious disease modelling. Oxford (UK): Oxford University Press; 2010.
7. Nishiura H, Linton NM, Akhmetzhanov AR. Serial interval of novel coronavirus (COVID-19) infections. Int J Infect Dis. 2020;93:284–6. https://doi.org/10.1016/j.ijid.2020.02.060
8. Tuite AR, Bogoch II, Sherbo R, Watts A, Fisman D, Khan K. Estimation of coronavirus disease 2019 (COVID-19) burden and potential for international dissemination of infection from Iran. Ann Intern Med. 2020. https://doi.org/10.7326/M20-0696

Address for correspondence: Isaac Chun-Hai Fung, Department of Biostatistics, Epidemiology and Environmental Health Sciences, Jiann-Ping Hsu College of Public Health, Georgia Southern University, PO Box 7989, Statesboro, GA 30460-7989 USA; email: cfung@georgiasouthern.edu; or Gerardo Chowell, Department of Population Health Sciences, School of Public Health, Georgia State University, Suite 662, Office 640B, Atlanta, GA 30303, USA; email: gchowell@gsu.edu.

Cluster of Coronavirus Disease Associated with Fitness Dance Classes, South Korea

Sukbin Jang, Si Hyun Han, Ji-Young Rhee

Author affiliation: Dankook University Hospital, Dankook University College of Medicine, Cheonan, South Korea

DOI: https://doi.org/10.3201/eid2608.200633

During 24 days in Cheonan, South Korea, 112 persons were infected with severe acute respiratory syndrome coronavirus 2 associated with fitness dance classes at 12 sports facilities. Intense physical exercise in densely populated sports facilities could increase risk for infection. Vigorous exercise in confined spaces should be minimized during outbreaks.

By April 30, 2020, South Korea had reported 10,765 cases of coronavirus disease (COVID-19) (*1*); ≈76.2% of cases were from Daegu and North Gyeongsang provinces. On February 25, a COVID-19 case was detected in Cheonan, a city ≈200 km from Daegu. In response, public health and government officials from Cheonan and South Chungcheong Province activated the emergency response system. We began active surveillance and focused on identifying possible COVID-19 cases and contacts. We interviewed consecutive confirmed cases and found all had participated in a fitness dance class. We traced contacts back to a nationwide fitness dance instructor workshop that was held on February 15 in Cheonan.

Fitness dance classes set to Latin rhythms have gained popularity in South Korea because of the high aerobic intensity (*2*). At the February 15 workshop, instructors trained intensely for 4 hours. Among 27 instructors who participated in the workshop, 8 had positive real-time reverse transcription PCR (RT-PCR) results for severe acute respiratory syndrome coronavirus 2, which causes COVID-19; 6 were from Cheonan and 1 was from Daegu, which had the most reported COVID-19 cases in South Korea. All were asymptomatic on the day of the workshop.

By March 9, we identified 112 COVID-19 cases associated with fitness dance classes in 12 different sports facilities in Cheonan (Figure). All cases were confirmed by RT-PCR; 82 (73.2%) were symptomatic and 30 (26.8%) were asymptomatic at the time of laboratory confirmation. Instructors with very mild symptoms, such as coughs, taught classes for ≈1 week after attending the workshop

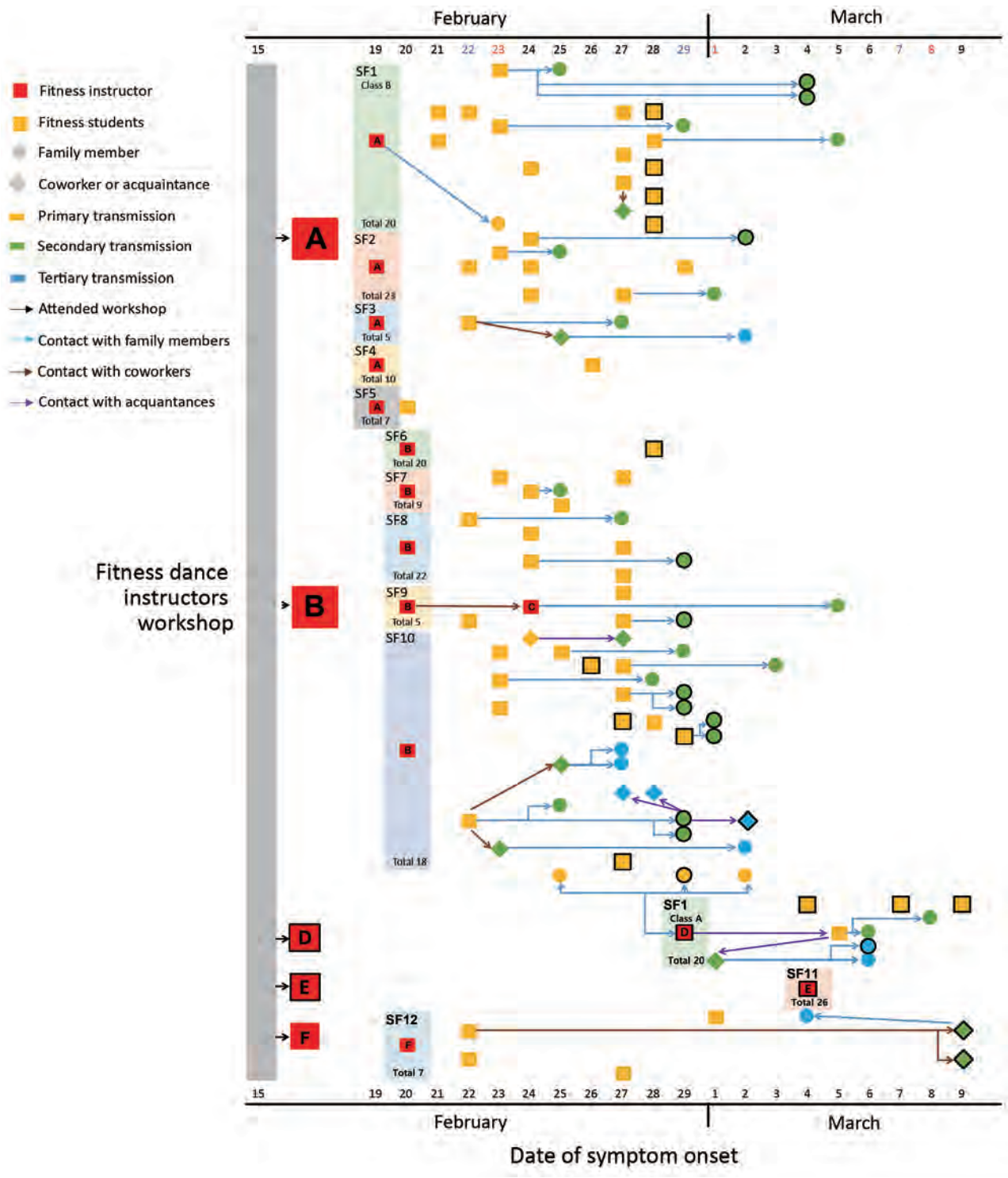

Figure. Case map of confirmed coronavirus disease (COVID-19) cases associated with fitness dance classes in Cheonan, South Korea, by date of symptom onset and relationship. Instructors outside of Cheonan are excluded. In 7 cases, transmission was suspected in the presymptomatic phase and the longest period before symptom onset was 5 days. None of the instructors had COVID-19 symptoms on the day of the workshop, but instructors from Daegu, which recently had a large outbreak, developed symptoms 3 days after the workshop. Sports facilities are represented by bars on the left with the number of students per class included. Bold outlines indicate a positive test for COVID-19 in a person in the presymptomatic phase.

(Appendix Figure 1, https://wwwnc.cdc.gov/EID/article/26/8/20-0633.App1.pdf). The instructors and students met only during classes, which lasted for 50 minutes 2 times per week, and did not have contact outside of class. On average, students developed symptoms 3.5 days after participating in a fitness dance class (*3*). Most (50.9%) cases were the result of transmission from instructors to fitness class participants; 38 cases (33.9%) were in-family transmission from instructors and students; and 17 cases (15.2%) were from transmission during meetings with coworkers or acquaintances.

Among 54 fitness class students with confirmed COVID-19, the median age was 42, all were women, and 10 (18.5%) had preexisting medical conditions (Appendix Table 1). The most common symptom at the time of admission for isolation was cough in 44.4% (24/54) of cases; 17 (31.5%) case-patients had pneumonia. The median time to discharge or end of isolation was 27.6 (range 13–66) days after symptom onset.

Before sports facilities were closed, a total of 217 students were exposed in 12 facilities, an attack rate of 26.3% (95% CI 20.9%–32.5%) (Appendix Table 2). Including family and coworkers, transmissions from the instructors accounted for 63 cases (Appendix Figure 2). We followed up on 830 close contacts of fitness instructors and students and identified 34 cases of COVID-19, translating to a secondary attack rate of 4.10% (95% CI 2.95%–5.67%). We identified 418 close contacts of 34 tertiary transmissions before the quarantine and confirmed 10 quaternary cases from the tertiary cases, translating to a tertiary attack rate of 2.39% (95% CI 1.30%–4.35%).

The instructor from Daegu who attended the February 15 workshop had symptoms develop on February 18 and might have been presymptomatic during the workshop. Evidence of transmission from presymptomatic persons has been shown in epidemiologic investigations of COVID-19 (*4*,*5*).

Characteristics that might have led to transmission from the instructors in Cheonan include large class sizes, small spaces, and intensity of the workouts. The moist, warm atmosphere in a sports facility coupled with turbulent air flow generated by intense physical exercise can cause more dense transmission of isolated droplets (*6*,*7*). Classes from which secondary COVID-19 cases were identified included 5–22 students in a room ≈60 m^2 during 50 minutes of intense exercise. We did not identify cases among classes with <5 participants in the same space. Of note, instructor C taught Pilates and yoga for classes of 7–8 students in the same facility at the same time as instructor B (Figure; Appendix Table 2), but none of her students tested positive for the virus. We hypothesize that the lower intensity of Pilates and yoga did not cause the same transmission effects as those of the more intense fitness dance classes.

A limitation of our study is the unavailability of a complete roster of visitors to the sports facilities, which might have meant we missed infections among students during surveillance and investigation efforts. Discovery of outbreak cases centered on exercise facilities led to a survey of instructors who participated in a fitness dance workshop and provided clues to identifying additional cases among students. Early identification of asymptomatic persons with RT-PCR–confirmed infections helped block further transmissions. Because of the increased possibility of infection through droplets, vigorous exercise in closely confined spaces should be avoided (*8*) during the current outbreak, as should public gatherings, even in small groups (*9*,*10*).

Acknowledgments

We thank the state, local, and territorial health department personnel for providing the reported coronavirus disease data; patients in Dankook University Hospital participating in interviews and providing data; and the Dankook University College of Medicine for their support. We also thank Editage (http://www.editage.co.kr) for English language editing.

About the Author

Dr. Jang is a clinical assistant professor in the Division of Infectious Diseases, Department of Medicine, Dankook University Hospital. His research interests include ecology of infectious disease, hospital infection control, and trauma related infections.

References

1. Korea Centers for Disease Control and Prevention. Current status of the coronavirus disease 2019 (COVID-19) outbreak in Republic of Korea [in Korean] [cited 2020 Apr 30]. http://ncov.mohw.go.kr
2. Vendramin B, Bergamin M, Gobbo S, Cugusi L, Duregon F, Bullo V, et al. Health benefits of Zumba fitness training: a systematic review. PM R. 2016;8:1181–200. https://doi.org/10.1016/j.pmrj.2016.06.010
3. Korea Centers for Disease Control and Prevention. Updates on COVID-19 in Korea as of 5 March 2020 [cited 2020 Mar 5]. https://www.cdc.go.kr/board/board.es?mid=a30402000000&bid=0030
4. Tong ZD, Tang A, Li KF, Li P, Wang HL, Yi JP, et al. Potential presymptomatic transmission of SARS–CoV–2, Zhejiang Province, China, 2020. Emerg Infect Dis. 2020;26:1052–4. https://doi.org/10.3201/eid2605.200198

5. Arons MM, Hatfield KM, Reddy SC, Kimball A, James A, Jacobs JR, et al. Presymptomatic SARS-CoV-2 infections and transmission in a skilled nursing facility. N Engl J Med. 2020 Apr 24 [Epub ahead of print]. https://doi.org/10.1056/NEJMoa2008457
6. Bourouiba L. Turbulent gas clouds and respiratory pathogen emission: potential implications for reducing transmission of COVID-19. JAMA. 2020 Mar 26 [Epub ahead of print]. https://doi.org/10.1001/jama.2020.4756
7. van Doremalen N, Bushmaker T, Morris DH, Holbrook MG, Gamble A, Williamson BN, et al. Aerosol and surface stability of SARS-CoV-2 as compared with SARS-CoV-1. N Engl J Med. 2020;382:1564–7. https://doi.org/10.1056/NEJMc2004973
8. Andrade A, Dominski FH, Pereira ML, de Liz CM, Buonanno G. Infection risk in gyms during physical exercise. Environ Sci Pollut Res Int. 2018;25:19675–86. https://doi.org/10.1007/s11356-018-1822-8
9. Musher DM. How contagious are common respiratory tract infections? N Engl J Med. 2003;348:1256–66. https://doi.org/10.1056/NEJMra021771
10. Ebrahim SH, Memish ZA. COVID-19 - the role of mass gatherings. Travel Med Infect Dis. 2020 Mar 9 [Epub ahead of print]. https://doi.org/10.1016/j.tmaid.2020.101617

Address for correspondence: Ji-Young Rhee, Division of Infectious Diseases, Department of Medicine, Dankook University Hospital, Dankook University College of Medicine, 201 Manghang-ro, Dongnam-ku, Chungcheongnam-do, South Korea; email: pluripotent@naver.com

Infectious SARS-CoV-2 in Feces of Patient with Severe COVID-19

Fei Xiao,[1] Jing Sun,[1] Yonghao Xu,[1] Fang Li,[1] Xiaofang Huang,[1] Heying Li, Jingxian Zhao, Jicheng Huang, Jincun Zhao

Author affiliations: Sun Yat-sen University, Zhuhai, China (F. Xiao); Guangzhou Medical University, Guangzhou, China (J. Sun, Y. Xu, F. Li, X. Huang, Jingxian Zhao, Jincun Zhao); Chinese Academy of Sciences, Guangzhou (H. Li); Guangzhou Customs District Technology Center, Guangzhou (J. Huang)

DOI: https://doi.org/10.3201/eid2608.200681

[1]These authors contributed equally to this article.

Severe acute respiratory syndrome coronavirus 2 was isolated from feces of a patient in China with coronavirus disease who died. Confirmation of infectious virus in feces affirms the potential for fecal–oral or fecal–respiratory transmission and warrants further study.

Severe acute respiratory syndrome coronavirus 2 (SARS-CoV-2) recently emerged in China, causing a major outbreak of severe pneumonia and spreading to >200 other countries (*1*). As of May 5, 2020, a total of 3,517,345 cases of coronavirus disease (COVID-2019) and 243,401 deaths had been reported to the World Health Organization (https://www.who.int/docs/default-source/coronaviruse/situation-reports/20200505covid-19-sitrep-106.pdf?sfvrsn=47090f63_2). The virus is believed to be spread by direct contact, fomites, respiratory droplets, and possibly aerosols (*2*). Viral RNA has been detected in feces and urine of some patients (*3*–*7*). Infectious virus was also isolated from urine of a patient with severe COVID-19 (*8*). However, it is unclear whether the virus in feces is infectious and might be an additional source for transmission.

This study was approved by the Health Commission of Guangdong Province and the Ethics Committees of Guangzhou Medical University to use patient and healthy donor sample specimens. On January 17, 2020, a 78-year-old man who had a history of recent travel to Wuhan, China, was admitted to the Fifth Affiliated Hospital of Sun Yat-Sen University because of a cough for 7 days and intermittent fever (Appendix Figure 1, panel A, https://wwwnc.cdc.gov/EID/article/26/8/20-0681-App1.pdf). Computed tomography of his chest showed multiple, ground-glass opacities (Appendix Figure 2). Nasopharyngeal and oropharyngeal swab specimens were positive for SARS-CoV-2 RNA by quantitative reverse transcription PCR (qRT-PCR).

On January 22, the patient's condition deteriorated and he was intubated. Ventilator-assisted breathing was instituted. The first feces specimen was collected on January 27 and was positive for viral RNA by qRT-PCR. Serial feces samples were collected on January 29, February 1, and February 7. All samples were positive for viral RNA (Appendix Figure 1, panel A). Viral antigen was also detected in gastrointestinal epithelial cells of a biopsy sample, as reported (*9*). The patient died on February 20.

We collected fecal specimens on January 29 to inoculate Vero E6 cells. Cycle threshold values for the fecal sample were 23.34 for the open reading frame 1lab gene and 20.82 for the nucleoprotein gene. A

cytopathic effect was visible in Vero E cells 2 days after a second-round passage (Appendix Figure 1, panel B). We extracted viral nucleic acid from virus culture supernatant by using the QIAamp Viral RNA Extraction Kit (QIAGEN, https://www.qiagen.com) and obtained full-length viral genome sequence (GenBank accession no. MT123292) by using next-generation sequencing. The sequenced showed 5 nt substitutions compared with the original Wuhan strain (GenBank accession no. NC045512.2) (Appendix Table).

We negatively stained culture supernatant and visualized by transmission electron microscopy. Viral particles that were visible were spherical and had distinct surface spike protein projections, consistent with a previously published SARS-CoV2 image (Appendix Figure, panel C) (*1*).

To estimate viral loads ($\log_{10}$ PFU equivalents/mL) in clinical samples from qRT-PCR cycle threshold values, we generated a standard curve from a serially diluted SARS-CoV-2 of known plaque titer. Viral loads quantified by using this method were viral RNA levels, not of infectious virus. The viral load was higher in feces than in respiratory specimens collected at multiple time points (17–28 days after symptom onset) (Appendix Figure, panel D). Isolation of virus from feces samples collected at later time points was not successful, although results for virus RNA remained positive, indicating only RNA fragments, not infectious virus, in feces of this patient collected at later time points of disease onset.

We collected feces specimens from 28 patients; 12, including the patient described in this report, were positive for viral RNA for ≥1 time point. We attempted to isolate SARS-CoV-2 virus from 3 of the viral RNA–positive patients. Results were successful for 2 of 3 patients, including the patient from this report, indicating that infectious virus in feces is a common manifestation of COVID-19.

The patient from this report had a high level of IgG against spike protein. Levels of nucleocapsid protein–specific antibodies were relatively lower. Spike protein (1,274 aa) is much larger than nucleoprotein protein (420 aa), which potentially contains more epitopes inducing specific antibody responses.

We also identified neutralization antibodies by using a focus reduction neutralization test. Neutralizing titers (50% focus reduction neutralization test) ranged from 1:1,065 to >1:4,860 at different time points (Appendix Figure, panel E). To show that isolated virus was infectious to susceptible cells, we tested fresh Vero E6 cells infected with the virus isolate by using indirect immunofluorescent assay and serum samples from the patient and a healthy donor. A positive reaction was only obtained with the patient serum (Appendix Figure 1, panel F).

Isolation of infectious SARS-CoV-2 in feces indicates the possibility of fecal–oral transmission or fecal–respiratory transmission through aerosolized feces. During the 2003 severe acute respiratory syndrome pandemic, 329 residents of a private housing estate in Hong Kong were infected; 42 died (*10*). Investigation of the building's structure showed that faulty sewage pipelines led to aerosolization of contaminated feces, which was believed to be the source of infection.

Our findings indicate the need for appropriate precautions to avoid potential transmission of SARS-CoV-2 from feces. Discharge and hospital cleaning practices should consider this possibility for critically ill patients or those who died who had high viral loads and are more likely to shed infectious virus.

Acknowledgments

We thank Nanshan Zhong and Malik Peiris for providing helpful discussions and critically reviewing the manuscript and the patient for participating in the study.

This study was supported by grants from The National Key Research and Development Program of China (2018YFC1200100), the National Science and Technology Major Project (2018ZX10301403), emergency grants for prevention and control of SARS-CoV-2 from the Ministry of Science and Technology (2020YFC0841400) and Guangdong Province (2020B111108001 and 2018B020207013).

About the Author

Dr. Xiao is a research scientist in the Department of Infectious Diseases, Guangdong Provincial Key Laboratory of Biomedical Imaging, Guangdong Provincial Engineering Research Center of Molecular Imaging, The Fifth Affiliated Hospital, Sun Yat-sen University, Zhuhai, Guangdong, China. His research interests focus on immunopathogenesis of infectious diseases in humans.

References

1. Zhu N, Zhang D, Wang W, Li X, Yang B, Song J, et al.; China Novel Coronavirus Investigating and Research Team. A novel coronavirus from patients with pneumonia in China, 2019. N Engl J Med. 2020;382:727–33. https://doi.org/10.1056/NEJMoa2001017
2. Chan JF, Yuan S, Kok KH, To KK, Chu H, Yang J, et al. A familial cluster of pneumonia associated with the 2019 novel coronavirus indicating person-to-person transmission: a study of a family cluster. Lancet. 2020;395:514–23. https://doi.org/10.1016/S0140-6736(20)30154-9
3. Guan WJ, Ni ZY, Hu Y, Liang WH, Ou CQ, He JX, et al.; China Medical Treatment Expert Group for Covid-19. Clinical characteristics of coronavirus disease 2019 in China.

N Engl J Med. 2020;382:1708–20. https://doi.org/10.1056/NEJMoa2002032
4. Pan Y, Zhang D, Yang P, Poon LL, Wang Q. Viral load of SARS-CoV-2 in clinical samples. Lancet Infect Dis. 2020; 20:411–2. https://doi.org/10.1016/S1473-3099(20)30113-4
5. Wu Y, Guo C, Tang L, Hong Z, Zhou J, Dong X, et al. Prolonged presence of SARS-CoV-2 viral RNA in faecal samples. Lancet Gastroenterol Hepatol. 2020;5:434–5. https://doi.org/10.1016/S2468-1253(20)30083-2
6. Wang W, Xu Y, Gao R, Lu R, Han K, Wu G, et al. Detection of SARS-CoV-2 in different types of clinical specimens. JAMA. 2020. https://doi.org/10.1001/jama.2020.3786
7. Zheng S, Fan J, Yu F, Feng B, Lou B, Zou Q, et al. Viral load dynamics and disease severity in patients infected with SARS-CoV-2 in Zhejiang province, China, January–March 2020: retrospective cohort study. BMJ. 2020;369:m1443. https://doi.org/10.1136/bmj.m1443
8. Sun J, Zhu A, Li H, Zheng K, Zhuang Z, Chen Z, et al. Isolation of infectious SARS-CoV-2 from urine of a COVID-19 patient. Emerg Microbes Infect. 2020;Apr 28:1–8. https://doi.org/10.1080/22221751.2020.1760144
9. Xiao F, Tang M, Zheng X, Liu Y, Li X, Shan H. Evidence for gastrointestinal infection of SARS-CoV-2. Gastroenterology. 2020;158:1831–1833.e3. https://doi.org/10.1053/j.gastro.2020.02.055
10. Yu IT, Li Y, Wong TW, Tam W, Chan AT, Lee JH, et al. Evidence of airborne transmission of the severe acute respiratory syndrome virus. N Engl J Med. 2004;350:1731–9. https://doi.org/10.1056/NEJMoa032867

Address for correspondence: Jincun Zhao, State Key Laboratory of Respiratory Disease, National Clinical Research Center for Respiratory Disease, Guangzhou Institute of Respiratory Health, the First Affiliated Hospital of Guangzhou Medical University, Guangzhou 510182, China, and Institute of Infectious Disease, Guangzhou Eighth People's Hospital of Guangzhou Medical University, Guangzhou 510060, China; email: zhaojincun@gird.cn or jczhao@gzhmu.edu.cn

Estimation of Coronavirus Disease Case-Fatality Risk in Real Time

Yang Ge, Shengzhi Sun

Author affiliations: The University of Georgia, Athens, Georgia, USA (Y. Ge); Boston University School of Public Health, Boston, Massachusetts, USA (S. Sun)

DOI: https://doi.org/10.3201/eid2608.201096

We ran a simulation comparing 3 methods to calculate case-fatality risk for coronavirus disease using parameters described in previous studies. Case-fatality risk calculated from these methods all are biased at the early stage of the epidemic. When comparing real-time case-fatality risk, the current trajectory of the epidemic should be considered.

We read with interest the research letter on estimating case-fatality risk for coronavirus disease (COVID-19) by Wilson, et al. (*1*). In their analyses, the authors estimated the case-fatality risk adjusted to a fixed lag time to death. They acknowledged that the calculated adjusted case-fatality risk (aCFR) might be influenced by residual uncertainties from undiagnosed mild COVID-19 cases and a shortage of medical resources. However, we believe the time-varying number of cumulative cases and deaths also should be considered in the epidemic profile.

Because of the exponential growth curve of the COVID-19 outbreak, the numbers of cumulative cases and cumulative deaths have been relatively close to each other in the early stages of the outbreak, leading to a much higher aCFR. As the outbreak progresses, the ratio of the cumulative cases and deaths declines, which reduces the aCFR. Thus, a higher aCFR does not necessarily indicate increased disease severity.

To test our hypothesis, we performed a simulation study by using a susceptible-infectious-recovered–death model and parameters set according to prior studies. We set the infectious period as 10 days (*2*); case-fatality risk as 3% (*3*); basic reproductive ratio (R_0) as 2.5 (*4*); recovery rate as 1/13 day (*5*), that is, 13 days from illness onset to recovery; and the population size as 1 million. We compared crude case-fatality risk, aCFR per Wilson et al.'s method, and aCFR per Mizumoto et al.'s method (*6*). Although the case-fatality risk calculated from these methods all are biased at the early stage of the epidemic, case-

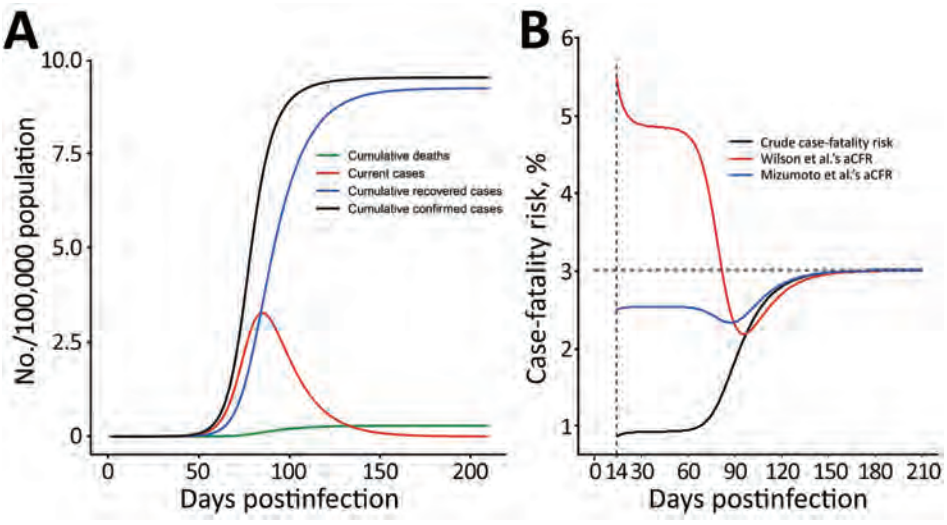

Figure. Progression of coronavirus disease outbreak and changes in the case-fatality risk by crude and adjusted rates. Crude case-fatality risk is the cumulative number of deaths on a given day divided by the cumulative number of cases on the same day. We set the infectious period as 10 days (*2*); case-fatality risk as 3% (*3*); basic reproductive ratio (R_0) as 2.5 (*4*); recovery rate as 1/13 day (*5*), that is, 13 days from illness onset to recovery; and the population size as 1 million. A) Changes in the number of subpopulations over time after the first infection. B) Changes in crude case-fatality risk after 13th day of exposure and aCFR calculated by using Wilson et al.'s method (*1*) and by using Mizumoto et al.'s method (*6*). aCFR, adjusted case-fatality risk.

fatality risk calculated from Mizumoto et al.'s method was closer to the true case-fatality risk of 3% (Figure).

In conclusion, we recommend the Mizumoto et al. method (*6*) to calculate aCFR in real time. When comparing real-time estimation of the case-fatality risk across countries and regions, our results indicate that the current trajectory of the epidemic should be considered, particularly if the epidemic is still in its early growth phase.

About the Authors

Mr. Ge is a PhD candidate in the Department of Epidemiology and Biostatistics at the University of Georgia, Athens, Georgia, USA. His research interests include infectious disease modeling and vaccine design.

Dr. Sun is a research scientist at the Boston University School of Public Health. His research focuses on estimating the impact of air pollution and climate change on human health.

References

1. Wilson N, Kvalsvig A, Barnard LT, Baker MG. Case-fatality risk estimates for COVID-19 calculated by using a lag time for fatality. Emerg Infect Dis. 2020 Mar 13 [Epub ahead of print]. https://doi.org/10.3201/eid2606.200320
2. Guan W-J, Ni Z-Y, Hu Y, Liang W-H, Ou C-Q, He J-X, et al. Clinical characteristics of coronavirus disease 2019 in China. N Engl J Med. 2020 Feb 28 [Epub ahead of print]. https://doi.org/10.1056/NEJMoa2002032
3. Novel Coronavirus Pneumonia Emergency Response Epidemiology Team. The epidemiological characteristics of an outbreak of 2019 novel coronavirus diseases (COVID-19) in China [in Chinese]. Zhonghua Liu Xing Bing Xue Za Zhi. 2020;41:145–51. https://doi.org/10.3760/cma.j.issn.0254-6450.2020.02.003
4. Li Q, Guan X, Wu P, Wang X, Zhou L, Tong Y, et al. Early transmission dynamics in Wuhan, China, of novel coronavirus–infected pneumonia. N Engl J Med. 2020 Jan 29 [Epub ahead of print]. https://doi.org/10.1056/NEJMoa2001316
5. World Health Organization. Report of the WHO-China Joint Mission on Coronavirus Disease 2019 (COVID-19). 2020 Feb 24 [cited 2020 Mar 27]. https://www.who.int/docs/default- source/coronaviruse/who-china-joint- mission-on-covid-19-final-report.pdf
6. Mizumoto K, Chowell G. Estimating risk for death from 2019 novel coronavirus disease, China, January–February 2020. Emerg Infect Dis. 2020 Mar 13 [Epub ahead of print]. https://doi.org/10.3201/eid2606.200233

Address for correspondence: Yang Ge, Department of Epidemiology and Biostatistics, University of Georgia, 101 Buck Rd, Athens, GA 30602-7396, USA; email: yang.ge@uga.edu; Shengzhi Sun, Department of Environmental Health, Boston University School of Public Health, 715 Albany St, Boston, MA 02118, USA; email: szsun@bu.edu

Secondary Transmission of Coronavirus Disease from Presymptomatic Persons, China

Weiwei Zhang,[1] Weibin Cheng,[1] Lei Luo,[1] Yu Ma, Conghui Xu, Pengzhe Qin, Zhoubin Zhang

Author affiliations: Guangzhou Center for Disease Control and Prevention, Guangzhou, China (W. Zhang, L. Luo, Y. Ma, C. Xu, P. Qin, Z. Zhang); Guangdong Second Provincial General Hospital, Guangzhou (W. Cheng)

DOI: https://doi.org/10.3201/eid2608.201142

We explored the secondary attack rate in different types of contact with persons presymptomatic for coronavirus disease (COVID-19). Close contacts who lived with or had frequent contact with an index case-patient had a higher risk for COVID-19. Our findings provide population-based evidence for transmission from persons with presymptomatic COVID-19 infections.

Coronavirus disease (COVID-19) caused by severe acute respiratory syndrome coronavirus 2 (SARS-CoV-2) is rapidly spreading across the globe. Some case reports and modeling studies suggest asymptomatic carriage of SARS-CoV-2 plays a role in transmission (*1*–*3*). Studies have shown that 30%–59% of SARS-CoV-2 infections are asymptomatic (*3*,*4*), which poses tremendous infection control challenges. To control asymptomatic infections, China implemented active case surveillance and enhanced social distancing measures, which include contact tracing, quarantine for key populations, medical observation, and curtailed social activities (*5*). However, additional information on the characteristics of presymptomatic transmission is needed to develop targeted control and prevention guidance.

We analyzed contact-tracing surveillance data collected during January 28–March 15, 2020, to explore the secondary attack rate from different types of contact with persons presymptomatic for COVID-19 in Guangzhou, China. Asymptomatic COVID-19 cases were found mainly through close contact screening, clustered epidemic investigations, follow-up investigation of infection sources, and active surveillance of key populations with travel or residence history in areas with continuous transmission of COVID-19 in China and abroad. We developed a case definition for presymptomatic COVID-19, criteria for close contact, and contact investigation and management guidelines (Appendix, https://wwwnc.cdc.gov/EID/article/26/8/20-1142.pdf). We estimated secondary attack rate (SAR) and 95% CI based on the proportion of COVID-19 incidence among close contacts. We calculated the mean reproductive number (R_0) from the number of secondary infections observed among close contacts of each index case. The study was approved by the ethics committee of Guangzhou Center for Disease Control and Prevention, which granted a waiver for informed consent. Data collection was conducted under the authority of the China Center for Disease Control and Prevention.

As of March 15, a total of 359 COVID-19 cases were confirmed in Guangzhou. Among them, 83 (23%) persons were asymptomatic at diagnosis; 71 (86%) of whom later developed symptoms. Among presymptomatic cases, 38 had ≥1 (range 1–90, median 4) close contact. We identified and included 369 close contacts in this study. Median age of close contacts was 35 years (range 0–93 years), 23.8% were family members of an index case, and 12 were confirmed to be infected via nucleic acid testing. Among them, 8 close contacts developed symptoms, and 4 were asymptomatic at the time of this study (Appendix Table).

The overall SAR was 3.3% (95% CI 1.9%–5.6%). The SAR among household contacts was 16.1% and was 1.1% for social contacts, and 0 for workplace contacts. Older close contacts had the highest SAR compared with other age groups; 8.0% in persons ≥60 years of age compared with 1.4%–5.6% in persons <60 years of age. Close contacts of asymptomatic index case-patients had the lowest SAR, 0.8%, but the SAR was 3.5% for those with mild symptoms, 5.7% for those with moderate symptoms, and 4.5% for those with severe symptoms. Close contacts that lived with an index case-patient had 12 times the risk for infection and those who had frequent contact with an index case-patient, >5 contacts during 2 days before the index case was confirmed, had 29 times the risk for infection (Table).

Our findings substantiate previous reports from China and Germany (*1*,*2*,*6*) and show that SARS-CoV-2 can be transmitted during asymptomatic COVID-19 infection period. The probability of infection increased substantially among close contacts who shared living environments or had frequent contact with an index case-patient, which underlines the need for prompt contact-based surveillance and social distancing (*7*). Our results also showed most secondary infections occurred in confined familial clusters and that persons ≥60 years of age appear to be more vulnerable to being infected. These results are consistent with previous reports on epidemiologic

[1]These first authors contributed equally to this article.

Table. Characteristics of and secondary attack rates among 369 close contacts of persons with presymptomatic coronavirus disease 2019, China*

Variable	No. contacts	No. infected	Attack rate, % (95% CI)	Relative risk (95% CI)
Sex				
M	217	5	2.3 (0.1–5.2)	Referent
F	152	7	4.6 (2.2–8.9)	2.1 (0.6–6.6)
Age				
≤17	46	2	4.3 (1.2–14.5)	Referent
18–30	104	3	2.9 (1.0–8.1)	0.7 (0.1–4.1)
31–40	72	1	1.4 (0.2–7.4)	0.4 (0.03–3.5)
41–50	68	1	1.5 (0.3–7.9)	0.4 (0.03–3.7)
51–60	54	3	5.6 (1.9–15.1)	1.3 (0.2–8.1)
≥61	25	2	8.0 (1.4–27.5)	1.9 (0.3–14.5)
Index case-patient status*				
Asymptomatic	119	1	0.8 (0.2–5.6)	Referent
Mild symptoms	141	5	3.5 (1.5–8.0)	4.3 (0.5–37.7)
Moderate symptoms	87	5	5.7 (2.5–12.8)	7.2 (0.8–62.7)
Severe symptoms	22	1	4.5 (0.8–21.8)	5.6 (0.3–93.4)
Contact mode				
Social interaction with friends or relatives	66	1	1.5 (0.3–8.1)	Referent
Lived together	62	10	16.1 (9.0–27.2)	12.5 (1.6–100.8)
Worked together	119	0	0	0
Social interaction with strangers	122	1	0.8 (0.2–4.9)	0.5 (0.03–8.7)
Contact frequency†				
Rare	149	1	0.7 (0.1–3.7)	Referent
Moderate	159	1	0.6 (0.1–3.5)	0.9 (0.1–15.1)
Frequent	61	10	16.4 (9.2–27.6)	29.0 (3.6–232.3)

*Status as of March 30, 2020, based on the person's clinical course assessed by a physician. Moderate symptoms included fever, respiratory symptoms, and radiographic evidence of pneumonia. Severe symptoms included breathing rate ≥30/min; oxygen saturation level ≤93% at rest; oxygen concentration level PaO_2/FiO_2 ≤300 mmHg (1 mmHg = 0.133kPa); lung infiltrates >50% within the past 24–48 h; respiratory failure requiring mechanical ventilation; septic shock; or multiple organ dysfunction or failure. All other symptomatic cases were classified as mild.
†Rare contact was defined as contacted with index cases <2 times during 2 days preceding confirmation of infection. Moderate contact was defined as contacted with index cases 3–5 times during 2 days preceding confirmation of infection. Frequent contact was defined as contacted with index cases ≥5 times during 2 days preceding confirmation of infection.

characteristics of 72,314 COVID-19 cases in China (*8*) and suggest that household-based isolation should be cautiously implemented for persons with asymptomatic suspected cases. We also noted that persons with asymptomatic infections appeared to be less effective in transmitting the virus. However, this finding should not discourage isolation and surveillance efforts. The R_0 in this cohort was 0.3 (95% CI 0.2–0.5), which was far smaller than the overall R_0 of 2.2 reported previously (*9*). This low transmission level could be the result of active surveillance, centralized quarantine, and forceful social-distancing strategies in Guangzhou.

Interpretation of the findings should be taken with caution, and several limitations influence our estimation of the SAR. First, the number of close contacts was limited because we only included those who had been reached, and asymptomatic infections might have been missed. Second, we excluded close contacts who were exposed to ≥2 confirmed COVID-19 case-patients. Third, the presymptomatic transmission period is not well defined.

Despite these limitations, our analysis provides valuable information on secondary transmission of SARS-CoV-2 in different types of contact with presymptomatic COVID-19 case-patients. Further evidence is needed to define the population characteristics, communicable period, and the volume and duration of viral shedding from persons with asymptomatic infections.

Acknowledgments

We thank Weiming Tang for reviewing and editing the article.

This study was supported by funding from the Project for Key Medicine Discipline Construction of Guangzhou Municipality (grant no. 2017-2019-07).

About the Author

Dr. W. Zhang is a senior public health physician at the Guangzhou Center for Disease Control and Prevention. Her research interests are health promotion and infectious disease epidemic modeling.

References

1. Bai Y, Yao L, Wei T, Tian F, Jin DY, Chen L, et al. Presumed asymptomatic carrier transmission of COVID-19. JAMA. 2020 Feb 21 [Epub ahead of print]. https://doi.org/10.1001/jama.2020.2565
2. Rothe C, Schunk M, Sothmann P, Bretzel G, Froeschl G, Wallrauch C, et al. Transmission of 2019-nCoV Infection

from an Asymptomatic Contact in Germany. N Engl J Med. 2020;382:970–1. https://doi.org/10.1056/NEJMc2001468
3. Nishiura H, Linton NM, Akhmetzhanov AR. Serial interval of novel coronavirus (COVID-19) infections. Int J Infect Dis. 2020;93:284–6. https://doi.org/10.1016/j.ijid.2020.02.060
4. Pan A, Liu L, Wang C, Guo H, Hao X, Wang Q, et al. Association of public health interventions with the epidemiology of the COVID-19 outbreak in Wuhan, China. JAMA. 2020 Apr 10 [Epub ahead of print]. https://doi.org/10.1001/jama.2020.6130
5. National Health Commission. Questions and answers about the prevention and control of asymptomatic cases infected by 2019-nCoV [in Chinese] 2020. [cited 2020 April 24]. http://www.nhc.gov.cn/jkj/s3578/202003/718c79c96f3e46409dd49303d41a00ef.shtml
6. Tong ZD, Tang A, Li KF, Li P, Wang HL, Yi JP, et al. Potential presymptomatic transmission of SARS-CoV-2, Zhejiang Province, China, 2020. Emerg Infect Dis. 2020;26:1052–4. https://doi.org/10.3201/eid2605.200198
7. Wang FS, Zhang C. What to do next to control the 2019-nCoV epidemic? Lancet. 2020;395:391–3. https://doi.org/10.1016/S0140-6736(20)30300-7
8. Novel Coronavirus Pneumonia Emergency Response Epidemiology Team. Vital surveillances: the epidemiological characteristics of an outbreak of 2019 novel coronavirus diseases (COVID-19)—China, 2020. China CDC Weekly. 2020;2: 113–122 [cited 2020 April 24]. http://weekly.chinacdc.cn/en/article/id/e53946e2-c6c4-41e9-9a9b-fea8db1a8f51
9. Li Q, Guan X, Wu P, Wang X, Zhou L, Tong Y, et al. Early transmission dynamics in Wuhan, China, of novel coronavirus-infected pneumonia. N Engl J Med. 2020;382:1199–207. https://doi.org/10.1056/NEJMoa2001316

Addresses for correspondence: Zhoubin Zhang or Pengzhe Qin, Guangzhou Center for Disease Control and Prevention, No.1 Qide road, Guangzhou, 510440, China; email gzcdczzb@gzcdc.org.cn or petgyy@gmail.com

Abdominal Visceral Infarction in 3 Patients with COVID-19

Giulia Besutti, Riccardo Bonacini, Valentina Iotti, Giulia Marini, Nicoletta Riva, Giovanni Dolci, Mariarosa Maiorana, Lucia Spaggiari, Filippo Monelli, Guido Ligabue, Giovanni Guaraldi, Paolo Giorgi Rossi, Pierpaolo Pattacini, Marco Massari

Author affiliations: Azienda Unità Sanitaria Locale di Reggio Emilia–Istituto di Ricovero e Cura a Carattere Scientifico di Reggio Emilia (AUSL–IRCCS), Reggio Emilia, Italy (G. Besutti, R. Bonacini, V. Iotti, G. Marini, N. Riva, G. Dolci, M. Maiorana, L. Spaggiari, P.G. Rossi, P. Pattacini, M. Massari); University of Modena and Reggio Emilia Clinical and Experimental Medicine PhD Program, Modena, Italy (G. Besutti, M. Maiorana); University of Modena and Reggio Emilia, Modena (R. Bonacini, G. Dolci, F. Monelli, G. Ligabue, G. Guaraldi)

DOI: https://doi.org/10.3201/eid2608.201161

A high incidence of thrombotic events has been reported in patients with coronavirus disease (COVID-19), which is caused by severe acute respiratory syndrome coronavirus-2 (SARS-CoV-2) infection. We report 3 clinical cases of patients in Italy with COVID-19 who developed abdominal viscera infarction, demonstrated by computed tomography.

Frequent thrombotic events, mostly pulmonary embolisms, have been reported in patients with coronavirus disease (COVID-19) (*1*–*4*). We describe 3 cases of COVID-19 complicated by abdominal visceral infarction that occurred in inhabitants of the Emilia Romagna region in northern Italy.

Patient 1, a 54-year-old male former smoker with a history of asthma and quiescent ulcerative colitis not receiving any treatment, was admitted to the emergency department (ED) on February 28, 2020, for syncope. He was discharged after undergoing chest radiography and brain computed tomography (CT), the results of which were unremarkable. He returned to the ED after 5 days for treatment of dyspnea, fatigue, and fever. Blood tests revealed decreased oxygen saturation (94%), increased C-reactive protein (CRP) level (5.38 mg/dL; reference <0.5 mg/dL), and lymphopenia (0.69 × 10^3 cells/mm^3; reference range 0.8–4 × 10^3 cells/mm^3). Chest CT scan demonstrated bilateral viral pneumonia, and nasopharyngeal and oropharyngeal swab specimens were positive for severe acute respiratory syndrome coronavirus 2 (SARS-CoV-2). He was hospitalized and treated with lopinavir/ritonavir (400/100 mg orally 2×/d), and hydroxychloroquine (200 mg orally 2×/d). He was discharged to home after 3 hospital days, on therapy; no anticoagulant prophylaxis was suggested. He was rehospitalized 6 days after discharge when he developed sharp right flank and lumbar pain, fever, and dysuria. Blood and urine tests revealed neutrophilia (9.9 × 10^3 cells/mm^3; reference range 1.6–7.5 × 10^3 cells/mm^3), increased lactate dehydrogenase (LDH) (1,507 U/L; reference range 28–378 U/L), increased CRP (1.43 mg/dL), and proteinuria (50 mg/dL). CT scan demonstrated a large right kidney arterial infarction (Figure, panel A). He was treated with low molecular weight

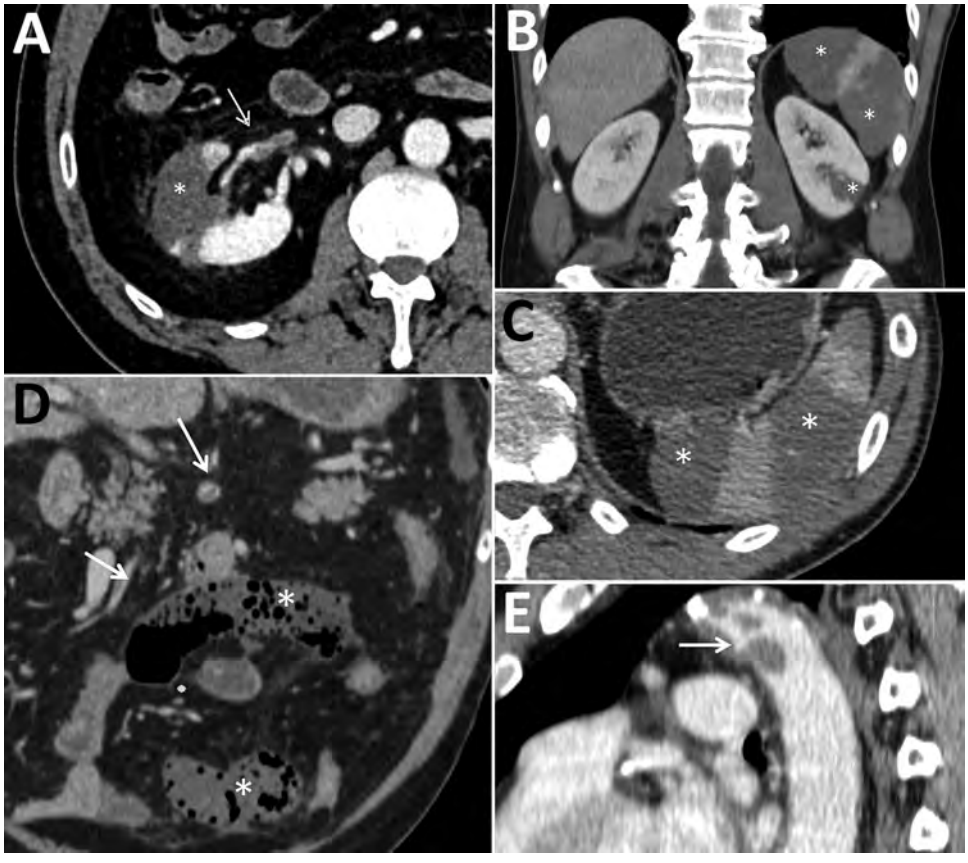

Figure. Abdominal contrast-enhanced computed tomography scans of 3 coronavirus disease patients with abdominal visceral infarction, Italy. A) Patient 1 (axial view) showing intraarterial thrombi in the renal artery (arrow) and kidney and splenic infarctions (asterisk), seen as large wedge-shaped hypodense parenchymal areas. B, C) Patient 2 (B, coronal view; C, axial view) showing kidney and splenic infarctions (asterisks), seen as large wedge-shaped hypodense parenchymal areas. D, E) Patient 3 (D, coronal view; E, sagittal view), showing intraarterial thrombi in the superior mesenteric artery and its branches (arrows in D) and thoracic descending aorta (arrow in E), as well as small bowel ischemia (asterisks in D), seen as small bowel loops with decreased or absent wall enhancement. In patients 1 and 2, scans did not show notable signs of atherosclerosis.

heparin (LMWH) (6,000 UI 2×/d) and discharged to home after 4 days.

Patient 2, a 53-year-old man with hypertension and a history of mitral valve replacement (June 2019), came to the ED on March 11, 2020, with fever, cough, and sore throat. At admission, he had decreased oxygen saturation (94%) and increased CRP (6.99 mg/dL). Chest CT scan demonstrated bilateral viral pneumonia, and nasopharyngeal and oropharyngeal swab specimens were positive for SARS-CoV-2. He was hospitalized and treated with lopinavir/ritonavir (400/100 mg orally 2×/d) and hydroxychloroquine (200 mg orally 2×/d); he also received 2 administrations of tocilizumab (8 mg/kg, an off-label use) on hospital day 3 because his respiratory function was worsening. Because of his previous mitral valve replacement, he was already being treated with antiplatelet prophylaxis with acetylsalicylic acid but not with anticoagulants. On hospital day 6 he reported severe left flank pain; blood tests revealed neutrophilia (11.74×10^3 cells/mm^3) and increased LDH (932 U/L) and CRP (4.42 mg/dL). CT scan demonstrated large infarcted areas involving the spleen and the left kidney (Figure, panels B,C). He was treated with LMWH (6,000 UI 2×/d) and discharged home after 7 days.

Patient 3, a 72-year-old man with stage 3 kidney failure, hypertension, previous myocardial infarction, and type 2 diabetes, came to the ED on March 25, 2020, with shortness of breath and dry cough. At admission, he had increased CRP (19.3 mg/dL) and high glucose level (1,000 mg/dL; reference <100 mg/dL) with severe metabolic acidosis. Nasopharyngeal and oropharyngeal swab specimens were positive for SARS-CoV-2. He was hospitalized, began antithrombotic prophylaxis with LMWH (4,000 UI 1×/d), and continued secondary prophylaxis with acetylsalicylic acid. He was transferred in the intensive care unit the day after admission; a few hours later, he developed severe abdominal pain. Blood tests revealed neutrophilia (17.69×10^3 cells/mm^3) and increased LDH (1,510 U/L), CRP (48 mg/dL), and D-dimer (6,910 ng/mL), with normal prothrombin time and activated partial thromboplastin time. Antiphospholipid antibodies were not detected. CT scan demonstrated small bowel ischemia associated with massive splenic infarction (Figure, panels D,E). He underwent resection of the ischemic bowel loop and splenectomy, was treated with heparin in continuous infusion, and was discharged from the ICU 2 days later. As of May 9, he was still hospitalized but his condition was improving.

Between the start of the SARS-CoV-2 outbreak in Reggio Emilia at the end of February and March 24, the province has had 460 hospitalizations in all hospitals. Among these, 2 (0.4%) patients (*1*,*2*) had acute ischemic events involving abdominal viscera; therefore, these events should not be considered too rare. Visceral infarction is probably a clinical manifestation of the prothrombotic state that has been described in patients with COVID-19 (*1*–*6*). Consistently, reports about pathological changes in organs other than the lungs describe parenchymal cells necrosis and small-vessel thrombosis (*7*).

The possibility of abdominal visceral infarction during COVID-19 has major implications in clinical practice. First, when patients with COVID-19 report severe abdominal pain, visceral infarction should be considered in differential diagnosis and taken into account in laboratory and imaging diagnostic workups. Second, this finding should further prompt the scientific community to stress the need to routinely use LMWH in patients with COVID-19 and to open the debate on the appropriate dosage. Finally, the prothrombotic state in patients with COVID-19 may justify therapeutic rather than prophylactic LMWH.

Acknowledgment

We thank Jacqueline Costa for English language editing.

About the Author

Dr. Besutti is a radiologist in Azienda USL–IRCCS of Reggio Emilia, Italy, and a PhD student in the clinical and experimental medicine PhD program, University of Modena and Reggio Emilia, Modena, Italy. Her primary research interest is about comorbidities in HIV-infected patients, especially involving the lungs, liver, and cardiovascular system.

References

1. Klok FA, Kruip MJHA, van der Meer NJM, Arbous MS, Gommers DAMPJ, Kant KM, et al. Incidence of thrombotic complications in critically ill ICU patients with COVID-19. Thromb Res. 2020 Apr 10 [Epub ahead of print]. https://doi.org/10.1016/j.thromres.2020.04.013
2. Griffin DO, Jensen A, Khan M, Chin J, Chin K, Saad J, et al. Pulmonary embolism and increased levels of d-dimer in patients with coronavirus disease. Emerg Infect Dis. 2020 Apr 29 [Epub ahead of print]. https://doi.org/10.3201/eid2608.201477
3. Khodamoradi Z, Boogar SS, Shirazi F, Kouhi P. COVID-19 and acute postpartum pulmonary embolism. Emerg Infect Dis. In press 2020.
4. Helms J, Tacquard C, Severac F, Leonard-Lorant I, Ohana M, Delabranche X, et al.; CRICS TRIGGERSEP Group (Clinical Research in Intensive Care and Sepsis Trial Group for Global Evaluation and Research in Sepsis). High risk of thrombosis in patients with severe SARS-CoV-2 infection: a multicenter prospective cohort study. Intensive Care Med. 2020 May 4 [Epub ahead of print]. https://doi.org/10.1007/s00134-020-06062-x
5. Huang C, Wang Y, Li X, Ren L, Zhao J, Hu Y, et al. Clinical features of patients infected with 2019 novel coronavirus in Wuhan, China. Lancet. 2020;395:497–506. https://doi.org/10.1016/S0140-6736(20)30183-5
6. Zhou F, Yu T, Du R, Fan G, Liu Y, Liu Z, et al. Clinical course and risk factors for mortality of adult inpatients with COVID-19 in Wuhan, China: a retrospective cohort study. Lancet. 2020;395:1054–62. https://doi.org/10.1016/S0140-6736(20)30566-3
7. Yao XH, Li TY, He ZC, Ping YF, Liu HW, Yu SC, et al. A pathological report of three COVID-19 cases by minimally invasive autopsies [in Chinese]. Zhonghua Bing Li Xue Za Zhi. 2020;49:E009.

Address for correspondence: Giulia Besutti, Radiology Unit, AUSL Reggio Emilia–IRCCS. Viale Risorgimento 80, 42123 Reggio Emilia, Italy; e-mail: giulia.besutti@ausl.re.it

Collateral Benefit of COVID-19 Control Measures on Influenza Activity, Taiwan

Shu-Chen Kuo, Shu-Man Shih, Li-Hsin Chien, Chao A. Hsiung

Author affiliation: National Health Research Institutes, Zhunan, Taiwan

DOI: https://doi.org/10.3201/eid2608.201192

Taiwan has strictly followed infection control measures to prevent spread of coronavirus disease. Meanwhile, nationwide surveillance data revealed drastic decreases in influenza diagnoses in outpatient departments, positivity rates of clinical specimens, and confirmed severe cases during the first 12 weeks of 2020 compared with the same period of 2019.

After the 2003 severe acute respiratory syndrome coronavirus epidemic, the government and public of Taiwan have been vigilant about the threat of emerging infectious diseases. The government of Taiwan took swift action to prevent coronavirus disease (COVID-19) importation and outbreaks (*1*). The public

has adhered well to control measures that included avoiding gatherings, maintaining social distance, mask wearing, hand and respiratory hygiene, temperature monitoring, and quarantine of high-risk and sick persons (Figure 1, panel A). Although the success of these measures for limiting COVID-19 transmission remains to be determined, nationwide surveillance has shown the rapid decline of influenza activity during the first 12 weeks of 2020 (through March 21) in Taiwan.

The Taiwan National Infectious Disease Statistics System (2), maintained by the Taiwan Centers for Disease Control, is an open data portal that provides nationwide surveillance data on infectious diseases (https://nidss.cdc.gov.tw). For this study, we analyzed data from outpatient department visits for selected syndromes, clinical specimen testing, isolated respiratory pathogens, and confirmed severe cases (Appendix, https://wwwnc.cdc.gov/EID/article/26/8/20-1192-App1.pdf). The institutional review board of the National Health Research Institutes approved this study (EC1051207-R4).

We compared changes across the first 12 weeks of 2020 with data from the same period of 2019 using simple linear regression. (The 9-day Lunar New Year holiday in week 6 of 2019, when most healthcare service was unavailable, resulted in extreme data; therefore, we excluded these data from analysis.) We saw fewer outpatient department visits for influenza-like illness (ILI) and ILI diagnoses per 1,000 visits during weeks 8–12 of 2020 compared with 2019 (Figure, panel A). The changes (slopes of the regression lines) of ILI visits (-8,061 vs. -590 per week; $p<0.05$) differed between 2020 and 2019, as did the changes in ILI diagnoses per 1,000 visits (-1.5 vs. -0.2 per week; $p<0.05$). The slopes of the regression lines

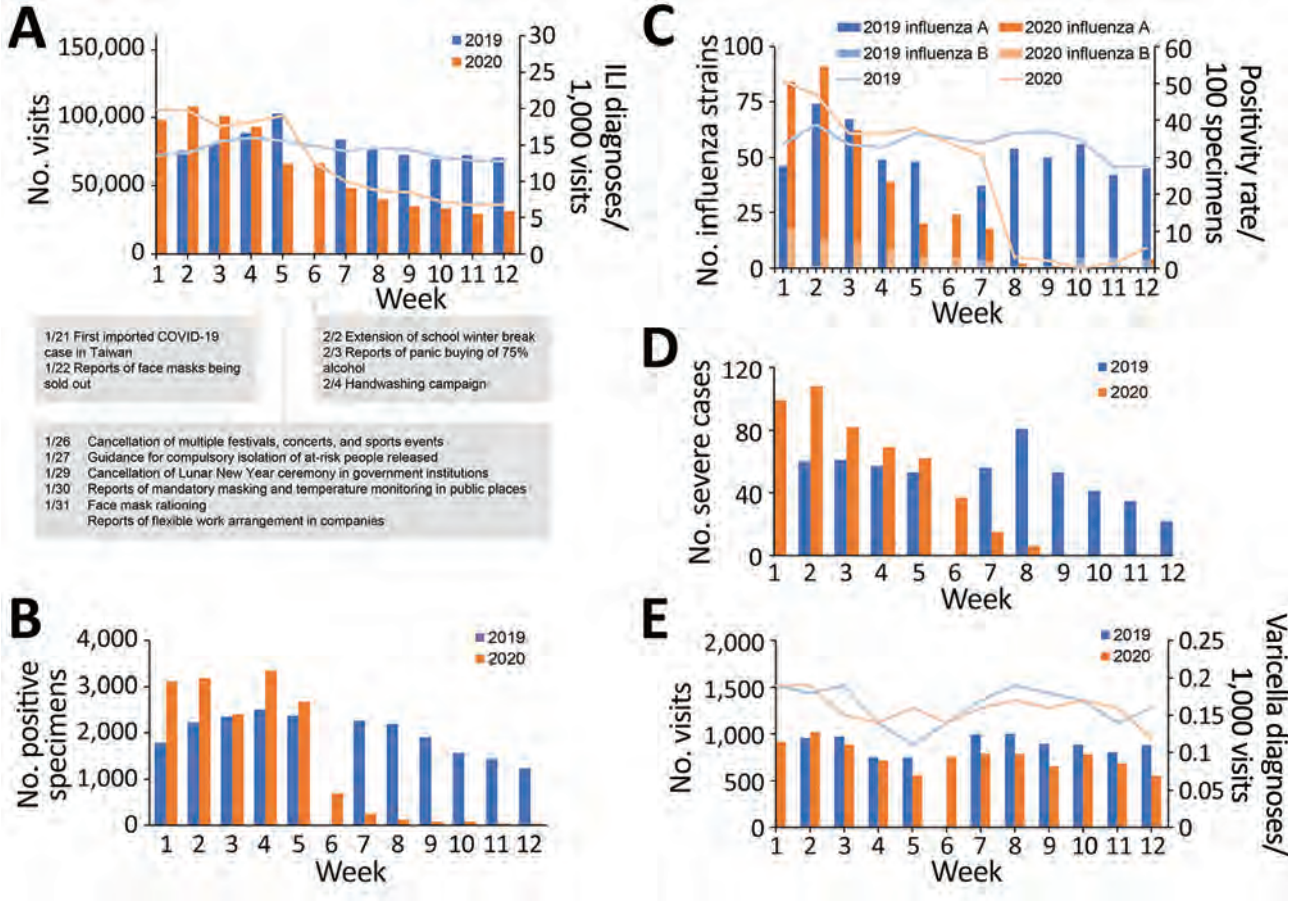

Figure. Influenza and varicella activity in Taiwan during the first 12 weeks of 2020 compared with the corresponding time period in 2019. A) Number of outpatient department visits in which the diagnosis of influenza-like illness (ILI) was made (bars) and the rate of ILI diagnoses per 1,000 visits (lines). Notable dates during the coronavirus disease pandemic are marked along the baseline. B) Number of specimens positive for influenza. C) Number of strains of influenza identified in commissioned laboratories (bars) and the number of positive specimens/total specimens positivity rate (lines). D) Number of laboratory-confirmed influenza cases with severe complications. E) Number of outpatient department visits in which the diagnosis of varicella infection was made (bars) and the rate of varicella diagnoses per 1,000 visits (lines). The 9-day Lunar New Year holiday in week 6 of 2019, when most healthcare service was unavailable, resulted in extreme data, which we excluded from the analysis.

for positive samples (-360 vs. -77 per week; p<0.05) also differed between 2020 and 2019 (Figure 1, panel B). Both the number of influenza strains isolated from clinical specimens in commissioned laboratories and the positivity rate dropped drastically in 2020; the trends were different from 2019 (p<0.05 for both) (Figure 1, panel C). The number of cases of confirmed influenza with severe complications decreased from 99 to 1 in 2020, compared with a decrease from 44 to 22 in 2019 (p<0.05) (Figure 1, panel D). In contrast, the number of outpatient department visits for varicella and the number of varicella diagnoses per 1,000 visits remained similar in 2020 and 2019 (p = 0.660 for outpatient department visits and p = 0.157 for varicella diagnosis) (Figure 1, panel E).

The functional healthcare and surveillance systems in Taiwan, the government's efforts to identify causes of ILI during the COVID-19 pandemic, and sufficient laboratory capacity ensure appropriate influenza testing and reporting of results. Healthcare avoidance during COVID-19 pandemic may be an important confounder for the results we reported. However, because of awareness of the similarities in symptoms between COVID-19 and influenza and the low number of COVID-19 patients in Taiwan (<200 cases as of March 21, 2020), patients with ILI would not avoid seeking medical help for a diagnosis. Healthcare avoidance also did not explain the lower number of severe influenza cases observed in 2020 (Figure 1, panel D). Therefore, we believe that the decreasing influenza activity in Taiwan in 2020 is the result of strict control measures that were established in response to COVID-19.

Acknowledgments

We thank the Taiwan Centers for Disease Control for making their data publicly available and I-Shou Chang for his comments regarding statistical methods.

This project was supported by an intramural grant from the National Health Research Institutes (IV-109-PP-01 and PH-109-GP-02).

About the Author

Dr. Kuo is an attending physician and associate investigator at the National Institute of Infectious Diseases and Vaccinology, National Health Research Institutes, Taiwan. His primary research interest involves infectious diseases and clinical microbiology.

References

1. Wang CJ, Ng CY, Brook RH. Response to COVID-19 in Taiwan: big data analytics, new technology, and proactive testing. JAMA. 2020;323:1341. https://doi.org/10.1001/jama.2020.3151
2. Jian SW, Chen CM, Lee CY, Liu DP. Real-time surveillance of infectious diseases: Taiwan's experience. Health Secur. 2017;15:144–53. https://doi.org/10.1089/hs.2016.0107

Address for correspondence: Shu-Chen Kuo, National Institute of Infectious Diseases and Vaccinology, National Health Research Institutes, 35 Keyan Rd, Zhunan, Miaoli County 35053, Taiwan; email: sckuo@nhri.edu.tw

Asymptomatic SARS-CoV-2 Infection in Household Contacts of a Healthcare Provider, Wuhan, China

Yi Luo,[1] Edwin Trevathan,[1] Zhengmin Qian, Yirong Li, Jin Li, Wei Xiao, Ning Tu, Zhikun Zeng, Pingzheng Mo, Yong Xiong, Guangming Ye

Author affiliations: Zhongnan Hospital, Wuhan University, Wuhan, China (Y. Luo, Y. Li, J. Li, Z. Zeng, P. Mo, Y. Xiong, G. Ye); Vanderbilt Institute for Global Health, Vanderbilt University Medical Center, Nashville, Tennessee, USA (E. Trevathan); Saint Louis University, St. Louis, Missouri, USA (Z. Qian); Central Hospital of Wuhan, Tongji Medical College, Huazhong University of Science and Technology, Wuhan (W. Xiao); Wuhan University Remin Hospital, Wuhan (N. Tu).

DOI: https://doi.org/10.3201/eid2608.201016

We found that all 5 asymptomatic household contacts of a Wuhan, China, physician with coronavirus disease had severe acute respiratory syndrome coronavirus 2 detected by PCR. The index patient and 2 contacts also had abnormal chest computed tomography scans. Asymptomatic infected household contacts of healthcare workers with coronavirus disease might be underrecognized.

Severe acute respiratory syndrome coronavirus 2 (SARS-CoV-2), the cause of the coronavirus disease (COVID-19) pandemic, is highly contagious and can put families of healthcare professionals at risk for both symptomatic COVID-19 and asymptomatic

[1]These first authors contributed equally to this article.

Table. Summary of laboratory results of a SARS-CoV-2–positive patient and 5 asymptomatic household contacts, Wuhan, China*

Laboratory test	Reference range	Patient 1	Contact 1	Contact 2†	Contact 3‡	Contact 4	Contact 5
C-reactive protein, mg/L	0–10	18.8	2.0	0.4	0.4	1.5	2.7
Leukocyte count, × 10^9 cells/L	3.5–9.5	6.68	6.89	4.79	6.86	3.54	5.84
Lymphocyte ratio, %	20–50	17.70	18.50	45.50	67.90	34.60	33.10
$CD19^+$ absolute count/μL	240–1317	140	147	626	767	271	299
ALT, U/L	7–45	45	11	520	16	15	7
AST, U/L	13–35	21	14	439	24	18	14
D-dimer, ng/mL	0–500	161	89	101	>3500	150	97

*ALT, alanine aminotransferase; AST, aspartate aminotransferase; SARS-CoV-2, severe acute respiratory syndrome coronavirus 2.
†Contact 2 had 4 serial negative throat swabs for SARS-CoV-2, and negative influenza A, influenza B, respiratory syncytial virus, parainfluenza virus, adenoviridae, Epistein-Barr virus, cucumber mosaic virus, mycoplasma, and chlamydia results. He had elevated AST and ALT and was negative for hepatitis A, B, C, and E; he had no jaundice or gastrointestinal symptoms. His AST and ALT returned to normal after 9 days of treatment with glycyrrhizinate 50 mg 3 times daily and vitamin C (0.2 g 3×/d).
‡Contact 3 had an elevated D-dimer level without anemia, bleeding, or evidence of a coagulopathy. She received vitamin C (0.2 g 3 ×/d). After the SARS-CoV-2 nucleic acid (throat swab) test was negative, her D-dimer level returned to normal (111 ng/mL).

SARS-CoV-2 infection with potential to infect others (*1*–*4*). Data regarding asymptomatic SARS-CoV-2 infection (*5*) among families of healthcare professionals can help inform healthcare management and the public health response during the COVID-19 pandemic. We describe the case of a physician in Wuhan, China, who had mildly symptomatic COVID-19 and the subsequent asymptomatic SARS-CoV-2 infection in all 5 of his household contacts.

The index patient (patient 1) was a 39-year-old nephrologist at Central Hospital of Wuhan who had onset of a dry cough on January 31, 2020, was admitted with fever on February 7, and was diagnosed with symptomatic SARS-CoV-2 infection on February 10. During January 31–February 6, patient 1 lived with 5 other immediate family members, all of whom were hospitalized on February 11 at Zhongnan Hospital of Wuhan University for ethics committee–approved (approval no. 2019125) medical studies, for which informed consent was obtained. The household contacts were his 37-year-old wife, a laboratory physician without patient contact at Zhongnan Hospital (contact 1); 7-year-old fraternal twins, who were in contact only with family because of school closure and social distancing (contacts 2 and 3); a retired 62-year-old grandfather, who was a current smoker in good health (contact 4); and a retired 64-year-old grandmother in good health (contact 5).

All household contacts underwent chest computed tomography scans and throat swabs for quantitative real-time reverse transcription PCR (qRT-PCR) tests for SARS-CoV-2 nucleic acid, in addition to other routine laboratory examinations (Table). qRT-PCR tests on stool specimens of contacts 1, 2, and 3 were positive for SARS-CoV-2. Contact 1 also was positive for SARS-CoV-2 on qRT-PCR tests of multiple serial throat swab specimens but negative for SARS-CoV-2 on IgM and IgG tests.

All 5 household contacts of patient 1 had laboratory evidence of SARS-CoV-2 infection but remained asymptomatic throughout the period of observation (February 11–March 1) (Figure, panel A). All household contacts who had throat swab specimens tested for SARS-CoV-2 were positive by PCR except for contact 2, who tested negative on 4 consecutive throat swab specimen tests for SARS-CoV-2 but whose stool specimen was positive for SARS-CoV-2; contact 2 also had elevated liver enzymes but no jaundice. Contact 3 had an elevated D-dimer level. These abnormal laboratory values resolved during observation (Table) and were not associated with clinical illness in either patient. Patient 1 and contacts 2 and 4 also had abnormal chest computed tomography scans consistent with SARS-CoV-2 infection (Figure, panel B).

Contact 1 underwent 11 serial throat swabs for SARS-CoV-2. Her case demonstrates the challenges of clinical interpretation qRT-PCR results for SARS-CoV-2. On 2 separate occasions, she had 2 consecutive negative results on throat swab specimens for SARS-CoV-2, only to revert back to having a throat swab specimen positive for SARS-CoV-2 (Figure, panel A). Contact 1 was the only family member who underwent serologic tests, which demonstrated low B lymphocyte counts but no detectable SARS-CoV-2–specific IgM or IgG. We cannot determine the cause or clinical significance of the lack of a detectable antibody response in contact 1 in our study, which differs from findings reported in other studies (*6*). The immunologic response after asymptomatic SARS-CoV-2 infection requires further study.

A likely source of infection for the 5 asymptomatic contacts was patient 1. Contact 1 had no patient contact and no known contact with COVID-19–positive co-workers, and contacts 2, 3, 4, and 5 were at their home in Wuhan and had no other substantial human contact during the period when they likely were infected. We identified no other likely source of infection. Our study could not determine the method of transmission between family contacts, but we did note the potential for respiratory transmission (e.g., through droplets), fecal–oral transmission, or both.

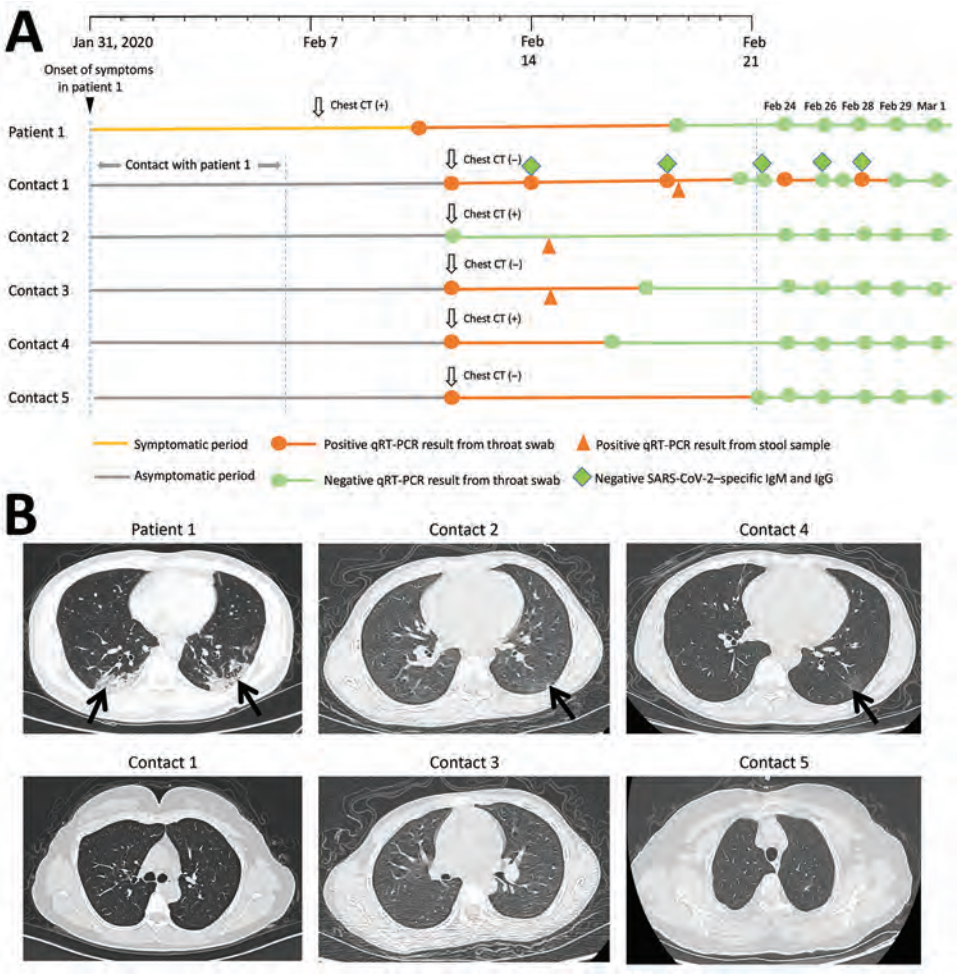

Figure. Timeline and CT images associated with a cluster of SARS-CoV-2 infections in a single household, Wuhan China. A) Timeline of key events, including laboratory tests, associated with SARS-CoV-2 infections in the index patient and 5 asymptomatic household contacts. B) Abnormal chest CT scans showing features consistent with SARS-CoV-2 infection (arrows) observed in the index patient and 2 household contacts (top row), compared with normal CT scans among the 3 other household contacts (bottom row). CT, computed tomography; qRT-PCR, quantitative real-time reverse transcription PCR; SARS-CoV-2, severe acute respiratory syndrome coronavirus 2.

An early report from China on 72,314 COVID-19 cases found that only 1% of SARS-CoV-2 infections were asymptomatic; however, asymptomatic close contacts were not routinely tested in that study (*7*). In our study, all 5 household contacts of a physician diagnosed with COVID-19 had laboratory evidence of infection but remained asymptomatic. This finding is consistent with emerging evidence that suggests that a substantial proportion of SARS-CoV-2 infections are asymptomatic (*1*,*8*,*9*).

In summary, this single-household study found a high attack rate for asymptomatic SARS-CoV-2 infection among the immediate family members of a symptomatic COVID-19 case-patient. The extent to which asymptomatic SARS-CoV-2 infections contribute to overall disease transmission is still unknown and warrants further study. We believe the potential for fecal–oral transmission also warrants investigation (*10*). Moreover, our experience indicates that screening symptomatic contacts with a single throat swab test for SARS-CoV-2 might lead to an underestimate of the rate of infection and that asymptomatic persons can repeatedly revert between positive and negative PCR results on throat specimens.

This study was supported by the Health Commission of Hubei Province Scientific Research Project (grant no. WJ2019H060) and the National Natural Science Foundation of China (grant no. 81501033).

About the Author

Dr. Luo is a laboratory physician specializing in respiratory infection pathogens at Zhongnan Hospital of Wuhan University, Wuhan, China. Her primary research interests are the epidemiology and diagnosis of infectious diseases.

References

1. Sutton D, Fuchs K, D'Alton M, Goffman D. Universal screening for SARS-CoV-2 in women admitted for delivery. N Engl J Med. 2020 Apr 13 [Epub ahead of print]. https://doi.org/10.1056/NEJMc2009316

2. Chan JF, Yuan S, Kok KH, To KK, Chu H, Yang J, et al. A familial cluster of pneumonia associated with the 2019 novel coronavirus indicating person-to-person transmission: a study of a family cluster. Lancet. 2020;395:514–23. https://doi.org/10.1016/S0140-6736(20)30154-9
3. Bai Y, Yao L, Wei T, Tian F, Jin DY, Chen L, et al. Presumed asymptomatic carrier transmission of COVID-19. JAMA. 2020;323:1406. https://doi.org/10.1001/jama.2020.2565
4. Ye F, Xu S, Rong Z, Xu R, Liu X, Deng P, et al. Delivery of infection from asymptomatic carriers of COVID-19 in a familial cluster. Int J Infect Dis. 2020 Apr 2 [Epub ahead of print]. https://doi.org/10.1016/j.ijid.2020.03.042
5. Hu Z, Song C, Xu C, Jin G, Chen Y, Xu X, et al. Clinical characteristics of 24 asymptomatic infections with COVID-19 screened among close contacts in Nanjing, China. Sci China Life Sci. 2020 Mar 4 [Epub ahead of print].
6. Du Z, Zhu F, Guo F, Yang B, Wang T. Detection of antibodies against SARS-CoV-2 in patients with COVID-19. J Med Virol. 2020 Apr 3 [Epub ahead of print]. https://doi.org/10.1002/jmv.25820
7. Wu Z, McGoogan JM. Characteristics of and important lessons from the coronavirus disease 2019 (COVID-19) outbreak in China: summary of a report of 72,314 cases from the Chinese Center for Disease Control and Prevention. JAMA. 2020;323:1239. https://doi.org/10.1001/jama.2020.2648
8. Mizumoto K, Kagaya K, Zarebski A, Chowell G. Estimating the asymptomatic proportion of coronavirus disease 2019 (COVID-19) cases on board the Diamond Princess cruise ship, Yokohama, Japan, 2020. Euro Surveill. 2020;25(10). https://doi.org/10.2807/1560-7917.ES.2020.25.10.2000180
9. Nishiura H, Kobayashi T, Suzuki A, Jung SM, Hayashi K, Kinoshita R, et al. Estimation of the asymptomatic ratio of novel coronavirus infections (COVID-19). Int J Infect Dis. 2020 Mar 13 [Epub ahead of print]. https://doi.org/10.1016/j.ijid.2020.03.020
10. Chen Y, Chen L, Deng Q, Zhang G, Wu K, Ni L, et al. The presence of SARS-CoV-2 RNA in feces of COVID-19 patients. J Med Virol. 2020 Apr 3 [Epub ahead of print]. https://doi.org/10.1002/jmv.25825

Address for correspondence: Guangming Ye, Department of Laboratory Medicine; Zhongnan Hospital of Wuhan University, 169 Donghu Rd, Wuhan 430071, China; email: fduser@163.com

Decreased Influenza Incidence under COVID-19 Control Measures, Singapore

Roy Jiunn Jye Soo, Calvin J. Chiew, Stefan Ma, Rachael Pung, Vernon Lee

Author affiliation: Ministry of Health, Singapore (R.J.J. Soo, C.J. Chiew, S. Ma, R. Pung, V. Lee); Saw Swee Hock School of Public Health, Singapore (V. Lee)

DOI: https://doi.org/10.3201/eid2608.201229

We compared indicators of influenza activity in 2020 before and after public health measures were taken to reduce coronavirus disease (COVID-19) with the corresponding indicators from 3 preceding years. Influenza activity declined substantially, suggesting that the measures taken for COVID-19 were effective in reducing spread of other viral respiratory diseases.

Public health measures, including public education and physical distancing, were implemented in Singapore to reduce transmission of coronavirus disease (COVID-19). However, instead of a lockdown, Singapore kept schools and workplaces open and did not advise the routine use of masks for persons who were well during the initial phase of the outbreak in January–February 2020. We examined the effect of these COVID-19 measures on influenza incidence as a proxy to determine the overall potential reduction in respiratory virus transmission.

We obtained routine sentinel surveillance data on influenza-like illnesses (ILI) from a national network of primary care clinics and the National Public Health Laboratory. ILI was defined as fever (≥38°C) and cough. Data included number of visits to government primary care clinics for ILI per day, ILI samples tested per week, and percentage influenza positivity. We estimated number of influenza cases per day by multiplying ILI visits per day by the proportion of ILI patients who tested positive for influenza, which better reflects influenza infection rates than either indicator alone (*1*).

We compared influenza activity between epidemiologic weeks 1–4 and weeks 5–9 of 2020. Most community-based COVID-19 measures were instituted after the first few cases were reported in epidemiologic week 4, and public awareness was increased (*2*). These measures included cancellation of large-scale events and precautions at schools (e.g., fewer assemblies, no interclass mixing, and staggered meal times) and workplaces (e.g., segregated teams and teleworking

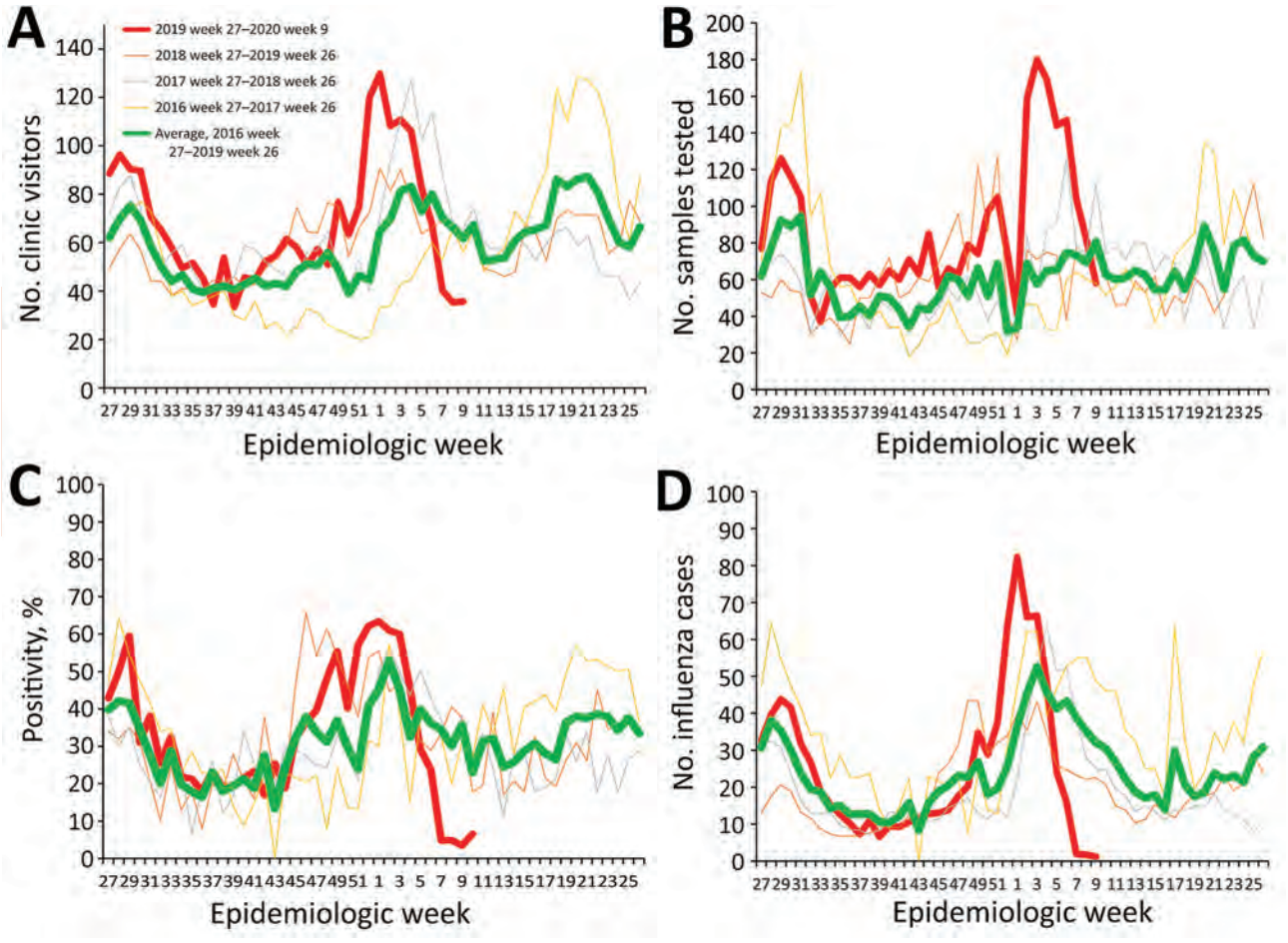

Figure. Indicators of influenza activity during the 2019–20 season (red line) compared with average of the preceding 3 years (green line), Singapore. A) Average number of visits per day to government primary care clinics for influenza-like illnesses, 2016–2020. B) Samples from patients with influenza-like illness tested per week, 2016–2020. C) Influenza positivity, 2016–2020. D) Estimated daily numbers of influenza cases, 2016–2020.

wherever possible). Intensive public education on personal hygiene and social responsibility included encouraging regular handwashing and seeking medical attention early when ill. To enable self-isolation and prevent spread, physicians were instructed to give certificates for 5 days of medical leave for patients who had respiratory symptoms but did not meet the COVID-19 suspect case definition.

We compared indicators of influenza transmissibility in 2020 against the average from corresponding periods in the 3 preceding epidemiologic years (2016–2019). We performed weekly paired difference *t*-test using R version 3.5.1 (https://www.r-project.org). Influenza activity peaked in epidemiologic week 1 of 2020 but declined to below the average of the preceding years by epidemiologic week 5 (Figure). Percentage influenza positivity decreased by 64% (p = 0.001) and estimated daily number of influenza cases decreased by 76% (p = 0.002) in epidemiologic weeks 5–9 of 2020 compared with the preceding years. In contrast, we saw no significant changes in any of the indicators, except percentage of influenza positivity (31%; p = 0.008), in epidemiologic weeks 1–4 of 2020 compared with preceding years.

Public health efforts to control COVID-19 probably reduced influenza transmission in February 2020 because both viruses have similar modes of transmission through respiratory and contact routes. Even if COVID-19 has a potentially higher basic reproduction number (R_0) than seasonal influenza (3), substantial reduction in transmission could reduce the impact of COVID-19 on healthcare capacity, thereby preventing excess deaths. Our modeling of the effective reproduction number for COVID-19 in Singapore in February 2020 (R. Pung, unpub. data) at 0.5–1 is

55%–77% lower than the mean estimated R_0 of 2.2 (4). This finding is consistent with the observed 76% reduction in influenza transmission.

Our study has several limitations. First, a decrease in influenza transmission is expected in February–March, given the yearly bimodal pattern of influenza incidence in Singapore (5). However, the decrease in 2020 is marked compared to previous years. Second, there could be fewer ILI visits to government clinics because of altered health-seeking behavior, or cases may be referred to hospitals and therefore not captured as ILI cases in clinics. However, these missed ILI cases would not affect the proportion positive for influenza. Third, we can infer similar effects on COVID-19 only if the transmission dynamics are similar to influenza.

In conclusion, we found a marked decline in ILI in Singapore after the implementation of public health measures for COVID-19. Our findings suggest that such measures are effective in reducing spread of viral respiratory diseases and could mitigate the impact of the COVID-19 pandemic.

About the Author

Dr. Soo is a preventive medicine resident in the National University Health System in Singapore. He obtained his medical degree from the National University of Singapore and is currently pursuing a Master of Public Health degree.

References

1. Lee VJ, Chen MI, Yap J, Ong J, Lim W-Y, Lin RTP, et al. Comparability of different methods for estimating influenza infection rates over a single epidemic wave. Am J Epidemiol. 2011;174:468–78. https://doi.org/10.1093/aje/kwr113
2. Singapore Government. Coronavirus disease 2019: cases in Singapore. A timeline of the confirmed cases in Singapore. 2020 [cited 2020 April 15]. https://www.gov.sg/article/covid-19-cases-in-singapore
3. World Health Organization. Q&A: Similarities and differences—COVID-19 and influenza. Geneva: The Organization; 2020 [cited 2020 April 15]. https://www.who.int/news-room/q-a-detail/q-a-similarities-and-differences-covid-19-and-influenza
4. Li Q, Guan X, Wu P, Wang X, Zhou L, Tong Y, et al. Early transmission dynamics in Wuhan, China, of novel coronavirus-infected pneumonia. N Engl J Med. 2020;382:1199–207. https://doi.org/10.1056/NEJMoa2001316
5. Chow A, Ma S, Ling AE, Chew SK. Influenza-associated deaths in tropical Singapore. Emerg Infect Dis. 2006;12:114–21. https://doi.org/10.3201/eid1201.050826

Address for correspondence: Vernon J. Lee, Communicable Diseases Division, Ministry of Health, Singapore, 12 College Rd, 169852, Singapore; email: Vernon_Lee@moh.gov.sg

SARS-CoV-2 Transmission from Presymptomatic Meeting Attendee, Germany

DirkJan Hijnen, Angelo Valerio Marzano, Kilian Eyerich, Corine GeurtsvanKessel, Ana Maria Giménez-Arnau, Pascal Joly, Christian Vestergaard, Michael Sticherling, Enno Schmidt

Author affiliations: Erasmus MC University Medical Center Rotterdam, Rotterdam, the Netherlands (D. Hijnen, C. GeurtsvanKessel); Fondazione IRCCS Ca' Granda Ospedale Maggiore Policlinico, Milan, Italy (A.V. Marzano); Università degli Studi di Milano, Milan (A.V. Marzano); Karolinska Institutet, Solna, Sweden (K. Eyerich); Universitat Autònoma de Barcelona, Barcelona, Spain (A.M. Giménez-Arnau); INSERM U—Rouen University Hospital, Rouen, France (P. Joly); Aarhus University Hospital, Aarhus, Denmark (C. Vestergaard); University Hospitals Erlangen, Erlangen, Germany (M. Sticherling); Lübeck Institute of Experimental Dermatology, Lübeck, Germany (E. Schmidt); University of Lübeck, Lübeck (E. Schmidt)

DOI: https://doi.org/10.3201/eid2608.201235

During a meeting in Munich, Germany, a presymptomatic attendee with severe acute respiratory syndrome coronavirus 2 infected at least 11 of 13 other participants. Although 5 participants had no or mild symptoms, 6 had typical coronavirus disease, without dyspnea. Our findings suggest hand shaking and face-to-face contact as possible modes of transmission.

We describe efficient spread of severe acute respiratory syndrome coronavirus 2 (SARS-CoV-2) resulting from contact with a presymptomatic infected person during a scientific advisory board meeting held February 20–21, 2020, in Munich, Germany; the country had <20 diagnosed coronavirus disease (COVID-19) cases at the time. Eight dermatologists from 7 countries and 6 scientists from the same company attended the meeting at a hotel in central Munich. The meeting was held in a room (≈70 m^2) with conventional radiators; a U-shaped setup of tables were separated by a central aisle >1 m wide. During the meeting, refreshments were served buffet style in the same room 4 times. In addition to 9.5 hours of discussions, the participants had dinner on February 20 in a nearby restaurant. Additional direct contacts between participants were handshakes during welcome and farewell with few short hugs without kisses. None of the participants, including the index patient (participant [Pt] 1), showed any signs of infection (e.g., coughing, sneezing, respiratory symptoms,

shivering, fever) before or during the meeting. No one wore a mask during the meeting. After the meeting, the index patient (Pt 1) shared a taxi with Pt 2, 4, and 9 for ≈45 min.

After returning home the evening of February 21, Pt 1 sought care for fever. Reverse transcription PCR was performed on throat and nasal swab specimens, and SARS-CoV-2 RNA was detected by established methods (*1*). The patient was admitted to the hospital for supportive care, although he had only moderate symptoms (Table, https://wwwnc.cdc.gov/EID/article/26/8/20-1235-T1.htm).

National authorities contacted most meeting participants on February 26 (Pt 7, 11–13) and 27 (Pt 2–6, 8–12); Pt 14 was contacted by a coworker. Twelve participants, including Pt 1, were tested for SARS-CoV-2 by PCR; 2 were not, Pt 9 because he showed no signs of infection and Pt 6 because testing was not available at his location (New York, NY, USA) at the time. Pt 6 later underwent ELISA testing, which showed IgA and IgG against the recombinant S1 domain of structural protein of SARS-CoV-2 (Euroimmun, https://www.euroimmun.com) (*2*). Excluding the index patient, in 10/11 tested participants, SARS-CoV-2 RNA was detected. In 1 participant, Pt 11, the PCR result for SARS-CoV-2 RNA was negative (Table). Thus, the index patient infected ≥11 (85%) of the 13 other participants.

All participants were isolated either in a hospital or at home with or without their families, regardless of the outcome of the first PCR test. These measures resulted in the subsequent infection of 14 additional persons (Table). Of the 12 infected participants, 2 (17%) had no symptoms, 3 (25%) experienced mild influenza-like symptoms, and 7 (58%) experienced a considerable reduction of their health, without dyspnea, classified as moderate COVID-19 (Table). None of the participants had a relevant medical history.

The index patient (Pt 1) was most likely infected by an outpatient he had examined in Milan, Italy, on February 18. The index patient reported that he had experienced no symptoms when attending the meeting. Probable transmission of SARS-CoV-2 from presymptomatic persons has been reported (*3*,*4*), with viral load levels in the nose similar to those of symptomatic patients (*5*). In contrast to severe acute respiratory syndrome coronavirus and influenza virus, the infectiousness of SARS-CoV-2 peaks on or before symptom onset (*6*).

The exact mode of transmission during the meeting remains elusive. At least 4 routes have been suggested: droplets during face-to-face contacts, aerosolized droplets (<5 μm) via air flow, fomites, and hand shaking (*4*,*7*–*9*). We identified face-to-face contacts lasting >5 min with the index patient and the 11 infected participants during 2 lunches (30 min each), 2 coffee breaks (15 min each), and the social dinner (sitting close to Pt 2, 4, 5, and 11). We also tracked Pt 1 sitting next to Pt 3 and Pt 6 during the meeting, and a 45-min taxi ride after the meeting (with Pt 2, 4, and 9) (Table). The index patient sat ≈2.60 m away from the closest participant opposite to him and had an average talk time during the meeting. Virus aerosolization in the relatively small room that was heated by conventional radiators appears to be possible in light of the duration of the meeting. Transmission via fomites appears to be less likely because few objects (bottles, coffee pots, forks) were shared by all participants during the breaks. Telephone communication with hotel management on April 20 revealed that none of the involved hotel staff were tested for SARS-CoV-2 and no staff member reported symptoms consistent with COVID-19.

Our findings indicate that hand shaking, aerosolization, and face-to-face contact may be relevant modes of transmission in this COVID-19 outbreak. Limitations include the lack of environmental samples and data about room ventilation and airflow patterns, as well as missing information about the infection status of Pt 9 and the inability to determine the actual impact of SARS-CoV-2 transmission from handshakes, droplets, and aerosolization.

Acknowledgments

We thank the company and the participating scientists for their contributions and support.

About the Author

Dr. Hijnen is a dermatologist, instructor, and researcher at Erasmus MC University Medical Center Rotterdam. His primary research interests are T-cell immunology and precision medicine in atopic dermatitis.

References

1. World Health Organization. Country & technical guidance—coronavirus disease (COVID-19) [cited 2020 May 7]. https://www.who.int/emergencies/diseases/novel-coronavirus-2019/technical-guidance
2. Okba NMA, Müller MA, Li W, Wang C, GeurtsvanKessel CH, Corman VM, et al. Severe acute respiratory syndrome coronavirus 2−specific antibody responses in coronavirus disease 2019 patients. Emerg Infect Dis. 2020 Apr 30 [Epub ahead of print].
3. Li P, Fu JB, Li KF, Chen Y, Wang HL, Liu LJ, et al. Transmission of COVID-19 in the terminal stage of incubation period: a familial cluster. Int J Infect Dis. 2020 Mar 6 [Epub ahead of print]. https://doi.org/10.1016/j.ijid.2020.03.027
4. Tong ZD, Tang A, Li KF, Li P, Wang HL, Yi JP, et al. Potential presymptomatic transmission of SARS-CoV-2, Zhejiang Province, China, 2020. Emerg Infect Dis. 2020;26:1052–4. https://doi.org/10.3201/eid2605.200198

5. Zou L, Ruan F, Huang M, Liang L, Huang H, Hong Z, et al. SARS-CoV-2 viral load in upper respiratory specimens of infected patients. N Engl J Med. 2020;382:1177–9. https://doi.org/10.1056/NEJMc2001737
6. He X, Lau EHY, Wu P, Deng X, Wang J, Hao X, et al. Temporal dynamics in viral shedding and transmissibility of COVID-19. Nat Med. 2020. https://doi.org/10.1038/s41591-020-0869-5
7. Cai J, Sun W, Huang J, Gamber M, Wu J, He G. Indirect virus transmission in cluster of COVID-19 cases, Wenzhou, China, 2020. Emerg Infect Dis. 2020 Mar 12 [Epub ahead of print]. https://doi.org/10.3201/eid2606.200412
8. Lu J, Gu J, Li K, Xu C, Su W, Lai Z, et al. COVID-19 outbreak associated with air conditioning in restaurant, Guangzhou, China, 2020. Emerg Infect Dis. 2020 Apr 2 [Epub ahead of print]. https://doi.org/10.3201/eid2607.200764
9. van Doremalen N, Bushmaker T, Morris DH, Holbrook MG, Gamble A, Williamson BN, et al. Aerosol and surface stability of SARS-CoV-2 as compared with SARS-CoV-1. N Engl J Med. 2020;382:1564–7. https://doi.org/10.1056/NEJMc2004973

Address for correspondence: DirkJan Hijnen, Erasmus MC University Medical Center Rotterdam, Department of Dermatology, Rotterdam, The Netherlands; email: d.hijnen@erasmusmc.nl

COVID-19 and Acute Pulmonary Embolism in Postpartum Patient

Zohre Khodamoradi, Shahrokh Sadeghi Boogar, Farnaz Kamali Haghighi Shirazi, Pariya Kouhi

Author affiliation: Shiraz University of Medical Sciences, Shiraz, Iran

DOI: https://doi.org/10.3201/eid2608.201383

We report a 36-year-old woman in Iran who sought care for left shoulder pain and cough 5 days after a scheduled cesarean section. Acute pulmonary embolism and coronavirus disease were diagnosed. Physicians should be aware of the potential for these concurrent conditions in postpartum women.

An outbreak of viral pneumonia that emerged in late 2019 and spread rapidly worldwide was named coronavirus disease (COVID-19) (*1*). COVID-19 is caused by severe acute respiratory syndrome coronavirus 2 (SARS-CoV-2). Two other viruses of this family, severe acute respiratory syndrome coronavirus and Middle East respiratory syndrome coronavirus, also have caused outbreaks globally (*1*).

Venous embolism has been associated with severe infection. Acute pulmonary embolism has been associated with severe acute respiratory syndrome coronavirus infections, but no cases have been reported with Middle East respiratory syndrome (*2*,*3*). A study reported a 75-year-old hospitalized woman with COVID-19 and pulmonary embolism (*4*). In addition, in 2 COVID-19–positive patients, 57 and 70 years of age, from Wuhan, China, computed tomography angiography (CTA) confirmed pulmonary embolism (*5*). Three cases of deep vein thrombosis with COVID-19 also have been reported (*6*).

Pregnancy increases the risk for venous embolism (*7*). Although approximately half of venous embolism occurs during pregnancy and half occurs during the postpartum period, the risk per day is greatest in the weeks immediately after delivery (*8*). We report a patient in Iran who sought care for cough and shoulder pain 5 days after an uncomplicated cesarean delivery in whom an acute pulmonary embolism and COVID-19 infection were subsequently diagnosed. The ethics committee of Shiraz University of Medical Sciences (Shiraz, Iran) approved the study.

A healthy 36-year-old nonsmoking woman (gravid 2, 1 term infant delivered, 1 abortion/miscarriage) underwent an elective scheduled caesarean section at 37 weeks 2 days of gestation after an uncomplicated pregnancy. The uncomplicated surgery resulted in the birth of a healthy infant. Mechanical prophylaxis to prevent deep vein thrombosis was used at delivery until ambulation. The woman was discharged on postpartum day 2 in a good condition. On postpartum day 5, she sought care for sudden onset left-side shoulder pain and dry cough. She stated that she did not have fever, myalgia, or diarrhea. On postpartum day 5, she experienced mild shortness of breath. During her pregnancy, she had no known history of contact with persons who had confirmed or suspected COVID-19.

At admission, physical examination revealed a blood pressure of 110/70 mm Hg, body temperature of 36.8°C, pulse rate of 92 beats/min, respiratory rate of 20 breaths/min, and oxygen saturation of 94% on ambient air. Her body mass index was 24.8 kg/cm^2. Her physical examination was otherwise unremarkable.

Laboratory test results showed a complete blood count and leukocyte differentials within reference ranges but elevated liver function tests, C-reactive

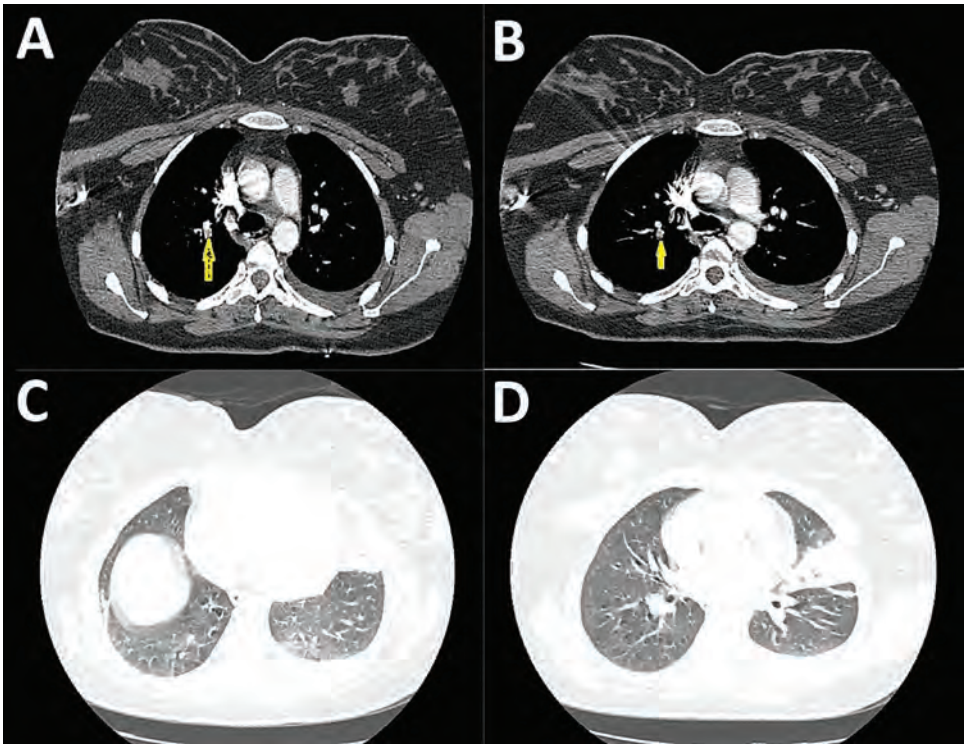

Figure. Thoracic computed tomography angiography of a 36-year-old postpartum woman with coronavirus disease and acute pulmonary embolism, Iran. A, B), Thoracic computed tomography angiography showing filling defect in the right side interlobar artery (arrow) and posterior basal segment and left-sided pleural effusion (arrow). C, D) Consolidation and ground-glass opacities affecting the left ligula and posterior recess.

protein level, and erythrocyte sedimentation rate. D-dimer was 800 μg/mL (reference <500 μg/mL). Results of her baseline electrocardiogram were unremarkable. She had a normal echocardiography with ejection fraction of ≈60%.

Because of the COVID-19 pandemic and the patient's report of cough, she underwent screening for SARS-CoV-2. Throat swab samples were positive for SARS-CoV-2 by real-time reverse transcription PCR. Moreover, because of her clinical features, history, risk for venous embolism, and high level of D-dimer, CTA was performed. Thoracic CTA on the first day of hospitalization showed emboli in the right side interlobar artery, posterior basal segment, and the lingular branch (Figure, panels A, B). Hampton hump in the right side posterior basal segment was consistent with lung infarction. CTA further revealed left-sided pleural effusion associated with new mixed consolidation and ground glass opacifications (Figure, panels C, D).

CTA findings were consistent with pneumonia, pulmonary embolism, and lung infarction. The patient was treated with enoxaparin (1 mg/kg subcutaneously 2×/d). She was discharged in good condition with enoxaparin for 6 months.

Multiple conditions made this patient susceptible to pulmonary embolism. Because inflammation and coagulation are related, infected patients have hypercoagulable state (*2*). Virchow's triad, which contributes to thrombosis, has 3 factors: venous stasis, hypercoagulability, and endothelial injury. Septic patients have criteria of Virchow's triad; cesarean section as a surgery contributed to Virchow's triad in this patienet because endothelial injury made the patient prone to embolic events (*7*–*9*).

The patient we report was young, was not critically ill or septic, and had no evidence of disseminated intravascular coagulation. Alteration in coagulation pathways during pregnancy increases the risk for embolic events. The risk in the immediate postpartum period is particularly high. Venous embolism is an important cause of maternal illness and death (*7*).

CTA or ultrasonography for deep vein thrombosis may be important for COVID-19–positive pregnant or postpartum patients who have signs or symptoms of possible venous embolism, given their potentially heightened risk. In this patient population, with an already elevated risk for venous embolism, physicians should be aware of the potential for concurrent mild COVID-19 and acute pulmonary embolism.

Acknowledgments

We thank Shiraz University of Medical Sciences and the Center for Development of Clinical Research of Nemazee Hospital and Nasrin Shokrpour for editorial assistance.

About the Author

Dr. Khodamoradi is an internal medicine resident in Shiraz University of Medical Sciences, Shiraz, Iran. Her primary research interests focus on internal medicine, gastroenterology, rheumatology, and cardiology.

References

1. Khodamoradi Z, Moghadami M, Lotfi M. Co-infection of coronavirus disease 2019 and influenza A: a report from Iran. Arch Iran Med. 2020;23:239–43. https://doi.org/10.34172/aim.2020.04
2. Tang N, Bai H, Chen X, Gong J, Li D, Sun Z. Anticoagulant treatment is associated with decreased mortality in severe coronavirus disease 2019 patients with coagulopathy. J Thromb Haemost. 2020;18:1094–9. https://doi.org/10.1111/jth.14817
3. Ng KH, Wu AK, Cheng VC, Tang BS, Chan CY, Yung CY, et al. Pulmonary artery thrombosis in a patient with severe acute respiratory syndrome. Postgrad Med J. 2005;81:e3. https://doi.org/10.1136/pgmj.2004.030049
4. Danzi GB, Loffi M, Galeazzi G, Gherbesi E. Acute pulmonary embolism and COVID-19 pneumonia: a random association? Eur Heart J. 2020 Mar 30:ehaa254; Epub ahead of print. https://doi.org/10.1093/eurheartj/ehaa254
5. Xie Y, Wang X, Yang P, Zhang S. COVID-19 complicated by acute pulmonary embolism. Radiology. Cardiothoracic Imaging. 2020;2:e200067. https://doi.org/10.1148/ryct.2020200067
6. Zhang Y, Xiao M, Zhang S, Xia P, Cao W, Jiang W, et al. Coagulopathy and antiphospholipid antibodies in patients with Covid-19. N Engl J Med. 2020;382:e38. https://doi.org/10.1056/NEJMc2007575
7. Clinton CM, Kuller JA, James AH. Prevention of postpartum venous thromboembolism. Obstet Gynecol Surv. 2019;74:601–6. https://doi.org/10.1097/OGX.0000000000000714
8. American College of Obstetricians and Gynecologists. ACOG practice bulletin no. 196: thromboembolism in pregnancy. Obstet Gynecol. 2018;132:e1–17. https://doi.org/10.1097/AOG.0000000000002706
9. Levi M, van der Poll T. Coagulation and sepsis. Thromb Res. 2017;149:38–44. https://doi.org/10.1016/j.thromres.2016.11.007

Address for correspondence: Shahrokh Sadeghi Boogar, Department of Internal Medicine, Shiraz University of Medical Sciences, Shiraz, Iran; email: sadeghi_sh@sums.ac.ir

Panton-Valentine Leukocidin–Secreting *Staphylococcus aureus* Pneumonia Complicating COVID-19

Claire Duployez, Rémi Le Guern, Claire Tinez, Anne-Laure Lejeune, Laurent Robriquet, Sophie Six, Caroline Loïez, Frédéric Wallet

Author affiliations: Centre Hospitalier Universitaire Lille, Lille, France (C. Duployez, R. Le Guern, C. Tinez, A.-L. Lejeune, L. Robriquet, S. Six, C. Loïez, F. Wallet); University of Lille (C. Duployez, R. Le Guern, A.-L. Lejeune)

DOI: https://doi.org/10.3201/eid2608.201413

Necrotizing pneumonia induced by Panton-Valentine leukocidin–secreting *Staphylococcus aureus* is a rare but life-threatening infection that has been described in patients after they had influenza. We report a fatal case of this superinfection in a young adult who had coronavirus disease.

Panton-Valentine leukocidin (PVL) is a cytotoxin produced by some strains of *Staphylococcus aureus*. These strains are responsible for primary skin infections and necrotizing pneumonia. This rare entity is mainly described in young immunocompetent patients with an influenza-like prodrome and has a high case-fatality rate (*1*,*2*). We report a case of necrotizing pneumonia induced by PVL-secreting methicillin-susceptible *S. aureus* in a patient infected with severe acute respiratory syndrome coronavirus 2 (SARS-CoV-2) and who had coronavirus disease (COVID-19).

In March 2020, during the SARS-CoV-2 outbreak in France, a man in his 30's who had no underlying conditions came to an emergency department because of fever, cough, and blood-streaked sputum that developed for 3 days. A diagnosis of pleuropneumonia was made, and antimicrobial therapy was initiated with cefotaxime plus metronidazole. Test results for *Streptococcus pneumoniae* and *Legionella pneumophila* serotype 1 urinary antigens were negative. A reverse transcription PCR specific for respiratory viruses also showed negative results.

The next day, further respiratory deterioration required transfer of the patient to an intensive care unit (ICU) for intubation, mechanical ventilation, and inotropic support. Spiramycin was added to the previous drug regimen. Chest computed tomography showed a parenchymal consolidation of the left

Figure. Chest computed tomography of a patient in France with Panton-Valentine leukocidin–secreting *Staphylococcus aureus* pneumonia complicating coronavirus disease, showing worsening of bilateral parenchymal damage with complete consolidation of the left lung, cavitary lesions suggestive of multiple abscesses, and appearance of areas of ground-glass opacities in the right lung

upper lung without ground-glass opacities commonly described for COVID-19 (*3*).

Four days after intubation, the condition of the patient had not improved. We performed a reverse transcription PCR specific for SARS-CoV-2 on an endotracheal aspirate by using the method developed by the National Reference Centre for Respiratory Viruses (Institut Pasteur, Paris, France). The PCR result was positive for SARS-CoV-2 (*4*). Chest computed tomography showed worsening of bilateral parenchymal damage with complete consolidation of the left lung, cavitary lesions suggestive of multiple abscesses, and appearance of areas of ground-glass opacities in the right lung (Figure). The chest radiograph also showed a left pleural effusion.

Bacteriological analysis of pleural drainage showed gram-positive cocci; the culture yielded monomicrobial *S. aureus*, which was identified by using matrix-assisted laser desorption/ionization time-of-flight mass spectrometry (Bruker Daltonics, https://www.bruker.com). The bacterial strain was resistant only to penicillin G (VITEK 2 System; bioMérieux, https://www.biomerieux.com). Because of this necrotizing pneumonia associated with acute respiratory distress syndrome, a PVL-producing strain was suspected. We confirmed PVL production by using a specific PCR as described by Deurenberg et al. (*5*).

We changed antimicrobial drug therapy to oxacillin plus clindamycin (for antitoxin effect) against methicillin-susceptible *S. aureus* and lopinavir/ritonavir (quickly stopped because of suspected toxicity) plus azithromycin against SARS-CoV-2. Three days later, given a lack of clinical improvement, antimicrobial therapy was changed to piperacillin/tazobactam plus linezolid (for antitoxin effect). Bronchoscopy showed that the left bronchial tree was obstructed by purulent secretions. Because of deterioration of respiratory, renal, and liver functions, venovenous extracorporeal membrane oxygenation and anticoagulation were initiated 10 days after ICU admission. Two days later, we performed upper left lobectomy, and antimicrobial drug therapy was incremented with meropenem, gentamicin, and linezolid. However, the patient died 17 days after his admission to the hospital.

PVL-secreting *S. aureus* necrotizing pneumonia is frequently preceded by an influenza-like infection (*6*), which might be a possible causative factor. Influenza virus is known to impede phagocytic killing and damage the bronchial epithelium, thus reducing secretin clearance and facilitating bacteria adhesion (*2*). It also induces an influx of immune cells to lung tissues, including neutrophils; the rapid killing of these cells by PVL and release of inflammatory mediators might promote disease development by damaging the epithelium (*7*,*8*). The association of PVL-secreting *S. aureus* and influenza virus has been reported (*6*,*9*). We report a PVL-secreting *S. aureus* superinfection in a patient who had COVID-19. Our findings indicate that the new SARS-CoV-2 is, in the same way, a facilitating factor for PVL-producing *S. aureus* necrotizing pneumonia.

In 2003, during the SARS-CoV outbreak, an increase in *S. aureus* superinfection (mostly methicillin-resistant *S. aureus* ventilator-acquired pneumonia) was described. Given common points between SARS-CoV-2 and previous coronaviruses, Lupia et al. discussed this issue for COVID-19 and suggested consideration of methicillin-resistant *S. aureus* coverage to reduce the risk of superinfection (*10*).

In PVL-producing *S. aureus* superinfection, prescribing antimicrobial drugs that have an antitoxin effect, such as clindamycin or linezolid, remains essential (*2*). Thus, in previously healthy young adults admitted to an ICU for COVID-19 and *S. aureus* superinfection, a PVL-producing strain should be assumed and treatment provided accordingly.

About the Author

Dr. Duployez is a microbiologist at Centre Hospitalier Universitaire Lille, Lille, France. Her primary research interest is medical diagnosis of bacterial diseases.

References

1. Gillet Y, Issartel B, Vanhems P, Fournet JC, Lina G, Bes M, et al. Association between *Staphylococcus aureus* strains carrying gene for Panton-Valentine leukocidin and highly lethal necrotising pneumonia in young immunocompetent patients. Lancet. 2002;359:753–9. https://doi.org/10.1016/S0140-6736(02)07877-7
2. Kreienbuehl L, Charbonney E, Eggimann P. Community-acquired necrotizing pneumonia due to methicillin-sensitive *Staphylococcus aureus* secreting Panton-Valentine leukocidin: a review of case reports. Ann Intensive Care. 2011;1:52. https://doi.org/10.1186/2110-5820-1-52
3. Kooraki S, Hosseiny M, Myers L, Gholamrezanezhad A. Coronavirus (COVID-19) outbreak: what the Department of Radiology should know. J Am Coll Radiol. 2020;17:447–51.
4. Bernard Stoecklin S, Rolland P, Silue Y, Mailles A, Campese C, Simondon A, et al.; Investigation Team. First cases of coronavirus disease 2019 (COVID-19) in France: surveillance, investigations and control measures, January 2020. Euro Surveill. 2020;25. https://doi.org/10.2807/1560-7917.ES.2020.25.6.2000094
5. Deurenberg RH, Vink C, Driessen C, Bes M, London N, Etienne J, et al. Rapid detection of Panton-Valentine leukocidin from clinical isolates of *Staphylococcus aureus* strains by real-time PCR. FEMS Microbiol Lett. 2004;240:225–8. https://doi.org/10.1016/j.femsle.2004.09.031
6. Jacquot A, Luyt CE, Kimmoun A, Levy B, Baux E; Fluvalentine Study group. Epidemiology of post-influenza bacterial pneumonia due to Panton-Valentine leucocidin positive *Staphylococcus aureus* in intensive care units: a retrospective nationwide study. Intensive Care Med. 2019;45:1312–4. https://doi.org/10.1007/s00134-019-05665-3
7. Niemann S, Ehrhardt C, Medina E, Warnking K, Tuchscherr L, Heitmann V, et al. Combined action of influenza virus and *Staphylococcus aureus* Panton-Valentine leukocidin provokes severe lung epithelium damage. J Infect Dis. 2012;206:1138–48. https://doi.org/10.1093/infdis/jis468
8. Löffler B, Niemann S, Ehrhardt C, Horn D, Lanckohr C, Lina G, et al. Pathogenesis of *Staphylococcus aureus* necrotizing pneumonia: the role of PVL and an influenza coinfection. Expert Rev Anti Infect Ther. 2013;11:1041–51. https://doi.org/10.1586/14787210.2013.827891
9. Riedweg-Moreno K, Wallet F, Blazejewski C, Goffard A. Successful management of Panton-Valentine leukocidine-positive necrotising pneumonia and A/H1N12009 influenzavirus coinfection in adult. BMJ Case Rep. 2014;2014:bcr2013201120. https://doi.org/10.1136/bcr-2013-201120
10. Lupia T, Scabini S, Mornese Pinna S, Di Perri G, De Rosa FG, Corcione S. 2019 novel coronavirus (2019-nCoV) outbreak: a new challenge. J Glob Antimicrob Resist. 2020;21:22–7. https://doi.org/10.1016/j.jgar.2020.02.021

Address for correspondence: Claire Duployez, Laboratoire de Bactériologie, Institut de Microbiologie, Centre de Biologie Pathologie, F-59037 Lille CEDEX, France; email: claire.duployez@chru-lille.fr

Pulmonary Embolism and Increased Levels of D-Dimer in Patients with Coronavirus Disease

Daniel O. Griffin, Alexandra Jensen, Mushmoom Khan, Jessica Chin, Kelly Chin, Jennifer Saad, Ryan Parnell, Christopher Awwad, Darshan Patel

Author affiliations: Columbia University Medical Center, New York, New York, USA (D.O. Griffin); Columbia University College of Physicians and Surgeons, New York (D.O. Griffin); Donald and Barbara Zucker School of Medicine at Hofstra/Northwell, Hempstead, New York, USA (A. Jensen, M. Khan, J. Chin, K. Chin, J. Saad, R. Parnell, C. Awwad, D. Patel)

DOI: https://doi.org/10.3201/eid2608.201477

We report 3 patients with coronavirus disease who had a decline in respiratory status during their hospital course that responded well to intravenous steroids and interleukin-6 receptor antagonist therapy. These patients later showed development of persistent hypoxia with increased levels of D-dimer levels and were given a diagnosis of pulmonary embolisms.

Coronavirus disease (COVID-19), caused by severe acute respiratory syndrome coronavirus 2, has been extensively reported since the outbreak in Wuhan, China, and can progress to involve major respiratory complications (*1*). Patients commonly have fever, cough, abdominal pain, and diarrhea.

During the second week of illness, decompensation occurs in some patients, possibly driven by the cytokine storm associated with increased levels of interleukin-6. We report 3 case-patients with COVID-19 who were improving after successful treatment during the critical period but showed development of pulmonary emboli (PEs) despite deep vein thrombosis (DVT) prophylaxis.

Three patients admitted to Northwell Plainview Hospital (Plainview, NY, USA) showed positive results for COVID-19 and had acute hypoxic respiratory failure secondary to COVID-19. All 3 patients received azithromycin and hydroxychloroquine, but their conditions continued to progress to more severe respiratory failure. During what was assumed to be the cytokine storm phase, on the basis of laboratory parameters and an increasing requirement for oxygen, the patients received intravenous steroids (solumedrol, 1–2 mg/kg/d for 5–8 d) and the interleukin-6 receptor antagonist tocilizumab (400 mg

Table. Characteristics of pulmonary embolism seen by CTA and increased levels of D-dimer in 3 patients with COVID-19, New York, USA*

Characteristic	Case-patient 1	Case-patient 2	Case-patient 3
Age, y	52	60	68
Risk factors	Allergic rhinitis, asthma	Chronic bronchitis, history of ovarian cancer, and history of provoked DVT	Hypertension, diabetes mellitus type 2
Smoking status	Former	Never	Never
BMI, kg/m^2	27.0	27.4	23.7
Creatinine clearance, mL/min	116	127.4	64
Day of symptoms, baseline/CTA	12/18	8/18	14/22
O_2 saturation, baseline/CTA	52% on RA/98% on NRB	92% on NC/91% on NC	94% on NRB/93% on NRB
D-dimer, μg/mL, baseline/CTA	2,283/9,698	221/2,563	33,318/1,554
Ferritin, μg/L, baseline/CTA	2,283/1,050	1,276/1,176	2,797/1,282
CRP, mg/L, baseline/CTA	32.30/0.42	11.89/0.66	8.88/0.25
Procalcitonin, ng/mL, baseline/CTA	0.19/0.05	0.05/0.13	0.23/NA
LDH, U/L, baseline/CTA	567/467	448/637	824/616
Neutrophil:lymphocyte ratio, baseline/CTA	10.58/11.75	6.6/7.5	7.67/14.99
ISTH score, day of CTA	≥5	≥5	≥5
VTE prevention	Enoxaparin, 40 mg 2×/d	Enoxaparin, 40 mg 2×/d	Enoxaparin, 40 mg/d
IMPROV score	0	3	1
Doses of tocilizumab	1	1	1
Methylprednisolone duration, d	8	5	5
Hydroxychloroquine duration, d	5	5	5
CTA read	Bilateral PE; filling defects most pronounced in the right lobar pulmonary artery extending to the first-order branches of the right lower lobe pulmonary artery; additional small filling defect identified within the right upper lobe, right middle lobe, and lingular pulmonary artery branches; diffuse scattered bilateral ground-glass opacities with areas of consolidation compatible with reported viral pneumonia COVID-19	Multiple bilateral segmental and subsegmental PE with suggestion of cardiac strain; bilateral scattered, predominantly peripheral ground-glass opacities with some interlobular septal thickening consistent with given history of COVID-19 pneumonia	Central filling defects compatible with acute pulmonary embolism in several segmental and subsegmental pulmonary arteries in the right upper lobe, right lower lobe, and left lower lobe; diffuse bilateral ground-glass opacities unchanged from previous imaging

*BMI, body mass index; COVID-19, coronavirus disease; CRP, C-reactive protein; CTA, computed tomography angiogram; DVT, deep vein thrombosis; IMPROV, International Medical Prevention on Venous Thrombosis; ISTH, International Society of Thrombosis and Haemostasis; LDH, lactate dehydrogenase; NA, not available; NC, nasal cannula; NRB, nonrebreather; PE, pulmonary embolus; RA, room air; RLL, right lower lobe; VTE, venous thromboembolism.

intravenously). Patients showed improvement and did not require intubation but later showed development of persistent hypoxemia with increases in levels of D-dimer. Computed tomography angiograms (CTAs) confirmed bilateral PEs, and the patients required supplemental oxygen (Table).

Case-patient 1, a 52-year-old male former smoker with a history of asthma, came to our hospital 12 days after symptom onset. At admission, he reported chest tightness, difficulty breathing, and was afebrile. His respiratory rate was 34 breaths/min, heart rate 87 beats/min, and blood pressure 117/67 mm Hg. The D-dimer level was 2,283 μg/mL at admission and increased to 9,698 μg/mL on hospital day 6. He had been receiving enoxaparin (40 mg/d subcutaneously) as venous thromboembolism (VT) prophylaxis. He had worsening hypotension, dyspnea on exertion, chest discomfort, and shortness of breath. CTA performed on symptom day 18 showed bilateral PEs. The patient was given enoxaparin (1 mg/kg subcutaneously 2×/d), transitioned to rivaroxaban, and discharged receiving supplemental oxygen.

Case-patient 2, a 60-year-old female nonsmoker with a history of chronic bronchitis, ovarian cancer postoophorectomy, and provoked DVT 18 years earlier, was admitted on day 8 of symptoms. At admission, she reported worsening cough, nausea, and loss of sense of smell. She was afebrile; her respiratory rate was 20 breaths/min, heart rate 106 beats/min, and blood pressure 145/68 mm Hg. The D-dimer level was 221 μg/mL at admission and 2,563 μg/mL on hospital day 10. She was given DVT prophylaxis (enoxaparin, 40 mg/d subcutaneously, increased to 2×/d on day 10 of illness). On day 18 of symptoms, she was persistently hypotoxic and had tachycardia

and hypotension. CTA showed multiple bilateral segmental and subsegmental PEs with suggestion of cardiac strain. The patient was given rivaroxaban and discharged receiving supplemental oxygen.

Case-patient 3, a 68-year-old male nonsmoker with a history of hypertension, and type 2 diabetes mellitus, was admitted on day 14 of symptoms. At admission, he reported cough, difficulty breathing, and progressive weakness. He was afebrile; his respiratory rate was 22 breaths/min, heart rate 107 beats/min, and blood pressure 144/92 mm/Hg, and he showed hypotoxicity. The D-dimer level was 33,318 μg/mL at admission and 1,554 μg/mL on hospital day-7. He was given DVT prophylaxis (enoxaparin, 40 mg/d subcutaneously). On day 22 of symptoms, he showed development of hypotension, and his oxygen saturation was <90% with a 100% nonrebreather mask. This finding prompted a CTA, which showed bilateral PEs on hospital day 3. The patient was given enoxaparin (1 mg/kg subcutaneously 2×/d) and showed improvement.

PEs can occur after the cytokine storm in COVID-19 patients, despite DVT prophylaxis. After initial improvements, patients might continue to have high or increasing oxygen requirements because of development of thromboembolic disease. Previous studies showed that low levels of platelets, increased levels of D-dimer, and increasing levels of prothrombin in COVID-19 were associated with poor outcome, which might be explained by thromboembolic complications in patients with severe disease (*2*). Platelet counts remained within reference ranges for 2 of our patients and only decreased for 1 patient. Two patients had increases in D-dimer levels, and the third patient was admitted with a highly increased D-dimer level.

Autopsy reports from COVID-19 patients have shown microthrombi in lungs and in other organs with associated foci of hemorrhage (*3*,*4*). These findings suggest that severe endothelial dysfunction, driven by the cytokine storm and associated hypoxemia, leads to disseminated intravascular coagulation, causing thromboembolic complications. In these patients, other parameters, such as the neutrophil–lymphocyte ratio, and inflammatory markers, including ferritin, C-reactive protein, and lactate dehydrogenase, were returning to reference levels despite increased D-dimer levels and increasing oxygen requirements. Standard dose DVT prophylaxis did not prevent this complication. This hypercoagulability was a consumptive coagulopathy and was not caused by an inhibitor, such as an anticardiolipin antibody; treatment with direct factor Xa inhibitors would be appropriate.

Although certain underlying conditions might have influenced the coagulation process in these patients, the hypothesis that hypercoagulability is driven by endothelial dysfunction is plausible. These case studies support the earlier observation that anticoagulation is associated with a decrease in mortality rates for COVID-19 patients (*5*). Monitoring disseminated intravascular coagulation and measurement of platelet counts, D-dimer and fibrinogen levels, and trending International Society of Thrombosis and Haemostasis scores might be beneficial for early diagnosis of PE in patients with COVID-19.

About the Author

Dr. Griffin is an instructor in clinical medicine and associate research scientist at Columbia University Medical Center, New York, NY. His primary research interests are HIV, stem cells, and malignancies.

References

1. Guan WJ, Ni ZY, Hu Y, Liang WH, Ou CQ, He JX, et al.; China Medical Treatment Expert Group for Covid-19. Clinical characteristics of coronavirus disease 2019 in China. N Engl J Med. 2020;NEJMoa2002032. https://doi.org/10.1056/NEJMoa2002032
2. Zhou F, Yu T, Du R, Fan G, Liu Y, Liu Z, et al. Clinical course and risk factors for mortality of adult inpatients with COVID-19 in Wuhan, China: a retrospective cohort study. Lancet. 2020;395:1054–62. https://doi.org/10.1016/S0140-6736(20)30566-3
3. Danzi GB, Loffi M, Galeazzi G, Gherbesi E. Acute pulmonary embolism and COVID-19 pneumonia: a random association? Eur Heart J. 2020;pii:ehaa254. https://doi.org/10.1093/eurheartj/ehaa254
4. Zuckier LS, Moadel RM, Haramati LB, Freeman L. Diagnostic evaluation of pulmonary embolism during the COVID-19 pandemic. J Nucl Med. 2020;pii:jnumed.120.245571. https://doi.org/10.2967/jnumed.120.245571
5. Tang N, Bai H, Chen X, Gong J, Li D, Sun Z. Anticoagulant treatment is associated with decreased mortality in severe coronavirus disease 2019 patients with coagulopathy. J Thromb Haemost. 2020Mar 27:10.1111/jth.14817.

Address for correspondence: Daniel O. Griffin, Division of Infectious Diseases, Department of Medicine, Columbia University Medical Center, 701 W 168th St, HHSC 1310, New York, NY 10032-3784, USA; email: dg2810@cumc.columbia.edu

Delayed Laboratory Response to COVID-19 Caused by Molecular Diagnostic Contamination

Ramona Mögling,[1] Adam Meijer,[1] Natasa Berginc, Sylvia Bruisten, Remi Charrel, Bruno Coutard, Isabella Eckerle, Vincent Enouf, Olav Hungnes, Gülay Korukluoglu, Thanos Kossyvakis, Andreas Mentis, Richard Molenkamp, Shaman Muradrasoli, Anna Papa, Fiona Pigny, Laurence Thirion, Sylvie van der Werf, Chantal Reusken

Author affiliations: National Institute for Public Health and the Environment, Bilthoven, the Netherlands (R. Mögling, A. Meijer, C. Reusken); Laboratory for Public Health Virology, Ljubljana, Slovenia (N. Berginc); Public Health Service of Amsterdam, Amsterdam, the Netherlands (S. Bruisten); Aix Marseille Université, Marseille, France (R. Charrel, B. Coutard, L. Thirion); University Hospital Geneva, Geneva, Switzerland (I. Eckerle, F. Pigny); Institut Pasteur, Paris, France (V. Enouf, S. van der Werf); Norwegian Institute of Public Health, Oslo, Norway (O. Hungnes); Public Health General Directorate of Turkey, Ankara, Turkey (G. Korukluoglu); Hellenic Pasteur Institute, Athens, Greece (T. Kossyvakis, A. Mentis); Erasmus Medical Center, Rotterdam, the Netherlands (R. Molenkamp, C. Reusken); Public Health Agency of Sweden, Slona, Sweden (S. Muradrasoli); Aristotle University of Thessaloniki, Thessaloniki, Greece (A. Papa)

DOI: https://doi.org/10.3201/eid2608.201843

The emergence of severe acute respiratory syndrome coronavirus 2 (SARS-CoV-2) created an exceptional situation in which numerous laboratories in Europe simultaneously implemented SARS-CoV-2 diagnostics. These laboratories reported in February 2020 that commercial primer and probe batches for SARS-CoV-2 detection were contaminated with synthetic control material, causing delays of regional testing roll-out in various countries.

Timely and reliable laboratory diagnosis is crucial for clinical care and to inform public health responses in the ongoing severe acute respiratory syndrome coronavirus 2 (SARS-CoV-2) pandemic (*1*). The laboratory response in Europe to emergence of SARS-CoV-2 appeared rapid at the country level; 38 laboratories in 24 European Union/European Economic Area countries had molecular testing already available by January 29, 2020, and an expected complete coverage of all European Union/European Economic Area countries by mid-February (*1*).

The first protocol for molecular detection, with a focus on envelope (E) and RNA-dependent RNA polymerase gene targets, was available on January 13, 2020 (*2*,*3*), and shared rapidly. Toward the end of January 2020, reports from laboratories in Europe indicated that commercial, custom-made primer and probe batches for SARS-CoV-2 detection might be contaminated with synthetic control material for the E gene target. This observation was disclosed within the expert laboratory network for Emerging Viral Diseases–LabNet (*4*) on February 5, 2020, and resulted in an alert and advice to perform a second target confirmation by the European Centre for Disease Prevention and Control (ECDC) on its website (*5*). A call for more detailed information was send out to assess the extent of the situation.

Ten laboratories from 8 countries in Europe reported PCR template contamination in commercially ordered primer and probe batches, which led to SARS-CoV-2 reverse transcription PCR (RT-PCR) signals in their no-template controls, and provided detailed information. Five additional laboratories (including addition of a ninth affected country) indicated that they received contaminated material but did not provide details.

Materials were ordered during January 13–February 28 from 8 companies offering custom nucleic acid synthesis. Delivery of contaminated oligonucleotides was reported during January 22–February 28 for 6 companies, including those that initially delivered contamination-free oligonucleotides until January 21 (Figure). The contamination issues concerned primer and probe batches for the E and the RNA-dependent RNA polymerase gene targets, as well as batches for nonrelated targets received on the same day. Others reported sporadic contamination. The extent of contamination varied strongly; reported cycle threshold values ranged from 23 to 39. The laboratories systematically excluded other, own laboratory-related, potential sources of contamination. None of the 10 laboratories ordered long synthetic DNA polymers.

Six laboratories indicated a delayed implementation of SARS-CoV-2 diagnostics. Three were central laboratories responsible for roll-out of diagnostic capability to regional and hospital laboratories within their country, which was therefore delayed by 7–14 days. Three laboratories indicated a delay in molecular test implementation of 2–7 days in their own facilities (Figure, panel C). One laboratory described a delay in final negative result reporting for 1 suspected

[1]These authors contributed equally to this article.

patient during a tense period in which the country did not have any cases.

The companies involved were informed. Some offered new batches free of charge, started to screen their products postproduction, or stopped production of long oligonucleotides. Others did not respond or denied that a problem existed. One company decontaminated its production facility.

The emergence of SARS-CoV-2 created an exceptional situation that demanded a rapid implementation of RT-PCRs. We hypothesize that the combined simultaneous and huge demand across Europe for primers, probes, and controls, related to the protocol of Corman et al. (*2*), might have led to production of primers and probes contaminated with synthetic controls. Initial limited access to positive controls (*1*) might have led to orders of long synthetic DNA polymers spanning SARS-CoV-2 RT-PCR target genes. In combination with extensive and simultaneous ordering of associated primers and probes, this ordering resulted in synthesis on the same production line within a short time span or in close proximity within some companies.

Companies that produce custom synthetic nucleotides need to be aware of these potential problems that might only appear in extreme situations, such as the massive laboratory response to SARS-CoV-2 at the end of January/beginning of February 2020 in Europe that was uniform and based on few available protocols (*2*). In normal circumstances, the common practice of synthesis of primers, probes, and long nucleic acids would not necessarily pose a major problem because different nucleic acids are randomly ordered and produced. However, in an emergency response scenario as described here, this common practice had consequences for an efficient laboratory and public health response.

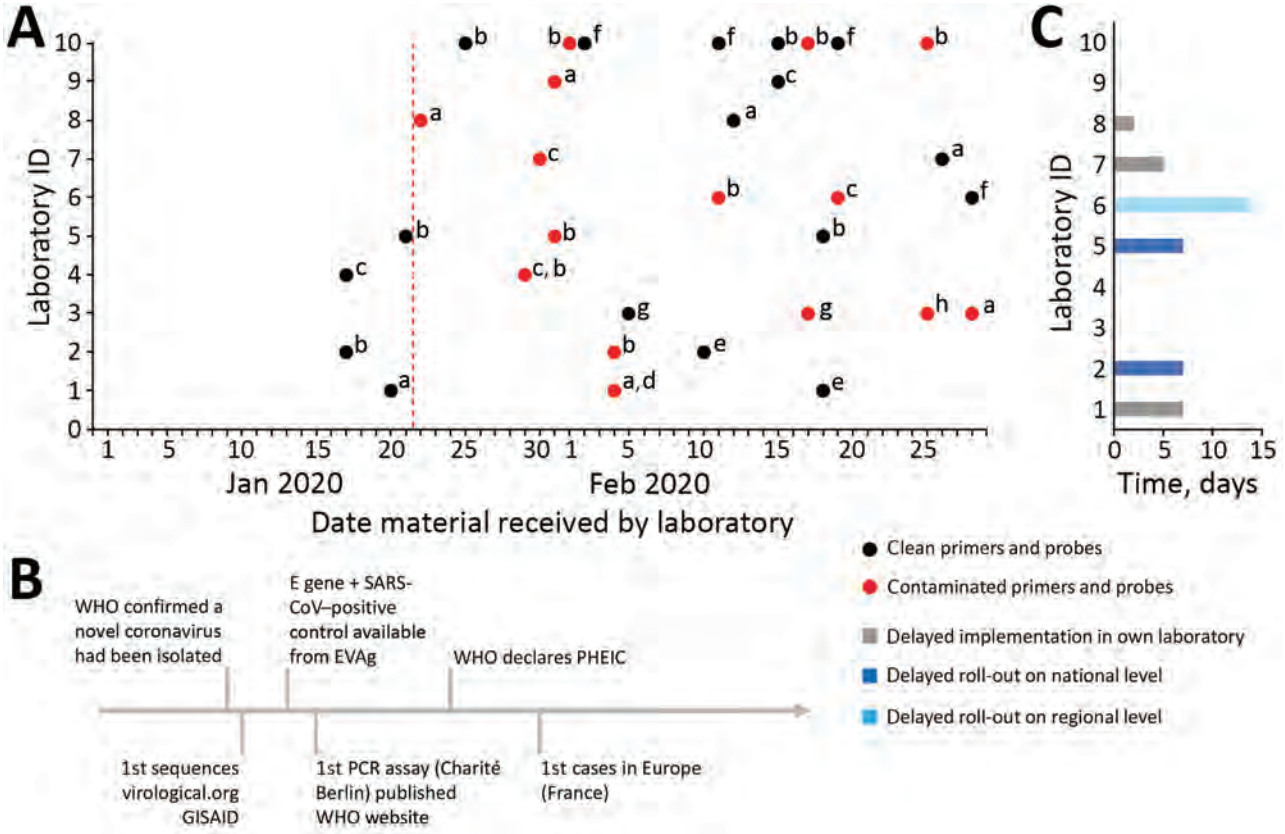

Figure. Timeline and extent of product and molecular diagnostic contamination issues in 10 laboratories in Europe during delayed laboratory response to COVID-19. A) Contamination status of commercially ordered primers and probes for molecular detection of SARS-CoV-2 based on Corman et al. (*2*). Red vertical dotted line indicates starting date of laboratories in Europe receiving contaminated commercial primers and probes. The letters a–h are unique identifiers for the 8 companies that produced the materials. B) Timeline of simultaneous hallmark events in the SARS-CoV-2 outbreak. C) Delay of implementation of SARS-CoV-2 diagnostic test in laboratories and delay of national or regional roll-out schemes per laboratory. Laboratories that indicated no delay had access to noncontaminated material from previous orders or cooperated with another laboratory. COVID-19, coronavirus disease; E, envelope; EVAg, European Virus Archive Global; GISAID, Global Initiative on Sharing All Influenza Data (http://gisaid.org); ID, identification; PHEIC, public health emergency of international concern; SARS-CoV, severe acute respiratory syndrome coronavirus; SARS-CoV-2, severe acute respiratory syndrome coronavirus 2; WHO, World Health Organization.

Comparison of ordered nucleic acids against sequence databases might inform the synthesis set-up at companies. This comparison could be combined with the already existing protocol for nucleic acid–synthesizing companies regarding synthesis of high-risk pathogens (*6*). Other measures might include separate production facilities for long and short nucleic acids. The necessity for this change was highlighted by a 16th laboratory that failed to order their primers and probes through explicit routing of a company to avoid contamination with popular PCR targets. E gene–contaminated primers and probes were received at the end of March 2020.

This report provides a warning to manufacturers of oligonucleotides and diagnostic laboratories alike to remain vigilant for contamination issues in popular RT-PCR reagents. Vigilance will help avoid delays in crucial laboratory responses now and in future outbreak events.

Acknowledgments

We thank Lisa Wijsman, Sharon van den Brink, Gabriel Goderski, and Bas van der Veer for providing technical assistance in the laboratory.

Emerging Viral Diseases–LabNet is supported by ECDC under Emerging Viral Diseases–LabNet Framework contract ECDC/2016/002. The European Virus Archive Global project is an H2020-INFRAIA-2019 program, project no. 871029 and is also supported by the Institut National de la Santé et de la Recherche Médicale through the Reacting (REsearch and ACTion Targeting emerging infectious diseases) initiative.

About the Author

Dr. Mögling is a research associate at the National Institute for Public Health and the Environment, Bilthoven, the Netherlands. Her primary research interests include (re) emerging viral infections and (inter)national laboratory preparedness and response activities.

References

1. Reusken CB, Broberg EK, Haagmans B, Meijer A, Corman VM, Papa A, et al.; On Behalf Of Evd-LabNet And Erli-Net. Laboratory readiness and response for novel coronavirus (2019-nCoV) in expert laboratories in 30 EU/EEA countries, January 2020. Euro Surveill. 2020;25. https://doi.org/10.2807/1560-7917.ES.2020.25.6.2000082
2. Corman VM, Landt O, Kaiser M, Molenkamp R, Meijer A, Chu DK, et al. Detection of 2019 novel coronavirus (2019-nCoV) by real-time RT-PCR. Euro Surveill. 2020;25. https://doi.org/10.2807/1560-7917.ES.2020.25.3.2000045
3. World Health Organization. Novel coronavirus. (2019-nCoV) technical guidance: laboratory guidance, 2020 [cited 2020 Mar 3]. https://www.who.int/emergencies/diseases/novel-coronavirus-2019/technical-guidance/laboratory-guidance
4. EVD-LabNet. EVD-LabNet, 2020 [cited 2020 Mar 5]. https://www.evd-labnet.eu/
5. European Centre for Disease Prevention and Control. Questions and answers regarding laboratory topics on SARS-CoV-2, 2020 [cited 2020 May 4]. https://www.ecdc.europa.eu/en/all-topics-z/coronavirus/threats-and-outbreaks/covid-19/laboratory-support/questions
6. International Gene Synthesis Consortium, 2020 [cited 2020 Mar 29]. https://genesynthesisconsortium.org

Address for correspondence: Chantal Reusken, National Institute for Public Health and the Environment, A. van Leeuwenhoeklaan 9, 3721 MA Bilthoven, the Netherlands; email: chantal.reusken@rivm.nl

Dengue Virus Type 1 Infection in Traveler Returning from Benin to France, 2019

Toscane Fourié,[1] Léa Luciani,[1] Sophie Amrane, Christine Zandotti, Isabelle Leparc-Goffart, Laetitia Ninove, Antoine Nougairède

Author affiliations: Aix Marseille Université, Marseille, France (T. Fourié, L. Luciani, S. Amrane, C. Zandotti, I. Leparc-Goffart, L. Ninove, A. Nougairède); French Armed Forces Biomedical Research Institute, Marseille (T. Fourié, I. Leparc-Goffart)

DOI: https://doi.org/10.3201/eid2608.200055

We investigated a case of dengue virus type 1 infection acquired in Benin. Phylogenetic analysis revealed the strain belongs to genotype V but clusters with Asian, rather than with known African, strains. Our finding suggests the introduction of Asian dengue virus in West Africa.

Dengue fever, a major public health concern throughout tropical and subtropical regions of the world, is a mosquitoborne disease caused by 4 distinct dengue virus (DENV) serotypes that share antigenic relationships (DENV-1–4).

[1]These authors contributed equally to this article.

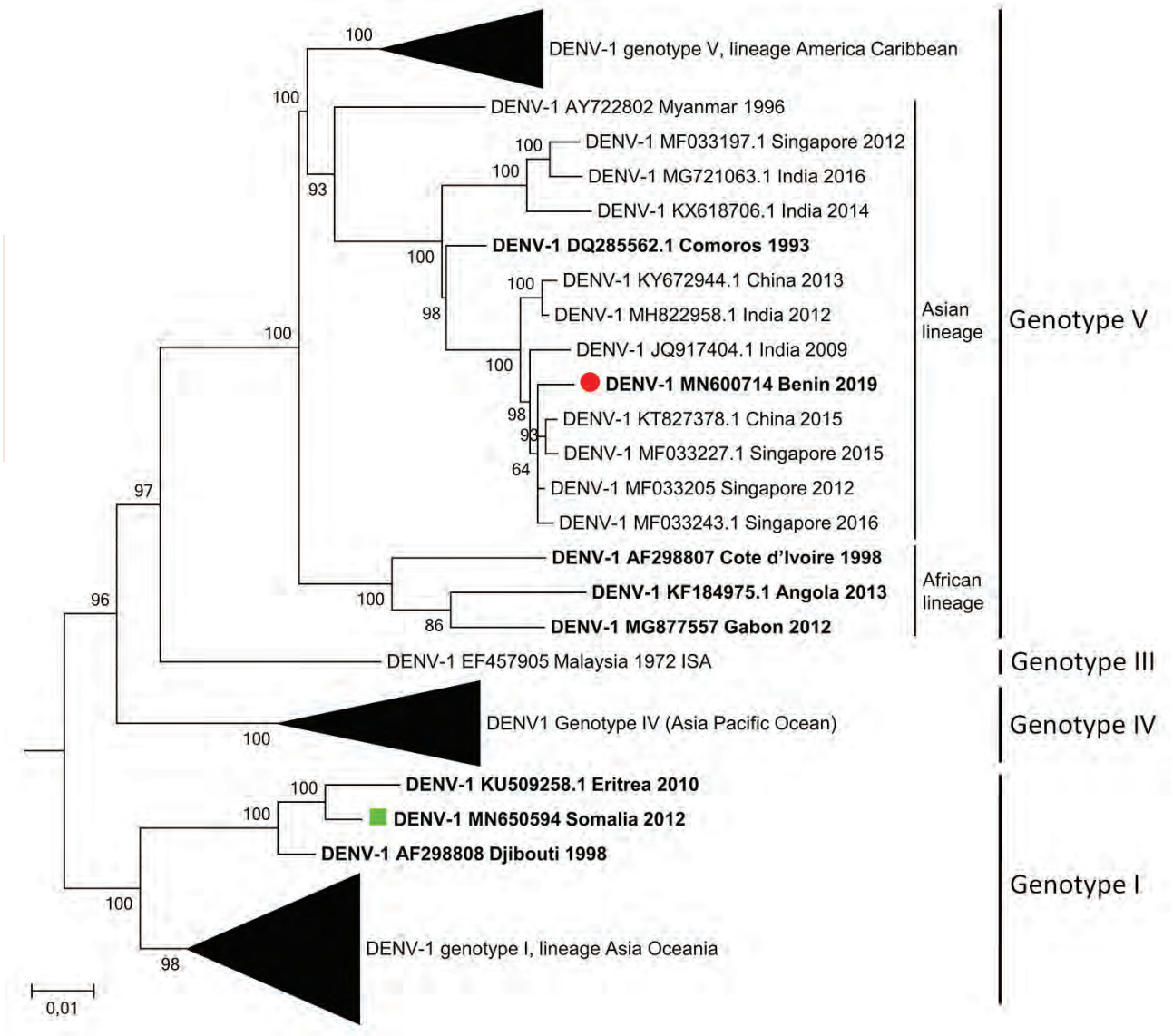

Figure. Maximum-likelihood phylogenetic tree of DENV-1 detected in a traveler who returned from Benin to France (red circle) along with other strains from Africa (bold), strain provided by the French National Reference Centre for Arbovirus (green square), and reference strains. The general time-reversible model (discrete γ distribution with evolutionarily Invariant sites) was used to construct the tree with 130 full-genome sequences. Bootstrap support values (percentage of 500 replicates) are shown at nodes. The tree was rooted with reference strains of DENV-2, DENV-3, and DENV-4 (not shown). Scale bar indicates nucleotide substitutions per site. DENV, dengue virus.

Although DENV is endemic to most countries in Africa, laboratory-confirmed dengue remains rare. Active transmission of DENV on the African continent lacks consistent molecular detection and characterization. In Benin, West Africa, probable cases of dengue fever have been described as far back as 1987 (*1*). In 2010, the first confirmed cases of dengue fever acquired in Benin were reported (*2*), and DENV-3 was identified (*3*). Since 2010, only a few cases have been reported in Benin (*4*). We investigated confirmed DENV-1 infection acquired in Benin in a traveler returning to France.

In February 2019, acute fever associated with intermittent headaches developed in a 16-year-old girl after she returned to her home in Marseille from a 10-day stay in urban Benin. She sought medical care 2 days after symptom onset and was hospitalized for suspected malaria at the public hospital of Marseille. She did not take antimalarial prophylaxis and did not experience symptoms during her stay in Benin. Physical examination revealed rash on her face, torso, and limbs.

At admission, laboratory results indicated a mild increase of aspartate transaminase (74 IU/L

[reference <25 IU/L]), a moderate increase in C-reactive protein (25 mg/L [reference <5 mg/L]), and hypokalemia (potassium 3.07 mmol/L [reference 3.5–4.5 mmol/L]). The rapid diagnostic test result for malaria was negative. We detected DENV nonstructural protein 1 antigen (SD Bioline Dengue Duo Combo kit; Alere [Abbott], https://www.alere.com) and DENV RNA (*5*) in the patient's serum collected at admission. Serotype-specific real-time reverse transcription PCR (*5*) identified DENV-1. DENV serology (ELISA; Euroimmun, https://www.euroimmun.com) showed absence of IgM and presence of IgG against DENV, suggesting the patient had been previously infected by other DENVs or serologically close flaviviruses. After 48 hours of hospitalization and symptomatic treatment (acetaminophen 2 g/d), the patient recovered without complications and was discharged. She and her mother (legal guardian) provided written consent to publish her clinical and biological data collected by the Assistance Publique Hôpitaux de Marseille during her stay.

We isolated DENV from a positive sample on C6/36 (American Type Culture Collection CRL-1660) cells. We obtained the complete viral genome sequence of this DENV-1 strain, named 2019/BJ/9943 (deposited in GenBank under accession no. MN600714), from cell culture supernatant using next-generation sequencing as previously described (*6*).

Phylogenetic analysis showed that the 2019/BJ/9943 strain belongs to DENV-1 genotype V (Figure). Within genotype V, American-Caribbean, Asian, and African clades are strongly associated with DENV strains detected in these specific geographic regions, suggesting a local dispersion of those viruses. The African clade of DENV-1 genotype V comprises only 3 full-genome sequences, all of which come from West Africa. Surprisingly, the 2019/BJ/9943 strain belongs to the Asian clade. The Asian clade already contains another strain from Africa isolated from the Comoros (an archipelago located between Madagascar and Mozambique) in 1993. Furthermore, a recent phylogenetic study in Nigeria based on envelop protein coding sequences suggests that certain DENV-1 genotype I strains from Nigeria cluster with strains from Cambodia (*7*). However, such partial sequences do not provide enough single-nucleotide polymorphisms for subgenotyping. In our study, full-genome phylogenetic analysis provides solid evidence that 2019/BJ/9943 strain is related to Asian strains.

Altogether, these data suggest repeated introductions of DENV-1 strains from Asia to Africa. Considering the lack of molecular data on DENV-1 strains from West Africa, it is difficult to estimate when the 2019/BJ/9943 strain was introduced to the continent from Asia. However, after the 2008 financial crisis, an increased number of migrant workers from China arrived in West Africa because of a rapid development of economic exchange and a gold rush in Ghana in 2013 (*8*). Additional molecular data from West Africa are needed to determine the effect of these population flows on the circulation of DENV between Asia and West Africa and to further clarify the epidemiology for this virus of serious public health concern.

Acknowledgments

We thank Geraldine Piorkowski and Karine Barthelemy for their help during sequencing experiments. We thank Camille Placidi for her technical contribution.

This work was supported by the European Virus Archive Goes Global Project (European Union—Horizon 2020 program under grant agreement no. 653316; http://www.european-virus-archive.com) and the French Armed Forces Biomedical Research Institute.

About the Author

Ms. Fourié is a PhD student at the Unité des Virus Emergents, Aix Marseille Université, Marseille, France. Her primary research interests include diagnostics of emerging viral infections. Dr. Luciani is a pharmacist medical biologist working at Assistance Publique Hôpitaux de Marseille and a PhD student at the Unité des Virus Emergents, Aix Marseille Université, Marseille, France. Her primary research interests include diagnostics of emerging viral infections.

References

1. Eisenhut M, Schwarz TF, Hegenscheid B. Seroprevalence of dengue, chikungunya and Sindbis virus infections in German aid workers. Infection. 1999;27:82–5. https://doi.org/10.1007/BF02560502
2. Gautret P, Botelho-Nevers E, Charrel RN, Parola P. Dengue virus infections in travellers returning from Benin to France, July–August 2010. Euro Surveill. 2010;15:19657.
3. Ujiie M, Moi ML, Kobayashi T, Takeshita N, Kato Y, Takasaki T, et al. Dengue virus type-3 infection in a traveler returning from Benin to Japan. J Travel Med. 2012;19:255–7. https://doi.org/10.1111/j.1708-8305.2012.00617.x
4. Loconsole D, Metallo A, De Robertis AL, Morea A, Quarto M, Chironna M. Seroprevalence of dengue virus, West Nile virus, chikungunya virus, and Zika virus in international travelers attending a travel and migration center in 2015–2017, southern Italy. Vector Borne Zoonotic Dis. 2018;18:331–4. https://doi.org/10.1089/vbz.2017.2260
5. Leparc-Goffart I, Baragatti M, Temmam S, Tuiskunen A, Moureau G, Charrel R, et al. Development and validation of real-time one-step reverse transcription-PCR for the

detection and typing of dengue viruses. J Clin Virol. 2009;45:61–6. https://doi.org/10.1016/j.jcv.2009.02.010
6. Baronti C, Piorkowski G, Leparc-Goffart I, de Lamballerie X, Dubot-Pérès A. Rapid next-generation sequencing of dengue, EV-A71 and RSV-A viruses. J Virol Methods. 2015;226:7–14. https://doi.org/10.1016/j.jviromet.2015.09.004
7. Ayolabi CI, Olusola BA, Ibemgbo SA, Okonkwo GO. Detection of dengue viruses among febrile patients in Lagos, Nigeria and phylogenetics of circulating dengue serotypes in Africa. Infect Genet Evol. 2019;75:103947. https://doi.org/10.1016/j.meegid.2019.103947
8. Wang Y, Wang X, Liu X, Ren R, Zhou L, Li C, et al. Epidemiology of imported infectious diseases, China, 2005–2016. Emerg Infect Dis. 2018;25:33–41. https://doi.org/10.3201/eid2501.180178

Address for correspondence: Antoine Nougairède, Faculté de médecine, 27 Bd Jean Moulin, 13005 Marseille, France; email: antoine.nougairede@univ-amu.fr

Outbreak of Human Metapneumovirus Infection in Zoo, Slovenia

Tina Uršič, Nika Lalek, Pavel Kvapil, Marjan Kastelic, Vasilij Cociancich, Irena G. Košnik, Miroslav Petrovec

Author affiliations: University of Ljubljana, Ljubljana, Slovenia (T. Uršič, V. Cociancich, M. Petrovec); Golnik University Clinic of Pulmonary and Allergic Diseases, Golnik, Slovenia (N. Lalek); Ljubljana Zoo, Ljubljana (P. Kvapil, M. Kastelic); National Institute of Public Health, National Laboratory of Health, Environment, and Food, Maribor, Slovenia (I.G. Košnik)

DOI: https://doi.org/10.3201/eid2608.200125

We report a case of human metapneumovirus infection that spread from humans to chimpanzees and back to humans. Bronchopneumonia developed in 4 of 6 members of a chimpanzee family, and 2 subsequently died. The chimpanzees' keeper also became ill. Sequencing showed 100% identity between virus sequences from chimpanzees and the keeper.

Apes are the closest nonhuman primate relative of humans and are therefore susceptible to many human pathogens. Chimpanzees have been kept at the Ljubljana Zoo in Slovenia since 1974. The zoo had never experienced a severe or fatal case of viral respiratory infection among the chimpanzee family, which consisted of 6 members (10, 11, 13, 15, 25, and 38 years of age). We report an outbreak of human metapneumovirus (hMPV) infection in chimpanzees and a zookeeper at this zoo.

This study was performed in accordance with the Helsinki Declaration. Written consent was obtained from the human patient and archived.

On June 19, 2013, four of the youngest chimpanzees at the zoo started showing signs of a cold (snorting, sneezing, and coughing). Veterinarians suspected a viral infection, but because of the possibility of secondary bacterial infection, the chimpanzees were given amoxicillin and clavulanic acid. The next day, clinical signs of pneumonia (apathy, dyspnea, and loss of appetite) appeared. The youngest chimpanzee died of respiratory failure on June 22; necropsy showed acute bronchopneumonia.

We tested animals for influenza A and B viruses, respiratory syncytial virus, hMPV, human coronaviruses (NL63, OC43, HKU1, and 229E), human bocavirus 1, human rhinoviruses, adenoviruses, and enteroviruses by using real-time reverse transcription PCR. Only hMPV was detected in nasal and throat swab specimens and lung tissue (*1*). The same day, the health of the other chimpanzees deteriorated.

The second-youngest chimpanzee that had signs of acute respiratory distress was sedated, ventilated, and given Ringer solution, bronchodilators, and intravenous antimicrobial drugs. However, it died on June 24 because of bronchopneumonia and pleural effusion, which was confirmed by necropsy.

In nasal and throat swab specimens and lung tissue, only hMPV and *Klebsiella pneumoniae* were detected. Histopathologic examination of hematoxylin and eosin–stained lung tissue samples of both chimpanzees that died showed severe bronchointerstitial pneumonia, including necrosis and sloughing of bronchial and bronchiolar epithelium; alveolar spaces filled with an exudate composed of foamy macrophages, neutrophils, and fibrin; and multifocal intraalveolar hemorrhage. In the second chimpanzee, we observed multifocal manifestations of bacilli-like bacteria. For the remaining 2 ill chimpanzees, clinical signs gradually disappeared in 6 days.

The keeper of the chimpanzees was a 31-year-old man, a nonsmoker who had a history of persistent allergic rhinoconjunctivitis and childhood asthma. He reported signs of a cold on June 21. His health deteriorated over the next 2 days; he had fever, sore

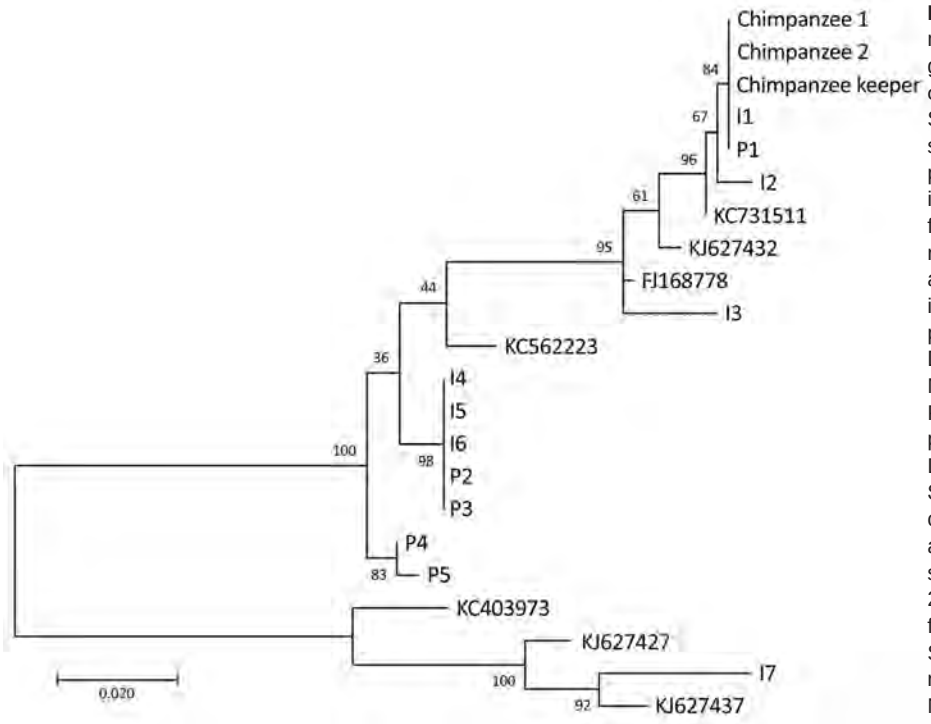

Figure. Phylogenetic tree of human metapneumovirus fusion protein gene fragments (518 bp) from chimpanzees and a keeper in a zoo, Slovenia, compared with randomly selected sequences from other patients with human metapneumovirus infections. Fusion protein gene fragments were inferred by using the maximum-likelihood method under a Tamura–Nei substitution model. I indicates sequences obtained from patients hospitalized at the Infectious Disease Department, University Medical Centre, Ljubljana, Slovenia; P indicates sequences obtained from patients hospitalized at the Pediatric Department at the same centre. Sequences I1–I7 are from samples collected during June 3–28, 2013, and sequences P1–P5 are from samples collected during June 4–July 2, 2013. All sequences were obtained from patients in the central region of Slovenia. Sequences with accession numbers were selected from GenBank. Numbers along branches are bootstrap values. Scale bar indicates nucleotide substitutions per site.

throat, chills, muscle and joint pain, headache, and a dry cough. He visited the emergency department of Golnik University Clinic of Pulmonology and Allergic Diseases on June 23.

A nasopharyngeal swab specimen showed only hMPV by PCR. A throat swab specimen was negative for pathogenic bacteria. On July 1, the patient was hospitalized because of chest tightness and wheezing. Examination detected inspiratory and expiratory wheezing with crepitations. High-resolution computed tomography showed localized mucus plugs in the bronchi for right posterior basal segments with segmental air trapping and no radiologic signs of asthma or bronchiolitis. He was given inhaled methylprednisolone and high-dose salbutamol and was discharged on July 4.

To confirm that the respiratory infection had spread from chimpanzees to their keeper, we performed real-time reverse transcription PCR and sequenced PCR products of part of the hMPV fusion protein gene (2). At the time of the hMPV outbreak among the chimpanzees, hMPV was circulating in Slovenia. Among 39 samples available for June 3–July 2 from the population in central Slovenia, we sequenced 12 samples with the lowest cycle threshold values to facilitate insight into the molecular epidemiology of circulating hMPV variants.

Sequencing analyses showed that virus sequences from the chimpanzees and keeper had 100% identity (Figure), as did 2 other sequences from 2 patients hospitalized during the virus outbreak at the zoo. These 2 sequences showed 99% identity with a previously reported sequence (GenBank accession no. KC731511). Alignment of all 15 sequences and phylogenetic analyses showed 7 unique sequences (GenBank accession nos. MN978917–23) among the 12 selected samples.

These cases are noteworthy because of how the infection spread. We assume that the chimpanzees acquired the virus from an infected child in a school or preschool group of children visiting the zoo as an end-of-year trip. The infection could have been spread by airborne route. Another possibility is that the chimpanzees acquired the virus from contaminated food of visitors; because of a narrow space (1.3 m) between visitors and the inner fence enclosing the chimpanzee cage, children could have thrown candies and other food onto the cage floor, and the chimpanzees might have eaten them.

Although the keeper had close contact with an ill chimpanzee and was probably infected by aerosols or body fluids from the chimpanzees, we cannot rule out the possibility that the keeper could have been infected by an infected adult human. We assume high infectivity pressure on the keeper, who fell ill only 2 days after the first chimpanzee started showing signs of respiratory infection. The keeper did not have children of his own and did not have close contact with children for at least 2 weeks before the incident.

This study was partially supported by the Slovenian Research Agency (Research Program P3-0083).

About the Author

Dr. Uršič is a research scientist at the Institute of Microbiology and Immunology, University of Ljubljana, Ljubljana, Slovenia. Her primary research interests are severe respiratory viral infections in children and the elderly, and molecular epidemiology studies.

References

1. Maertzdorf J, Wang CK, Brown JB, Quinto JD, Chu M, de Graaf M, et al. Real-time reverse transcriptase PCR assay for detection of human metapneumoviruses from all known genetic lineages. J Clin Microbiol. 2004;42:981–6. https://doi.org/10.1128/JCM.42.3.981-986.2004
2. Reiche J, Jacobsen S, Neubauer K, Hafemann S, Nitsche A, Milde J, et al. Human metapneumovirus: insights from a ten-year molecular and epidemiological analysis in Germany. PLoS One. 2014;9:e88342. https://doi.org/10.1371/journal.pone.0088342

Address for correspondence: Tina Uršič, Institute of Microbiology and Immunology, Faculty of Medicine, University of Ljubljana, Zaloška 4, 1000 Ljubljana, Slovenia; email: tina.ursic@mf.uni-lj.si

mcr-Positive *Escherichia coli* ST131-H22 from Poultry in Brazil

Andre Becker S. Saidenberg, Marc Stegger, Lance Bradley Price, Thor Bech Johannesen, Maliha Aziz, Marcos P.V. Cunha, Andrea M. Moreno, Terezinha Knöbl

Author affiliations: University of São Paulo, São Paulo, Brazil (A.B.S. Saidenberg, M.P.V. Cunha, A.M. Moreno, T. Knöbl); George Washington University, Washington, DC, USA (M. Stegger, L.B. Price, M. Aziz); Statens Serum Institut, Copenhagen, Denmark (M. Stegger, T.B. Johannesen)

DOI: https://doi.org/10.3201/eid2608.191724

Escherichia coli sequence type (ST) 131 is of concern because it can acquire antimicrobial resistance and cause extraintestinal infections. *E. coli* ST131-*H*22 sublineage appears capable of being transmitted to humans through poultry. We report on multidrug-resistant ST131-*H*22 poultry isolates in Brazil closely related to international human and poultry isolates.

The pandemic, extraintestinal, pathogenic *Escherichia coli* multilocus sequence type (MLST) 131 lineage has emerged extensively, gaining notoriety for its extensively multidrug-resistant ST131-*H*30 sublineage (*1*). Whereas ST131-*H*30 appears to be transmitted primarily from person to person, the *H*22 sublineage may be transmitted zoonotically through poultry and cause urinary tract infections and urosepsis (*2*,*3*). We report isolating ST131-*H*22 strains that are multidrug resistant (MDR), meaning that they are resistant to ≥3 classes of antimicrobials (*4*), carrying mobile colistin-resistance (*mcr*) determinants from poultry in Brazil, the largest poultry-exporting country in the world.

We collected 64 *E. coli* strains from poultry with colibacillosis cases from 2 different farms in the same geographic region of Brazil and screened them by PCR for the ST131 clonal group (*5*). PCR detected 6 ST131 isolates (2 from the first farm, 4 from the second), which we whole-genome sequenced (BioProject no. PRJNA398035). We determined phenotypic antimicrobial susceptibility with disk diffusion testing, except for isolates carrying the *mcr* gene, which we tested using broth microdilution (*6*).

We trimmed the reads and used QUAST (http://quast.sourceforge.net) to evaluate the quality of assemblies (contig lengths and expected genome sizes). We assembled DNA sequences with SPAdes (http://cab.spbu.ru/software/spades), then determined the serotype, phylogroup, MLST, *fimH* protein type, virulence gene profile, plasmid replicons, and markers of antimicrobial resistance for each isolate *in silico* using the ABRicate virulence factors database (https://github.com/tseemann/abricate) and ResFinder/PlasmidFinder tools from CGE (https://cge.cbs.dtu.dk/services). Genes were identified with a minimum of ≥95% of identity and coverage.

We identified all isolates as O25:H4-ST131-*H*22, all belonging to phylogroup B2. We generated a maximum-likelihood phylogeny tree on the basis of core-genome single-nucleotide polymorphisms, including the 6 isolates from Brazil and 140 ST131-*H*22 sequences from EnteroBase (http://enterobase.warwick.ac.uk) and a previous study (*2*), using the Northern Arizona SNP Pipeline (https://tgennorth.github.io/NASP/) aligned against *E. coli* JJ1886 ST131-*H*30 (GenBank

accession no. CP006784) (Appendix, https://wwwnc.cdc.gov/EID/article/26/8/19-1724-App1.pdf). The 6 isolates from poultry were nested within a clade of intermingled poultry and human clinical isolates within the overall international isolates (Figure, panel A). The isolates from Brazil were closely related to ST131-*H*22 avian pathogenic *E. coli* isolates from poultry in the United States and those from a human urinary tract infection in Australia (Figure, panel B). Identical virulence factors and plasmid replicons were observed among 4 β-lactamase positive isolates and between 2 isolates missing the β-lactamase genes but

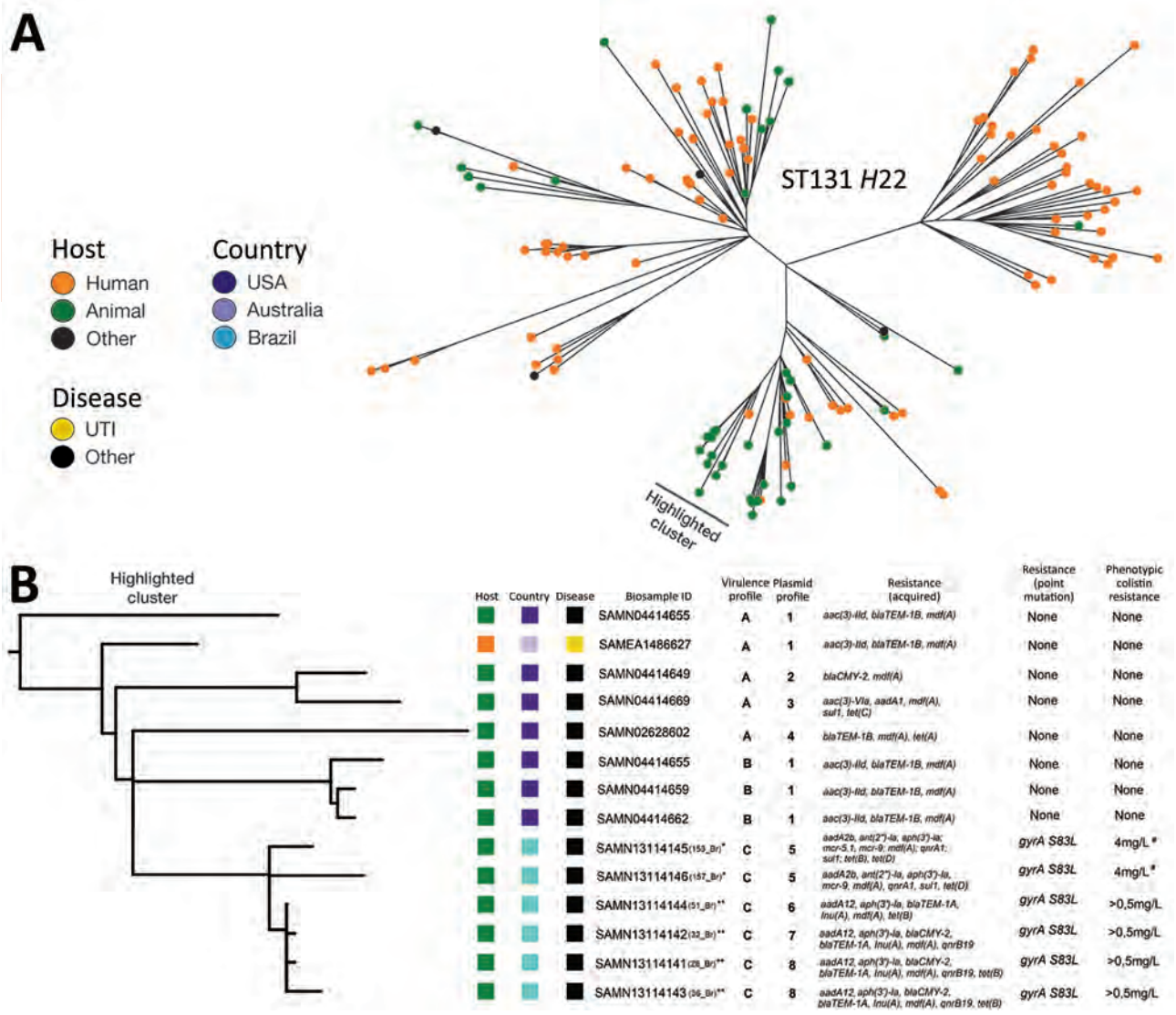

Figure. Phylogenetic analysis of *Escherichia coli* ST131-*H*22 isolates from poultry in Brazil and reference sequences. A) Unrooted phylogeny of 146 *E. coli* ST131-*H*22 isolates based on core genome single-nucleotide polymorphisms with the host origin outlined. The cluster containing closely related isolates to the 6 isolates from Brazil is highlighted. B) Rooted phylogeny of closely related isolates from retail meat with APEC and a human isolate with our 6 APEC isolates. The highlighted cluster includes a partial depiction of the tree including the data on host, country, and disease (urinary tract infection or other). Clusters containing the study's isolates have their individual identification in parenthesis. Asterisks indicate farm origins (*, farm 1; **, farm 2). Virulence factors profiles are identified as groups A: *cvi/cva, ent, fimA-H, ibeA, irp1/2, iroN, iucD,iss, kpsM, ompA, tsh;* B: *cvi/cva, ent, fimA-H, ibeA, irp1/2, iroN, iucD, iss, kpsM, ompA*; and C: *cvi/cva, ent, fimA-H, fyuA, ibeA, irp1/2, iroN, iucD, iss, kpsM, ompA, tsh*. Plasmid profiles are identified by group: 1: IncFIB, IncFIC(FII), IncI1; 2: IncFIB, IncFIC(FII), IncFII, IncI1; 3: IncFIB, IncFIC(FII), IncFII, IncHI2, IncHI2A, IncI1; 4: IncFIB, IncFIC(FII), IncI1, IncN; 5: IncFIB, IncFIC(FII), IncFII, IncFII(pCoo), IncHI2, IncHI2A; 6: IncFIB, IncFIC(FII), IncFII, IncHI2, IncHI2A; 7: IncFIB, IncFII, IncI1, IncX1; and 8: IncFIB, IncFIC(FII), IncFII, IncI1, IncX1. Phenotypic colistin-resistance is indicated by the symbol # for the 2 colistin-resistance *mcr* genes positive isolates, showing resistance according to 2018 Clinical Laboratory Standards Institute (https://clsi.org/) clinical breakpoints. APEC, avian pathogenic *E. coli*; ID, identification; ST, sequence type; UTI, urinary tract infection.

carrying *mcr* colistin–resistance determinants. All 6 isolates had MDR profiles, phenotypically confirmed (data not shown except for those from colistin microdilution method) (Figure, panel B).

The ST131-*H*22 lineage, while currently not as common as the *H*30 sublineage as a cause of community-acquired infections, does present a public health challenge because it colonizes poultry flocks, contaminating retail poultry products, and carries *mcr* colistin–resistance genes (*3*). The enormity and rapid growth of poultry production, in which many developing countries use antimicrobials extensively (*5*), and its zoonotic potential, make ST131-*H*22 worthy of specific attention (*2*).

Findings from our phylogenetic analyses of a global collection of ST131-*H*22 isolates from humans and poultry support findings from previous studies (*2*,*3*) and underscore the zoonotic potential of this virulent sublineage. Given that Brazil annually processes 13.8 million poultry products and exports 3.8 million kilograms (*4*), these findings warrant further examination to assess potential zoonotic spillover in Brazil and poultry-importing countries. Until such studies are conducted, the zoonotic potential of ST131-*H*22 in flocks in Brazil cannot be quantified.

The discovery of *mcr* mobile colistin resistance determinants in food animals has renewed attention to the potential risks of widespread antimicrobial use in livestock. In Latin America, *mcr-5* has been found in poultry in Paraguay (9). The description of the *mcr-9* homologue from humans in the United States and horses in Sweden has raised attention to another *mcr* gene with potential for global spread (*10*). Both *mcr* variants in this study, 153_Br and 157_Br, showed phenotypic resistance (*6*) and came from the same farm (Figure, panel B). Interestingly, 153_Br carried both *mcr-5.1* and *mcr-9* variants. These isolates may portend a more widespread problem within poultry flocks in Brazil.

Isolates from this study showed resistance to all of the World Health Organization's highest priority critically important antimicrobial classes (Figure, panel B) (*8*). Analysis of the absence of tetracycline resistance (*tet*[B]/[D]) in 1 of our isolates (Figure, panel B) indicates partial plasmid loss (data not shown).

Use of colistin as a growth promoter in livestock was banned in Brazil in November 2016, although it continued being therapeutically used in poultry up to 2018 (*7*). Therefore, *mcr*-encoding *H*22 strains could be selected out of the population over time. Further restrictions will have to be implemented to combat the growing resistance of *E. coli* in poultry in Brazil to critically important antimicrobial drugs (*4*).

Our findings suggest that poultry in Brazil may serve as a reservoir for MDR extraintestinal pathogenic *E. coli* carrying mobile colistin-resistance determinants. These findings highlight the need for better antimicrobial stewardship and surveillance systems to determine the prevalence of MDR *E. coli* ST131-*H*22 in these poultry flocks and clarify the risks posed to domestic and international poultry consumers.

Acknowledgments

The authors wish to thank the invaluable support provided with the laboratory processing of samples for whole-genome sequencing by the Department of Bacteria, Parasites and Fungi of the Statens Serum Institut (SSI), Denmark.

This research was sponsored in part by FAPESP (2011/18204, and 2014/11523-7) and in part by the Coordenação de Aperfeiçoamento de Pessoal de Nível Superior - Brasil (CAPES - Finance Code 001- André Becker S. Saidenberg - PhD student).

About the Author

Dr. Becker Saidenberg is a PhD student and researcher at the College of Veterinary Medicine, University of São Paulo, São Paulo, Brazil. He is engaged in microbiological studies focused on poultry and wildlife and the zoonotic aspects connected to the animal-human interface.

References

1. Manges AR. *Escherichia coli* and urinary tract infections: the role of poultry-meat. Clin Microbiol Infect. 2016;22:122–9. https://doi.org/10.1016/j.cmi.2015.11.010
2. Liu CM, Stegger M, Aziz M, Johnson TJ, Waits K, Nordstrom L, et al. *Escherichia coli* ST131-*H*22 as a foodborne uropathogen. mBio. 2018;9:e00470–18. https://doi.org/10.1128/mBio.00470-18
3. Roer L, Overballe-Petersen S, Hansen F, Johannesen TB, Stegger M, Bortolaia V, et al. ST131 fim*H*22 *Escherichia coli* isolate with a bla_{CMY-2}/IncI1/ST12 plasmid obtained from a patient with bloodstream infection: highly similar to *E. coli* isolates of broiler origin. J Antimicrob Chemother. 2019;74:557–60. https://doi.org/10.1093/jac/dky484
4. Van Boeckel TP, Brower C, Gilbert M, Grenfell BT, Levin SA, Robinson TP, et al. Global trends in antimicrobial use in food animals. Proc Natl Acad Sci U S A. 2015;112:5649–54. https://doi.org/10.1073/pnas.1503141112
5. Doumith M, Day M, Ciesielczuk H, Hope R, Underwood A, Reynolds R, et al. Rapid identification of major *Escherichia coli* sequence types causing urinary tract and bloodstream infections. J Clin Microbiol. 2015;53:160–6. https://doi.org/10.1128/JCM.02562-14
6. Clinical and Laboratory Standards Institute. Performance standards for antimicrobial susceptibility testing; 28th informational supplement (M100–S28). Wayne (PA): The Institute; 2018.

7. Brazil. Governmental Normative Instruction IN-45. Diario Oficial da Uniao. 2016. Nov 11 [cited 2020 Mar 20]. http://www.in.gov.br/materia/-/asset_publisher/Kujrw0TZC2Mb/content/id/22078290/do1-2016-11-30-instrucao-normativa-n-45-de-22-de-novembro-de-2016-22078259
8. World Health Organization. Critically important antimicrobials for human medicine. 2011 [cited 2019 Oct 21]. http://apps.who.int/iris/bitstream/10665/77376/1/9789241504485%20eng.pdf
9. Nesporova K, Jamborova I, Valcek A, Medvecky M, Literak I, Dolejska M. Various conjugative plasmids carrying the *mcr-5* gene in *Escherichia coli* isolates from healthy chickens in Paraguay. J Antimicrob Chemother. 2019;74:3394–7. https://doi.org/10.1093/jac/dkz317
10. Börjesson S, Greko C, Myrenås M, Landén A, Nilsson O, Pedersen K. A link between the newly described colistin resistance gene *mcr-9* and clinical *Enterobacteriaceae* isolates carrying bla_{SHV-12} from horses in Sweden. J Glob Antimicrob Resist. 2020;20:285–9. https://doi.org/10.1016/j.jgar.2019.08.007

Address for correspondence: Andre Becker S. Saidenberg, University of São Paulo, Av. Prof. Orlando Marques de Paiva, 87, 05508-270, São Paulo, Brazil; email: andresaidenberg@usp.br

Heartland Virus in Lone Star Ticks, Alabama, USA

Brent C. Newman, William B. Sutton, Abelardo C. Moncayo, Holly R. Hughes, Ali Taheri, Thomas C. Moore, Callie J. Schweitzer, Yong Wang

Author affiliations: Tennessee State University, Nashville, Tennessee, USA (B.C. Newman, W.B. Sutton, A. Taheri); Tennessee Department of Health, Nashville (A.C. Moncayo, T.C. Moore); Centers for Disease Control and Prevention, Fort Collins, Colorado, USA (H.R. Hughes); US Department of Agriculture, Huntsville, Alabama, USA (C.J. Schweitzer); Alabama Agricultural and Mechanical University, Huntsville (Y. Wang)

DOI: https://doi.org/10.3201/eid2608.200494

We detected Heartland virus (HRTV) in lone star nymphs collected in 2018 in northern Alabama, USA. Real-time reverse transcription PCR selective for the small segment of the HRTV genome and confirmatory sequencing of positive samples showed high identity with HRTV strains sequenced from Tennessee and Missouri.

Heartland virus (HRTV) is an emerging pathogenic phlebovirus first identified in the United States in 2009 and now reported in 15 states (*1*,*2*). Nymphal lone star ticks (*Amblyomma americanum*) are considered the primary vectors of HRTV, and a variety of domestic and endemic mammalian species are potential amplification hosts of this virus (*2*,*3*). Although *A. americanum* ticks are well-established throughout the eastern, southeastern, and midwestern United States, their range is expanding northward and westward, most likely because of increased host availability and abundance, changes in environmental and climatic conditions, and adaptive genetic variation (Figure, panel A) (*4*). We tested for HRTV in *A. americanum* ticks collected in Alabama, USA, a state within the range of this vector where HRTV has not been documented previously from ticks.

From June 1, 2018, through August 31, 2018, we collected ticks as previously described (*5*) in the William B. Bankhead National Forest, Alabama (34.2270°N, 87.3461°W; Figure, panel B). In preparation for pathogen screening, we separated ticks into pools. Nymph tick pools ranged from 1 to 5 tick(s) of the same species per pool. We screened adult ticks individually (i.e., 1 adult tick per pool) (Appendix Table, https://wwwnc.cdc.gov/EID/article/26/8/19-0494-App1.pdf). We did not include larvae in pathogen screening. We used molecular methods to extract viral RNA and detect the small (S) segment of the HRTV genome using the HRTV-4 primer and probe set (*6*) in tick pools (Appendix Table). We sequenced HRTV-4–positive samples using the Ion Torrent Personal Genomic Machine system (Life Technologies, https://www.thermofisher.com) at the Centers for Disease Control and Prevention (CDC; Fort Collins, CO, USA) as described previously (*7*). We obtained sequences of the HTRV S segment of other HRTV samples and strains from the GenBank database, and aligned sequences using the MUSCLE alignment tool (https://www.ebi.ac.uk/Tools/msa/muscle) in MEGA software (*8*). We also included a closely related severe fever with thrombocytopenia syndrome virus isolate from the GenBank database as an outgroup for this analysis. We used a maximum-likelihood tree approach with 1,000 bootstrap replications to generate the genetic relationships between the Alabama samples and the other HRTV samples available through the GenBank database.

We collected 964 ticks, of which 921 were *A. americanum* (872 nymphs, 22 adult males, and 27 adult females) and 43 were *Dermacentor variabilis* (20 adult males and 23 adult females). We tested

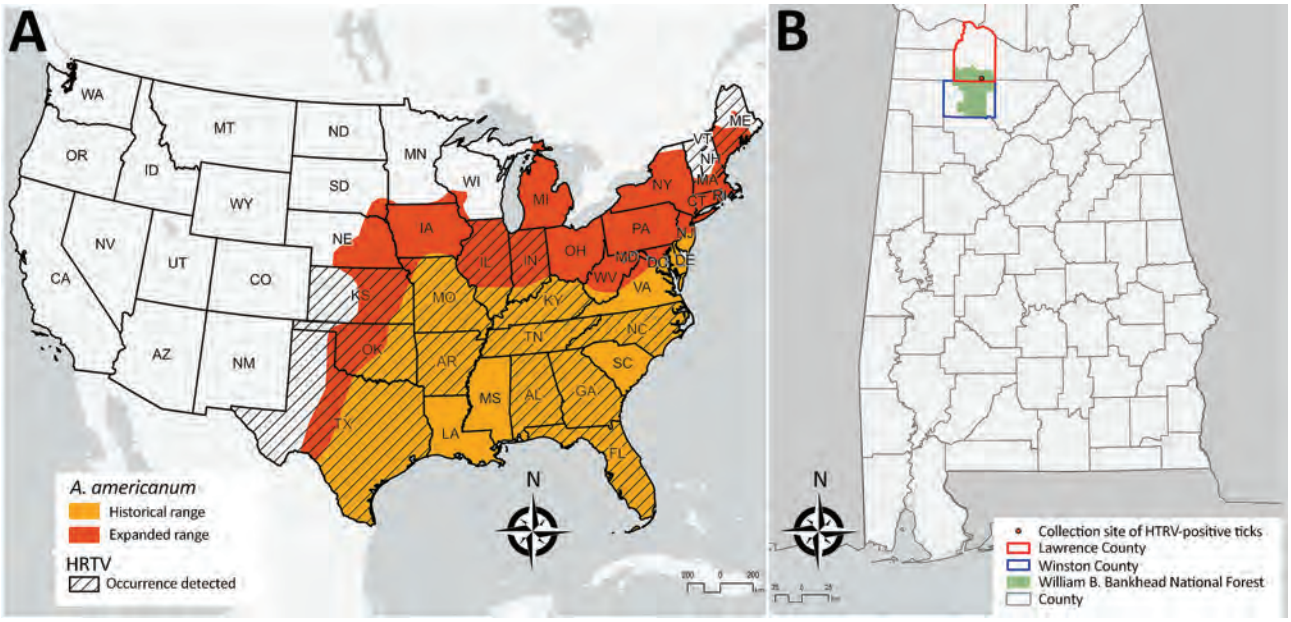

Figure. Distribution of HRTV and range of *Amblyomma americanum* ticks. A) Geographic distribution of Heartland virus, United States, 2009–2020 (*1*,*2*) with historical and expanded range of *A. americanum* ticks adapted from (*4*). B) Location of the William B. Bankhead National Forest within Lawrence and Winston Counties, Alabama, and collection site of the HRTV-positive *A. americanum* nymphs. All maps were created by using ArcGIS Pro 2.5 (ESRI, https://www.esri.com/en-us/home). HRTV, Heartland virus.

the ticks in 337 screened tick pools (Appendix Table). We amplified HRTV-4 from 5 pools that each contained 4 *A. americanum* nymphs. Therefore, the bias-corrected maximum-likelihood estimate of the infection rate (*9*) in questing *A. americanum* nymphs collected from the William B. Bankhead National Forest during 2018 was 0.58 (95% CI 0.21–1.27) and minimum infection rate (*9*) was 0.57 (95% CI 0.07–1.07) per 100 ticks screened on the basis of 235 nymph pools tested. To confirm results, we randomly selected homogenate from 3 of 5 HRTV-4–positive pools and submitted 3 individual RNA samples for sequencing at CDC. Sequencing RNA directly from tick homogenate confirmed HRTV in each of the 3 pools. Although we did not obtain whole-genome sequences, we identified partial coding sequences of all 3 HRTV segments in each pool. Maximum-likelihood phylogenetic inference of 730 nt of the S segment confirmed the BLAST analysis (https://blast.ncbi.nlm.nih.gov/Blast.cgi) and placed the generated HRTV S segment (submitted under GenBank accession no. MT052710) in a well-supported clade with HRTV strains previously described in Missouri and Tennessee (Appendix Figure).

Our findings of HRTV in *A. americanum* ticks in Alabama update knowledge of the virus' distribution in the United States (Figure, panel A). Our findings also suggest *A. americanum* nymphs are the primary vectors of HRTV. As the geographic range of *A. americanum* continues to expand, we encourage enhanced surveillance and screening for HRTV to provide a more accurate and up-to-date understanding of where this tickborne virus probably occurs in the United States. Treatment for HRTV infection is limited to supportive care only; clinical data from the southeastern United States show that Heartland virus has a 10% death rate (*10*). Surveillance of HRTV in tick vector species is necessary to gain a comprehensive understanding of the environmental determinants that may put humans at risk for encountering the vector and to identify the geographic host range (both current and potential) of this emerging pathogen in the United States.

Acknowledgments

We thank Allison Cochran for forest stand access and logistical support at the William B. Bankhead National Forest and Stuart Robertson and Alexander Binney for field sampling assistance. We also thank Amy Lambert for enabling collaboration and sample sequencing for this research, Javier Monzón for permission to recreate his *A. americanum* range map, and Suzanne Wade for help creating the maps.

This study was supported by the US Department Agriculture, National Institute of Food and Agriculture 1890 Institution Teaching, Research and Extension Capacity Building Grants Program.

About the Author

Mr. Newman is a PhD candidate in biological sciences at Tennessee State University, Nashville, Tennessee. His interests are landscape genomics, the function of biodiversity in vectorborne disease ecology, and application of One Health concepts to wildlife parasitology.

References

1. Centers for Disease Control and Prevention, National Center for Emerging and Zoonotic Infectious Diseases, Division of Vector-Borne Diseases. Heartland virus disease (Heartland): statistics & maps. 2018 Oct 22 [cited 2020 Feb 11]. https://www.cdc.gov/heartland-virus/statistics/index.html
2. Riemersma KK, Komar N. Heartland virus neutralizing antibodies in vertebrate wildlife, United States, 2009–2014. Emerg Infect Dis. 2015;21:1830–3. https://doi.org/10.3201/eid2110.150380
3. Bosco-Lauth AM, Panella NA, Root JJ, Gidlewski T, Lash RR, Harmon JR, et al. Serological investigation of Heartland virus (Bunyaviridae: *Phlebovirus*) exposure in wild and domestic animals adjacent to human case sites in Missouri 2012–2013. Am J Trop Med Hyg. 2015;92:1163–7. https://doi.org/10.4269/ajtmh.14-0702
4. Monzón JD, Atkinson EG, Henn BM, Benach JL. Population "and evolutionary genomics of *Amblyomma americanum*, an expanding arthropod disease vector. Genome Biol Evol. 2016;8:1351–60. https://doi.org/10.1093/gbe/evw080
5. Newman BC, Sutton WB, Wang Y, Schweitzer CJ, Moncayo AC, Miller BT. A standardized method for the construction of a tick drag/flag sampling approach and evaluation of sampling efficacy. Exp Appl Acarol. 2019;79:433–46. https://doi.org/10.1007/s10493-019-00429-6
6. Savage HM, Godsey MS Jr, Lambert A, Panella NA, Burkhalter KL, Harmon JR, et al. First detection of Heartland virus (Bunyaviridae: *Phlebovirus*) from field collected arthropods. Am J Trop Med Hyg. 2013;89:445–52. https://doi.org/10.4269/ajtmh.13-0209
7. Hughes HR, Russell BJ, Lambert AJ. First complete genome sequences of Anopheles A virus of the genus *Orthobunyavirus*. Genome Announc. 2017;5:e01331–17. https://doi.org/10.1128/genomeA.01331-17
8. Kumar S, Stecher G, Li M, Knyaz C, Tamura K. MEGA X: molecular evolutionary genetics analysis across computing platforms. Mol Biol Evol. 2018;35:1547–9. https://doi.org/10.1093/molbev/msy096
9. Biggerstaff BJ. PooledInfRate, version 4.0: a Microsoft Office add-in to compute prevalence estimates from pooled samples. Fort Collins (CO): Centers for Disease Control and Prevention; 2009 [cited 2020 Apr 16]. https://www.cdc.gov/westnile/resourcepages/mosqsurvsoft.html
10. Hevey MA, O'Halloran JA, Jagger BW, Staples JE, Lambert AJ, Panella AJ, et al. Heartland virus infection in a heart transplant recipient from the Heartland. Transpl Infect Dis. 2019;21:e13098. https://doi.org/10.1111/tid.13098

Address for correspondence: Brent C. Newman, Department of Agricultural and Environmental Sciences, 3500 John A. Merritt Blvd, Nashville, TN 37209, USA; email: bnewman1@my.tnstate.edu

Visceral Leishmaniasis Caused by *Leishmania donovani* Zymodeme MON-37, Western Ghats, India

Prasanta Saini, N. Pradeep Kumar, P.M. Ajithlal, Aswathy Joji, K.R. Rajesh, K.J. Reena, Ashwani Kumar

Author affiliations: Indian Council of Medical Research–Vector Control Research Centre (Field Station), Kottayam, India (P. Saini, N.P. Kumar, P.M. Ajithlal, A. Joji); Government Medical College, Thrissur, India (K.R. Rajesh); District Medical Officer, Thrissur (K.J. Reena); Indian Council of Medical Research–Vector Control Research Centre, Puducherry, India (A. Kumar)

DOI: https://doi.org/10.3201/eid2608.200557

During 2015–2019, we recorded 10 patients with indigenous cases of visceral leishmaniasis caused by *Leishmania donovani* in Western Ghats, a region in India to which visceral leishmaniasis is not endemic. The parasite involved in 4 of these infections was of the MON-37 zymodeme strain, which normally causes cutaneous leishmaniasis in this region.

Leishmaniasis is a neglected tropical disease, caused by *Leishmania* parasites and transmitted by phlebotomine sand flies, which manifests in 3 primary clinical forms: visceral (VL), also known as kala-azar; cutaneous (CL); and mucocutaneous (*1*). The lack of continuous active surveillance, indefinite array of symptoms, resemblance to other infections, and diverse clinical manifestations may lead to misdiagnosis of this disease, especially in areas to which it is not endemic (*2*). Despite the reduction in VL reported by the National Kala-azar Elimination Programme, emergence or resurgence is being recorded in different regions of India (*3*,*4*). During 2003, two indigenous cases of VL were reported from Kerala (*5*). We report the occurrence of 10 additional indigenous cases of VL from the foothills of the Western Ghats in Kerala during March 2015–October 2019 (Figure). Ethics clearance for this study was obtained from the Indian Council of Medical Research–Vector Control Research Centre (approval no. IHEC-0119/R/M).

The patients exhibited clinical symptoms of VL, such as hepatosplenomegaly, fever, malaise, pancytopenia, anemia, emaciation, and anorexia. They tested negative for other microbial infections, such as HIV and tuberculosis. Histopathologic examination of bone marrow aspirates detected Leishman Donovan bodies within the macrophages. Results of serologic diagnosis with a Kalazar Detect rK39 rapid test kit (InBiOS,

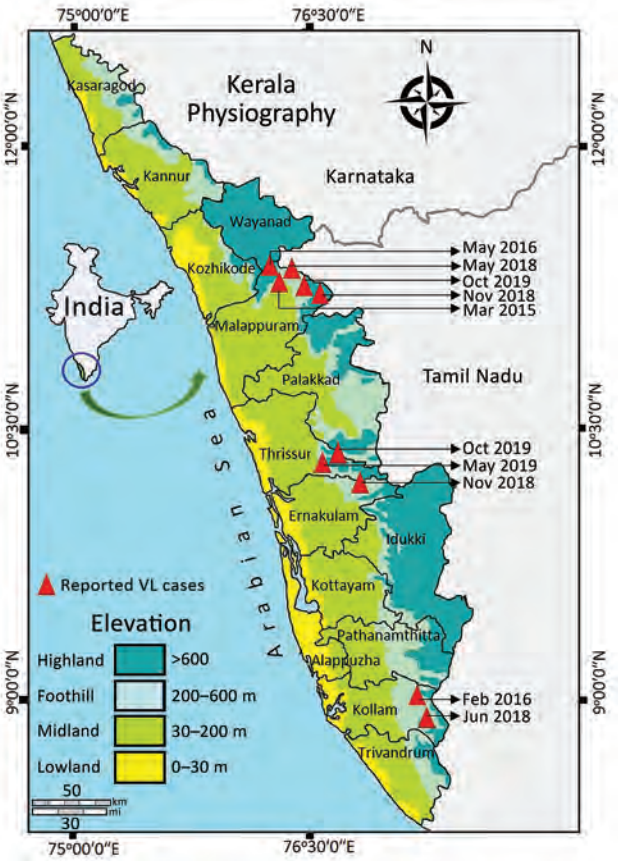

Figure. Spatial distribution and detailed timeline of VL cases in the foothills of Western Ghats, Kerala, India. VL, visceral leishmaniasis.

https://inbios.com) were also positive. We performed molecular diagnosis (*6*) on bone marrow and trephine biopsy samples from 4 of 10 patients. Among the other 6 patients, 3 were unwilling to provide samples; the other 3 patients died after diagnosis.

PCR amplification of a kinetoplast DNA minicircle gene, restriction fragment-length polymorphism analysis of the 3′ untranslated region Hsp70 and DNA sequencing of Hsp70 gene amplicons (GenBank accession no. MT010559) characterized the parasites involved in the cases to be *Leishmania donovani*. Further genetic analysis of 6-phosphogluconate dehydrogenase gene sequences (A976G) indicated that the parasite belonged to the zymodeme MON-37 (GenBank accession no. MT010560). This strain is known to cause CL in the tribal belt of Western Ghats of Kerala (*6*) as well as in Sri Lanka (*7*). Thus, our investigations evinced that MON-37 zymodeme *L. donovani* is involved in both CL (*6*) and VL manifestations in the foothills of the Western Ghats, whereas MON-2 zymodeme of *L. donovani* caused VL in other VL-endemic zones across eastern India (*8*). Also, MON-37 has been characterized from an autochthonous VL case in Sri Lanka (*9*). These uncommon phenomena warrant further investigation.

We treated the patients with an intravenous infusion of 1 dose of liposomal amphotericin B (10 mg/kg). Seven patients recovered completely; 1 patient, who was not responsive to the treatment and later died, was subsequently diagnosed with acute myeloid leukemia. Detailed treatment records were unavailable for the other 2 deceased patients.

We monitored the recovered patients once every 3 months beginning with the commencement of treatment. We did not detect any relapse of symptoms or post–Kala-azar dermal leishmaniasis. Although rK39 antibodies have been documented to persist up to 5 years after treatment, immediate contacts of the VL patients tested negative for clinical symptoms of this disease and for rK39 antibodies by rK39 rapid diagnostic test.

Entomologic investigations were carried out within a 0.5 km radius around the patients' residences every 3 months for 1 year. *Phlebotomus argentipes* was the predominant sand fly species recorded. No natural infection with *Leishmania* parasites was detected in the sampled specimens; however, this result could be because of the limited number of cross-sectional entomologic surveys carried out and the long incubation period of *Leishmania* parasites. To control the vector population, indoor residual spraying with lambda cyhalothrin 10% wettable powder formulation was performed in and around houses, in all villages where cases had been reported.

All of these patients lived in either tribal colonies or villages located in the foothills of Western Ghats, which encompasses one of the world's major biodiversity hotspots. The region is characterized by its tropical climate, conserved forest ecosystem, low human activity, humid and shady microhabitats, and mud houses and is therefore highly conducive to sand fly breeding and proliferation. Epidemiologic surveys recorded that all of the patients lived in unplastered, humid, and poorly lit houses, which also serve as optimal resting sites for sand flies (*10*). The patients had histories of frequent visits to deep forest areas to collect forest products for their livelihoods. In addition, their reluctance to use protective clothing and insect repellents escalated their exposure to sand fly bites. Because of the difficulty of accessing these thickly forested regions, vector control activities using adulticidal insecticides have remained suspended in this region since the successful elimination of malaria during the 1960s.

None of the patients had a history of travel to other VL-endemic regions of the country or direct contact with persons from those regions, suggesting that these

infections were indigenous. The occurrence of 10 VL cases in Kerala, a nonendemic state, during 2015–2019 suggests the need to adopt management strategies, including active surveillance, for leishmaniasis in the region. These actions would facilitate the successful implementation of guidelines from the ongoing National Kala-azar Elimination Programme in India.

Acknowledgments

We are grateful to Abidha Suresh and Jessu S. Mathew for their technical help and to the Directorate of Health Services, Government of Kerala, India, for facilitating the study.

This study is being funded by the Indian Council of Medical Research, New Delhi (Grant No. 6/9-7(213)/2019-ECD-II).

Authors hereby declared that no conflict of interest is involved in this study.

About the Author

Dr. Saini has more than 10 years of research experience in the field of parasitology and is a scientist at the Indian Council of Medical Research–Vector Control Research Centre, India. His major research interests include vectorborne diseases and their control.

References

1. World Health Organization. Leishmaniasis [cited 2020 Mar 3]. Geneva: The Organization; 2020. https://www.who.int/en/news room/fact-sheets/detail/leishmaniasis
2. Boettcher JP, Siwakoti Y, Milojkovic A, Siddiqui NA, Gurung CK, Rijal S, et al. Visceral leishmaniasis diagnosis and reporting delays as an obstacle to timely response actions in Nepal and India. BMC Infect Dis. 2015;15:43. https://doi.org/10.1186/s12879-015-0767-5
3. World Health Organization. Operational guidelines on kala-azar (visceral leishmaniasis) elimination in India—2015. Geneva: The Organization; 2015 [cited 2020 Feb 20]. https://www.who.int/leishmaniasis/burden/Operational_guidelines_on_kala_azar_elimination_in_India.pdf
4. Thakur L, Singh KK, Shanker V, Negi A, Jain A, Matlashewski G, et al. Atypical leishmaniasis: a global perspective with emphasis on the Indian subcontinent. PLoS Negl Trop Dis. 2018;12:e0006659. https://doi.org/10.1371/journal.pntd.0006659
5. Kesavan A, Parvathy VK, Thomas S, Sudha SP. Indigenous visceral leishmaniasis: two cases from Kerala. Indian Pediatr. 2003;40:373–4 https://www.ncbi.nlm.nih.gov/pubmed/12736419.
6. Kumar NP, Srinivasan R, Anish TS, Nandakumar G, Jambulin gam P. Cutaneous leishmaniasis caused by *Leishmania donovani* in the tribal population of the Agasthyamala Biosphere Reserve forest, Western Ghats, Kerala, India. J Med Microbiol. 2015;64:157–63. https://doi.org/10.1099/jmm.0.076695-0
7. Kariyawasam UL, Selvapandiyan A, Rai K, Wani TH, Ahuja K, Beg MA, et al. Genetic diversity of *Leishmania donovani* that causes cutaneous leishmaniasis in Sri Lanka: a cross sectional study with regional comparisons. BMC Infect Dis. 2017;17:791. https://doi.org/10.1186/s12879-017-2883-x
8. Thakur CP, Dedet JP, Narain S, Pratlong F. *Leishmania* species, drug unresponsiveness and visceral leishmaniasis in Bihar, India. Trans R Soc Trop Med Hyg. 2001;95:187–9. https://doi.org/10.1016/S0035-9203(01)90160-9
9. Ranasinghe S, Zhang WW, Wickremasinghe R, Abeygunasekera P, Chandrasekharan V, Athauda S, et al. *Leishmania donovani* zymodeme MON-37 isolated from an autochthonous visceral leishmaniasis patient in Sri Lanka. Pathog Glob Health. 2012;106:421–4. https://doi.org/10.1179/2047773212Y.0000000054
10. Srinivasan R, Kumar NP, Jambulingam P. Detection of natural infection of *Leishmania donovani* (Kinetoplastida: Trypanosomatidae) in *Phlebotomus argentipes* (Diptera: Psychodidae) from a forest ecosystem in the Western Ghats, India, endemic for cutaneous leishmaniasis. Acta Trop. 2016; 156:95–9. https://doi.org/10.1016/j.actatropica.2016.01.010

Address for correspondence: Prasanta Saini, ICMR-Vector Control Research Centre (Field Station), 5-D, Skyline River Valley, Collectorate PO, Kottayam, Kerala, India; email: prasantasaini09@gmail.com

Cryptosporidium baileyi Pulmonary Infection in Immunocompetent Woman with Benign Neoplasm

Żaneta Kopacz, Martin Kváč, Paweł Piesiak, Magdalena Szydłowicz, Andrzej B. Hendrich, Bohumil Sak, John McEvoy, Marta Kicia

Author affiliations: Wroclaw Medical University, Wroclaw, Poland (Ż. Kopacz, P. Piesiak, M. Szydłowicz, A.B. Hendrich, M. Kicia); Biology Centre of the Czech Academy of Sciences, České Budějovice, Czech Republic (M. Kváč, B. Sak); University of South Bohemia, České Budějovice (M. Kváč); North Dakota State University, Fargo, North Dakota, USA (J. McEvoy)

DOI: https://doi.org/10.3201/eid2608.201117

Cryptosporidium baileyi, a bird-specific parasite, infects gastrointestinal, pulmonary, and urinary tracts of its host. We report on a *C. baileyi* infection associated with pulmonary hamartoma in an immunocompetent patient in Poland. Further work is needed to investigate the association between *Cryptosporidium* infections and tumors.

Cryptosporidium is a global protozoan parasite infecting wild, agricultural, and domestic vertebrates, and humans. Most infections lead to a gastrointestinal illness characterized by diarrhea (*1*). In addition, in birds, *C. baileyi* and *C. avium* parasites cause pulmonary infection (*2*). In humans, respiratory cryptosporidiosis is mostly associated with immunodeficiency, but several cases in immunocompetent children with intestinal cryptosporidiosis also have been reported (*3*,*4*). We describe a *C. baileyi* infection associated with a lung hamartoma in an immunocompetent patient.

The Human Research Ethics Committee of Wroclaw Medical University (Wroclaw, Poland) approved the use of diagnostic samples and corresponding patient data for this study (permit no. KB648/2014). The patient provided written informed consent for conduct of the studies and publication of the results.

In June 2015, a 51-year-old immunocompetent woman living in a rural area of Poland was admitted to a hospital with a suspected spinal injury. In addition to confirming the spinal injury, a solitary pulmonary nodule (SPN), 1.3–1.8 cm, in the third segment of the right lung upper lobe was detected by chest radiography and computed tomography (Figure, panels A, B). The lesion was of high density and had well-defined borders. The patient was referred to the Department of Pulmonology and Lung Cancers of Wroclaw Medical University for a nodule differential diagnosis. A bronchoscopy performed in July 2015 included biopsy samples for histology and cytology and a bronchial washings (BW) sample for acid-fast bacilli examination. We did not detect any changes in the bronchial trees, vocal cords, or trachea. Histologic and cytologic examination showed low cell count material, and the cells of the nodule lacked features of malignant process. The BW was negative for acid-fast bacilli. A second chest radiograph and bronchoscopy performed before surgery in September 2015 to remove the SPN showed a normal bronchial tree without anatomic changes and a slight increase in size of the SNP (1.5–2.0 cm). The SPN was removed by wedge resection in video-assisted thoracoscopic surgery after stabilization of the spine.

Before and during hospitalization, the patient was in good physical condition, afebrile, and without signs or symptoms of pulmonary and gastrointestinal infection. She reported no chronic diarrhea or cough in recent years. Blood count data, acid-base balance, gasometry, and spirometry did not deviate from mean values. She had no palpable lymphadenopathy. Except for the SPN, medical history was unremarkable. The patient was not undergoing immunosuppressive treatment and did not have an autoimmune disease. She was discharged 1 week after surgery in good general condition.

A paraffin-embedded tissue sample from the removed mass was diagnosed as a bronchial

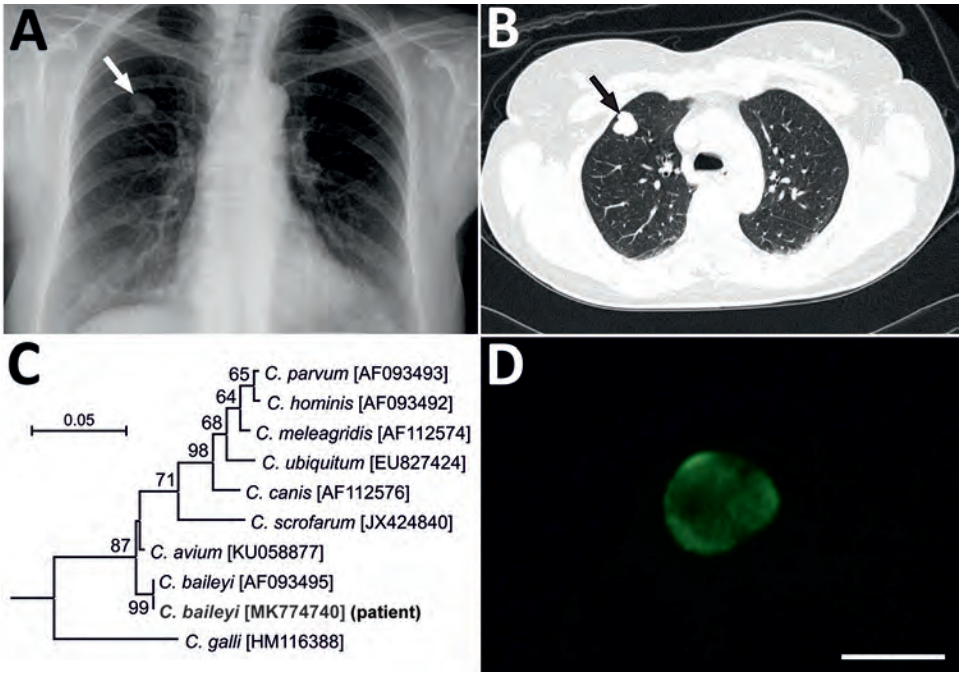

Figure. Findings from a 51-year-old immunocompetent woman with a benign neoplasm and *Cryptosporidium baileyi* pulmonary infection, Poland, 2015. A) Chest radiography in posterior-anterior position. A tumor, 13 × 18 mm with well-defined boundaries, is visible in the third segment of the upper right lung (arrow). B) Patient's lung tomogram. Tumor is visible in the right lung (arrow). C) Maximum log likelihood tree based on partial sequences of gene coding small subunit rRNA of *Cryptosporidium*, including sequences obtained in this study (bold). Scale bar indicates nucleotide substitutions per site. D) *Cryptosporidium* oocyst detected in patient's bronchial washings after immunofluorescent labeling with excitation and emission spectrum peak wave lengths of 495 nm/519 nm. Scale bar indicates 5 μm.

hamartoma. The BW was tested for pulmonary pathogens using individual conventional PCR (*Chlamydia pneumoniae*, *Mycoplasma pneumoniae*, *Legionella pneumophila*, *Cryptosporidium*, *Encephalitozoon*, and *Enterocytozoon*) and real-time PCR (*Pneumocystis jirovecii*). To identify *Cryptosporidium*, we extracted DNA from the BW and amplified a partial sequence of the small-subunit rRNA of *Cryptosporidium* (*5*) and sequenced it in triplicate. We inferred relationships to sequences from known species/genotypes from maximum-likelihood phylogenies (MEGA X, https://www.megasoftware.net). Bootstrap support for branching was based on 1,000 replications. A BW smear was labeled with genus-specific fluorescein isothiocyanate–conjugated antibodies (indirect fluorescent antibody Crypto cel; Cellabs Pty Ltd., https://www.cellabs.com.au).

The small-subunit sequence (GenBank accession no. MK774740) for the patient isolate was identical to that of a *C. baileyi* isolate from chickens (GenBank accession no. AF093495) (Figure, panel C). Microscopic examination of the BW smear showed oocysts measuring 5.2–5.5 μm with typical green fluorescence after labeling with FITC-conjugated anti-*Cryptosporidium* oocyst wall antibody (Figure, panel D).

We report an unusual case of human respiratory *C. baileyi* infection in an immunocompetent woman with hamartoma. Previously, a presumptive *C. baileyi* infection had been reported in the lungs, trachea, larynx, esophagus, whole intestine, gallbladder, and urinary tract of an immunodeficient man with HIV (*6*). Although not confirmed by sequence analysis, the finding that oocysts were infective for chickens supports the identification.

Immunocompetence is a critical determinant of the clinical course of *Cryptosporidium* infection. Intestinal cryptosporidiosis can be devastating to immunodeficient persons (*7*) and can involve extraintestinal sites (*6*). Pulmonary cryptosporidiosis in immunocompetent humans typically manifests as a cough and dyspnea, and concurrent intestinal infection is frequently reported (*3*,*4*). Consistent with this, the overwhelming majority of respiratory cases in humans have been caused by *C. parvum* and *C. hominis*, the major causes of intestinal cryptosporidiosis (*3*,*4*,*8*). Respiratory *Cryptosporidium* infection in birds is mostly asymptomatic but can result in high rates of death in association with other etiologic agents (*2*). The patient in this study did not report direct contact with birds but might have been exposed to wild bird excretions occupationally through work in an orchard. The hamartoma could have created an environment that supported the *C. baileyi* infection. *C. meleagridis* parasites were recently detected around a colon adenocarcinoma in an immunocompetent patient who, similarly, did not have symptoms typically associated with cryptosporidiosis (*9*). Alternatively, experimental evidence suggests that *Cryptosporidium* parasites can cause neoplastic changes in immunocompromised animals and in cells cultured in vitro, consistent with a role in carcinogenesis (*10*).

This work was supported by the Grant for Young Scientists of Wroclaw Medical University, Poland (STM.A060.17.038) and the Czech Science Foundation (18-12364S).

About the Author

Dr. Kopacz is a research scientist at the Department of Biology and Medical Parasitology, Wroclaw Medical University. Her research focuses on opportunistic parasites, including microsporidia, *Cryptosporidium* spp., and *Pneumocystis jirovecii* in humans and animals.

References:

1. Plutzer J, Lassen B, Jokelainen P, Djurković-Djaković O, Kucsera I, Dorbek-Kolin E, et al. Review of *Cryptosporidium* and *Giardia* in the eastern part of Europe, 2016. Euro Surveill. 2018;23:1–23. https://doi.org/10.2807/1560-7917.ES.2018.23.4.16-00825
2. Nakamura AA, Meireles MV. *Cryptosporidium* infections in birds—a review. Rev Bras Parasitol Vet. 2015;24:253–67. https://doi.org/10.1590/S1984-29612015063
3. Sponseller JK, Griffiths JK, Tzipori S. The evolution of respiratory cryptosporidiosis: evidence for transmission by inhalation. Clin Microbiol Rev. 2014;27:575–86. https://doi.org/10.1128/CMR.00115-13
4. Mor SM, Tumwine JK, Ndeezi G, Srinivasan MG, Kaddu-Mulindwa DH, Tzipori S, et al. Respiratory cryptosporidiosis in HIV-seronegative children in Uganda: potential for respiratory transmission. Clin Infect Dis. 2010;50:1366–72. https://doi.org/10.1086/652140
5. Xiao L, Morgan UM, Limor J, Escalante A, Arrowood M, Shulaw W, et al. Genetic diversity within *Cryptosporidium parvum* and related *Cryptosporidium* species. Appl Environ Microbiol. 1999;65:3386–91. https://doi.org/10.1128/AEM.65.8.3386-3391.1999
6. Ditrich O, Palkovic L, Stěrba J, Prokopic J, Loudová J, Giboda M. The first finding of *Cryptosporidium baileyi* in man. Parasitol Res. 1991;77:44–7. https://doi.org/10.1007/BF00934383
7. Mead JR, Arrowood MJ. Treatment of cryptosporidiosis. In: Cacciò SM, Widmer G, editors. *Cryptosporidium*: parasite and disease. Heidelberg (Germany): Springer: 2014. p. 455–88.
8. Reina FTR, Ribeiro CA, Araújo RS, Matté MH, Castanho REP, Tanaka II, et al. Intestinal and pulmonary infection by *Cryptosporidium parvum* in two patients with HIV/AIDS. Rev Inst Med Trop São Paulo. 2016;58:21. https://doi.org/10.1590/S1678-9946201658021
9. Kopacz Ż, Kváč M, Karpiński P, Hendrich AB, Sąsiadek MM, Leszczyński P, et al. The first evidence of *Cryptosporidium meleagridis* infection in a colon adenocarcinoma from an immunocompetent patient. Front Cell Infect Microbiol. 2019;9:35. https://doi.org/10.3389/fcimb.2019.00035

10. Benamrouz S, Conseil V, Chabé M, Praet M, Audebert C, Blervaque R, et al. *Cryptosporidium parvum*–induced ileo-caecal adenocarcinoma and Wnt signaling in a mouse model. Dis Model Mech. 2014;7:693–700. https://doi.org/10.1242/dmm.013292

Address for correspondence: Żaneta Kopacz, Department of Biology and Medical Parasitology, Wrocław Medical University, ul. J. Mikulicza-Radeckiego 9, 50-367 Wrocław, Poland; email: zaneta.kopacz@umed.wroc.pl

COMMENT LETTERS

Intact *Mycobacterium leprae* Isolated from Placenta of a Pregnant Woman, China

Ajay Vir Singh, Harpreet Singh Pawar, Rajbala Yadav, Devendra Singh Chauhan

Author affiliation: Indian Council of Medical Research–National JALMA Institute for Leprosy and Other Mycobacterial Diseases, Agra, India

DOI: https://doi.org/10.3201/eid2608.191149

To the Editor: Chen et al. (*1*) reported intact *Mycobacterium leprae* in homogenate of placenta of a pregnant woman with untreated histoid leproma, highlighting the effectiveness of the placental barrier in stopping vertical transmission of leprosy (Hansen disease). However, reports in the published literature indicate that this claim is not absolutely correct.

Several early studies provided evidence of transplacental transmission of *M. leprae*; these studies revealed *M. leprae* in umbilical cords (25/104) (*2*) and cord blood (10/12) (*3*) of neonates born to mothers with leprosy, as well as in the placentae (57/104 and 9/12) (*2*,*3*) of those mothers (*2*,*3*). Furthermore, transplacental infection with *M. leprae* has been supported by an increased concentration of IgA in cord blood (*4*) and *M. leprae* IgA and IgM in cord serum (*5*) of babies of mothers with leprosy. These observations indicate that in some mothers with leprosy, whole *M. leprae*, its antigens, or both can cross the placenta, possibly inducing the fetal immune system to produce antibodies against *M. leprae* antigens. Therefore, we believe that vertical transmission of *M. leprae* is a complex, uncommon, and multifactorial event that might depend on the presence of *M. leprae* in maternal blood, maternal and fetal immune responses, fetal gestational age at infection, and other placental factors.

Consequently, the claim of Chen et al. (*1*) needs to be read with attention to the limitations of the underlying data and might not be generalizable to all mothers with leprosy. Further studies are needed to clarify the mechanisms of transplacental transmission of leprosy. The follow-up care of newborns of mothers with leprosy is necessary for early detection of the disease and to ensure appropriate general healthcare, especially considering that babies of mothers with leprosy have lower fetoplacental weights, slower growth, more fatal infections, and higher rates of infant mortality than those of mothers without leprosy.

References

1. Chen Z, Kuang Y, Jiang H, Zhang W, Shi Y, Chokkakula S, et al. Intact *Mycobacterium leprae* isolated from placenta of a pregnant woman, China. Emerg Infect Dis. 2019;25:1604–7. https://doi.org/10.3201/eid2508.190114
2. Pineda EV. The presence of *Mycobacterium leprae* in the placenta and umbilical cord. J Philipp Med Assoc. 1928;VIII:67–70.
3. Sugai T, Monobe J. Uber histologische befunde in der placenta tuberkulose und leprakranker. zentralblatt für bakteriol-ogie, Parasitenkunde. Infektionskrankheiten und Hygiene. 1913;13:262.
4. Melsom R, Duncan ME, Bjune G. Immunoglobulin concentration in mothers with leprosy and in healthy controls and their babies at the time of birth. Lepr Rev. 1980;51:19–28. https://doi.org/10.5935/0305-7518.19800004
5. Melsom R, Harboe M, Duncan ME, Bergsvik H. IgA and IgM antibodies against *Mycobacterium leprae* in cord sera and in patients with leprosy: an indicator of intrauterine infection in leprosy. Scand J Immunol. 1981;14:343–52. https://doi.org/10.1111/j.1365-3083.1981.tb00574.x

Address for correspondence: Ajay Vir Singh, Department of Microbiology and Molecular Biology, ICMR-National JALMA Institute for Leprosy and Other Mycobacterial Diseases, Agra, Uttar Pradesh, Pin-282001, India; email: avsjalma@gmail.com

The Practice of Wearing Surgical Masks during the COVID-19 Pandemic

Cho-Han Chiang, Cho-Hung Chiang, Cho-Hsien Chiang, Yee-Chun Chen

Author affiliations: National Taiwan University College of Medicine, Taipei, Taiwan (Cho-Han Chiang, Y.-C. Chen); Fu-Jen Catholic University, Taipei (Cho-Hung Chiang); Chung Shan Medical University, Taichung, Taiwan (Cho-Hsien Chiang); National Taiwan University Hospital, Taipei (Y.-C. Chen)

DOI: https://doi.org/10.3201/eid2608.201498

To the Editor: We read with interest the meta-analysis conducted by Xiao et al. (*1*) that found no significant reduction in influenza transmission with the use of surgical masks in the community, based on 10 randomized controlled trials. Nevertheless, mechanistic studies found that surgical masks could prevent transmission of human coronavirus and influenza virus infections if worn by infected persons (*2*). The authors pointed out the limitations of their study: small sample size and suboptimal adherence in the mask-wearer group (*1*). Recommendations on masks in the community vary across countries during the coronavirus disease (COVID-19) pandemic (*3*); studies have reported mixed results (*2*,*4*,*5*).

Epidemiologic data may provide an alternative insight. As of April 3, 2020, Taiwan recorded 348 COVID-19 cases (1.46/100,000 population), of which 48 (13.8%) were local cases. Singapore recorded 1,114 cases (19.07/100,000 population), of which 572 (51.3%) were local cases. Taiwan and Singapore both employed stringent measures. Taiwan recommended the use of masks early in the pandemic. In contrast, Singapore did not recommend the use of masks until April 3 and initiated its Stay Home policy on April 7.

Before the 2003 severe acute respiratory syndrome coronavirus epidemic in Taiwan, only persons with open tuberculosis wore masks in public. During the epidemic, wearing a mask in public was stigmatized. Thereafter, we educated the public to wear masks as a practice of respiratory hygiene. Although evidence is limited for their effectiveness in preventing transmission of severe acute respiratory syndrome coronavirus 2, either for source control or to reduce exposure, the wearing of masks by healthy persons may prevent potential asymptomatic or presymptomatic transmission (*3*). This marginal reduction in transmission may produce substantial results, particularly when it is implemented early. Taiwan had the foresight to create a large stockpile of medical and surgical masks; other countries or regions might now consider doing so as part of future pandemic plans (*3*).

About the Author

Mr. Chiang is a medical student at National Taiwan University. His primary research interests are epidemiology and prevention of communicable diseases.

References

1. Xiao J, Shiu EYC, Gao H, Wong JY, Fong MW, Ryu S, et al. Nonpharmaceutical measures for pandemic influenza in nonhealthcare settings—personal protective and environmental measures. Emerg Infect Dis. 2020;26:967–75. https://doi.org/10.3201/eid2605.190994
2. Leung NHL, Chu DKW, Shiu EYC, Chan KH, McDevitt JJ, Hau BJP, et al. Respiratory virus shedding in exhaled breath and efficacy of face masks. Nat Med. 2020 Apr 3 [Epub ahead of print]. https://doi.org/10.1038/s41591-020-0843-2
3. Feng S, Shen C, Xia N, Song W, Fan M, Cowling BJ. Rational use of face masks in the COVID-19 pandemic. Lancet Resp Med. In press 2020. https://doi.org/10.1016/S2213-2600(20)30134-X
4. Ng K, Poon BH, Kiat Puar TH, Shan Quah JL, Loh WJ, Wong YJ, et al. COVID-19 and the risk to health care workers: a case report. Ann Intern Med. 2020 Mar 16 [Epub ahead of print]. https://doi.org/10.7326/L20-0175
5. Bae S, Kim MC, Kim JY, Cha HH, Lim JS, Jung J, et al. Effectiveness of surgical and cotton masks in blocking SARS–CoV-2: a controlled comparison in 4 patients. Ann Intern Med. 2020 Apr 6 [Epub ahead of print]. https://doi.org/10.7326/M20-1342

Address for correspondence: Yee-Chun Chen, Department of Internal Medicine, National Taiwan University Hospital No. 7 Chung-Shan South Rd, Taipei, Taiwan; email: yeechunchen@gmail.com

Infections among Contacts of Patients with Nipah Virus, India

Chong Tin Tan, Kum Thong Wong

Author affiliation: University of Malaya, Kuala Lumpur, Malaysia

DOI: https://doi.org/10.3201/eid2608.190722

To the Editor: Kumar et al. recently reported 3 asymptomatic, seropositive persons with Nipah virus (NiV) among 279 contacts of 18 NiV-infected patients (*1*). In the 1998–1999 NiV outbreak in Malaysia, asymptomatic, seropositive persons, most of whom were farm workers and soldiers involved in pig culling, also were identified (*2*,*3*). Furthermore, some additional cases might not have been detected among patients who had mild, nonencephalitic symptoms (e.g., fever, influenza-like illness). Up to 16% of asymptomatic, seropositive persons exhibited lesions in their brain magnetic resonance imaging (MRI) scans, albeit a slightly smaller number than in patients with acute NiV encephalitis (*2*). These discrete, small high-signal lesions in the cerebrum were best seen on fluid-attenuated inversion recovery images (*2*). In another study, a seropositive nurse who was exposed only to patients also had similar brain lesions visible on an MRI scan, suggesting person-to-person transmission (*4*). Whether late-onset NiV encephalitis (i.e., encephalitis in an asymptomatic or mildly symptomatic person) would develop in any of these persons, especially those with brain lesions visible on MRI scan, is unknown. In another cohort, approximately 5% of asymptomatic or mildly symptomatic persons (*5*) had febrile encephalitis characterized by headache, seizures, focal neurologic signs, and cerebrospinal fluid pleocytosis, a set of symptoms and signs distinct from acute NiV encephalitis. In patients who survived acute NiV encephalitis, a clinicopathologically similar relapsing encephalitis has also been reported (*5*). The death rate was ≈20% during the clinical course of late-onset/relapsing NiV encephalitis (5).

Physicians should consider using brain MRI to identify subclinical brain lesions in asymptomatic, seropositive Nipah patients. Moreover, physicians should advise patients of the possibility that late-onset encephalitis might occur months or even years after virus exposure (*5*). New treatments are in development or on trial, so patients with these complications may be offered access to effective treatments.

References

1. Kumar CPG, Sugunan AP, Yadav P, Kurup KK, Aarathee R, Manickam P, et al. Infections among contacts of patients with Nipah virus, India. Emerg Infect Dis. 2019;25:1007–10. https://doi.org/10.3201/eid2505.181352
2. Tan KS, Ahmad Sarji S, Tan CT, Abdullah BJ, Chong HT, Thayapran T, et al. Patients with asymptomatic Nipah virus infection may have abnormal cerebral MR imaging. Neurology Journal of Southeast Asia. 2000;5:69–73.
3. Ali R, Mounts AW, Parashar UD, Sahani M, Lye MS, Isa MM, et al. Nipah virus among military personnel involved in pig culling during an outbreak of encephalitis in Malaysia, 1998–1999. Emerg Infect Dis. 2001;7:759–61. https://doi.org/10.3201/eid0704.017433
4. Tan CT, Tan KS. Nosocomial transmissibility of Nipah virus. J Infect Dis. 2001;184:1367. https://doi.org/10.1086/323996
5. Chong HT, Tan CT. Relapsed and late-onset Nipah encephalitis, a report of 3 cases. Neurology Journal of Southeast Asia. 2003;8:109–12.

Address for correspondence: Kum Thong Wong, Department of Pathology, Faculty of Medicine, University of Malaya, 50603 Kuala Lumpur, Malaysia; email: wongkt@um.edu.my

Retraction: Novel Orthobunyavirus Causing Severe Kidney Disease in Broiler Chickens, Malaysia, 2014–2017

Vilmos Palya, Edit Walkóné Kovács, Szilvia Marton, Tímea Tatár-Kis, Balázs Felföldi, Barbara Forró, Marianna Domán, Krisztián Bányai

Author affiliations: Ceva-Phylaxia Veterinary Biologicals Co. Ltd., Budapest, Hungary (V. Palya, E.W. Kovács, T. Tatár-Kis, B. Felföldi); Hungarian Academy of Sciences, Budapest (S. Marton, B. Forró, M. Domán, K. Bányai)

DOI: https://doi.org/10.3201/eid2608.202331

To the Editor: We would like to retract our article Novel Orthobunyavirus Causing Severe Kidney Disease in Broiler Chickens, Malaysia, 2014–2017 from the June 2019 issue of Emerging Infectious Diseases (*1*). We assert that research was performed in good faith, that all the experimental data contained in the article are well founded and scientifically valid, and that there was no scientific misconduct. However, we subsequently were made aware of further information about the epidemiologic and clinical observations made locally in Malaysia, which brings into question the geographic location where the noted virus originated. Thus, we request this article's retraction.

Reference

1. Palya V, Kovács E, Marton S, Tatár-Kis T, Felföldi B, Forró B, et al. Novel orthobunyavirus causing severe kidney disease in broiler chickens, Malaysia, 2014–2017. Emerg Infect Dis. 2019;25:1110–7. https://dx.doi.org/10.3201/eid2506.181661

Address for correspondence: Vilmos Palya, Ceva-Phylaxia Veterinary Biologicals Co. LTD, Scientific Support and Investigation Unit, Szállás u. 5, Budapest 1107, Hungary; email: vilmos.palya@ceva.com

Human Parasitic Diseases: A Diagnostic Atlas

Lawrence R. Ash, Thomas C. Orihel; American Society for Clinical Pathology Press, Chicago, Illinois, USA, 2019; ISBN-10: 0891896775; ISBN-13: 9780891896777; Pages: 688; Price: $249.29

Human Parasitic Diseases: A Diagnostic Atlas is a comprehensive and invaluable resource for parasitologists, microbiologists, pathologists, and infectious disease practitioners. Lawrence R. Ash, PhD, and Thomas C. Orihel, PhD, have curated a beautiful photographic series of common and rare parasites shown in tissue, blood, feces, and free-living forms. Organized by phylum, genera, and species, this book provides detailed yet practical assistance in identifying and diagnosing human parasitic diseases. Each section starts with a brief overview of the epidemiology, life cycle, transmission, and clinical manifestations of the parasite, detailed enough to orient the reader to the clinical relevance of the pathogen without distracting from its macroscopic and microscopic diagnostic features. The authors provide up-to-date references of each parasite's clinical manifestations and diagnostic procedures.

In addition to the beautiful, high-quality photomicrographs, the authors supplement the book with detailed diagrams clarifying the key microscopic diagnostic features. These details enable the reader to differentiate between closely related parasites.

This book offers many unique aspects. First, the authors provide multiple images comparing subtle differences in the appearance of the same parasite, which will reassure anyone who has struggled to identify a blood smear of a parasite that does not quite fit the textbook example. These images emphasize the subtlety of microscopic identification and pattern recognition. Second, this atlas emphasizes the appearance of parasites in histologic findings and tissue. The authors acknowledge the difficulty of making a histologic diagnosis on the basis of fragments of larger parasites or those that have degenerated in tissues. Third, the book contains a 1911 Arthur Looss quote emphasizing the interconnectedness of animal and human parasites and highlighting the need to consider animal pathogens that have rarely infected humans. This perspective is relevant in a world with increasingly immunosuppressed patients and unprecedented levels of travel and global trade. Therefore, this book is a compelling reference volume for pathologists and microbiology or clinical infectious disease training programs.

Particularly useful for today's clinical infectious diseases practitioners is the last section of the book, which covers artifacts for which macroscopic or microscopic appearance could be easily confused even by an experienced pathologist. This section is a helpful reminder of the diagnostic challenges facing clinicians seeing patients who believe they have an infestation but in whom no parasite can be found.

I will certainly use this atlas as a reference and training guide and will most likely browse through its pages before recertification examinations. Any reader with an inclination towards parasitology will appreciate the authors and their colleagues' fascinating careers in this field.

Tonya Crook

Author affiliation: Penn State Health Milton S. Hershey Medical Center, Hershey, PA, USA

DOI: https://doi.org/10.3201/eid2608.200270

Address for correspondence: Tonya Crook, Penn State Health Milton S. Hershey Medical Center, 500 University Dr, Hershey, PA 17033, USA; email: tcrook@pennstatehealth.psu.edu

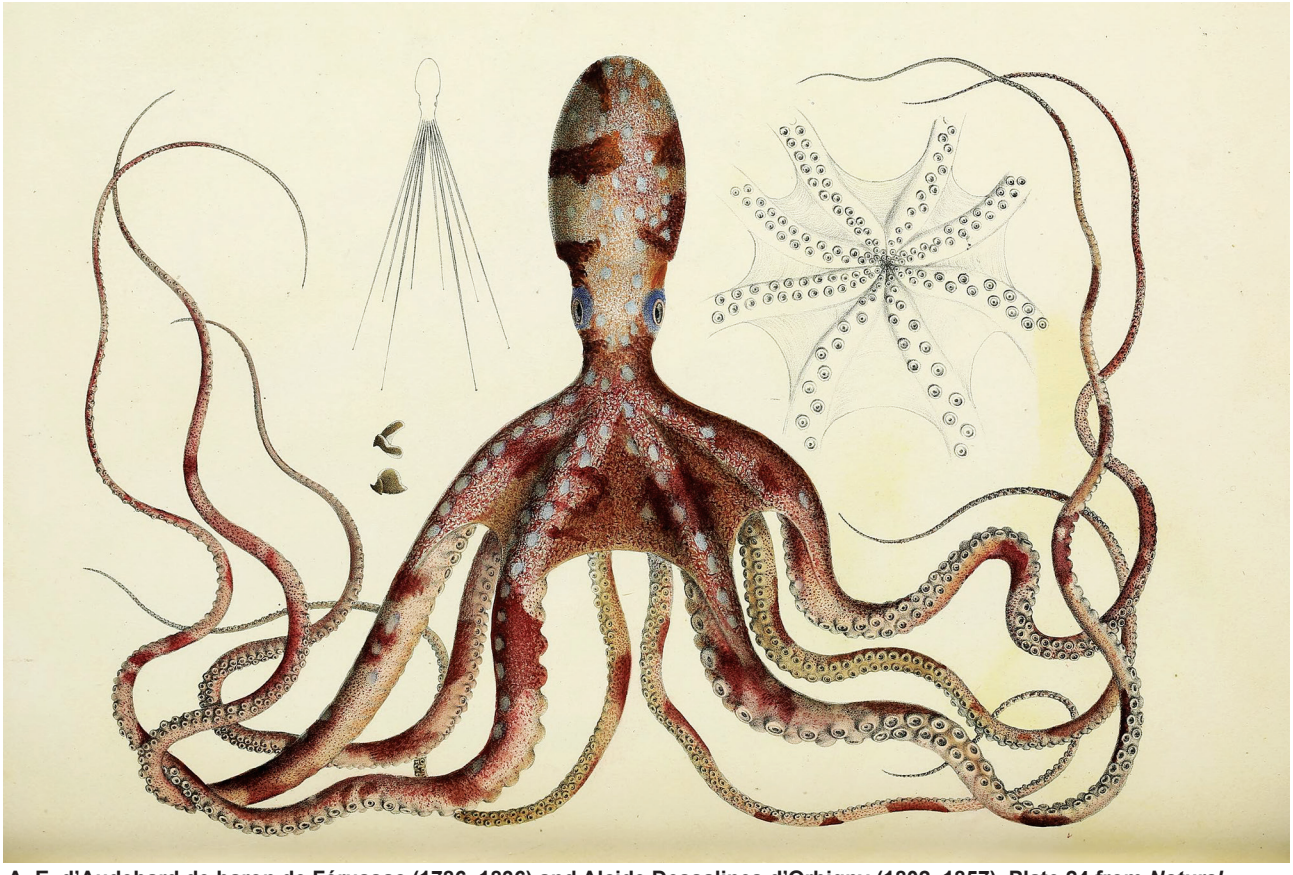

A. E. d'Audebard de baron de Férussac (1786–1836) and Alcide Dessalines d'Orbigny (1802–1857). Plate 24 from *Natural, general and particular history of the acetabuiferous cephalopods living* (1835). Ink on paper. Public domain image from Biodiversity Heritage Library. Holding institution: Smithsonian Libraries, Washington, DC, USA.

The Curious Case of the Cephalopod Parasites

Byron Breedlove

This month's cover illustration of an octopus comes from the book *Natural, General and Particular History of the Acetabuiferous Cephalopods Living* (see the bibliography for the full title). This voluminous study of cephalopods was completed by a pair of 19th century French naturalists, though not exactly as collaborators. A.E. d'Audebard de baron de Férussac wrote the introduction and the first 11 parts; Alcide Dessalines d'Orbigny revised and completed the book. Férussac, a professor of geography and statistics at the École d'état-major in Paris, is now chiefly recognized for his studies of molluscs. D'Orbigny, a professor of paleontology at the Paris Muséum National d'Histoire Naturelle, collected natural specimens from South America and corresponded with Charles Darwin.

Completed in the 1830s, this detailed illustration does not identify the species of octopus represented, though it is most likely a common octopus, which would have been 1–3 feet long and weighed 10–20 pounds. Nonetheless, it displays the animal's characteristic features: bulbous head, wide-angled eyes that provide a panoramic view, 8 whip-like arms festooned with suckers, and mottled and flecked colors. One companion image resembling a multipronged compass protractor reveals the scale and reach of

Author affiliation: Centers for Disease Control and Prevention, Atlanta, Georgia, USA

DOI: https://doi.org/10.3201/eid2608.AC2608

the straightened arms, and on first glance, a second drawing of the creature's underside could pass for a splayed umbrella.

An undeserved reputation for ferocity and belligerence has been foisted on the octopus. In the first century CE, Pliny the Elder decried, "no animal is more savage in causing the death of a man in the water." The air of mystery attached to these intelligent, curious creatures befits them, no doubt spurred by their physical appearance. Anthropologist Roland Burrage Dixon references a Hawaiian creation myth that describes a primordial ocean in which "swims the octopus, the lone survivor from an earlier world."

Given their outward appearance, labeling these creatures as alien or otherworldly does not seem farfetched. Examining their anatomy does not dispel those notions. Their arms, which contain more neurons than their brains, collect and convey an array of sensory information and may even have distinct personalities. Of their three hearts, two move blood from their gills and the third circulates their blood. Their blue blood is tinted by the copper-transporting protein hemocyanin, which is more efficient than hemoglobin for transporting oxygen in frigid and oxygen-poor ocean water.

Octopuses are acknowledged for their adeptness at solving intricate problems and using tools, curiosity, and even mischief. Able to mimic colors and textures and to squeeze into astonishingly compact spaces, these cephalopods excel as both hunters and survivalists. Science writer Katherine Harmon Courage writes, "The boneless octopus must avoid becoming lunch for sharks, eels, fish and even killer whales. But not all of the organisms that feed on octopuses are such charismatic megafauna."

Parasitic organisms occur in all animal species, are as diverse as their host species, and derive their sustenance, during at least part of their lifecycles, at the expense of their hosts. This ubiquitous template of coexistence has persisted and evolved and given rise to euryxenous parasites that infect a spectrum of unrelated hosts; stenoxenous parasites that prefer closely related hosts; and oioxenous parasites that limit themselves to single species of host. Among the latter two types is a phylum of highly specialized parasites known as Rhombozoa or Dicyemida, which dwell only in the kidneys of cephalopods.

Some of the estimated 250–300 known species of octopus are so similar that researchers differentiate them by examining those parasites. Courage writes, "These microorganisms are often unique not just to the octopus but also to a particular species of octopus. In fact, these very specific, kidney-dwelling species can even be used to tell one octopus species from another. (With such variable physical attributes, octopus specimens can be difficult to parse.)"

Parasites can cause a range of diseases in humans, domestic animals, and wildlife. Myriad parasitic infections range from asymptomatic to mild to severe to fatal. They are encountered by hosts of every species on every continent and in every body of water. A confluence of factors—including deforestation, urbanization, and development, international travel and tourism, contemporary agricultural practices, and displacement of wildlife, sanitation problems, and growing antimicrobial and insecticide resistance—encumbers efforts to control parasitic infections. Discerning the abundance, diversity, specialization, and history of parasitic organisms, such as the curious case of the finicky Rhombozoa, may yield information with potential to improve our understanding of other parasitic infections.

Bibliography

1. Centers for Disease Control and Prevention. About parasites [cited 2020 Jun 23]. https://www.cdc.gov/parasites/about.html
2. Combes C. Parasitism: the ecology and evolution of intimate interactions. Chicago: University of Chicago Press; 2001. p. 55–7.
3. Costantino G. The octopus…the monster that isn't. Biodiversity Heritage Library [cited 2020 May 23]. https://blog.biodiversitylibrary.org/2014/10/the-octopusthe-monster-that-isnt.html
4. Courage KH. Octopuses make food for weird critters. Scientific American [cited 2020 Apr 28]. https://blogs.scientificamerican.com/octopus-chronicles/octopuses-make-food-for-weird-critters/
5. Courage KH. Octopus!: the most mysterious creature in the sea. New York: Current, 2015. p. 70–5.
6. Dixon RB. Myths of origins and the deluge. In: Oceanic mythology. Boston: Marshall Jones; 1916. p. 15–6 [cited 2020 Jun 28]. https://archive.org/details/oceanicmytholog02dixogoog
7. Ellis R. Monsters of the sea. New York: Alfred A. Knopp Inc.; 1994. p. 261.
8. Férussac AE, d'Orbigny AD. Natural, general and particular history of the living acetabuiferous cephalopods, and fossils: including: the zoological and anatomical description of these molluscs, details on their organization, their manners, their habits, and the history of the observations of which they were the object from the earliest times to the present day [in French] [cited 2020 Apr 28]. https://www.biodiversitylibrary.org/item/274151
9. Montgomery S. The soul of an octopus: a surprising exploration into the wonder of consciousness. New York: Atria Books; 2016. p. 1–2, 48–50, 158–61.

Address for correspondence: Byron Breedlove, EID Journal, Centers for Disease Control and Prevention, 1600 Clifton Rd NE, Mailstop H16-2, Atlanta, GA 30329-4027, USA; email: wbb1@cdc.gov

UPCOMING ISSUE

EMERGING INFECTIOUS DISEASES®

Vol. 26 No. 9 • September 2020 • Coronaviruses

- Seroepidemiologic Study Designs for Determining SARS-COV-2 Transmission and Immunity
- Disparate Effects of Invasive Group A *Streptococcus* on Native Americans
- Polyclonal *Burkholderia cepacia* Complex Outbreak in Peritoneal Dialysis Patients Caused by Contaminated Aqueous Chlorhexidine and Documented by Genomic Sequencing
- Pathology and Pathogenesis of SARS-CoV-2 Associated with Fatal Coronavirus Disease, United States
- Severe Acute Respiratory Syndrome Coronavirus 2 Prevalence, Seroprevalence, and Exposure Among Evacuees from Wuhan, China, 2020
- Encephalopathy and Encephalitis Associated with Cerebrospinal Fluid Cytokine Alterations and Coronavirus Disease, Atlanta, Georgia, USA, 2020
- Outbreak of *Saprochaete clavata* Infections through Dishwashers in a Cancer Center
- Association of Biosecurity and Hygiene Practices with Environmental Contamination with Influenza A Viruses in Live Bird Markets, Bangladesh
- Risk-Based Estimate of Human Fungal Disease Burden, China
- Molecular Description of a Novel *Orientia* Species Causing Scrub Typhus in South America
- Evaluation of World Health Organization–Recommended Hand Hygiene Formulations
- Heterogeneity of Dengue Illness in Community-Based Prospective Study, Iquitos, Peru
- Isolation, Sequence, Infectivity, and Replication Kinetics of Severe Acute Respiratory Syndrome Coronavirus 2
- Incidence and Seroprevalence of Avian Influenza among a Cohort of Backyard Poultry Growers, Egypt, August 2015–March 2019
- Hepatitis E Virus Genotype 7 RNA and Antibody Kinetics in Naturally Infected Dromedary Calves, United Arab Emirates
- Detection of Severe Acute Respiratory Syndrome Coronavirus 2 RNA on Surfaces in Quarantine Rooms
- Clinicopathologic and Immunohistochemical Findings from Autopsy of Patient with COVID-19, Japan
- Lyme Borreliosis with Scalp Eschar Mimicking Rickettsial Infection
- Large Outbreak of Coronavirus Disease among Wedding Attendees, Jordan
- Carbapenemase-Producing Gram Negative Bacteria in Andalusia, Spain, 2014–2018
- Enterovirus D68 Subclade B3 in Children with Acute Flaccid Paralysis in West Africa, 2016
- Role of Wildlife in Emergence of Ebola Virus, Kaigbono (Likati), Democratic Republic of the Congo, 2017
- Emergence of pstS-Null Vancomycin-Resistant *Enterococcus faecium* clone ST1478, Canada, 2013–2018
- Clusters of Coronavirus Disease in Communities, Japan, January–April 2020
- Sequence Type Changes Associated with Decreasing Macrolide-Resistant *Mycoplasma pneumoniae,* Japan
- Mycobacterial Testing Trends, United States, 2009–2015
- Persistence of Severe Acute Respiratory Syndrome Coronavirus 2 in Aerosol Suspensions
- Updated Estimates of Chronic Conditions Affecting Risk for Complications from Coronavirus Disease, United States
- Oxacillinase-181 Carbapenemase-Producing *Klebsiella pneumoniae* in Neonatal Intensive Care Unit, Ghana, 2017–2019
- Latent Tuberculosis Screening Using Electronic Health Record Data
- Typhus Group Rickettsiosis, Brazilian Amazon
- Information-Accessing Behavior During Zika Virus Outbreak, United States, 2016
- *Clostridioides difficile* in COVID-19 Patients, Detroit, Michigan, USA, March–April 2020
- Acute Cerebral Stroke with Multiple Infarctions and COVID-19, France, 2020
- Large SARS-CoV-2 Outbreak Caused by Asymptomatic Traveler, China

Complete list of articles in the September issue at http://www.cdc.gov/eid/upcoming.htm

Earning CME Credit

To obtain credit, you should first read the journal article. After reading the article, you should be able to answer the following, related, multiple-choice questions. To complete the questions (with a minimum 75% passing score) and earn continuing medical education (CME) credit, please go to http://www.medscape.org/journal/eid. Credit cannot be obtained for tests completed on paper, although you may use the worksheet below to keep a record of your answers.

You must be a registered user on http://www.medscape.org. If you are not registered on http://www.medscape.org, please click on the "Register" link on the right hand side of the website.

Only one answer is correct for each question. Once you successfully answer all post-test questions, you will be able to view and/or print your certificate. For questions regarding this activity, contact the accredited provider, CME@medscape.net. For technical assistance, contact CME@medscape.net. American Medical Association's Physician's Recognition Award (AMA PRA) credits are accepted in the US as evidence of participation in CME activities. For further information on this award, please go to https://www.ama-assn.org. The AMA has determined that physicians not licensed in the US who participate in this CME activity are eligible for AMA PRA Category 1 Credits™. Through agreements that the AMA has made with agencies in some countries, AMA PRA credit may be acceptable as evidence of participation in CME activities. If you are not licensed in the US, please complete the questions online, print the AMA PRA CME credit certificate, and present it to your national medical association for review.

Article Title

Tuberculosis in Internationally Displaced Children Resettling in Harris County, Texas, USA, 2010–2015

CME Questions

1. You are seeing a 13-year-old girl who recently emigrated from Afghanistan for a well-child check. What does the Centers for Disease Control and Prevention (CDC) recommend regarding tuberculosis (TB) screening for this patient?

A. No screening is needed without symptoms or known TB exposures
B. Only an interferon-gamma release assay (IGRA) is required
C. Only a tuberculin skin test (TST) is required
D. A TST should be applied, and a positive test should be confirmed with an IGRA

2. The patient's mother reports that she had a positive TST at the US consulate 4 months ago, before departing Afghanistan. What was the approximate rate of discrepant test results between TSTs and IGRAs in the current study?

A. 20%
B. 30%
C. 40%
D. 60%

3. What can you tell this family about the results of TB testing in the current study?

A. The rate of any positive TB test was 22%
B. Only 40% of children with a positive TB test were ultimately diagnosed with TB infection
C. About 1% of children were diagnosed with TB disease
D. 10% of children with TST-positive/IGRA-negative testing eventually developed TB disease

4. Which one of the following variables was most associated with a higher TST or IGRA in the current study?

A. Immigration classification
B. Female sex
C. Age between 2 and 13 years of age
D. Immigration from Southeast Asia vs other regions

Earning CME Credit

To obtain credit, you should first read the journal article. After reading the article, you should be able to answer the following, related, multiple-choice questions. To complete the questions (with a minimum 75% passing score) and earn continuing medical education (CME) credit, please go to http://www.medscape.org/journal/eid. Credit cannot be obtained for tests completed on paper, although you may use the worksheet below to keep a record of your answers.

You must be a registered user on http://www.medscape.org. If you are not registered on http://www.medscape.org, please click on the "Register" link on the right hand side of the website.

Only one answer is correct for each question. Once you successfully answer all post-test questions, you will be able to view and/or print your certificate. For questions regarding this activity, contact the accredited provider, CME@medscape.net. For technical assistance, contact CME@medscape.net. American Medical Association's Physician's Recognition Award (AMA PRA) credits are accepted in the US as evidence of participation in CME activities. For further information on this award, please go to https://www.ama-assn.org. The AMA has determined that physicians not licensed in the US who participate in this CME activity are eligible for AMA PRA Category 1 Credits™. Through agreements that the AMA has made with agencies in some countries, AMA PRA credit may be acceptable as evidence of participation in CME activities. If you are not licensed in the US, please complete the questions online, print the AMA PRA CME credit certificate, and present it to your national medical association for review.

Article Title

Sporadic Creutzfeldt-Jakob Disease among Physicians, Germany, 1993–2018

CME Questions

1. Your patient is a 65-year-old male retired surgeon with early signs of dementia and ataxic gait. On the basis of the analysis of occupational data of patients with sporadic Creutzfeldt-Jakob disease (sCJD) in Germany by Hermann and colleagues, which one of the following statements about the occurrence of sCJD among physicians in Germany from 1993 to 2016 is correct?

A. The number of reported physicians with sCJD was 0.26% from 1993 to 2016
B. The rate of reported physicians with sCJD remained stable over time
C. In 2017 to 2018, physicians had a 2.6-fold increase for reported sCJD, using the total German population as a control group
D. Of probable/definite sCJD cases aged at least 35 years from June 1993 to December 2016 with occupational data, 0.5% were physicians

2. According to the analysis of occupational data of patients with sCJD in Germany by Hermann and colleagues, which one of the following statements about risk factors for sCJD among physicians in Germany from 1993 to 2018 is correct?

A. The rate of sCJD in 2017 to 2018 was higher among neurosurgeons than among other physicians
B. Of all physicians with sCJD from 1993 to 2018, 64% were surgeons, but in 2018, only 31% of physicians with sCJD were surgeons
C. Surgeons with sCJD were more likely to have short disease duration than nonsurgeon physicians with sCJD
D. A single hospital in Germany had a disproportionately high number of physicians with sCJD

3. On the basis of the analysis of occupational data of patients with sCJD in Germany by Hermann and colleagues, which one of the following statements about clinical implications of the occurrence of sCJD among physicians in Germany from 1993 to 2016 is correct?

A. Larger multinational studies are needed to confirm greater sCJD risk in German physicians in recent years and to clarify whether this is a general or a country-specific phenomenon
B. No risk factors for sCJD have previously been established
C. Results of previous studies all showed increased risk for sCJD in health professionals
D. Case-control studies have shown that orthopedic surgeons had slightly elevated risk for sCJD